

NAVAL POSTGRADUATE SCHOOL

Monterey, California



SYSTEMATIC AND INTEGRATED APPROACH TO
TROPICAL CYCLONE TRACK FORECASTING:
PART III:
TRAITS KNOWLEDGE BASE FOR JTWC TRACK
FORECAST MODELS IN THE WESTERN NORTH PACIFIC

Lester E. Carr, III and Russell L. Elsberry

June 1999

Approved for Public Release; Distribution Unlimited.

Prepared for: Office of Naval Research
Code 322MM, Arlington, VA 22217

SPAWARSYSCOM
Code PWM185, San Diego, CA 92110-3127

DTIC QUALITY INSPECTED 4

19990714 014

Naval Postgraduate School
Monterey, California 93943-5000

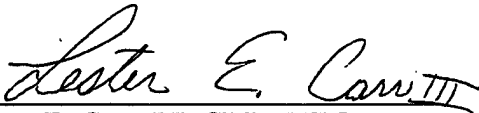
Rear Admiral R. C. Chaplin
Superintendent

Richard S. Elster
Provost

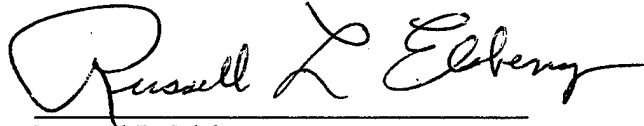
This report was prepared for the Joint Typhoon Warning Center (JTWC) at the Naval Pacific Meteorology and Oceanography Center (NPMOC). Funding was provided by the Office of Naval Research Marine Meteorology Program and Space Warfare Systems Command.

Reproduction of all or part of the report is authorized.

This report was prepared by:

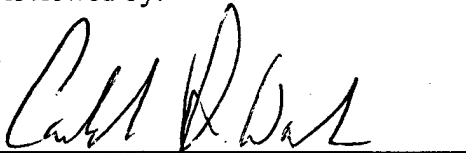


Lester E. Carr, III, CDR, USN
Research Associate
Professor of Meteorology



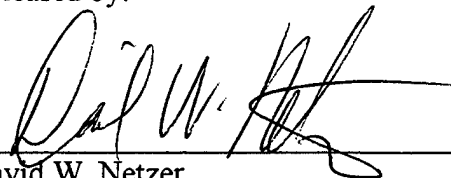
Russell L. Elsberry
Professor of Meteorology

Reviewed by:



Carlyle H. Wash, Chairman
Department of Meteorology

Released by:



David W. Netzer
Dean of Research

REPORT DOCUMENTATION PAGE

Form Approved
OMB No. 0704-0188

Public reporting burden for this collection of information is estimated to average 1 hour per response, including the time for reviewing instructions, searching existing data sources, gathering and maintaining the data needed, and completing and reviewing this collection of information. Send comments regarding this burden estimate or any other aspect of this collection of information, including suggestions for reducing this burden, to Washington Headquarters Services, Directorate for Information Operations and Reports, 1215 Jefferson Davis Highway, Suite 1204, Arlington, VA 22202-4302, and to the Office of Management and Budget, Paperwork Reduction Project (0704-0188), Washington, DC 20503.

1. AGENCY USE ONLY (Leave blank)

2. REPORT DATE

June 1999

3. REPORT TYPE AND DATES COVERED

Interim 10/98 - 5/99

4. TITLE AND SUBTITLE Systematic and Integrated Approach to Tropical Cyclone Track Forecasting: Part III: Traits Knowledge Base for JTWC Track Forecast Models in the Western North Pacific

5. FUNDING NUMBERS

N0003998WRDF125

6. AUTHOR(S)

Lester E. Carr, III, and Russell L. Elsberry

7. PERFORMING ORGANIZATION NAME(S) AND ADDRESS(ES)

Naval Postgraduate School, Department of Meteorology
589 Dyer Rd., Room 245
Monterey, CA 93943-5114

8. PERFORMING ORGANIZATION
REPORT NUMBER

9. SPONSORING/MONITORING AGENCY NAME(S) AND ADDRESS(ES)

SPAWAR Office of Naval Research
PWM 185 Code 322MM
San Deigo, CA 92110-3127 800 N. Quincy St.
Arlington, VA 22217

10. SPONSORING/MONITORING
AGENCY REPORT NUMBER

11. SUPPLEMENTARY NOTES

The views expressed in this report are those of the author and do not reflect the official policy or position of the Department of Defense.

12a. DISTRIBUTION/AVAILABILITY STATEMENT

Approved for Public Release; Distribution Unlimited

12b. DISTRIBUTION CODE

13. ABSTRACT (Maximum 200 words)

All highly erroneous NOGAPS and GFDN track forecasts (72-h error > 300 n mi) in the western North Pacific during 1997 are examined and responsible error mechanisms are identified using the conceptual models of the Systematic Approach Meteorological Knowledge Base. An important and encouraging result of this research is that only six error mechanisms account for 84% (91 of 108) of the poor NOGAPS track forecasts, and only three error mechanisms account for 68% (61 of 90) of the poor GFDN track forecasts. The indications and characteristics of these frequently recurring error mechanisms in the forecast tracks and fields of the models are thoroughly documented and one or more illustrative case studies are provided for each error mechanism. This documentation is organized into a 5-level preliminary Model Traits Knowledge Base for use by TC forecasters when applying the Systematic Approach to formulate the official track forecast. The results of this research also provide model developers and researchers at FNMOC, NRL Monterey, and GFDL with specific information needed to improve the TC track forecasting performance of the NOGAPS and GFDN models.

14. SUBJECT TERMS

Tropical cyclone track forecasting; Tropical cyclone motion

15. NUMBER OF PAGES

227

16. PRICE CODE

17. SECURITY CLASSIFICATION
OF REPORT

UNCLASSIFIED

18. SECURITY CLASSIFICATION
OF THIS PAGE

UNCLASSIFIED

19. SECURITY CLASSIFICATION
OF ABSTRACT

UNCLASSIFIED

20. LIMITATION OF ABSTRACT

NONE

TABLE OF CONTENTS

Acknowledgments	iii
List of Tables	iv
List of Figures	v
 1. Introduction	 1
a. Systematic Approach background	1
b. Report overview	11
1) Purpose	11
2) Methodology	11
3) Results overview	13
4) Report format	14
 2. Binary cyclone interactions	 19
a. Direct cyclone interaction	19
1) Description	19
2) Frequency and characteristics	21
3) Case studies	25
4) Impact on other objective guidance	35
5) Summary	36
b. Indirect cyclone interaction	39
1) Description	39
2) Frequency and characteristics	41
3) Case studies	47
4) Impact on other objective guidance	47
5) Summary	47
 3. Beta effect-related processes	 48
a. Ridge Modification by the Tropical cyclone (RMT)	48
1) Description	48
2) Frequency and characteristics	48
3) Case studies	50
4) Impact on other objective guidance	58
5) Summary	58
b. Reverse trough formation (RTF)	60
1) Description	60
2) Frequency and characteristics	61
3) Case study: Typhoon Rosie (10W)	61
4) Impact on other objective guidance	64
5) Summary	64
c. Tropical Cyclone initial Size (TCS)	64
1) Description	64
2) Impact on other objective guidance	73
3) Summary	73

4. Midlatitude-related processes	75
a. Midlatitude System Evolutions (MSE)	75
1) Description	75
2) Frequency and characteristics	77
3) Case Studies	78
4) Impact on other objective guidance	81
5) Summary	84
b. Response to Vertical wind Shear (RVS)	85
1) Description	85
2) Frequency and characteristics	87
3) Case studies	90
4) Impact on other objective guidance	94
5) Summary	97
c. Baroclinic Cyclone Interaction (BCI)	98
1) Description	98
2) Frequency and characteristics	99
3) Case studies	101
4) Impact on other objective guidance	108
5) Summary	110
5. Conclusion	113
a. Summary of results	113
b. Application to Typhoon Rex (06W) in 1998	114
c. A preliminary Model Traits knowledge base	114
d. Future plans	117
Appendix A	
Appendix B: Case Study of Typhoon Rex (06W) in 1998	
a. TC motion synopsis	199
b. Error mechanism synopsis	199
c. Selected illustrations of error mechanisms	206
d. Conclusion	224
References	225

Acknowledgments. This research has been sponsored from the beginning by the Office of Naval Research Marine Meteorology Program, and more recently by the Space Warfare Systems Command. The authors gratefully acknowledge the crucial assistance and many valuable contributions made by personnel at the Naval Pacific Meteorology and Oceanography Center (NPMOC)/Joint Typhoon Warning Center and the NPMOC, Pearl Harbor, Hawaii. Appreciation is extended to CAPT T. Aldinger and LTC W. Stapler for their support of this research and for making available personnel and facilities at NPMOC/JTWC during the development of this research. Mark Boothe provided a thorough review of the manuscript, which was expertly prepared by Mrs. Penny Jones.

LIST OF TABLES

Table		Page
1.1	NOGAPS 72-h track forecasts during 1997 with FTE > 300 n mi.	14
1.2	As in Table 1.1, except for GFDN 72-h track forecasts	15
1.3	Frequencies of causes of large NOGAPS and GFDN track errors	16
2.1	cases of excessive DCI in the western North Pacific during 1997	24
2.2	Summary of important aspects and illustration key for E-DCI	38
2.3	JTWC maximum wind speed and 35-kt radii for Ivan and Joan	43
3.1	Cases of erroneous RMT in the western North Pacific during 1997	50
3.2	Summary of important aspects and illustrations key for E-RMT	60
3.3	Tropical cyclone structure and movement of Paka and the NOGAPS and GFDN forecast track errors	68
4.1	Cases of erroneous MSE in the western North Pacific during 1997	78
4.2	Summary of important aspects and illustration key for E-MCG	85
4.3	Cases of erroneous RSV in the western North Pacific during 1997	88
4.4	NOGAPS 72-h FTE, ATE, and CTE for 18-20 April 1997	88
4.5	Summary of important aspects and illustration key for E-RVS	98
4.6	Cases of erroneous BCI in the western North Pacific during 1997	101
4.7	Summary of important aspects and illustration key for E-BCI	111
4.8	Summary of important aspects and illustration key for I-BCI	112
5.1	Five-level framework of Model Traits knowledge base	115
5.2	Level 1 of the Model Traits knowledge base indicating error mechanisms	115
5.3	Level 2 of the Model Traits knowledge base listing forecast indications	116
5.4	Levels 3,4, and 5 of Model Traits knowledge base	116
B.1	NOGAPS and GFDN FTEs > 300 n mi and assigned error mechanisms	204

LIST OF FIGURES

Figure	Page
1.1. Overall conceptual framework for the Systematic Approach	2
1.2. General framework of the Meteorological knowledge base	3
1.3. Idealized model tracks with a consensus track	5
1.4. Meteorological knowledge base for western North Pacific	9
1.5. New synoptic patterns and synoptic regions	10
1.6. Frequency of occurrence of 72-h track errors for NOGAPS and GFDN	12
2.1. Conceptual model of Direct Cyclone Interaction (DCI)	20
2.2. Schematics of excessive-DCI contributing to large errors	22
2.3. Track of TC Nestor and five NOGAPS track forecasts	28
2.4. Satellite infrared imagery for Nestor (07W)	30
2.5. Satellite infrared imagery for TC Winnie	32
2.6. Satellite water vapor imagery for TC Rosie	35
2.7. Satellite IR image and track of TC Amber	36
2.8. Best-track and four objective track forecasts during E-DCI	37
2.9. Conceptual model for ICI on eastern TC	40
2.10. Conceptual model for ICI on western TC	40
2.11. Best-track and selected model forecast tracks for TC Joan	42
2.12. Satellite infrared imagery for Ivan and Joan	45
2.13. Best-track and selected model forecast tracks for TC Ivan	46
3.1. Conceptual model of Ridge Modification by a TC (RMT)	49
3.2. Erroneous RMT conceptual model	49
3.3. Best-track and selected model forecast tracks for TC Tina	53
3.4. Best-tracks of TC Victor and TC Tina	53
3.5. Best-track and selected model forecast tracks for TC Bing	55
3.6. Best-tracks of TC Amber and TC Bing	56
3.7. Sea-level pressure analyses and 66-h forecasts for GFDN model	57
3.8. Best-track and selected objective technique forecasts for TC Tina	59
3.10. Conceptual model for a reverse trough formation	62
3.11. Satellite infrared imagery for TC Rosie	63
3.12. Best-track and selected model forecast tracks for TC Rosie	65
3.13. Best-track of Rosie and selected objective technique track forecasts	66
3.14. Right and left semi-circle 35-kt wind radii and corresponding GFDN and NOGAPS FTEs	67
3.15. Satellite IR imagery for TC Paka during 13-18 December 1997	69
3.16. Best-track and selected model track forecasts for TC Paka	70
3.17. Sea-level pressure fields for GFDN analysis of Paka and subsequent forecasts	72
3.18. Best-track of Paka and selected objective technique track forecasts	74
4.1. Schematic of Midlatitude System Evolutions (MSE) leading to track errors	76
4.2. Best-track and selected model track forecasts for TC Mort	80
4.3. Best-track of TC Joan and selected objective technique track forecasts	82
4.4. Best-track of TC Mort and selected objective technique track forecasts	83

Figure	Page
4.5. Conceptual model for Response to Vertical wind Shear leading to track errors	86
4.6. NOGAPS 48- and 72-h 500 mb wind forecasts for TC Isa	89
4.7. Satellite IR imagery for TC Nestor	91
4.8. Best-track for TC Nestor and two sets of NOGAPS and GFDN forecasts	93
4.9. Best-track and selected model track forecasts for TC Paka	94
4.10. Satellite IR imagery for TC Paka during 19-22 December 1997	95
4.11. Best-track for TC Nestor and selected objective technique track forecasts	96
4.12. Best-track for TC Paka and selected objective technique track forecasts	97
4.13. Schematics of two stages of Baroclinic Cyclone Interaction	100
4.14. Satellite IR imagery for TC Peter	103
4.15. Best-track and selected model track forecasts for TC Peter	105
4.16. Best-track and selected model track forecasts for TC Yule	106
4.17. Satellite IR imagery for TC Yule	107
4.18. Best-track for TC Peter and selected objective technique track forecasts	109
4.19. Best-track for TC Yule and selected objective technique track forecasts	110
B.1. Best-track for TC Rex	200
B.2. Satellite IR imagery for TC Rex from 24 – 29 August 1998	201
B.3. Satellite IR imagery for TC Rex from 30 August – 2 September 1998	202
B.4. Satellite IR imagery for TC Rex from 3-8 September 1998	203
B.5. Best-track and selected model forecast tracks for TC Rex	205
B.6. Best-track and selected model forecast tracks for TC Rex	207
B.7. NOGAPS 500-mb wind forecasts and verifying analyses for 1200 UTC 24 August	208
B.8. NOGAPS sea-level pressure forecasts and verifying analyses for 1200 UTC 24 August 1998	210
B.9. NOGAPS and GFDN sea-level pressure forecasts and verifying analyses for 0000 (0600) UTC 26 August 1998	212
B.10. NOGAPS and GFDN sea-level pressure forecasts and verifying analyses for 0000 (0600) UTC 29 August 1998	216
B.11. NOGAPS and GFDN 500 mb wind forecasts and verifying analyses for 0000 (0600) UTC 29 August 1998	218
B.12. NOGAPS and GFDN sea-level pressure forecasts and verifying analyses for 0000 (0600) UTC 3 September 1998	220
B.13. NOGAPS and GFDN sea-level pressure forecasts and verifying analyses for 0000 (0600) UTC 4 September 1998	222

1. Introduction

a. Systematic Approach background

1) Objective. The long-range objective of the Systematic and Integrated Approach to Tropical (TC) Cyclone Track Forecasting (hereafter the Systematic Approach) project is to bring about significant quantitative and qualitative improvements in official TC track forecasts. Desired quantitative improvements include: lower average forecast track errors (FTE), official FTE's that are consistently better than the FTEs of the objective track forecast guidance available to the forecaster, and a reduction in the number of track forecasts that have very large FTEs (commonly referred to as "busts"). Unlike track forecasts provided by objective guidance (i.e., models), each official track forecast is accompanied by a subjective conceptual picture or "meteorological scenario" in the mind of the forecaster. This conceptual picture provides the meteorological basis for the official track forecast. The meteorological reasoning behind the official forecast is routinely conveyed in both written and verbal forms (e.g., prognostic reasoning messages and phone discussions) to other meteorologists and non-meteorologists to help them understand and properly respond to the forecast. Thus, the meteorological reasoning of the forecaster is a highly important, albeit qualitative, component of the official track forecast. The Systematic Approach is designed to help the TC forecaster develop a meteorological basis for the official track forecast that reflects dynamically-sound, state-of-the-science understanding of tropical cyclone motion and track prediction.

2) Concept. In the conceptual framework of the Systematic Approach (Fig. 1.1), the official track forecast results from the application of knowledge bases (right column) to various sources of information (left column) via a series of evaluation and formulation processes (center column). The most important components of the Systematic Approach are the TC Meteorological knowledge base and the Forecast Model Traits knowledge base. For reasons explained below, the Model Traits knowledge base is divided into two parts: Numerical Model Traits and Objective Technique Traits (Fig. 1.1). The Meteorological knowledge base is a set of conceptual models (Fig. 1.2) by means of which the forecaster may assemble a conceptual picture to explain observed (and predicted) TC motion in terms of:

- (i) environment structure that is comprised of a synoptic pattern and region, which determine the large-scale steering flow that to first order is responsible for TC motion;
- (ii) TC structure that consists of a maximum wind speed (intensity), which affects the vertical depth of the TC and thus how it responds to environmental steering; and a horizontal size or extent, which affects how the TC interacts with, and potentially alters, the environment; and
- (iii) one or more "transitional mechanisms" that may or may not depend on the presence of the TC, and that act to change (i.e., transition) the structure of the TC environment from one pattern/region combination to another, and thus change the steering flow primarily responsible for the motion of the TC.

SYSTEMATIC APPROACH CONCEPTUAL FRAMEWORK

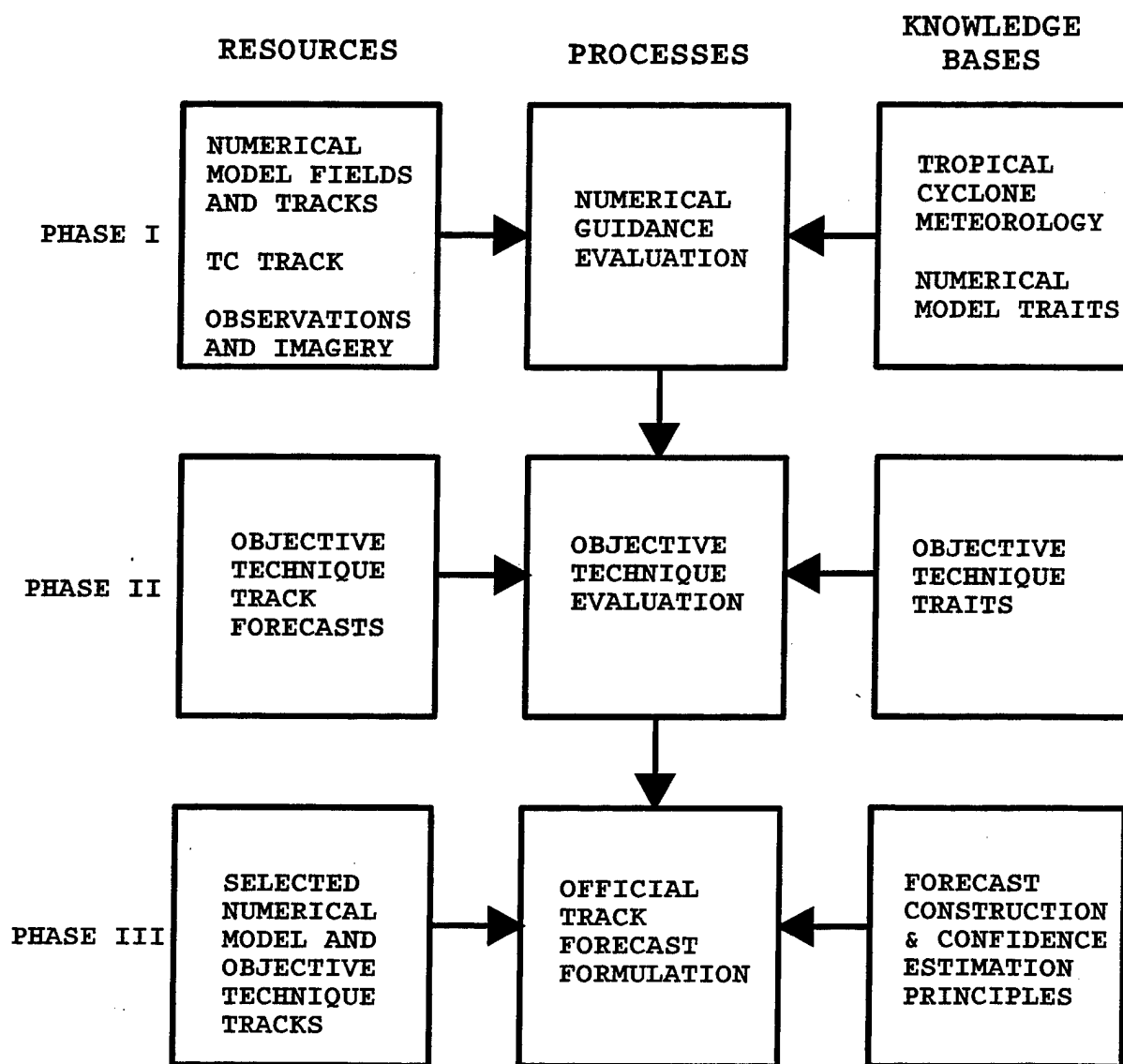


Fig. 1.1. Overall conceptual framework for the Systematic Approach to Tropical Cyclone Track Forecasting in three phases. This report primarily addresses the Numerical Model Traits Knowledge Base in the upper right.

Meteorological Knowledge Base Framework

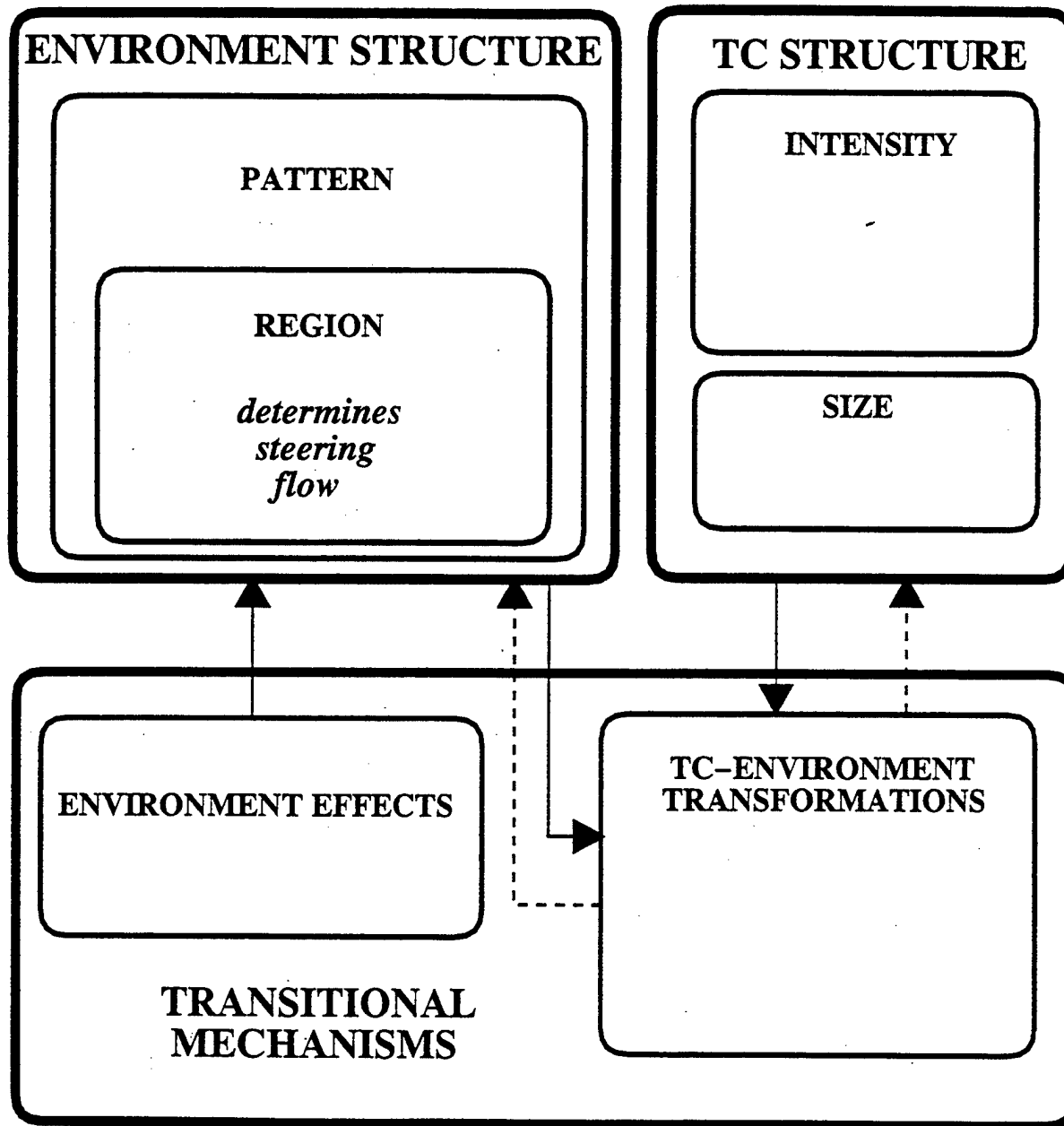


Fig. 1.2. General framework of the Meteorological Knowledge Base of the Systematic Approach, which can be adapted to each tropical cyclone basin.

The Numerical Model Traits knowledge base (Fig. 1.1) follows naturally from the assumption that the error characteristics of TC track forecasting models (whether simple or complex) are not random, but rather depend systematically on the particular meteorological situation responsible for the motion of the TC at any time. Examples that support this premise, and which are familiar to any TC forecaster, include: (i) improved accuracy and closer agreement of track forecast models when the TC is equatorward of the subtropical ridge as compared to when the TC is at or near the ridge axis; (ii) typically poorer-than-normal model performance when two or more TCs are in proximity; and (iii) periods when there are consistently good forecasts, then consistently poor forecasts, and then consistently good forecasts again. The Numerical Model Traits knowledge base of the Systematic Approach is comprised of the results of a systematic evaluation of the performance of available track forecast models in the various scenarios of TC-environment interaction described by the Meteorological knowledge base.

A distinction is made between the Numerical Model Traits and Objective Technique components of the Model Traits knowledge base, because only numerical TC forecast models have analysis and forecast fields that the forecaster can use to characterize the model-depicted TC-environment scenario that accounts for the model's track forecast. Thus, a numerical model track can be associated with a conceptual picture derived directly from the model's prediction fields. By contrast, other objective techniques such as regression equation models and steering models provide only a track, and thus tend to be "black boxes." The conceptual picture to explain the track forecast by such techniques must be obtained indirectly via the forecast fields of the numerical model on which the techniques depend. That is, the conceptual picture developed to explain the numerical model track using the forecast fields from the model may also adequately account for the tracks of an objective technique, if the track forecast by the technique is similar to the numerical model track.

Given the above, the basic idea of the Systematic Approach is to enable the forecaster to systematically:

- (i) employ the Meteorological knowledge base to classify and form a conceptual picture of the current and numerically-forecast meteorological situation;
- (ii) employ the Model traits knowledge base to identify the available numerical TC track forecast models (and associated objective techniques) that are likely to be acceptably accurate or unacceptably inaccurate based on past performance characteristics in similar situations; and
- (iii) formulate an official track forecast that represents an informed, selective consensus of only those model track forecasts deemed to be acceptably accurate.

To help the reader to visualize how the Systematic Approach is intended to assist the forecaster, consider the idealized distributions of model 72-h track forecasts in Fig. 1.3. All actual distributions of model forecasts can be viewed by the forecaster as constituting either:

Idealized Model Track Forecast Distributions

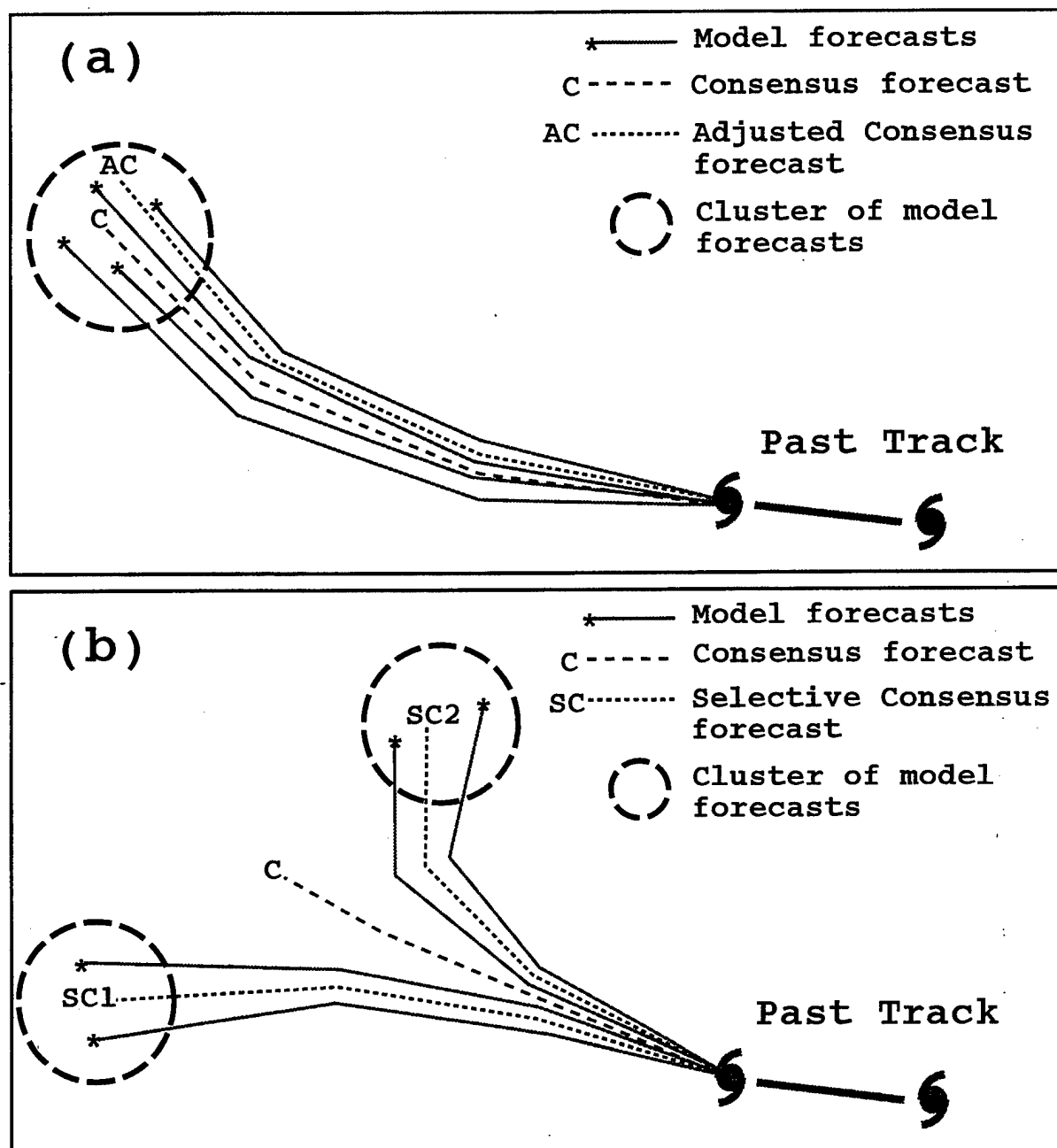


Fig. 1.3. Idealized model tracks (solid lines) with a consensus track (labelled C, dashed) and a hypothetical adjusted consensus (AC, dotted). In panel (a), the model tracks essentially are consistent and fall into a single cluster (heavy dashed circle). In panel (b), the tracks fall into two clusters in which the selective consensus is the average of the tracks in that cluster.

(i) a single cluster with a single associated meteorological scenario that explains all of the model tracks (Fig. 1.3a); or

(ii) two or more clusters, with each cluster corresponding to a particular meteorological scenario that explains the model tracks in that cluster (Fig. 1.3b).

It is emphasized that:

(i) although very distinct clusters are shown in Fig. 1.3a and b for purpose of illustration, in reality the clusters can be quite "fuzzy," which may cause the forecaster to not assign a two-cluster classification to the distribution of model forecast tracks; and

(ii) although clustering by forecast direction is illustrated in Fig. 1.3b, the clusters may be distinguished by any combination of speed and direction, and may only contain one forecast track.

In the case of a single cluster, an official track forecast that closely conforms to the consensus of all the model tracks (Fig. 1.3a; track C) will usually be the best option for the forecaster, and is the most likely to result in the lowest errors on average (Goerss 1998). In this situation, for which the forecast positions of all the models agree well, application of the Systematic Approach Meteorological and Model Traits knowledge bases to discern subtle differences among the individual model forecast fields is not likely to consistently result in an improvement to a simple consensus forecast. In a minority of cases, model track forecasts in relatively good agreement may all have a qualitatively similar bias. In these situations, an adjusted consensus (AC) track forecast may make a modest improvement on the simple consensus forecast. Regardless of whether a simple consensus or adjusted consensus results from a single model track forecast cluster, the Systematic Approach process will still be qualitatively useful for formulating a consistent dynamically-informed explanation (conceptual picture) that accounts for the predicted TC motion.

In the case of two track clusters, a simple consensus average track (Fig. 1.3b; track C) down the middle may not be consistent with any of the meteorological scenarios represented by the individual clusters, and thus may not be meteorologically justifiable. If the track clusters have large directional differences, the simple consensus forecast will necessarily have a slow bias (illustrated in Fig. 1.3b). Given two track forecast clusters, one cluster usually represents the actual track better than the other cluster. In other words, it is very unlikely that both clusters will depart from reality equally, particularly if the separation distance between the cluster centroids is large. As a result, it is more likely that a selective consensus (Fig. 1.3b; tracks SC1 or SC2) of the members of one of the clusters will have lower forecast errors than the simple consensus of all the available track forecasts. It is especially in these cases that the Systematic Approach concept is expected to greatly help the forecaster to decide which selective consensus is the better choice on which to base the official track forecast. So long as the same meteorological conditions continue to apply, the official forecasts should follow this scenario so that shift-to-shift consistency in the official track forecasts is achieved. Only when it is clear that the actual meteorological condition differs from this scenario should the official track forecast be changed to the other track cluster.

As will be shown later, it will be relatively straightforward in some cases to determine that the meteorological scenario that represents a particular track cluster is highly unlikely to verify (say for example track SC1 in Fig. 1.3b). In such cases, the selective consensus based on the remaining cluster of tracks (track SC2) logically becomes the basis for the official track forecast. In other situations, the forecaster may use the Systematic Approach process to identify two scenarios that may be equally likely to verify. This is still very useful information, despite the fact that the forecaster must still select one selective consensus or the other to be the basis for the official track forecast. Via the prognostic reasoning that accompanies each official forecast, the forecaster can communicate that the current situation appears to have a low degree of predictability and alert the recipients of the TC warning of the possible occurrence of an alternate scenario, as represented by the selective consensus of the model track forecast cluster not used for the official track forecast.

3. Development progress. Since the first presentation at the 1994 Annual Tropical Cyclone Conference in Tokyo that introduced the idea, the Systematic Approach project has gone through several evolutionary stages. In Part I of this Naval Postgraduate School (NPS) technical report series (Carr and Elsberry 1994; hereafter Part I), the motivation and a conceptual framework for the Systematic Approach were introduced, and a proposed TC motion Meteorological knowledge base applicable to the western North Pacific was developed. The main body of Part I included many case studies to illustrate the potential of the Meteorological knowledge base to explain a wide variety of TC tracks. The scientific bases for the knowledge were documented in the Appendices to Part I that synthesized results from observational, theoretical, and numerical studies in the literature. In addition, the authors incorporated some original research to explain several modes of TC motion in the western North Pacific that were not (or adequately) addressed in the literature.

To assess the effectiveness of the proposed Meteorological knowledge base, a five-year (1989-1993) climatological data base of pattern/region and transitional mechanism assignments was developed (Carr et al. 1995) using primarily 500-mb analyses from the Navy Operational Global Atmospheric Prediction System (NOGAPS), satellite imagery, and TC tracks prepared by the Joint Typhoon Warning Center (JTWC). In addition, a reproducibility test was conducted to determine how well scenario assignments made by novices to the Systematic Approach compared to those made by the developers of the Systematic Approach. This assessment process led to a number of refinements and additions to the meteorological knowledge base proposed in Part I that have been documented in Part II of this technical report series (Carr et al. 1995; hereafter Part II).

Some of the research by the authors leading to the development of a western North Pacific meteorological knowledge base has been published in journal articles. Carr and Elsberry (1995) investigate interactions between TCs and monsoon gyres that lead to severe TC track changes. Carr and Elsberry (1997) formulate a physically-based model for TC outer wind structure that is then used to model beta-effect propagation as a function of TC size, and also to generate the peripheral anticyclone that contributes to poleward turns. Carr et al. (1997a) present observational evidence for three modes of binary TC interaction. Finally, Carr and Elsberry (1998) investigate quantitative properties of the three modes of TC interaction (rotation sense and rate, separation distance, etc.) and develop objective criteria by which to alert forecasters of the possible onset of different modes of TC interaction. To provide a single document that incorporates the essential information from the technical reports and journal articles cited above in a form more useful to the forecaster, a technical report entitled "Condensed and Updated Meteorological Knowledge Base for the Western

North Pacific" (Carr et al. 1997b; hereafter CMKB) has recently been published. The particular set of conceptual models that have been developed to account for observed TC motion in the western North Pacific is shown in Fig. 1.4. Most of these models are defined and illustrated in the CMKB.

Concurrent with the development of the Systematic Approach in the western North Pacific, the approach has been extended to other basins. Two M. S. theses have investigated adaptation of the western North Pacific Meteorological knowledge base to the eastern and central Pacific (White 1995) and the Atlantic (Kent 1995). Because these studies provided preliminary support for the applicability of the Systematic Approach to all TC basins, the names of some of the Meteorological knowledge base conceptual models were modified to facilitate global application (e.g., using the term poleward vice northward). Recently, Boothe (1997) extended the work of White in the eastern and central Pacific by increasing the size of the data base, and tabulating the frequency of recurring environment transitions and responsible transitional mechanisms. In addition, a collaborative effort with the Australian Bureau of Meteorology adapted the western North Pacific Meteorological knowledge base for use in the Southern Hemisphere and produced a 4-year (1994-1997) climatological data base of pattern/region and transitional mechanism assignments (Bannister et al. 1997). Recently, a second collaborative effort was completed and resulted in some refinements to the Southern Hemisphere Meteorological knowledge base and a doubling of the size of the climatological data base to 8 years (1992-1998). These results are documented in Bannister et al. (1998).

The new Environment Structure terminology in Fig. 1.4 (upper left) is illustrated in the synoptic patterns and regions in Fig. 1.5. In the Standard (S) pattern, the previous Weakened Ridge (WR) region has been replaced by a Poleward Flow (PF) region, and the previous Dominant Ridge (DR) has been replaced by a Tropical Easterlies (TE) region. An Equatorward Flow (EF) region has also been added to account for equatorward tracks. Although the Multiple TC pattern has now been dropped, the EF and PF regions of that pattern have been completely subsumed in the S pattern (Fig. 1.5). In the Poleward (P) pattern, the previous Poleward-Oriented (PO) has been replaced by the PF region, and two new synoptic regions called Equatorial Westerlies (EW) and EF have been added. Similar region name changes from PO to PF and DR to TE have also been made in the Gyre (G) synoptic pattern. Finally, a new Midlatitude (M) synoptic pattern has been introduced with PF and EF regions in addition to the Midlatitude Westerlies (MW) region.

Other changes in the Transitional Mechanisms in Fig. 1.4 will be described later in this report. For example, the previous TC Interactions (DTI, STI, and ITI) have been generalized to the interaction of a TC with another cyclone (hence DCI, SCI, and ICI). The Baroclinic Cyclone Interaction (BCI) will be described in section 4c, and the Midlatitude System Evolutions (MSE) with its four variations involving Cyclogenesis (MCG), Cyclolysis (MCL), Anticyclogenesis (MAG), and Anticyclolysis (MAL) is introduced in section 4a.

Meteorological Knowledge Base for the Western North Pacific

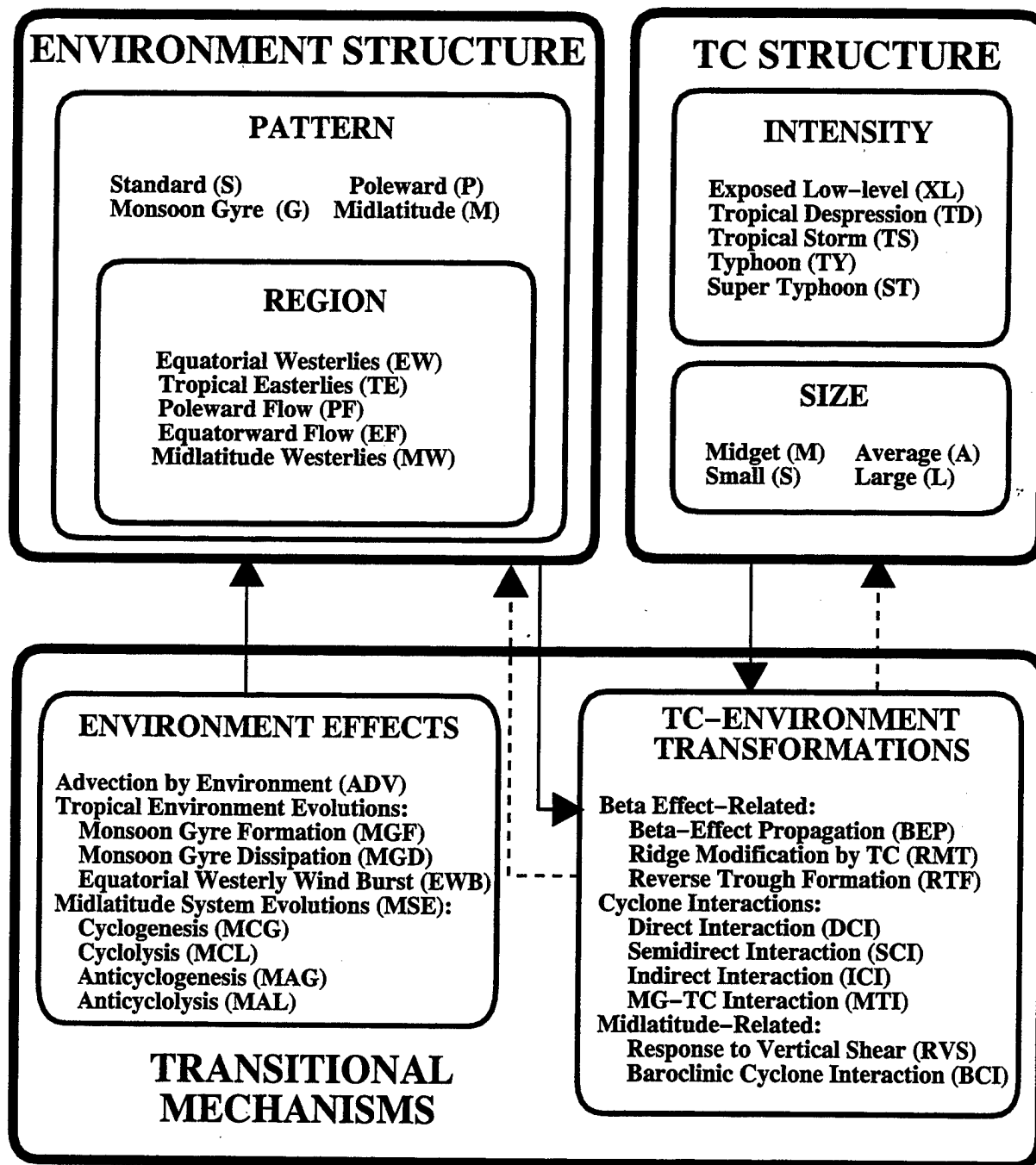


Fig. 1.4. Specific example of the Meteorological knowledge base in Fig. 1.2 for the western North Pacific. As indicated in the text, this knowledge base has recently been updated.

WESTERN NORTH PACIFIC SYNOPTIC PATTERNS AND REGIONS

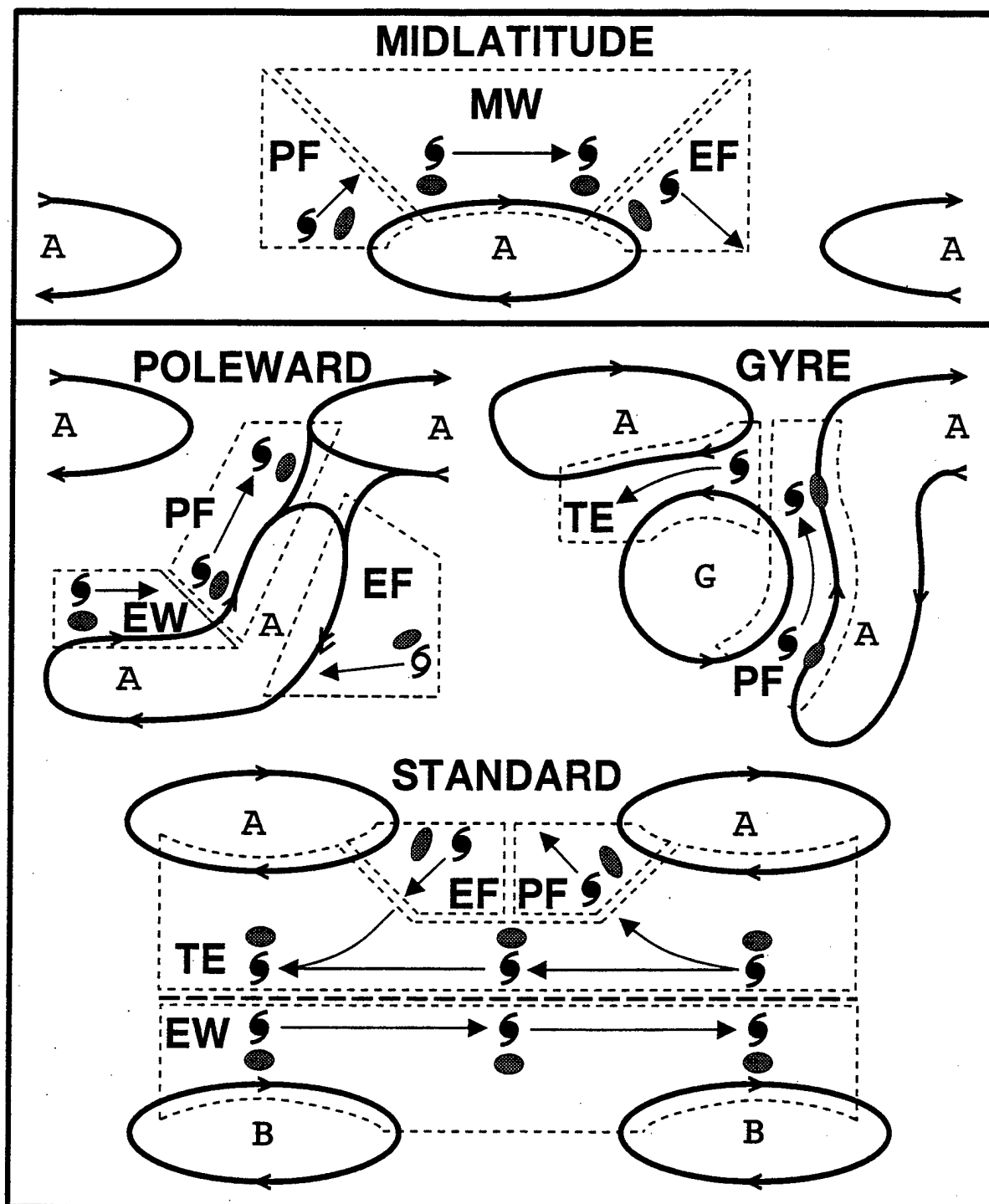


Fig. 1.5 New synoptic patterns (Standard, Poleward, Gyre, and Midlatitude) and synoptic regions (see text and Fig. 1.4 for definitions) for the western North Pacific.

b. Report overview

1) Purpose. The focus of the Part I, Part II, and CMKB reports was the development of the Meteorological knowledge base for the western North Pacific. The purpose of this report is to document the second major component of the Systematic Approach: a Model Traits knowledge base that describes how objective TC track forecast guidance available to the forecasters at JTWC performs in the western North Pacific. In particular, this report will focus on the identification and analysis of instances when highly erroneous forecasts have been made by one or both of the numerical models run by the U.S. Navy: NOGAPS and the U.S. Navy version of the Geophysical Fluid Dynamics Laboratory model (GFDN). Such documentation is a necessary step to successfully recognize highly erroneous numerical model track forecasts on a real-time basis, and either discard or greatly modify such objective forecasts when formulating the official track forecast. That is, a knowledge of when specific model track forecasts are likely to be highly erroneous will permit the forecaster to formulate an official track forecast that reflects an informed adjusted or selective consensus of the remaining numerical model tracks (as discussed in the Systematic Approach Concept section above), as opposed to using an indiscriminate simple consensus of all available track guidance.

The emphasis is on the traits of NOGAPS and GFDN since currently only the forecast fields of these two models are available for analysis and interpretation by the JTWC forecaster. However, some limited description will be provided on the traits of the other objective TC track forecasting techniques employed by JTWC, as well as the numerical models: the Japanese Global Spectral Model (JGSM); the Japanese Typhoon Model (JTYM); and the UK Meteorological Office Global Model (EGRR), even though only the tracks are available to JTWC forecasters.

2) Methodology. The data base for this study consists of the NOGAPS and GFDN forecast tracks and fields for all 1997 western North Pacific TCs except Linda (30W). Linda was omitted since all 72-h NOGAPS and GFDN forecasts verified in the North Indian Ocean, which is treated as a climatologically distinct region for the purpose of the Systematic Approach. The analysis is limited to 1997 as this is the first year that both NOGAPS and GFDN fields were available from the Master Environmental Library (MEL) at the Naval Research Laboratory--Monterey. The distribution of the 72-h forecast track errors (FTE) of NOGAPS (denoted NGPS by JTWC) and GFDN for the 1997 western North Pacific TC season are shown in Fig. 1.6. To maximize the sample sizes in Fig. 1.6, the objectively-determined (via the NOGAPS and GFDN TC tracking algorithms) forecast positions archived in the Automated Tropical Cyclone Forecast (ATCF) System data base are supplemented by some manually-determined positions from the model fields. Specifically, whenever a closed pressure center and collocated closed 850-mb wind center were evident in the 72-h forecast fields, a missing 72-h position was added. This manual tracking technique resulted in the addition of 35 NOGAPS 72-h forecast positions, but none for GFDN. In a number of instances, the GFDN model integration terminated before 72 h because the TC approached the boundary of the model domain. If the GFDN did reach 66 h and a definite TC circulation was evident in the GFDN 66-h forecast field, a 72-h position was derived by simple extrapolation. This technique resulted in five 72-h forecast positions being added to the database.

Notice that neither the NOGAPS nor GFDN FTE histograms are normally distributed. Rather, the distributions are skewed toward the large FTEs that pose a serious problem for the

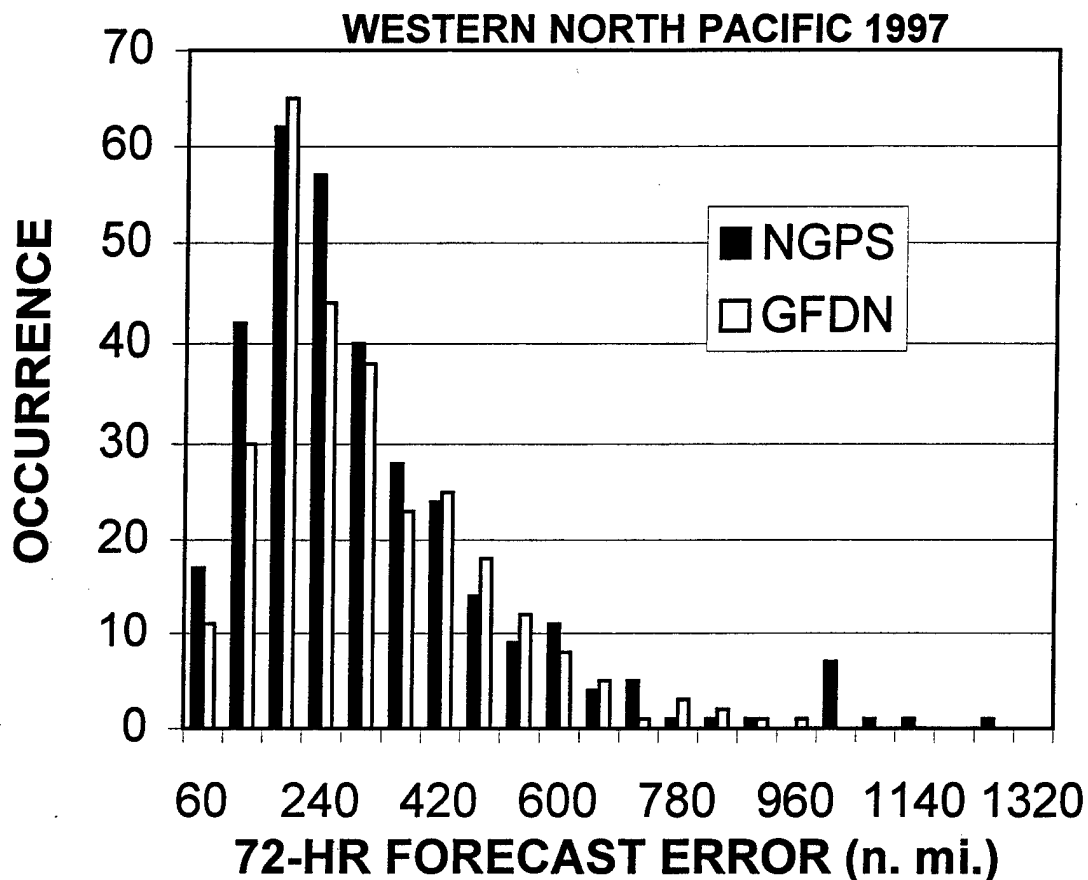


Fig. 1.6. Frequency of occurrence of 72-h track errors for the NOGAPS (solid) and GFDN (open) forecasts of western North Pacific TCs during 1997.

forecaster. Even though the largest FTE for NOGAPS (1226 n mi) is significantly larger than that for GFDN (931 n mi), the percent of 72-h forecasts with a 300 n mi or greater FTE is very similar (33.1% for NOGAPS and 34.5% for GFDN). Since a FTE of 300 n mi is twice the magnitude of the average 72-h FTE goal of 150 n mi that JTWC is trying to attain, this FTE value is defined as the lower limit for highly erroneous track forecast. For each FTE greater than 300 n mi, a subjective evaluation was conducted of the forecast fields of both models and visible, infrared, and water vapor imagery to determine if a plausible physical mechanism could be identified to account for the large FTE. The results of this analysis are the basis for a NOGAPS and GFDN forecast traits knowledge base.

The analysis process described above also provides a *de facto* test of the capability of the western North Pacific Meteorological knowledge base of the Systematic Approach to describe model-predicted TC motion as well as actual motion. Of interest in this regard is the fraction of poor NOGAPS or GFDN track forecasts:

- (i) that could be plausibly explained in terms of a TC motion mechanism already included in the western North Pacific Meteorological knowledge base;
- (ii) that could be plausibly explained in terms of a physical mechanism not contained in the western North Pacific Meteorological knowledge base; or
- (iii) for which no plausible physical explanation could be found.

3) Results overview. The results of the above evaluation process are listed by TC number and the model initial time for NOGAPS and GFDN in Tables 1.1 and 1.2, respectively. The meanings and frequencies of the "cause" acronyms in these tables are provided in Table 1.3. Although each of these track error sources will be described in detail in the following chapters, an overview is presented here to provide a perspective on the relative frequency from various error sources.

Erroneous binary cyclone interactions (Table 1.3; rows 1- 4) were by far the most frequent cause of poor NOGAPS and GFDN 72-h forecasts, and accounted for 42 (39%) and 36 (36%) of the large FTE cases, respectively. The three types of cyclone interactions listed are analogous to the three types of TC-TC interactions described in Carr et al. (1997), except that in the numerical model predictions the second cyclone was not always a TC. Excessive Direct Cyclone Interaction (E-DCI) was remarkably prevalent, and degraded more forecasts than any other single phenomenon by roughly a 2-to-1 margin for NOGAPS and 3-2 margin for GFDN. Those poor forecasts occurred during 18 separate periods involving 14 TCs in the western North Pacific in 1997. By contrast, evaluation of the TC tracks and NOGAPS analyses indicated that track-altering DCI actually occurred only twice in 1997; i.e., real DCI is a rare event in relation to these model-predicted events.

Table 1.1. All NOGAPS 72-h track forecasts for western North Pacific TCs (except Linda) during 1997 that resulted in a forecast track error (FTE) exceeding 300 n mi. The meanings of the acronyms in the "Cause" columns are provided in Table 1.3. The appearance of ????? in the "Cause" column indicates that a dynamical explanation for the large FTE could not be readily discerned.

NOGAPS 72-H FORECASTS EXCEEDING 300 N MI IN 1997							
TC	DATE	FTE	CAUSE	TC	DATE	FTE	CAUSE
02W	97041700	338	?????	12W	97073100	547	
02W	97041912	502	E-RVS	12W	97073112	665	
02W	97042000	687		12W	97080100	739	
04W	97050700	688	E-DCI	12W	97080112	502	E-RMT
04W	97050712	497		12W	97080200	517	
04W	97050800	308		12W	97080212	311	
05W	97052612	360	E-DCI	12W	97080600	326	I-BCI
05W	97052700	378		12W	97080612	396	
05W	97052712	327		12W	97080700	572	
05W	97052900	317	E-DCI	13W	97080100	343	?????
05W	97052912	394		14W	97080812	392	E-DCI
06W	97052712	385	E-DCI	14W	97081600	403	E-DCI
06W	97052800	384		14W	97081612	390	
06W	97052900	391		14W	97081700	570	
06W	97052912	420	E-RVS	14W	97081712	786	
06W	97053000	557		15W	97081900	334	I-BCI
07W	97060600	377	E-RMT	15W	97081912	431	
07W	97061100	541	E-DCI	18W	97082112	590	E-RMT
07W	97061200	600	E-RVS	18W	97082712	319	E-DCI
07W	97061212	354	E-BCI	19W	97082800	307	E-RMT
08W	97061612	372	I-MAL	19W	97082812	393	
08W	97061700	423		19W	97090212	640	I-BCI
08W	97061712	598		19W	97090300	478	E-BCI
08W	97061800	342		21W	97091312	508	E-RMT
09W	97062600	569	I-BCI	21W	97091400	535	
09W	97062612	1019		21W	97091412	493	
09W	97062700	1226		23W	97092100	428	E-BCI
10W	97071900	458	E-RTF	23W	97092112	303	
10W	97071912	363		24W	97092212	460	E-DCI
10W	97072000	474		24W	97092300	306	
10W	97072600	459	E-BCI	24W	97092500	328	E-DCI
11W	97072800	961	E-DCI	24W	97092612	326	I-BCI
11W	97072812	1087		27W	97101400	320	E-RMT
11W	97072912	880		27W	97101600	357	
11W	97073000	1019		27W	97101700	427	E-RTF
12W	97073012	609	E-DCI	27W	97101712	582	
27W	97101800	404		27W	97101812	301	
27W	97101812	301		27W	97101912	381	E-SCIW
27W	97101912	406		27W	97102000	500	
27W	97102012	500		27W	97102100	462	E-RVS
27W	97102112	597		27W	97102200	642	
27W	97102200	1016		27W	97102212	407	E-RTF
28W	97101712	682		28W	97101800	395	
28W	97101812	355	E-BCI	28W	97102112	327	
28W	97102200	337		28W	97102212	345	E-DCI
29W	97102712	335	E-MAG	29W	97110312	393	
29W	97110400	308		29W	97110412	680	E-RVS
29W	97110500	584	I-BCI	29W	97110512	1073	
29W	97110600	372	E-DCI	02C	97091312	382	
02C	97091400	1017	E-DCI	02C	97091400	986	
05C	97120700	961		05C	97120712	443	
05C	97120712	362		05C	97120800	453	
05C	97120800	303		05C	97120812	390	E-TCS
05C	97120900	330		05C	97121000	321	
05C	97121000	321		05C	97121400	473	
05C	97121412	500		05C	97121512		
05C	97121512			05C	97121600		
05C	97121600			05C	97121612		

Table 1.2. As in Table 1.1, except for GFDN 72-h track forecasts. The appearance of ??? NF in the "Cause" column indicated that a meteorological explanation for the large FTE could not be provided owing to the nonavailability of forecast fields from the GFDN model, and the GFDN forecast track was highly dissimilar to the NOGAPS forecast track.

GFDN 72-H FORECASTS EXCEEDING 300 N MI IN 1997											
TC	DATE	FTE	CAUSE	TC	DATE	FTE	CAUSE	TC	DATE	FTE	CAUSE
01W	97012006	439	???NF	14W	97080906	344	E-DCI	28W	97102106	500	
02W	97041418	355	E-MCG	14W	97081618	502	E-DCI	28W	97102118	540	E-BCI
02W	97041718	406	???NF	14W	97081706	551		28W	97102206	360	
02W	97042006	434	???NF	14W	97081718	636		28W	97102218	343	
02W	97042018	724		14W	97081806	544		29W	97110306	346	E-MCG
03W	97042218	569	???NF	14W	97081818	786		29W	97110506	368	E-BCI
04W	97050706	501	E-DCI	15W	97081918	628	I-BCI	29W	97110518	491	
05W	97052606	411	E-DCI	18W	97082206	322	E-DCI	29W	97110606	391	
05W	97052618	673		19W	97083006	466	I-RMT	29W	97110618	471	
05W	97052906	738	E-DCI	19W	97083118	378	E-MCG	31W	97111106	408	E-MCG
06W	97052718	455	E-DCI	19W	97090106	360		31W	97111118	427	
06W	97053006	365	E-RVS	19W	97090218	480	E-BCI	31W	97111206	312	
07W	97060606	343	E-RMT	21W	97091318	437	E-RMT	31W	97111218	304	
08W	97061606	402	E-DCI	21W	97091618	339	I-BCI	31W	97111306	376	
08W	97061706	358	I-MAL	22W	97092118	408	?????	31W	97111318	646	
08W	97061718	464		24W	97092406	326	E-DCI	02C	97091406	481	???NF
09W	97062318	324	E-DCI	24W	97092418	365		05C	97120706	473	E-DCI
09W	97062706	398	E-BCI	24W	97092618	302	???NF	05C	97120718	501	
10W	97072018	318	E-DCI	27W	97101518	413	I-ICIW	05C	97120806	373	
10W	97072506	365	???NF	27W	97102006	309	E-SCIW	05C	97120818	312	
10W	97072518	410	E-BCI	27W	97102106	318	E-MCG	05C	97120906	389	
10W	97072606	462		27W	97102118	355		05C	97121318	497	E-TCS
11W	97072706	337	E-DCI	27W	97102218	431		05C	97121406	324	
11W	97072718	503		28W	97101506	392	E-ICIE	05C	97121418	354	
11W	97072806	637		28W	97101518	376		05C	97121506	473	
11W	97072818	798		28W	97101606	315		05C	97121518	554	
11W	97072906	931		28W	97101706	389	E-RTF	05C	97121606	741	
11W	97073006	339	???NF	28W	97101718	571		05C	97121618	849	
12W	97073018	434	E-DCI	28W	97101806	601	E-MCG	05C	97121706	409	
12W	97073106	445		28W	97101818	590		05C	97121718	592	
12W	97073118	439		28W	97101906	432		05C	97121806	512	I-RVS
12W	97080106	439		28W	97101918	516		05C	97121818	482	
13W	97073118	433	?????	28W	97102018	367		05C	97121906	380	

Table 1.3. Meanings and frequencies of the causes of large NOGAPS and GFDN forecast track errors during 1997. If two numbers are listed, the first (second) is the number of times the phenomenon occurred excessively (insufficiently) in the model and corresponds to the E (I) prefixes in Tables 1.1 and 1.2.

CAUSES OF NOGAPS OR GFDN 72-H FORECAST TRACK ERRORS GREATER THAN 300 N MI		NUMBER OF FORECASTS	
Phenomenon Name	Acronym	NOGAPS	GFDN
Direct Cyclone Interaction	DCI	39-0	31-0
Semi-direct Cyclone Interaction	SCI		
SCI on Western TC	SCIW	3-0	1-0
SCI on Eastern TC	SCIE	0-0	0-0
Indirect Cyclone Interaction	ICI		
ICI on Eastern TC	ICIE	0-0	3-0
ICI on Western TC	ICIW	0-0	0-1
Ridge Modification by TC	RMT	12-0	2-1
Reverse Trough Formation	RTF	10-0	2-0
Response to Vertical wind Shear	RVS	10-0	1-3
Baroclinic Cyclone Interaction	BCI	8-12	11-2
Midlatitude System Evolutions	MSE		
Midlatitude CycloGenesis	MCG	0-0	19-0
Midlatitude CycloLysis	MCL	0-0	0-0
Midlatitude AnticycloGenesis	MAG	3-0	0-0
Midlatitude AnticycloLysis	MAL	0-4	0-2
Tropical Cyclone Initial Size	TCS	5-0	9-0
Not discernable or explainable		2	2
Fields not available		0	9
All causes		108	99

Ridge Modification by a TC (RMT) and Reverse Trough Formation (RTF) are a manifestation of the beta effect and involve the development of an anticyclone eastward and equatorward of the TC (RMT) or TCs (RTF) that facilitates poleward motion (Carr and Elsberry 1997). Erroneous prediction of these two phenomena together degraded 22 (20%) NOGAPS track forecasts, but only 5 (5%) GFDN track forecasts.

Response to Vertical wind Shear (RVS) and Baroclinic Cyclone Interaction (BCI) represent the competing negative and positive dimensions of TC interaction with the midlatitudes. The RVS process tends to decrease the intensity of the TC, which usually results in a decrease in translation speed as the TC responds to environmental steering over a shallower layer. The BCI process tends to deepen, or at least maintain the strength, of the circulation via transition into an extratropical cyclone, which affects the motion of the TC. Erroneous prediction of these two phenomena together degraded 30 (28%) NOGAPS and 17 (17%) GFDN track forecasts.

The errors associated with the influences of Midlatitude Cyclogenesis (MCG), Midlatitude Anticyclogenesis (MAG), and Midlatitude Anticyclolysis (MAL), along with Midlatitude Cyclolysis (MCL) (which was not associated with any poor forecasts in 1997), relate the structure and movement of midlatitude features (i.e., troughs, ridges, cyclones and anticyclones) to changes in environmental steering of the TC. That is, the model forecast has clearly misrepresented midlatitude features in a manner that is consistent with the character of the TC track error. Together these error mechanisms accounted for the degradation of 21 (21%) GFDN forecasts, but only 7 (6%) NOGAPS track forecasts.

Incorrect Tropical Cyclone initial Size (TCS) was responsible for the degradation of 5 (5%) NOGAPS and 9 (9%) GFDN track forecasts. All of these poor track forecasts were attributed to an overly large initial size of the TC in the models, which was possibly due to an overly large 35-kt radius in the JTWC warnings during a period when the TC was translating rapidly westward (up to 17 kt).

Only 2 (2%) NOGAPS and 2 (2%) GFDN forecasts with large 72-h errors were considered to have no discernable physical explanation. It is noteworthy that the largest of these four forecast errors was only 433 n mi. In other words, a discernable physical explanation could be provided for virtually all of the forecasts with very large FTEs. Since being able to readily discern a plausible reason for an erroneous track forecast is a necessary (but not sufficient) condition for anticipating such errors in an operational setting, this is considered to be a very encouraging result.

The error mechanisms in the first nine rows of Table 1.3 are related to TC-Environment Transformations in the Meteorological knowledge base (Fig. 1.4; lower right), and in each case the TC circulation interacts significantly with the surrounding environment. By contrast, the error mechanisms in the next four rows involve large-scale midlatitude processes to which the TC is a comparatively passive respondent. Thus, a very important finding is that the vast majority (87%) of highly erroneous NOGAPS track forecasts and a significant majority (59%) of highly erroneous GFDN track forecasts may be attributed primarily to misrepresentations of phenomena that depend sensitively on the fidelity with which the structure of the TC is represented in the model. Furthermore, in the first nine rows of Table 1.3, it was usually excessive interaction of the TC with the environment that was the cause for the poor forecast. It is also significant that E-MCG was responsible for 19 (19%) of highly erroneous GFDN track forecasts, but no highly erroneous NOGAPS track forecasts. This difference suggests that perhaps some tuning of the GFDN model is necessary to function more effectively when using NOGAPS initial and boundary conditions.

These findings have important ramifications for operational TC forecasting and numerical TC forecast model development. For the forecaster, it means that particular attention should be paid to evaluating the numerical TC model forecasts for indications of excessive interaction with the environment. For the numerical modeler, it means that if continued improvements are to be achieved in the numerical prediction of western North Pacific TC tracks, then significant effort must be directed toward achieving improved (i.e., usually less vigorous) model representations of TC structure and interaction with the environment (particularly with other cyclones).

4) Report format. Sections 2 through 4 address the mechanisms cited in Table 1.3 as causes of large FTEs by NOGAPS and/or GFDN. The order in which the various mechanisms are

discussed corresponds roughly to when in the life cycle of a typical TC these processes are typically manifest. Each of these sections includes a conceptual depiction and description of the phenomenon, a brief discussion of the frequency and important characteristics of the phenomenon, one or more illustrative case studies, and a brief summary. The key illustration vehicle in the case study subsections is a comparison/verification diagram that uses a 12-panel, 2-page spread to depict: (i) the track forecasts of NOGAPS, GFDN and other numerical models available to JTWC; (ii) the NOGAPS and GFDN forecasts fields that generated the illustrated track forecasts; and (iii) NOGAPS analyses at the times that the NOGAPS and GFDN forecast fields verify. The 12-panel diagrams are collected into Appendix A to improve readability and practical utility of report. If desired, the reader may separate Appendix A from the main body of the report and put it into a binder that can be opened to the appropriate 12-panel figure being cited in the text.

Although the emphasis of Sections 2-4 is after-the-fact scientific analysis and explanation of phenomena that have been identified as causes for large FTEs in NOGAPS and GFDN, some attention will also be given to real-time detection of these processes by the forecaster in the course of operational TC forecasting. Application of these concepts to explain the large track errors in the model guidance for Typhoon Rex during 1998 is described in Appendix B.

Section 5 provides an overview of the key findings that have resulted from this research, which forms a preliminary Numerical Model Traits knowledge base. How such a Numerical Model Traits knowledge base, and the underlying Meteorological knowledge base, may be used by the forecaster to formulate an official track forecast that consistently accounts for expected errors in objective TC track forecast guidance as part of the Systematic Approach methodological framework (Fig. 1.1) will be described in a future report.

2. Binary Cyclone Interactions

According to Table 1.3, all three of the modes of binary cyclone interaction (i.e., direct, semi-direct, and indirect) defined by Carr et al. (1998) were identified as causes for highly degraded track forecasts by NOGAPS and/or GFDN. Because erroneous direct cyclone interaction (DCI) was responsible for roughly one third of the highly erroneous NOGAPS and GFDN track forecasts in 1997, this phenomenon is thoroughly discussed and illustrated in Section 2a. The three NOGAPS and one GFDN forecasts degraded by erroneous semi-direct cyclone interaction (SCI) on the western TC involved only one TC. This semi-direct case was rather unrepresentative in that the TC was poleward of the subtropical ridge, rather than equatorward as depicted in the CMKB (see p. 98), and thus is not described here. The four GFDN forecasts degraded by indirect cyclone interaction (ICI) also involved only one TC. However, this ICI case is important because it involves a very evident under-forecast of TC size that is apparently a unique capability of GFDN owing to the high resolution of the innermost grid. Under-representation of TC size by GFDN was also determined to be responsible for the one instance of insufficient RMT shown in Table 1.3 (discussed later in Section 3a), which suggests that under-representation of TC size is a recurring (albeit infrequent) trait of GFDN forecasts that the forecaster should be aware of, and thus warrants discussion in this report.

a. Direct cyclone interaction (DCI)

1) Description. Recall from Table 1.3 that excessive Direct Cyclone Interaction (E-DCI) was identified to be the primary cause for highly erroneous 72-h track forecasts 39 times for NOGAPS and 31 times for GFDN, which accounted for roughly one third of the poor NOGAPS and GFDN forecasts in 1997. By contrast, not one instance of insufficient DCI (I-DCI) was identified.

The E-DCI phenomenon occurs when a numerical model forecasts the TC circulation to directly interact with an adjacent cyclonic circulation such that the predicted interaction is either false (i.e., does not occur in reality) or is significantly more vigorous than in reality. A conceptual model of the phenomenon is shown in Fig. 2.1a-d. The concept of DCI is analogous to the Direct TC Interaction (DTI) described by Carr et al. (1997) and in the CMKB (pp. 103-104), except that the adjacent cyclone is not necessarily a JTWC-designated TC. If real, the other cyclone may be: (i) a named TC or a precursor tropical disturbance; (ii) a tropical disturbance that does not actually develop into a named TC; or (iii) an upper-tropospheric circulation of mid-latitude origin.

Notice that the conceptual model of E-DCI involves both a rotation of the two cyclones and a possible merger into one circulation that is usually larger in size than the analyzed TC. The TC in Fig. 2.1 is depicted as the larger, and thus more dominant, circulation into which the second cyclone merges. In this case, the TC track forecast by the model may be only moderately affected by the interaction, since such an interaction depends on the strength of the other cyclone. It is also possible that the second cyclone will be analyzed and forecast in the model to be the dominant circulation into which the TC tends to merge. In this case, the track forecast by the model will often exhibit a definite cyclonic loop, and the forecast track may be prematurely terminated owing to excessive weakening of the model TC as it merges with the overly strong adjacent cyclone.

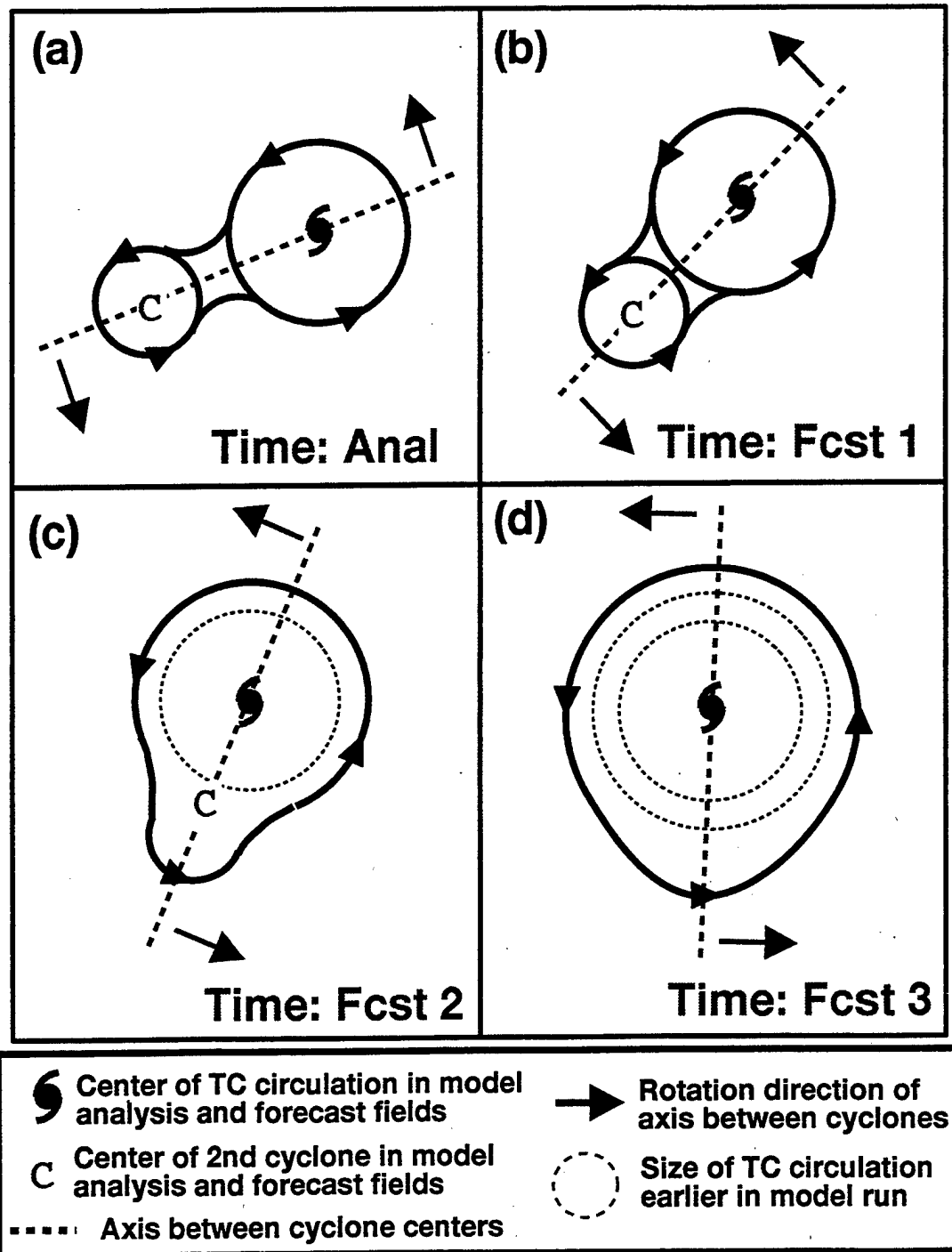


Fig. 2.1. Conceptual model of Direct Cyclone Interaction (DCI) in which a TC circulation interacts with another cyclone (C) to cause a counter-clockwise (Northern Hemisphere) rotation of the axis between the cyclone centers (heavy dashed line) and a possible merger of the two cyclones in which the combined circulation becomes larger with time (panels c and d). The TC may also be the smaller of the two cyclones, or the model may be applied to two TCs of similar sizes in which the tracks of both TCs will be affected.

Reasons for E-DCI with another real cyclonic circulation include: (i) too large a horizontal extent and associated outer wind strength of the TC and/or the other cyclone in the initial analysis, or during the forecast period (Fig. 2.2a); (ii) mis-location of the TC and/or the other cyclone in the initial analysis, or during the forecast such that the separation of the two cyclones is smaller than in reality (Fig. 2.2b); and (iii) overly deep penetration of an upper-level midlatitude circulation into the lower troposphere where it can affect the steering of the TC (Fig. 2.2c).

It is also possible for numerical models to forecast E-DCI between the TC and a fictitious cyclone. This situation is basically a variant of Fig. 2.2a. This scenario was found to be relatively rare in this 1997 sample of NOGAPS and GFDN forecasts.

Another situation that has been occasionally observed in NOGAPS, but not in GFDN, is a self-interaction caused by a significant difference between the TC location in the first-guess field and the synthetic TC cyclone inserted during the data assimilation cycle (Fig. 2.2d). As a result, the NOGAPS initial analysis contains two non-collocated representations of the same TC that will then tend to rotate around each other during the early stages of the model integration. This phenomenon may occur when: (i) the JTWC position, about which the synthetic observations are centered, is significantly offset from the initial position in the 12-h NOGAPS forecast that serves as the first-guess for the analysis; or (ii) a significant relocation of the JTWC analysis position or short-term forecast occurs between two successive synoptic times. These situations less likely to occur in the GFDN because normally the TC is effectively removed by filtering the global model analysis before a model-compatible vortex is inserted at the warning position.

2. Frequency and characteristics. In the 1997 sample of NOGAPS and GFDN track forecasts, 18 periods (based on model initialization time) were identified when E-DCI occurred sometime during the model integration (Table 2.1). The 18 periods of model-predicted E-DCI involved only 14 TCs, since two distinct periods of model-predicted E-DCI occurred during the existence of Marie (05W), three during Winnie (14W), and two during Amber (18W). Notice that the durations of E-DCI in Table 2.1 are usually longer than in Tables 1.1 and 1.2. The reason for this difference is that Table 2.1 identifies the periods when the E-DCI phenomenon was considered to be affecting model track forecasts FTEs without regard to FTE magnitude, whereas Tables 1.1 and 1.2 list only the model initialization times for which a 72-h FTE exceeding 300 n mi occurred.

In contrast to the frequent occurrence of E-DCI, the observational study of TC interaction by Carr et al. (1998; their Table 1) determined that actual direct TC interaction (DTI) involving mutual influence occurred only three times in seven years, or about once every two years. If the 1997 season is representative, model-predicted E-DCI occurs considerably more often than real mutual DTI. This difference has very important ramifications for TC forecasting. Specifically, given that the forecaster can in real-time discern the occurrence of DCI in a numerical model, the probability is high that the predicted DCI is false, or at least excessive. Therefore, the forecaster is justified in either ignoring or giving low weight to the forecast track of that numerical model when formulating the official track forecast. The case studies that follow will show that E-DCI is comparatively easy to identify if the forecaster knows what clues to look for and has access to the proper model fields and field-display tools.

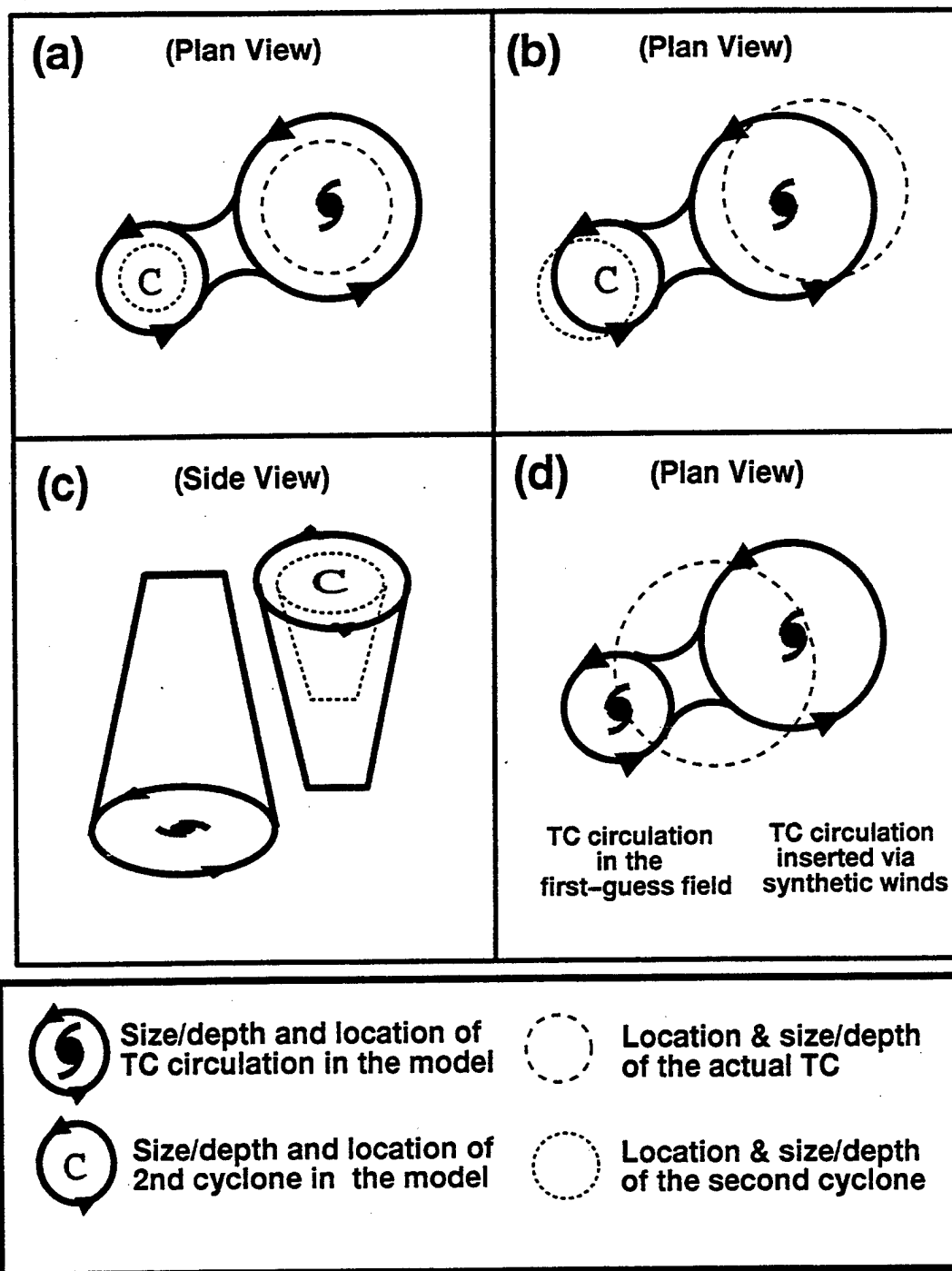


Fig. 2.2. Schematics of excessive-DCI (E-DCI) contributing to large TC errors. (a) Both the TC and the cyclone (C) have too large circulations in the numerical model, which leads to DCI as in Fig. 2.1. (b) Mislocations of the TC and C in the model such that the separation distance is small enough to lead to a DCI. (c) A DCI in which an overly large and deep upper-tropospheric cyclone extends into the middle troposphere such that it establishes an erroneous steering current across the warm-core TC circulation that decreases in strength with elevation. (d) Dual TC circulations in the numerical model introduced by synthetic TC observations being inserted sufficiently far from the location of the TC circulation in the first-guess field from the previous 12-h forecast.

Based on model initialization time (Table 2.1; column 2), the number of model integrations affected by E-DCI ranged from as few as one to as many as eleven (Table 2.1; last row) consecutive model runs; that is, over a period of more than three days. With the exception of TC 05W (Table 2.1; rows 2-3), the TC environment structure during the period of E-DCI was classified as being Standard/Tropical Easterlies (S/TE), Standard/Poleward Flow(S/PF), Poleward/Poleward Flow (P/PF), or a transitional state between two of these pattern/region combinations (Table 2.1, column 3). In two of the cases in which the pattern/region classifications were P/PF, the TC was at a relatively low latitude. Thus, the E-DCI phenomenon almost always occurred in this sample when the TC was moving westward in the vicinity of the equatorial or monsoon trough, or recently had turned poleward, but was still in proximity to the tropical easterlies. Notice that only during the second period of E-DCI affecting Amber (18W) was there actual direct TC interaction (DTI) occurring. Thus, the E-DCI in this one case was an exaggeration of an actual interaction of the TC with another cyclone (Cass). In the other 17 cases, the E-DCI was deemed to be false.

In 12 (67%) of the cases, the TC was a moderate tropical storm (< 50 kt) or depression when the E-DCI period commenced (Table 2.1, column 4). This fact is consistent with the expectation that a numerical model misrepresentation of a nearby cyclone would have a greater impact on the model-predicted track of a weak TC. The second cyclone was a tropical cyclonic circulation (either a TC, TC precursor, or non-developing disturbance) in 13 of the cases, and a midlatitude upper-level cyclone in three cases (Table 2.1, column 5). When the second cyclone in the model was a non-developing disturbance (11 times), a circulation was evident in the satellite imagery (e.g., weakly organized convection) at some time during the model integration for all cases except Marie (06W) and Oliwa (02C). All three cases of E-DCI involving a midlatitude cyclone had clear satellite indications of the other cyclone (or trough), particularly in the water vapor channel. Thus, for the time period studied, NOGAPS and GFDN were much more likely to over-develop a real second cyclone than to falsely develop a possibly nonexistent cyclone (two times).

In 13 of 15 cases that involved a second tropical circulation (including designated, probable, or false entries in column 5), that cyclone was located in the west or south quadrant of the affected TC (Table 2.1, column 6) as in Fig. 2.2a. In the two other cases, the opposite orientation occurred with the second tropical circulation to the east. If the second circulation is initially to the west (east) and E-DCI occurs, the model forecast track will usually have a poleward (equatorward) bias. Not surprisingly, E-DCI involving an upper-level circulation originating in the midlatitudes began with the second circulation in the northern semicircle of the affected TC. In the three E-DCI cases with an asterisk in column 6, a significant mis-positioning of the TC toward the E-DCI source apparently caused, or at least contributed, to the E-DCI situation.

Of the 18 periods of E-DCI listed in Table 2.1, degradation of the forecast tracks of NOGAPS and GFDN, NOGAPS but not GFDN, and GFDN but not NOGAPS occurred 12, 2, and 4 times, respectively (Table 2.1, column 7). When both NOGAPS and GFDN were affected by E-DCI, the degree of degradation was usually greater in NOGAPS. Although forecast fields were not available from the Global Spectral Model and Typhoon Model run by Japan (designated JGSM and JTYM by JTWC), or the UK Met Office global model (designated EGRR by JTWC), it appeared on the basis of forecast track similarities that one or more of these models were affected by E-DCI in 10 of the 18 cases (Table 2.1, column 8). This presumed frequency of occurrence of E-DCI in these other models is probably an underestimation because only the cases of large NOGAPS and/or

Table 2.1. Cases of model-predicted Excessive Direct Cyclone Interaction (E-DCI) in the western North Pacific during 1997.

TC No	Starting times of affected model runs ¹	Synoptic Environment of TC	Intensity during interaction ²	Nature of Second cyclone ³	Location of second cyclone ⁴	Models affected	
						JTWC ⁵	Others ⁶
04W	May 07/00 → 08/12	S/TE	25 → 45	PTC	WSW	N,G	(E,S)
05W	May 26/00 → 27/12	S/EW → P/PF	25	PTC	WNW	G,N	N/A
05W	May 29/00 → 29/12	P/PF → S/PF	45	ULC	NW	G,N	
06W	May 27/12 → 29/00	S/TE → P/PF	30 → 45	FTC	SW*	N,G	S,T,E
07W	Jun 10/12 → 11/00	S/TE → S/PF	140 → 130	Pre-08W	SW	N	
08W	Jun 16/06	S/PF	40	ULC	NW	G	
09W	Jun 23/18	S/TE → P/PF	35	PTC	W	G	
10W	Jul 20/00 → 22/00	S/TE → P/PF	70 → 100	ULC	NNE	G,(N)	(E)
11W	Jul 27/00 → 30/00	P/PF	30 → 45	Pre-12W	SW*	N,G	E,T,S
12W	Jul 30/12 → 01/12	S/TE	30 → 50	PTC	E	N,G	
14W	Aug 08/00 → 10/00	S/TE	25 → 65	PTC	W	N,(G)	E,(S)
14W	Aug 09/06 → 10/06	S/TE	35 → 75	PTC	E	G	
14W	Aug 16/00 → 18/00	S/TE	85 → 75	Pre-17W	WSW	N,G	T
18W	Aug 22/06	S/TE-ICIE	60	PTC	W	G	
18W	Aug 26/00 → 29/06	S/TE-DCI	85 → 105	20W	W	N,(G)	(T)
02C	Sep 13/00 → 14/00	S/TE → S/PF	105 → 95	FTC	S	N	
24W	Sep 22/12 → 25/00	S/TE → P/PF	30 → 55	PTC	WSW*	N,G	E,(S,T)
05C	Dec 07/00 → 10/00	S/TE	45 → 50	PTC	SW	N,G	E,S

Footnotes:

1. The date and times (UTC) indicated in column 2 give the starting times of the first and last model run affected noticeably by E-DCI. For example, in the case of Nestor (07W) two model runs were affected by E-DCI and had starting times of 1200 UTC 10 June 1997 and 0000 UTC 11 June 1997, respectively. If more than one model was affected by E-DCI, the period for the model that was affected the longest (most model runs) is given.
2. Intensities in column 4 are in kt, and correspond to the values at the beginning and end of the DCI period shown in column 2.
3. PTC = Probable Tropical Circulation, or FTC = False Tropical Circulation. A probable (false) assignment is made if the existence of the disturbance is (is not) supported by discernible convection in satellite imagery. ULC = Upper Level Circulation, which is usually a cut-off low originating from the mid-latitudes; ##W = a JTWC-designated TC that is involved in the E-DCI; pre = a precursor to a JTWC-designated TC that is involved in the E-DCI.
4. The set of letters is the compass direction from the TC involved in the DCI when the interaction begins. The presence of an asterisk indicates that a significant error in the position of the TC (relative to the final best track position) toward the location of the second cyclone appeared to cause or influence the E-DCI.
5. N = Navy Operational Global Atmospheric Prediction System (NOGAPS); G = Geophysical Fluid Dynamics Laboratory TC Model as run by the U.S. Navy. Parentheses indicates that degradation to the forecast track was visibly evident, but did not result in an 72-h FTE greater than 300 n mi.
6. S = Japanese Global Spectral Model (JGSM); T = Japanese Typhoon Model (JTYM); E = UK Met Office Global Model (EGRR). No fields were available for these models. The existence of E-DCI was inferred from the behavior of the forecast tracks during periods that E-DCI was determined to have occurred in NOGAPS and/or GFDN via examination of forecast fields. Parentheses and the order of presentation have the same meaning as in footnote 5.

GFDN errors have been investigated. It seems likely that other periods may have existed when E-DCI could have been degrading one or more of the non-U.S. models, but not NOGAPS and/or GFDN. In summary, Table 2.1 suggest that an erroneous track forecast owing to E-DCI is a relatively frequent problem, and seems to be ubiquitous in the sense that it apparently affects diverse models.

3. Case Studies. The primary purpose of the case studies in this section is to illustrate the important aspects and variations of the E-DCI phenomenon. During the course of the discussion, some attention will be given to clues that the forecaster can use in real-time to detect and account for expected degradations to numerical model track forecasts.

The first case of Typhoon Nestor (07W) illustrates E-DCI that affected only NOGAPS and involved a second real tropical circulation. This case also shows how E-DCI is manifest in sea-level pressure forecast fields when the TC is much more intense than the second cyclone, as well as the characteristic sudden changes in the model track forecasts at the beginning and end of the E-DCI period. The second case of Typhoon Winnie (14W) illustrates with 500 mb wind fields the appearance of E-DCI with two other tropical circulations that affect a relatively weak TC. This case also shows that E-DCI may affect both NOGAPS and GFDN, and by inference, the accuracy of the other numerical model track forecasts available to JTWC. The third case of Typhoon Rosie (10W) provides an example of E-DCI that involves an upper-level trough/cyclone that is over-developed by more than one model. Finally, the Typhoon Amber (18W) case is instructive as a situation in which actual asymmetric mutual DTI occurs between Amber and Cass (20W) (asymmetric because Amber is larger than Cass), but several numerical models predict an excessive degree of merging that degrades the track forecasts for Amber. No clear examples of E-DCI involving the synthetic wind observation and model first-guess circulations as in Fig. 2.2d were identified during the 1997 season. For a clear example of this phenomenon, the reader is referred to the case of Typhoon Fred (1994) as presented in Schnabel (1998).

The Nestor case will be presented in greater detail to illustrate how the onset and cessation of E-DCI is manifest in model forecast fields and tracks. The remaining examples will be presented in less detail.

a) Typhoon Nestor (07W). For this TC, the NOGAPS track forecasts were affected by E-DCI for two model runs initiated at 1200 UTC 10 June and 0000 UTC 11 June 1997 (Table 2.1, row 3), although only the second degraded forecast resulted in a FTE exceeding 300 n mi (Table 1.1). A comparison/verification of the NOGAPS and GFDN¹ sea-level pressure forecasts from integrations initiated at 0000 and 0600 UTC 10 June, respectively, is given in Fig. A.1a-l in Appendix A to provide a context for the period of E-DCI that affects subsequent NOGAPS integrations. At this time, the NOGAPS and GFDN track forecasts, as well as the JGSM and JTYM tracks, are in close agreement (Fig. A.1a). That is, they form a single tight cluster as in Fig. 1.3a. Not surprisingly, the consensus of the 72-h positions is quite accurate, which is usually (but not always) the case when model track forecasts are tightly clustered. As expected, generally good

¹ Comparison of NOGAPS and GFDN forecasts separated by 6 hours is necessary because computational limitations at the Fleet Numerical Oceanography and Meteorology Center where the models are run permits integrations of NOGAPS only at 0000 and 1200 UTC, and GFDN only at 0600 and 1800 UTC.

agreement also exists among the NOGAPS forecast fields (Fig. A.1e-h), the corresponding GFDN forecast fields (Fig. A.1i-l), and the verifying NOGAPS analysis fields (Fig. A.1b-d). However, subtle differences exist that have an important bearing on the ensuing period of E-DCI that will affect NOGAPS.

Both the NOGAPS 72-h and GFDN 66-h forecast fields (Fig. A.1h and l, respectively) have an extensive area of pressures less than 1008 mb to the south of Nestor where the verifying NOGAPS analysis (Fig. A.1d) has the pressure above 1008 mb over the same area. In addition, a lobe of sub-1004 mb pressure that extends to the WSW from Nestor in the NOGAPS 48-h field (Fig. A.1g) appears to rotate to the SSW in the 72-h field (Fig. A.1h). Notice that no such pressure lobe is evident in the corresponding GFDN 42-h and 66-h forecasts (Fig. A.1k-l). This cyclonically rotating lobe of low pressure is a manifestation of E-DCI as depicted in Fig. 2.1. However, as evidenced by the near collocation of the NOGAPS and GFDN track forecasts (Fig. A.1a), the E-DCI is not sufficiently severe in this NOGAPS integration to noticeably degrade the accuracy of the TC track forecast.

A comparison/verification of the NOGAPS and GFDN sea-level pressure forecasts initiated at 1200 and 1800 UTC 10 June, respectively, is presented in Fig. A.2a-l. At this time, the NOGAPS track is slow and to the left of the actual track of Nestor (Fig. A.2a). The corresponding 72-h FTE is 282 n mi, which represents a sharp increase from an 80 n mi FTE just 12 h earlier. In retrospect, the NOGAPS track forecast is now a noticeable outlier to the left of the cluster of tracks formed by the other models, rather than being part of a tight track cluster as was the case 12 h earlier. In real-time, the forecaster could either view the distribution of forecast numerical model forecast tracks as a single cluster that is broader than 12 h previously, or two clusters distinguished primarily by track direction (as in Fig. 1.3b), with one cluster comprised solely of the NOGAPS track, and the other cluster comprised of the remaining model tracks.

The change in the relationship of the NOGAPS track forecast to the GFDN track (as well as the other tracks) is an important clue to the forecaster, who should then search for a suitable explanation by comparing the NOGAPS and GFDN forecast fields. Notice that the rotation and degree of extension of the sub-1004 mb lobe to the south and west of Nestor in the NOGAPS forecast fields has become more pronounced at 48 h and 72 h (Fig. A.2g-h). Although a low pressure extension is evident to the south of Nestor in the GFDN 42-h forecast (Fig. A.2k), a separate, albeit weak, low pressure area to the south of Nestor is predicted at 66 h (Fig. A.2l). Also, the rotating lobe of sub-1004 mb pressure evident in the NOGAPS forecast is absent in the GFDN forecast. Thus, the westward shift of the NOGAPS track forecast relative to the GFDN track (Fig. A.2a) is explainable in terms of E-DCI that occurs in the NOGAPS, but not the GFDN forecast.

Comparison of the NOGAPS and GFDN forecast fields with the verifying NOGAPS analyses (Fig. A.2b-d) confirms that both NOGAPS and GFDN are over-developing the second cyclone to the south. Also, the horizontal extent of the low pressure area representing Nestor is significantly larger in the NOGAPS forecast fields (Fig. A.2f-h) than in the corresponding GFDN fields (Fig. A.2j-l). Thus, this case of E-DCI in the NOGAPS forecast is consistent with the conceptual model in Fig. 2.2a, in which excessive interaction occurs because both cyclones have larger horizontal extents in the NOGAPS forecast fields than in reality. Presumably, the more compact representation of Nestor in the high resolution GFDN model was sufficient to preclude E-

DCI, even though the second cyclone is forecast to be too strong. The similarity of the JGSM, JTYM, and EGRR tracks to the GFDN track suggests that the E-DCI phenomenon was probably not present in those models.

Comparison/verification of the subsequent 0000 and 0600 UTC 11 June NOGAPS and GFDN forecasts of Nestor (Fig. A.3a-l) reveals a qualitatively similar situation. However, the NOGAPS forecast track is now shifted so far west and south of the other model tracks (Fig. A.3a) that the forecaster should recognize that the distribution of tracks manifests more than one cluster (as in Fig. 1.3b). The NOGAPS 72-h FTE at this time has increased to about 541 n mi since the accelerating recurvature of the actual TC was not predicted. By contrast, the GFDN forecast track is very close to the actual track of Nestor with only a moderately slow bias, and the JGSM track has a moderately fast and right bias. Whereas there continues to be no indication of E-DCI in the GFDN fields (Fig. A.3i-l), the cyclonically rotating lobe of sub-1004 mb pressure is even more evident in the 48-h and 72-h NOGAPS forecast fields (Fig. A.3g-h).

A comparison/verification of the 1200 and 1800 UTC 11 June NOGAPS and GFDN forecasts is provided in Fig. A.4a-l. Notice that the accuracy of the NOGAPS forecast has suddenly and dramatically improved (72-h FTE is 126 n mi). Also, the NOGAPS track is now a member of a tight cluster that also includes the GFDN, JGSM, and EGRR forecasts, but not the JTYM (which represents a single-member cluster distinguished by a significantly slower translation speed) (Fig. A.4a). The forecaster should note this sudden change in the character of the NOGAPS track forecast and its relationship to the other numerical model tracks, and check the NOGAPS forecast fields to verify that the period of E-DCI has ended. As expected, the rotating lobe of low pressure is no longer evident in the NOGAPS 48-h and 72-h forecasts (Fig. A.4g-h). Notice also that both the 72-h NOGAPS and 66-h GFDN forecasts represent the second cyclone as a distinct, broad area of sub-1008 mb pressure (Fig. A.4h and l) that is much larger than in the verifying NOGAPS analysis (Fig. A.4d).

Consider the progression of the 72-h positions of the NOGAPS track forecasts initiated during the period 1200 UTC 9 to 1200 UTC 11 June 1997 (Fig. 2.3). Before the period of E-DCI, the 72-h positions of forecast tracks A and B are quite accurate and represent a steady progression to the NNW along the actual track of Nestor. During the period of E-DCI, the progression of the 72-h forecast positions of tracks B through D has changed to a WSW trend. The dramatic jump from the 72-h position of forecast D to that of E in Fig. 2.3 represents the absence (or dramatic reduction in the degree) of E-DCI in the 1200 UTC 11 June NOGAPS integration and the resumption of accurate track forecasts by NOGAPS. The knowledge that E-DCI may have a sudden onset and cessation is an important clue to help the forecaster detect the phenomenon.

Consider the possible interpretation the forecaster could give to the WSW trend of the 72-h forecast positions in tracks B-D in Fig. 2.3. This trend could be interpreted to mean that Nestor will turn to the left and stall at the subtropical ridge axis. While this is a potential scenario, the forecaster should be alerted to evaluate the NOGAPS forecast fields and TC track in relation to the GFDN forecast fields and TC track, which was a member of a cluster of forecast tracks that did not turn left and stall in the ridge (Figs. 1.3b and A.3a). The forecaster would note that the 48- and 72-h NOGAPS forecasts from 1200 UTC 10 June (Fig. A.2g-h) are consistent in time with regard to

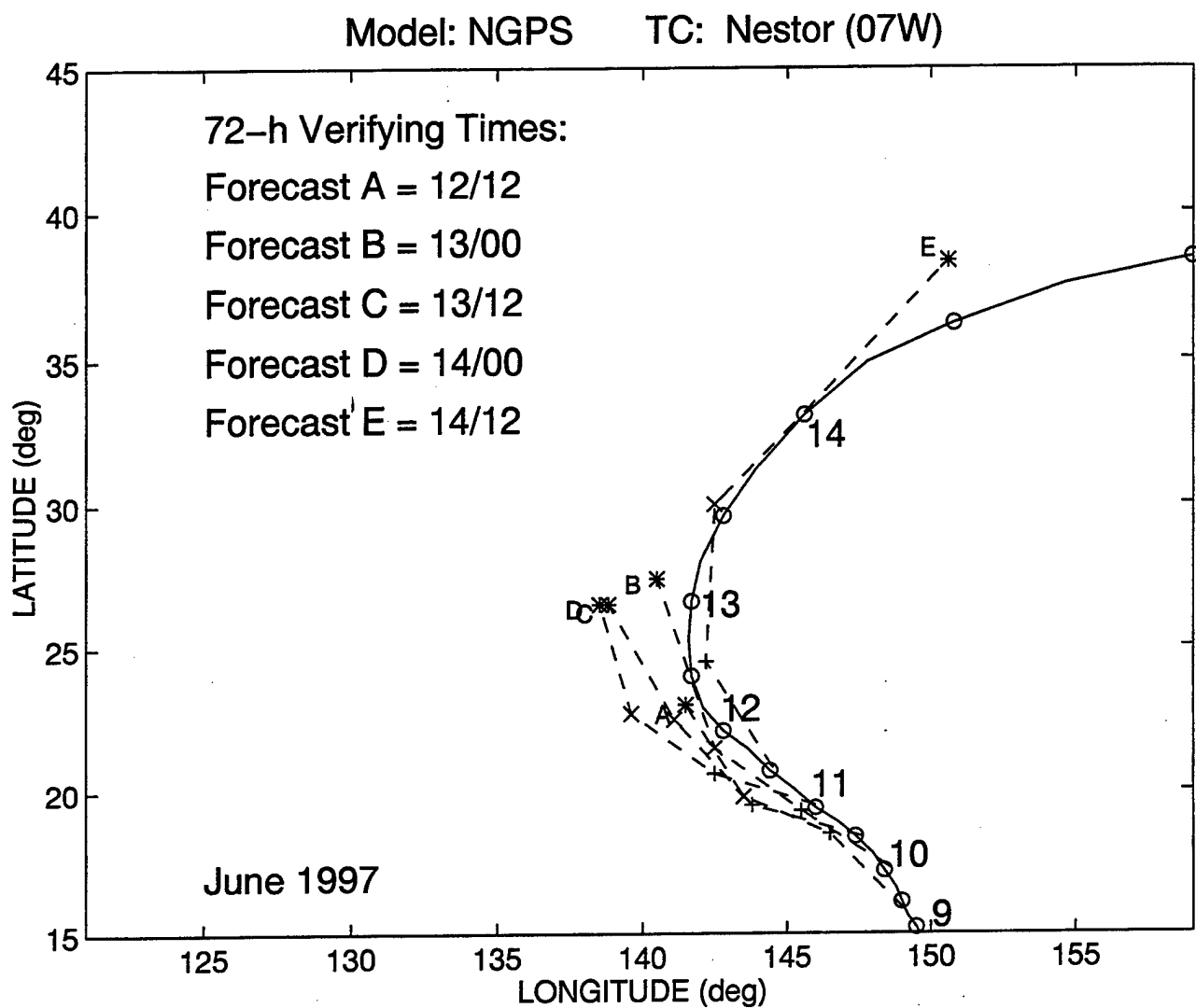


Fig. 2.3 Track (solid, circles each 12 h) of TC Nestor (07W) during 0000 UTC 9 June to 0000 15 June 1997 and sequence of five NOGAPS 72-h track forecasts labeled A-E verifying at times shown in the inset. The forecast tracks have a cross (+) at the 24-h position, an x at the 48-h position, and an asterisk at the 72-h position.

developing a lobe in the sea-level pressure that rotates cyclonically as in the previous forecast. The same comment would apply to the 48- and 72-h NOGAPS forecasts from 0000 UTC 11 June (Fig. A.3g-h). Although the corresponding GFDN fields also have low sea-level pressures to the south, no cyclonically rotating lobe is present and Nestor is forecast as a compact center moving poleward by 72 h (Fig. A.2j-l). This scenario is repeated in the subsequent GFDN forecast (Figs. A.3j-l). If after examining the NOGAPS and GFDN forecast fields at the 500 mb steering level, the forecaster could not find any differences that would adequately explain a stall by Nestor due to some other mechanism (e.g., an amplifying midlatitude ridge to the north of the TC), then invoking the E-DCI mechanism as the explanation for the stall would be justifiable.

In a uniform background flow, one would expect two cyclones that are directly interacting to exhibit cyclonic looping tracks. By contrast, the curvature of forecast tracks C and D in Fig. 2.3 is still anticyclonic, which the forecaster could interpret as evidence against the existence of E-DCI in the NOGAPS forecasts. To avoid this misinterpretation, the forecaster must also recognize that the predicted environment of Nestor is undergoing a transition from a Standard/Tropical Easterlies (S/TE) synoptic structure to Standard/Poleward Flow (S/PF), and thus is providing a non-uniform steering that acts to turn Nestor anticyclonically toward the north. As a result, the effect of E-DCI in this case is to lessen the degree of anticyclonic turning in the degraded NOGAPS track forecasts, rather than cause outright cyclonic motion.

The source of E-DCI in NOGAPS is listed in Table 2.1 (column 5) as pre-08W. This determination was based on satellite imagery (Fig. 2.4a-d). Increasing convective activity to the south and west of Nestor is evident, and this disturbance eventually organizes by the 14th (Fig. 2.4d) into the precursor to Typhoon Opal (08W). Notice that at 0000 UTC 11 June, which is the initialization time for the NOGAPS run most affected by E-DCI (Fig. A.3a), the convection to the southwest of Nestor shows no significant organization and is separated from Nestor by more than 10° lat (Fig. 2.4a). These are important clues to the forecaster that the direct cyclone interaction in the NOGAPS forecast is in all likelihood false, since: (i) observed cases of mutual direct interaction between TCs that includes merger only occurs at separation distances less than 10° lat. (Carr et al. 1998; Table 1); and (ii) a tropical disturbance with a cyclonic circulation vertically and horizontally extensive enough to have a significant DCI influence should be accompanied by a reasonably organized convective cloud mass.

b) Typhoon Winnie (14W). Three separate periods of model-predicted E-DCI were identified for Typhoon Winnie (Table 2.1). The first period affected model runs initiated at 0000 UTC 8 through 0000 UTC 10 August. A comparison/verification of the NOGAPS and GFDN 500-mb wind fields and TC track forecasts initiated at 1200 UTC and 1800 UTC 8 August, respectively, is presented in Fig. A.5a-l. Since Winnie is moving west-northwest in the relatively uniform flow of a S/TE environment (Table 2.1), the E-DCI occurring in the NOGAPS and GFDN forecasts is clearly manifest as cyclonically curved tracks (Fig. A.5a). Notice that the directions to the NOGAPS and GFDN 24-h forecast positions depart dramatically from the recent motion vector of the TC. The combination of a poor agreement between the short-term forecast and recent TC motion, and the clear cyclonic curvatures to the 72-h position, are important clues to the forecaster that the forecast fields should be examined for indications of E-DCI. Even though the inference is made in the absence of forecast fields, the agreement of the short-term UKMO (denoted EGRR in Fig. A.5a) track with Winnie's recent motion, and the lack of significant cyclonic curvature

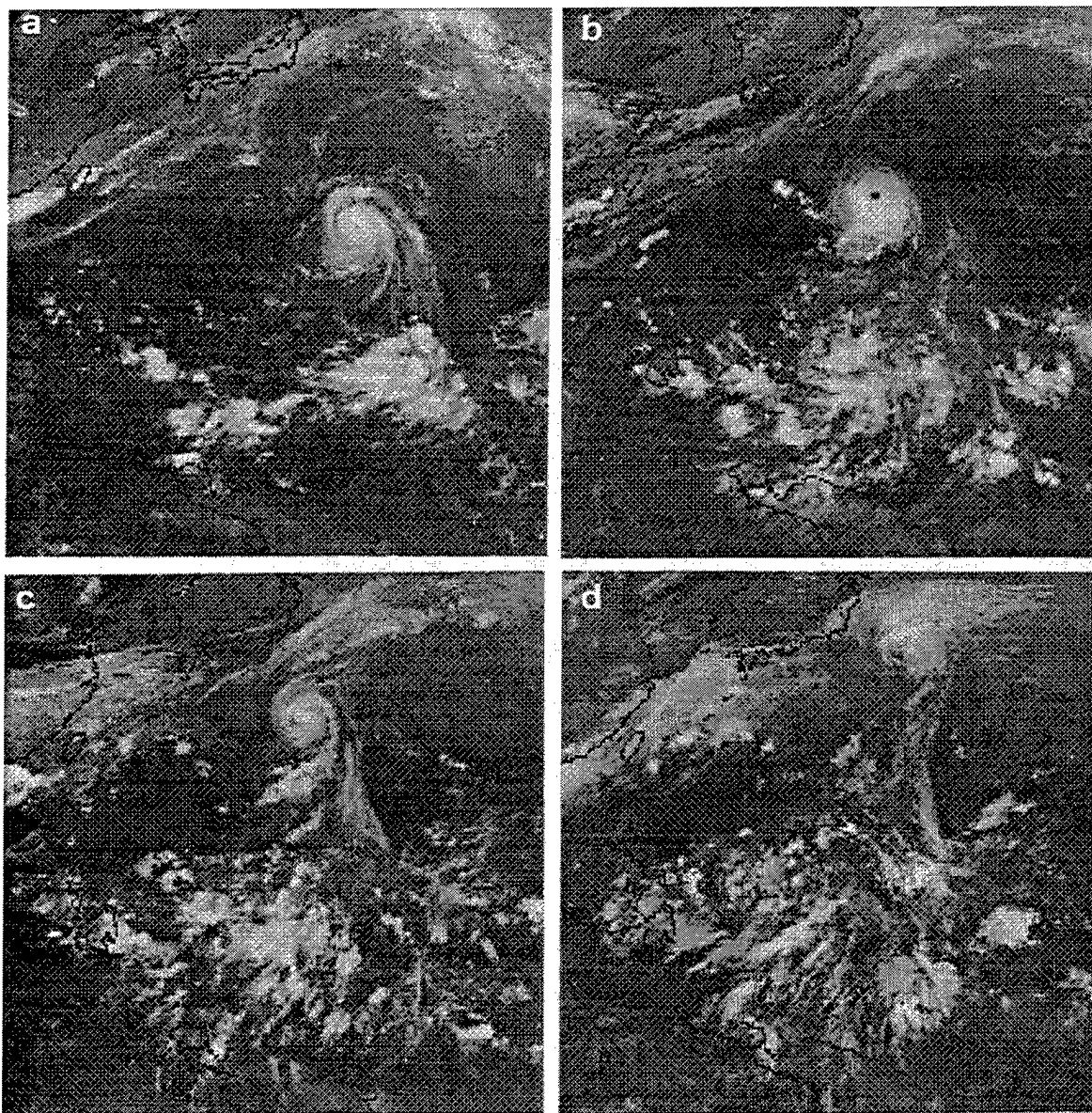


Fig. 2.4. Satellite infrared imagery for TC Nestor (07W) and a disturbed convective area to the south that later becomes 08W. The images are at 0000 UTC on (a) 11, (b) 12, (c) 13, (d) 14 June 1997.

suggests that E-DCI is not occurring to a significant degree in the UKMO model. In the NOGAPS and GFDN analysis fields (Fig. A.5e and i), an extensive cyclone appears about 15-17° lat. to the west-southwest of Winnie. Despite a separation distance that well exceeds the limit for real DCI, the two circulations rotate and merge into one very large circulation in the NOGAPS forecast fields (Fig. A.5f-h). Although the corresponding GFDN forecast fields (Fig. A.5j-l) have the extensive western cyclone dissipating as it merges with Winnie, a third, smaller cyclone forms at 18 h (Fig. A.5j) between Winnie and the larger western cyclone, and this cyclone clearly interacts and merges with the TC (Fig. A.5k-l).

In the verifying NOGAPS analyses (Fig. A.5b-d), the western cyclone/trough does not appear to interact significantly with Winnie, but rather remains in roughly the same location and dissipates as Winnie passes to the north and deepens. Although the Winnie circulation in the NOGAPS analysis is large at 1200 UTC 11 August (Fig. A.5d), it is still smaller than the size of the cyclone formed by the merger of Winnie and the other cyclone(s) in the corresponding NOGAPS 72-h and GFDN 66-h forecast fields (Fig. A.5h and i, respectively).

The 500-mb wind analysis/forecast fields and TC tracks generated by subsequent NOGAPS and GFDN forecasts initiated at 0000 UTC and 0600 UTC 9 August, respectively (Fig. A.6a-l), reveal some significant changes from the previous comparison. In Fig. A.6a, notice that the direction to the 24-h NOGAPS forecast position now agrees closely with recent movement of Winnie, and the track no longer exhibits the cyclonic curvature of the previous NOGAPS track (Fig. A.5a). These changes are important clues to the forecaster that the 0000 UTC 9 August NOGAPS forecast track is likely to be more trustworthy than the previous track. By contrast, the GFDN track exhibits an extremely tight cyclonic loop that should alert the forecaster to look for an explanation in the GFDN forecast fields. Because the JGSM track now has an cyclonic curvature similar to the NOGAPS and GFDN tracks 12 h ago, it is inferred that the JGSM integration is being degraded by E-DCI. Unfortunately, no JGSM fields are available to confirm this inference. Notice also that the UKMO (EGRR) track has a moderate cyclonic curvature that was not present 12 h ago. This change should alert the forecaster to the possibility that this forecast is also moderately affected by E-DCI.

The NOGAPS forecast fields (Fig. A.6f-h) still have symptoms of an E-DCI with the large cyclone to the southwest, particularly at 24 h when Winnie exhibits more of a northeast-southwest elongation than in the verifying analysis (Fig. A.6b). In the GFDN forecast fields (Fig. A.6j-l), Winnie and the intervening third cyclone begin to interact as before (Fig. A.6j). However, a prominent, and completely different cyclone develops to the east from 42 h to 66 h and merges with Winnie (Fig. A.6k-l), which accounts for the sharply cyclonic turn and near-stall in the GFDN track in Fig. A.6a. This instance of E-DCI accounts for the second entry for 14W in Table 2.1.

The satellite images during 9-12 August (Fig. 2.5a-d) have an extensive area of poorly-organized, and weakening convection to the west-southwest of Winnie that corresponds roughly to the large western cyclone in both the GFDN and NOGAPS analyses. A smaller, rapidly organizing area of convection to east of Winnie that corresponds to the disturbance that the GFDN model forecasts to develop. Thus, both of the above instances of E-DCI appear to have been with actual weak tropical circulations that were over-developed by the NOGAPS and GFDN models, but did not develop into JTWC-designated TCs.

c) *Typhoon Rosie (10W)*. As listed in Table 2.1, E-DCI involving Typhoon Rosie and an upper-level cyclonic circulation (ULC) affected the TC track forecasts initiated at 0000 UTC 20 through 1200 UTC 23 July 1997. The comparison/verification of the NOGAPS and GFDN 500-mb wind analyses and forecasts for 1200 and 1800 UTC 20 July in Fig. A.7a-l provides a representative illustration of this case. Notice that a large rightward bias develops in the NOGAPS track after 48 h and the GFDN track after 42 h (Fig. A.7a). Although the tracks of the other numerical models are less affected, all are right-of-track after 24 h and fast at 72 h.

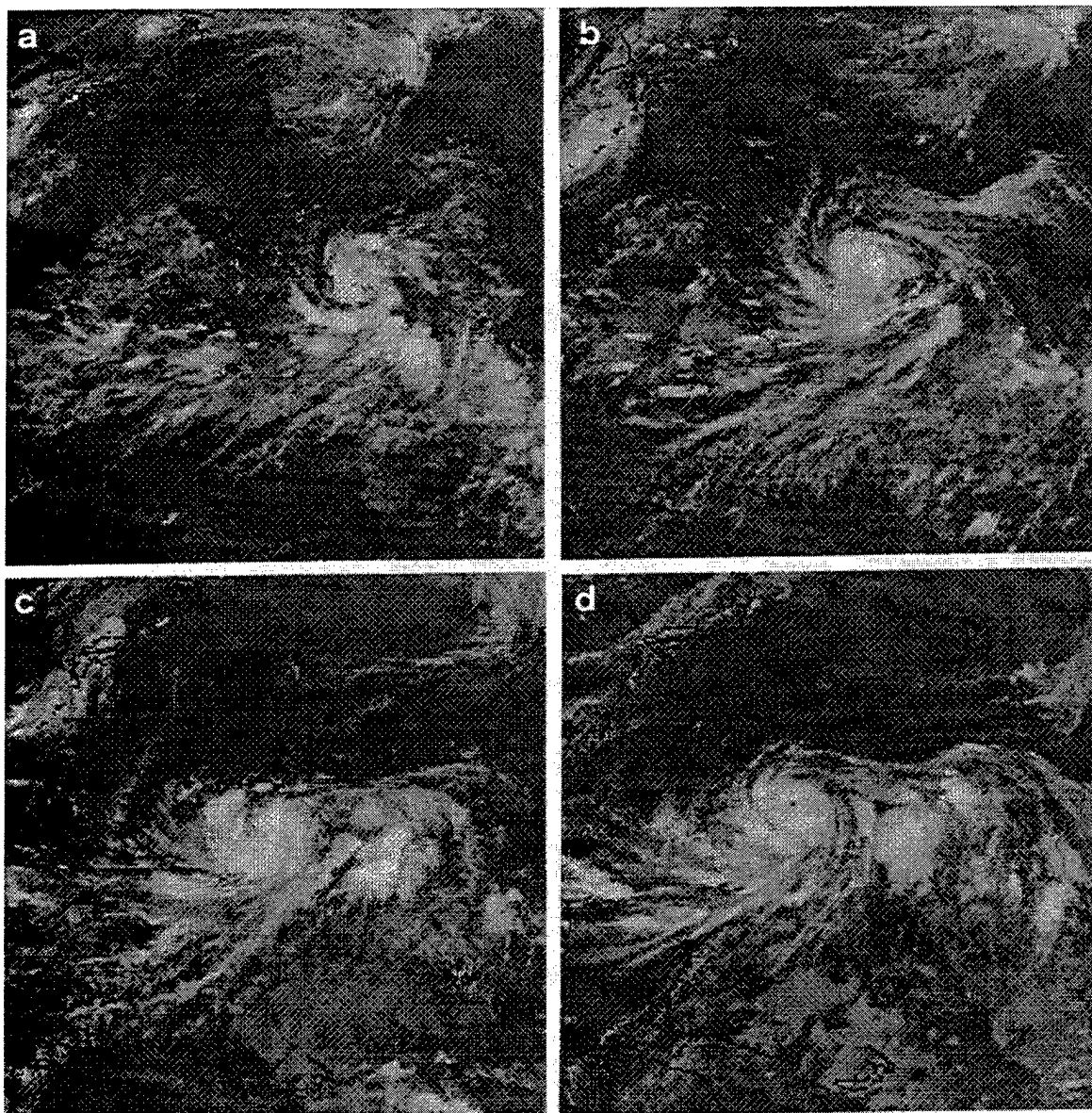


Fig. 2.5. Satellite imagery as in Fig. 2.4, except for TC Winnie at (a) 1200 UTC 9 August and 0000 UTC on (b) 10, (c) 11, and (d) 12 August.

The corresponding NOGAPS and GFDL forecast fields (Fig. A.7f-h and j-l, respectively) clearly show an ULC that forms from a trough to the north-northeast of Rosie moves southwestward into the vicinity of Rosie, where a direct interaction between the two cyclones is predicted to occur during 48 h and 72 h. In the NOGAPS 24-h forecast field (Fig. A.7f), the ULC is already about 3° lat. south of the verifying position (Fig. A.7b), which presumably facilitated an E-DCI with Rosie that takes place later in the model integration. In addition, the horizontal extent of the ULC is larger in the 48-h forecast than in the verifying analysis (compare Figs. A.7g and c, respectively). Examination of the 700- and 850-mb winds (not shown) of the same NOGAPS

integration reveals that the circulation of the ULC extends lower into the troposphere in the NOGAPS forecasts than in the verifying analyses. Thus, the E-DCI affecting the NOGAPS forecast has elements of three of the conceptual models in Figs. 2.2. That is, E-DCI occurred because the model over-forecast the size of at least one cyclone (Fig. 2.2a), brought the cyclones too close together (Fig. 2.2b), and over-represented the depth of the ULC (Fig. 2.2c).

Consider the distribution of track forecasts in Fig. A.7a and how the forecaster could use an awareness of the E-DCI phenomenon and knowledge of model error traits to insightfully interpret the distribution. As the E-DCI occurs in the NOGAPS 48- and 72-h forecasts (Fig. A.7g-h), the strength of the ULC weakens faster than Rosie, and Rosie becomes the dominant circulation. By contrast, the ULC in the GFDN 42 and 66-h forecasts (Fig. A.7k-l) strengthens significantly, and becomes dominant with respect to Rosie. These differences in the forecast evolution of the two cyclones explain why the latter portion of the GFDN track forecast is well to the right of (and also more degraded than) the NOGAPS track (Fig. A.7a). Notice that the JGSM, JTYM, and EGRR tracks are all to the left of the NOGAPS and GFDN tracks (Fig. A.7a). Although the JTWC forecasters did not have the fields for these models, a reasonable inference would be that these other models were either: (i) less affected by E-DCI; or (ii) unaffected by E-DCI. If the first inference is made, then all five of the 72-h forecast positions could be treated as one cluster that has been made "fuzzy" by a phenomenon that is affecting all of the forecasts to varying degrees. This would be an example of where the forecaster could make an official forecast that reflects an adjusted consensus (AC) (recall Fig. 1.3a) of all the available numerical model track forecasts, but assigns them varying weights. Alternately, the forecaster may make the judgment that the JGSM, JTYM, and EGRR models were unaffected by the E-DCI phenomenon identified in the NOGAPS and GFDN models. In this case, the suite of five tracks would be treated as two separate clusters, and the official forecast would be based only on the selective consensus (SC) of the three western-most tracks.

As listed in Table 1.2, only the GFDN track forecast initiated at 1800 UTC 20 July 1997 was highly degraded by E-DCI. After the fact, the E-DCI phenomenon could be identified as continuing until 1200 UTC 23 July 1997 (Table 2.1), even though the effect did not result in 72-h FTEs exceeding 300 n mi. The comparison/verification of the NOGAPS and GFDN 500-mb wind analyses and forecasts for 1200 and 1800 UTC 22 July in Fig. A.8a-l provides a representative illustration of this period of weak E-DCI. In the 24-h NOGAPS and 18-h GFDN forecast fields (Fig. A.8f and j, respectively), the ULC to the north-northeast is closer to the TC than in the verifying NOGAPS analysis (Fig. A.8b), which indicates that E-DCI is still occurring. Weak troughing that rotates cyclonically around the TC is evident in the subsequent NOGAPS and GFDN forecast fields (Fig. A.8g-h and k-l, respectively), but not in the verifying analyses (Fig. A.8c-d), which is further evidence of weak E-DCI. Notice also that the NOGAPS and GFDN forecast tracks curve more cyclonically after 48-h than the verifying best track (Fig. A.8a).

That the E-DCI in the NOGAPS and GFDN forecasts at this time is weak is confirmed by the close agreement of the 72-h forecast positions with the verifying best-track position (Fig. A.8a). Notice also the excellent agreement among the 72-h positions of the five numerical model forecast tracks. This is an important clue to the operational forecaster that, should the signature of E-DCI be detected in the model forecast fields, the phenomenon is weak and not likely to be causing significant track forecast degradation. Because of the sensitivity of the E-DCI to the analyzed and

forecast structure of the two cyclones, and differences among the data assimilation schemes and physics of the five models, it is not very likely that significant E-DCI would occur in all five models with equal effect, and thus very likely that the model tracks will not be in good agreement. Thus, by checking for degree of forecast track consistency, the forecaster can avoid a false alarm of significant E-DCI based on analysis of the model fields alone.

With the benefit of hindsight, it is relatively straightforward to determine that the interaction between Rosie and the ULC predicted by the NOGAPS and GFDN models (and possibly to a lesser extent by the other numerical models) did not occur. However, the forecaster must make such a determination without knowing the future track of the TC, if he/she is to successfully employ the kind of forecast track analysis presented in the preceding paragraphs. A key issue is whether TCs and ULCs interact at all in nature. Whereas TCs in the Eastern/Central Pacific and Atlantic basins (White 1995 and Kent 1995, respectively) have been observed to orbit very large, deep cutoff lows, the authors know of no cases in the western North Pacific in which an ULC clearly altered the track of a TC owing to DCI. Thus, it seems very improbable that model-predicted DCI involving an ULC would actually verify. An additional indication to the forecaster that no significant interaction would likely occur in the Rosie case is provided by 0000 UTC water vapor images during 20-23 July (Fig. 2.6a-d). The trough that evolves north of Rosie does not have the well-defined signature expected of a circulation feature sufficiently deep to affect the motion of a TC.

d) *Typhoon Amber (18W)*. As indicated in Table 2.1, an E-DCI involving Typhoon Amber (18W) and Tropical Storm Cass (20W) degraded the NOGAPS and GFDN (and by inference, JTJM) track forecasts of Amber (but not Cass) initiated at 0000 UTC 26 through 0000 UTC 28 August. This is the only one of the 18 cases of E-DCI observed in 1997 that was a misrepresentation of an actual DTI (versus a false forecast of DCI). The comparison/verification of the NOGAPS and GFDN 500-mb wind analyses and forecasts for 1200 and 1800 UTC 27 August in Fig. A.9a-l illustrate this case. Notice that the five numerical model track forecasts may be segregated into clusters comprised of NOGAPS/GFDN and JGSM/JTJM/EGRR (Fig. A.9a). Both the NOGAPS (Fig. A.9e-h) and GFDN models (Fig. A.9i-l) predict that Amber (eastern TC) and Cass (western TC) will undergo very vigorous mutual (two-way) DTI that results in a merger after about 48 h. In the verifying NOGAPS analyses (Fig. A.9b-d), the rotation rate of the two TCs about a midpoint is much slower and they are still separated by about 5° lat. after 72 h (66 h).

Given that the forecaster recognizes that NOGAPS and GFDN models are predicting a DTI of Amber and Cass, the key question is whether the official forecast should reflect: (i) the more vigorous interaction represented by the consensus of the NOGAPS and GFDN tracks that involves a significant deflection of Amber's track toward Cass; or (ii) the less vigorous interaction represented by the consensus of the other three tracks, which involves only a modest acceleration in response to the influence of Cass. A useful, independent source of information is the geostationary satellite IR image at 1200 UTC 27 August (Fig. 2.7a), which reveals that Cass has a much smaller cloud signature than Amber. Given the separation distance between the two cyclones, this suggests that the track of Amber will likely be little affected by an interaction with Cass, and that a selective consensus based on the JGSM/JTJM/EGRR cluster would be more accurate in this case. Interestingly, the JTJM track 12 h later agrees more with NOGAPS and GFDN (Fig. 2.7b), which

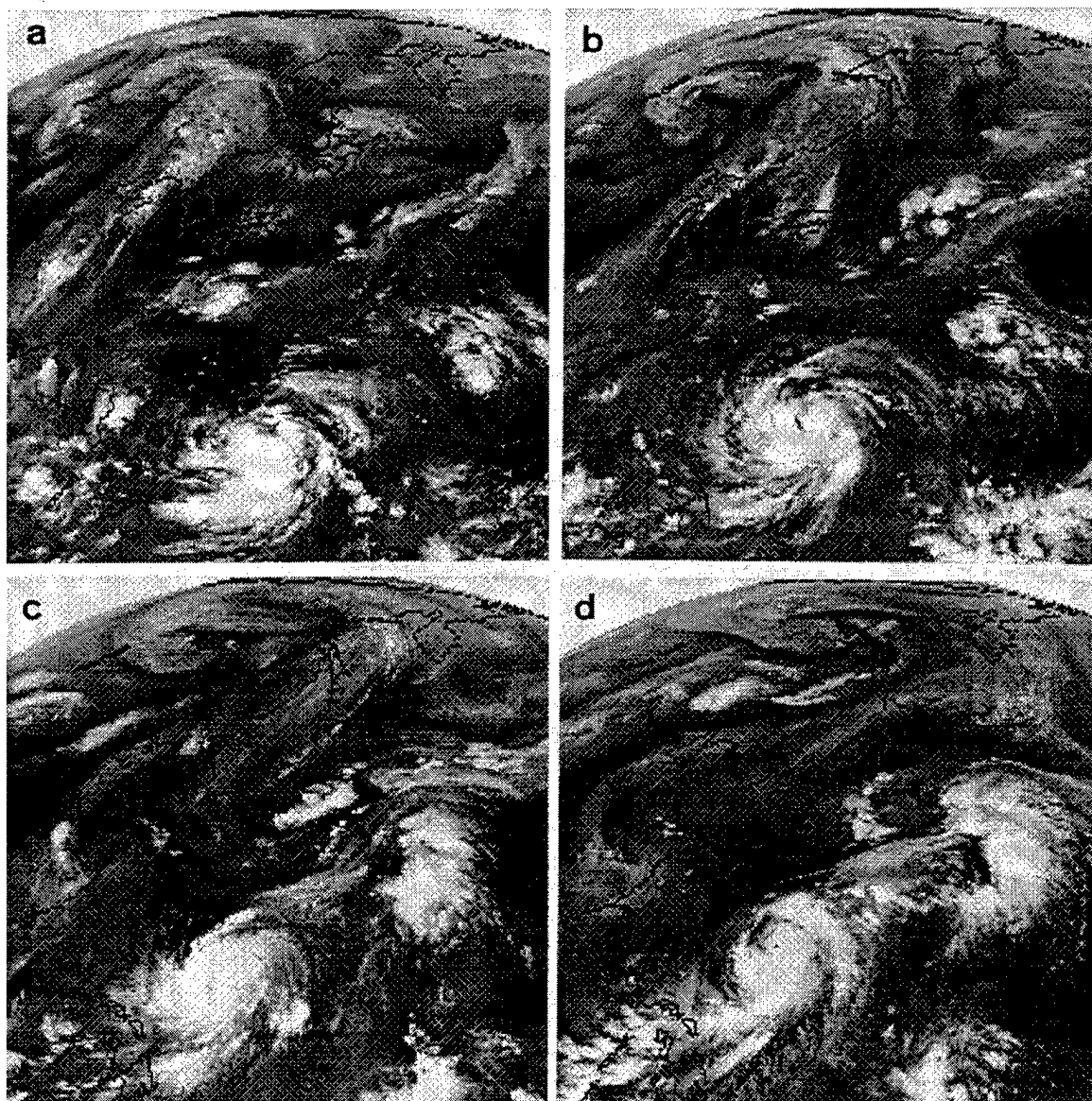


Fig. 2.6. Satellite water vapor images for TC Rosie at 0000 UTC on (a) 20, (b) 21, (c) 22, and (d) 23 July 1997.

still have a significant left bias. This change illustrates the inherent sensitivity of the E-DCI phenomenon, and also emphasizes that simply aligning the official forecast to follow the "majority opinion" of the numerical models will not always produce the best forecast when a E-DCI scenario is occurring.

4) Impact on other objective guidance. The performance of the NOGAPS-dependent objective track forecast techniques at times when E-DCI occurred in the NOGAPS forecast is shown in Fig. 2.8a-d, which may be compared with the corresponding NOGAPS tracks in Figs. A.3a, A.5a, A.7a, and A.9a, respectively. In each case, the shallow (SBAM) and medium (MBAM) depth steering models are significantly degraded in a manner similar to the NOGAPS forecast. The deep steering model (FBAM) also appears to be affected, but usually to a significantly less degree. The statistical-dynamical model CSUM does not appear to be significantly affected in the cases of

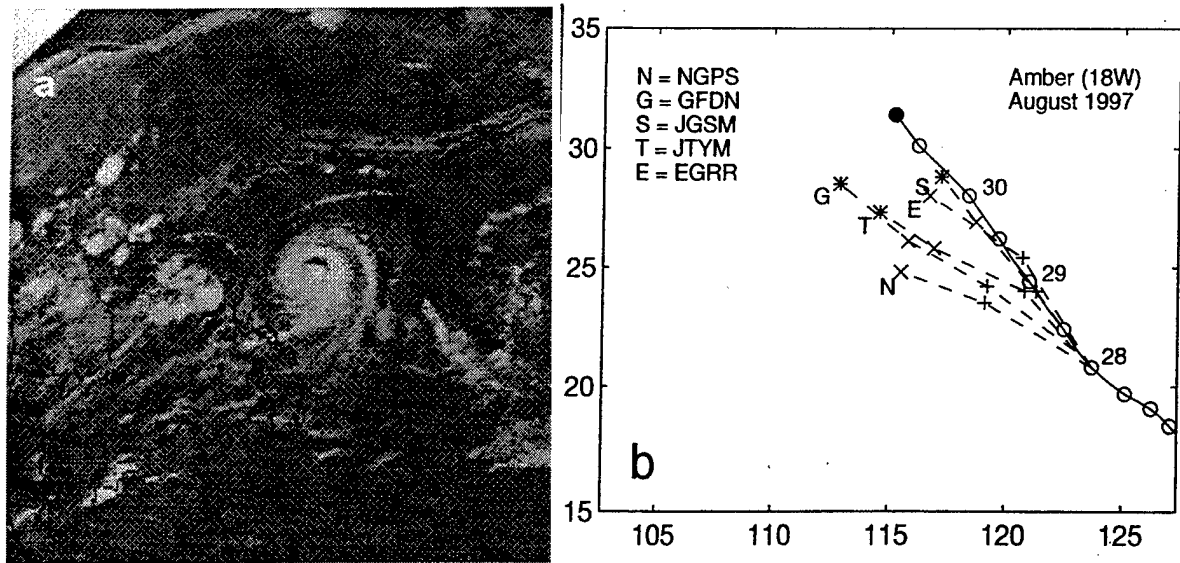


Fig. 2.7. (a) Satellite IR image as in Fig. 2.4, except for Amber at 1200 UTC 27 August, and (b) best-track of Amber during 1200 UTC 26 August to 1200 UTC 30 August and five numerical model track forecasts (see inset) initiated at 0000 UTC (models N, S, and E) or 0600 UTC (models G and T) 28 August 1997. The forecast tracks have a cross (+) at the 24-h (18-h) position, an x at the 48-h (42-h) position, and an asterisk at the 72-h (66-h) position for models initiated at 0000 (0600) UTC. Circles are best track positions every 12 h, and solid circle is the verifying position for the 72-h (66-h) forecast for models initiated at 0000 (0600) UTC.

Winnie and Rosie (Fig. 2.8b and c, respectively) and produces very accurate 72-h forecasts. The CSUM tracks for Nestor and Amber (Fig. 2.8a and d, respectively) are inaccurate. However, the TC in these cases is undergoing a turn at the initialization time of the model, and CSUM has a known tendency to under-forecast poleward turns. Thus, the poor performance of the model for these two cyclones is probably more a reflection of a performance characteristic peculiar to the CSUM as opposed to being a manifestation of E-DCI.

5) Summary. Table 2.2 is a summary of the key aspects of the E-DCI phenomenon, its indications in numerical model fields and tracks, and its impact on various models available to the JTWC forecaster. Where appropriate, a citation is given to identify the figure(s) that illustrates the pertinent point. Notice that the key indicator in Table 2.2 (bold type) to the forecaster that E-DCI is degrading a NOGAPS or GFDN track forecast is the presence in the sea-level pressure and/or mid-to-lower tropospheric wind fields of a second cyclonic feature that rotates cyclonically about, and tends to merge with, the TC.

A key result for the forecaster is that whereas DCI seems to occur relatively frequently in numerical models (e.g., 18 periods, involving 14 TCs, and which degraded 39 NOGAPS forecasts and 31 GFDN forecasts in 1997), vigorous track-altering direct interactions between real TCs and other cyclones appear to be rare. Therefore, pending any new information to the contrary, the forecaster will normally be justified in treating any model-predicted DCI as E-DCI, and either

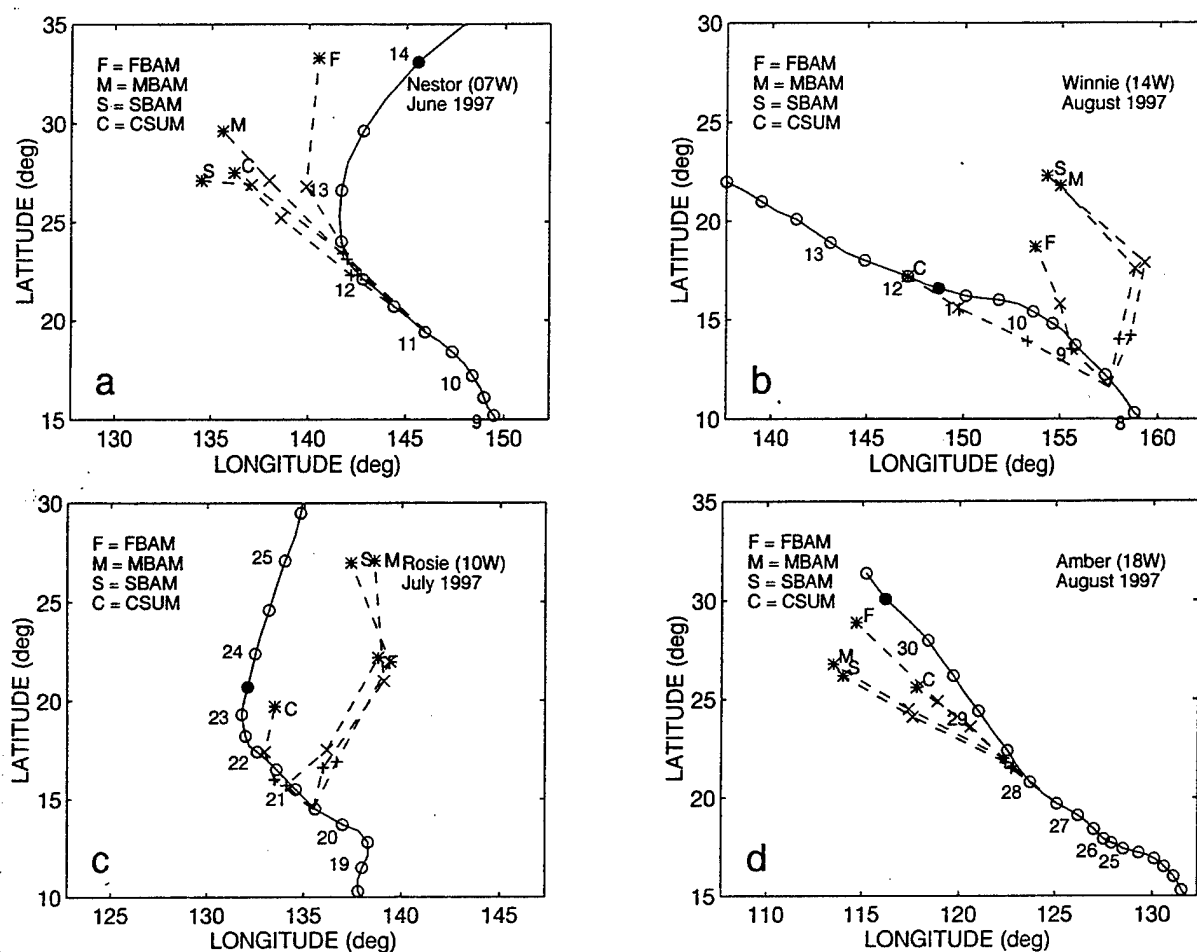


Fig. 2.8 Best-track and four objective technique track forecasts (see inset) during periods of E-DCI in the NOGAPS forecast of (a) Nestor at 0000 UTC 11 June, (b) Winnie at 1200 UTC 8 August, (c) Rosie at 1200 UTC 20 July, and (d) Amber at 1200 UTC 27 August 1997.

rejecting or giving low weight to the track forecast of that model. Since E-DCI is relatively easy to identify, and according to Table 1.3 accounted for about one third of all poor 72-h forecasts produced by the NOGAPS (39 of 108) and the GFDN (31 of 99) models in 1997, using the Systematic Approach to detect and account for this phenomenon in the future has the potential to considerably reduce the number of official track forecasts with large FTEs.

Table 2.2 Summary of important aspects and illustration key for the E-DCI phenomenon.

Aspect	Description	Figure
Conceptual model	False/excessive orbiting and merger of TC and a nearby cyclone due to mutual advection and shearing by one or both cyclone circulations.	2.1
Frequency	18 periods involving 14 TCs and significantly degrading 39 (31) NOGAPS (GFDN) forecasts in the western North Pacific during 1997	Table 2.1
Environment	Usually occurs when TC is in vicinity of active equatorial (monsoon) trough that contains other weak disturbances in vicinity	2.5a
Variations of the Phenomenon	<p>May be caused by:</p> <ul style="list-style-type: none"> (i) too large a size/depth of the TC and/or second cyclone; (ii) mislocation of TC and/or second cyclone; or (iii) self-interaction between the TC in 1st-guess field and the synthetic observations cyclone located at a different position. <p>Second cyclone may be:</p> <ul style="list-style-type: none"> (i) another TC or precursor usually located to the west and south; (ii) a real or false tropical non-developing tropical disturbance; usually located to the west and south; occasionally to the east; or (iii) an upper-level cyclone of midlatitude origin and located north of the TC, and that becomes large and deep in the model. 	<p>2.2a,c 2.2b 2.2d</p> <p>2.4a, 2.9a 2.5a-d</p> <p>2.8a-d</p>
Indications in numerical model fields	<p>In streamline fields:</p> <ul style="list-style-type: none"> - a closed cyclone or an area of streamline troughing that rotates about and merges to some degree with the TC circulation <p>In sea-level pressure fields:</p> <ul style="list-style-type: none"> - a closed low or a trough that rotates about and merges to some degree with the TC circulation 	<p>A.5e-l A.7e-l</p> <p>A.3e-h</p>
Numerical model levels affected	<p>500 mb and below if 2nd cyclone is a tropical disturbance</p> <p>WARNING: Best level varies from case to case. In weaker cases the DCI indication may appear at only one level. Check all levels!</p> <p>500 mb and above if 2nd cyclone is midlatitude cyclone or TUTT cell</p>	
Indications in numerical model tracks	<ul style="list-style-type: none"> - cyclonic curvature or looping (if interaction is vigorous); often results in first 24-h forecast that deviates significantly from persistence - sudden changes in temporal progression of 72-h forecast positions at onset and cessation - deflection toward 2nd cyclone compared to unaffected model tracks - significant translational acceleration toward 2nd cyclone - significant translational deceleration if TC was initially moving, or forecast to move away from 2nd cyclone 	<p>A.5a, A.6a</p> <p>2.3</p> <p>A.9a 2.7b A.6a</p>
Relative impact on numerical models	Usually affects both NOGAPS and GFDN, but may affect only one. Often seems to affect JSGM, JTYM, and EGRR when either NOGAPS or GFDN is affected.	Table 2.1 2.7a-d
Relative impact on other objective guidance	<ul style="list-style-type: none"> - BAMs are usually degraded as much as or more than NOGAPS; SBAM and MBAM are usually affected more than FBAM - CSUM usually not affected; accuracy of track depends on synoptic situation (performs best in S/TE) 	<p>2.11a,c 2.13a,c 2.11b,d 2.11b,d</p>

b. Indirect cyclone interaction (ICI)

1) Description. The conceptual model for indirect cyclone interaction on an eastern TC (ICIE) is shown in Fig. 2.9. The ICIE model is analogous to the ITIE conceptual model developed by Carr et al. (1998) and used in the CMKB (see p. 88). In the more general case of ICIE, the western cyclone may be any large cyclonic circulation (such as a large TC, monsoon gyre, deep midlatitude trough or cut-off low) that tends to generate a strong peripheral anticyclone to the southeast. In a barotropic, beta-plane model, this anticyclone is a result of Rossby wave dispersion of the large western cyclone (cf. Carr and Elsberry 1998; their Fig. 12c). However, baroclinic influences may have a significant role in the development of this anticyclone in the atmosphere. Excessive ICIE (E-ICIE) occurs when the numerical model predicts that this peripheral anticyclone generated by the western cyclone will force the eastern TC to take a more equatorward track than in reality. This situation tends to occur when the anticyclone is predicted to be too strong and/or the eastern TC is predicted to be too small. Only the GFDN model was affected by this phenomenon in 1997. Conversely, insufficient ICIE (I-ICIE) occurs when the numerical model predicts that track of the eastern TC will be less equatorward than in reality either because the eastern TC is too large or the peripheral anticyclone of the western cyclone is too weak. This phenomenon was not responsible for degrading track forecasts by either NOGAPS or GFDN in 1997, but is a physical possibility.

The conceptual model for indirect cyclone interaction (ICI) on a western TC (ICIW) is shown in Fig. 2.10. The ICIW model is analogous to the ITIW conceptual model developed by Carr et al. (1997) and used in the CMKB (see p. 92). In the case of ICIW, the eastern cyclone may be any cyclonic circulation (such as a TC or TUTT cyclone) that can act to erode or preclude the development of a significant peripheral anticyclone associated with the western TC. Insufficient ICIW (I-ICIW) occurs when the model predicts that the western TC will track more poleward than in reality because the eastern cyclone does not sufficiently inhibit (or preclude) the development of a significant peripheral anticyclone associated with the western TC. Only the GFDN model was affected by this phenomenon in 1997. Conversely, excessive ICIW (E-ICIW) occurs when the model predicts that the western TC will track less poleward than in reality because the eastern cyclone is too effective in weakening or precluding the development of the peripheral anticyclone of the western TC. This phenomenon was not responsible for degrading track forecasts by either the NOGAPS or the GFDN models in 1997, but is a physical possibility.

Erroneous Model-predicted Indirect Cyclone Interaction on Eastern TC (ICIE)

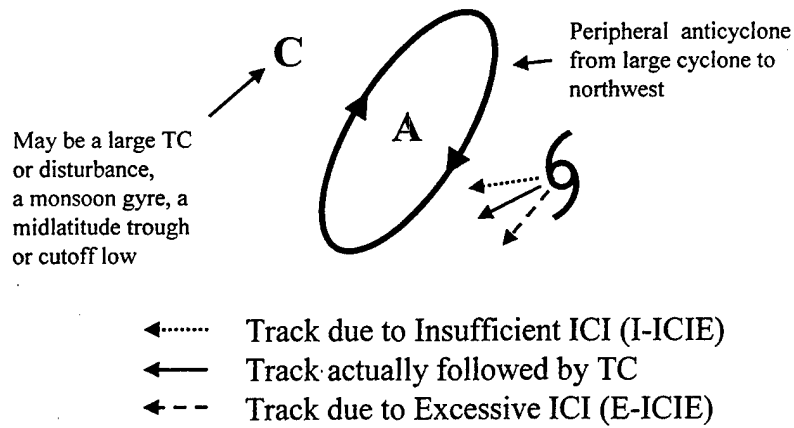


Fig. 2.9. Conceptual model as in Fig. 2.2 when large forecast track errors are associated with insufficient (dotted arrow) or excessive (dashed arrow) Indirect Cyclone Interaction on eastern TC (ICIE).

Erroneous Model-predicted Indirect Cyclone Interaction on Western TC (ICIW)

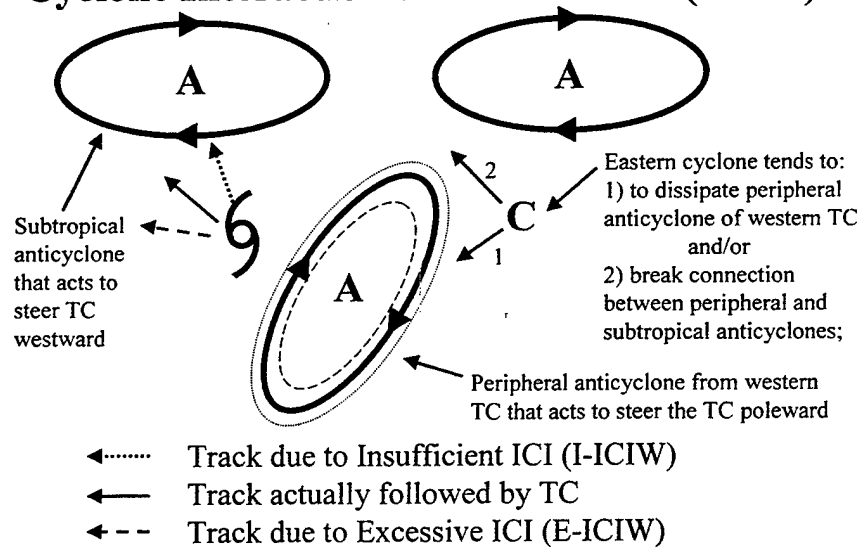


Fig. 2.10. Conceptual model as in Fig. 2.9, except for erroneous ICI on the western TC.

2) Frequency and characteristics. In the western North Pacific during 1997, only three GFDN forecasts for Typhoon Joan (28W) were degraded by E-ICIE arising from Typhoon Ivan (27W) to the west, and only one GFDN forecast for Typhoon Ivan (27W) was degraded by I-ICIW associated with Typhoon Joan (28W) to the east. The size of the sample is presently too small to warrant comments about frequency and characteristics. Such an analysis must be deferred until additional years of NOGAPS and GFDN track forecasts can be evaluated.

3) Case studies. The Typhoon Joan (28W) case illustrates E-ICIE occurring in the GFDN model only, and the Typhoon Ivan (27W) case illustrates I-ICIW in the GFDN model only. Both of these cases involve misrepresentations of TC size that appear to be a result of the particular TC initial condition specification used in the GFDN model.

a) Typhoon Joan (28W). The relationships of the five numerical model forecast tracks to the actual track of Joan during the period 0000 UTC 15 October to 1200 UTC 16 October 1997 are shown in Fig. 2.11a-d. Notice that for the first three synoptic times the GFDN forecast is an outlier with a track toward the west-southwest, whereas the other four model tracks are oriented toward the west-northwest. By contrast, the GFDN forecast initiated at 1800 UTC 16 October is in good agreement with the other models. A comparison/verification of 500 mb wind fields for the 1200 UTC 15 October NOGAPS and 1800 UTC 15 October GFDN forecasts is shown in Fig. A.10a-l. In both the NOGAPS and GFDN analyses (Fig. A.10e and i, respectively), an anticyclone appears between Joan and Ivan to the west. The presence of this anticyclone and the slight equatorward turn of Joan at 0000 UTC 15 October (Fig. A.10a) indicate that weak ITIE occurs during 15 October.

Notice in the GFDN forecast fields (Fig. A.10j-l) that the anticyclone between Ivan and Joan remains connected with the subtropical anticyclone to the north of Joan, and thus continually subjects Joan to equatorward steering. That is, ITIE continues to occur in GFDN model throughout the forecast, and the left bias of the GFDN forecast track (Fig. A.10a) confirms that the predicted TC interaction is too strong. In the corresponding NOGAPS forecast fields (Fig. A.10f-h), a large peripheral anticyclone forms to the southeast of Ivan. However, this anticyclone becomes separated from the subtropical anticyclone to the north of Joan, which allows Joan to move west-northwestward between the peripheral anticyclone and the subtropical anticyclone. Thus, ITIE does not continue to occur in the NOGAPS forecasts. Although the NOGAPS track forecast has a poleward bias, the actual track of Joan also becomes increasingly poleward after 0000 UTC 16 October, which indicates that the period of real ITIE from Ivan has concluded.

A plausible explanation for the excessively equatorward GFDN tracks is revealed from the comparison/verification of sea-level pressure from the 1200 UTC 15 October NOGAPS and 1800 UTC 15 October 1997 GFDN forecasts (Fig. A.11a-l). Notice that the sizes of Joan and Ivan are nearly the same in the NOGAPS sea-level pressure analysis (Fig. A.11e). By contrast, Joan is about four times smaller than Ivan in the GFDN analysis (Fig. A.11i), and is very small in an absolute sense. As shown in Table 2.3, the JTWC 35-kt wind radii at 1200 UTC 15 October for both Joan and Ivan were also quite small ($\sim 1^\circ$ lat. radius). Thus, it appears that the TC initial condition specification for the GFDN analysis for Joan successfully removed the larger circulation for Joan analyzed by NOGAPS and replaced it with a spin-up vortex that more closely adheres to the JTWC-specified wind radii. Recall that the TC initial condition specification process is not applied

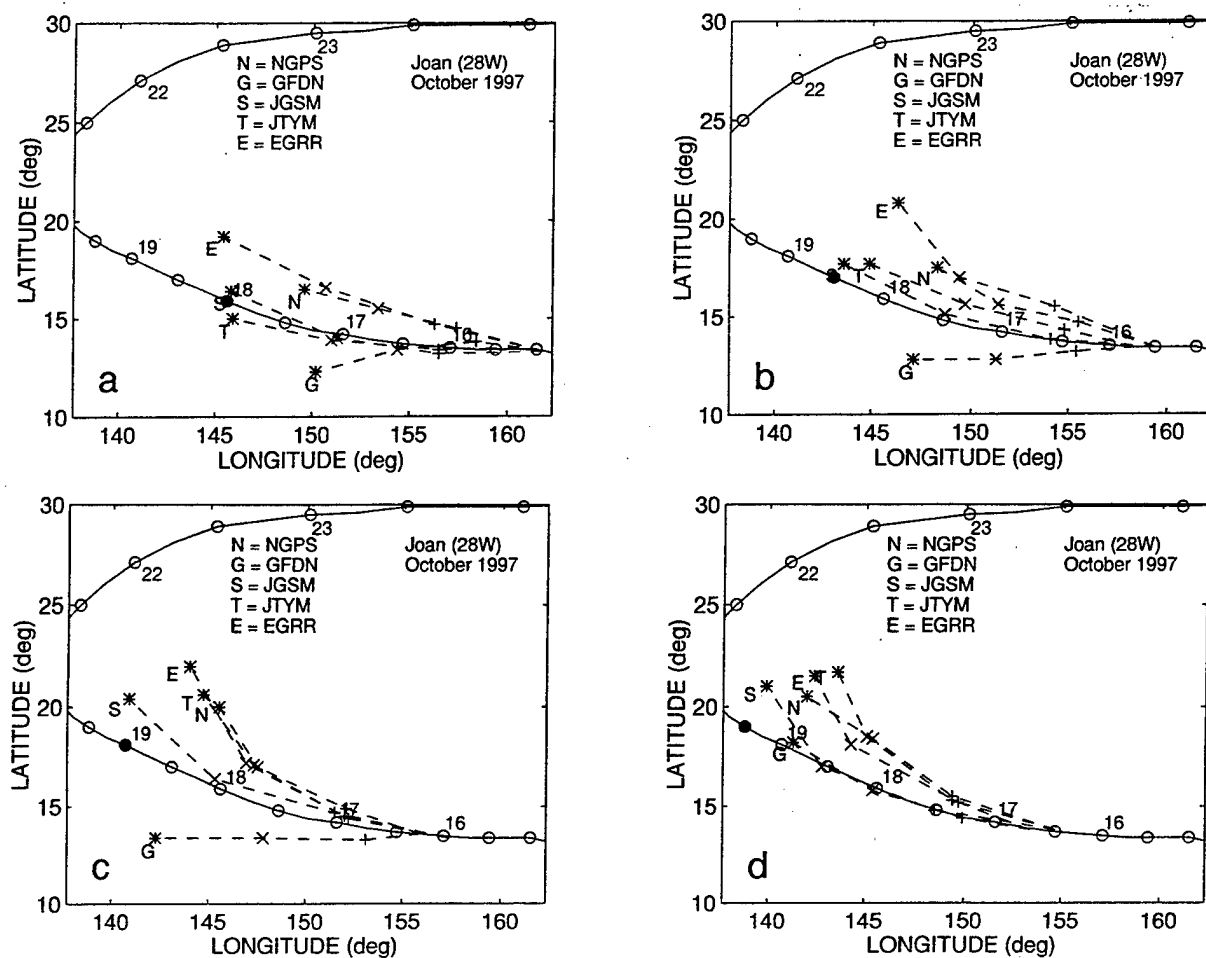


Fig. 2.11. Best-track and selected model forecast tracks (see inset) as in Fig. 2.7b, except for TC Joan (28W) on (a) 0000 UTC and (b) 12 UTC 15 October, and (c) 0000 UTC 16 and (d) 1200 UTC 16 October 1997.

to other TCs in the GFDN model, so that the size of Ivan in the GFDN integration with Joan as the target TC remains unchanged from the NOGAPS analysis. The differing initial condition treatment of Joan and Ivan in the GFDN track forecast for Joan creates an imbalance that does not exist in reality, and this size imbalance is maintained in the GFDN sea-level pressure forecast fields (Fig. A.11j-l). The comparatively large size of Ivan in the GFDN model generates a peripheral anticyclone that has an equatorward deflection of the track of Joan that is excessive. As a result, the GFDN track forecast for Joan has an equatorward bias in agreement with the E-ICIE conceptual model (Fig. 2.9, dashed arrow).

Table 2.3 JTWC maximum wind speed (V_m) and 35-kt radius (R_{35}) estimates for Ivan and Joan. The first (second) number in the wind radius columns is the radius of the strong (weak) semi-circle.

Date/Hours (UTC)	Ivan V_m (kt)	Ivan R_{35} (n mi)	Joan V_m (kt)	Joan R_{35} (n mi)
971015/0000	55	40/30	45	50/40
971015/1200	70	60/50	60	50/40
971016/0000	85	85/70	85	70/55
971016/1200	90	90/50	125	110/90

Recall that the equatorward bias in the three GFDN track forecasts for Joan from 0000 UTC 15 October to 0000 UTC 16 October (Fig. 2.11a-c) abruptly vanishes in the 1800 UTC 16 October GFDN forecast (Fig. 2.11d). The NOGAPS and GFDN 500-mb wind forecasts that correspond to the tracks in Fig. 2.11d are shown in Fig. A.12. Notice that although the peripheral anticyclone develops well to the southeast of Ivan in the GFDN forecast fields (Fig. A.12j-l), this anticyclone does not become connected to the subtropical anticyclone to the north of Joan. As a result, the synoptic pattern in the GFDN 72-h forecast field (Fig. A.12l) is very similar to the 72-h NOGAPS forecast (Fig. A.12h) and the verifying NOGAPS analysis (Fig. A.12d). The reduced influence of the peripheral anticyclone from Ivan removes the equatorward steering of Joan. The improved track forecast by the GFDN for 1800 UTC 16 October is consistent with the increased size of Joan relative to Ivan in the sea-level pressure analysis (Fig. A.13i). This increased size of Joan in the GFDN analysis is consistent with the 35-kt wind radius specification by JTWC (Table 2.3; row 4) that is roughly twice as large as the radius specified 24 h earlier (Table 2.3; row 2). Although the size of Joan is still noticeably smaller than for Ivan in the GFDN forecast fields (Fig. A.13j-l), the difference is apparently small enough to not cause a degradation in the GFDN track forecast for Joan.

Satellite imagery of both Ivan and Joan during the period when the GFDN track was an equatorward outlier relative to the other numerical models (Fig. 2.12a-d) represents an operationally useful indication to the forecaster that both of the TCs were rather small and similar in size. This information would have helped the forecaster to recognize the inequity in sizes of the TCs in the GFDN analysis if it had been available to the forecaster, and perhaps that the sizes of both TCs were too large in the NOGAPS analyses (which were available).

In summary, this case illustrates how a track forecast error can occur in the GFDN model because the TC initial condition specification is applied only to the target TC, and not to any other TCs in the domain. The problem may be exacerbated when a small 35-kt wind radius is specified, because the higher resolution of the GFDN model permits the specification of a significantly smaller vortex than in the NOGAPS model. In principle, this kind of problem could affect NOGAPS in a binary TC situation if an erroneous analysis of the size of only one TC results because synthetic TC observations were rejected, or were highly unrepresentative. In the Ivan and Joan case, both TCs were small, and both sets of synthetic TC observations did not result in reductions in the overly large representations of both circulations that originated from the background fields from the 12-h NOGAPS forecast. Since the sizes of both TCs were in error, the effect was a "balanced" error with regard to the RMT process. That is, the increased rate of

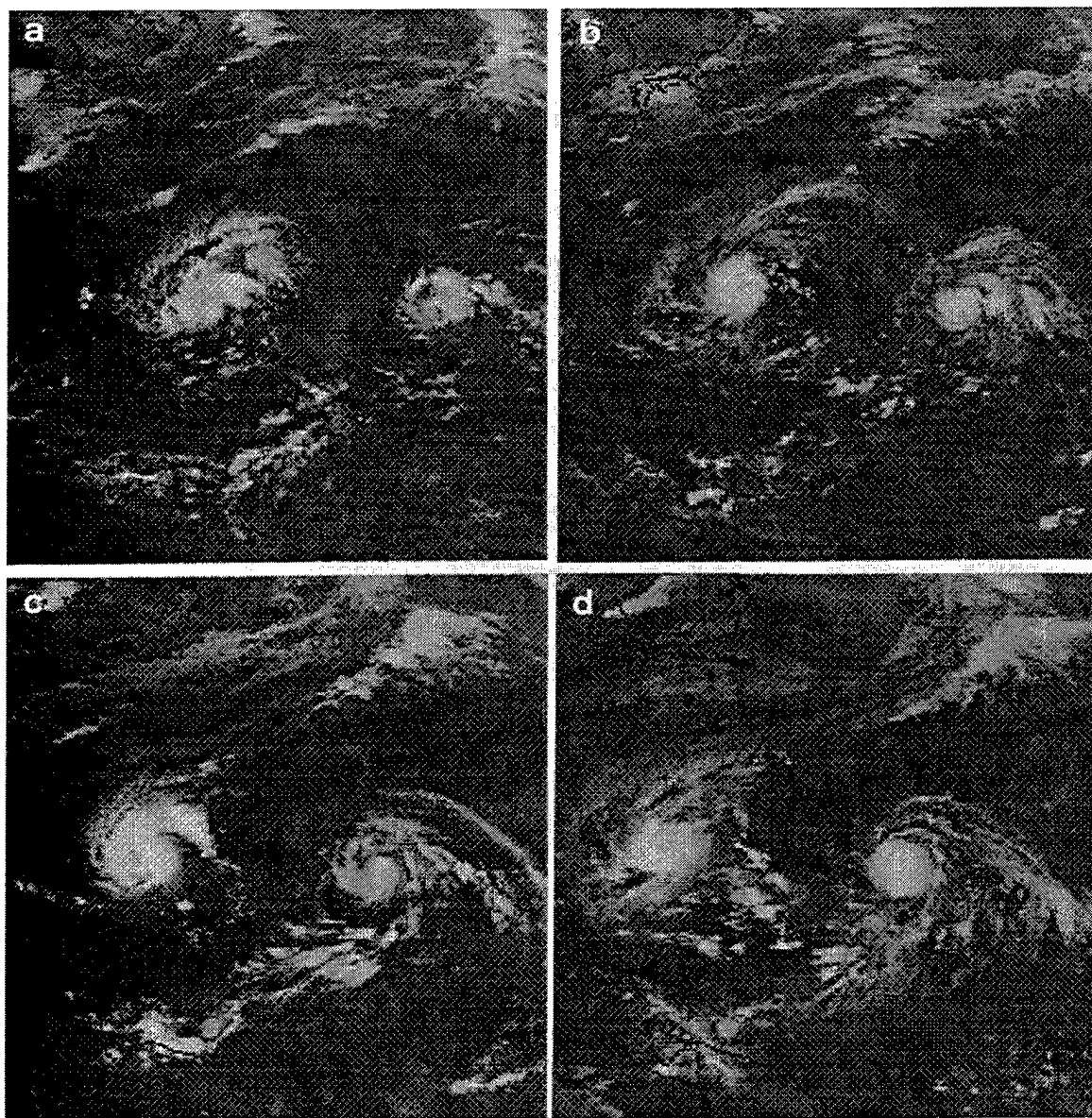


Fig. 2.12. Satellite infrared imagery as in Fig. 2.4, except for TCs Ivan (western) and Joan (eastern) at (a) 0000 UTC and (b) 1200 UTC 15 October, and (c) 0000 UTC and (d) 1200 UTC 16 October 1997.

peripheral anticyclone generation by Ivan was apparently offset by an increased tendency by Joan to erode that peripheral anticyclone, which thus kept the situation in balance.

b) Typhoon Ivan (27W). The relationships of the five numerical model forecast tracks to the actual track of Ivan during the period 0000 UTC 15 October to 1200 UTC 16 October 1997 are shown in Fig. 2.13a-d. Notice that the GFDN forecast initiated at 1800 UTC 15 October has a significant poleward bias relative to the NOGAPS track forecast and the verifying best track (Fig.

2.13b). Comparison of the NOGAPS and GFDN 500-mb wind forecasts (Fig. A.14e-h and i-l, respectively) corresponding to the tracks in Fig. 2.13b reveals differences in environment structure that explain the differences in the track forecasts. In the GFDN 42-h forecast field (Fig. A.14k), the peripheral anticyclone generated by Ivan develops a clear connection with the subtropical anticyclone to the north of Joan and an isotach maximum appears to the east of Ivan. These changes are coincident with a poleward turn in the GFDN track (Fig. A.14a), which indicates that the environment structure of Ivan has transitioned from S/TE to P/PF.

In the NOGAPS 48-h and 72-h forecast fields (Fig. A.14g-h), the peripheral anticyclone of Ivan actually becomes increasingly separated from the subtropical anticyclone to the north of Joan, presumably due to the encroachment of Joan's circulation. The agreement of the NOGAPS forecasts with the verifying analyses (Fig. A.14c-d) indicates that the apparently greater influence of Joan on the peripheral anticyclone of Ivan in the NOGAPS forecast is representative. By inference, an insufficient influence by Joan on the peripheral anticyclone of Ivan was predicted by the GFDN model. That is, there was insufficient ICIW (I-ICIW) on Ivan by Joan in GFDN in accordance with the conceptual model that includes an unrepresentatively large anticyclone (Fig. 2.10, dotted ellipse) that steers the western TC too strongly poleward (Fig. 2.10, dotted arrow).

A comparison of the sea-level pressure fields from the 1800 UTC GFDN and 1200 UTC 15 October NOGAPS forecasts (Fig. A.15) reveals the reason for I-ICIW in the GFDN forecast for Ivan. Notice the size of the sea-level pressure pattern for Joan in the GFDN forecast is too small and the lowest pressure never goes below 1004 mb. By contrast, the NOGAPS model maintains a somewhat larger and deeper circulation for Joan (compared to the GFDN model) that apparently leads to ICIW that is sufficient to keep the 500-mb peripheral anticyclone of Ivan from becoming connected to the anticyclone to the north of Joan (Fig. A.14h).

A comparison of the 500-mb wind fields from the 0000 UTC 16 October NOGAPS and 0600 UTC 16 October GFDN forecasts is shown in Fig. A.16a-l. Notice that the sudden improvement in the accuracy of the GFDN track forecast (Fig. A.16a) compared to 12 hours previously corresponds to a failure of the peripheral anticyclone generated by Ivan to connect with the subtropical anticyclone in the GFDN 72-h forecast (Fig. A.16l). In the corresponding GFDN sea-level pressure forecast fields (Fig. A.17i-l), a larger circulation for Joan is maintained compared to the GFDN forecast 12 h earlier (Fig. A.15i-l). Notice that this circulation compares better with the size of Joan in the corresponding NOGAPS sea-level pressure forecasts (Fig. A.17f-h). Apparently, both of these circulations are adequately large to create sufficient ICIW to preclude a poleward track change in either model, although both representations of Joan are significantly smaller than in the verifying NOGAPS analyses (Fig. A.17b-d).

Recall that in the case of Joan discussed in the previous subsection, a considerable difference existed in the size of the TC in the NOGAPS (Fig. A.11e) and the GFDN (Fig. A.11i) analyses. This difference occurred because the GFDN TC initial condition is supposed to completely remove the NOGAPS-analyzed TC circulation and replace it with a GFDN model-consistent spin-up vortex. When the actual TC is small, the GFDN-analyzed size of the TC should be smaller than in the NOGAPS model simply due to differences in horizontal resolution. If the area of sub-1008 mb pressures is used as a measure of TC size in the case of Ivan, then the TC is essentially the same size in both model analyses (e.g., compare Fig. A.15e with Fig. A.15i, and Fig.

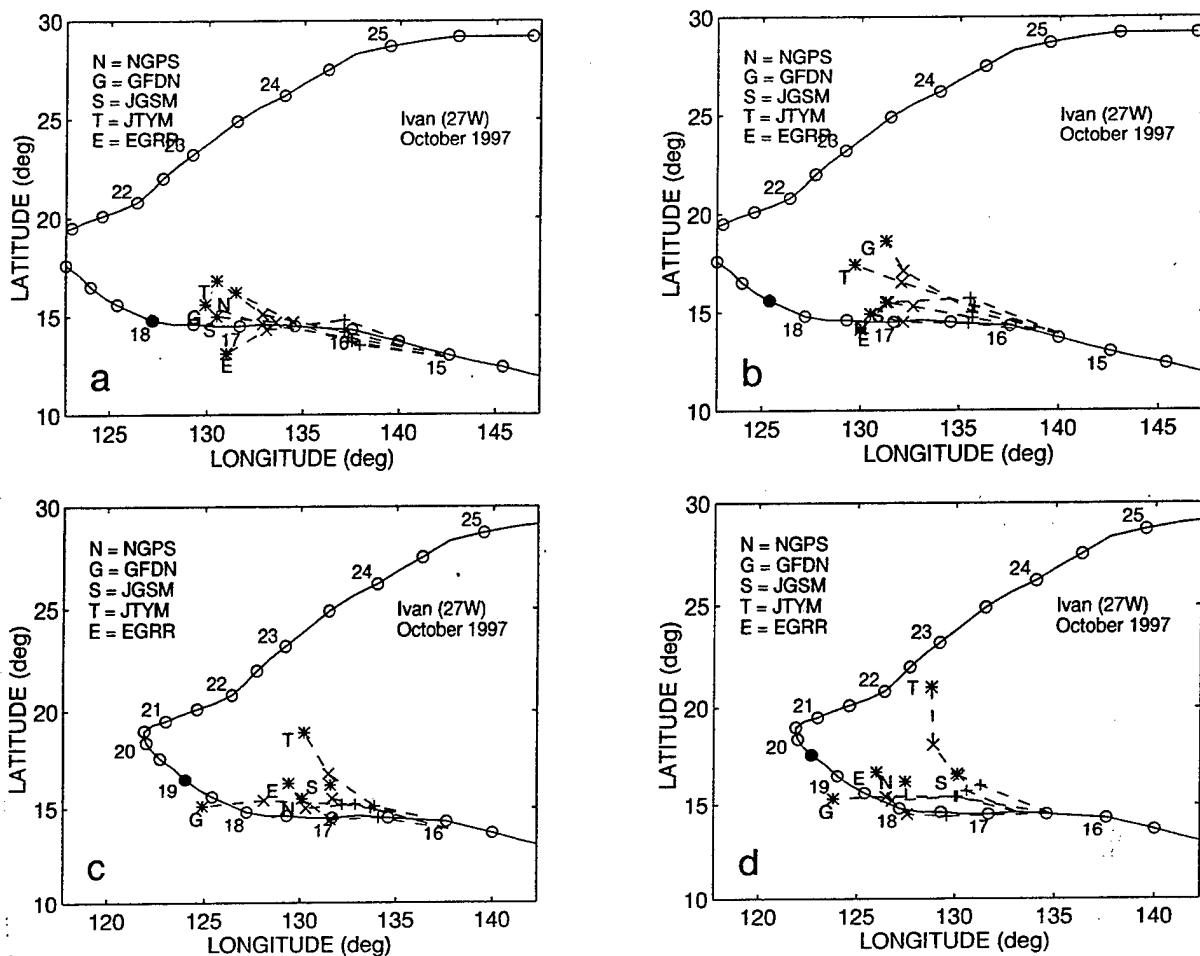


Fig. 2.13. Best-track and selected model forecast tracks (see inset) as in Fig. 2.7b, except for TC Ivan (27 W) on (a) 0000 UTC and (b) 1200 UTC 15 October, and (c) 0000 UTC and (d) 1200 UTC 16 October 1997.

A.17e with Fig. A.17i). However, notice that the areas of sub-1004 mb pressures are considerably smaller in the GFDN analyses compared to the NOGAPS analyses. The interpretation of this observation is that the GFDN TC initial condition specification was not completely successful in removing the larger NOGAPS-analyzed TC circulation before inserting the smaller GFDN spin-up vortex. This failure to completely remove the larger NOGAPS-analyzed TC circulation would tend to cause excessive RMT in the GFDN forecasts, which in conjunction with the severe under-representation of Joan in the 1800 UTC 15 October GFDN forecast (Fig. A.15j-l), would have contributed to the poleward bias in the GFDN track forecast (Fig. A.15a). The criteria in the GFDL initial condition specification that determines the size of the TC vortex that is to be removed from the global model analysis was established using Atlantic TCs that form in a trade-wind environment. Western North Pacific TCs tend to be larger than Atlantic TCs, and usually form in a monsoon environment that is very different from the Atlantic environment. The case of Ivan suggests that different TC-size specification criteria may be necessary to effectively remove western North Pacific TCs from the NOGAPS analysis prior to insertion of the spin-up vortex in the GFDN analysis.

4) Impact on other objective guidance. Since the cases of erroneous ICI affected only GFDN during 1997, no impact was noted on the objective techniques that depend on NOGAPS.

5) Summary. Although erroneous ICI was infrequent in 1997, the observed cases seem to be clearly associated with inconsistencies or weaknesses in how the TC initial condition specification in the GFDN model handles TCs that are actually small, but are overly large in the NOGAPS analysis. Thus, these cases serve to emphasize that the forecaster must carefully evaluate the analyses of both models to identify erroneous and inconsistent representations of TC size, particularly when binary TCs are present that may falsely interact if the TC sizes are incorrect.

3. Beta effect-related processes

The error mechanisms in Table 1.3 that involve the beta effect are Ridge Modification by the TC (RMT), Reverse Trough Formation (RTF), and TC initial Size (TCS). All of these error mechanisms are associated with the well-established dependence of the beta effect (both propagation and wave train generation) on TC size. Although excessive TCS, which occurred only in the case of TY Paka, actually degrades model forecast tracks via the E-RMT mechanism, it is treated separately since it results from erroneous specification of TC size that is forced into the numerical model *analysis* by the forecaster. By contrast, it will be seen that all instances of erroneous RMT in the NOGAPS and GFDN forecasts are associated with erroneous *forecasts* of the TC size by the model. Another important reason to make a distinction between erroneous RMT and TCS is that NOGAPS forecasts were more likely to be degraded by erroneous RMT and RTF (Table 3.1, rows 5 and 6) than the GFDN forecasts, whereas GFDN forecasts were degraded more often than NOGAPS forecasts during the period of E-TCS in the Paka case (Table 1.3, row 12).

a. Ridge Modification by the Tropical Cyclone (RMT)

1. Description. The concept of erroneous RMT in a dynamical model is analogous to the RMT phenomenon described in the CMKB (p. 70) and shown in Fig. 3.1, except that the phenomenon occurs either to an excessive (E-RMT) or an insufficient (I-RMT) degree. The usual numerical model forecast errors are that the environment of the TC will transition from S/TE to P/PF more rapidly or more slowly than in reality. In principle, erroneous RMT may occur in any situation in which the size of the TC is not properly represented by a numerical model. For the western North Pacific TC forecasts during 1997 evaluated in this study, all the instances of erroneous RMT occurred when the TC was embedded in the Rossby wave train of a large cyclonic circulation to the west and north (Fig. 3.2). This cyclonic circulation (e.g., a second large TC, a large monsoonal disturbance or gyre, or a midlatitude cutoff low or trough with a southwest-to-northeast orientation) generates a peripheral anticyclone to the northwest of the affected TC. If the steering flow associated with this anticyclone causes the TC to move south of west, then indirect cyclone interaction (ICIE) is actually occurring, and the TC would be in the Equatorward Flow (EF) region of a Poleward (P) synoptic pattern (Fig. 1.5). Because energy propagates to the southeast (in the Northern Hemisphere) from the cyclonic circulation to the anticyclone circulation to the TC in the wave train, the TC and its associated peripheral anticyclone also tend to grow in horizontal extent. In this scenario, the environment structure of the TC often undergoes a transition from S/TE or P/EF (if ICIE has been causing equatorward motion) to P/PF. When E-RMT (I-RMT) occurs in a numerical model, the southeastward (Northern Hemisphere) propagation of energy is more (less) vigorous than in reality. When excessive growth of the peripheral anticyclone to the southeast of the TC occurs as in Fig. 3.2, the TC will have a forecast track that is poleward of the actual track. A TC that is embedded in a Rossby wave usually does turn poleward, but the predicted turn is premature (delayed/missed) in a model in which E-RMT (I-RMT) is occurring.

2) Frequency and characteristics. The phenomenon of erroneous RMT in NOGAPS and/or GFDN resulted in degraded 72-h track forecasts for seven cases during 1997 (Table 3.1, column 1). The environment structure of the TC when the erroneous RMT occurred in the model was always S/TE (Table 3.1, column 3), and in one case (18W) ITIE was influencing the track of the TC. The track forecasts of the model(s) were degraded by excessive RMT (E-RMT) in every case except

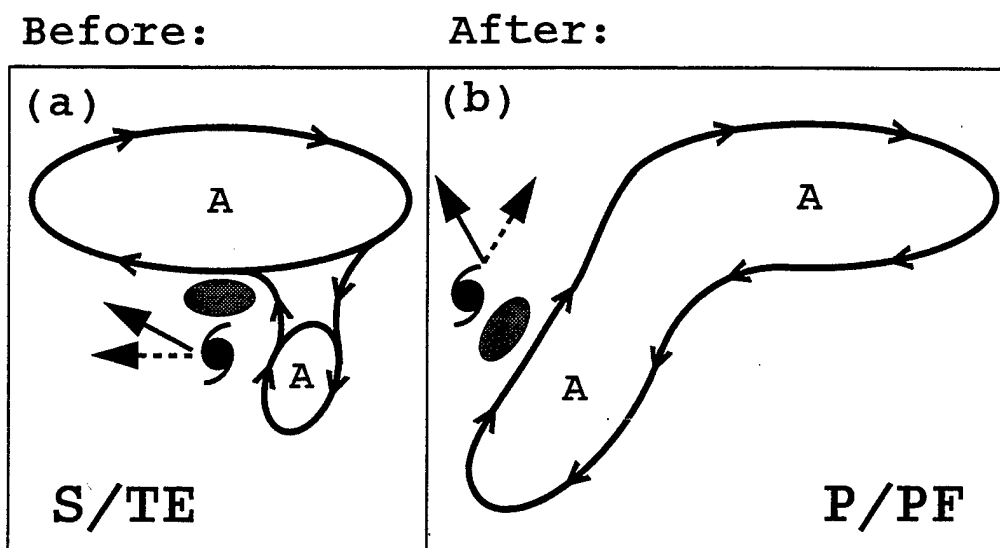


Fig. 3.1. Conceptual model as in Fig. 2.1 for the Ridge Modification by a TC (RMT) transformation from the (Before) Standard/Tropical Easterlies (S/TE) to the (After) Poleward/Poleward Flow (P/PF) synoptic pattern/region. A smaller (larger) TC will move along the dashed (solid) arrow because of the beta-effect propagation.

Erroneous Model-predicted Ridge Modification by the TC (RMT)

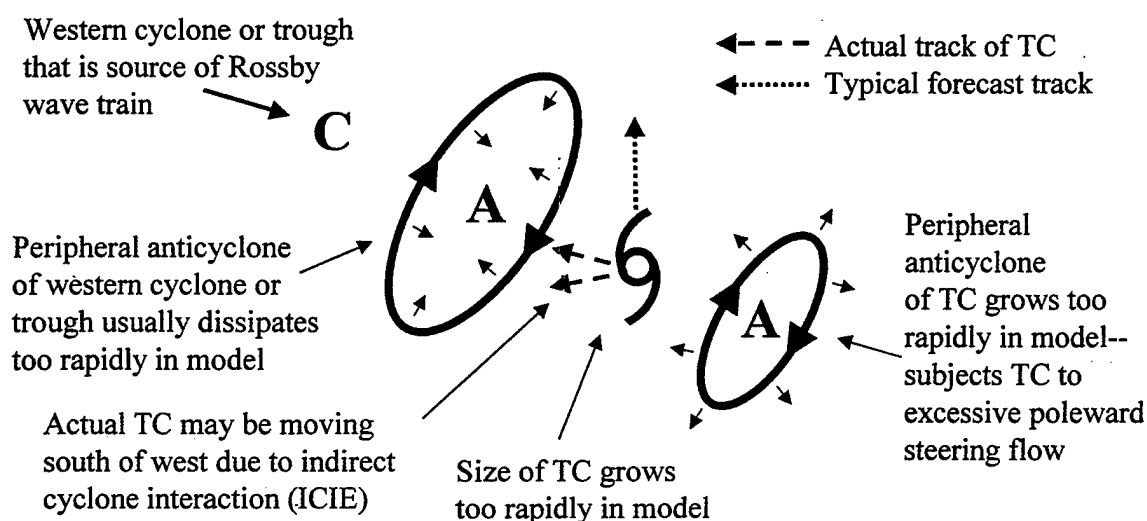


Fig. 3.2. Erroneous RMT as in Fig. 3.1 influencing the forecast track of a TC embedded in the wave train of another cyclone (c) to the northwest (Northern Hemisphere). If the Rossby wave dispersion leads to an overly large peripheral anticyclone trailing the TC, the TC track error will be poleward (dotted arrow).

Table 3.1. Cases of erroneous model-predicted Ridge Modification by the TC (RMT) in the western North Pacific during 1997. See Table 2.1 for explanatory footnotes.

TC No	Starting times of affected model runs ¹	Synoptic Environment of affected TC	Degree Of RMT	Identity of second cyclone ³	Distance (° lat.) & bearing (°) to second cyclone	Models affected	
						JTWC ⁵	Others ⁶
07W	Jun 06/00-06/06	S/TE	Excessive	FTC	15.0° @ 283°	G,N	
12W	Aug 01/12-02/12	S/TE	Excessive	13W	18.4° @ 278°	N,(G)	(S,T)
18W	Aug 21/12	S/TE - ICIE	Excessive	17W	19.4° @ 286°	N,	
19W	Aug 28/00-28/12	S/TE	Excessive	18W (20W)	32.7° @ 294°	N,(G)	E
19W	Aug 30/06	S/TE → P/PF	Insufficient	18W (20W)	23.9° @ 301°	G	
21W	Sep 13/12-14/12	S/TE	Excessive	02C	30.8° @ 288°	N,G	
27W	Oct 13/12-16/12	S/TE	Excessive	Trough	N/A	N	T

the GFDN forecast for Bing (19W) that was initiated at 0600 UTC 30 August, which involved I-RMT (Table 3.1, column 4). Whereas the cyclonic circulation to the west (Fig. 3.2) was a designated TC in five of the seven cases, it was a false tropical circulation in the case of Nestor (07W) (Table 3.1; column 5). Since the wave train is usually triggered by an overly large cyclonic circulation to the west, it is not surprising that this cyclone is frequently a named TC. In each of these cases, the cyclone that generates the wave train is located to the west-northwest at distances ranging from roughly 15° to 30° lat. (Table 3.1; column 6).

The case of Ivan (27W) was somewhat different in that the western cyclone was a midlatitude trough that caused the subtropical ridge axis to have a west-southwest-to-east-northeast slope as in Fig. 3.2. Although the Ivan case was unique in the 1997 data set, the authors have identified instances in other basins of wave trains that seem to be initiated by midlatitude troughs that have the proper tilt. Another case was that of Typhoon Rex during 1998 as described in Appendix B. These cases provide sufficient justification to invoke the wave train mechanism as a provisional explanation for the poor NOGAPS forecast for Ivan.

Notice that during the six cases of excessive RMT (E-RMT) when the NOGAPS forecast was significantly degraded (i.e., FTE > 300 n mi), the GFDN forecasts were more likely to be either moderately degraded (i.e., FTE < 300 n mi; denoted by parentheses), or not degraded at all (Table 3.1; column 7). This predominance in NOGAPS errors may occur because the western cyclone and/or the eastern TC are more likely to be too large due to the relatively coarse resolution of NOGAPS, which may then excite excessively strong Rossby wave trains. In three cases, it appeared that the other agency numerical model forecasts available to JTWC were also degraded to some extent (Table 3.1, column 8).

3) Case studies. The case studies of Typhoons Tina (12W) and Bing (19W) provide typical illustrations of E-RMT occurring for a TC embedded in the wave train of another TC (Fig. 3.2). The Bing case includes the sole instance of I-RMT degrading the GFDN track forecast. The case of Ivan (27W), for which there is a closed cyclone to the west-northwest, is briefly discussed. Although the primary purpose of the case studies is to illustrate the important aspects and variations of the erroneous RMT, some clues will also be given to real-time detection of the phenomenon.

a) *Typhoon Tina (12W)*. A comparison/verification of the 500-mb wind fields and TC tracks from the NOGAPS and the GFDN forecasts initiated at 0000 UTC 2 August and 0600 UTC 2 August, respectively, is provided in Fig. A.18a-l. In the initial fields of both models (Fig. A.18e and i), the circulations of Tina (eastern TC) and Victor (western TC) are roughly 20° long. apart and oriented east-southeast to west-northwest with anticyclonic flow between the TCs, which is consistent with the conceptual model in Fig. 3.2. In the verifying NOGAPS analyses over the next three days (Fig. A.18b-d), the peripheral anticyclone of Victor is present to the northwest of Tina, and a peripheral anticyclone also develops to the southeast of Tina. The shift of the isotach maximum from north to northeast of Tina (Fig. A.18d) and the increasingly poleward track of Tina (Fig. A.18a) indicate that a transition from a S/TE to a P/PF pattern/region is in progress for Tina in accordance with the RMT conceptual model (Fig. 3.1).

During the NOGAPS integration (Fig. A.18f-h), the circulation of Victor dissipates rapidly and the peripheral anticyclone of Victor that is initially to the northwest (southwest) of Tina dissipates slowly (rapidly), and a more pronounced peripheral anticyclone appears to the southeast of Tina. The isotach maximum is predicted to shift to the east-southeast of Tina in the 72-h forecast field (Fig. A.18h). This sequence of events is consistent with excessive energy propagation in the wave train conceptual model (Fig. 3.2), and represents a more rapid transition from S/TE to P/PF than occurred in the analysis sequence (Fig. A.18b-d). As a result, the NOGAPS forecast track is significantly east of the verifying best track (Fig. A.18a). By contrast, the GFDN forecast fields (A.18j-l) are more similar to the NOGAPS verifying analyses, and the GFDN track forecast does not have as much of a poleward bias.

A comparison/verification of the sea-level pressure fields and TC tracks from the NOGAPS and the GFDN forecasts initiated at 0000 UTC and 0600 UTC 2 August, respectively, is provided in Fig. A.19a-l. Although the minimum sea-level pressure of Tina actually increases until 48 h in the NOGAPS forecast, the size of TC circulation expands considerably (Fig. A.19e-h) and exceeds the horizontal extent of the TC in the verifying analyses (Fig. A.19b-d). Notice that both the GFDN- and the NOGAPS-predicted circulations for the western TC (Victor) do not dissipate as rapidly as in the verifying analyses, which suggests that the overly large circulation of Victor may have generated too strong a wave train in the GFDN and NOGAPS forecast fields. It is hypothesized that this excessively strong wave train in the NOGAPS prediction propagates energy too fast to the southeast, which causes an overly rapid growth of Tina, and in turn the peripheral anticyclone of Tina to the southeast. Whereas the NOGAPS model is presumably affected more because of its relatively coarse horizontal resolution, the GFDN model is hypothesized to be affected less because its higher resolution maintains a smaller TC that is less susceptible to stimulation by the overly strong Rossby wave train from Victor.

The forecaster may be alerted to a potential problem by the more eastward NOGAPS track relative to the other dynamical models. The difference in the TC structure forecast by the NOGAPS model (rising minimum sea-level pressure, but expansion of the area with sub-1008 mb pressures) and the GFDN model (increasing intensity without significant expansion of the sub-1008 mb pressure area) would present a dilemma without the hindsight available here (Fig. A.19b-d). Given the normally high sea-surface temperatures in this low-latitude, open-ocean region, the filling minimum sea-level pressure in NOGAPS would seem to be less likely to verify than the deepening trend in the GFDN forecast. Given the wave train conceptual model in Fig. 3.2, the forecaster

would have a physically-based explanation for the NOGAPS forecast structure, and thus a reason to reject the NOGAPS track.

The five numerical model tracks for Tina for four consecutive synoptic times from 1200 UTC 1 August to 0000 UTC 3 August (Fig. 3.3) illustrate the temporal progression of the E-RMT phenomenon. The first three sets of tracks are during the period with 72-h NOGAPS FTEs greater than 300 n mi. Although the NOGAPS model had the worst performance during this period, the other global models (JSGM and EGRR) also exhibited a significant right-of-track bias. By contrast, the GFDN and JTYM regional models tended to perform better during the period, possibly owing to their higher resolution as suggested above. During the period of E-RMT for NOGAPS (and perhaps the other models), the left-most forecast track agreed very well with the actual track of the TC. In other words, the left edge of the envelope formed by the ensemble of numerical model forecast tracks would have been the best predictor of the future track of the TC during the period of NOGAPS degradation due to E-RMT. Because this relationship has been repeatedly observed by the authors, it may be useful to forecasters.

Whereas the spread of the numerical model track ensemble is large early in the period of E-RMT (Fig. 3.3a-b), it is considerably smaller near the end of the period (Fig. 3.3c-d). The large spread results when some of the models are highly degraded by the E-RMT phenomenon (e.g., the global models), and others are not (e.g., the regional models). As the error-producing phenomenon ceases, the models tend to perform more consistently (assuming of course that some other error mechanism does not come into play), which results in a smaller spread in the ensemble of tracks. The decrease in ensemble spread in Fig. 3.3c-d corresponds well with the dissipation of the western TC (Victor) after landfall (Fig. 3.4), which might be expected from the wave train conceptual model (Fig. 3.2) since Victor is hypothesized to have been the source of the track-altering wave train. Consequently, the peripheral anticyclone from the western TC (Victor) will tend to dissipate rapidly when its source no longer exists. If the western TC has generated a particularly large peripheral anticyclone, the cessation of the E-RMT phenomenon in the model may lag the dissipation of the western TC by a day or so because the very large anticyclone may dissipate more slowly than its source TC.

b) Typhoon Bing (19W). A comparison/verification of the 500-mb wind fields and TC tracks from the NOGAPS and GFDN forecasts initiated at 1200 UTC and 1800 UTC 28 August 1997, respectively, is shown in Fig. A.20a-l. As in the case of Tina and Victor, the east-southeast to west-northwest orientation of Bing and Amber/Cass and the intervening anticyclone in the initial NOGAPS and GFDN analyses (Fig. A.20e,i) agree well with the conceptual model in Fig. 3.2. In the NOGAPS forecast fields (Fig. A.20f-h) and the GFDN forecast fields (Fig. A.20j-l), Bing turns poleward as the peripheral anticyclone to its southeast amplifies, which causes an environment structure change from S/TE to P/PF that does in fact occur (Fig. A.20b-d). Whereas the GFDN track forecast is quite accurate through 48 h (Fig. A.20a), the NOGAPS track forecast has a significant poleward bias by 24 h (Fig. A.20a). Notice that the NOGAPS 24-h forecast (Fig. A.20f) has an isotach maximum to the southeast of Bing that is more prominent than in either the GFDN 24-h forecast field (Fig. A.20j) or the verifying analysis (Fig. A.20b).

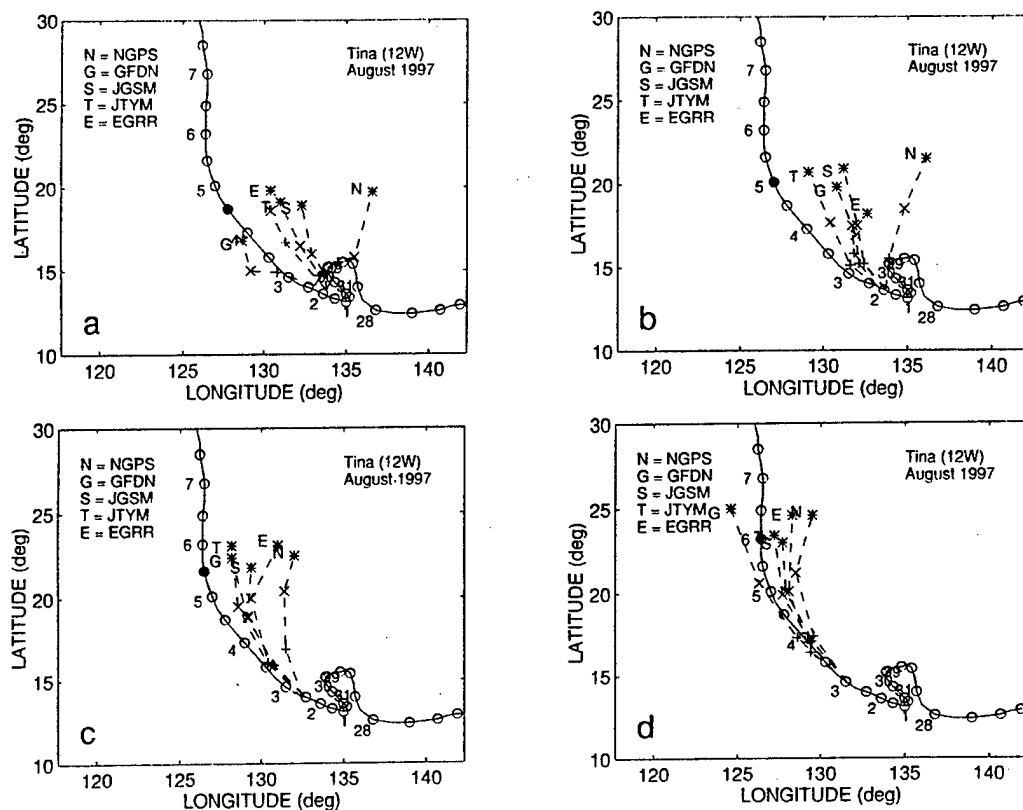


Fig. 3.3. Best-track and selected model forecast tracks (see inset) as in Fig. 2.7b, except for TC Tina at (a) 1200 UTC 1 August, (b) 0000 UTC and (c) 1200 UTC 2 August, and (d) 0000 UTC 3 August 1997.

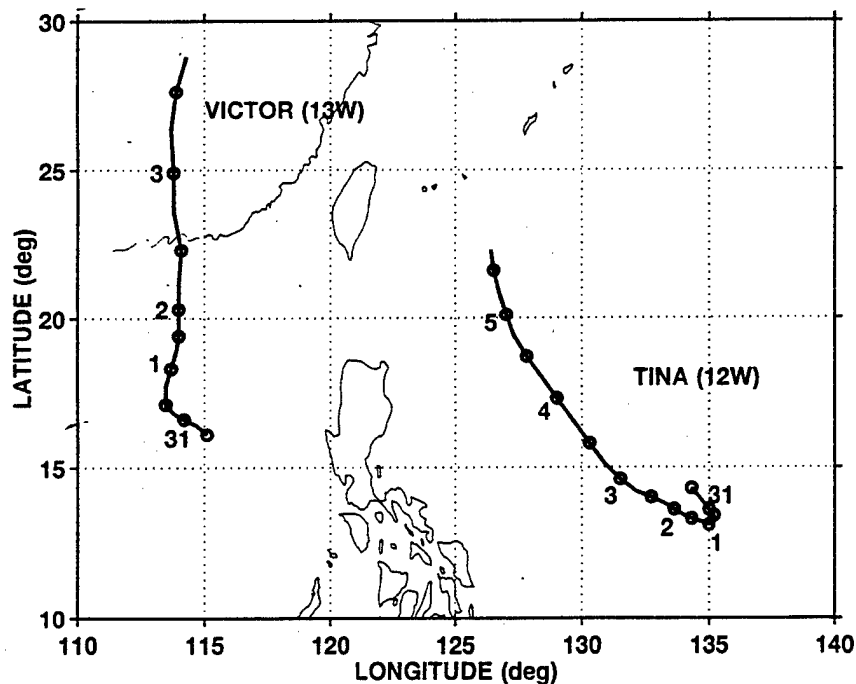


Fig. 3.4. Best-tracks of Victor (13W) and Tina (12W) during 1200 UTC 30 July to 1200 UTC 5 August 1997.

Applying the wave train E-RMT conceptual model (Fig. 3.2), the premature transition of the environment of Bing in the NOGAPS forecast is expected to be associated with excessive growth of the eastern TC. That such an excessive growth did in fact occur in the NOGAPS forecast is confirmed by Fig. A.21a-l, which is a comparison/verification of sea-level pressure fields from the same NOGAPS and GFDN integrations as in Fig. A.20. Whereas the size of Bing in the NOGAPS forecast fields (Fig. A.21f-h) is considerably larger than in the verifying analyses (Fig. A.21b-d), the size of Bing in the GFDN forecast fields (Fig. A.21i-l) remains commensurate with the verifying analyses. In contrast to the previous case, the NOGAPS model predicts a decrease in minimum sea-level pressure as well as an increase in the extent of the area with sub-1008 mb sea-level pressures.

Comparisons of the five numerical model tracks available to JTWC for six consecutive synoptic times from 0000 UTC 28 August to 1200 UTC 30 August (Fig. 3.5a-f) illustrate the temporal progression of the E-RMT effect on numerical model track forecasts for Bing. The first three comparisons are during the period that either the NOGAPS or the UKMO (EGRR) models had 72-h FTEs of greater than 300 n mi. Unfortunately, the JGSM and JTYM tracks are missing during this period. As in Fig. 3.3a-c, the left-most track in the ensemble tends to agree well with the verifying best track. By 1200 UTC 29 August (Fig. 3.5d), the spread of the 72-h positions has decreased and the ensemble envelope is approximately centered on the verifying best track. This time corresponds well with the landfall of Amber (and Cass) over Asia (Fig. 3.6), which is when the peripheral anticyclone being generated by Amber would be expected to begin dissipating.

Notice that the GFDN forecast track: (i) is in reasonably good agreement with the other model forecasts initiated at 1200 UTC 29 August (Fig. 3.5d); (ii) is considerably to the west and slower than the other model forecasts for 0000 UTC 30 August (Fig. 3.5e); and (iii) then is in good agreement with the other model forecasts at 1200 UTC 30 August (Fig. 3.5f). The lack of temporal consistency of GFDN forecast tracks may be explained by comparing the extent of Bing's circulation in the GFDN analysis and 66-h forecast fields of sea-level pressure for these three synoptic times (Fig. 3.7a-f). Although the extent of Bing's circulation increases with time in the three analyses (Fig. 3.7a,c,e), the extent of the TC in the GFDN model is smaller at 66 h in the second integration compared to the first integration (compare Fig. 3.7d and b), and larger in the third integration compared to the second integration (compare Fig. 3.7f and d). The correspondence of an anomalous forecast of smaller TC size and an anomalous left track bias in the GFDN run for 0600 UTC 30 August is consistent with the conceptual model of I-RMT (Fig. 3.2). By contrast, the corresponding NOGAPS 72-h sea-level pressure forecasts had a consistently large circulation size for Bing (not shown), which is consistent with the persistent right-of-track bias in Fig. 3.5d-f.

c) *Typhoon Ivan (27W)*. Four sets of dynamical model track forecasts from 0000 UTC 15 October to 1200 UTC 16 October 1997 for Ivan (27W) were presented in Fig. 2.13. Notice that the tracks from the later NOGAPS, JGSM, and EGRR forecasts exhibit a significant slow bias and a premature poleward turn. The premature poleward turn in the 0000 UTC 16 October NOGAPS track forecast (Fig. 2.13c) is consistent with the development of an overly strong peripheral anticyclone to the southeast of the TC in the 500-mb wind forecast fields (Fig. A.16f-h) compared to the verifying analyses (Fig. A.16b-d). Notice that the isotach maximum in the NOGAPS 72-h wind forecast (Fig. A.16h) is to the southeast of the TC, whereas in the verifying NOGAPS analysis (Fig. A.16d) the isotach maximum is still to the northeast of the TC. These differences are

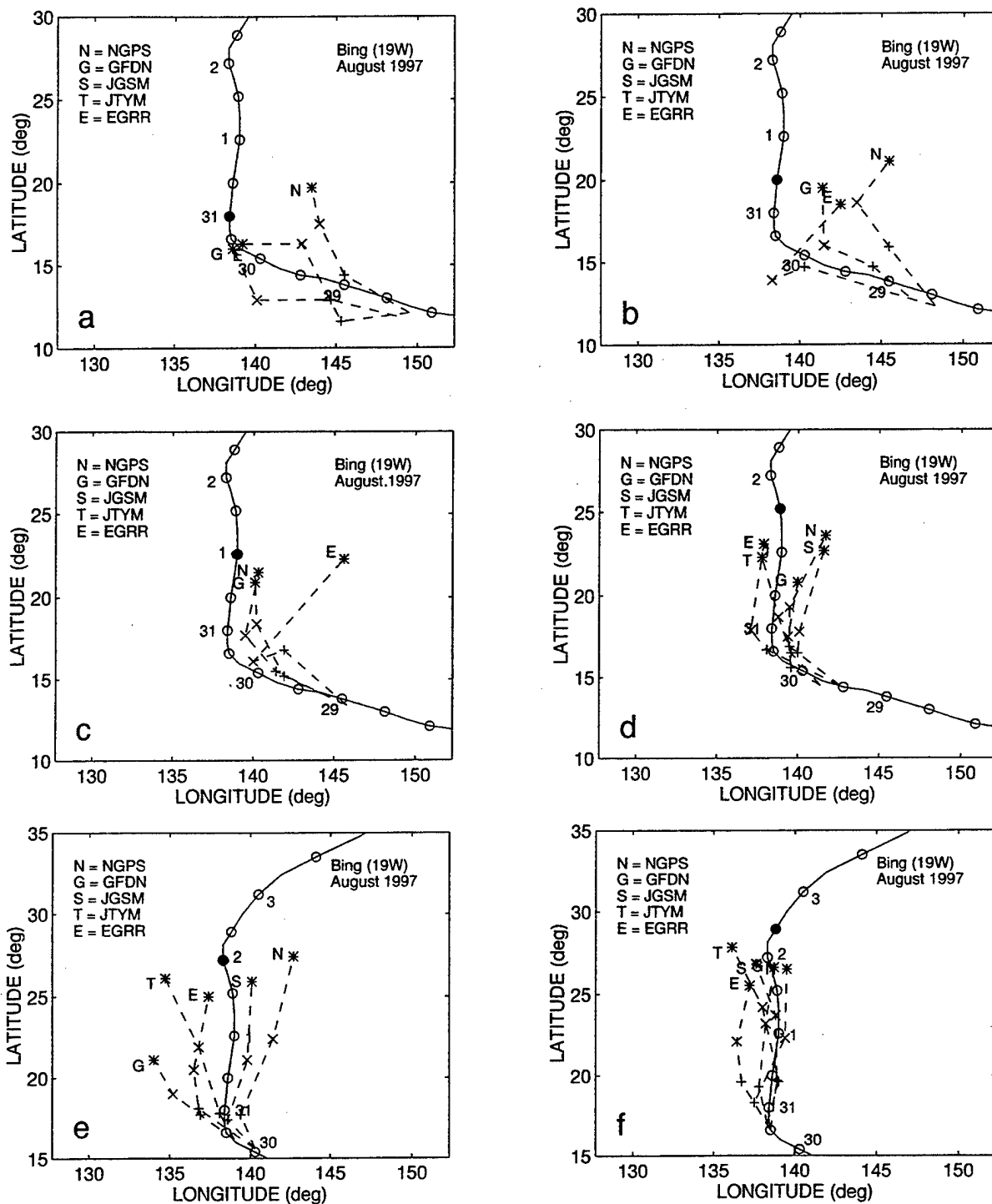


Fig. 3.5. Best-track and selected model forecast tracks (see inset) as in Fig. 2.7b, except for TY Bing at (a) 0000 UTC and (b) 1200 UTC 28 August, (c) 0000 UTC and (d) 1200 UTC 29 August, and (e) 0000 UTC and (f) 1200 UTC 30 August 1997.

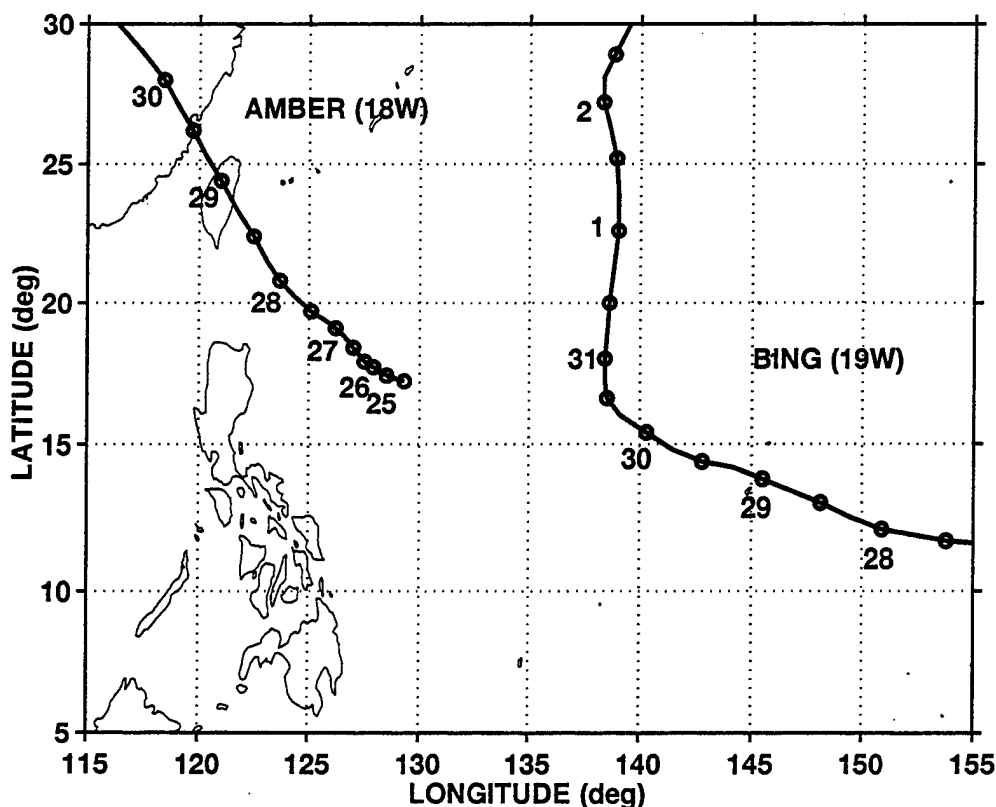


Fig. 3.6. Best-tracks of Amber (18W) and Bing (19W) during 1200 UTC 24 August to 1200 UTC 2 September 1997.

indicative of E-RMT in the NOGAPS forecast, which is leading to a premature transition from a S/TE to a P/PF pattern/region combination. In the GFDN forecast fields (Fig. A.16j-l), a much weaker peripheral anticyclone develops to the southeast of the TC. As a result, the 66-h forecast field (Fig. A.16l) is very similar to the verifying NOGAPS analysis (Fig. A.16d), and the 66-h locations of the Ivan and Joan circulations in the GFDN integration with Ivan as the target TC agree well with the corresponding locations in the verifying analysis. According to barotropic theory, the E-RMT error should be the consequence of an excessive TC size in the model analysis and/or excessive growth of the TC during the forecast. In fact, the size of Ivan in the NOGAPS sea-level pressure forecasts (Fig. A.17f-h) is much larger than in the verifying analyses (Fig. A.17b-d). By contrast, the sizes of both TC circulations remain constant in the GFDN sea-level pressure forecasts (Fig. A.17j-l).

Notice the prominent anticyclone to the northwest of Ivan at about 20°N, 121°E in the 48-h NOGAPS 500-mb wind forecast (Fig. A.16g). This anticyclone, together with Ivan and the peripheral anticyclone southeast of Ivan form a northwest-to-southeast-oriented circulation that resembles the wavetrain in Fig. 3.2, except a distinct cyclone is not evident to the northwest of the anticyclone northwest of Ivan. This sequence of circulations does not appear as prominently in the

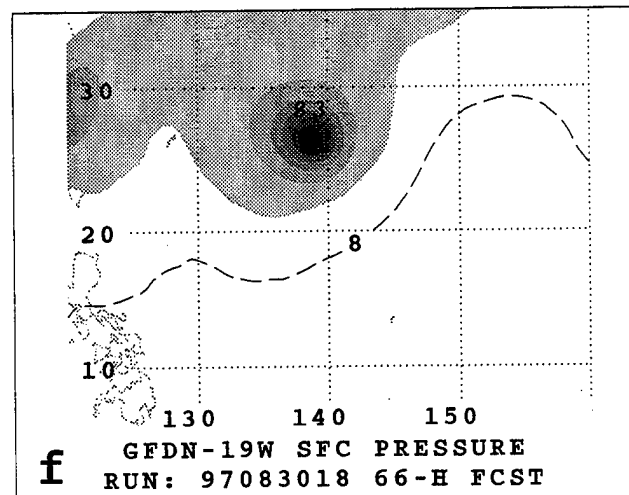
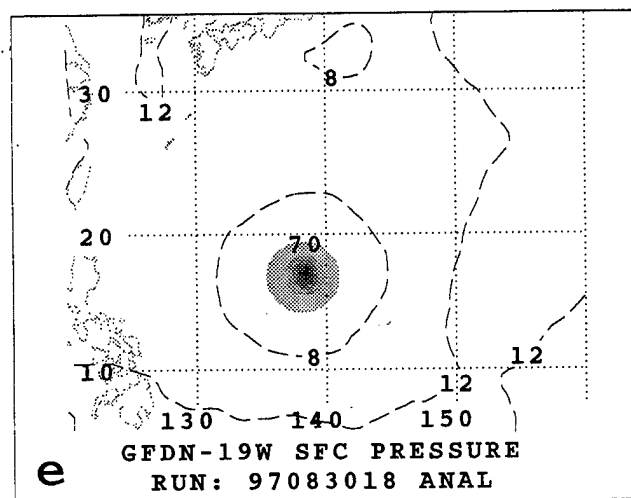
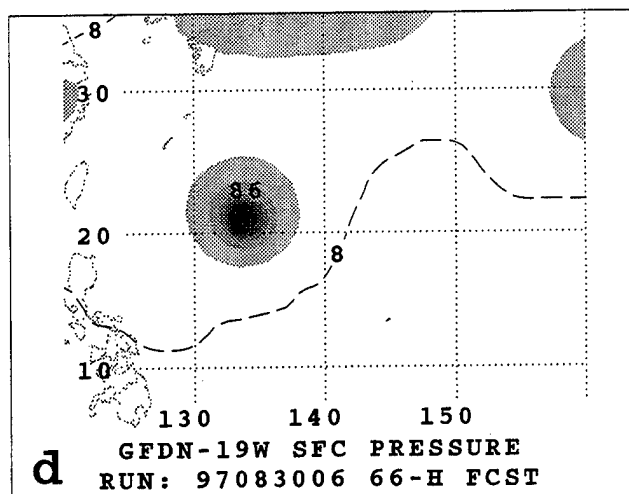
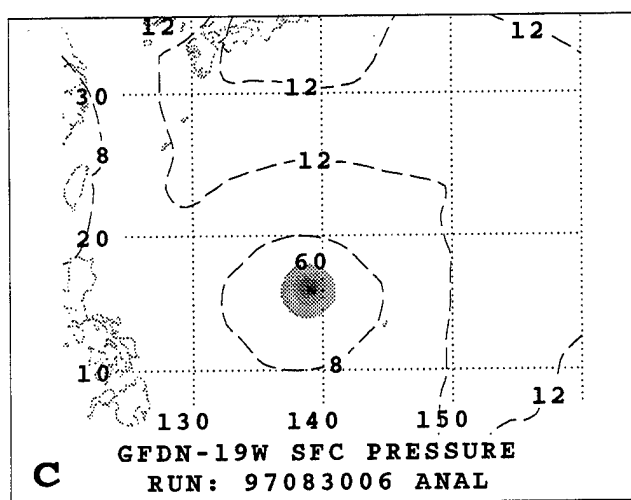
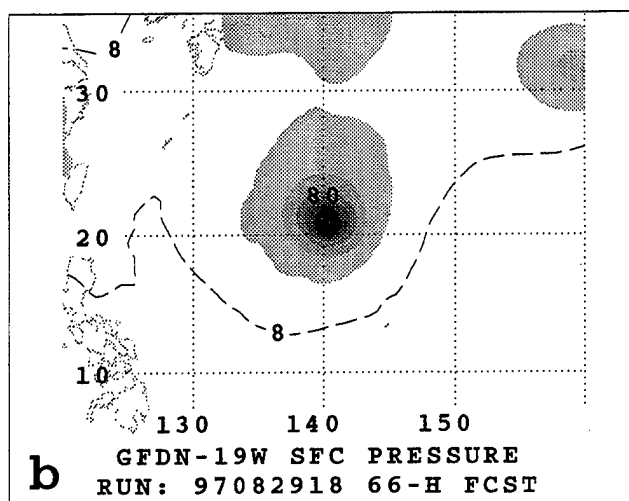
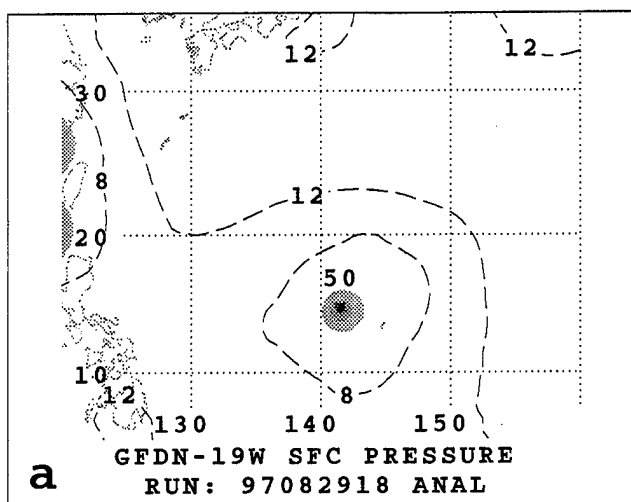


Fig. 3.7. Sea-level pressure analyses (left column) and corresponding 66-h forecasts (right column) for the GFDN model at the initial times of (a-b) 1800 UTC 29 August, (c-d) 0600 UTC 30 August, and (e-f) 1800 UTC 30 August 1997.

corresponding GFDN forecast (Fig. A.16k), and is not evident in the verifying NOGAPS analysis (Fig. A.16c). In addition, the dissipation (growth) of the anticyclone to the northwest (southeast) of Ivan from 48 h to 72 h in the NOGAPS forecast (compare Fig. A.16g and h) would be consistent with a southeastward propagation of energy through the wavetrain, and would provide an explanation for the slowing and poleward turn in the NOGAPS track forecast for Ivan (Fig. A.16a). All of these indicators are consistent with the wavetrain conceptual model (Fig. 3.2), except for the absence of a prominent cyclone to the northwest of Ivan in the initial NOGAPS analysis (Fig. A.16e). However, midlatitude southwesterlies to the northwest of Ivan may imply the presence of a broad trough farther to the northwest (not shown). As a result, the subtropical ridge axis has a west-southwest to east-northeast tilt that may have been conducive, along with the presumably overly large size of Ivan, to triggering an excessive wavetrain energy propagation in the NOGAPS forecast. Although this explanation is somewhat speculative, the authors are aware of other examples of midlatitude troughs triggering Rossby-like wave trains that are then associated with consistently poleward track forecast biases by the numerical models (e.g., the Rex case in Appendix B). The Ivan case is included here to alert the forecaster to the possibility of such phenomena, and encourage further research into the wavetrain phenomenon.

4) Impact on other objective guidance. When E-RMT occurred in the NOGAPS forecasts of Typhoons Tina and Bing, the impact on objective forecast techniques that utilize NOGAPS forecast fields is illustrated in Figs. 3.8 and 3.9, respectively. In both cases, the shallow (SBAM) and medium (MBAM) steering models exhibit a right bias similar to that of NOGAPS, which reflects the erroneously strong poleward steering component contributed by the overly strong anticyclone to the southeast. This right bias for the SBAM and MBAM ceases at or shortly after the western TC makes landfall, as was observed for the NOGAPS track forecasts. Although the deep steering model (FBAM) track does not have a similar bias in these two cases, its performance appears to be degraded-- possibly for reasons unrelated to the E-RMT phenomenon.

The statistical-dynamical model CSUM persistently forecasts a northwestward track in both cases (Figs. 3.8 and 3.9), and thus does not appear to experience any degradation as a result of E-RMT in the NOGAPS forecasts. In the case of Tina (Fig. 3.8a-d), CSUM provides a reasonably accurate forecast of the TCs gradual poleward turn. In the case of Bing (Fig. 3.9a-d), CSUM does a poor job of forecasting the relatively sharp poleward turn by the TC. This error is not related to the E-RMT occurring in NOGAPS. Rather, it is well-known trait that CSUM is not particularly skillful in predicting sharp poleward turns during a S/TE to P/PF transition.

5) Summary. Table 3.2 is a summary of the key aspects of the Rossby wavetrain E-RMT phenomenon, the indications in numerical model fields and tracks, and the impact on various models available to the JTWC forecaster. A key result for the forecaster is that the wavetrain E-RMT phenomenon frequently occurs in NOGAPS, and causes a significant degradation in the track forecast, whereas GFDN is usually not affected or only moderately affected. Even if the other numerical model forecasts are not available, the differences in the NOGAPS and GFDN forecast tracks will be an important clue that a problem may be occurring. The key indicator that E-RMT is occurring in the NOGAPS forecast, and that the S/TE-P/PF transition is premature, is significant growth of the size of the TC in the sea-level pressure forecasts (Table 3.2; bold type), particularly when such growth does not also occur in the GFDN forecast.

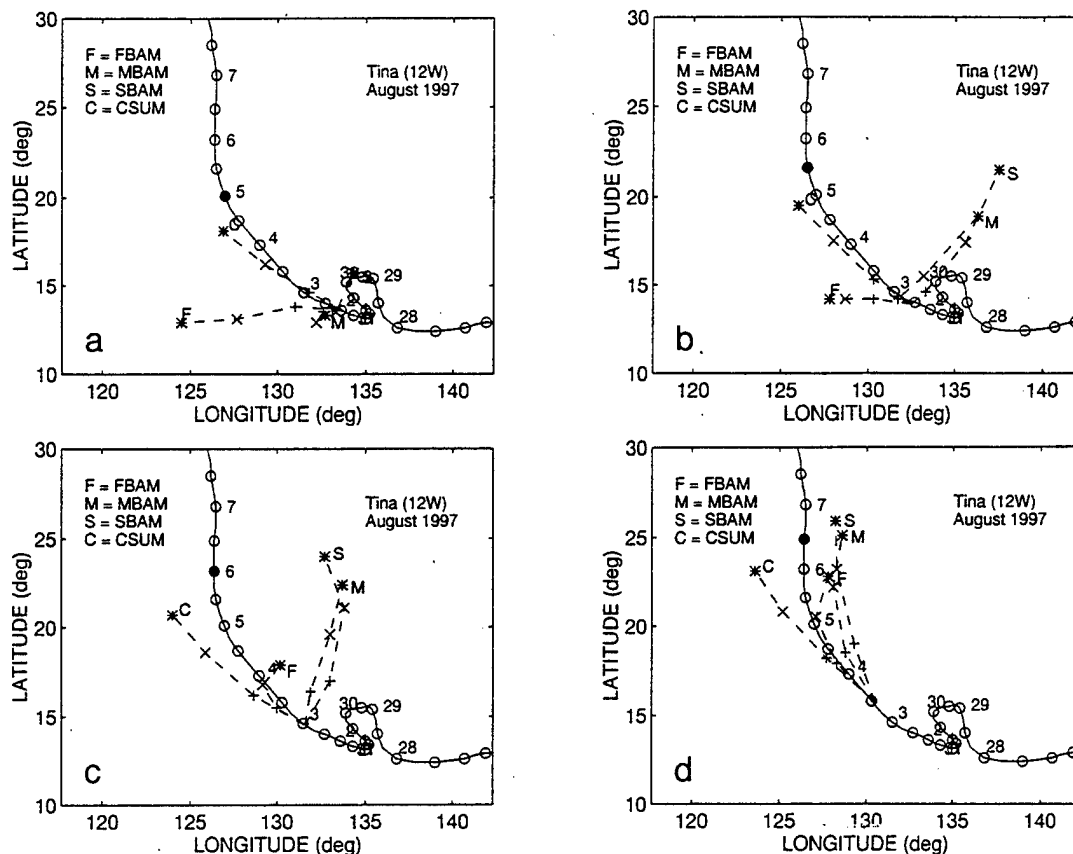


Fig. 3.8. Best-track and selected objective technique forecasts (see inset) for TC Tina as in Fig. 3.3b-d for panels a-c, and (d) at 1200 UTC 3 August.

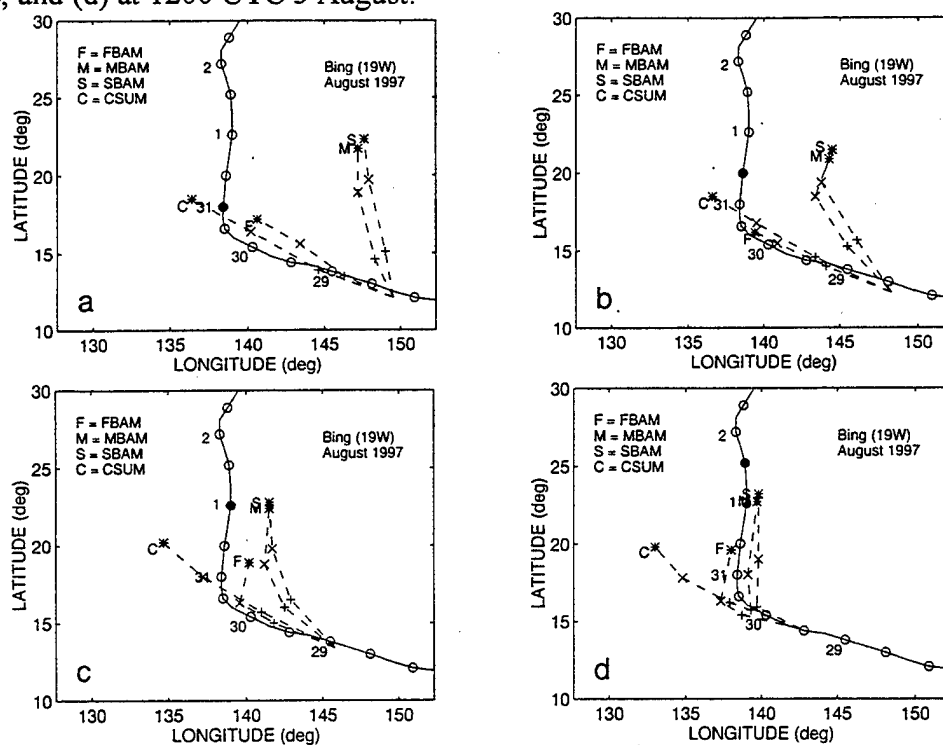


Fig. 3.9. Best-track and selected objective technique forecasts (see inset) for TC Bing as in Figs. 3.5a-d.

Table 3.2. Summary of important aspects and illustration key for the phenomenon of Excessive Ridge Modification by TC (E-RMT).

Aspect	Description	Figure
Conceptual model	Excessive growth of an eastern TC and its peripheral anticyclone due to the influence of the Rossby wave train from a second cyclone to the north and west.	3.2
Frequency	7 periods involving 6 TCs, significantly degrading 12 NOGAPS forecasts, but only 3 GFDN forecasts in the western North Pacific during 1997	Table 3.1
Environment	Standard Pattern/Tropical Easterlies Region (S/TE) usually with a large TC to west and north (actual ICIE is probably occurring if eastern TC is tracking south of west or moving slower than normal)	Table 3.1
Variations of the Phenomenon	Western cyclone is: <ul style="list-style-type: none"> Usually another large TC of depression intensity or higher; Occasionally may be a false model-generated TC; or Could possibly be a monsoon gyre, a cut-off midlatitude cyclone, or a midlatitude trough with a southwest to northeast tilt conducive to generating a Rossby wave train. 	Table 3.1 Table 3.1 3.2
Indications in numerical model fields	In streamline fields: <ul style="list-style-type: none"> Rapid amplification of peripheral anticyclone to southeast of affected TC and rotation of isotach maximum from northern to eastern quadrant Rapid dissipation of the anticyclone between the affected TC and the western cyclone In sea-level pressure fields: <ul style="list-style-type: none"> Significant growth of the eastern TC circulation 	A.18e-h A.20e-h A.19e-h A.21e-h
Indications in numerical model tracks	<ul style="list-style-type: none"> Immediate, sharp turn onto a poleward-oriented track Significant poleward bias at short forecast intervals 	3.3a-c 3.5a-c
Relative impact on numerical models	<ul style="list-style-type: none"> Global models more affected Regional models usually less affected, and GFDN may not be degraded at all 	3.3, 3.5
Relative impact on other objective guidance	<ul style="list-style-type: none"> BAMs are usually degraded as much as or more than NOGAPS; SBAM and MBAM are usually degraded more than FBAM CSUM usually not affected. The accuracy of CSUM will depend on how sharp the actual transition from S/TE to P/PF will be. 	3.8, 3.9

b. Reverse Trough Formation (RTF)

1) **Description.** The Reverse Trough Formation (RTF) conceptual model is shown in Fig. 3.10, (see also CMKB p. 74). The phenomenon of RTF occurs when the eastern TC is at approximately the same latitude as the western TC such that the peripheral anticyclones (each of which is a manifestation of RMT) of the two TCs can constructively superpose to produce one large anticyclone. When this occurs, both TCs tend to recurve simultaneously, or near simultaneously. When a numerical model predicts excessive RTF (E-RTF), the RTF processes either occur prematurely or falsely in the model and the predicted track is poleward compared to reality. When a model predicts insufficient RMT (I-RMT), the RTF process that occurs in nature takes place too slowly in the model or not at all, so that the poleward turn is predicted too late or not at all.

2) Frequency and characteristics. During 1997, E-RTF was responsible for degraded forecasts of three TCs: Rosie (10W), Ivan (27W), and Joan (28W). In the Rosie case, E-RTF occurred only in the NOGAPS forecast in association with over-development of the TC and a monsoonal disturbance to the west, when in actuality a reverse trough did not develop. In the cases of Ivan and Joan, a reverse trough involving the TCs did develop, but E-RTF in the NOGAPS forecast resulted in a premature recurvature of both TCs. In the GFDN forecast with the inner grid centered on Joan, E-RTF also occurred and degraded the tracks of Joan (and also Ivan) in the model. However, E-RTF did not occur in the GFDN forecast with the inner grid centered on Ivan, and thus did not degrade track prediction of either TC in the model. The Ivan/Joan case emphasizes that the GFDN integrations for two simultaneously existing TCs can predict very different interactions of the two TCs, which complicates the forecaster's evaluation process.

3) Case study: Typhoon Rosie (10W). A comparison/verification of the 500-mb wind fields and TC tracks from the NOGAPS and GFDN forecasts initiated at 0000 UTC and 0600 UTC 19 July 1997, respectively, is shown in Fig. A.22a-l. The NOGAPS track forecast has a large poleward and eastward bias relative to the best track, and is an outlier compared to the forecast tracks of the other four numerical models (Fig. A.22a). Notice the weak cyclone to the west of Rosie (asterisk) in the verifying NOGAPS analyses (Fig. A.22b-d) as well as in both the NOGAPS and GFDN forecasts (Fig. A.22 f-h, and i-l, respectively). Satellite infrared images for 19-22 July (Fig. 3.11a-d) verify an area of poorly organized convection initially over the Philippine islands moves west during the period.

In the NOGAPS forecasts, an extensive isotach maximum develops to the south of Rosie by 24 h, and then south of the western cyclone by 48 h, in association with the development of a large equatorial buffer eddy. As a result, the NOGAPS model predicts a strongly poleward track for Rosie, and the cyclone to the west remains roughly quasi-stationary between the eastward steering of the equatorial eddy and the westward steering from the subtropical anticyclone to the north. This poleward track in the NOGAPS forecast fields is consistent with the development of a peripheral anticyclone as in the RTF conceptual model (Fig. 3.10). By 48 h in the GFDN integration (Fig. A.22k), isotach maxima have developed south of both Rosie and the disturbance to the west. However, the equatorial buffer is not as extensive, and the two isotach maxima are not connected, as in the NOGAPS 48-h forecast (Fig. A.22g). Nevertheless, the strength of the eastward steering associated with the equatorial eddy to the south of the western cyclone kept the eddy over the Philippines, rather than drifting to the west (Fig. A.22d). That is, a reverse-oriented (southwest to northeast) monsoon trough did not occur in nature as in the NOGAPS forecast (Fig. A.22h), or to a smaller extent in the GFDN forecast (Fig. A.22l). This E-RTF involving Rosie and a probable tropical circulation (PTC) resulted in a significantly degraded (FTE > 300 n mi) NOGAPS track forecast, and a moderately degraded (FTE < 300 n mi) GFDN track forecast as in Fig. A.22a.

In the corresponding sea-level pressure fields, the size of Rosie in the NOGAPS forecasts (Fig. A.23f-h) becomes considerably larger than in the verifying NOGAPS analyses (Fig. A.23b-d), but the size of Rosie in the GFDN forecasts (Fig. A.23j-l) is slightly smaller than in the verifying analyses. In both the NOGAPS and GFDN forecasts, the disturbance to the west of Rosie is over-developed. The overly large sizes of the TC and the western cyclone in the NOGAPS forecast cause significant E-RTF. Because the size of Rosie in the GFDN forecast remained sufficiently

REVERSE TROUGH FORMATION (RTF) CONCEPTUAL MODEL

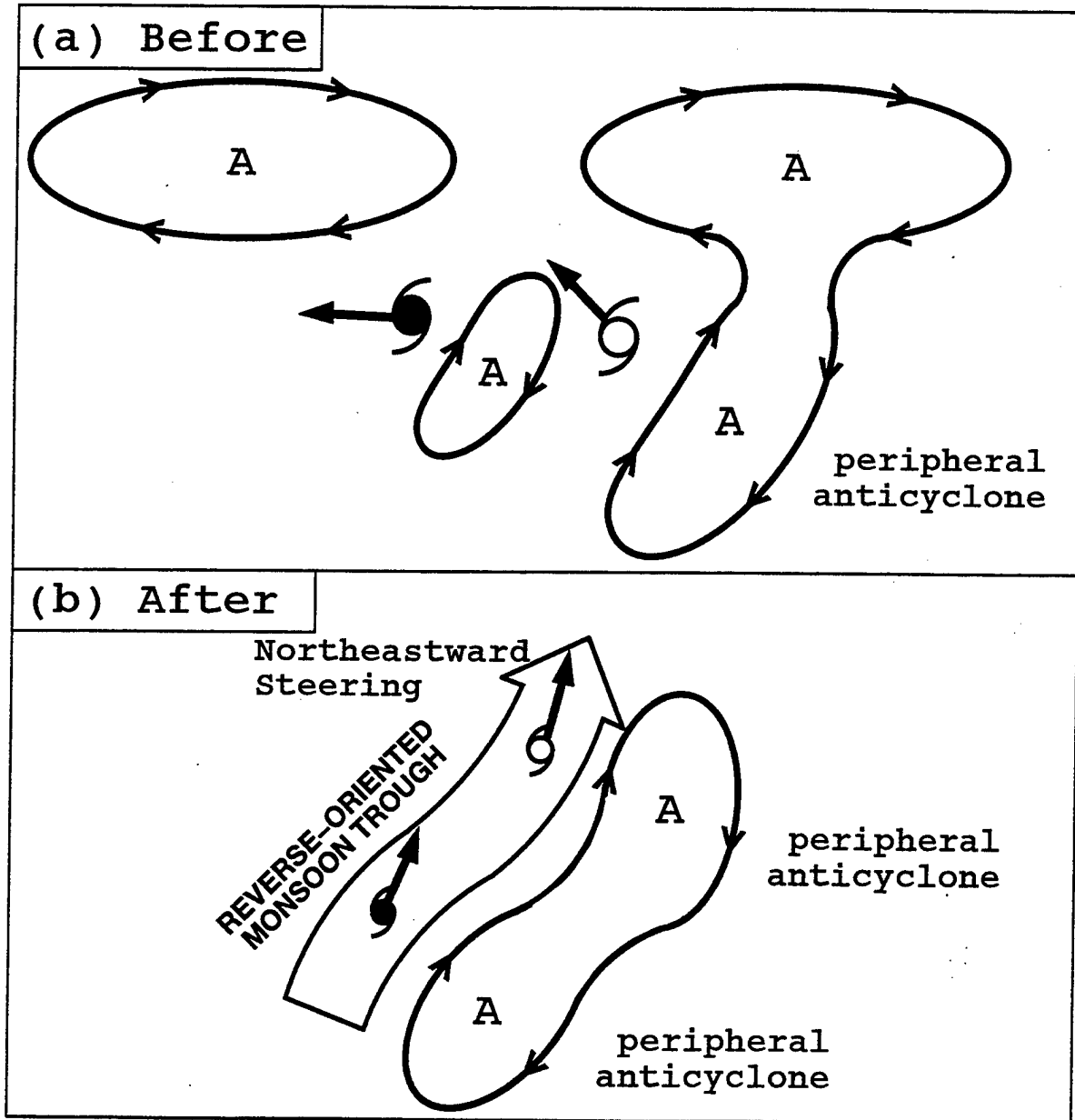


Fig. 3.10 Conceptual model as in Fig. 3.2, except for a reverse trough formation (RTF) in which two initially east-west oriented TCs become aligned more southwest to northeast in a reverse-oriented monsoon trough with an extensive anticyclone also oriented southwest to northeast so that both TCs change to more poleward track.

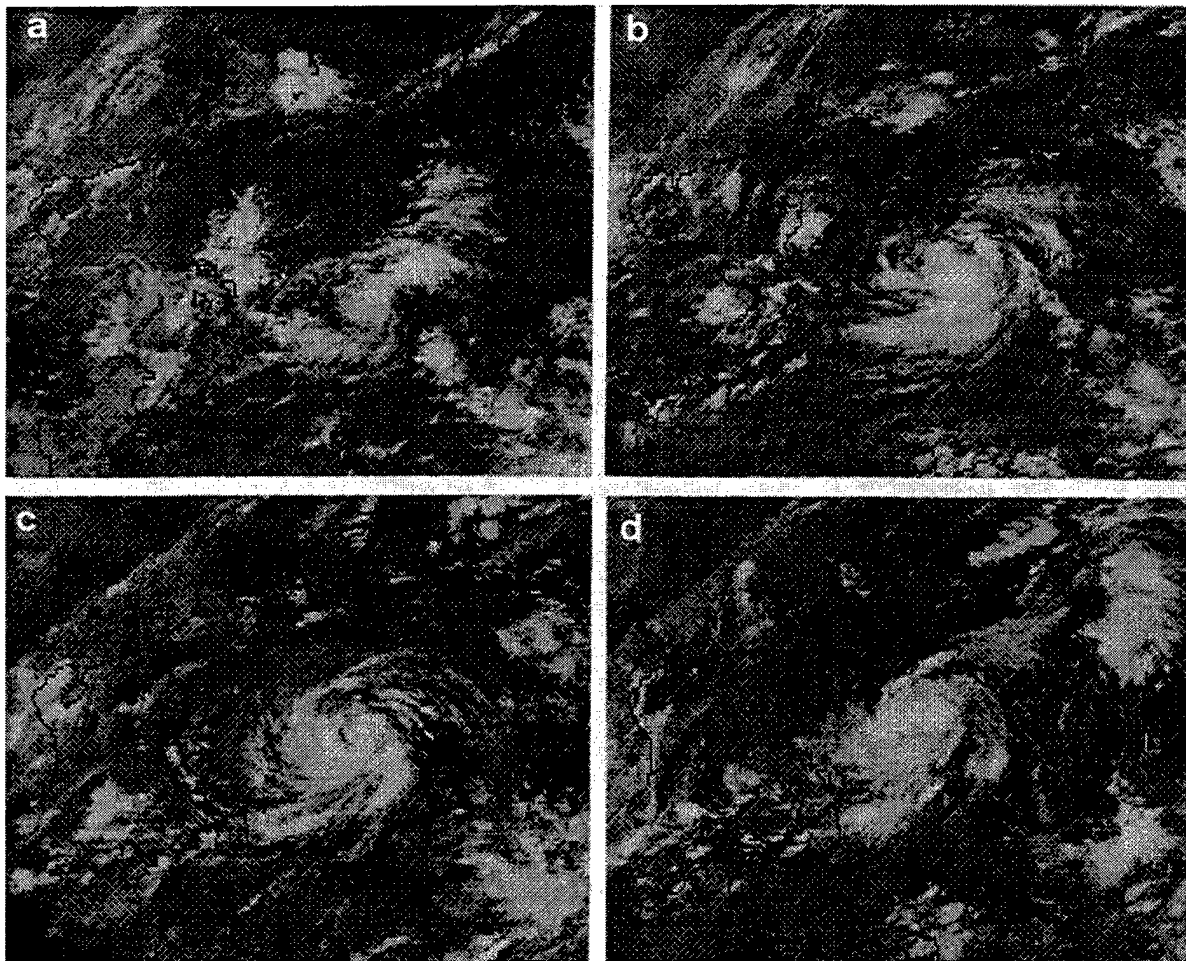


Fig. 3.11 Satellite IR imagery as in Fig. 2.4, except for TC Rosie at 0000 UTC on (a) 19, (b) 20, (c) 21, and (d) 22 July 1997.

small, a significant E-RTF event (i.e., FTE > 300 n mi) did not occur, despite the over-development of the western cyclone.

As indicated in Table 1.1, E-RTF significantly degraded three NOGAPS forecast tracks during the period 0000 UTC 19 to 0000 UTC 20 July 1997. During this period (Fig. 3.12a-c), the NOGAPS tracks had a consistent poleward and eastward bias relative to the tracks of the other four numerical models. The forecaster should notice that the tracks of the other four models are either along or to the right of the TC track. Just as in the GFDN forecast described above, those tracks with a rightward bias are probably affected by E-RTF to some extent. As a result, the actual TC track falls along the left side of the envelope formed by all of the model tracks. Recall that a

similar relationship of the ensemble envelope and the track of the TC occurred for Tina and Bing when E-RMT was occurring (Figs. 3.3 and 3.5, respectively).

Whereas the right and poleward bias in the NOGAPS forecasts suddenly diminishes at 1200 UTC 20 July (Fig. 3.12d), the accuracy of the GFDN forecast becomes highly degraded. At this time, the E-RTF has essentially ceased in the NOGAPS forecast. However, E-DCI that involves an upper-level cyclone (ULC) has become the dominant error mechanism in the GFDN forecast of Rosie. This E-DCI only moderately degraded the NOGAPS forecast (72-h FTE < 300 n mi), but significantly degrades the GFDN forecast (72-h FTE > 300 n mi), as described in the case study in Section 2. The ULC that will eventually be the source of E-DCI in the GFDN forecast from 1200 UTC 20 July is already present in the earlier forecast, i.e., to the north of Rosie in the 66-h GFDN forecast, and in the NOGAPS 72-h forecast, and in the verifying NOGAPS analysis (Figs. A.22l, h, and d, respectively). Thus, E-DCI may be starting to occur by the end of the 0000 UTC 19 July NOGAPS integration. However, this E-DCI cannot be the error mechanism primarily responsible for the poor NOGAPS track forecast in Fig. A.22a, since the NOGAPS forecast already has a significant east and poleward bias by 48 h in the integration (Fig. A.22g) when no indication of the ULC to the north of the TC is evident in the model forecast.

4) Impact on other objective guidance. During the period that the NOGAPS track forecasts were degraded by E-RTF (Fig. 3.12a-c), the tracks of the steering models that are based on the NOGAPS fields were similarly degraded (Fig. 3.13a-c). However, CSUM tracks appear largely unaffected. Although the CSUM track for 1200 UTC 19 July had a significant right bias, this was attributed to a general ineffectiveness of statistical-dynamic models in forecasting sharp track changes. The 1200 UTC 20 July tracks of the steering model forecasts remain highly degraded (Fig. 3.13d) despite a significant improvement in the accuracy of the NOGAPS track (Fig. 3.12d). As noted above, E-DCI has started to be a significant error mechanism, and as noted in Table 2.2, an E-DCI typically degrades the NOGAPS steering model forecasts more than the NOGAPS forecast from which the steering is derived.

5) Summary. The impact of E-RTF on the numerical model track forecast is very similar to the E-RMT cases (compare Table 1.3; rows 5 and 6) in that the number of degraded tracks was significantly greater for the NOGAPS model than for the GFDN model. Similar numbers of NOGAPS tracks were degraded by E-RMT (12) and E-RTF (10), despite a smaller number of TCs in the case of E-RTF. In addition, the poleward track bias during an E-RTF event in the NOGAPS model is qualitatively similar to that during an E-RMT event (e.g., compare Figs. 3.3 and 3.12). Finally, the summary of the key aspects of the E-RMT phenomenon (Table 3.2), including the indications in numerical model fields and tracks, and the impacts on various models available to the JTWC forecaster, are also generally applicable to E-RTF. As in the case of E-RMT, the key indicator (bold type) that E-RTF is causing a premature transition from a S/TE to P/PF environmental structure is the considerable growth of the TC circulation in the NOGAPS sea-level pressure forecast relative to the GFDN sea-level pressure forecast.

c. Tropical Cyclone initial Size (TCS)

1. Description. As listed in (Table 1.3), five NOGAPS and nine GFDN 72-h forecasts with FTEs exceeding 300 n mi were attributed to excessive TC initial size. All of these forecasts were

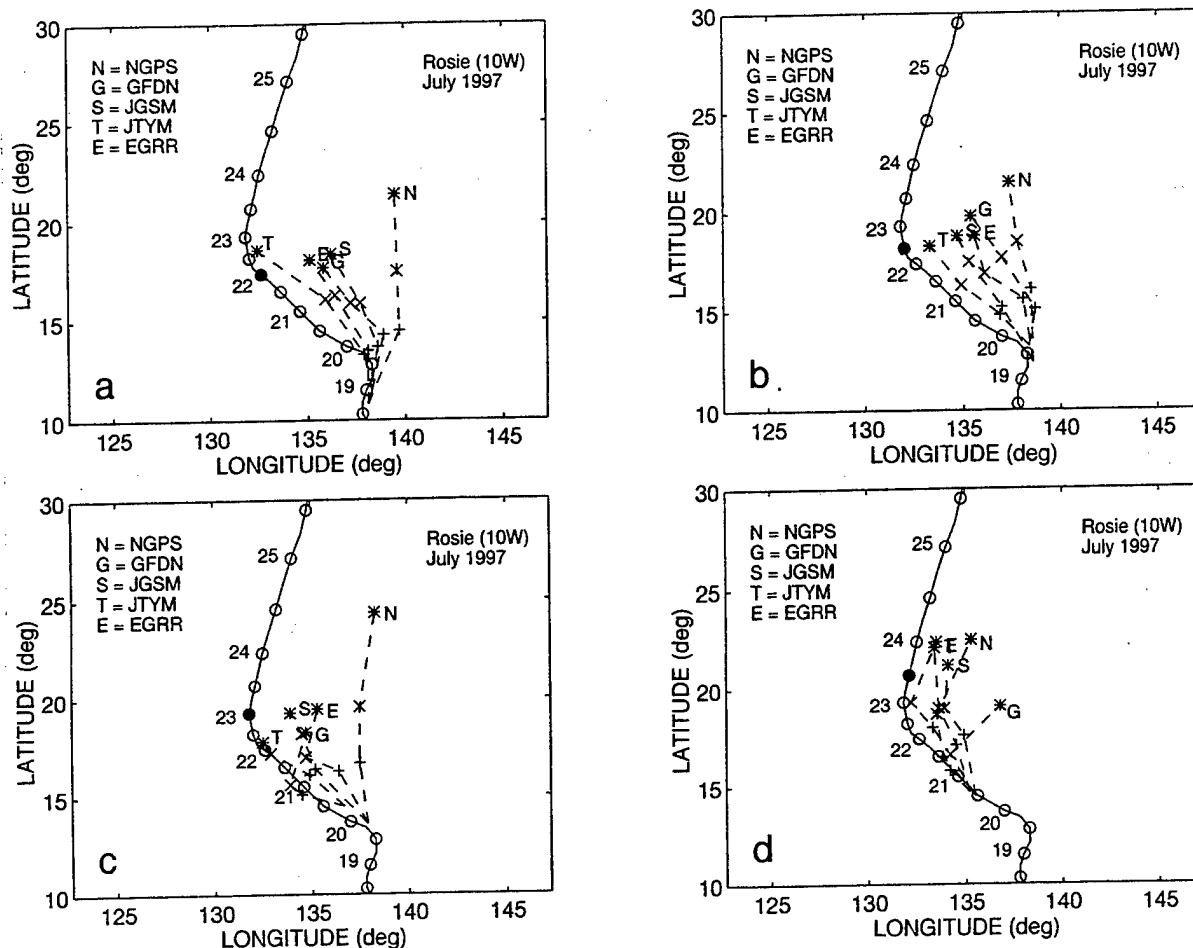


Fig. 3.12 Best-track and selected model forecast tracks (see inset) as in Fig. 2.7b, except for TC Rosie at (a) 0000 UTC and (b) 1200 UTC 19 July, and (c) 0000 UTC and 1200 UTC 20 July 1997.

for Typhoon Paka (05C) during 13-19 December 1997 (see Tables 1.1 and 1.2). Justification for attributing the large track errors to an excessive TCS (E-TCS) is based on a correlation between the size/asymmetry of the JTWC 35-kt wind radius (which is used to initialize the TC in both the NOGAPS and GFDN models) and the 72-h FTEs during 11-19 December 1997 (Fig. 3.14 and Table 3.3). Prior to 1200 UTC 13 December, the average 35-kt radius between right and left semi-circles is essentially constant at 115 n mi, and with one exception the 72-h FTEs for both the NOGAPS and GFDN models are well below 200 n mi. Beginning at 1200 UTC 13 December and continuing through 1200 UTC 16 December, the average 35-kt wind radius becomes as large as 155 n mi due to increasing right semi-circle radii in the JTWC warning messages. Notice that the NOGAPS (GFDN) FTEs are as large as 500 (849) n mi during this period. Although the JTWC forecasters presumably increased the right semi-circle 35-kt radius when it became imbedded in stronger environmental steering (notice the rapid translation speed of Paka during 12-14 December in Table 3.3), this was not accompanied by a decrease in the left-side radius.

By presumably over-specifying the increase in the northern 35-kt wind radius, or perhaps under-specifying the decrease in the southern 35-kt wind radius, an increase in the size is specified

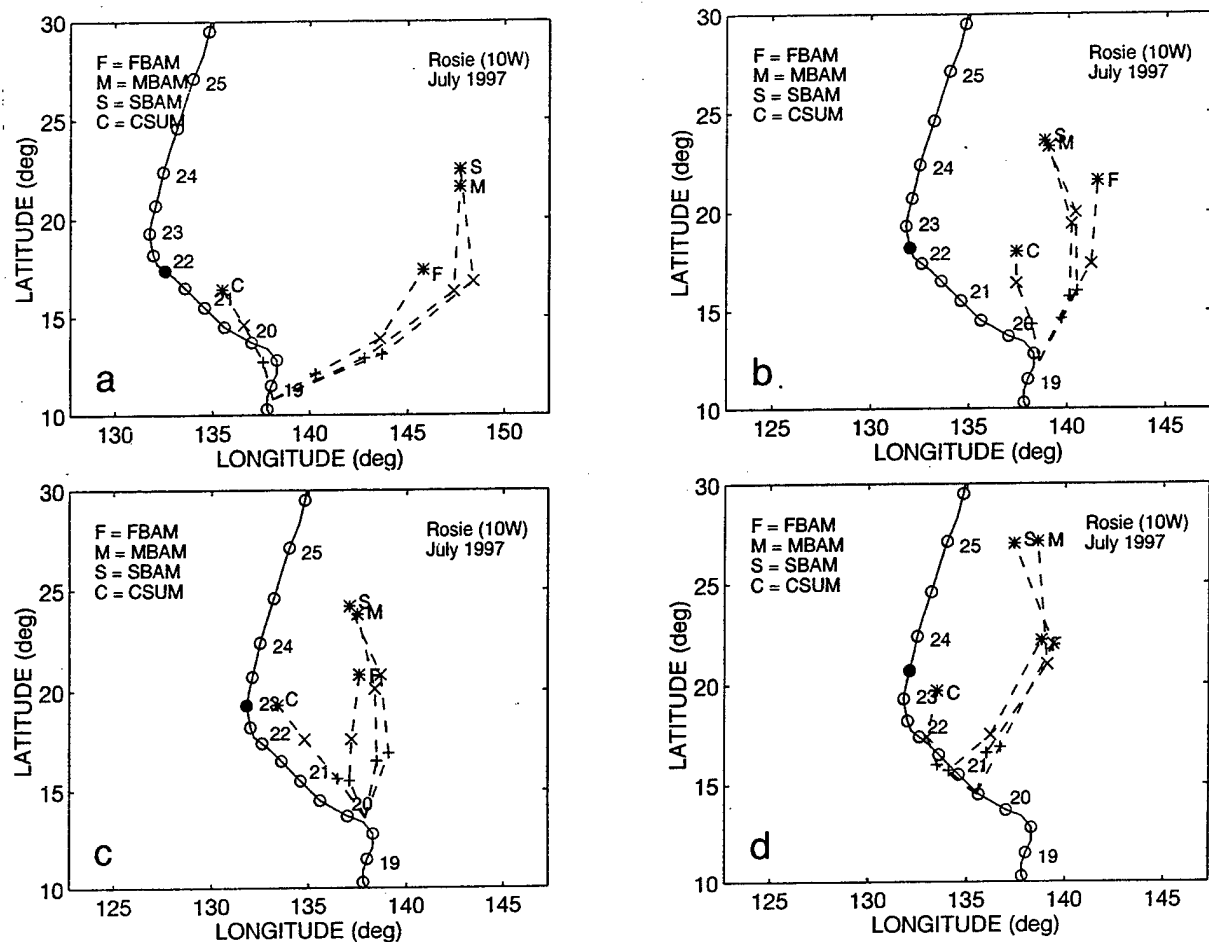


Fig. 3.13. Best-track of Rosie and selected objective technique track forecasts (see inset) for same times as in Fig. 3.12.

for Paka in the initial conditions of the NOGAPS and the GFDN models. Whereas an increase in the size of Paka may indeed have occurred, the overall cloud pattern for Paka in the satellite infrared imagery (Fig. 3.15a-f) shows no sign of a significant increase that might be expected to accompany such an increase in size. Another possible explanation is using a linear weighting of the right-side and left-side 35-kt wind radii to determine the size of the TC in NOGAPS and GFDN. Adding (subtracting) the large translation speed of Paka on the right (left) side to a nonlinear tangential wind profile (more rapid increases toward the center) is not well represented by simply specifying the profile based on the average of the right-side and left-side radii. The degree of over-estimation is larger when a small, intense TC has a translation speed that is a significant fraction of 35 kt. Whereas the period of increasingly large FTEs might be attributed to an increase in TC intensity to as much as 140 kt (Table 3.3), a later period of intensification to an even higher 160 kt is not accompanied by larger FTEs in NOGAPS. Thus, the tentative hypothesis is that the large FTEs are a result of an improper initial condition specification in the numerical models of the size of a small, but very intense, TC such as Paka.

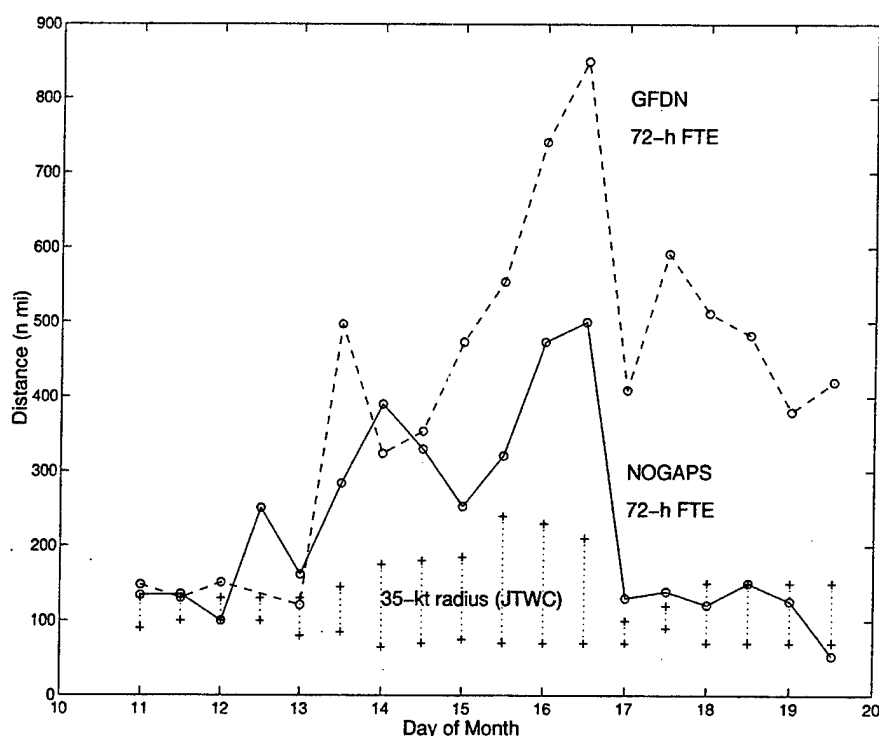


Fig. 3.14. Right (upper cross) and left (lower cross) semi-circle 35-kt wind radii warnings from JTWC during 11-19 December and the corresponding GFDN (dashed) and NOGAPS (solid) 72-h FTEs of the model integrations that were initialized with these 35-kt wind values.

After the sudden decrease in the right semi-circle 35-kt wind radius at 0000 UTC 17 December (Fig. 3.14), the average 35-kt wind radius is roughly constant at 110 n mi, and the NOGAPS 72-h FTEs are again consistently below 200 n mi. Although the corresponding GFDN FTEs remain large, a significant drop in magnitude occurs from 1200 UTC 16 to 0000 UTC 17 December as the average 35-kt wind radius is suddenly decreased by about 40%. These large GFDN FTEs are attributed to an increasing environmental vertical wind shear that will eventually contribute to weakening and dissipation of Paka, as manifest by translation speed as the steering is at lower elevations beginning 20 December. As indicated in Table 1.2, insufficient Response to Vertical wind Shear (I-RVS) was identified as the principal cause of the large GFDN 72-h FTEs by 0000 UTC 18 December. That is, the vortex in the GFDN model remained too strong (and too deep) and thus was advected too much by strong upper-tropospheric winds when Paka had actually been vertically decoupled and was being advected by weak lower-tropospheric steering.

During the period (1200 UTC 13 to 1200 UTC 16 December) with large 72-h FTEs, false forecasts of recurvature are found in both the NOGAPS and GFDN forecasts (e.g., Fig. 3.16c-e), whereas Paka actually continued to have a persistent west-northwest track. A comparison/verification of the 500-mb wind fields and TC tracks from the NOGAPS and GFDN forecasts initiated at 0000 UTC and 0600 UTC 16 December 1997, respectively, reveals the reason for these false recurvature forecasts (Fig. A.24a-l). In both the initial NOGAPS and GFDN analyses (Fig. A.24e and i, respectively), a prominent peripheral anticyclone is southeast of the TC. Notice also that the isotach maximum is to the east-northeast of the TC in the NOGAPS analysis,

Table 3.3 Tropical cyclone structure and movement of Typhoon Paka (05C) and the NOGAPS and GFDN forecast track errors during 11-19 December 1997. The GFDN FTEs are for the integration initiated 6 h after the synoptic time in the first column. Asterisks indicate the period when a distinct correlation exists between the 35-kt wind radius and the FTE magnitude.

Date/Time (UTC)	Intensity (kt)	Translation Speed (kt)	35-kt wind radius (n mi)	NOGAPS 72-h FTE (n mi)	GFDN 72-h FTE (n mi)
971211/0000	80	6	130/90	134	148
971211/1200	105	6	130/100	135	130
971212/0000	105	8	130/100	100	151
971212/1200	115	9	130/100	251	N/A
971213/0000	105	12	130/80	162	121
971213/1200	105	15	145/85 *	284 *	497 *
971214/0000	115	17	175/65 *	390 *	324 *
971214/1200	120	17	180/70 *	330 *	354 *
971215/0000	140	15	185/75 *	253 *	473 *
971215/1200	140	12	240/70 *	321 *	554 *
971216/0000	120	9	230/70 *	473 *	741 *
971216/1200	125	7	210/70 *	500 *	849 *
971217/0000	125	9	100/70	130	409
971217/1200	145	7	120/90	139	592
971218/0000	160	9	150/70	121	512
971218/1200	135	8	150/70	150	482
971219/0000	115	9	150/70	126	380
971219/1200	115	7	150/70	53	420

and is particularly evident to the east of the TC in the GFDN analysis. Thus, both the NOGAPS and GFDN analyses have the TC in the Poleward Flow (PF) region of a Poleward (P) pattern. In reality, Paka is moving just north of west (Fig. A.24a) at about 9 kt (Table 3.3), which indicates that the TC is actually in the Tropical Easterlies (TE) of the Standard (S) pattern.

This discrepancy between the model-analyzed environment structure and the actual environment structure implied by the motion of Paka may be explained in terms of barotropic beta-effect theory and modeling. Owing to the presumably erroneous expansion of the JTWC 35-kt wind radii beginning 1200 UTC 13 December, excessive RMT (E-RMT) has been occurring in the NOGAPS forecasts that is expected to cause a S/TE to P/PF transition. For example, notice in Fig. 3.16b the decreased translation by 48 h in the NOGAPS forecast track and the poleward turn at 48 h in the GFDN. Since the data assimilation cycle of NOGAPS uses the 6-h forecast as the first-guess field for the next analysis, the series of erroneous specifications of the TC structure contaminates each subsequent initial analysis. The larger and larger TC vortex in the NOGAPS initial conditions and forecasts leads to earlier poleward deflections in the track forecast (note poleward turns in Fig. 3.16c in the NOGAPS and GFDN tracks at 24 h and 48 h, respectively). If a persistent E-RMT is generated from consistently erroneous large initial TC sizes, eventually the erroneous environment structure will dominate in the model analysis (i.e., Fig. A.24e and i); and the movement of the TC in the model will be highly erroneous virtually from the start of the model run (see Fig. 3.16d, which corresponds to the fields in Fig. A.24). Recall that the GFDN initial TC specification has an environment from the off-time NOGAPS analysis on which a spin-up TC vortex is imposed. If the overly large TC structure in the NOGAPS analysis is not removed as part

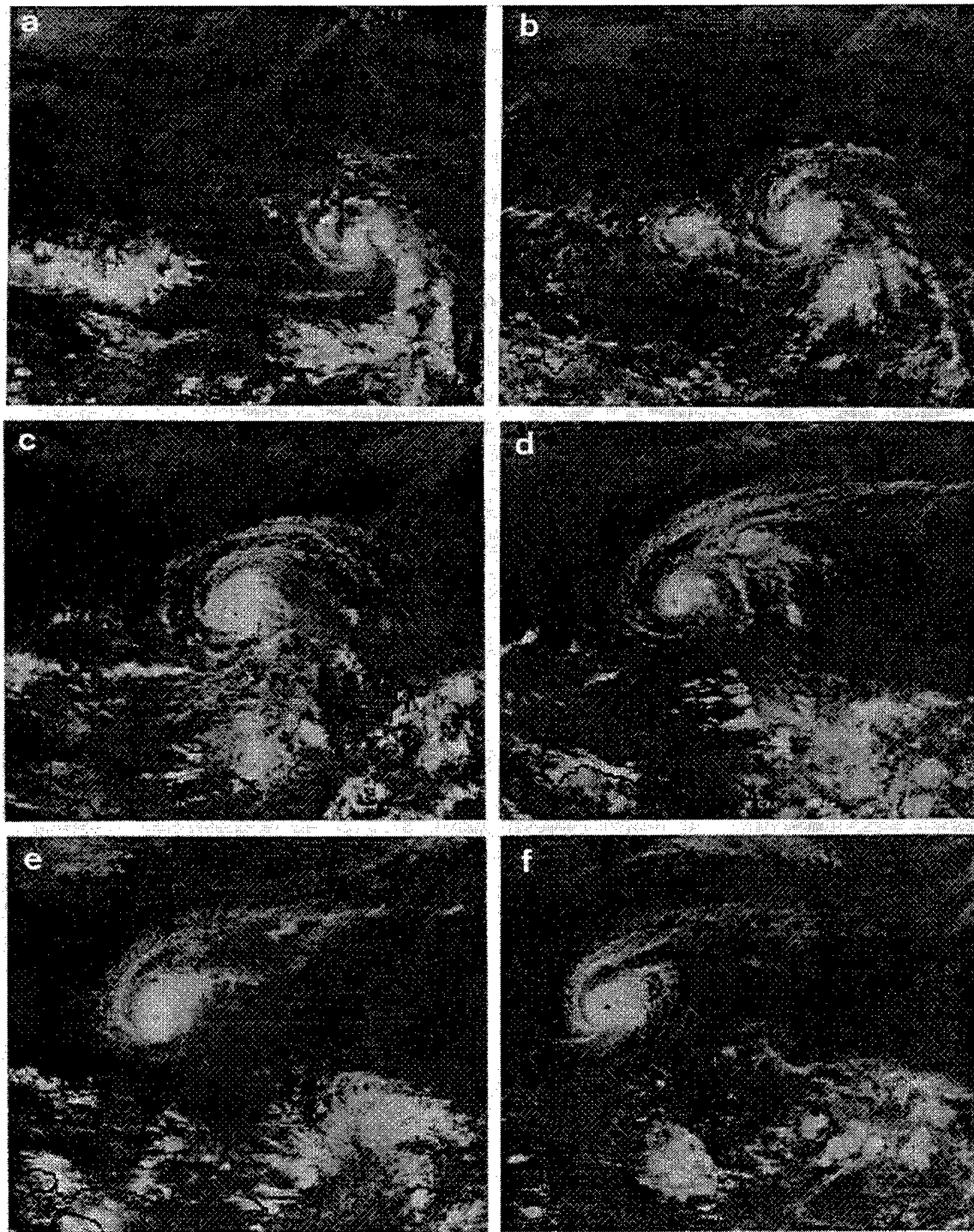


Fig. 3.15. Satellite IR imagery as in Fig. 2.4, except for TC Paka at 0000 UTC on (a) 13, (b) 14, (c) 15, (d) 16, (e) 17, and (f) 18 December 1997.

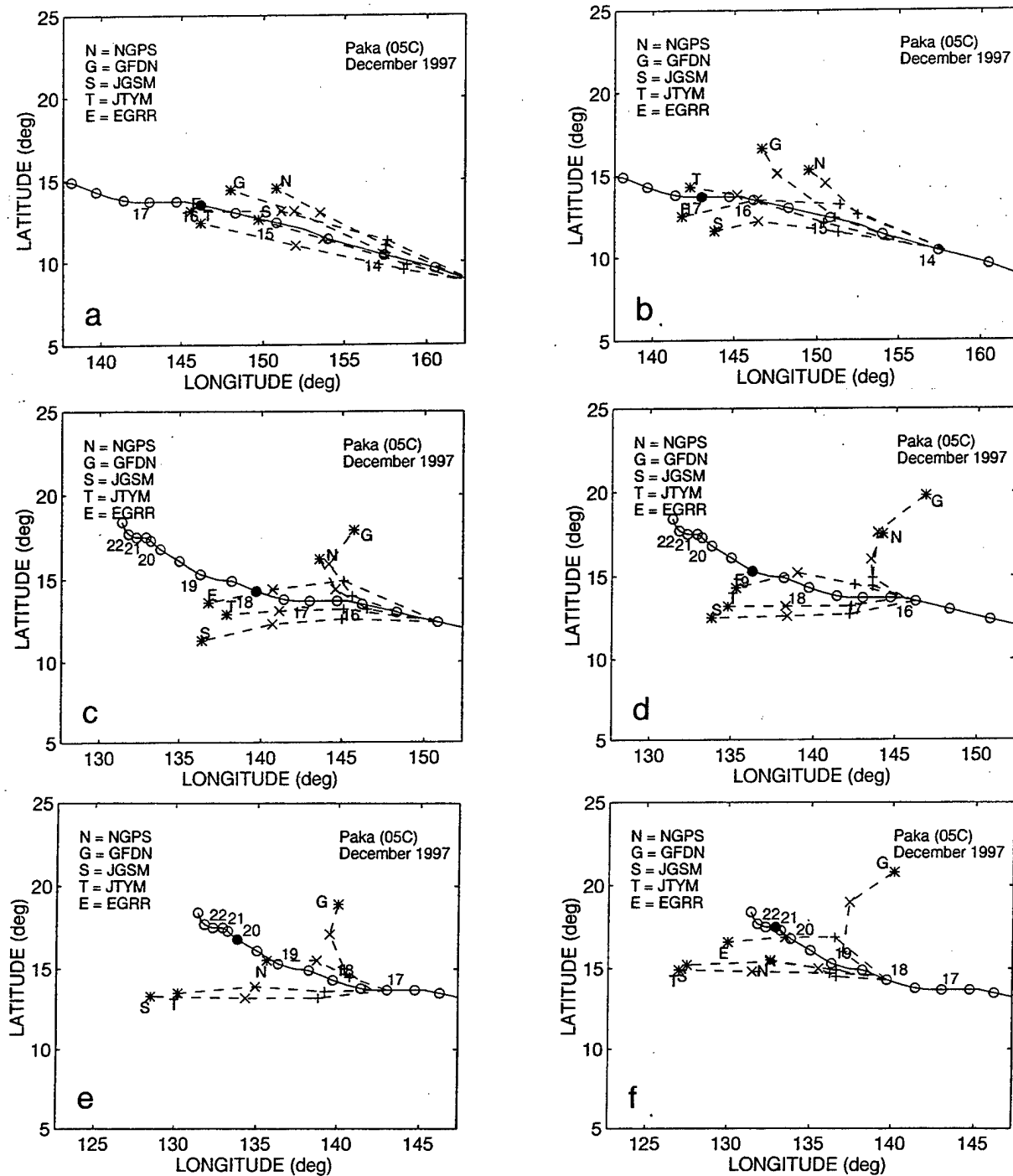


Fig. 3.16. Best-track and selected model track forecasts (see inset) as in Fig. 2.7b, except for TC Paka at 0000 UTC on (a) 13, (b) 14, (c) 15, (d) 16, (e) 17, and (f) 18 December 1997.

of this GFDN initial TC specification, the GFDN model will also suffer a qualitatively similar track forecast degradation.

The differences in how the GFDN and NOGAPS models are initialized provide a probable explanation for why the GFDN track forecasts for Paka were consistently worse than the NOGAPS forecasts. Whereas the NOGAPS model is initialized with a symmetric TC vortex, it is assumed that the first-guess field includes the beta gyres. If the sum of the background flow at the 13 TC synthetic observation locations does not equal the recent motion vector, a correction vector is added to each of the 13 synthetic observations to improve the early track prediction. In the GFDN initial TC specification, the TC vortex in the NOGAPS analysis is presumably removed before insertion of a symmetric TC vortex and beta gyres that are consistent with the TC size specified in the JTWC wind radii warning. If an excessive TC size is specified by JTWC, then excessively strong beta gyres will be inserted into the GFDN analysis. Since these gyres may be superposed on any gyre remnants from the background NOGAPS analysis that has not been removed by the GFDN initial specification, anomalously fast beta-effect propagation that even exceeds that in NOGAPS can occur. (Note: During the 1998 typhoon season, the portion of the GFDN initial TC specification related to beta gyres has been changed. In that change, the asymmetric circulation at 12 h from the prior GFDN forecast is extracted and inserted at the new TC position. What effect this will have on the GFDN track forecasts is unknown, but is not expected to be large. If too large TC sizes are specified, the GFDN model will probably experience a degree of track degradation similar to NOGAPS, as opposed to having been much worse as in the Paka case.)

When the right semi-circle 35-kt wind radius is suddenly reduced at 0000 UTC 17 December to half the size 12 h earlier (Table 3.3), the accuracy of the NOGAPS forecast track dramatically improves, and the GFDN forecast continues to be degraded. A comparison/verification of the 500-mb wind fields and TC tracks from the NOGAPS and GFDN forecasts initiated at 0000 UTC and 0600 UTC 17 December 1997, respectively (Fig. A.25a-l), reveals the reason for this dissimilar response by the models. In the NOGAPS analysis (Fig. A.25e), the size of the TC circulation is similar to that in the NOGAPS analysis 24 h earlier (Fig. A.24e), which indicates that insertion of weaker synthetic TC observations based on the reduction in average 35-kt wind radius have not been fully effective in offsetting the size of the TC circulation coming from the NOGAPS first-guess field. Consequently, E-RMT still occurs, so that a poleward bias is evident in the 24-h forecast track (Fig. A.25a), and transition from S/TE to P/PF appears imminent (Fig. A.25f; note isotach to east of TC). By 48 h in the NOGAPS forecast (Fig. A.25g and h), the center of the low-level TC circulation (asterisk) appears separated from the 500-mb circulation, which indicates that the TC in the model is rapidly weakening. As a result of this anomalous weakening (and shallowing) of the TC in the NOGAPS model, the low-level circulation has a westward track (Fig. A.25a) in response to easterlies at lower levels, even though the 500-mb environment conforms to the Poleward pattern. A continuation of the excessive TC weakening in the NOGAPS forecast initiated at 0000 UTC 18 December (not shown) probably accounts for the equatorward bias of that NOGAPS track forecast (Fig. 3.16f). However, this error does not result in an FTE that exceeds 300 n mi.

In the GFDN analysis (Fig. A.25i), the size of the TC circulation is remarkably smaller than in the GFDN analysis 24 h earlier (Fig. A.24i), which indicates the GFDN initial TC specification has been successful in removing the erroneously large TC circulation from the NOGAPS analysis 6

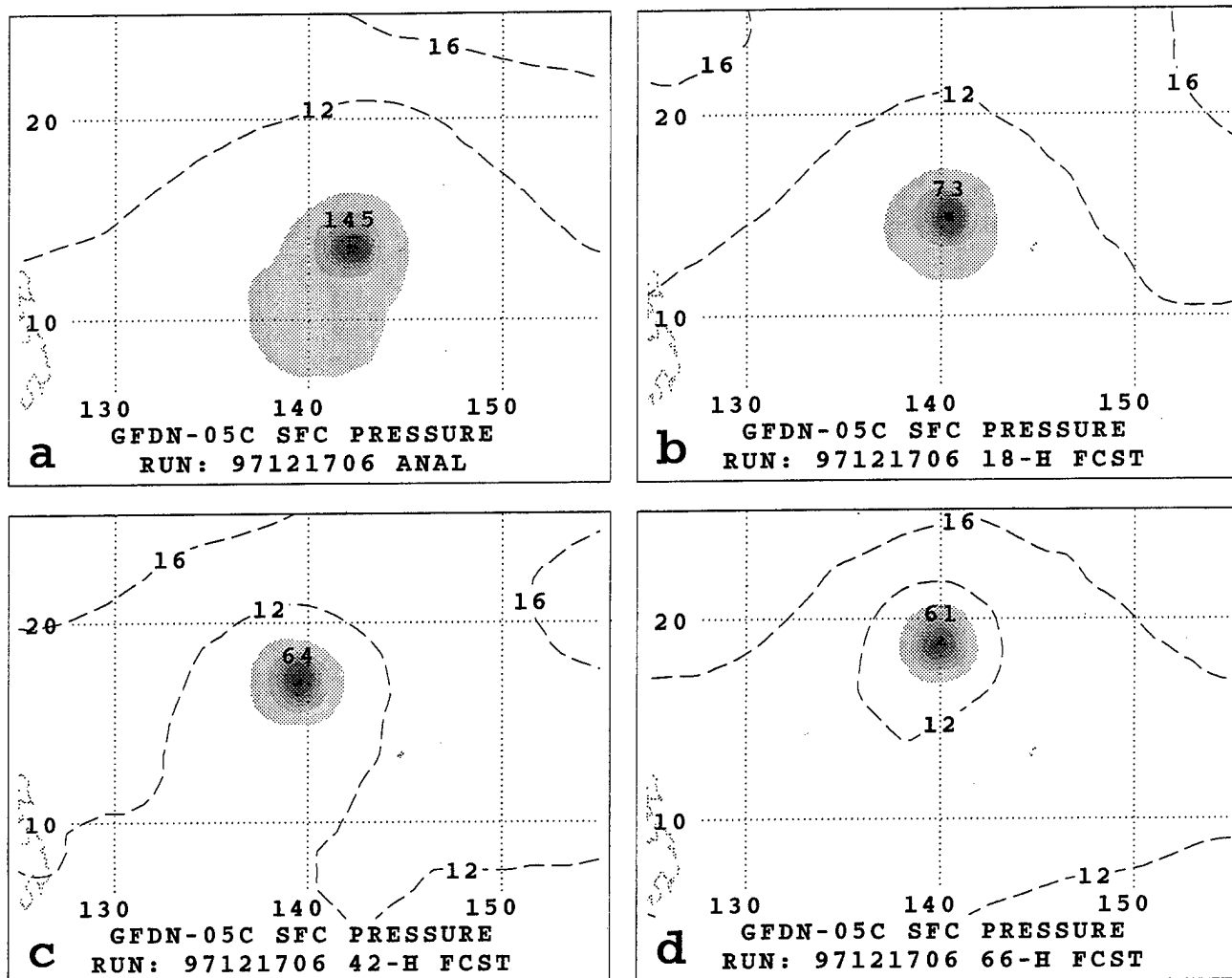


Fig. 3.17 Sea-level pressure fields as in Fig. A.1a-l for the GFDN (a) analysis at 0600 UTC 17 December 1997, and subsequent (b) 18-h, (c) 42-h, and (d) 66-h forecasts.

h after Fig. A.25e. However, an overly strong Rossby wave train is still evident in the peripheral anticyclone that is a residual of the overly strong beta gyres generated in prior forecasts. Since the GFDN initial condition specification is designed to remove only the TC, these gyres remain in the TC environment. Notice also that a cyclonic eddy appears near 8°N, 140°E in the GFDN analysis (Fig. A.25i), where an odd lobe of sub-1008 mb pressures also occurs in the corresponding sea-level pressure analysis (Fig. 3.17a). Notice that the lobe of low pressure disappears by 18 h in the GFDN forecast (Fig. 3.17b), and the size of the TC decreases considerably throughout the GFDN forecast (Fig. 3.17b-d). These features provide further evidence that an overly large, and unrepresentatively shaped, TC vortex remains in the GFDN analysis field (Fig. A.25i). These problems with specifying the initial conditions, combined with the fact that an intense (and thus vertically extensive) vortex will usually be maintained in the GFDN model, provide a probable explanation for why the erroneous recurvature problem continues in the GFDN forecast. Even though less track degradation occurs (Fig. A.25a) compared to the earlier forecast (Fig. A.24a), insufficient RVS (I-RVS) is probably becoming a contributing factor, and will eventually become the dominant error mechanism for the GFDN model (Table 1.2). Recall that the erroneous TCS in

the NOGAPS forecast of Paka led to a poleward track into large vertical shear, which reduced the steering level such that a compensating effect occurred. The error due to E-TCS creating a poleward deflection in the GFDN track is not offset by the vertical shear reducing the steering level since the intense vortex in the GFDN resists the shear effect.

2) Impact on other objective guidance. During 13-16 December 1997, when large 35-kt wind radii in the right semi-circle were being specified by JTWC (Fig. 3.14), and the track forecasts of NOGAPS were being increasingly degraded by E-TCS (Fig. 3.16a-d), the tracks of the steering models were also becoming increasingly degraded (Fig. 3.18a-d). During this period the shallow BAM (SBAM) tended to be the most degraded, which is not surprising since errors in TC size would be expected to have the greatest impact in the mid-to-lower troposphere where the cyclonic circulation of the TC is the largest. Even though the right semi-circle 35-kt wind radius had been dramatically reduced at 0000 17 December, the tracks of the steering models (particularly SBAM) continued to be degraded (Fig. 3.18e), which is again attributed to the time required for the deleterious effects of E-TCS to be purged from the NOGAPS initial condition via the data assimilation system. Notice the inter-relationships among the steering models undergo a fundamental change from 17 to 18 December 1997 (Fig. 3.18e and f, respectively), with the SBAM (FBAM) track having the most equatorward (poleward) bias relative to the track of the TC. This change indicates that the effect of E-TCS is now largely gone from the NOGAPS forecasts that are the basis of these steering models on 18 December. As will be discussed in Section 4, this spread of the FBAM, MBAM, and SBAM tracks is indicative of increasing vertical wind shear. The poor GFDN forecasts on and after 0000 UTC 18 December 1997 (see Fig. 3.16f) are a result of insufficient RVS (I-RVS) compared to the actual conditions, since Paka dissipated at 1200 UTC 22 December without recurving (Fig. A.18f). Throughout the period when the steering models were degraded by E-TCS, the tracks of CSUM were consistently accurate.

3) Summary. The degraded forecasts of the NOGAPS and GFDN models due to E-TCS in the Paka case emphasize that the 35-kt wind radii warnings issued by JTWC can greatly impact the accuracy of the numerical model TC track forecasts. This case also raises important questions about the effectiveness of current procedures for specifying the initial TC circulation in the numerical models. For example, the wind radii specified in JTWC warnings are for the surface winds over the ocean to alert ships and islands of the approaching damaging winds. However, the motion of the TC and its interaction with the environment depend on the TC vortex structure throughout the troposphere, which may not be particularly well-represented by the horizontal distribution of surface winds. This case of E-TCS arises because these surface winds influence the initial structure of the TC in the NOGAPS and GFDN models. As the TC moves in a stronger environmental flow (and thus the translation speed increases), the 35-kt wind radius will be increased (decreased) on the right (left) side even if the symmetric vortex wind structure is unchanged. Part of the problem in this case may be due to mis-interpreting the increase in the right semi-circle 35-kt wind radius as an increase in the vortex size versus an environmental flow increase. A rethinking of how best to specify the TC initial structure in the numerical models is needed, particularly in light of significant increases in cloud- and water vapor-tracked winds that may currently define the *outer* wind distribution of the TC with sufficient representativeness to reduce the dependency on synthetic TC observations in the NOGAPS model and a constrained spin-up vortex in the GFDN model.

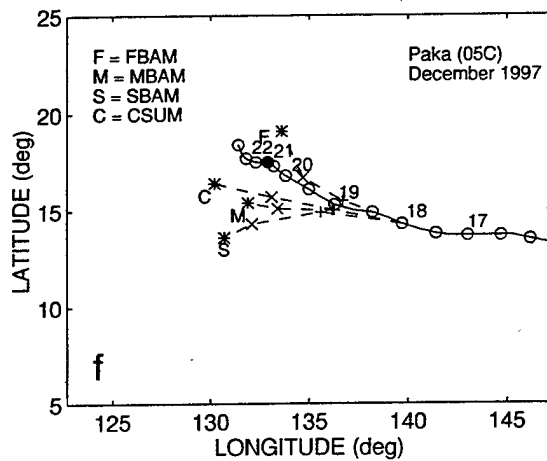
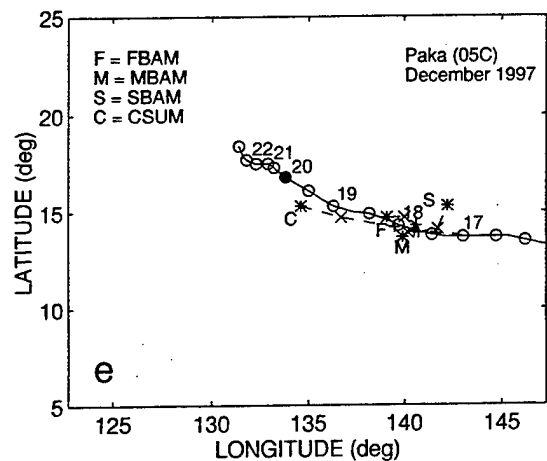
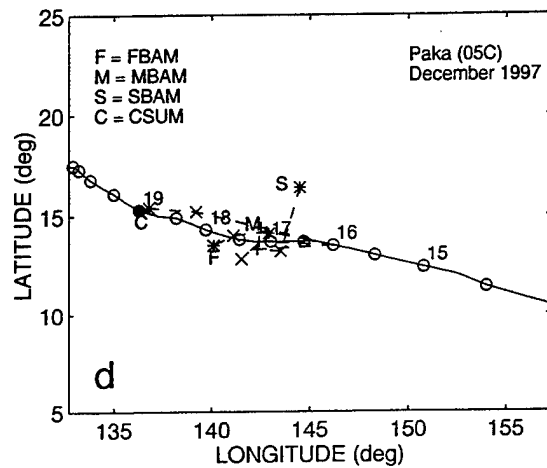
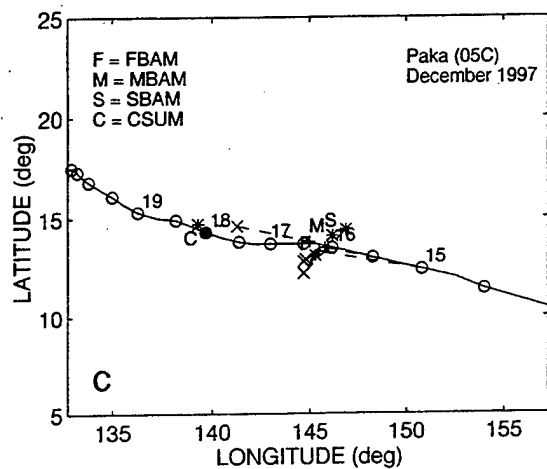
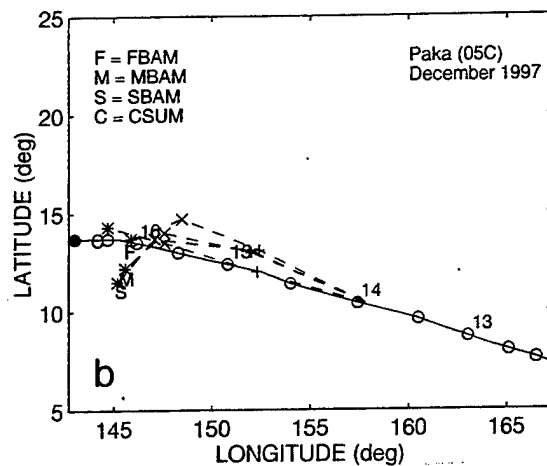
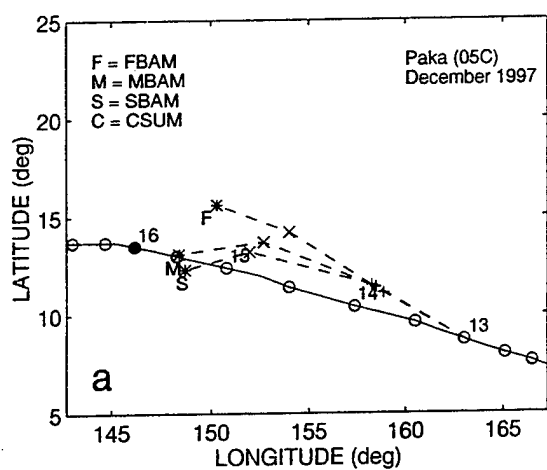


Fig. 3.18 Best-track of Paka and selected objective technique track forecasts (see inset) for same times as in Fig. 3.16.

4. Midlatitude-related processes

The error mechanisms in Table 1.3 that involve midlatitude-related processes are Response to Vertical wind Shear (RVS), Baroclinic Cyclone Interaction (BCI), and Midlatitude System Evolutions (MSE). All processes for which TC interaction with the environment is an inherent factor (i.e., all error mechanisms except MSE) are grouped together in Table 1.3. In this section, MSE will be addressed first, followed by RVS and BCI, for two reasons. First, this order presents the error mechanisms in order of increasing complexity from both conceptual and operational perspectives. Second, the order of presentation here generally follows the order that the midlatitude-related error mechanisms will typically become a factor during the TC lifecycle. It is emphasized that all three error mechanisms may be simultaneously operative to varying degrees. However, the authors have found that for most of the poor forecasts evaluated clear indications exist that one of the three mechanisms is primarily responsible for the degraded track forecast.

a. Midlatitude System Evolutions

1) Description. The fundamental idea of Midlatitude System Evolutions (MSE) is one of changes to the TC steering flow due to development, dissipation, and/or movement of midlatitude features (cyclones, troughs, anticyclones, or ridges) that occur essentially *independent of the TC*. Idealized conceptual models for the four basic kinds of MSE are illustrated in Fig. 4.1.

When Midlatitude CycloGenesis (MCG) takes place, the TC labeled A in Fig. 4.1a that has been tracking essentially westward in the Tropical Easterlies (TE) steering flow equatorward of the subtropical ridge (STR) axis may be turned onto a more poleward heading as the developing midlatitude trough or cyclone “breaks” the ridge and creates more poleward flow in the vicinity of the TC (Fig. 4.1b). That is, sufficient MCG may result in an environment structure transition from S/TE to S/PF (Fig. 1.6). Similarly, a TC that is poleward of the STR axis (Fig. 4.1a; labeled B) and moving northeastward in the PF region when MCG takes place may then undergo directional and/or speed changes as the developing trough/cyclone alters the direction and strength of the midlatitude flow in which the TC is embedded (Fig. 4.1b). If MCG changes only the translation speed of the TC, then it will remain in the M/PF pattern/region combination (Fig. 1.6), or perhaps change to the M/MW pattern/region. However, a vigorous MCG may change the direction of environmental steering sufficiently that a region transition may occur within the M Pattern (e.g., from MW to PF region as suggested in Fig. 4.1b). For simplicity of depiction, Midlatitude Cyclolysis (MCL) is simply depicted in Fig. 4.1 as the reverse of MCG. However, the reader should not construe this to imply that no fundamental differences exist between MCG and MCL.¹ If MCG (MCL) occurs to a greater or lesser extent in a numerical TC forecast model than in reality such that a significant FTE results, then Excessive (E) or Insufficient (I) MCG (MCL) is considered to have occurred.

¹ It is acknowledged, for example, that latent heat release usually makes an important contribution to cyclogenesis, but not to anticyclogenesis.

Midlatitude System Evolutions (MSE)

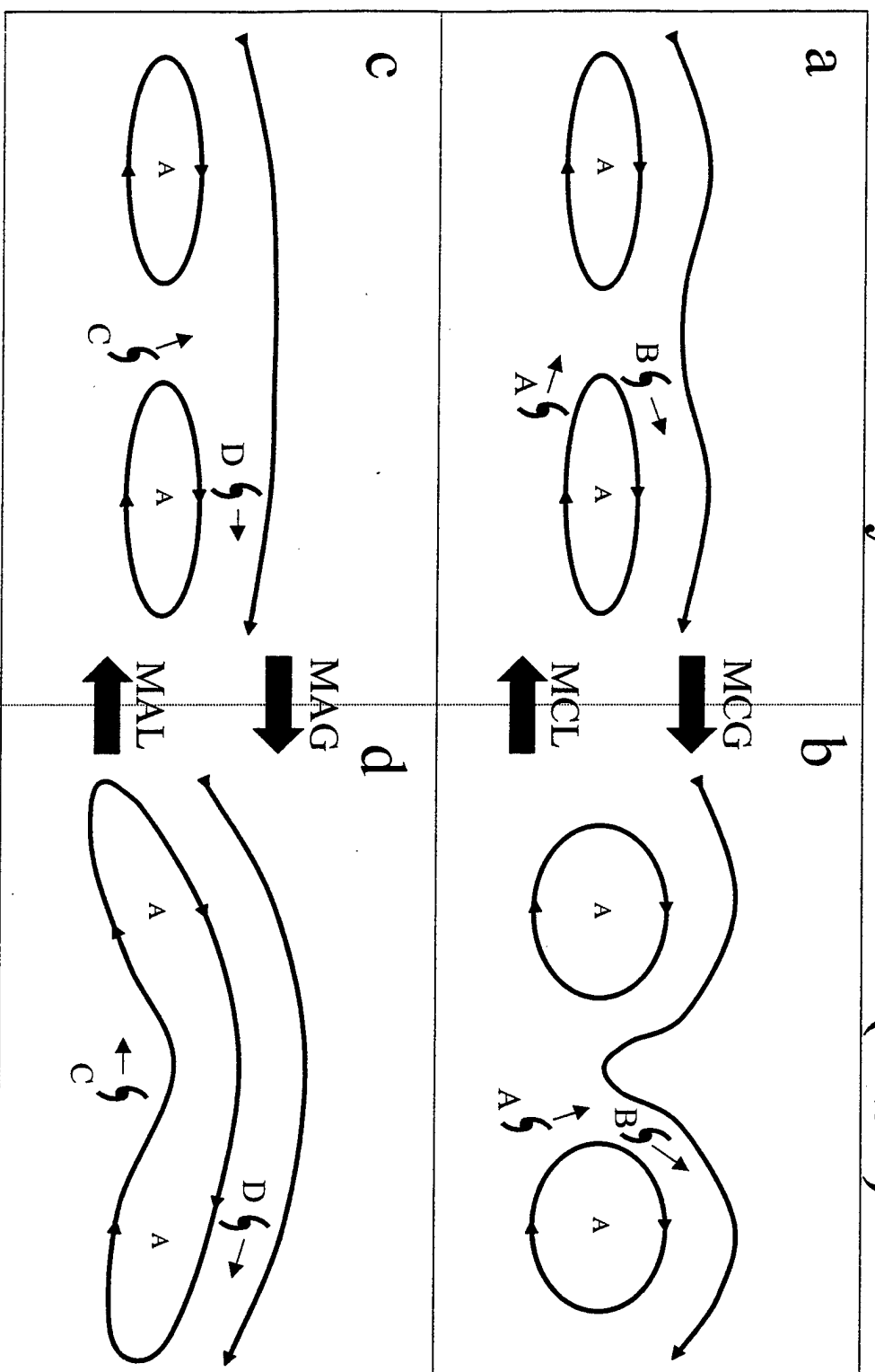


Fig. 4.1. Schematics of the Midlatitude System Evolutions (MSE) that may lead to large TC track errors. The deepening of the midlatitude trough from panel a to panel b depicts Midlatitude Cyclogenesis (MCL) and the reverse order (panel b to panel a) implies Midlatitude Anticyclogenesis (MAL). Similarly, the midlatitude anticyclone change poleward of the TC from panel c to panel d depicts Midlatitude Anticyclogenesis (MAL) and the reverse order (panel d to panel c) implies Midlatitude Cyclogenesis (MCL).

When Midlatitude AnticycloGenesis (MAG) takes place, a TC labeled C in Fig. 4.1c that has been tracking northwestward in the PF region southeast of a weakness in the STR may be turned westward (or even south of west) as the developing midlatitude ridge/anticyclone increases the strength of the STR poleward of the TC. If the STR builds sufficiently in association with MAG, then the TC labelled C will be subjected to predominantly easterly or even northeasterly steering (Fig. 4.1d), i.e., may have a change in environment structure from S/PF to S/TE or S/EF (Fig. 1.6). When such a MAG event takes place, the TC labeled D in Fig. 4.1d that has been moving eastward and/or poleward in the midlatitude flow poleward of the STR axis may undergo directional and/or speed changes as the midlatitude developing ridge/anticyclone alters the direction and strength of the midlatitude flow in which the TC is embedded. If MAG changes only the translation speed of the TC, then it will remain in either a M/PF or M/MW pattern/region combination (Fig. 1.6). If MAG changes the direction of environmental steering sufficiently, then a region transition can occur within the M Pattern (e.g., from MW to EF region as suggested in Fig. 4.1d). For simplicity, Midlatitude Anticyclolysis (MAL) is simply treated as the reverse of MAG in Fig. 4.1. If MAG (MAL) occurs to a greater or lesser extent in a numerical TC forecast model than in reality such that a significant FTE results, then Excessive (E) or Insufficient (I) MAG (MAL) is considered to have occurred.

In the schematics of Fig. 4.1, the midlatitude features are depicted as developing without moving. Actually, it may primarily be the approach or retreat of a non-developing midlatitude trough or ridge that causes a change in the steering flow and thus in the TC motion. For these schematics, either movement or development of midlatitude features will be considered as potential methods to affect the steering flow on the TC. It is also emphasized that a variety of TC track changes can occur depending of the location of the TC relative to the pertinent midlatitude features, and depending on changes in the amplitude and/or orientation of the midlatitude features. That is, the four MSE depictions in Fig. 4.1 must be treated as highly flexible templates that may have to be adjusted with respect to shape, location, and number of midlatitude features to explain particular TC tracks, or as it may be predicted by a model. Recall again that the MSE conceptual model is used for explaining differences between a model forecast and the movement of the TC, or between two numerical model track forecasts, for situations in which TC interaction with its environment does not seem to be a determining factor in the motion (i.e., one of the TC-environment transitional mechanisms in lower right box in Fig. 1.4).

It is also noted that when a MSE process alters the motion of a TC equatorward of the STR axis, it is by indirectly altering the structure of the STR in the vicinity of the TC. Whereas this phenomenon was formerly called STR Modulation (SRM) in the Systematic Approach Meteorological knowledge base (see CMKB p. 8, 155-166), the four MSE processes in the schematics in Fig. 4.1 are a more general treatment of both the direct and indirect influences of the midlatitude circulation on the TC steering flow.

2) Frequency and Characteristics. Erroneous MSE in the NOGAPS and/or GFDN forecasts resulted in large degradations in the 72-h track forecasts for seven TCs in 1997 (Table 4.1, column 1). It is somewhat surprising that the TC was equatorward of the STR axis in a S/TE environment at the analysis time in five of the seven cases (Table 4.1; column 3), since the more poleward position (labeled B in Fig. 4.1a) might have been expected to be more favored. Other mechanisms to be described below tend to be more important when the TC is poleward of the STR axis. By far

the most frequently occurring erroneous MSE was E-MCG (Table 4.1; column 4), which significantly degraded track forecasts for five TCs. The error mechanisms I-MAL and E-MAG each affected one TC, and no instances of erroneous MCL were noted in the NOGAPS or GFDN forecasts during 1997.

Table 4.1. Cases of erroneous Midlatitude System Evolutions (MSE) in the western North Pacific during 1997. See Table 1.3 and the text for meaning of the acronyms in column 4, and Table 2.1 for explanatory footnotes.

TC No	Starting times of affected model runs ¹	Initial synoptic environment of affected TC	Type of erroneous Midlatitude System Evolutions (MSE)	Models affected	
				JTWC ⁵	Others ⁶
02W	Apr 13/12-14/12	S/TE	Excessive-MCG	G,(N)	E,(T)
08W	Jun 16/00-18/00	S/PF	Insufficient-MAL	N,G	E,T
19W	Aug 31/18-02/06	P/PF	Excessive-MCG	G,(N)	
27W	Oct 21/06-22/18	P/PF → M/PF	Excessive-MCG	G,(N)	
28W	Oct 18/06-21/06	S/TE → P/PF	Excessive-MCG	G,(N)	
29W	Nov 02/12-04/12	S/TE → S/PF	Excessive-MAG	N	
31W	Nov 10/18-13/18	S/TE	Excessive-MCG	G,(N)	

Two very useful results are: (i) that every instance of E-MCG occurred in GFDN (Table 4.1; column 5); and (ii) that whenever E-MCG occurred in a GFDN forecast, a similar misrepresentation of MSE was also evident in the NOGAPS forecast fields, although not with sufficient severity to cause a 72-h FTE greater than 300 n mi (as denoted by the parentheses). Thus, detection of a situation in which the NOGAPS forecast includes a midlatitude cyclogenesis that may be affecting the TC track should trigger a close examination for E-MCG in the GFDN forecast, which may result in a significantly degraded track. This consistent difference between the two models can be used to advantage by the forecaster in the near-term. In the longer term, a consistent problem of moderate E-MCG in the NOGAPS model that apparently contributes to a significant E-MCG event in the GFDN forecast needs to be thoroughly investigated and corrected in both models, especially as this one error source was responsible for 19 of 99 poor GFDN track forecasts (Table 1.3).

3) Case Studies. The Joan (28W) case provides a clear illustration of E-MCG that occurs in both the NOGAPS and GFDN forecasts, but only with sufficient severity in the GFDN model that the track forecast is highly degraded. The Mort (31W) case provides an illustration of E-MCG in which comparatively subtle differences exist in the NOGAPS and GFDN 500-mb wind field forecasts, but very noticeable differences are found in the sea-level pressure forecasts. This characteristic emphasizes the utility of comparing the NOGAPS and GFDN sea-level pressure fields for indications of E-MCG.

a) Typhoon Joan (28W). As listed in Table 4.1, E-MCG was responsible for degrading GFDN track forecasts for Joan over a three-day period. During 19-20 October, the impact of E-MCG on the GFDN track is a very evident as a persistent fast and poleward bias relative to the actual track of Joan. For example, the comparison/verification of the 500-mb wind fields and

NOGAPS and GFDN TC track forecasts initiated 1200 UTC and 1800 UTC 19 October, respectively (Fig. A.26a-l), provides a typical illustration of how this error mechanism degrades the GFDN forecasts. The 66-h GFDN forecast position is far to the northeast of the other model positions, as well as the verifying position of the TC (Fig. A.26a). In the GFDN 500-mb wind forecasts (Fig. A.26j-l), a midlatitude cyclone appears to the northwest of the TC in the 18-h forecast, deepens and moves eastward to a position due north of the TC by 42 h, and then weakens by 66 h. Notice also that in the 66-h forecast the TC is embedded in an elongated wind maximum exceeding 40 kt. In the corresponding NOGAPS 500-mb wind forecasts (Fig. A.26f-h), the midlatitude cyclone is forecast to undergo a similar evolution, and by 72 h the TC is embedded in a wind maximum that is not as strong as in the GFDN forecast (compare Fig. A.26h with A.26l). In the verifying NOGAPS analyses (Fig. A.26b-d), the weaker isotach maximum to the south of the midlatitude cyclone at 1200 UTC 21 October (Fig. A.26c) compared to the corresponding NOGAPS and GFDN forecasts (Fig. A.26g and k, respectively) indicates that weaker cyclone development occurred than in the model forecasts. At 1200 UTC 22 October (Fig. A.26d), the TC is embedded in much weaker midlatitude westerlies than in the corresponding NOGAPS and GFDN forecasts (Fig. A.26h and l, respectively). Notice that the TC structure remains vertically coherent and compact throughout the 72-h forecast period, even though it is embedded in midlatitude westerlies at some distance south of the midlatitude cyclone by 72 h. As discussed in the next two sections, these indications suggest that the TC is not interacting significantly with the midlatitude environment in either the model or in reality. The evolutions depicted by both model forecasts and the verifying analyses are consistent with the conceptual model of MCG causing TC recurvature into the midlatitude westerlies (Fig. 4.1a to b), and that E-MCG has occurred with sufficient severity to degrade the GFDN 72-h forecast.

In the corresponding sea-level pressure fields (Fig. A.27a-l), notice that the midlatitude cyclone to the north of Joan is deeper and extends more equatorward in the GFDN forecast (Fig. A.27j-l) than in the NOGAPS forecast (Fig. A.27f-h), which in turn depict a midlatitude cyclone that is deeper and more extensive than in the verifying NOGAPS analyses (Fig. A.27b-d). As a result, the region between the two cyclones has lower sea-level pressures in the GFDN forecast than in the NOGAPS forecast and in the verifying NOGAPS analyses. Given hydrostatic equilibrium in the 1000 - 500 mb column, significantly lower mid-tropospheric heights, and thus stronger midlatitude westerlies, are expected in the GFDN forecast compared to the NOGAPS forecast and verifying analyses. As described in the analysis of E-RMT in section 3, differences in sea-level pressure between the NOGAPS and GFDN forecasts may serve as an expedient, and highly discernable, indicator that E-MCG is occurring in the GFDN forecast. Given the indications of E-MCG in the GFDN sea-level pressure forecast fields in this case, and that the GFDN 66-h position is a distinct outlier relative to a tight cluster of the positions of the other models (Fig. A.27a), the forecaster would be justified in heavily weighting the official forecast toward a selective consensus that excludes the GFDN forecast. The resultant 72-h forecast position would be a significant improvement over a consensus including all five models.

b) *Typhoon Mort (31W)*. As indicated in Table 4.1, E-MCG was responsible for degrading GFDN track forecasts for Mort over a three-day period. The large 72-h FTEs were a result of a persistent tendency in the GFDN forecasts for a recurvature or stair-step track for Mort, whereas all

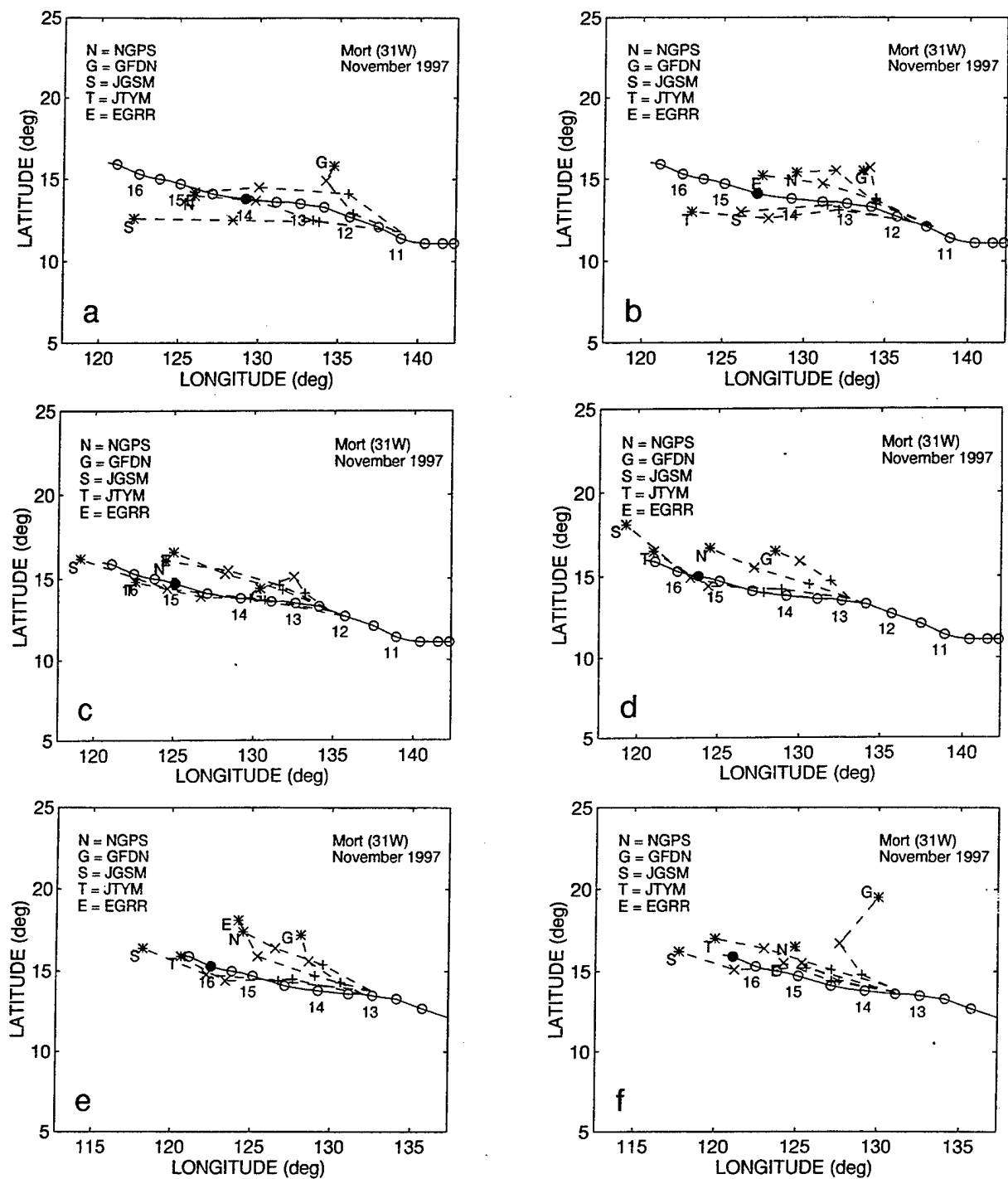


Fig. 4.2. Best-track and selected model track forecasts (see inset) as in Fig. 2.7b, except for TC Mort at (a) 0000 UTC and (b) 1200 UTC 11 November, (c) 0000 UTC and (d) 1200 UTC 12 November, and (e) 0000 UTC and (f) 1200 UTC 13 November 1997.

of the other numerical models forecast a steady west-northwestward motion (Fig. 4.2a-f). Comparisons/verifications of the 500-mb wind and the sea-level pressure fields with the NOGAPS and GFDN TC track forecasts initiated 0000 UTC and 0600 UTC 11 November, respectively, are provided in Fig. A.28a-l and A.29a-l, respectively. Whereas a broad, weak troughing in the midlatitude westerlies is found poleward of Mort in the 42-h GFDN 500-mb wind forecast (Fig. A.28k), no clear troughing or ridging is found in the 48-h NOGAPS 500-mb wind forecast (Fig. A.28g), and in the verifying NOGAPS analysis (Fig. A.28c) there is broad, weak ridging. As a result of these differences, the STR circulations northeast and northwest of Mort are weaker and displaced more equatorward in the GFDN forecast compared to either the NOGAPS forecast or the verifying NOGAPS analysis. These differences among the two model 72-h forecasts and the verifying analysis are greater (compare Fig. 28l,h, and d), although the differences are still subtle. By contrast, the midlatitude low to the north of Mort is quite noticeably deeper in the 66-h GFDN sea-level forecast fields (Fig. A.29k-l) than in the corresponding NOGAPS forecasts (Fig. A.29g-h) or in the verifying NOGAPS analyses (Fig. A.29c-d).² Due to these differences in the development of the midlatitude low, the break in the subtropical ridge to the north of Mort is much larger in the 42-h GFDN track forecast than in the 48-h NOGAPS forecast or verifying analysis (compare Fig. A.29k,g, and c). The weaker STR in the GFDN sea-level pressure is a reflection of a weaker STR throughout the lower troposphere.

Given some indicators of E-MCG in the GFDN sea-level pressure forecast fields, and that the GFDN is the only model predicting recurvature, the forecaster may be justified in excluding the GFDN track from consideration when formulating the official forecast. However, a selective consensus of numerical model tracks that excludes only the GFDN track would be fast and actually be less accurate than a simple consensus of all the numerical models, owing to a very fast track forecast by the JGSM. Without the JGSM digital fields for examination, it is not possible to determine the likely cause of this fast track. In the next subsection, it will be shown that including the steering models and CSUM, which are normally skillful in the TE region, will result in a forecast as good as the simple consensus, which would mitigate the negative influence of the fast JGSM track in the consensus.

4) Impact on other objective guidance. Although E-MCG occurred in only the GFDN model with sufficient severity to result in highly degraded 72-h track forecasts (Tables 1.3 and 4.1), a weak E-MCG was present in the corresponding NOGAPS forecast. This weak E-MCG could potentially degrade the forecast tracks of the steering models and/or CSUM that depend on the NOGAPS forecast fields, even if the NOGAPS track forecast was not significantly degraded. However, track forecasts by these objective techniques for Joan during 19-20 October (Fig. 4.3a-f) and Mort during 11-13 November (Fig. 4.4a-f) provide strong evidence to the contrary. In the case of Joan, the three steering models produced very similar forecasts from 0000 UTC 19 to 1200 UTC 20 October and the consensus of their 72-h positions was highly accurate (Fig. 4.3a-d). Beginning at 0000 UTC 21 October, the FBAM track had a fast bias, whereas the average of the MBAM and

² Although the 0000 UTC 14 November NOGAPS sea-level pressure analysis was missing from the MEL archive from which the model fields illustrated in this report were obtained, the authors have verified independently that the 1004-mb low near 36°N, 146°E in the NOGAPS 72-h forecast field (Fig. A.29h) was significantly (>4 mb) weaker in the verifying NOGAPS analysis.

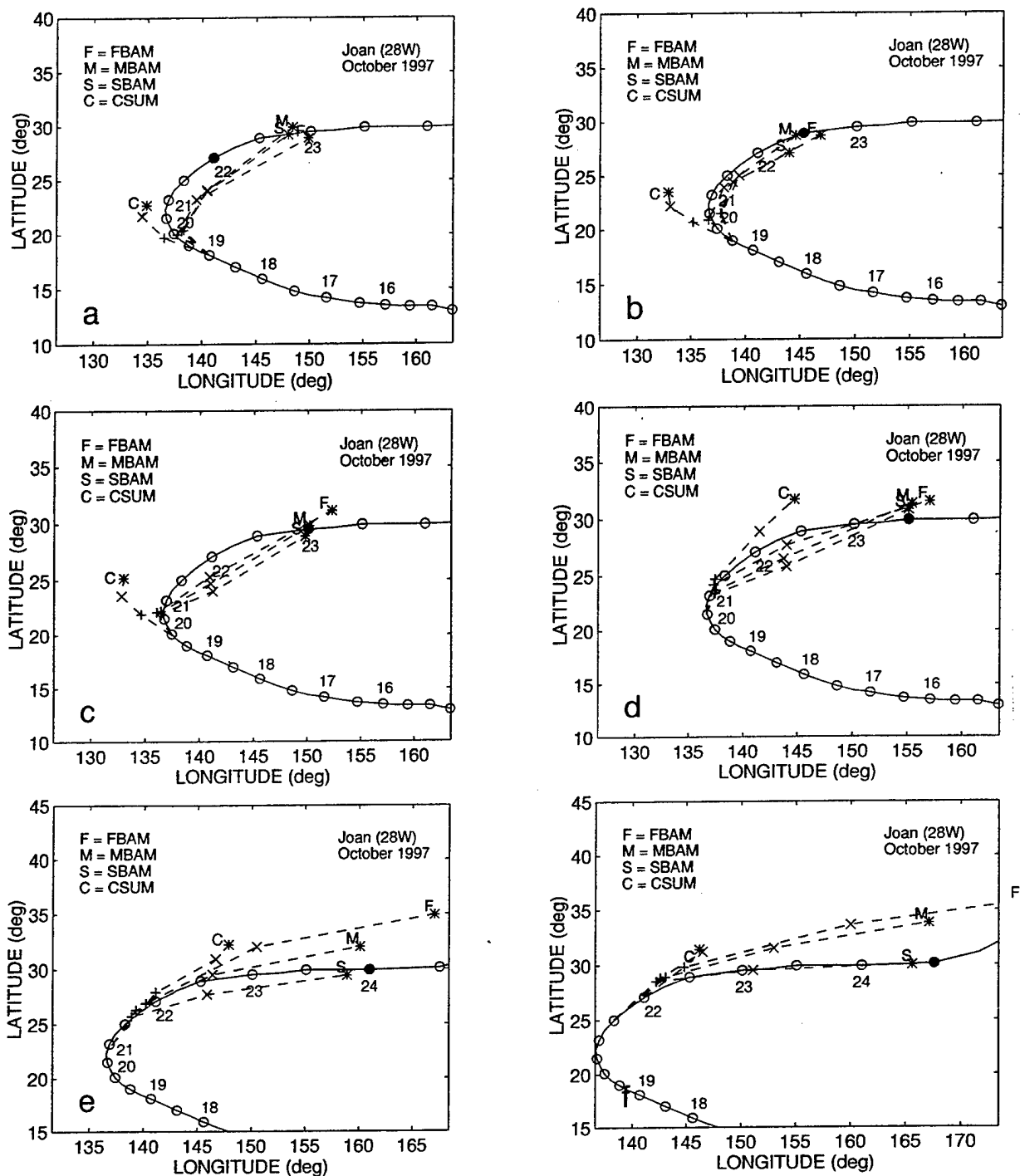


Fig. 4.3. Best-track and selected objective technique tracks (see inset) as in Fig. 2.3, except for TC Joan at (a) 0000 UTC and (b) 1200 UTC 19 October, (c) 0000 UTC and (d) 1200 UTC 20 October, and (e) 0000 UTC and (f) 1200 UTC 21 October 1997.

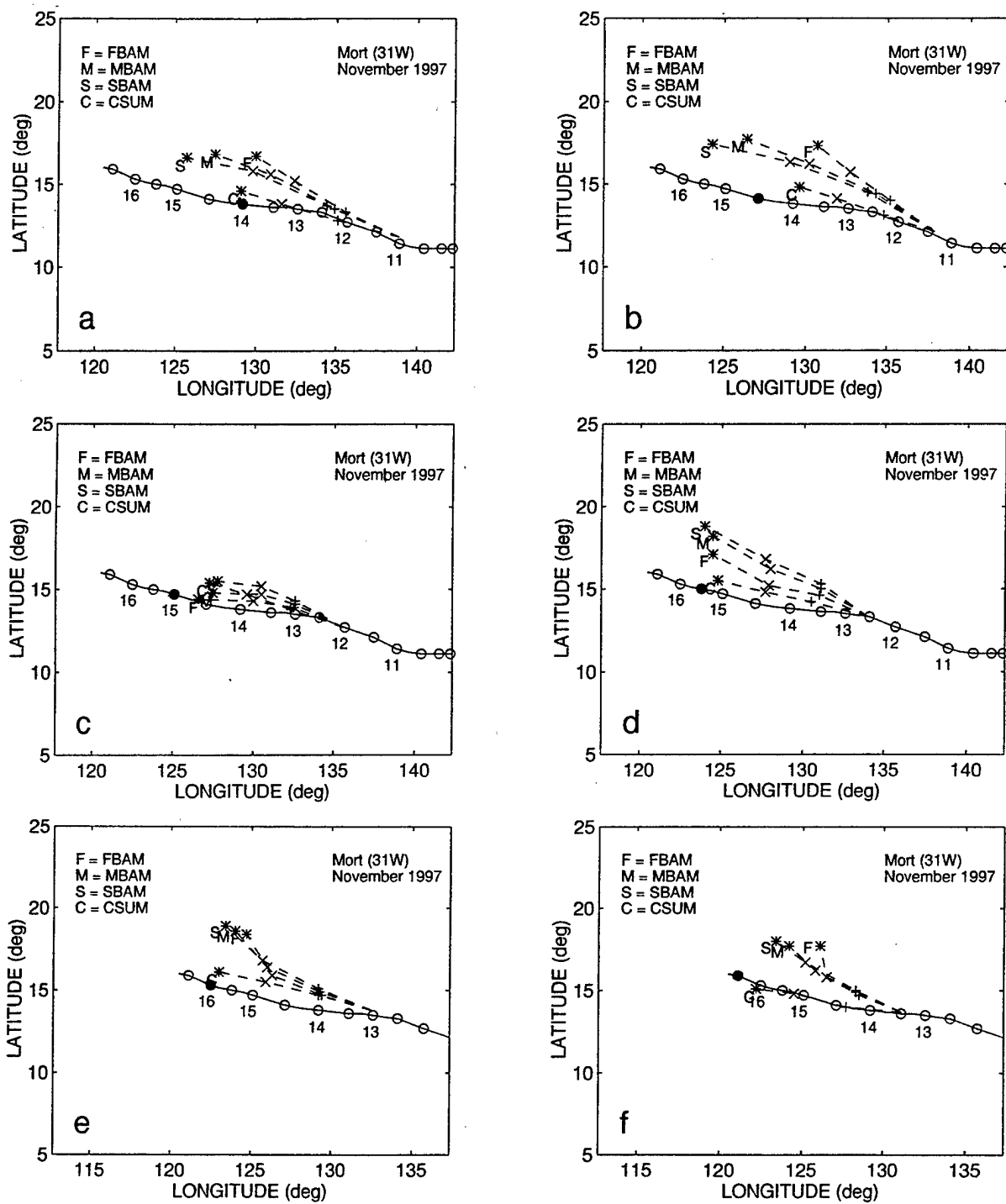


Fig. 4.4. Best-track and selected objective technique tracks (see inset) for TC Mort for same times as in Fig. 4.2

SBAM tracks provided a highly accurate forecast (Fig. 4.3e-f). The increasingly fast bias of the FBAM track is to be expected after the TC recurves since the FBAM uses a 1000-100 mb deep-layer mean wind, which is usually much deeper than the cyclonic circulation of the TC after recurvature. Since the GFDN track forecasts were even faster than the FBAM during 19-20 October, this would tend to rule out I-RVS as the responsible mechanism, and thus support an E-MCG error mechanism assignment. This comparison emphasizes how the three steering models can be used as an important diagnostic tool by the forecaster. By contrast, the CSUM forecasts were consistently slow to recurve Joan, which is not consistent with the fast track biases that should result from the influence of an E-MCG in the NOGAPS forecasts. Rather, the poor performance of the CSUM during the recurvature of Joan is a well-known bias of the model.

In the case of Mort, the CSUM provides highly accurate forecasts for the entire period (Fig. 4.4), which is consistent with the expected skill of this model for straight-moving TCs. A consensus of the SBAM, MBAM, and FBAM steering models has a persistent poleward bias, but no appreciable speed bias until 1200 UTC 13 November (Fig. 4.4f). Although the steering models begin to show signs of impending recurvature after 0000 UTC 13 November, they are not degraded any more than the NOGAPS forecasts, and much less than the GFDN forecasts (Fig. 4.2e-f). Notice also that the track forecasts of the three steering models are very similar throughout the period of Fig. 4.4, which is a useful diagnostic that no significant vertical wind shear is predicted by the NOGAPS model in the vicinity of Mort. This fact tends to confirm that the poor GFDN forecasts were not due to Insufficient Response to Vertical wind Shear (I-RVS), which also can cause false recurvatures when the TC is near the axis of a thin STR. The case study of Typhoon Paka in the next section provides an illustration of vertical shear that is revealed by the three steering models having very dissimilar tracks. In the Paka case, the GFDN false recurvature forecasts (with tracks that are very similar to the false recurvature forecasts in the Mort case) will be attributed to I-RVS. The point is that the spread (or lack of spread) of the SBAM, MBAM, and FBAM tracks provides a clue as to the environmental vertical shear in the NOGAPS forecast, which can help distinguish between track error mechanisms.

5) Summary. Table 4.2 is a summary of the key aspects of the E-MCG phenomenon, which is the only one of the four kinds of MSE to occur with sufficient frequency to permit a meaningful summary of characteristics. The table includes the indications in numerical model fields and tracks, and the impact on various models available to the JTWC forecaster. A key result for the forecaster is that the E-MCG error mechanism is a source of frequent track forecast degradation only in the GFDN model, and when degradation occurs in the GFDN forecast, the NOGAPS track forecast is usually not significantly degraded. Even if the non-U.S. numerical model forecasts are not available, the differences in the NOGAPS and GFDN forecast tracks will be an important clue that a problem is occurring. The key indicator that E-MCG is occurring in the GFDN forecast is excessive deepening (compared to NOGAPS) in the sea-level pressure of a midlatitude low to the north of the TC (Table 4.2; bold type).

Table 4.2 Summary of important aspects and illustration key for the phenomenon of Excessive Midlatitude CycloGenesis (E-MCG).

Aspect	Description	Figure
Conceptual model	Excessive development of a midlatitude trough/cyclone that alters the speed and/or direction of the environmental steering at the location of the TC	4.1a → b
Frequency	5 periods involving 5 TCs, significantly degrading 19 GFDN forecasts, but no NOGAPS forecasts in the western North Pacific during 1997.	Table 4.1 Table 1.3
Environment	Usually in TE region near a weakness in the STR, or in the PF region just north or south of the STR axis.	Table 4.1
Variations of the Phenomenon	<ul style="list-style-type: none"> If the TC is equatorward of the STR axis, E-MCG indirectly alters the steering at the location of the TC by altering the structure of the intervening STR If the TC is poleward of the subtropical ridge, E-MCG directly alters the steering flow at the location of the TC. 	4.1 a→b TC #1 4.1a→b TC #2
Indications in numerical model fields	<p>In 500-mb streamline fields:</p> <ul style="list-style-type: none"> Development of a deeper trough/cyclone in the affected model compared to an unaffected model. This difference is sometimes subtle. <p>In sea-level pressure fields:</p> <ul style="list-style-type: none"> Development of a deeper low in the affected model compared to an unaffected model. This difference is usually quite distinct. 	A.26g-h,k-l A.28g-h,k-l A.27g-h,k-l A.29g-h,k-l
Indications in numerical model tracks	<ul style="list-style-type: none"> Direction and/or speed bias relative to the tracks of non-affected numerical models in a sense that is consistent with location of the E-MCG relative to the TC, and the expected impact on environmental steering. 	A.26a A.28a
Relative impact on numerical models	<ul style="list-style-type: none"> Only GFDN track has been observed to be frequently degraded. E-MCG indications are also present in NOGAPS fields whenever GFDN is degraded, but NOGAPS track suffers little degradation 	4.2
Relative impact on other objective guidance	<ul style="list-style-type: none"> BAMS and CSUM will not normally experience any degradation Actual accuracy of CSUM will depend on synoptic situation. 	4.3 and 4.4 4.3 vs 4.4

b. Response to Vertical wind Shear (RVS)

1. **Description.** A conceptual model of erroneous RVS is given in Fig. 4.5a-d. It is assumed that a significant difference in the vertical depth and the associated intensity exists between the actual TC and model-predicted TC in the presence of vertically-sheared environmental flow (Fig. 4.5b), so that the model representation of the TC will have a different translation speed (Fig. 4.5a). Typically, the difference between the actual and model-depicted vertical structure of the TC tends to become greater with increasing forecast interval (Fig. 4.5d), which results in increasing differences in translation speeds, and thus TC track errors (Fig. 4.5c). Insufficient RVS (I-RVS) is said to be occurring in the model if the model-depicted vertical structure of the TC is too deep and upright (i.e., not tilted) compared to reality, which will result in a track forecast that is too fast. Conversely, Excessive RVS (E-RVS) is said to be occurring in the model if the model-depicted vertical structure of the TC is too shallow and excessively tilted, which will result in a track forecast that is too slow.

Response to Vertical Wind Shear (RVS) Conceptual Model

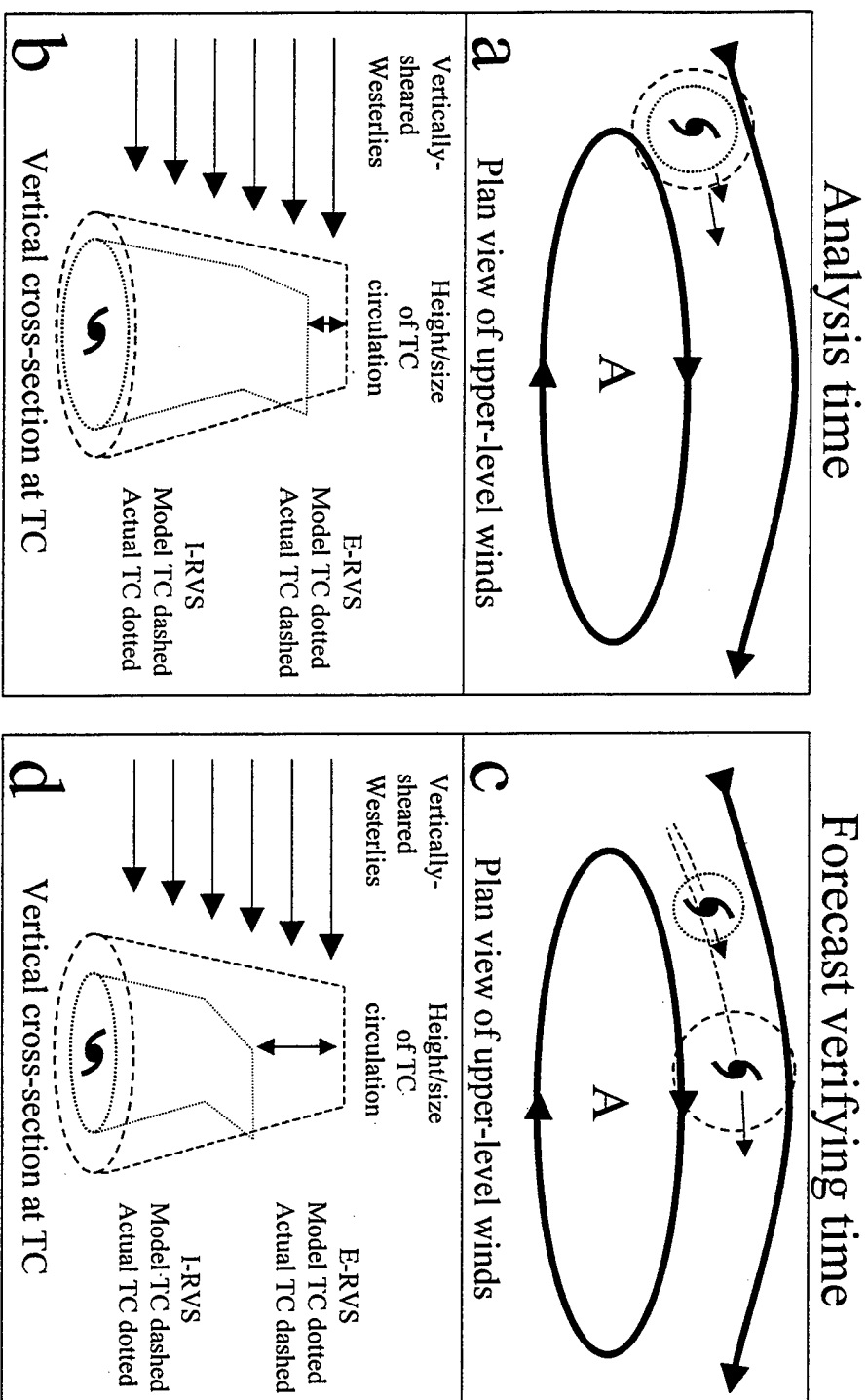


Fig. 4.5. Conceptual model as in Fig. 4.1, except for the Response to Vertical wind Shear (RVS) of a TC in a numerical model. (a). Plan view of the 500-mb environmental flow and (b) vertical cross-section along the vertical wind shear vector through the TC with different vertical (and presumably horizontal) extents in the model and in nature at analysis time. (c)-(d) Corresponding plan view and vertical cross-section at verification time in which excessive RVS (E-RVS) causes the vortex to be too shallow (panel d, dotted) and the track to have a slow bias (panel c, dotted). Insufficient RVE (I-RVS) leads to a vortex that is too deep and a fast track bias (dotted lines in panels (c and d).

Although the depictions of the RVS contain some basic similarities to the MSE conceptual model (e.g., compare TC labeled B in Fig. 4.1a with Fig. 4.5a), the two situations are fundamentally different with regard to the response of the TC structure to the environmental flow. The RVS mechanism is invoked in situations in which differences in the TC structural response to environmental vertical wind shear best explain forecast track differences. The four MSE mechanisms are applied when significant differences in environmental steering, which are not essentially related to the presence of the TC and do not result in TC vertical structure differences, seem to best explain differences in forecast track.

A thorough analysis of either the real or the model TC circulation RVS would require a time-consuming evaluation of multiple levels and cross-sections through both the real and model TC. Such an analysis of the model TC might be difficult to accomplish under the time constraints of operational TC forecasting, and the forecaster does not have access to full-resolution model fields that would better reveal the structure of the TC in the model. In addition, observations of the TC structure are not available in the western North Pacific owing to the lack of aircraft reconnaissance. Thus, it is proposed that an expedient means to infer RVS-induced changes in the vertical structure of the TC is to compare the sea-level pressure forecasts. Assuming hydrostatic equilibrium and thermal wind balance, a positive correlation may be expected between the vertically integrated wind strength and the minimum sea-level pressure of the model TC. This correlation is represented Fig. 4.5b and d in that the TC circulation with less vertical extent has a smaller sea-level pressure pattern (dotted) compared to the TC circulation with more vertical extent (dashed).

2) Frequency and characteristics. Erroneous RVS in the NOGAPS and/or GFDN models resulted in degraded 72-h track forecasts for six TCs in 1997 (Table 4.3, column 1). Although all cases of erroneous RVS during 1997 occurred in the spring or fall (Table 4.3; column 2), the sample is too small to rule out the possibility that the problem is independent of season. With one exception, the TC was in the Poleward Flow (PF) region of either a Standard (S) or Poleward (P) pattern when the erroneous RVS began to occur (Table 4.3; column 3). That is, the TC was in the vicinity of a break in the subtropical ridge. Even though the late season Paka (05C) was still in the Tropical Easterlies (TE) region south of the STR axis (Table 4.3; row 6), the thin meridional extent of the subtropical ridge to the north resulted in exposure to upper-tropospheric southwesterly winds. Excessive RVS (E-RVS) occurred for five of the TCs, and insufficient RVS (I-RVS) occurred in one case (Table 4.3, column 4).

A potentially very useful E-RVS characteristic that leads to highly degraded NOGAPS 72-h FTEs is that the trough that represents the 500-mb circulation of the TC becomes noticeably displaced down-shear of the low-level center in the 48- to 72-h forecast fields (Table 4.3; column 5). When the 500-mb circulation and low-level centers remain closely aligned throughout the forecast period (and no other error mechanism is operative), the NOGAPS track forecast is reasonably accurate. This correlation is clearly illustrated by a comparison of the 48- and 72-h 500-mb NOGAPS forecasts initiated at 0000 UTC and 1200 UTC 19 April and 0000 UTC 20 April 1997 (Fig. 4.6a-b, c-d, and e-f, respectively) with the 72-h FTEs for Typhoon Isa (02W) (Table 4.4). Notice that in the 0000 UTC 19 April NOGAPS forecast fields (Fig. 4.6a-b), the location of the low-level wind center is well-aligned with the location of the 500-mb cyclone or

Table 4.3. Cases of erroneous Response to Vertical wind Shear (RVS) in the western North Pacific during 1997. See Table 2.1 for explanatory footnotes.

TC No	Starting times of Affected model runs ¹	Initial synoptic Environment of affected TC	Character of Response to Vertical Shear	500-mb circulation displaced downshear of low-level center	Models affected	
					JTWC ⁵	Others ⁶
02W	Apr 18/12-20/00	S/PF	Excessive	Yes (48 h, 72 h)	N	
06W	May 29/12-30/00	P/PF	Excessive	Yes (48 h, 72 h)	N,G	S
07W	Jun 12/00	S/PF	Excessive	Yes (48 h)	N	
27W	Oct 21/00-22/12	P/PF → M/MW	Excessive	No	N	E,S,T
29W	Nov 05/00	S/PF	Excessive	Yes (72 h)	N	S
05C	Dec 18/06-19/06	S/TE	Insufficient	No	G	E

Table 4.4. NOGAPS 72-h Forecast Track Error (FTE), Along-Track Error (ATE) and Cross-Track Error (CTE) for the period 18-20 April 1997.

Date/Time (UTC)	72-h FTE (n mi)	72-h ATE (n mi)	72-h CTE (n mi)
970418/0000	179	-83	159
970418/1200	211	-192	86
970419/0000	274	-218	116
970419/1200	502	-473	170
970420/0000	687	-659	194

trough axis at 48 h and 72 h. Although the 72-h FTE for this NOGAPS run is still below 300 n mi (Table 4.4, row 3), a steady increase in 72-h FTE has been occurring in the previous NOGAPS forecasts (Table 4.4; rows 1-2). In the 1200 UTC 19 April NOGAPS forecast fields (Fig. 4.6c-d), the 72-h 500-mb trough axis is clearly displaced down-shear of the low-level center. Similarly, the 500-mb trough axis is clearly displaced down-shear of the low-level center at 48 h and 72 h in the 0000 UTC 20 April forecast fields (Fig. 4.6e-f). The NOGAPS 72-h FTEs for both of these forecasts are well over 300 n mi (Table 4.4; rows 4-5), and represent a dramatic degradation in accuracy compared to the previous three forecasts. Further evidence that the larger NOGAPS 72-h FTEs beginning with the 1200 UTC 18 April forecast are a result of E-RVS is that these errors are primarily a result of large negative (slow) Along-Track Errors (ATE) rather than cross-track errors (Table 4.4; compare columns 3-4). That is, a TC embedded in strong (but nearly uni-directional) midlatitude vertical wind shear that is predicted to have an E-RVS will be too shallow and thus will have a steering flow over a shallower depth. Thus, the predicted motion is slower than for the actual TC, but will be in the same general direction.

Whereas nine NOGAPS forecasts (see list in Table 1.3 and Table 4.3; column 6, rows 1-5) involving five TCs were degraded by E-RVS, only one GFDN forecast was degraded by E-RVS. Only GFDN forecasts were degraded by I-RVS, and all of these forecasts were for Paka (05C in Table 4.3). In four of the six cases in which erroneous RVS degraded the NOGAPS and/or GFDN forecasts, the tracks of JGSM, JTYM, and/or EGRR were similarly degraded (Table 4.3, column 7), which indicates that erroneous RVS may have been responsible.

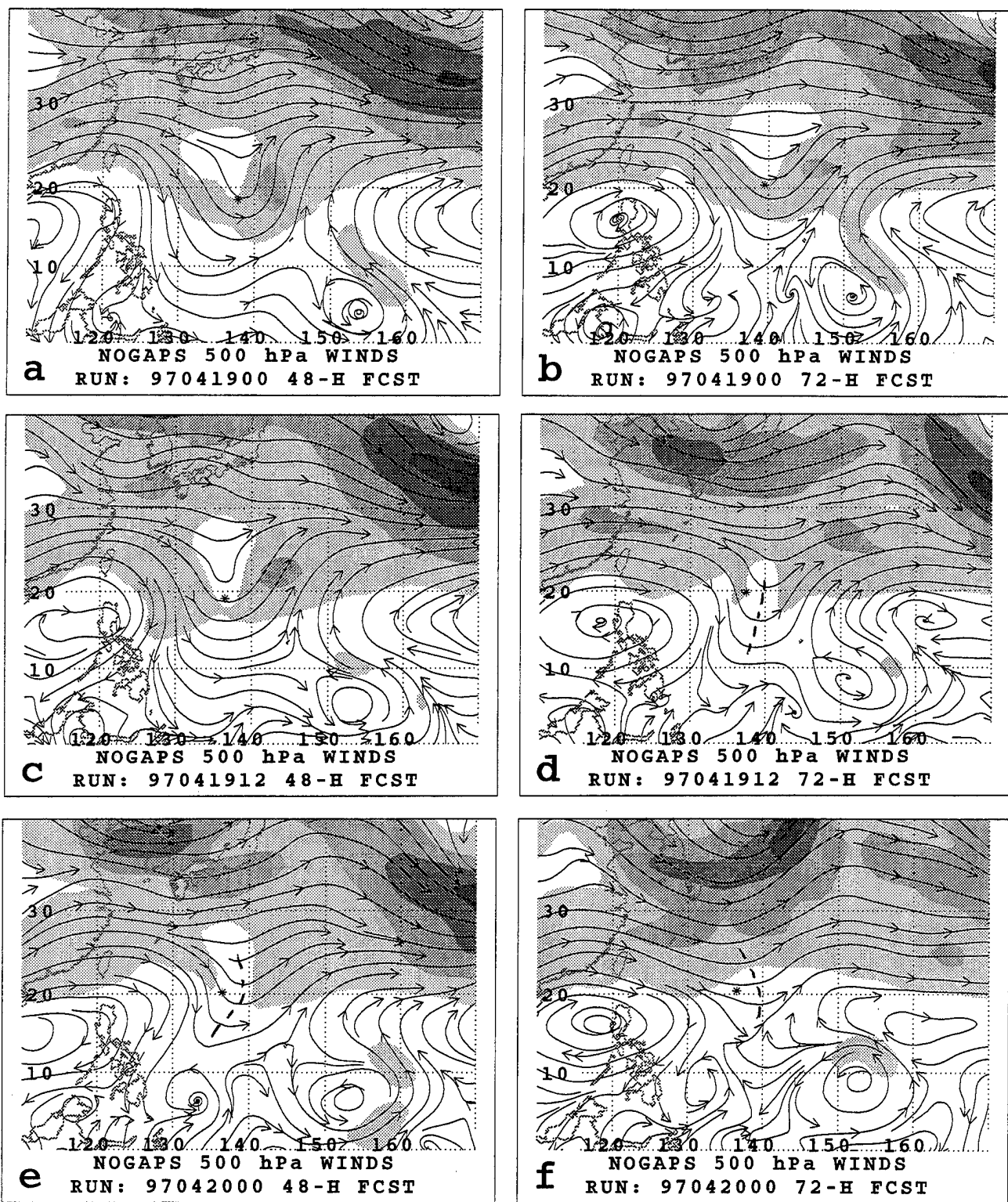


Fig. 4.6. NOGAPS 48- (left column) and 72-h (right column) 500-mb wind forecasts for TC Isa initiated at (a)-(b) 0000 UTC 19 April, (c)-(d) 1200 UTC 19 April, and (e)-(f) 0000 UTC 20 April 1997. Notice that the 500-mb trough (dashed line) is displaced to the east of the low-level center (asterisk) in panels (d) through (f).

3) Case studies. In the Nestor (07W) case, E-RVS significantly degrades the NOGAPS track, but not the GFDN track. The Paka (05C) case illustrates I-RVS causing significant degradation of the GFDN forecast track, but not the NOGAPS forecast.

a) *Typhoon Nestor (07W)*. A comparison/verification of the NOGAPS and GFDN 500-mb wind fields and TC track forecasts initiated 0000 UTC and 0600 UTC 12 June, respectively, is provided in Fig. A.30a-l. Notice that the NOGAPS 72-h position forecast lags far behind the verifying best-track position as well as the GFDN and other numerical model track forecasts (Fig. A.30a). Notice in the 48-h NOGAPS 500-mb forecast field (Fig. A.30g) that the TC appears to be in a trough with an isotach maximum to the east, but the trough axis is several degrees to the east of the 1000-mb wind center (asterisk). In the 72-h NOGAPS forecast field (Fig. A.30h), no distinct 500-mb trough is found above the 1000-mb wind center. In the verifying 48- and 72-h NOGAPS analyses (Fig. A.30c-d), the best-track position (asterisk) is closely aligned with a 500-mb trough axis that has an isotach maximum to the east.³ Satellite infrared images (Fig. 4.7a-d) corresponding to the NOGAPS analysis sequence (Fig. A.26e,b-d) suggest that Nestor maintains an intense, highly organized central convection through the period of the 48-h NOGAPS forecast (Fig. 4.7c). Such an organized convective signature indicates that a coherent vertical structure still exists, and is to be contrasted with the distorted convective cloud mass that occurs when vertical wind shear has destroyed the vertical integrity of the TC (cf. Fig. 4.10c and related text in next subsection). Such differences between the NOGAPS forecasts and verifying analyses and imagery are consistent with the E-RVS conceptual model in Fig. 4.5d in which the dotted circulation represents the model TC and the dashed circulation represents the actual TC.

In the GFDN 500-mb wind forecasts (Fig. A.30j-l), the TC centers (asterisks) are vertically aligned with the 500-mb TC circulation throughout the 66-h period, which is one indicator that E-RVS is not occurring in the GFDN forecast. Actually, the GFDN 42- and 66-h forecasts have a stronger TC vortex (closed cyclones) at 500 mb than in the verifying NOGAPS analyses (only open waves). Although this more intense and vertically coherent vortex structure might indicate the possibility of I-RVS, the accuracy of the GFDN 66-h forecast position (Fig. A.30a) suggests that I-RVS must not be occurring to a significant degree. One interpretation is that the GFDN model is representing the TC structure with sufficient realism to permit an accurate track forecast even in this vertically sheared environmental flow, whereas the TC intensity in the 500-mb NOGAPS analyses is being under-represented because of the 1° lat./long. resolution.

The corresponding NOGAPS and GFDN sea-level pressure fields and TC track forecasts initiated at 0000 UTC and 0600 UTC 12 June, respectively, is provided in Fig. A.31a-l. Notice that the minimum sea-level pressure in the NOGAPS 24-h forecast field (Fig. A.31f) is approximately 8 mb higher than in the verifying analysis (Fig. A.31b), and the NOGAPS 24-h forecast position lags behind the other numerical model forecasts and the actual location of the

³ It should be noted that insertions of synthetic TC observations in the NOGAPS analysis may lead to an under-representation of the vertical tilt of the TC in a vertically sheared environment, since the synthetic observations always specify a vertical structure. The degree of under-representation would depend on the extent to which the objective analysis and data assimilation process accepts the synthetic observations.

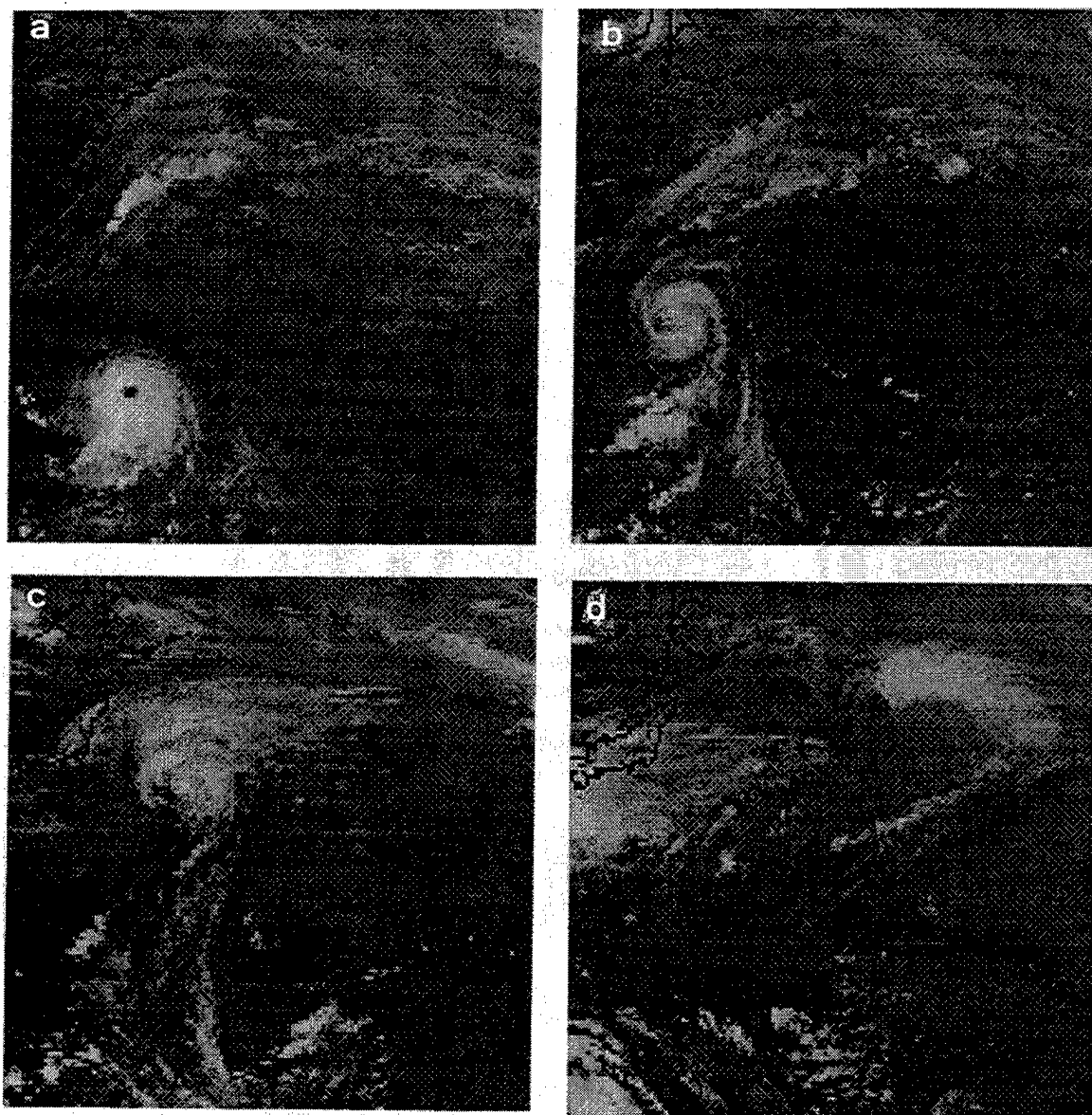


Fig. 4.7. Satellite IR imagery as in Fig. 2.5, except for TC Nestor at 0000 UTC on (a) 12, (b) 13, (c) 14, and (d) 15 June 1997.

TC (Fig. A.31a). Similarly, the minimum sea-level pressure is higher and the outermost closed isobar is lower in the NOGAPS 72-h forecast field (Fig. A.31h) than in the verifying analysis (Fig. A.31d), which is consistent with the lack of a cyclonic circulation for Nestor in the corresponding NOGAPS 500-mb wind forecast (Fig. A.30h). By contrast, Nestor appears as a deep low in the GFDN sea-level pressure forecast (Fig. A.31j-l), which is consistent with the robust cyclonic circulation that appears in the corresponding 500-mb wind forecasts (Fig. A.30j-l).

In summary, the conceptual model in Fig. 4.5 appears to explain the slow NOGAPS track forecasts owing to a weakening and increasingly shallow TC vortex in the presence of vertically-sheared westerlies. By contrast, the GFDN model maintains an intense and vertically-deep TC vortex that moves more quickly in response to a deeper layer of westerlies. Whereas these verifying analyses would not be available in real-time, the forecaster would be able to compare the NOGAPS and GFDN sea-level pressure forecasts for Nestor discussed above with those initiated 12 h earlier (see Fig. A.4e-h and i-l). Such a comparison would reveal that the later GFDN forecast has a sea-level pressure evolution that is very similar to the earlier run, and has a consistent track in that the 66-h forecast position is northeast of the 66-h position from the 12 h earlier forecast (Fig. 4.8). By contrast, the later NOGAPS 72-h minimum sea-level pressure forecast is dramatically weaker than in the earlier 72-h forecast, and the 72-h position is several degrees to the southwest of the 72-h position from the earlier run. Such a change over 12 h is a “flag” to the forecaster that at least one of the NOGAPS track forecasts may be highly erroneous. This is an example in which the “outlier” NOGAPS track forecast in Fig. A.31a may be identified to have anomalously changed over just 12 h. The highly dissimilar sea-level pressure evolutions in the two NOGAPS forecasts, and the important indicator of an eastward displaced 500-mb trough relative to the low-level center position would provide the forecaster with sufficient justification to invoke the E-RVS conceptual model (Fig. 4.5) and discount the NOGAPS track forecast in Fig. A.31a. Since the two GFDN forecasts are consistently grouped with several other numerical models (compare Fig. A.4a and Fig. A.31a), a selective consensus excluding the NOGAPS forecast and only involving the models that agree with the GFDN track is likely to be the best basis for the official track forecast.

b) Typhoon Paka (05C). Whereas the GFDN track forecasts from 0000 UTC 18 to 1200 UTC 19 December 1997 (Fig. 4.9a-d) consistently predict that the TC will recurve, the other numerical models forecast a continued westward movement, except for one recurvature forecast by the UKMO (EGRR) model (Fig. 4.9d). The actual TC continues to move steadily west-northwest until 20 December when a quasi-stationary west-northwest motion ensues. Satellite infrared imagery during 19-22 December (Fig. 4.10a-f) reveal the reason for the translation deceleration. As the convective cloud mass of the TC weakens in response to vertical wind shear (Fig. 4.10a-d), the cloud mass is advected down-shear, which leaves the completely exposed low-level circulation more than 5° lat. up-shear at 1200 UTC 21 December (Fig. 4.10e). The effect of the separation of the deep convective cloud mass and upper-level circulation from the low-level circulation is to lower significantly the effective steering level of the TC, so that the motion depends more on weaker lower-tropospheric winds rather than the strong jet-level winds. The interpretation is that the I-RVS conceptual model (Fig. 4.5) is applicable here, in that the GFDN model erroneously recurved Paka because the predicted TC circulation in this high-resolution model was too deep and vertically coherent. Conversely, the more accurate NOGAPS track would suggest that a more representative RVS occurred in that model.

To confirm this I-RVS interpretation for the GFDN forecast, a comparison/verification of the NOGAPS and GFDN 500-mb and 850-mb wind fields and TC track forecasts initiated at 0000 UTC and 0600 UTC 19 December, respectively, are provided in Fig. A.32a-l and Fig. A.33a-l, respectively. Notice that a nearly closed cyclone still appears in the 42-h 500-mb GFDN wind forecast (Fig. A.32k) over the low-level center, and that west-southwesterly environmental winds are impinging on the TC. The change in the GFDN forecast track from a poleward to a northeast-

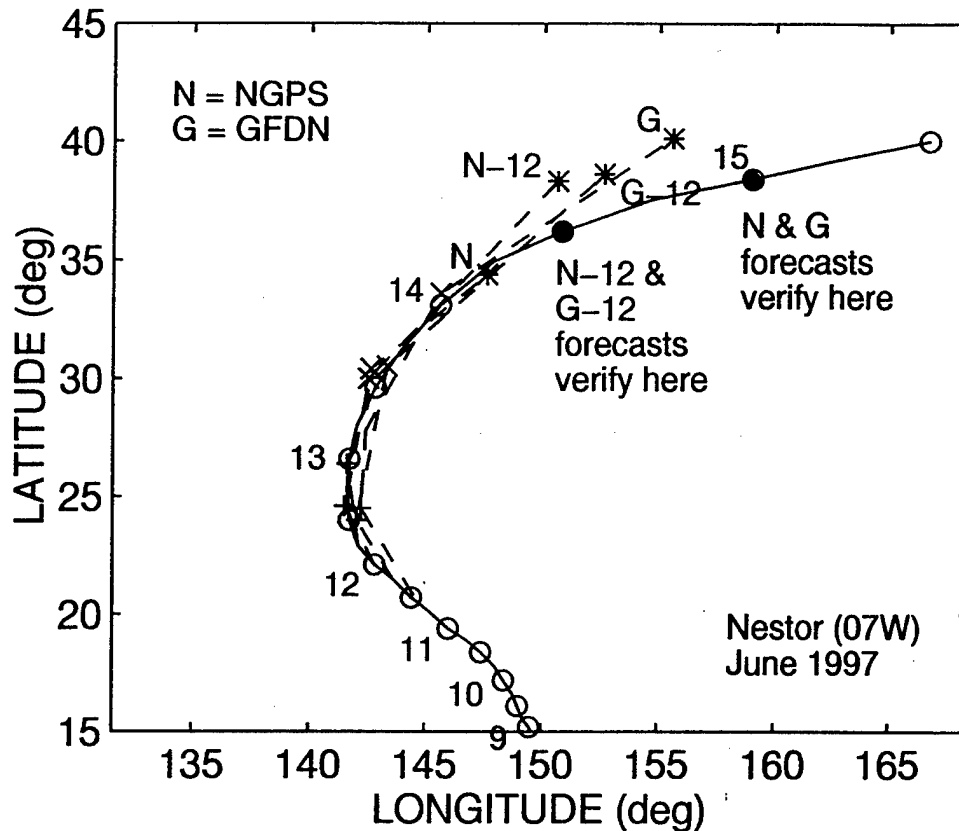


Fig. 4.8. Best-track and two sets of NOGAPS and GFDN track forecasts where N-12 refers to an initial time of 1200 UTC 11 June and N initial time is 0000 UTC 12 June 1997. Similarly, the G-12 initial time is at 1800 UTC 11 June and the G initial time is at 0600 UTC 12 June 1997.

ward direction at 42 h (Fig. A.32a) is strong evidence that the effective steering level of the model TC is still near 500 mb at that time in the model integration. In the corresponding 48-h NOGAPS 500-mb wind forecast (Fig. A.32g), only a weak 500-mb trough is evident, and the displacement of the trough down-shear of the low-level center is an indicator that the upper-level TC circulation is now decoupled. The steady west-northwest NOGAPS track through 48 h (Fig. A.32a) indicates that the effective steering level in the NOGAPS model has been much lower in the troposphere. That the TC in the NOGAPS model is responding more to lower-tropospheric steering until at least 48 h in the integration is supported by the NOGAPS 850-mb wind forecast fields (Fig. A.33f-h) that have the TC in easterly flow around the subtropical anticyclone cell to the north (Fig. A.33g). Even though the 18-h GFDN 850-mb wind forecast (Fig. A.33j) also has a weak anticyclone to the north of the TC, the predicted TC track is almost due north from 18 h to 42 h (Fig. A.33a). This discrepancy between the direction of low-level steering and the track of the TC in the GFDN model supports the hypothesis that the motion of the TC is heavily influenced by upper-level environmental steering.

Although the verifying 0000 UTC 21 December NOGAPS analysis (Fig. A.32c) for the two forecasts has a 500-mb cyclone directly over the low-level center, recall that the insertion of synthetic observations into the NOGAPS data assimilation cycle can force a potentially unrealistic vertical structure in the initial conditions. However, satellite imagery at 0000 UTC 21 December (Fig. 4.10c) has a highly distorted convective cloud mass that is indicative of a

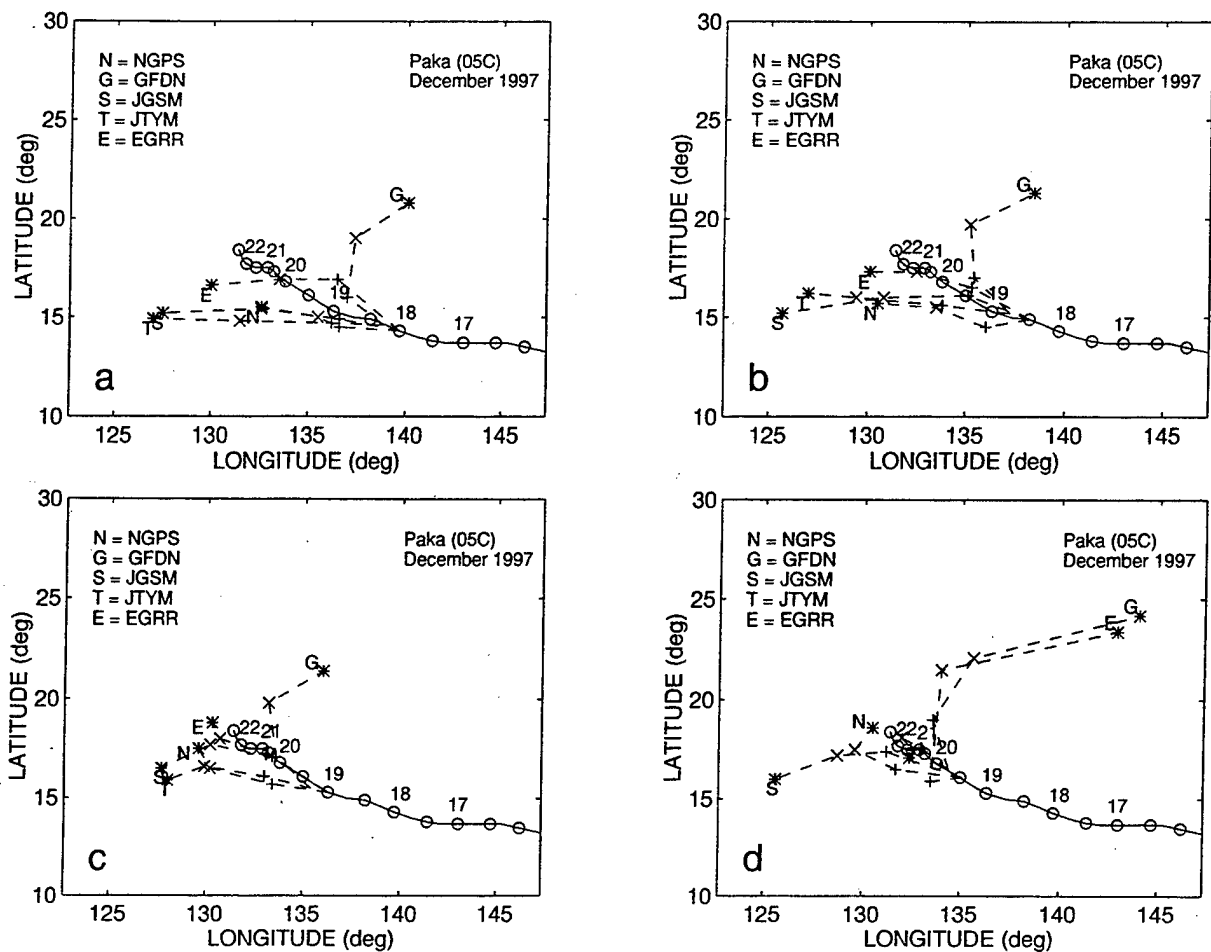


Fig. 4.9. Best-track and selected model track forecasts (see inset) as in Fig. 2.7b, except for TC Paka at (a) 0000 UTC and (b) 1200 UTC 18 December, and (c) 0000 UTC and (d) 1200 UTC 19 December 1997.

partially exposed low-level circulation, and the imagery 12 h later (Fig. 4.10e) reveals a fully exposed low-level circulation. Thus, a reasonable conclusion is that in this NOGAPS forecast the RVS was sufficiently representative of the actual situation to result in a 72-h FTE of less than 300 n mi. By contrast, the GFDN forecast appears to have been affected by I-RVS, which resulted in a large 72-h FTE.

4. Impact on other objective guidance. Since the RVS conceptual model in Fig. 4.5 should be applied to situations in which the interior TC structure responds to the environmental wind shear influence without necessarily altering the environment, it should be expected that objective techniques that depend on the NOGAPS forecast of the environment will not be significantly degraded by an erroneous RVS in the NOGAPS forecast. Since the three steering model tracks reflect the NOGAPS representation of the steering over different depths,⁴ differences in the three 72-h forecast positions provide a useful indication of the average

⁴ 1000-100mb for FBAM; 850-300mb for MBAM; and 850-700mb for SBAM.

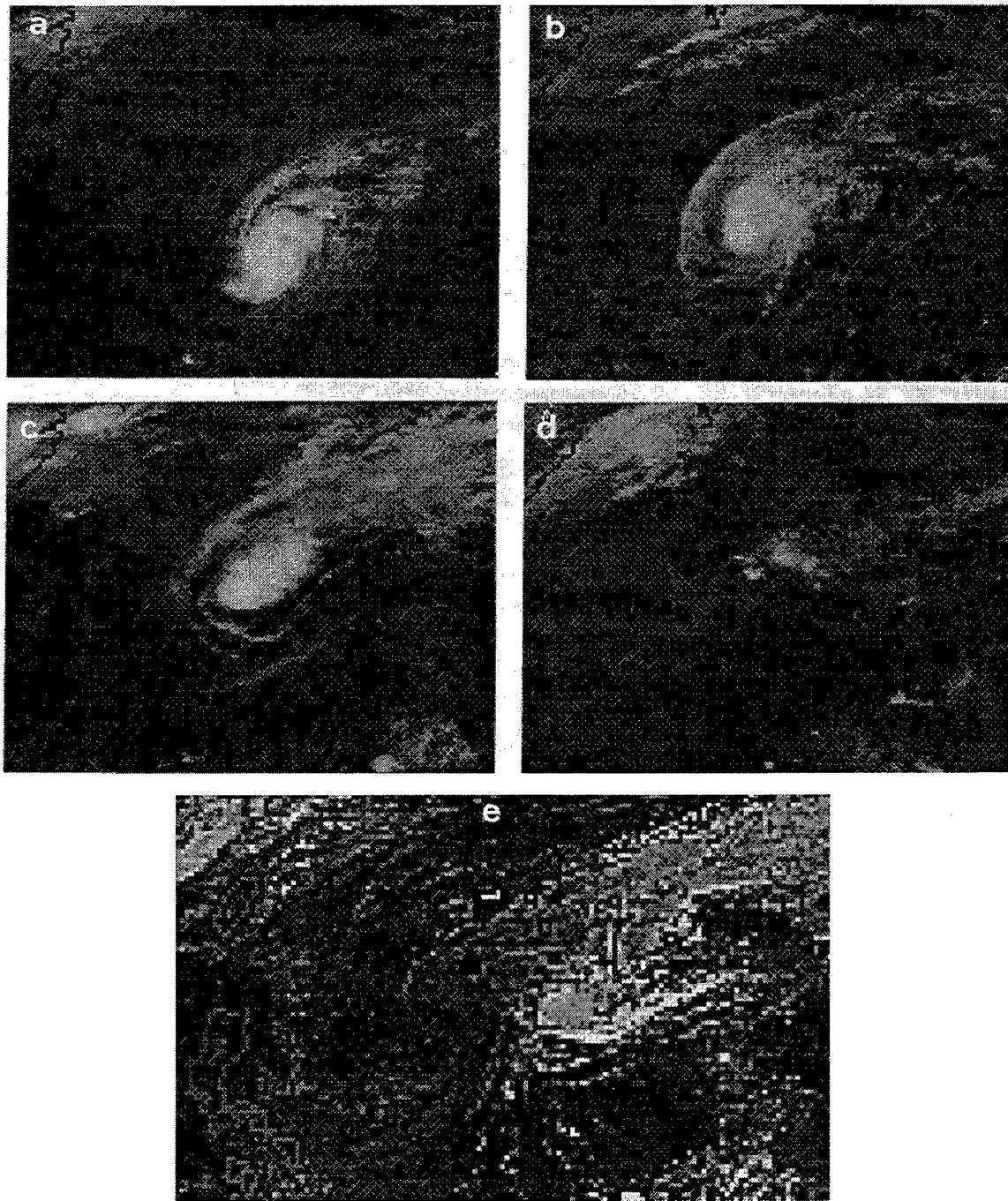


Fig. 4.10. Satellite IR imagery as in Fig. 2.5, except for TC Paka at 0000 UTC on (a) 19, (b) 20, (c) 21, and (d) 22 December 1997. (e) An enhancement of the 1200 UTC 21 December image to illustrate the low-level center of Paka after the vertical decoupling has occurred.

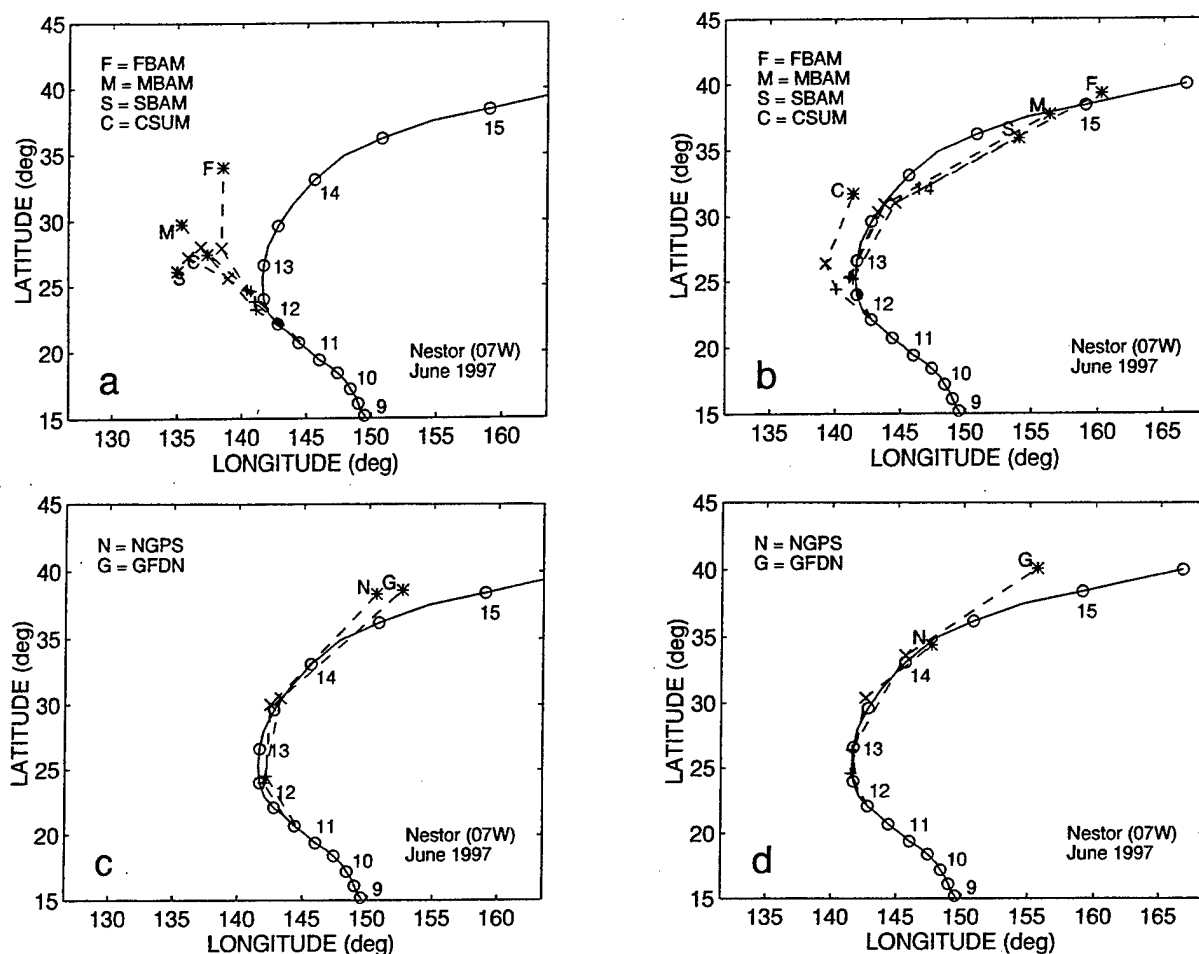


Fig. 4.11. Best-track and (a)-(b) selected objective technique and (c)-(d) NOGAPS and GFDN track forecasts (see insets) for TC Nestor at (a)-(c) 1200 UTC 11 June and (b)-(d) 0000 UTC 12 June 1997.

direction and magnitude of environmental vertical wind shear during the 72-h forecast period. In the case of TC Nestor, the spreads of the 72-h positions are similar and not particularly large for the 1200 UTC 11 June and 0000 UTC 12 June steering model forecasts (Fig. 4.11a and b, respectively). The northeastward progression of the two corresponding GFDN 66-h forecast positions (Fig. 4.11c-d) is consistent with the temporal steadiness of the vertical wind shear implied by the steering models, whereas the large westward displacement of the second NOGAPS forecast relative to the first forecast is not. Thus, evaluation of the magnitude and variation of the environmental shear in this case supports the conclusion that it is likely the slow NOGAPS track forecast in Fig. 4.11d that is erroneous (due to E-RVS) than the more rapid GFDN track forecast (due to I-RVS). Also, the modest magnitude of unidirectional vertical wind shear in this TC Nestor case also would seem to be unlikely to produce a sudden shear-induced separation of the convective cloud mass from the low-level circulation.

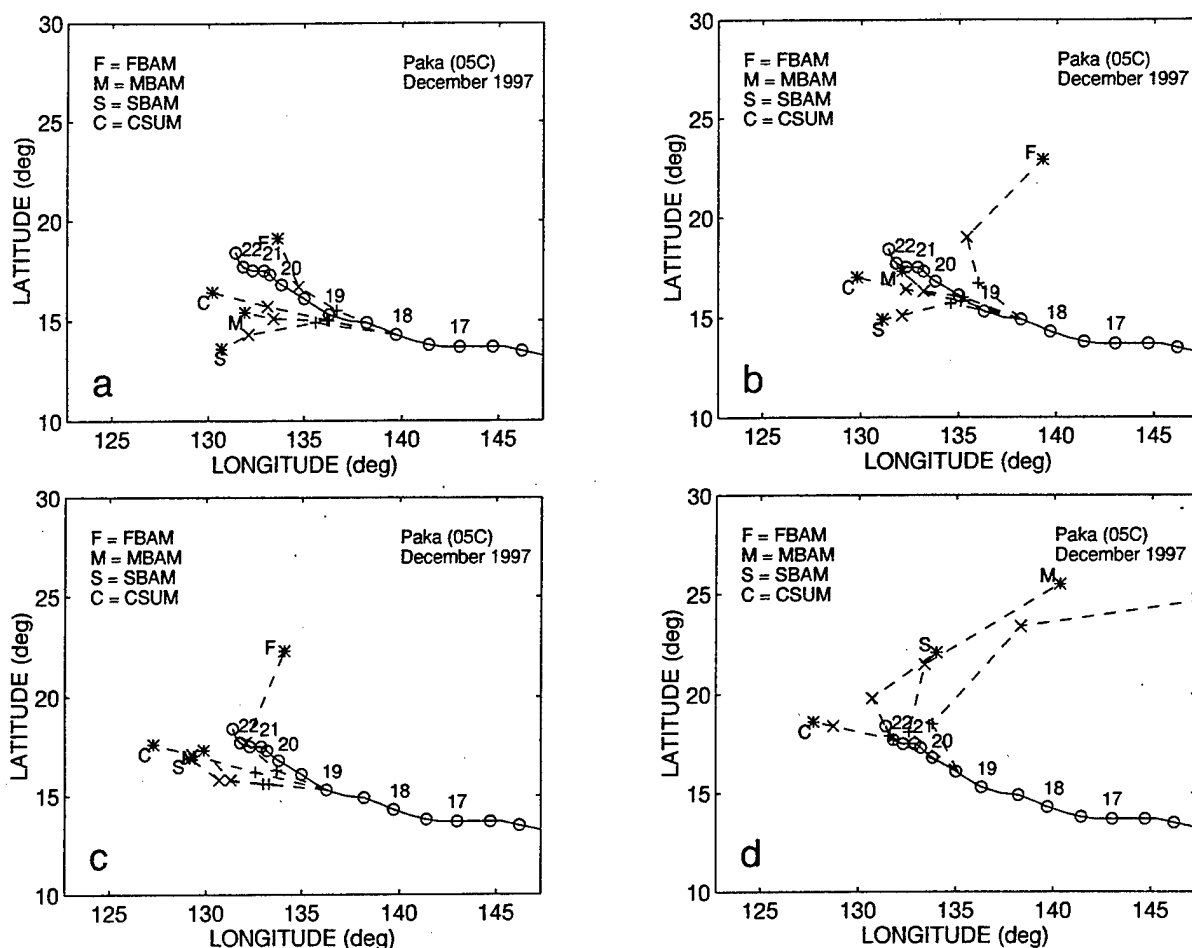


Fig. 4.12. Best-track and selected objective technique tracks (see inset) for Paka at (a) 0000 UTC and (b) 1200 UTC 18 December, and (c) 0000 UTC and 1200 UTC 19 December 1997.

In the Paka case, the magnitude of vertical wind shear implied by the spread in the three steering model forecasts increases dramatically from 0000 UTC 18 to 0000 UTC 19 December (Fig. 4.12a-c) and from 1200 UTC 18 to 1200 UTC 19 December (Fig. 4.12b-d).⁵ The dramatic increases in spread are consistent with the fact that Paka did shear apart and dissipate (and did not recurve). These indications of environmental vertical wind shear that may be inferred from the spread in the three steering model forecasts should be investigated as an indicator of whether or not the TC will be sheared apart.

5. Summary. Table 4.5 is a summary of the key aspects of the E-RVS phenomenon. The I-RVS did not occur with sufficient frequency to permit a similar summary of characteristics. The table includes the indications in numerical model fields and tracks, and the impacts on various models available to the JTWC forecaster. A key result for the forecaster is that the E-RVS error mechanism is a recurring source of degradation only in the NOGAPS forecasts, whereas only one GFDN forecast during 1997 was degraded by E-RVS. Thus, even if other

⁵ Comparisons of forecasts that are 24 h apart are used since there appears to be a clear diurnal variation in the magnitude of the wind shear.

Table 4.5. Summary of important aspects and illustration key for the phenomenon of Excessive Response to Vertical wind Shear (E-RVS).

Aspect	Description	Figure
Conceptual model	Excessive weakening and shallowing of the TC in response to vertical wind shear in the midlatitude environment, which results in the TC moving in response to an excessively shallow steering layer.	4.5
Frequency	5 periods involving 5 TCs, significantly degrading 9 NOGAPS forecasts, but only 1 GFDN forecast in the western North Pacific during 1997.	Table 4.3 Table 1.3
Environment	TC usually in PF region just north or south of STR axis at start of model integration.	Table 4.3
Indications in numerical model fields	<p>In 500-mb streamline fields:</p> <ul style="list-style-type: none"> Displacement of 500-mb circulation of TC (usually a trough) several degrees down-shear of low-level center at 48 h to 72 h in model integration. <p>In sea-level pressure fields:</p> <ul style="list-style-type: none"> Increase in minimum sea-level pressure in model TC to 1000 mb or more by 72 h. 	4.6, A.30g A.31h
Indications in numerical model tracks	<ul style="list-style-type: none"> Significant slow speed, but typically little directional bias, relative to tracks of unaffected numerical models. 	A.30a
Relative impact on numerical models	<ul style="list-style-type: none"> NOGAPS usually degraded, but not GFDN. Other global models occasionally degraded, but not JTYM 	4.3
Relative impact on other objective guidance	<ul style="list-style-type: none"> BAMS usually not affected. Accuracy of each BAM depends on what steering layer the TC is responding to; FBAM is usually too fast once initial position of TC is north of STR axis. CSUM usually slow until after recurvature due to inherent bias, but not due to E-RVS in the NOGAPS. 	4.11b 4.11b

numerical model forecasts are not available, the differences in the NOGAPS and GFDN forecast tracks will be an important clue that a problem is occurring. The key indicator that E-RVS is occurring in the NOGAPS is displacement of the 500-mb TC circulation several degrees longitude down-shear of the low-level center when no such displacement occurs in the GFDN forecast (Table 4.5; bold type). In addition, the spread in the three steering model forecasts provides indications of the magnitude of vertical wind shear in the NOGAPS forecast. Additional study is required to determine if vertical shear implied by the steering model tracks can be used to infer the likelihood of a severe RVS of the actual TC.

c. Baroclinic Cyclone Interaction

1. Description. Erroneous Baroclinic Cyclone Interaction (BCI) in the numerical model is said to occur when extratropical transition is either over- or under-predicted such that a significant TC track error results (Fig. 4.13). In a potential extratropical transition scenario, the TC is in the vicinity of the mid-tropospheric subtropical ridge axis with a midlatitude trough to the north or northwest, and an upper-tropospheric jet maximum is to the northeast of the TC (Fig 4.13a). The right entrance (or left exit) region of the jet maximum has an enhanced upper-

tropospheric divergence that tends to produce corresponding areas of lower-tropospheric convergence and cyclogenesis that may appear to accelerate the TC northeastward toward the location of maximum cyclogenetic tendency (Fig. 4.13b). Concurrently, poleward (equatorward) flow on the east (west) side of the TC in the presence of a large-scale meridional temperature gradient results in warm (cold) temperature advection (Fig. 4.13b) that may amplify the upper-level trough/ridge pattern via a process called self-amplification or self-development (Fig. 4.13c). To the extent that the TC becomes constructively aligned with a midlatitude area of baroclinic cyclogenesis, significant deepening occurs and the TC undergoing extratropical transition develops frontal characteristics (Fig. 4.13d). Since the lower-tropospheric warm and cold temperature advection (Fig. 4.13b) affects the structure of the mid-tropospheric winds that steer the TC, a vigorous BCI event may have a significant impact on the TC track (Fig. 4.13d; see arrows). Typically, the greater the deepening of the TC that is undergoing extratropical transition, the more poleward will be the track owing to the BCI-induced amplification of the mid-tropospheric ridge to the northeast of the TC. However, the BCI process can result in various combinations of direction and speed changes depending on the tilt of the midlatitude trough and the orientation of the midlatitude trough relative to the TC. Excessive BCI (E-BCI) is said to occur when the extratropical transition process occurs more vigorously (or falsely) in the model compared to reality. Conversely, Insufficient BCI (I-BCI) is considered to occur when the extratropical transition process occurs less vigorously (or not at all) in the model compared to reality.

2. Frequency and characteristics. Erroneous BCI in the NOGAPS and/or GFDN models resulted in degraded 72-h track forecasts for 11 TCs during 1997 (Table 4.6, column 1), so that erroneous BCI is second only to E-DCI (see Table 2.1) in terms of number of TCs affected. Recall from Table 1.3 that this BCI degraded 20 NOGAPS forecasts and 13 GFDN forecasts, which makes BCI the second most frequent error mechanism in NOGAPS (after E-DCI) and third most frequent in GFDN (after E-DCI and E-MCG). With the exception of only two TCs, the TC was in, or transitioning from, the Poleward Flow (PF) region of either a Standard (S) or Poleward (P) synoptic pattern (Table 4.6; column 3). Periods of both I-BCI and E-BCI occurred at different times in the life cycles for seven TCs (Table 4.6; column 4). For five of the fourteen cases, indications of an erroneous RVS event preceded the period of erroneous BCI such that the RVS contributed to the severity of the erroneous BCI (Table 4.6; column 5). This connection between the RVS and BCI is to be expected since the baroclinity of the midlatitude environment that enables baroclinic development is also associated with vertical wind shear. For three of the TCs, track errors caused by Midlatitude System Evolutions (MSE) led to a situation that then contributed to erroneous BCI. In terms of number of TCs affected, I-BCI degraded the NOGAPS forecasts much more often than the GFDN forecasts (Table 4.6; column 6, rows 1-7). However, the occurrences of E-BCI were more even between the models (Table 4.6; column 6, rows 8-14). In six of the 14 cases in which erroneous BCI degraded the NOGAPS and/or GFDN forecasts, the JGSM, JTYM, and/or EGRR tracks were similarly degraded, which suggests that erroneous BCI may have been responsible (Table 4.6; column 7). The reader is reminded that separate analysis of tracks from these other models might identify BCI-affected cases for which the NOGAPS and GFDN forecasts were not also degraded.

Baroclinic Cyclone Interaction (BCI)

Conceptual Model

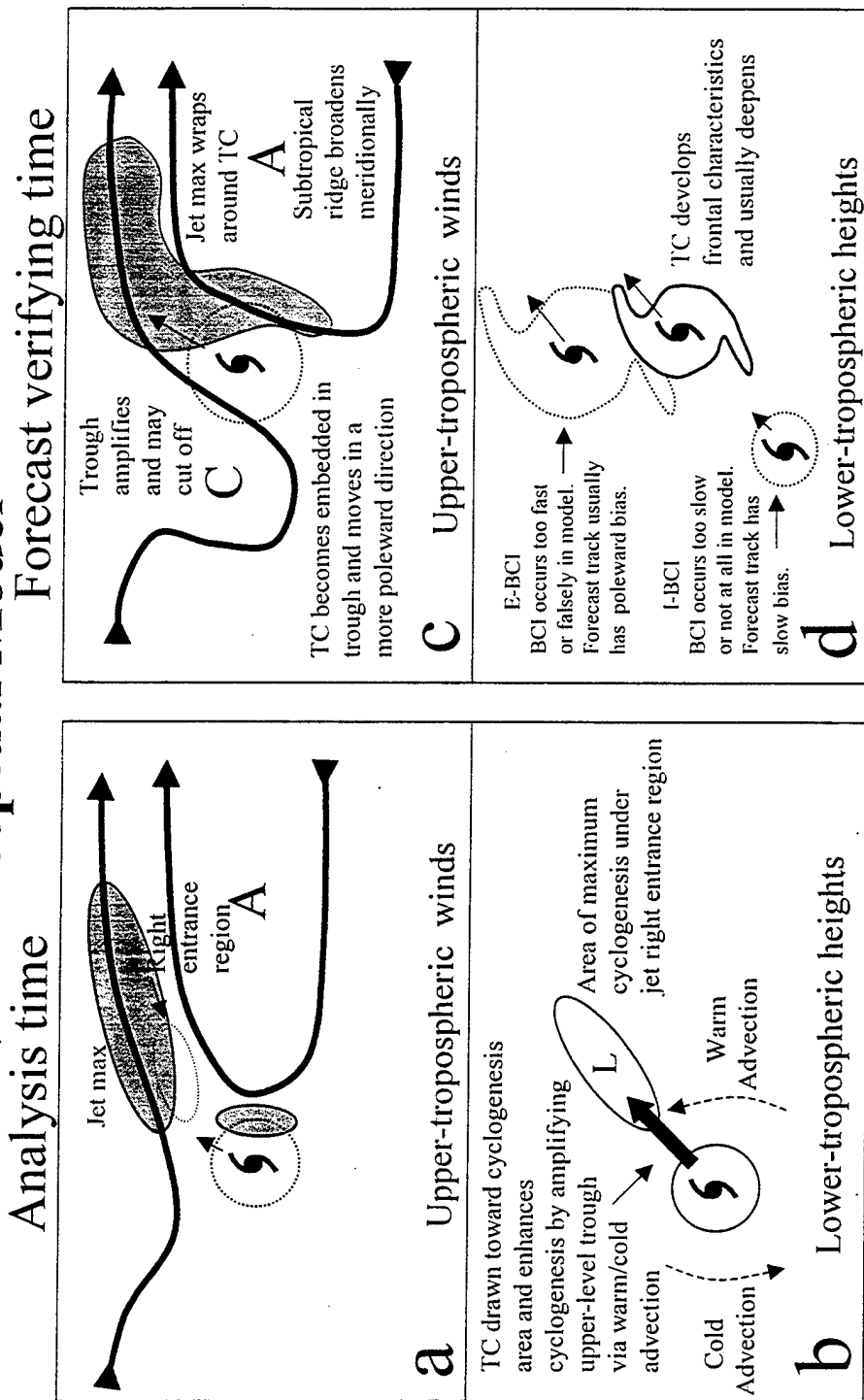


Fig. 4.13. Schematics of two stages of Baroclinic Cyclone Interaction with a recurving TC that is potentially undergoing extratropical transition. Because the TC circulation has not been included, the blending of the environment flow (heavy streamlines) with the TC (dotted circle) in panel c would wrap around the TC. Modifications in the lower tropospheric thermal structure (panels b and d) lead to changes in the environmental steering of the TC (panel c). Excessive BCI usually results in a more poleward track bias and insufficient BCI results in a slow track bias (panel d).

Table 4.6. Cases of erroneous Baroclinic Cyclone Interaction (BCI) in the western North Pacific during 1997. See Table 2.1 for explanatory footnotes.

TC No	Starting times of Affected model runs ¹	Initial synoptic Environment of affected TC	Character of baroclinic interaction	Indications of contributing error mechanisms	Models affected	
					JTWC ⁵	Others ⁶
09W	Jun 26/00-27/00	P/PF	Insufficient	E-RVS	N	S,T,E
12W	Aug 06/00-07/00	P/PF	Insufficient	I-MCG	N	(S)
15W	Aug 19/00-20/12	P/PF	Insufficient	E-RVS (NOGAPS)	N,G	S,E,T
19W	Sep 02/12	P/PF	Insufficient	None	N	
21W	Sep 16/00-17/00	S/TE	Insufficient	None	G (N)	
24W	Sep 26/00-26/12	P/PF S/TE	Insufficient	None	N	S,E,T
29W	Nov 05/12-06/00	S/PF → M/PF	Insufficient	E-RVS	N	
07W	Jun 12/12	S/PF	Excessive	None	N	
09W	Jun 27/06	P/PF	Excessive	I-RVS & E-MCG	G	
10W	Jul 25/18-26/06	P/PF S/TE	Excessive	I-RVS	N,G	
19W	Sep 02/18-03/00	P/PF → M/PF	Excessive	E-MCG	G,N	
23W	Sep 21/00-21/12	S/TE	Excessive	None	N	
28W	Oct 21/12-22/18	P/PF → M/PF	Excessive	None	G,N	T,E
29W	Nov 04/18-06/18	S/PF → M/PF	Excessive	I-RVS	G	T,E

From the perspective of the forecaster attempting to discern whether one or both of two dissimilar numerical model forecast tracks is degraded by I-BCI or E-BCI, the distribution of degraded GFDN and NOGAPS forecasts in Table 4.6 does not look particularly promising. For example, the double entries for 09W, 19W, and 29W indicate instances of GFDN forecasts that have been degraded by E-BCI, whereas the preceding NOGAPS forecast was degraded by E-BCI. Moreover, in the case of 19W, a NOGAPS forecast that was degraded by I-BCI was immediately followed by a forecast degraded by E-BCI (Table 4.6; compare column 6 for the two 19W entries). These instances indicate that the BCI process is highly sensitive to the forecast TC structure and its environment, which includes both the approaching midlatitude trough/ridge and the subtropical ridge. Thus, multiple interactions are potentially affecting the TC evolution and track, which suggests that the predictability of BCI is low. Such knowledge is still useful to the forecaster. For example, it may be advisable that when the forecaster discerns that BCI is occurring to widely varying degrees in most or all of the models, it may be more difficult in this case to establish that an outlier should be eliminated. The fallback strategy may be to base the official forecast on a simple consensus of all of the models, instead of a selective consensus based on any one cluster of tracks. The accompanying prognostic reasoning message should indicate that more than one scenario is possible depending on the outcome of the potential BCI event that involves the TC, the subtropical anticyclone, and the midlatitude circulation. In addition to the most likely scenario, an alternate scenario should be described with an indication of what features should be monitored to decide which scenario is developing. The following case studies illustrate some of this BCI variability and the magnitudes of large FTEs that are possible.

3. Case studies. In the Peter (09W) case, the NOGAPS track forecast is degraded during a 48-h period because E-RVS occurs and this leads to I-BCI, whereas only one GFDN track forecast is degraded because E-MCG (and likely I-RVS) occurs that leads to E-BCI. The Yule

(15W) case shows how the sensitivity of the BCI process can result in poor temporal continuity of consecutive numerical model forecasts depending on the degree to which the TC and midlatitude system interact. Both the Peter and Yule cases illustrate the complexity of the inter-related processes, the range of predicted outcomes, and thus the difficulty of forecasting scenarios that involve real or predicted BCI.

a) *Typhoon Peter (09W)*. A comparison/verification of the NOGAPS and GFDN sea-level pressure (500-mb wind) fields and TC track forecasts initiated at 0000 UTC and 0600 UTC 27 June, respectively, is provided in Fig. A.34a-l (Fig. A.35a-l). Both the NOGAPS 72-h and the GFDN 66-h position forecasts lag behind the verifying best-track position. In the NOGAPS sea-level pressure analyses of 1200 UTC 28 June and 0000 UTC 29 June (Fig. A.34b and c), midlatitude cyclogenesis occurs to the northeast of the TC, which generates a low pressure area that overlaps the TC and is manifest by an elongation of the isobar pattern toward the area of cyclogenesis. A merger of the two systems has occurred in the 0000 UTC 30 June NOGAPS analysis (Fig. A.34d), since the isobar pattern of Peter is again symmetric. Notice also that significant deepening has occurred from 29 to 30 June. The cyclogenesis appears to be in response to a midlatitude trough with an associated 500-mb jet maximum to the northeast of the TC near 38°N, 143°E at 0000 UTC 27 June (Fig. A.35e). In the NOGAPS 500-mb wind analyses (Fig. A.35e, b-d), the TC becomes embedded in the jet maximum and the maximum wraps around the southeast periphery of the TC. Notice that the strength of the 500-mb midlatitude cyclone increases significantly from 29 June (panel c) to 30 June (panel d). These NOGAPS analyses of sea-level pressure and 500-mb wind are consistent with the Baroclinic Cyclone Interaction (BCI) conceptual model (Fig. 4.13). Satellite infrared imagery from 1200 UTC 27 to 0000 UTC 30 June (Fig. 4.14a-f) confirms that an extratropical transition of Typhoon Peter actually took place, with the cloud pattern acquiring distinct frontal characteristics at 1200 UTC 29 June (Fig. 4.14e).

In the NOGAPS sea-level pressure forecasts (Fig. A.34f-h), low-level cyclogenesis occurs to the northeast of Peter (panel f), and Peter and the low-level cyclone then appear to form an elongated trough (panel g). However, the mid-latitude low is forecast (panel h) to develop significantly separate from Peter, which drifts slowly eastward rather than becoming part of the developing midlatitude cyclone. Notice that in the NOGAPS 48-h forecast of sea-level pressure (panel g) neither the TC nor the low pressure area to the northeast are as deep as in verifying analysis (panel c). Whereas the interaction of the TC and the jet maximum in the NOGAPS 500-mb wind forecasts (Fig. A.35f-h) is qualitatively similar to the verifying analyses (Fig. A.35b-d), the forecast development for the midlatitude cyclone at 72 h (panel h) is clearly less than in the verifying analysis (panel d). These evolutions in the NOGAPS forecasts of sea-level pressure and 500-mb wind are consistent with the conceptual model of Insufficient BCI (I-BCI) in Fig. 4.13d. Notice that the minimum sea-level pressure for Peter is weaker in the NOGAPS 36-h forecast (Fig. A.34f) than in the verifying analysis (Fig. A.34b). In addition, the area of +40-kt winds at 500 mb that is present to the southeast of Peter in the verifying analysis (Fig. A.35b) is absent in the 36-h forecast (Fig. A.35f). Both of these differences indicate that the TC is too weak in the NOGAPS forecast. Since at this point in the forecast the TC is beginning to recurve, E-RVS appears to be occurring in NOGAPS, which results in a slow motion bias that probably contributes to I-BCI later in the 72-h forecast period (as noted in Table 4.6; row 1, column 5).

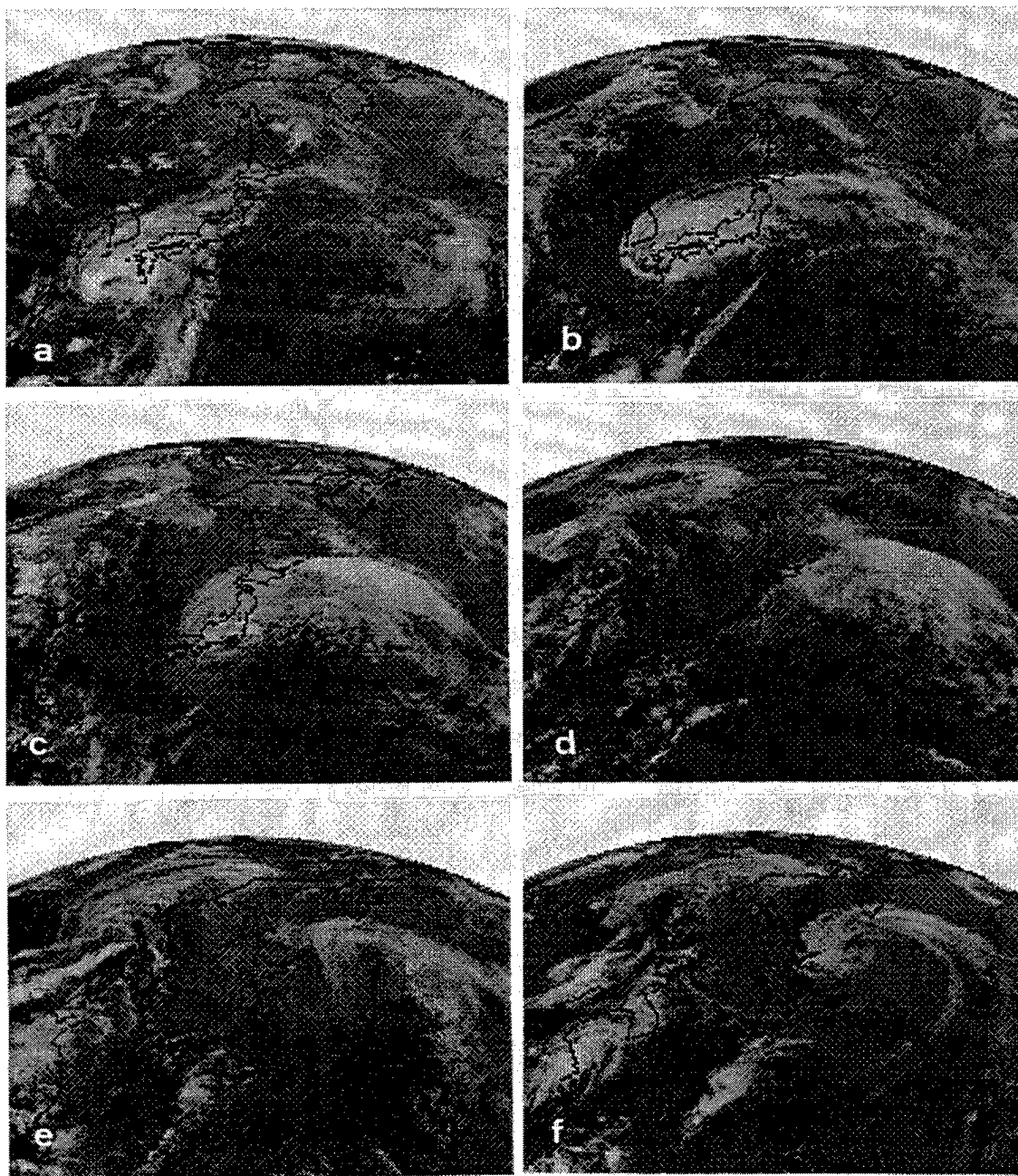


Fig. 4.14. Satellite IR imagery as in Fig. 4.2, except for TC Peter at (a) 1200 UTC 27 June, (b) 0000 UTC and (c) 1200 UTC 28 June, (d) 0000 UTC and (d) 1200 UTC 29 June, and (f) 0000 UTC 30 June 1997.

In the GFDN sea-level pressure forecasts (Fig. A.34j-l), interaction of the TC and the low-level cyclone occurs at a faster rate than in the NOGAPS forecasts or in the verifying analyses. Whereas the locations of the midlatitude low and the TC can still be distinguished in the NOGAPS 48-h forecast (panel g) and the verifying analysis (panel c), the cyclones seem to have completely merged in the GFDN 42-h forecast (panel k). The resultant cyclone in the GFDN 66-h forecast is larger and deeper than in either the NOGAPS 72-h forecast (panel h) or the verifying analysis (panel d). This evolution in the GFDN forecast is consistent with the conceptual model of Excessive BCI (E-BCI) depicted in Fig. 4.13d. Notice that the lobe of low sea-level pressures 10°-15° long. to the northeast of Peter is deeper and more extensive in the GFDN 30-h forecast (Fig. A.34j) than in either the NOGAPS 36-h forecast (Fig. A.34f) or the NOGAPS verifying analysis (Fig. A.34b). Thus, it appears that E-MCG occurs early in the GFDN forecast, which then contributes to E-BCI later in integration (as noted in Table 4.6; row 9, column 5).

Whereas the NOGAPS track forecasts initiated from 0000 UTC 26 to 1200 UTC 27 June (Fig. 4.15a-d) were consistently and highly degraded by I-BCI, the response of the other numerical models was variable. Although the 0600 UTC 27 June GFDN forecast track was moderately degraded (note the longitudinal scale is small in this case) by E-BCI, the subsequent forecast was very accurate (Fig. 4.15c and d, respectively). Based on similarities in the forecast tracks, the other three non-U.S. numerical models appeared to be highly degraded by BCI on 0000 UTC and 1200 UTC 26 June (Fig. 4.15a-b). At 0000 UTC 27 June (Fig. 4.15c), the JGSM and EGRR tracks improve dramatically, but the JTYM track remains degraded in a similar manner to the NOGAPS track. As with the JGSM track earlier, the JTYM track forecast on 1200 UTC 27 June is a dramatic improvement (Fig. 4.15d). Such variability in the track forecast accuracy of all the models highlights the inherent complexity and probable low predictability of the extratropical transition process.

b) *Typhoon Yule (15W)*. Whereas I-BCI is listed in Table 4.6 as the cause of highly degraded numerical model track forecasts initiated over a 48-h period from 0000 UTC 19 to 1200 UTC 20 August 1997, Table 1.1 (Table 1.2) lists only two (one) time(s) early in that period when the NOGAPS (GFDN) track was degraded. The longer period listed in Table 4.6 accounts for variability in the performance of the NOGAPS and GFDN models as well as clear indications that the other numerical model tracks were also being sporadically degraded by I-BCI (Fig. 4.16a-d). For example, the 0600 UTC 19 August GFDN forecast track was accurate and faster than all other model tracks (Fig. 4.16a), but 12 h later was inaccurate and slower than all other model tracks (Fig. 4.16b). However, the following two GFDN forecasts (Fig. 4.16c-d) are only slightly slow with 72-h FTEs that are much less than 300 n mi. Other indications of non-consistent behavior include the slow JGSM and JTYM track forecasts for 0000 UTC 20 August (Fig. 4.16c) that dramatically improve for 1200 UTC 20 August (Fig. 4.16d). Also, the UKMO model track (EGRR) was slow at 0000 UTC 19 August (Fig. 4.16a) and then was poleward of the verifying positions on 20 August (Fig. 4.16c-d). Satellite infrared imagery during 19-24 August (Fig. 4.17a-f) shows that Yule underwent a vigorous interaction with a midlatitude system that resulted in extratropical transition into a deep low that JTWC estimated to have 65-kt sustained winds.

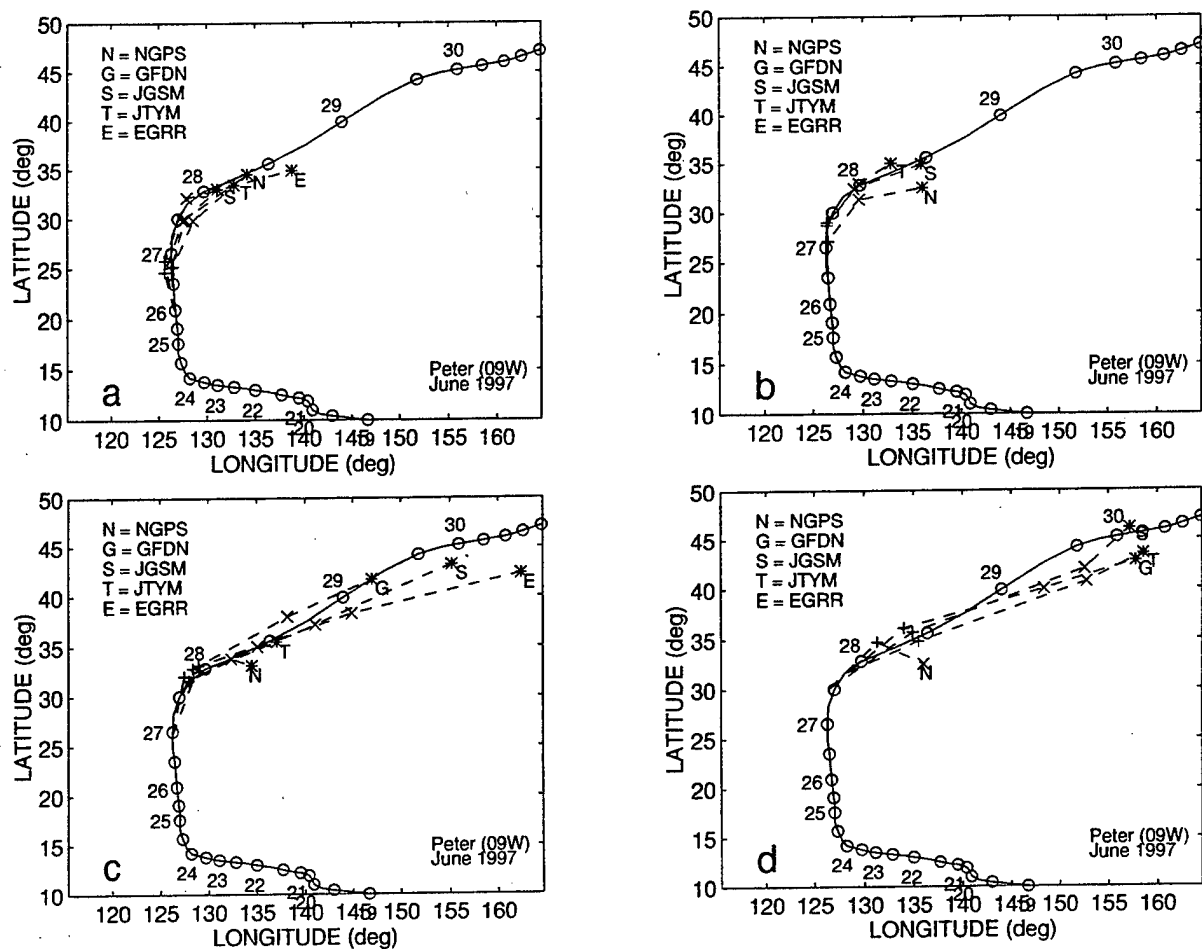


Fig. 4.15. Best-track and selected model track forecast (see inset) as in Fig. 2.7b, except for TC Peter at (a) 0000 UTC and (b) 1200 UTC 26 June, and (c) 0000 UTC and (d) 1200 UTC 27 June 1997.

A comparison/verification of the NOGAPS and GFDN sea-level pressure (500-mb wind) fields and TC track forecasts initiated at 1200 UTC and 1800 UTC 19 August 1997, respectively, in Fig. A.36a-l (Fig. A.37a-l) illustrates a case when both the NOGAPS and GFDN forecasts were poor. In the 48- and 72-h NOGAPS and GFDN forecasts, midlatitude cyclogenesis is manifest as an area of troughing that extends north-northeast of the TC in the sea-level pressure fields (Fig. A.36g-h and k-l, respectively). Midlatitude cyclogenesis is also evident in the verifying 1200 UTC 22 August sea-level pressure analysis (Fig. A.36d) as an apparent interaction of the TC with the midlatitude system. In the corresponding NOGAPS 500-mb wind analyses (Fig. A.37c-d), the TC becomes increasingly embedded in the poleward flow southeast of the developing midlatitude cyclone, which explains the significant poleward acceleration of TC Yule after 1200 UTC 21 August (Fig. A.37a). By contrast, even though the TC again appears to become embedded in an upper-level cyclone in both the NOGAPS and GFDN 500-mb wind forecasts (Fig. A.37h and l, respectively), apparently the interaction was not sufficiently vigorous to accelerate the TC poleward. Thus, both NOGAPS and GFDN track forecasts appear to have been degraded by I-BCI according to the conceptual model in Fig. 4.13. A reasonable explanation for the I-BCI in the NOGAPS forecast is that E-RVS (acting as a contributing error mechanism) resulted in a 24-h forecast of minimum sea-level pressure that is 8 mb higher than in

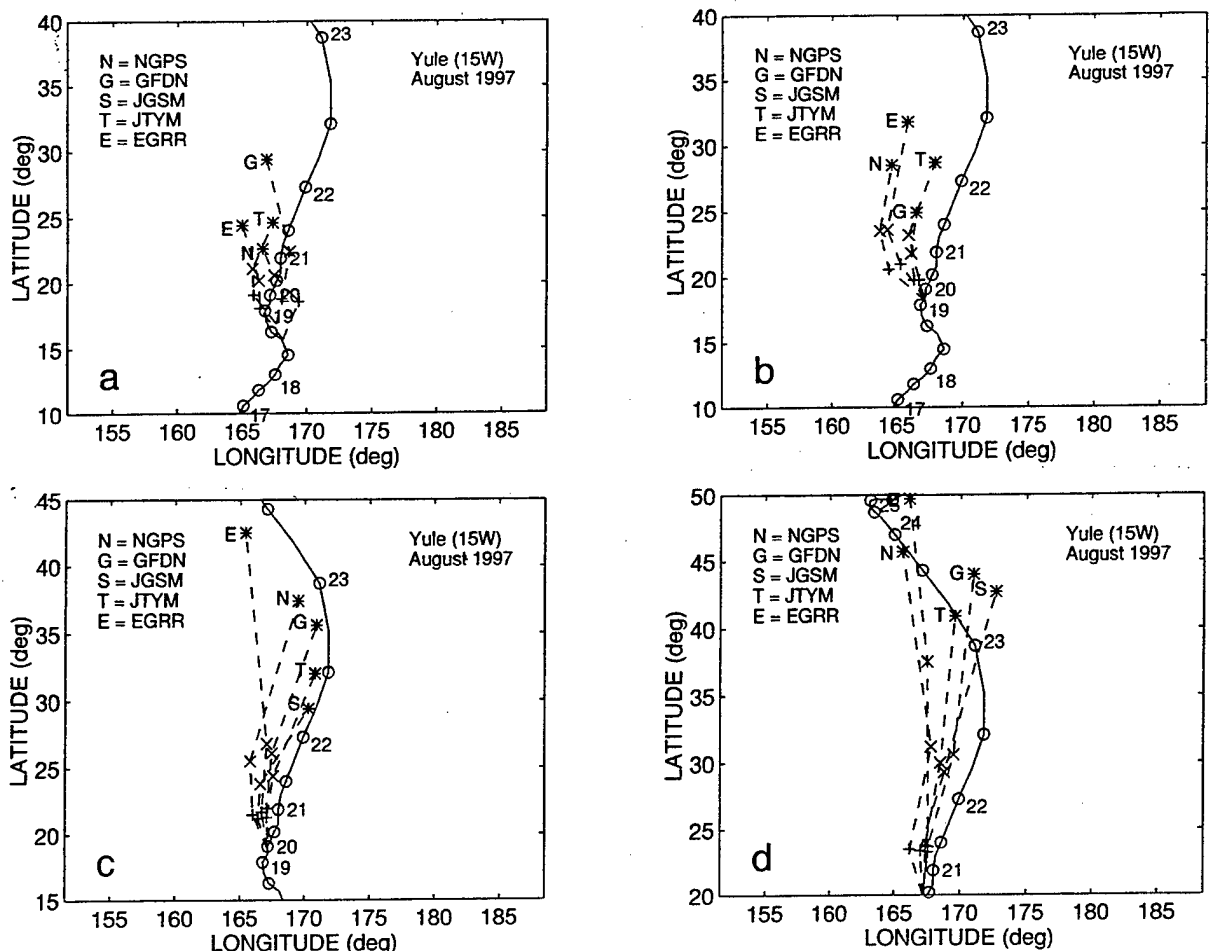


Fig. 4.16. Best-track and selected model track forecasts (see inset) as in Fig. 2.7b, except for TC Yule at (a) 0000 UTC and (b) 1200 UTC 19 August, and (c) 0000 UTC and (d) 1200 UTC 20 August 1997.

the verifying NOGAPS analysis (compare Fig. A.36f and b). As a result of the weaker and less vertically extensive TC circulation, the NOGAPS track forecast has a slow bias that apparently keeps the TC from being translated to a position relative to the midlatitude system for vigorous baroclinic interaction to occur. However, the GFDN forecast of the TC maintains a very deep sea-level low (Fig. A.36j-l) and strong a cyclone at 500 mb (Fig. A.37j-l), which preclude assigning E-RVS as a contributing error mechanism. Moreover, the upper-level cyclone into which the TC becomes embedded in the GFDN forecast looks very similar to the corresponding NOGAPS forecast and verifying analyses. Apparently some very subtle errors in GFDN with regard to the evolution of the TC, midlatitude cyclone, and/or their interaction was responsible for the I-BCI.

A comparison/verification of the NOGAPS and GFDN sea-level pressure (500-mb wind) fields and TC track forecasts initiated at 0000 UTC and 0600 UTC 20 August 1997, respectively, in Fig. A.38a-l (Fig. A39a-l) illustrates a period when both the NOGAPS and GFDN models had accurate forecasts. In the 24-h and 48-h NOGAPS sea-level pressure forecasts (Fig. A.38f-g), the minimum pressure of the TC is again predicted to be much higher than in the verifying analyses (Fig. A.38b-c), and seems to be the cause of a equatorward forecast track bias at 48 h (Fig. A.38a). Nevertheless, the TC interacts sufficiently with the midlatitude cyclogenesis to overcome the slow track bias at 48 h and merge with the midlatitude cyclone by 72 h (Fig. A.38h). The

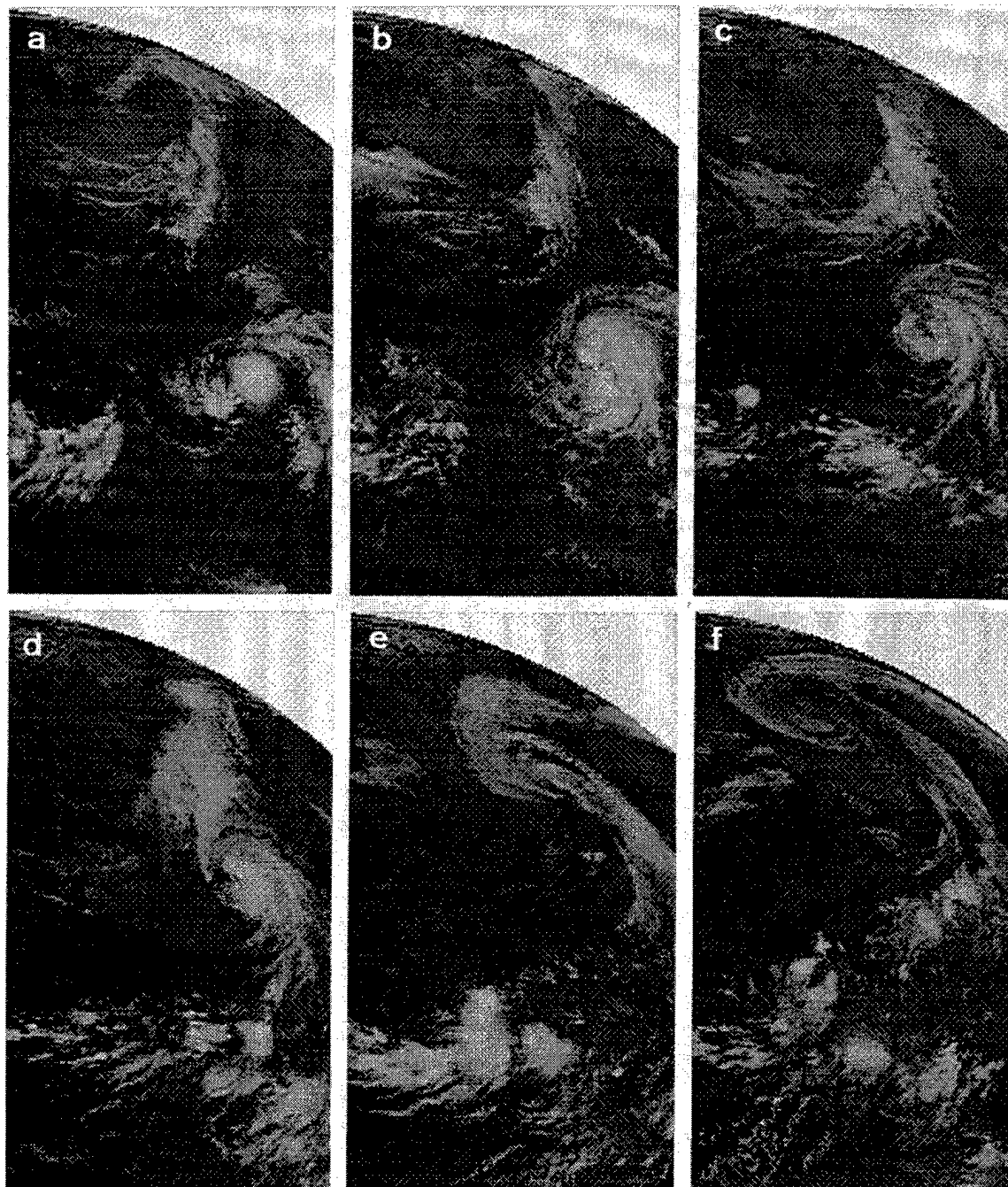


Fig. 4.17. Satellite IR imagery as in Fig. 2.5, except for TC Yule undergoing extratropical transition at 0000 UTC on (a) 19, (b) 20, (c) 21, (d) 22, (e) 23, and (f) 24 August 1997.

GFDN sea-level pressure forecasts for both the TC and the midlatitude cyclogenesis (Fig. A.38j-k) are not distinctly different from the previous forecast (Fig. A.36j-k), and yet this is a much more accurate 72-h track forecast (Fig. A.38a). Similarly, the midlatitude cyclones to the northwest of the TC in the 66-h GFDN forecast, the 72-h NOGAPS forecast, and the verifying NOGAPS analysis (Fig. A.39l, h, and d, respectively) are not noticeably different from their counterparts 12 h earlier (Fig. A.37l, h, and d, respectively), other than with regard to the location of the TC. Such similarities between the forecast fields from two consecutive models runs that have somewhat different TC track errors highlight the sensitivity of the BCI process.

4. Impact on other objective guidance. During 26-27 June when the NOGAPS track forecasts for Peter were consistently degraded by I-BCI (Fig. 4.15a-d), the corresponding track forecasts of the three steering models were similarly degraded (Fig. 4.18a-d, respectively). This similarity is consistent with the BCI conceptual model (Fig. 4.13). That is, an erroneous prediction of baroclinic interaction between the TC and its environment should be expected to result in erroneous steering model tracks, since the model-predicted evolution of the mid-tropospheric environmental steering of the TC is dependent on the degree to which the TC and environment interact. Another example is the similarity of the NOGAPS and the three steering model track forecasts for TC Yule during 19-20 August (Fig. 4.16a-d and 4.19a-d, respectively), when the accuracy of the NOGAPS tracks varies considerably. Specifically, the slow bias of the 0000 UTC and 1200 UTC 19 August NOGAPS track forecasts (Fig. 4.16a-b) is matched by a qualitatively similar poor performance by the corresponding steering model forecasts (Fig. 4.19a-b). However, the improved accuracy of the 0000 UTC and 1200 UTC 20 August NOGAPS track forecasts (Fig. 4.16c-d) is matched by a qualitatively similar improvement in the accuracy of the corresponding steering model track forecasts (Fig. 4.19c-d).

The similarity of the NOGAPS track forecast accuracy with these three steering models that depend on the NOGAPS-predicted fields provides a contrast with the dissimilarity of the steering model tracks during an erroneous RVS event (Fig. 4.10). Recall that when the NOGAPS track forecast for Nestor was being degraded by E-RVS (Fig. 4.11d), the consensus position of the steering models was essentially unaffected (Fig. 4.11b). The presence of environmental vertical wind shear may be inferred in Fig. 4.11b by the down-shear spread of the SBAM, MBAM, and FBAM tracks. If an excessive RVS occurs in the NOGAPS forecast and results in a shearing of the model TC vortex such that the steering level becomes much shallower, a slow NOGAPS track bias is expected. The interpretation of the NOGAPS-steering model track dissimilarity in the RVS case is that the vertical structure change in the model vortex does not feed back to change the environment that "drives" the steering model track forecasts. Rather than the model vortex experiencing a rather passive response as in the RVS conceptual model, the interaction (or lack of interaction) of the vortex and the environment during a BCI event may change the environmental steering that drives the SBAM, MBAM, and FBAM track forecasts. This suggests that comparison of the NOGAPS and steering models may provide insight as to which error mechanism is most likely to be responsible for a NOGAPS track forecast that appears to be erroneous.

Although the CSUM forecasts for Peter were consistently poor during 26-27 June (Fig. 4.18a-d) as was the case for the NOGAPS track forecasts (Fig. 4.16a-d), the similarity is

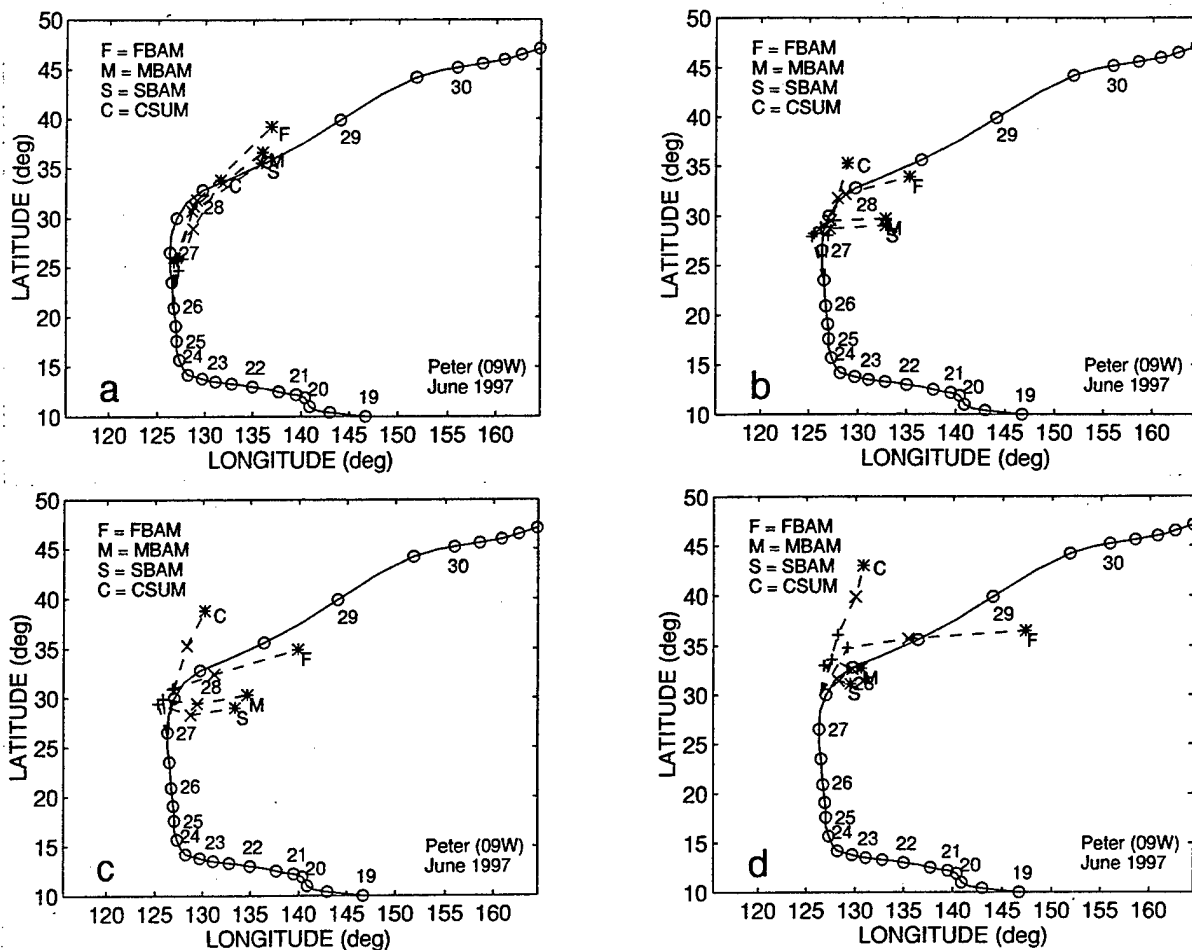


Fig. 4.18. Best-track and selective objective technique track forecasts (see inset) for TC Peter for the same four forecasts in Fig. 4.15 during which the NOGAPS track forecasts were degraded by I-BCI.

considered to be coincidental, i.e., it is attributed to the well-known inability of the CSUM to skillfully forecast recurvature. Support for this interpretation comes from the case of Yule when a variable response to BCI is occurring in NOGAPS. Notice that on 0000 UTC and 1200 UTC 19 August, CSUM has accurate forecasts when the NOGAPS track forecasts are inaccurate (Fig. 4.16a-b and 4.19a-b, respectively). The "on-the ridge" equation set of CSUM is generally accurate when the poleward motion is steady as in this case. However, when Yule is accelerating as in the 0000 UTC 20 August forecast, CSUM has an inaccurate forecast when the NOGAPS model has an accurate forecast (Fig. 4.16a-b and 4.19a-b, respectively). Thus, the correlation of the CSUM and NOGAPS track forecast does not seem to provide clues about the likely NOGAPS performance; rather, the forecaster needs to recognize the situations when CSUM is likely to provide accurate or inaccurate guidance.

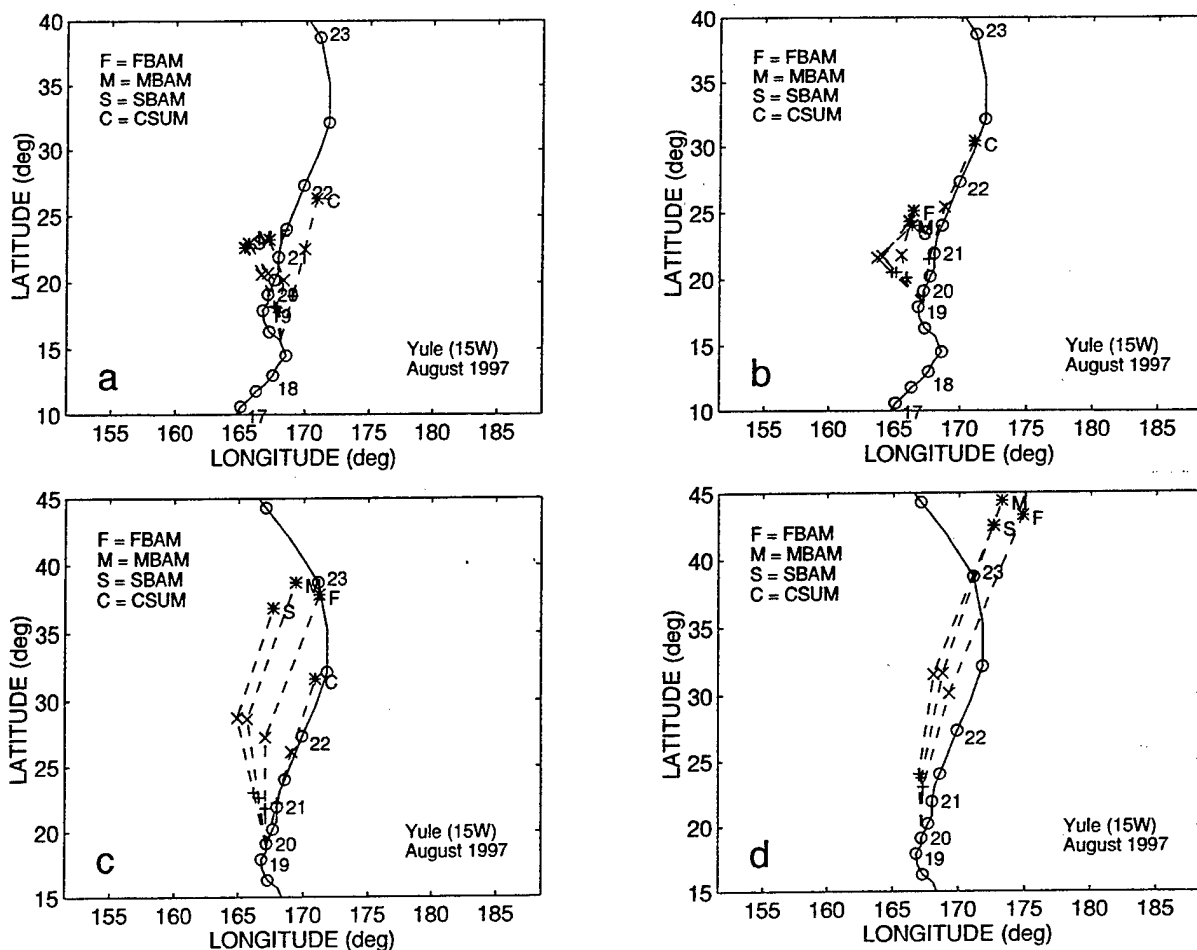


Fig. 4.19 Best-track and selected objective technique track forecasts (see inset) for TC Yule for the same times as in Fig. 4.16.

5. Summary. Tables 4.7 and 4.8 provide summaries of the key aspects of the E-BCI and I-BCI phenomena. The tables include the indications in the numerical model fields and TC tracks, and the impacts on the various models available to the JTWC forecaster. A key result for the forecaster is that similar to erroneous DCI events, erroneous BCI tends to occur simultaneously in the NOGAPS and GFDN forecasters. Whereas erroneous DCI was always found to be excessive in both the NOGAPS and GFDN forecasts during 1997, the simultaneous occurrence of I-BCI in the NOGAPS forecast and E-BCI in the GFDN forecast was not an uncommon situation during 1997. Based on forecast track similarities, it also appears that the other numerical models behave similarly (e.g., E-BCI is apparently occurring in the UKMO model (EGRR) while I-BCI is apparently occurring in the JGSM and JTYM forecasts for the case in Fig. 4.16c. In addition, occurrence of erroneous BCI tends to have little temporal continuity, with alternating accurate and inaccurate predictions, and even examples of changes from E-BCI to I-BCI between consecutive forecasts in the same model. For this sample, the 72-h FTEs resulting from I-BCI were typically much larger than those resulting from E-BCI, which suggests that the best official forecast might be one that gives more weight to those members of

Table 4.7. Summary of important aspects and illustration key for Excessive Baroclinic Cyclone Interaction (E-BCI).

Aspect	Description	Figure
Conceptual model	Excessive interaction of TC with a midlatitude cyclone/trough due to a misrepresentation of TC structure evolution, midlatitude cyclone evolution, or the model's handling of the baroclinic self-development process.	4.13
Frequency	7 periods involving 7 TCs, significantly degrading 8 NOGAPS forecasts and 11 GFDN forecasts in the western North Pacific during 1997.	Table 4.6 Table 1.3
Environment	TC usually in PF region just north or south of STR axis at start of model integration.	Table 4.6
Indications in numerical model fields	<p>In 500-mb streamline fields:</p> <ul style="list-style-type: none"> • Over-development and displacement of mid-tropospheric midlatitude cyclone toward TC, and premature embedding of TC into southerly flow on southeast flank of midlatitude cyclone. <p>In sea-level pressure fields:</p> <ul style="list-style-type: none"> • Excessive lowering minimum sea-level pressure and expansion of the size of the TC. 	A.35k vs c A.34l vs d A.40h vs d
Indications in numerical model tracks	<ul style="list-style-type: none"> • Variable depending on orientation of TC and midlatitude system: * For an example of a slow bias see: * For an example of a fast bias see: 	A.34a A.40a
Relative impact on numerical models	<ul style="list-style-type: none"> • NOGAPS and GFDN can be degraded. • Other models probably can be degraded, but only EGRR and JTYM observed in 1997. 	4.15, 4.16 4.16
Relative impact on other objective guidance	<ul style="list-style-type: none"> • BAMS usually degraded in the same sense as NOGAPS. • CSUM usually not affected, but generally does not have much skill in scenario where BCI occurs (recurvature). 	4.17, 4.18 4.17, 4.18

the track ensemble that manifest the stronger BCI. However, the case of Typhoon Rex (06W) during 1998 in which extratropical transition was delayed (see Appendix B) had larger errors in the models that forecast the most vigorous E-BCI, and the only model that did not forecast any BCI achieved consistently smaller 72-h FTEs. This variability among the BCI cases suggest that potential extratropical transition situations, which involve interactions among the midlatitude circulations, the subtropical anticyclone circulation, and the TC, are difficult to forecast accurately. None of the numerical models available to JTWC could be relied upon to provide consistently accurate TC forecast tracks in all of these BCI situations. Until a better understanding of model traits with regard to BCI is achieved, a simple consensus of all the numerical model tracks may be generally preferable to a selective consensus as the basis for the official track forecast when the implications of erroneous BCI are not clear.

Table 4.8 Summary of important aspects and illustration key for Insufficient Baroclinic Cyclone Interaction (I-BCI).

Aspect	Description	Figure
Conceptual model	Insufficient interaction of TC with a midlatitude cyclone/trough to due a misrepresentation of TC structure evolution, midlatitude cyclone evolution, or the model's handling of the baroclinic self-development process.	4.13
Frequency	7 periods involving 7 TCs, significantly degrading 12 NOGAPS forecasts and 2 GFDN forecasts in the western North Pacific during 1997.	Table 4.6 Table 1.3
Environment	TC usually in PF region just north or south of STR axis at start of model integration.	Table 4.6
Indications in numerical model fields	<p>In 500-mb streamline fields:</p> <ul style="list-style-type: none"> Under-development and displacement of mid-tropospheric midlatitude cyclone toward TC, and slow and failed embedding of TC into southerly flow on southeast flank of midlatitude cyclone. <p>In sea-level pressure fields:</p> <ul style="list-style-type: none"> Typically manifested by the appearance of an overly extended trough to the northeast of the TC. 	<p>A.35h vs d A.37h vs d</p> <p>A.34g vs c A.36h vs d</p>
Indications in numerical model tracks	<ul style="list-style-type: none"> Slow, and sometimes very slow along-track bias 	4.15, 4.16
Relative impact on numerical models	<ul style="list-style-type: none"> NOGAPS much more likely to be degraded than GFDN in 1997. Other three numerical models apparently degraded in 1997. 	4.15, 4.16 4.15, 4.16
Relative impact on other objective guidance	<ul style="list-style-type: none"> BAMS usually degraded in the same sense as NOGAPS CSUM usually not affected, but generally does not have much skill in scenario where BCI occurs (recurvature). 	4.17, 4.18 4.17, 4.18

5. Conclusion

a. Summary of results

This report (sections 1 – 4) documents an extensive research effort that has: (i) examined all highly erroneous (i.e., 72-h FTE > 300 n mi) NOGAPS and GFDN track forecasts in the western North Pacific during 1997; (ii) identified the principal error mechanisms that caused the error using the conceptual models of the Systematic Approach Meteorological knowledge base for the western North Pacific; and (iii) documented the frequency and characteristics of the identified error mechanisms and presented illustrative case studies. To the authors' knowledge, this project is the first of its kind, and is a much needed complement to the traditional statistical measures of TC track forecast model performance, e.g., mean and standard deviations of vector error, along-track and cross-track error, etc.

An important and encouraging result of this research is that only six error mechanisms (E-DCI, E-RMT, E-RTF, E-RVS, E-BCI and I-BCI) account for 84% (91 of 108) of the poor NOGAPS track forecasts, and only three error mechanisms (E-DCI, E-MCG, E-BCI) account for 68% (61 of 90¹) of the poor GFDN track forecasts in the western North Pacific in 1997 (from Table 1.3). With only one exception (E-RTF in NOGAPS, which is essentially a binary TC variation of E-RMT), every one of these error mechanisms had five or more episodes that involved a total of eight or more degraded forecast tracks. By contrast, every one of the other error mechanisms in Table 1.3 had only one episode (i.e., involved only one TC), with no more than a total of four² degraded track forecasts.

This research has immediate utility in terms of providing model developers and researchers at FNMOC, NRL Monterey, and GFDL with specific information needed to improve the TC track forecasting performance of the NOGAPS and GFDN models. Specifically, the tendency of:

(i) both NOGAPS and GFDN to over-develop weak tropical disturbances in the vicinity of the TC needs to be corrected to reduce the number of highly degraded TC track forecasts due to E-DCI in both models;

(ii) NOGAPS to excessively grow a TC and its peripheral anticyclone in response to forcing by the Rossby wave train of another large cyclone to the northwest needs to be corrected to reduce the number of highly degraded TC track forecasts due to E-RMT and E-RTF;

(iii) GFDN to significantly over-forecast midlatitude cyclogenesis that is also being moderately over-forecast by NOGAPS needs to be corrected to reduce the number of highly degraded TC track forecasts due to E-MCG;

¹ Excludes the nine GFDN forecasts for which no fields were available to make a determination of the likely error mechanism.

² Excludes special case of E-TCS during Paka, which was probably more a result of an avoidable mis-specification of the TC synthetic observations than due to inherent problems in either the NOGAPS or GFDN models.

(iv) NOGAPS to over-weaken the TC in the presence of vertical wind shear needs to be corrected to reduce the number of highly degraded track forecasts due to E-RVS; and

(v) both NOGAPS and GFDN to sporadically over- or under-forecast the rate of extratropical transition by the TC needs to be corrected to reduce the number of highly degraded track forecasts due to E-BCI and I-BCI in both models.

b. Application to Typhoon Rex (06W) in 1998

Typhoon Rex had a complex, sinuous northeastward track from 23 August to 9 September 1998. During much of that period, the NOGAPS, GFDN, and EGRR track forecasts were highly inaccurate, which resulted in exceptionally large JTWC official track forecast errors. As a result, the JTWC requested that FNMOC and NPS conduct research to identify the influences that were responsible for the complex track of the TC, and the reasons for the many highly erroneous NOGAPS and GFDN track forecasts. The anomalous Typhoon Rex motion, and the persistently unsatisfactory performance of the numerical model TC forecasts, provide an illustration of the conceptual models of the Meteorological knowledge base, and especially the error mechanism conceptual models documented in this report. Appendix B provides an analysis that identifies the probable reasons for the several unusual turns of Rex, and explains the highly erroneous NOGAPS and GFDN tracks in terms of the error mechanism concepts arising from this research.

c. A preliminary Model Traits knowledge base

Within the context of the Systematic Approach to TC track forecasting, this research is the raw material for a preliminary Model Traits knowledge base for the western North Pacific. Although a formal implementation of the Model Traits knowledge base will be included in the Systematic Approach Expert System (SAES) that is currently under development, the basic elements of the knowledge base are described here in terms of a five-level framework (Table 5.1). The following discussion illustrates how the operational forecaster would typically access the knowledge base.

Whenever the spread and clustering of the track forecasts (i.e., as in Fig. 1.3b) indicate it is likely that one or more of the numerical models is significantly degraded, the forecaster needs to first identify which error mechanism(s) is the most likely source(s) of degradation. The first level of the Model Traits knowledge base (Table 5.2) provides the forecaster information as to which error mechanisms are frequent sources of large NOGAPS and GFDN track forecast errors. This table indicates whether it is probable that the error mechanism will be manifest in a qualitatively similar manner in both the NOGAPS and GFDN fields (as in the cases E-DCI and E-BCI), or will more likely appear in the fields of only one of the models (rest of the entries in Table 5.1). Given that the NOGAPS forecast is degraded by a particular error mechanism, the BAMs and/or CSUM may or may not be degraded (Table 5.1). With the exception of E-RTF, which involves the mis-prediction of a very large anticyclone to the southeast of both TCs, the CSUM is insensitive to NOGAPS degradations by these frequently occurring error mechanisms. This information about the CSUM can be particularly useful to the forecaster in situations in which most of the numerical model tracks appear to be degraded, so that the forecaster may be compelled to depart from the normal policy of

Table 5.1 Five-level framework of the Systematic Approach Model Traits knowledge base.

Level	Knowledge	Location
1	Identity of frequently occurring error mechanisms and affected models	Table 5.2
2	Key field and track indications of the frequently occurring error mechanisms	Table 5.3
3	Detailed characteristics of a particular error mechanism	Table listed in column 2 of Table 5.4
4	Selected illustrations of a particular error mechanism	Figures identified by column 3 of Table 5.4
5	Thorough discussion and illustration of a particular error mechanism	Case studies identified in column 4 of Table 5.4

Table 5.2 Level 1 of the Model Traits knowledge base indicating error mechanisms that frequently (F) degrade JTWC track forecast model guidance. In the rows for Beta and Advection Models (FBAM, MBAM, and SBAM) and the CSUM, the designator F means frequently degraded when NOGAPS is degraded by the same error mechanism.

Model Name	Error Mechanism Frequency of Occurrence						
	E-DCI	E-RMT	E-RTF	E-MCG	E-RVS	E-BCI	I-BCI
NOGAPS	F	F	F		F	F	F
GFDN	F			F		F	
BAMs	F	F	F			F	F
CSUM			F				

giving high weight to the numerical forecast guidance.

Given this summary of the frequently occurring error mechanisms, the forecaster must then be aware of the key indications of the error mechanisms in the forecast fields and forecast tracks of the affected models, which are summarized in the second level of the Model Traits knowledge base (Table 5.3). Although manifestations of the error mechanisms are usually present in both the sea-level pressures and the 500-mb (or lower if the TC is weak) winds, the most readily detectable indications for six of the seven error mechanisms are in the sea-level pressure fields. Depending on his/her experience level or knowledge of specific error mechanisms, the forecaster may desire to have access to: (i) more detailed information on error mechanism characteristics and frequency; (ii) selected illustrations that will help the forecaster identify certain aspects of the phenomenon; and/or (iii) detailed case studies that thoroughly illustrate an error mechanism phenomenon in the context of the lifecycle of the TC. These increasingly detailed sets of information are in levels 3-5 of the Model Traits knowledge base (Table 5.4). Whereas only levels 1 – 4 typically would be accessed by the TC forecaster, level 5 would be heavily accessed during training and post-analysis when operational time constraints are not a factor.

Table 5.3. Level 2 of the Model Traits knowledge base including summaries of the key forecast field and forecast track indications for each of the frequently occurring error mechanisms.

Error Mechanism	FORECAST FIELD INDICATIONS (in affected model compared to verifying analyses or unaffected model forecast fields)		FORECAST TRACK INDICATIONS (in affected models compared to actual TC track and tracks of unaffected models)
	In sea-level pressure	In 500-mb winds	
E-DCI	Lobe of low SLP that rotates cyclonically around and tends to merge with the TC	Cyclonic rotation of trough or cyclone around the TC. May appear at lower levels	Displacement toward 2 nd cyclone manifested as an acceleration, deceleration, or turning track depending on past motion of TC and bearing to 2 nd cyclone.
E-RMT	Significant growth of the TC circulation	Early transition of environment pattern from S to P/PF	More poleward-oriented track. Usually means a more right track and slow track bias compared to unaffected models.
E-RTF	Significant growth of one or both TCs in the SLP	Early transition of environment pattern from S to P/PF	Earlier and sharper recurvature of west TC. Earlier and faster recurvature of east TC.
E-MCG	Over-development of midlatitude low 15°-30° poleward of TC	Excessive midlatitude troughing poleward of TC	Earlier poleward turn if TC initially equatorward of STR axis. Various direction and speed changes may occur if TC is initially poleward of STR.
E-RVS	More rapid filling of minimum pressure of TC to above 1004-mb by 48 to 72 h	Displacement of TC circulation (trough) > 2° lat. downshear of low-level center.	Slow track bias that usually becomes larger with increasing forecast interval.
E-BCI	More rapid merging and/or excessive deepening of interacting TC and midlatitude low	Over-deepening of midlatitude trough and more displacement toward TC (effect may be subtle or absent)	Usually a poleward track bias. Fast or slow speed bias depending on orientation of midlatitude cyclone and transitioning TC.
I-BCI	Low pressure trough due to midlatitude cyclogenesis that extends northeast from TC	Under-deepening of midlatitude trough and less displacement toward TC (effect may be subtle or absent)	Usually a large, and sometimes extremely large, slow track error, but typically not much of an across-track error.

Table 5.4. Levels 3, 4, and 5 of the Model Traits knowledge base, which are the sources from this technical report of increasingly detailed information of the seven most frequent occurring error mechanisms, including summaries of characteristics, selected illustrations, and case studies, respectively.

	Level 3	Level 4	Level 5
Error Mechanism	Summary of characteristics	Conceptual model and selected illustrations (page)	Detailed case studies (pages)
E-DCI	Table 2.2	Table 2.2 figure citations (38)	25 - 35
E-RMT	Table 3.2	Table 3.2 figure citations (60)	50 - 58, B.1 - 206 - 210
E-RTF	Table 3.2	Table 3.2 figure citations (60)	61 - 64
E-MCG	Table 4.2	Table 4.2 figure citations (85)	78 - 81
E-RVS	Table 4.5	Table 4.5 figure citations (98)	90 - 94
E-BCI	Table 4.7	Table 4.7 figure citations (111)	101 - 104, 210 - 214
I-BCI	Table 4.8	Table 4.8 figure citations (112)	101 - 108, 214

This Model Traits knowledge base must be regarded as preliminary as it is based on the detailed analysis of only one year of highly erroneous NOGAPS and GFDN track forecasts. Some refinements to the knowledge base are expected as additional years are studied.

d. Future plans

One limitation of the present study is that it is for the NOGAPS and GFDN large 72-h FTEs for western North Pacific TCs during 1997 only, although Appendix B is an examination of the errors for Typhoon Rex during 1998. Several efforts are planned to expand this study:

(i) The cases of large 72-h FTEs of the UKMO and ECMWF models will be examined for the 1997 western North Pacific TCs to determine if the error mechanisms are the same or if new error mechanisms are isolated;

(ii) All cases of large 72-h FTEs of the NOGAPS, GFDN, UKMO, and ECMWF models for the western North Pacific TCs during 1998 will be examined to determine whether the error mechanisms are similar to those during 1997;

(iii) All cases of large 72-h FTEs of the NOGAPS, GFDN, UKMO, and the ECMWF models for the Southern Hemisphere TCs during the 1997-1998 and 1998-1999 seasons will be examined to determine if the same error mechanisms apply; and

(iv) Cases of large 72-h FTEs by NOGAPS, GFDL, UKMO, and the ECMWF models for Atlantic TCs during the 1997 and 1998 seasons will be examined for detection of similar error mechanisms.

Upon completion of these studies, a more confident case can be made regarding the applicability of the error mechanisms described in this report.

A second limitation of the present study is that it is retrospective. A test of near-real time recognition of these error mechanisms is planned that will make use of the Systematic Approach Expert System for the western North Pacific TCs. The specific goal is to enable the forecaster to recognize the likely erroneous dynamical model guidance using the conceptual models described in this report. Validation and refinement of the preliminary Model Traits knowledge base summarized in section 5 will be a byproduct of this test.

In the overall conceptual framework of the Systematic Approach concept (Fig. 1.1), the purpose of the Numerical Model Traits and Objective Technique Traits knowledge bases (Fig 1.1; top-right and middle-right boxes, respectively), is to enable the forecaster to perform the Numerical Guidance Evaluation and Objective Guidance Evaluation processes (Fig. 1.1; upper two boxes of middle row). The goal is to identify a subset of trustworthy numerical model and objective track forecasts (Fig. 1.1; bottom-left box) on which to base the official track forecast. A knowledge base consisting of track forecast construction and confidence estimation principles and techniques (Fig. 1.1; bottom-right box) will be formulated to assist the forecaster in skillfully

formulating an official track forecast (Fig. 1.1; bottom-center box) that reflects some type of consensus of the selected numerical model tracks (as in Fig. 1.3) and objective technique tracks (Fig. 1.1; bottom-left box). Research to develop this third basic knowledge base is in progress.

Appendix A

On the following pages are large 12-panel figures that are referred to in the main body of the report, but have been collected here to improve the readability of the report. The format of the figures is as follows:

(i) panel a depicts the JTWC best-track of the TC (solid line and circles) and the forecast tracks generated by the global models NOGAPS, JGSM, and EGRR initiated at 0000 or 1200 UTC, and generated by the regional models GFDN and JTYM at 6 h after the global models. The 24- (plus), 48- (cross), and 72-h (asterisk) positions are shown for the global models, and the 18-, 42-, and 66-h positions are shown for the regional models. The closed circle on the best track denotes the verifying position for the 72-h global and 66-h regional forecasts;

(ii) panels e-h are the 00-, 24-, 48-, and 72-h forecast fields for NOGAPS;

(iii) panels i-l are the 00-, 18-, 42-h, and 66-h forecast fields for the GFDN model initiated 6 h after the NOGAPS forecast appear in panels e-h; and

(iv) panels b-d are the verifying NOGAPS analyses for the corresponding NOGAPS and GFDN forecast fields.

The conventions used in the figures are:

(i) for panels displaying sea-level pressure, the shading starts for a pressure of 1008 mb with an increment of 4 mb below 1008 mb;

(ii) for panels displaying upper-level winds, the shading starts at a wind speed of 20 kt with an increment of 20 kt;

(iii) for the analysis fields, the asterisk is the JTWC best-track position of the TC and the number above the asterisk is the JTWC intensity of the TC; and

(iv) for the forecast fields, the asterisk is the NOGAPS or GFDN forecast position for the TC and the number above the asterisk (GFDN only) is the GFDN maximum wind speed of the TC.

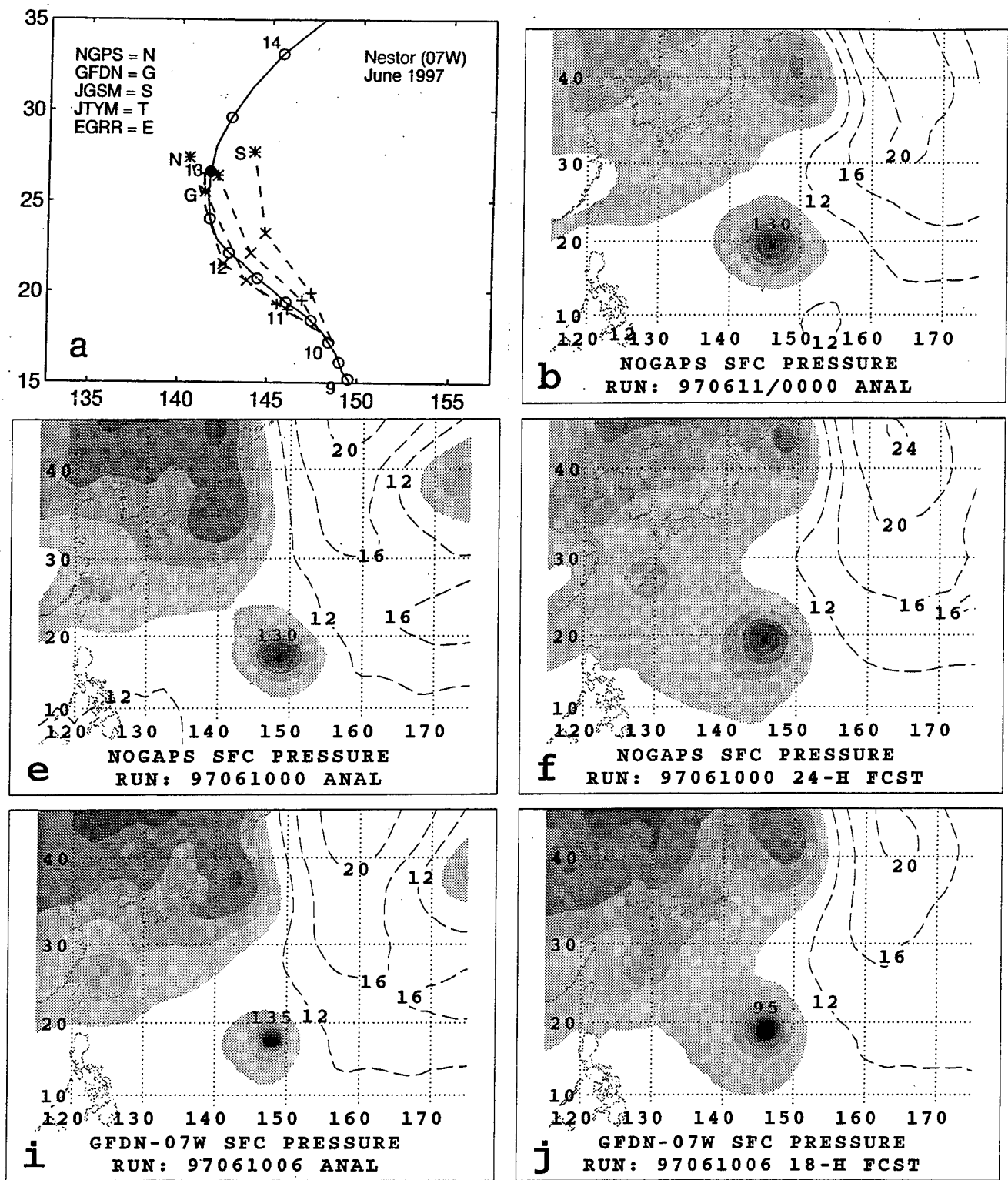


Fig. A.1. (a - j). Comparison/verification of the NOGAPS and GFDN tracks and sea-level pressure forecasts for Nestor initiated at 0000 and 0600 UTC 10 June 1997. See page A-1 for additional details.

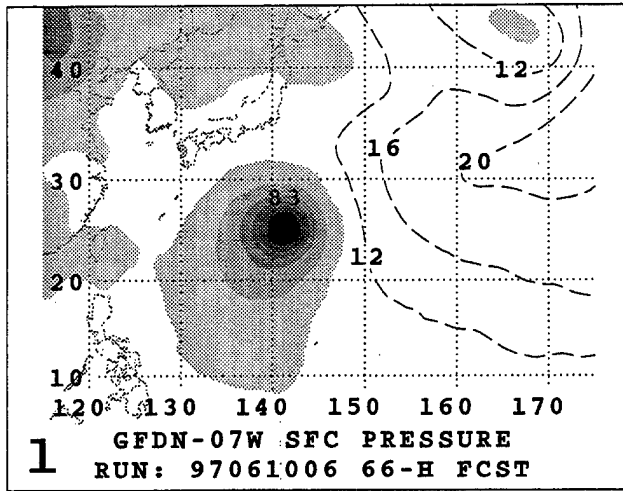
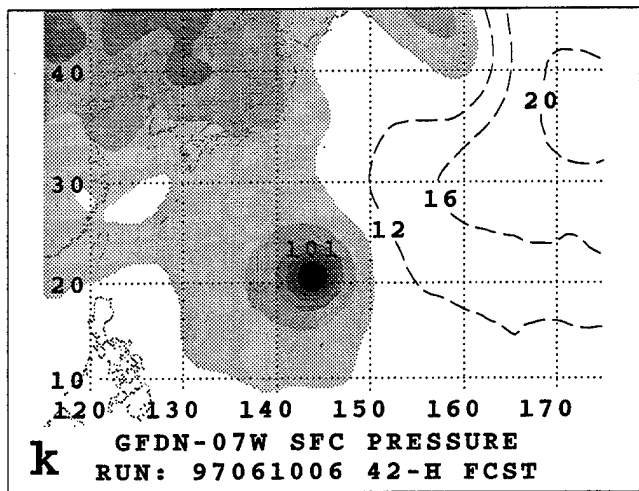
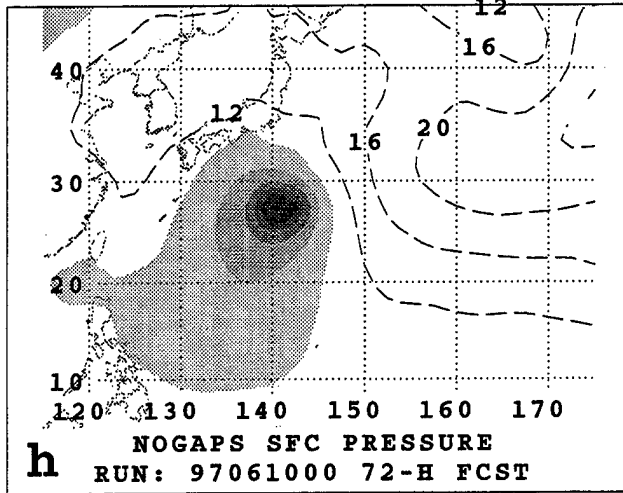
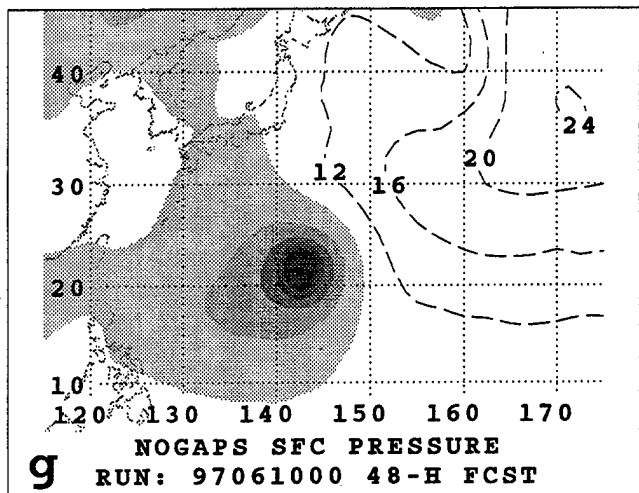
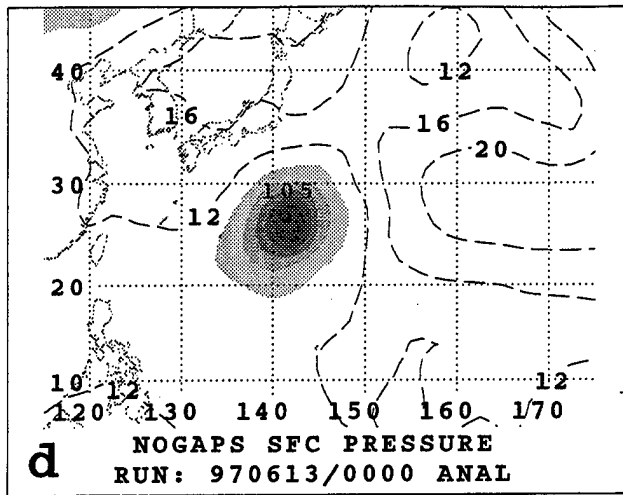
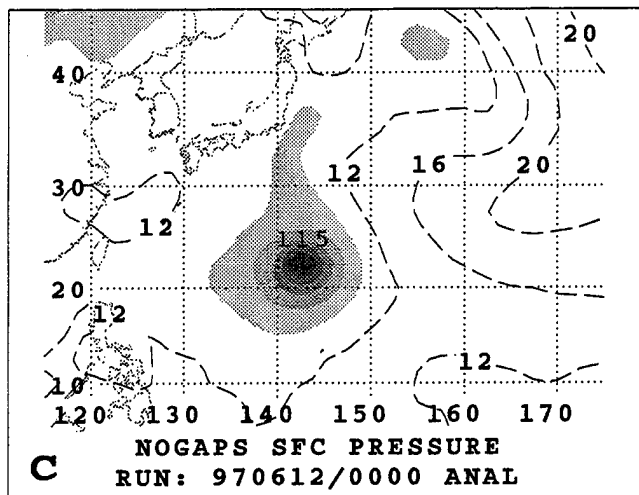


Fig. A.1. (continued)

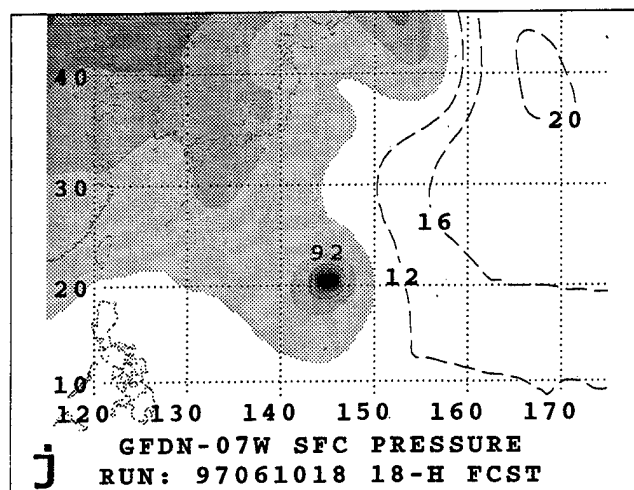
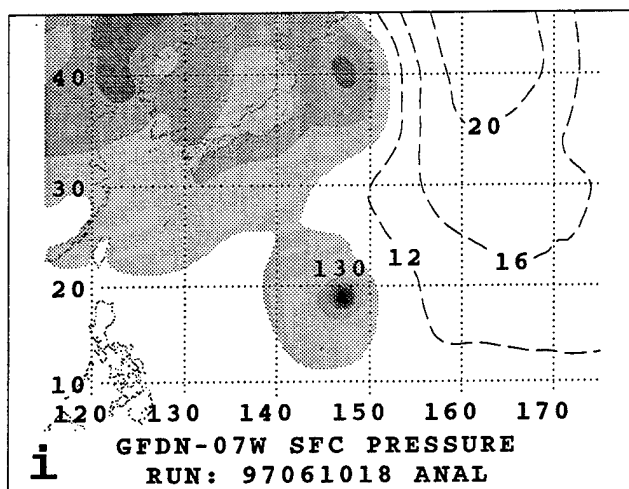
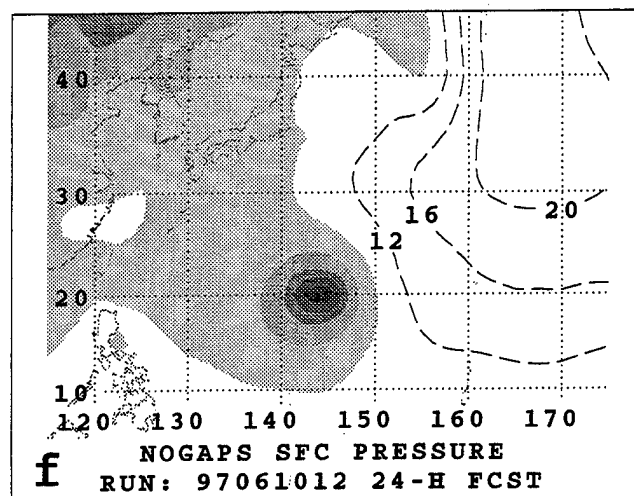
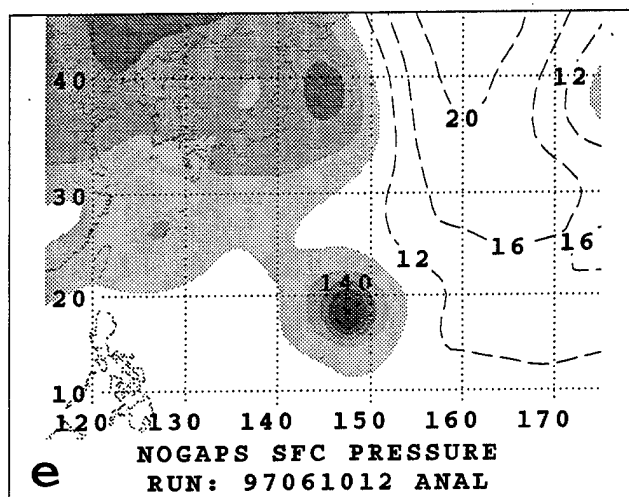
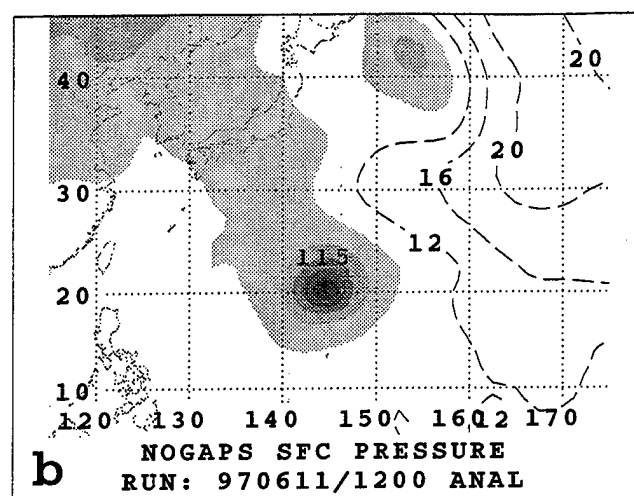
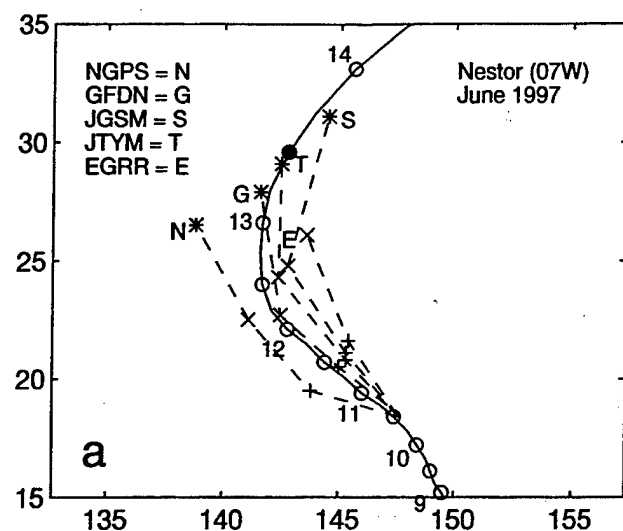


Fig. A.2. (a-l) As in Fig. A.1, except for sea-level pressure forecasts for Nestor initiated at 1200 and 1800 UTC 10 June 1997.

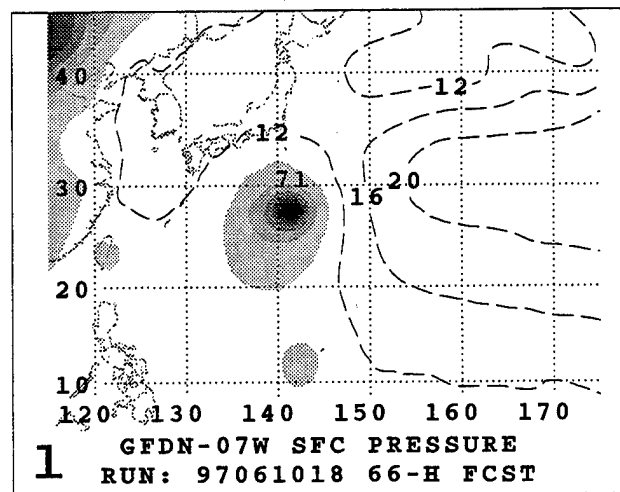
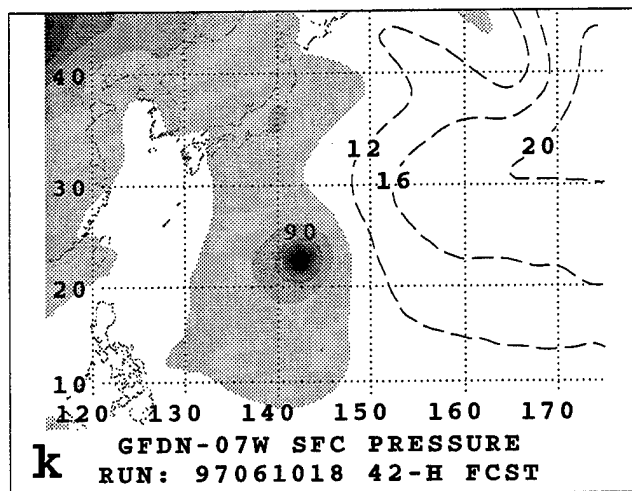
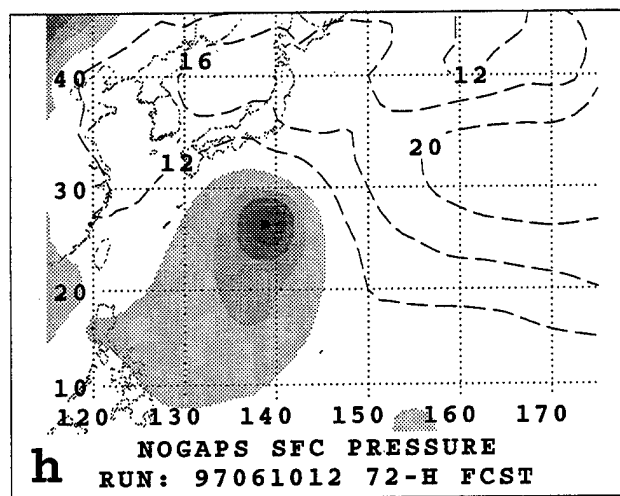
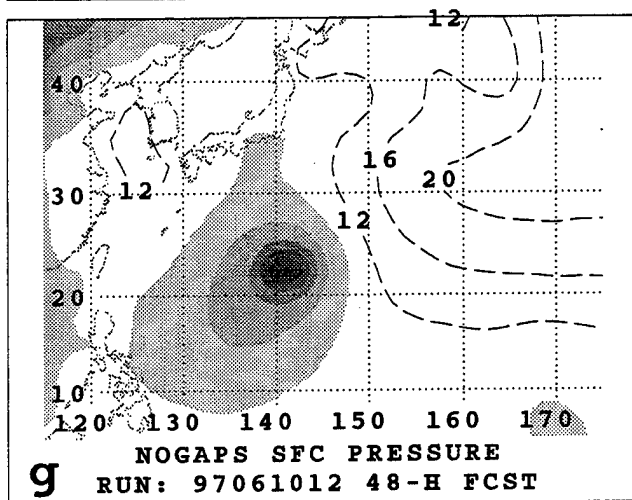
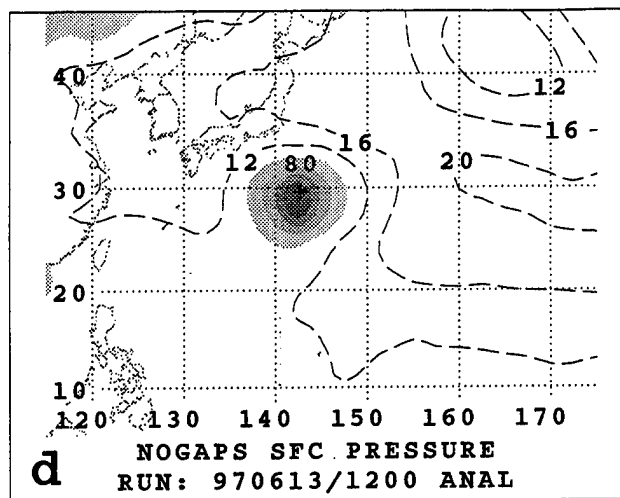
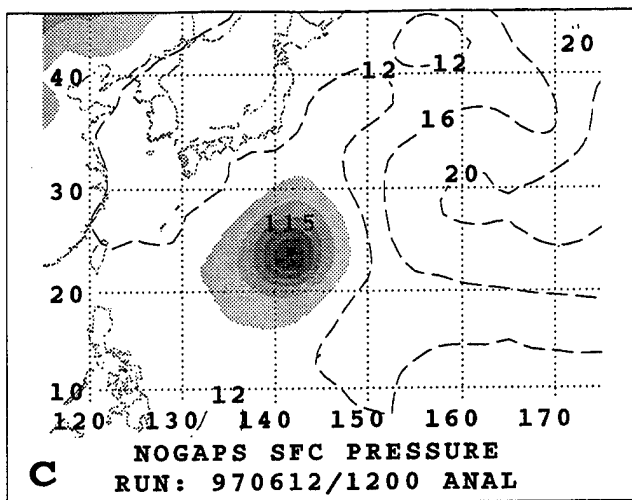


Fig. A.2. (continued)

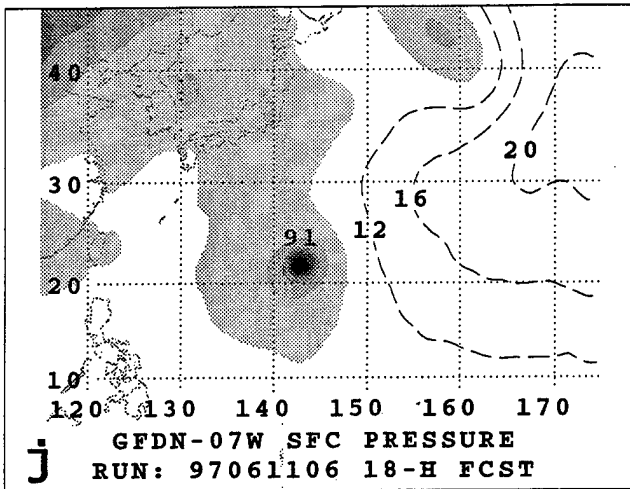
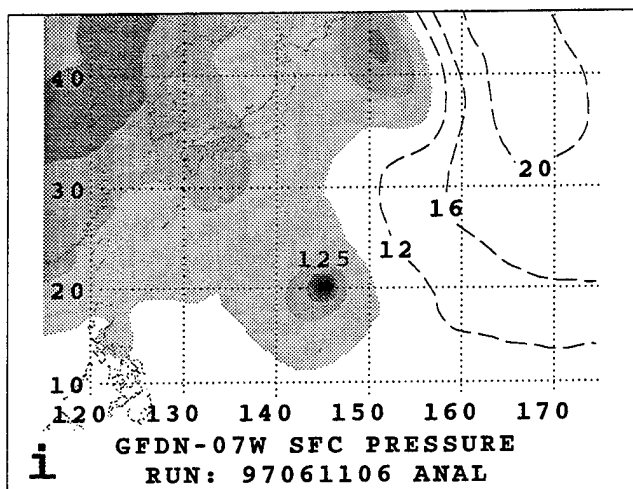
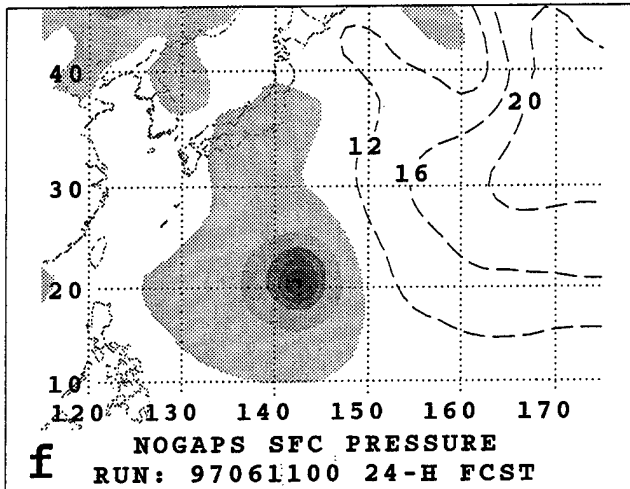
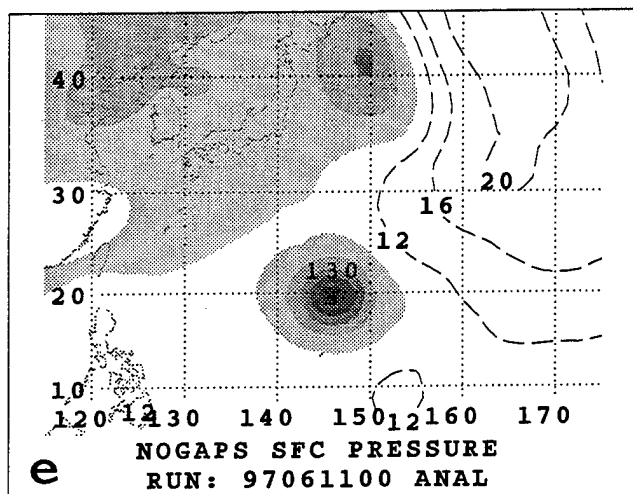
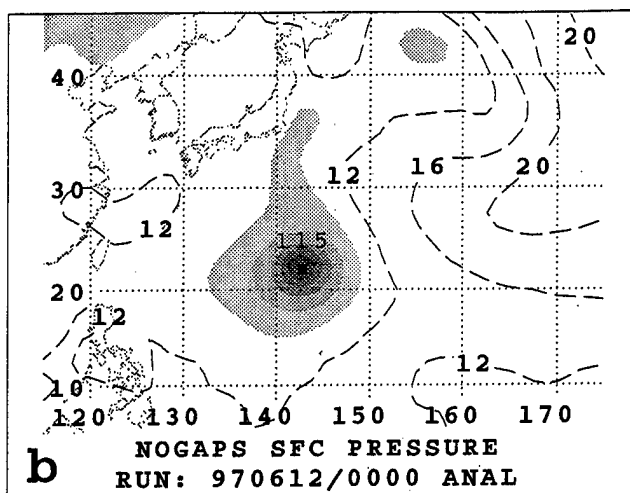
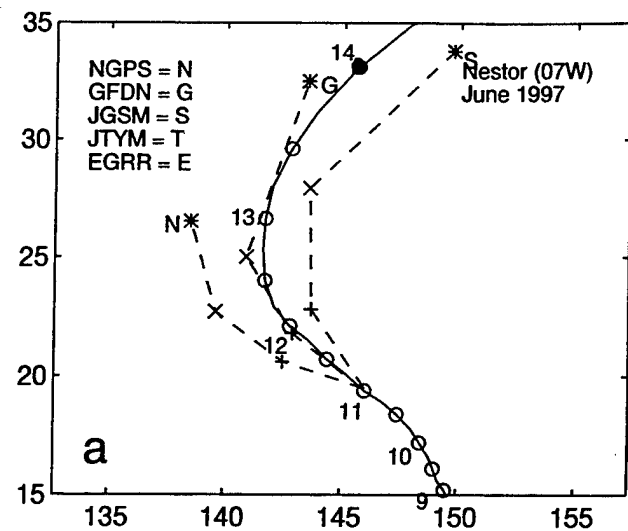


Fig. A.3. (a-l) As in Fig. A.1, except for sea-level pressure forecasts for Nestor initiated at 0000 and 0600 UTC 11 June 1997.

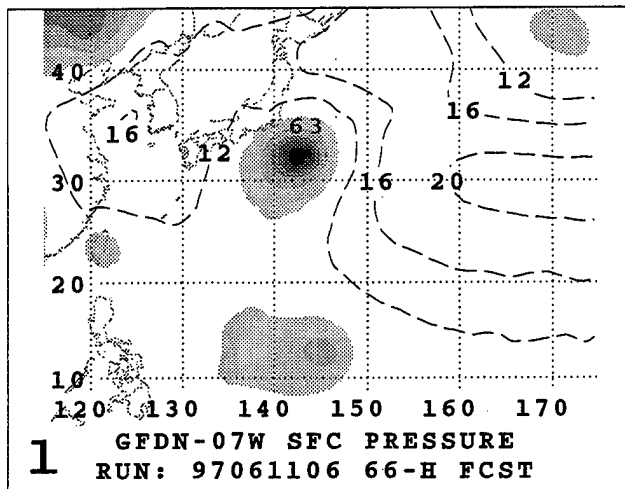
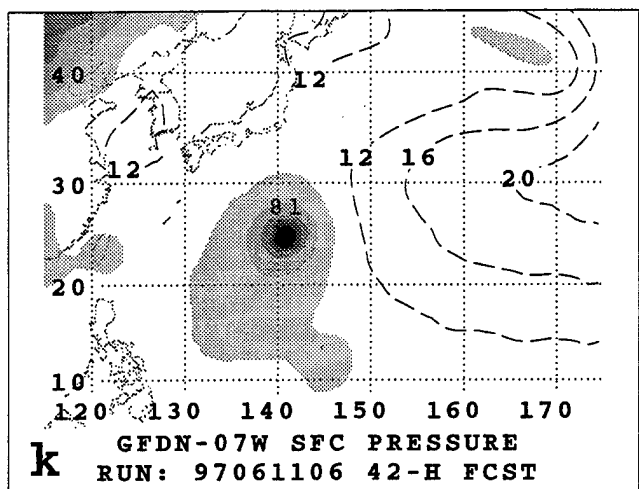
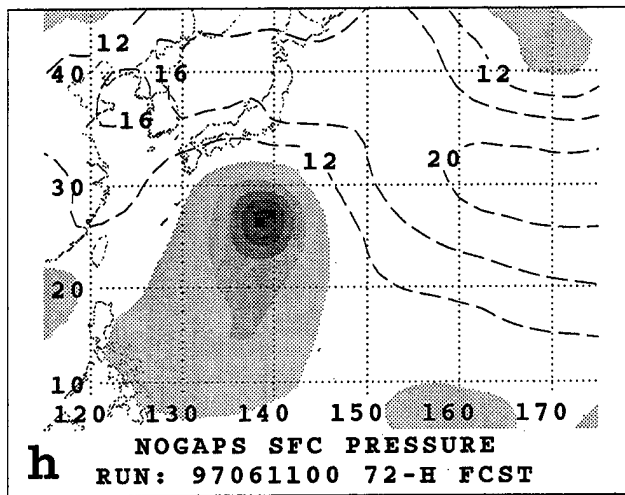
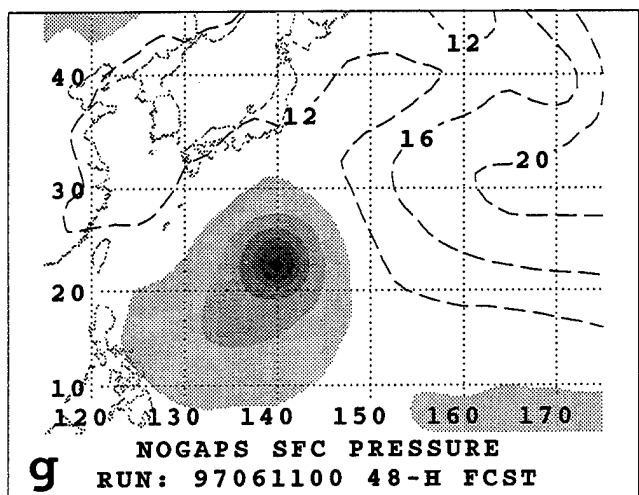
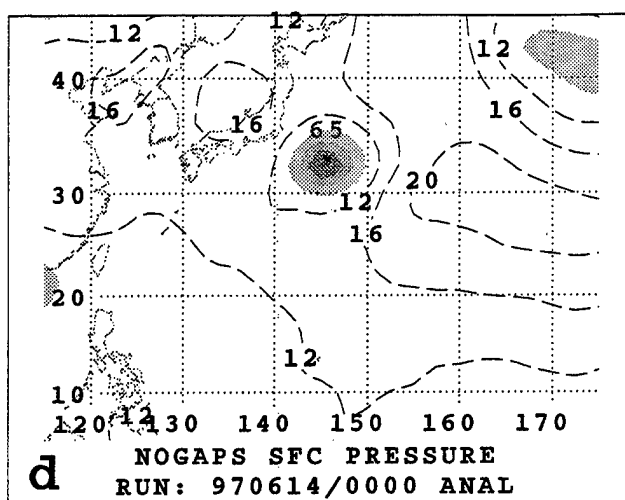
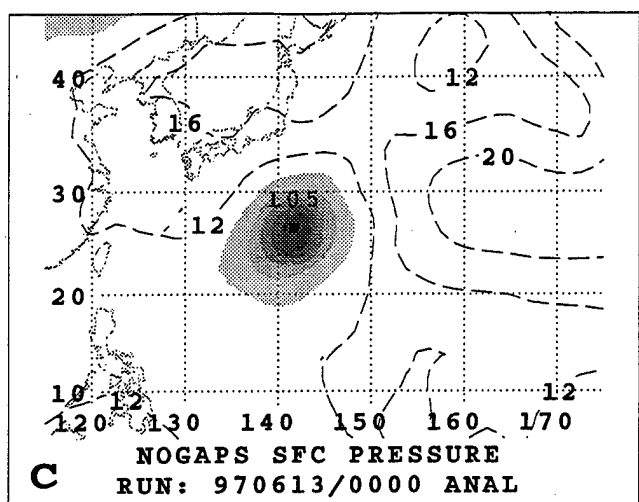


Fig. A.3. (continued)

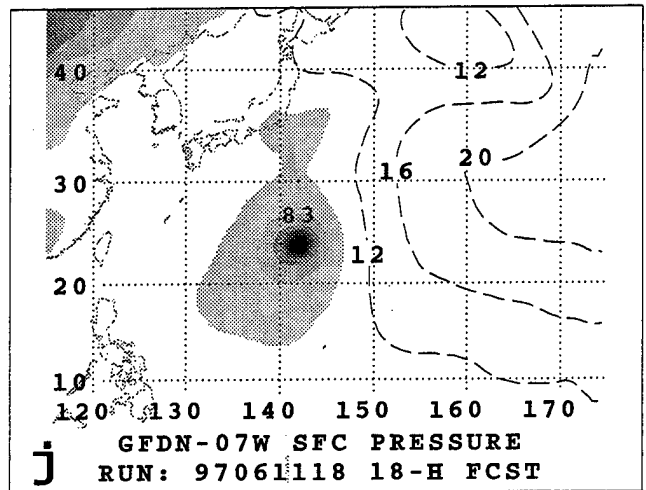
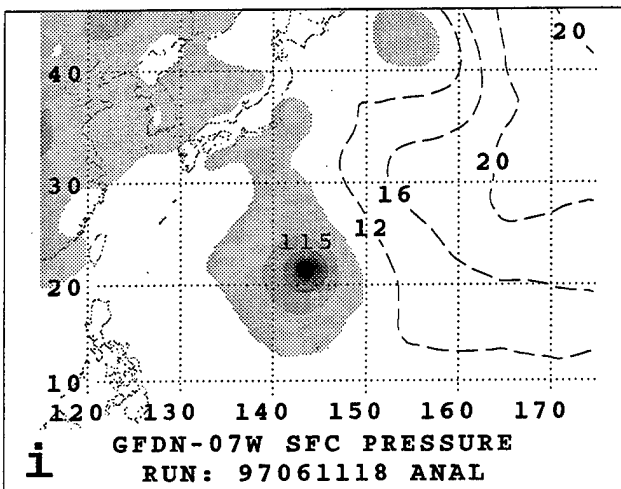
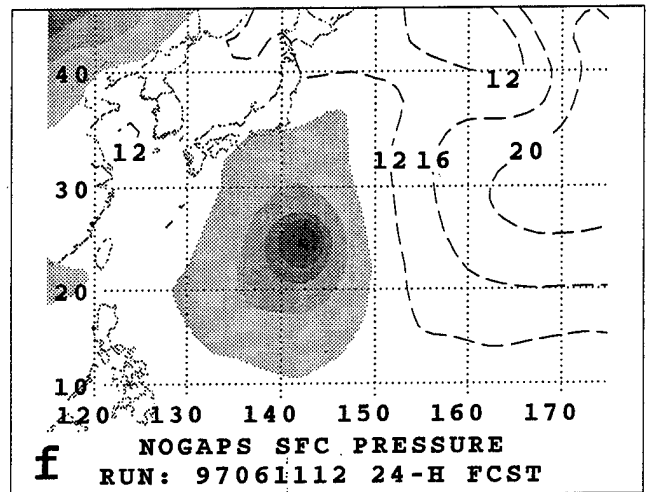
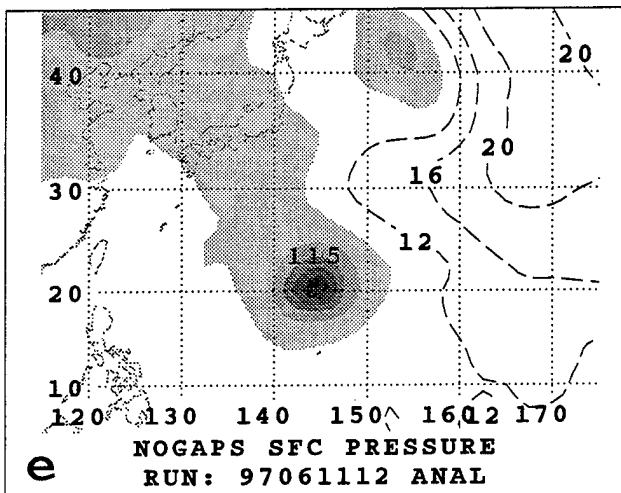
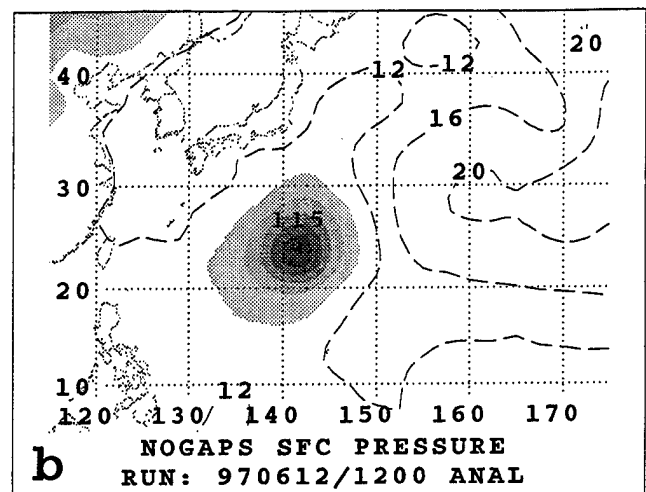
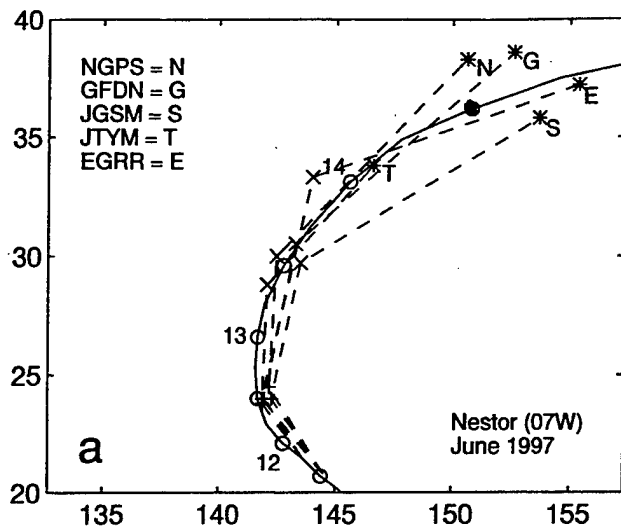


Fig. A.4. (a-l) As in Fig. A.1, except for sea-level pressure forecasts for Nestor initiated at 1200 and 1800 UTC 11 June 1997.

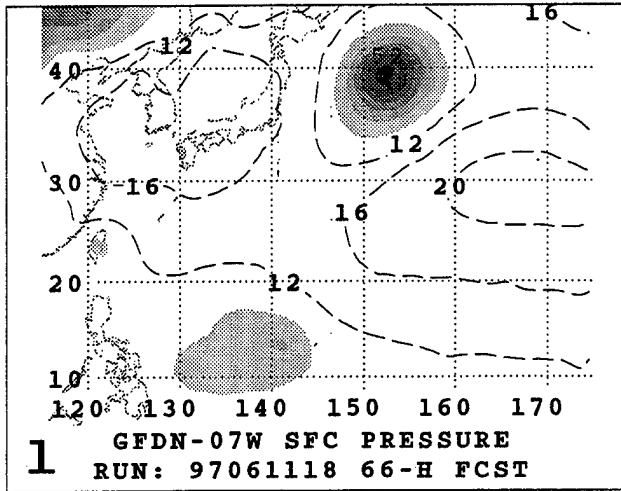
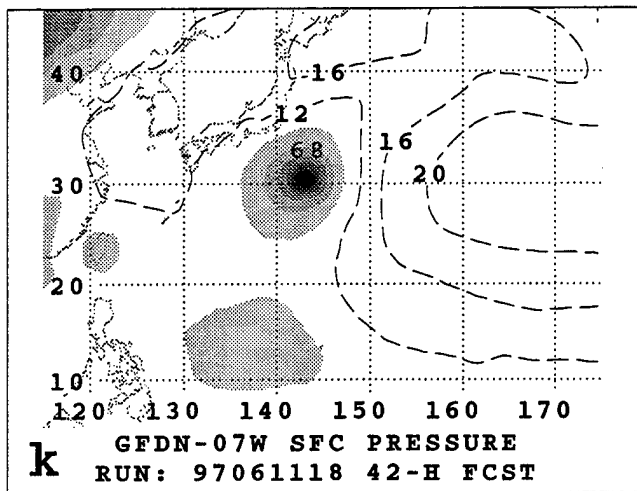
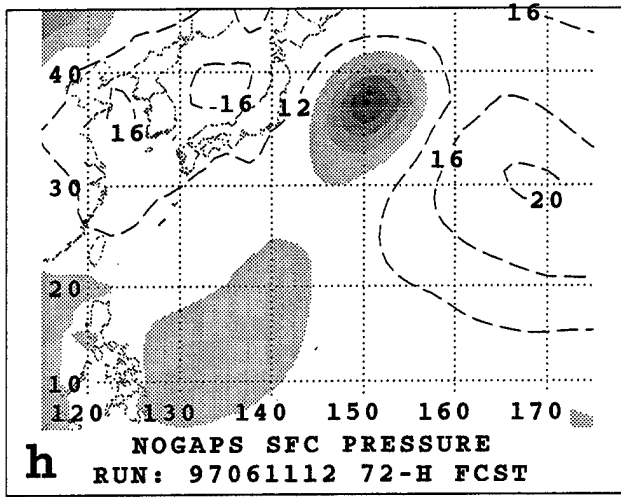
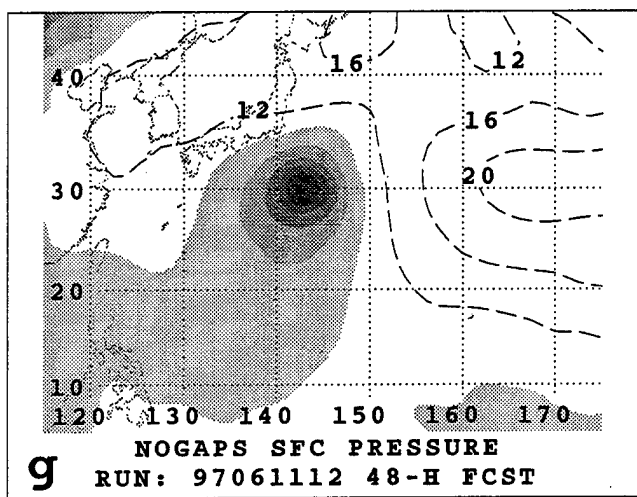
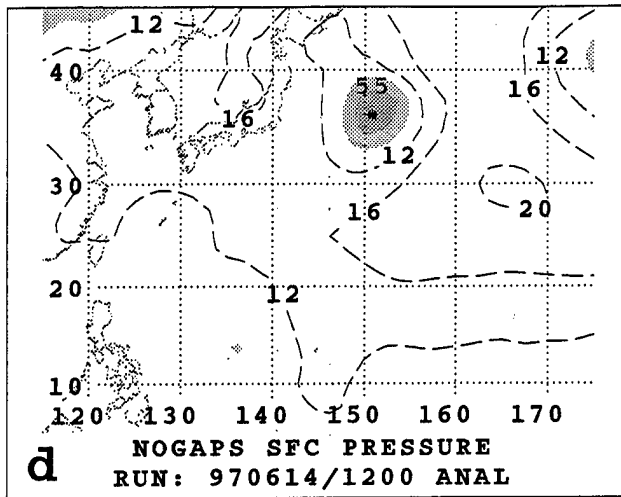
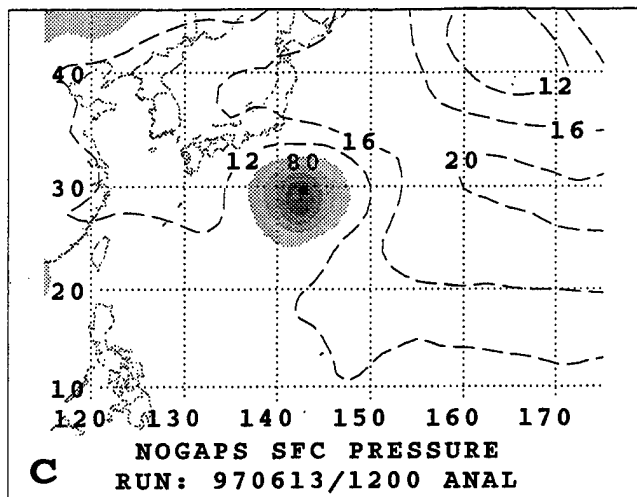


Fig. A.4. (continued)

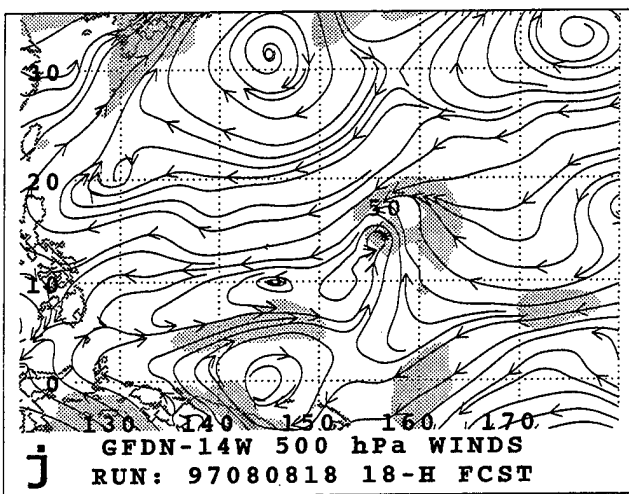
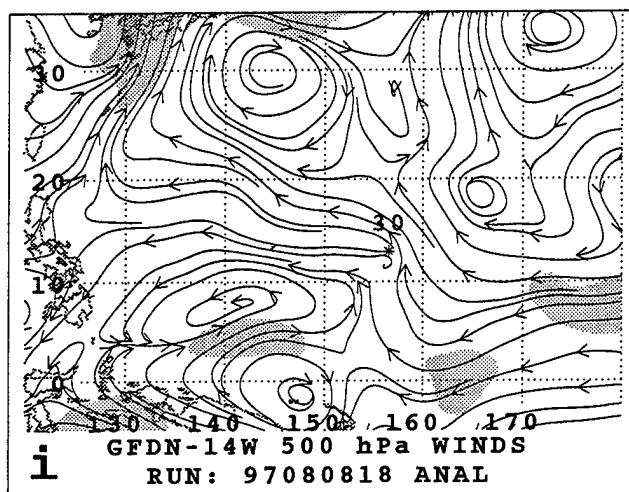
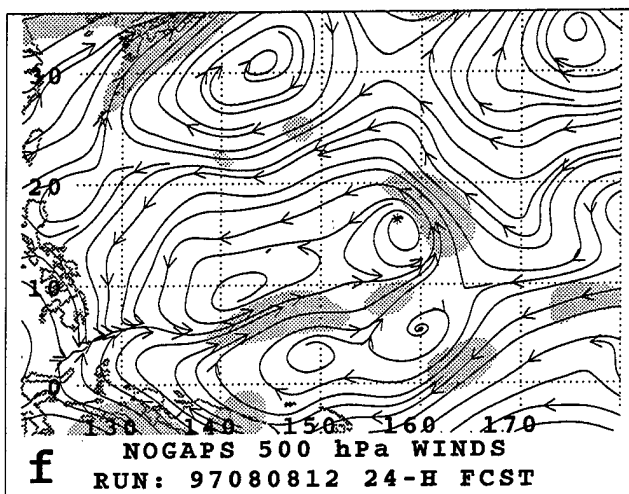
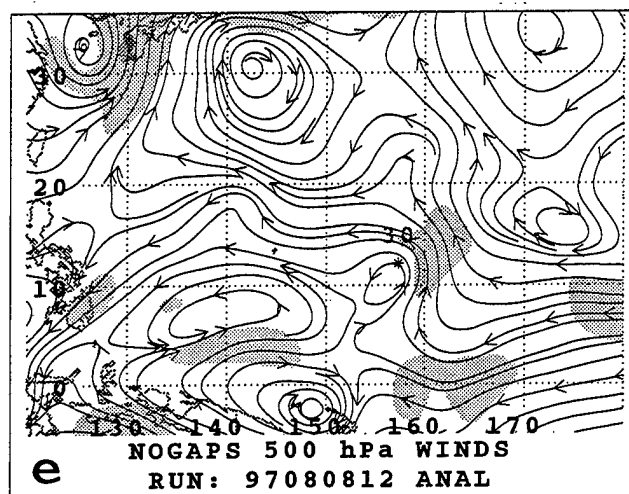
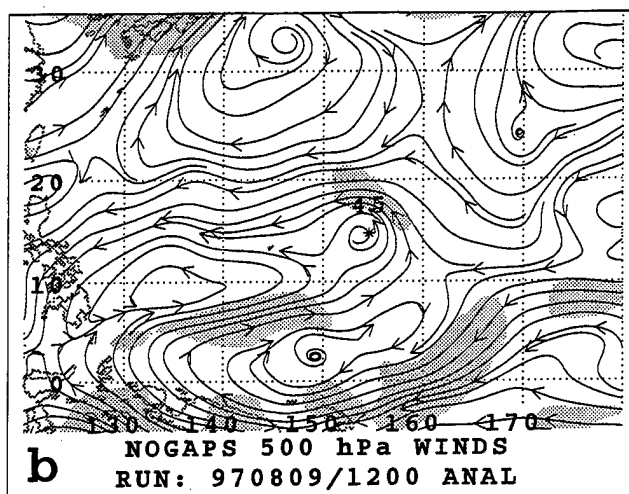
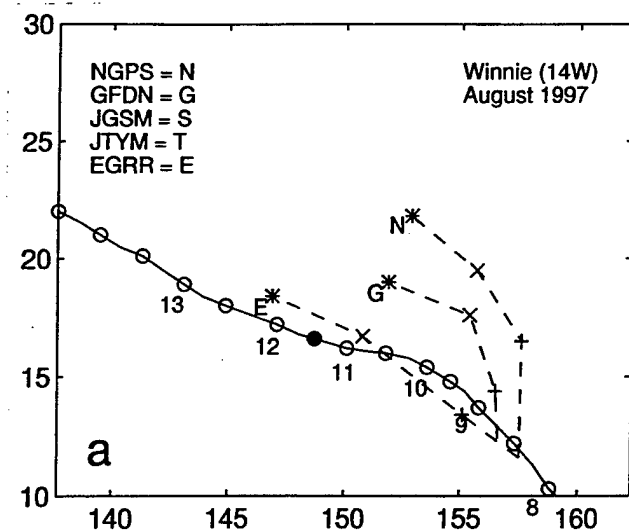


Fig. A.5. (a-l) As in Fig. A.1, except for 500-mb wind forecasts for Winnie initiated at 1200 and 1800 UTC 8 August 1997.

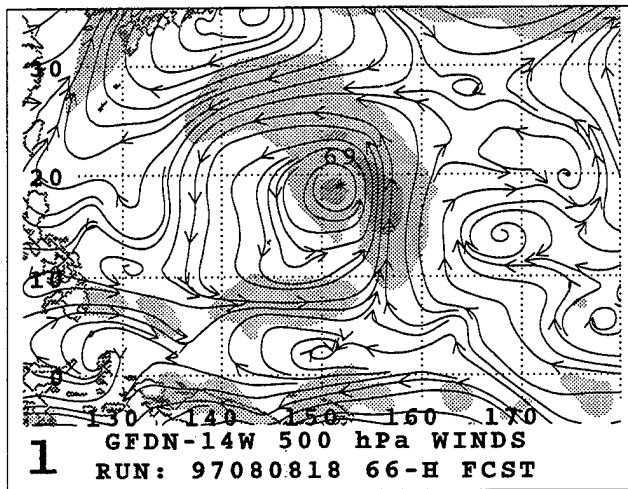
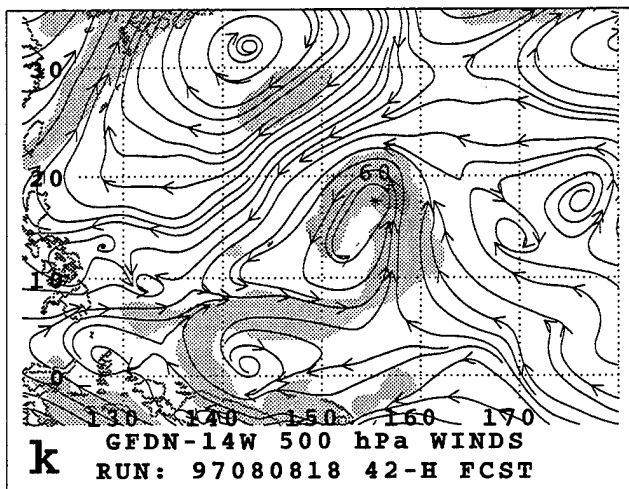
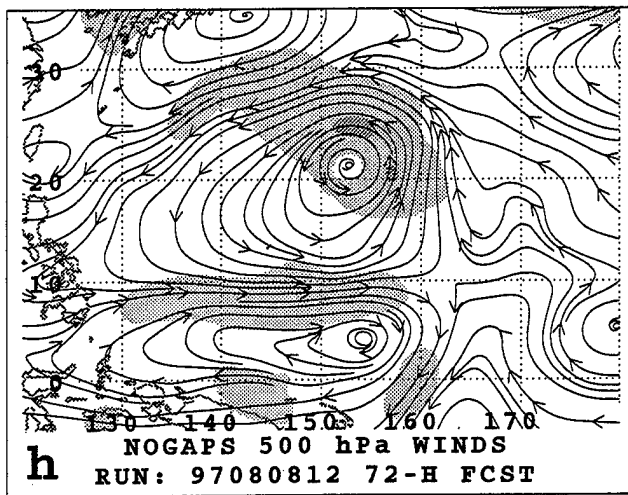
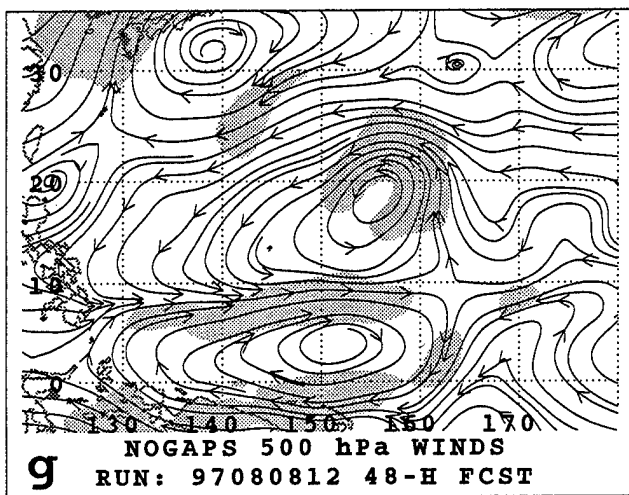
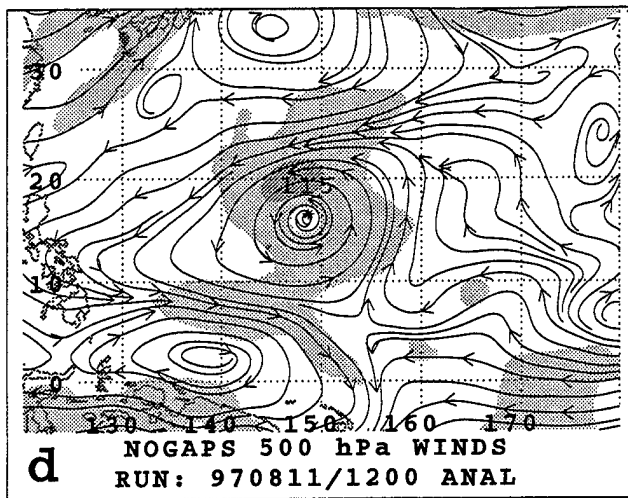
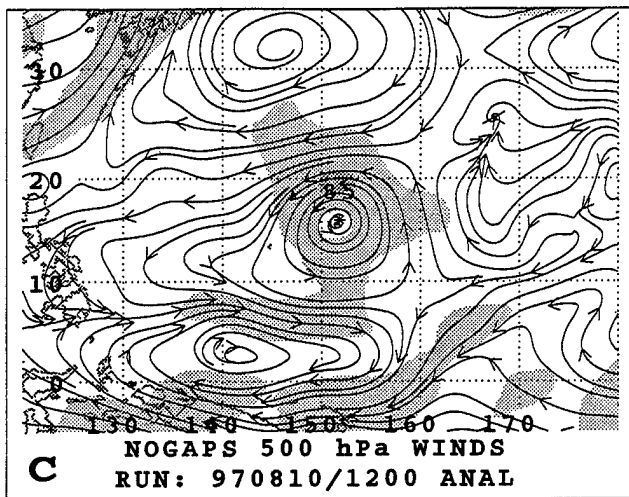


Fig. A.5. (continued)

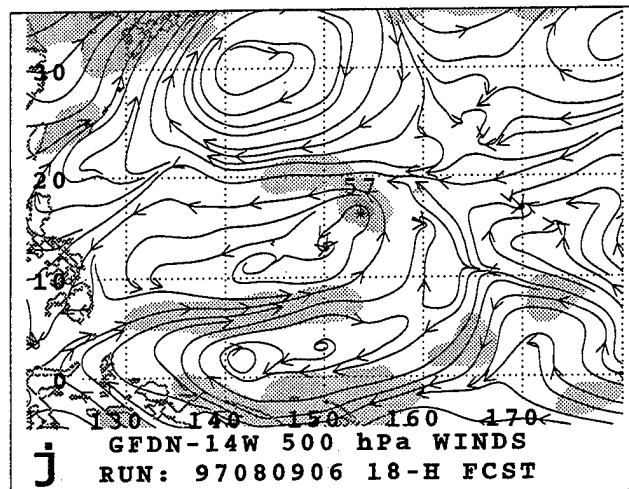
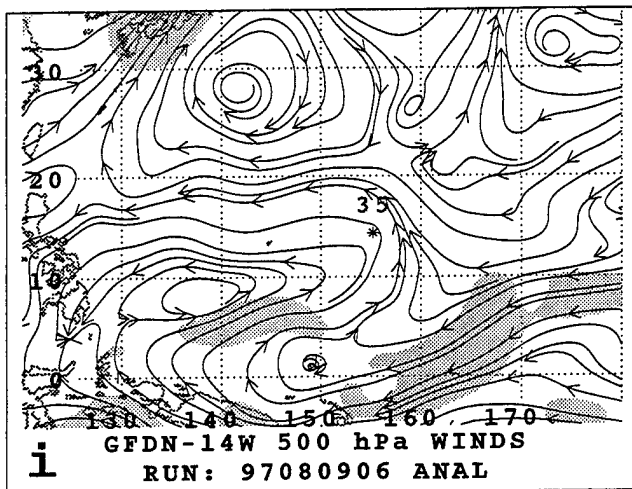
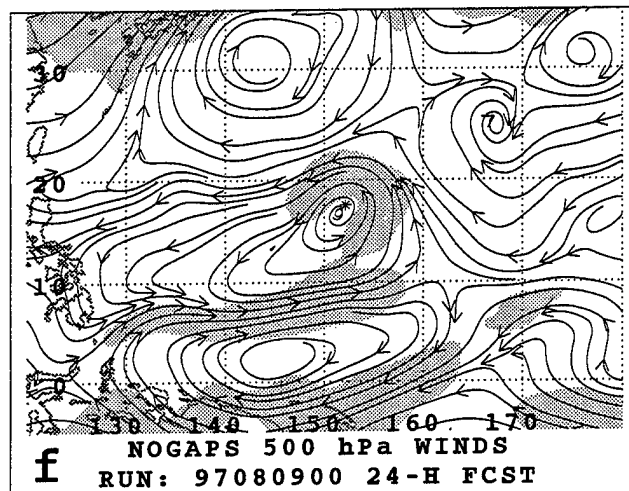
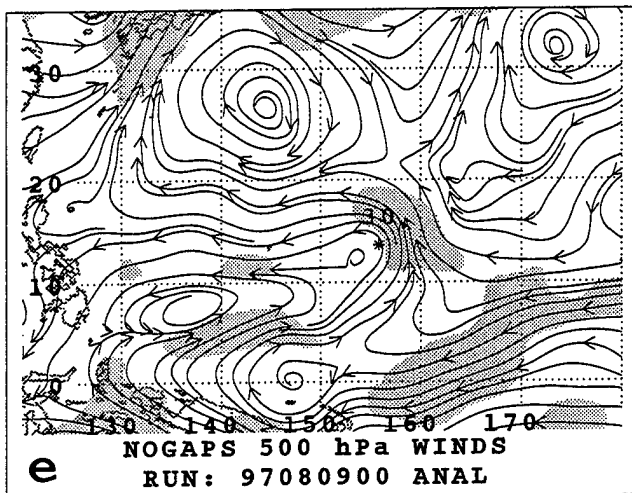
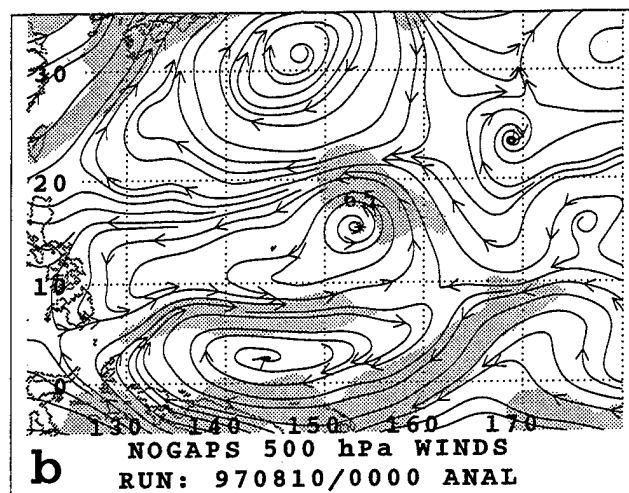
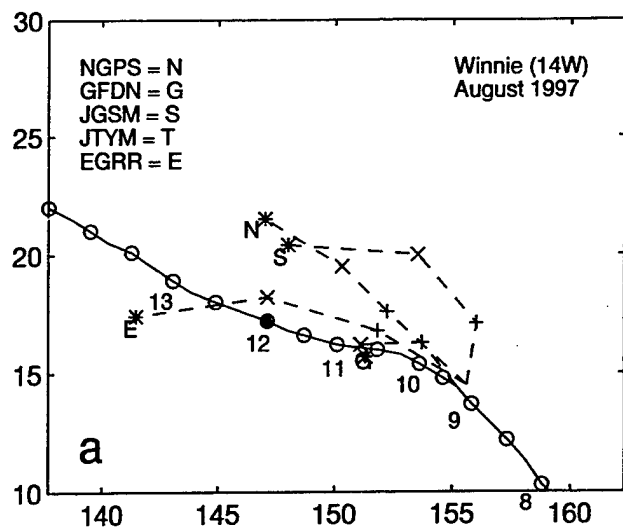


Fig. A.6. (a-l) As in Fig. A.1, except for 500-mb wind forecasts for Winnie initiated at 0000 and 0600 UTC 9 August 1997.

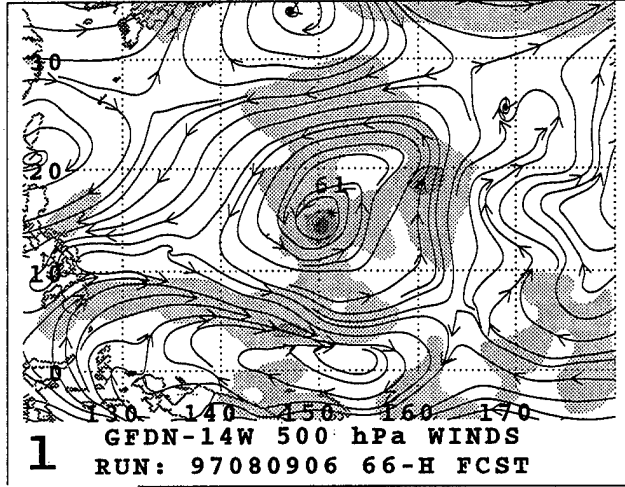
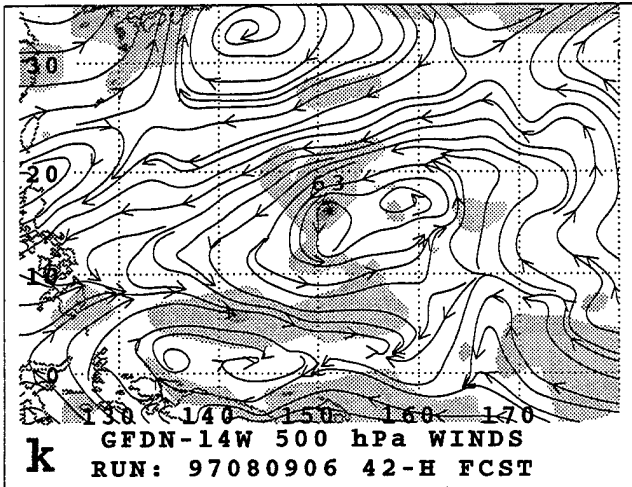
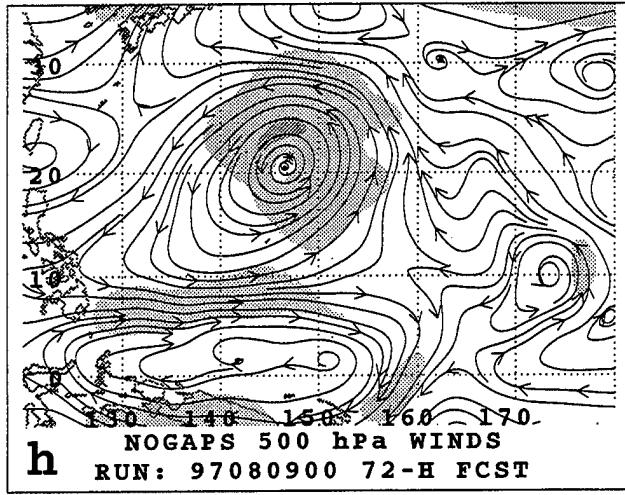
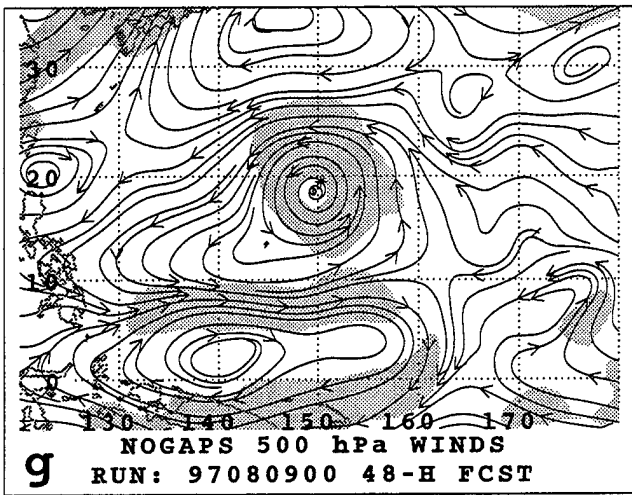
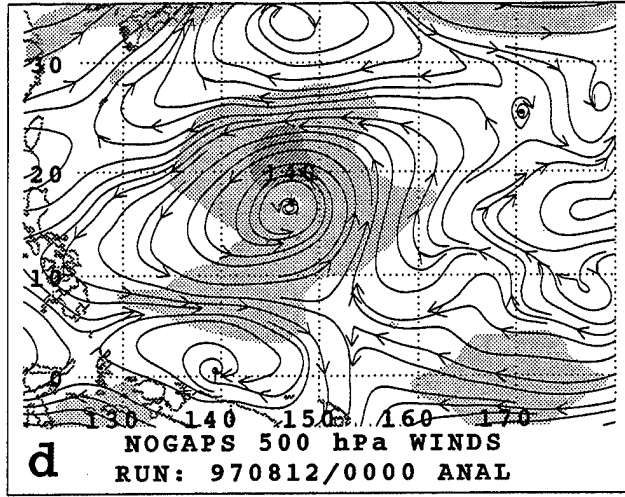
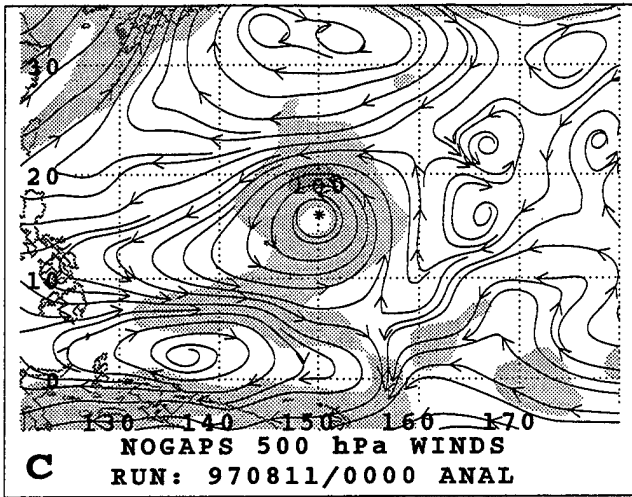


Fig. A.6. (continued)

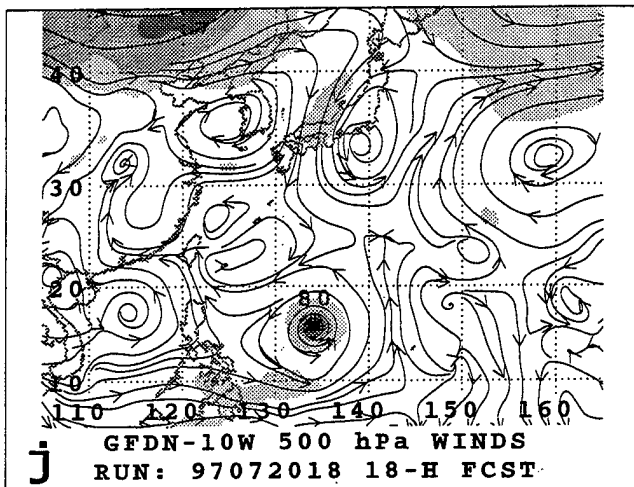
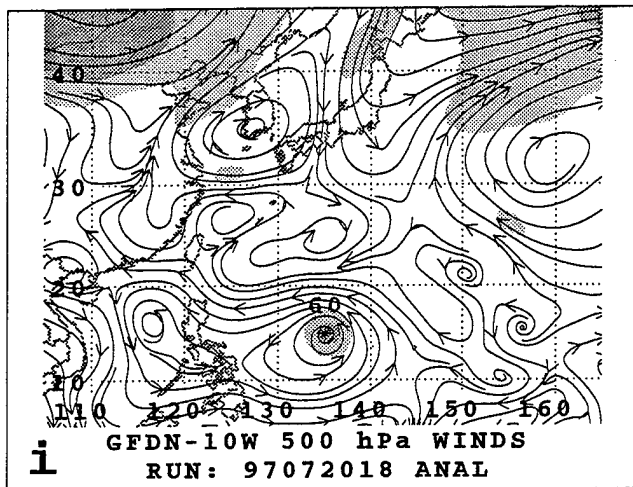
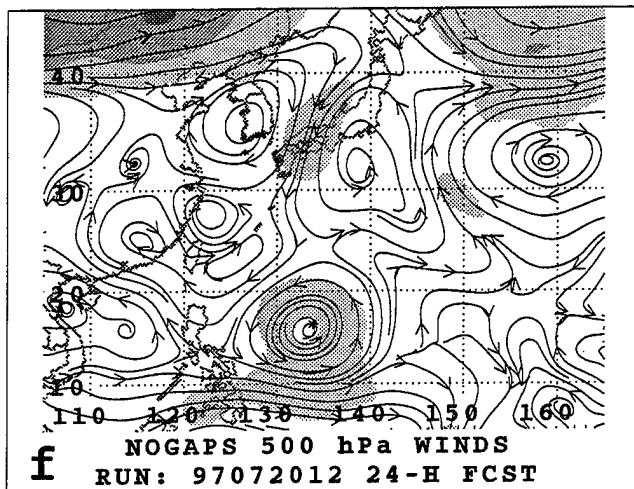
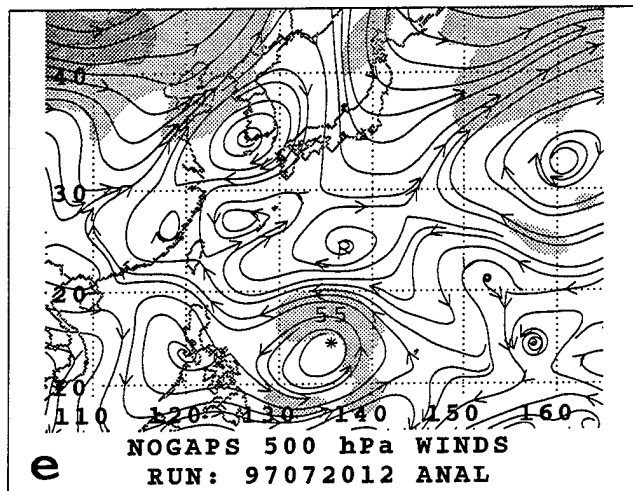
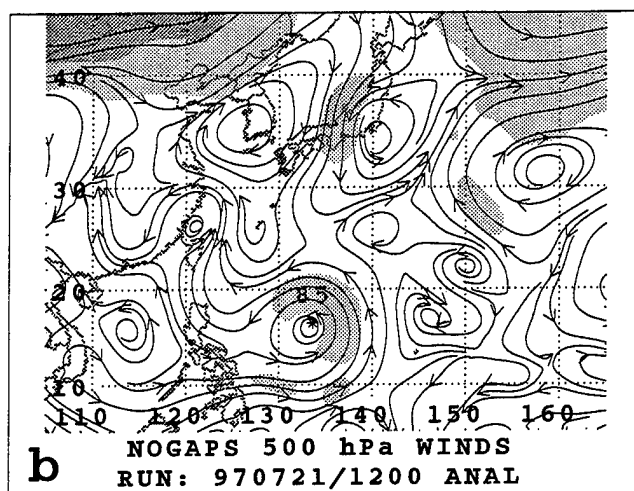
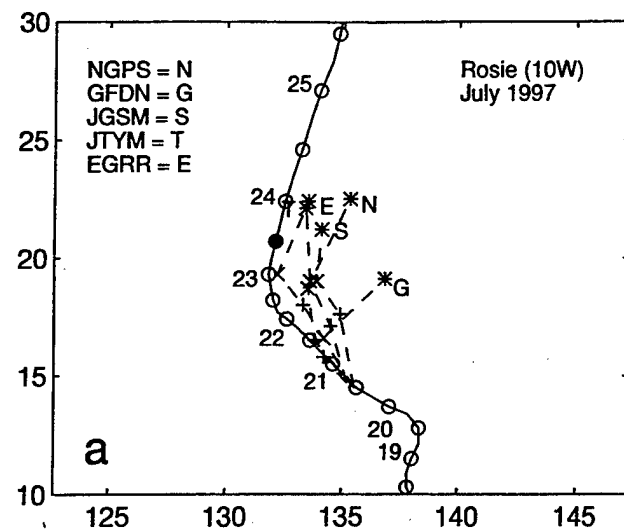


Fig. A.7. (a-l) As in Fig. A.1, except for 500-mb wind forecasts for Rosie initiated at 1200 and 1800 UTC 20 July 1997.

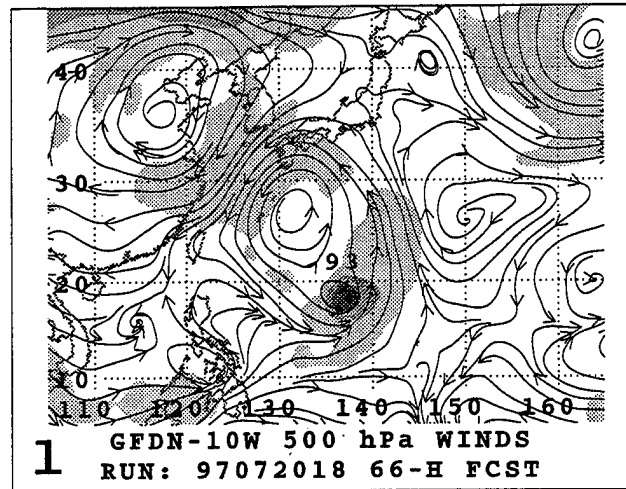
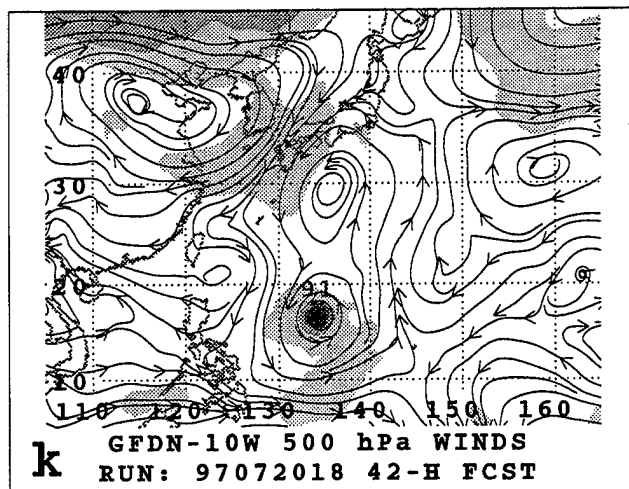
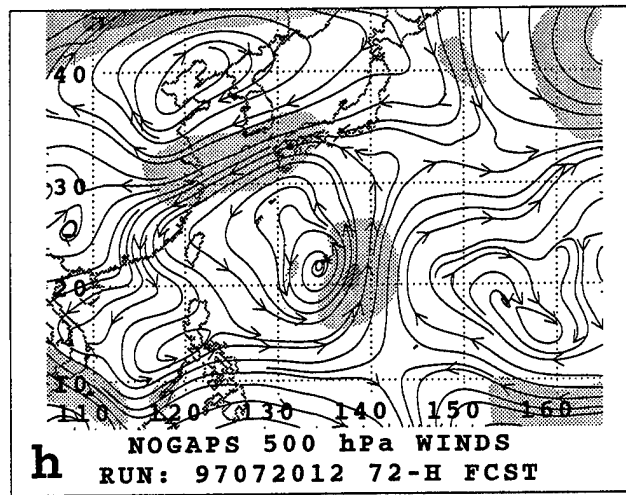
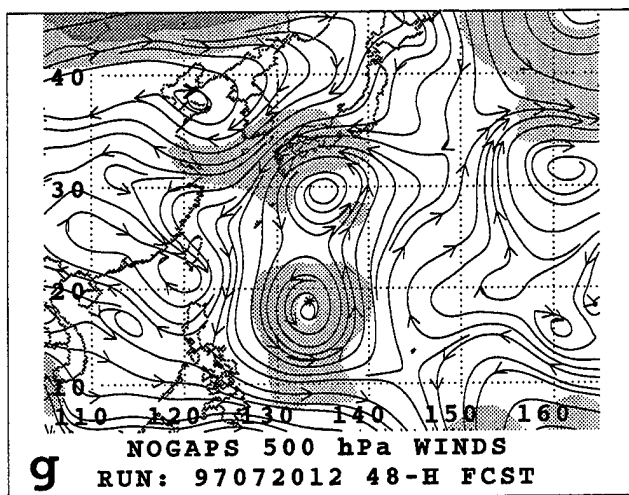
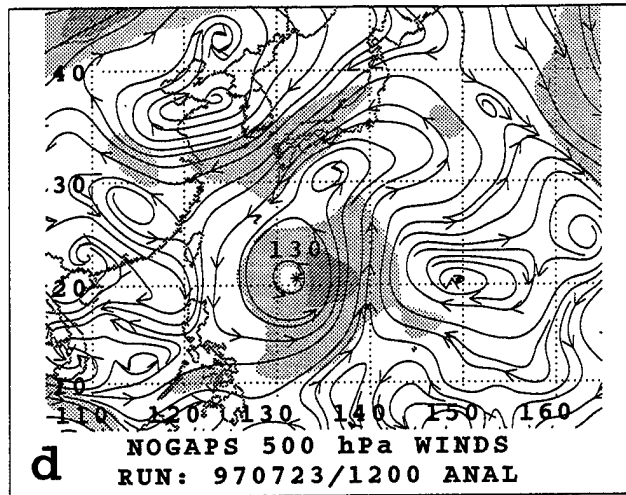
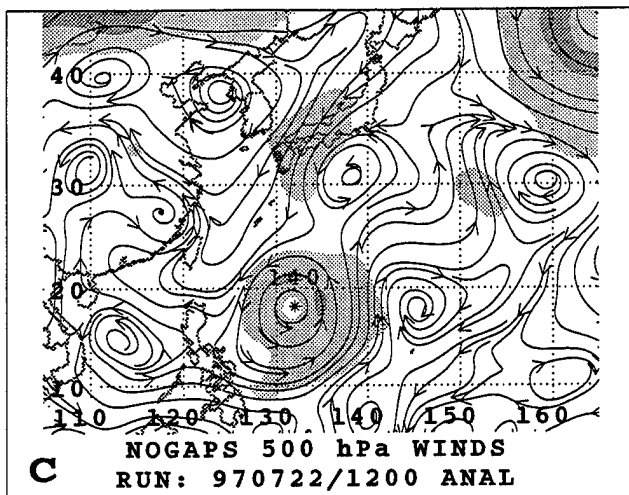


Fig. A.7. (continued)

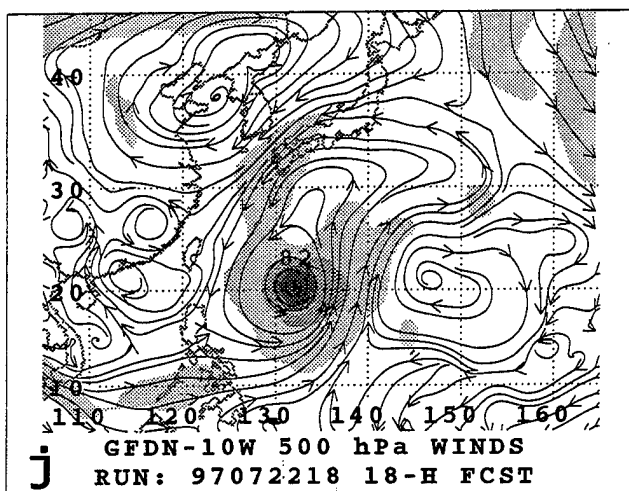
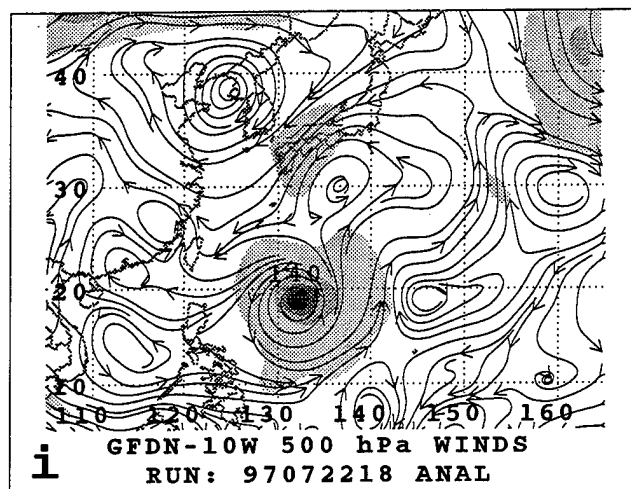
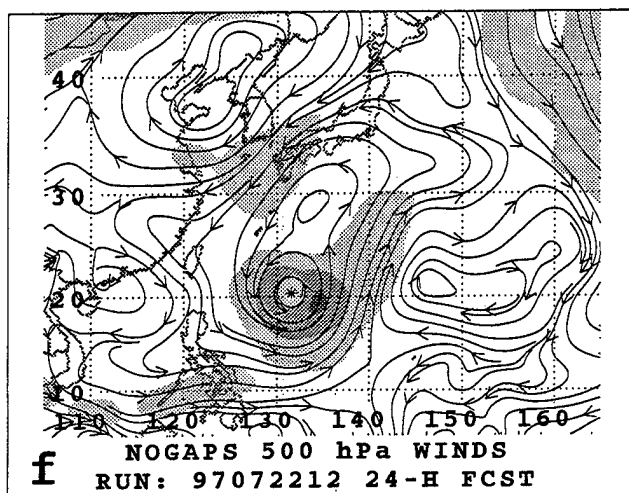
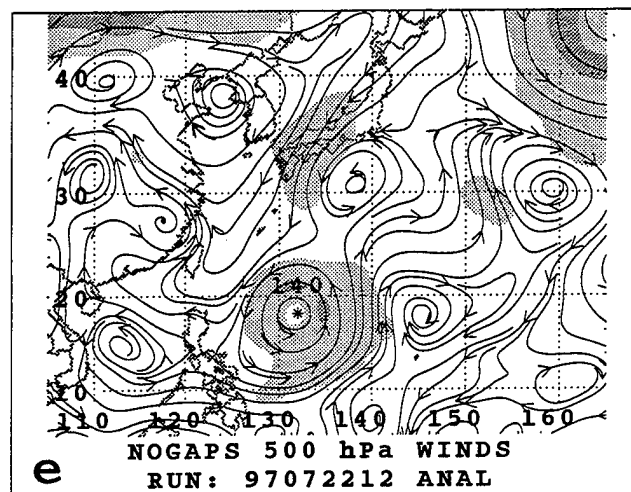
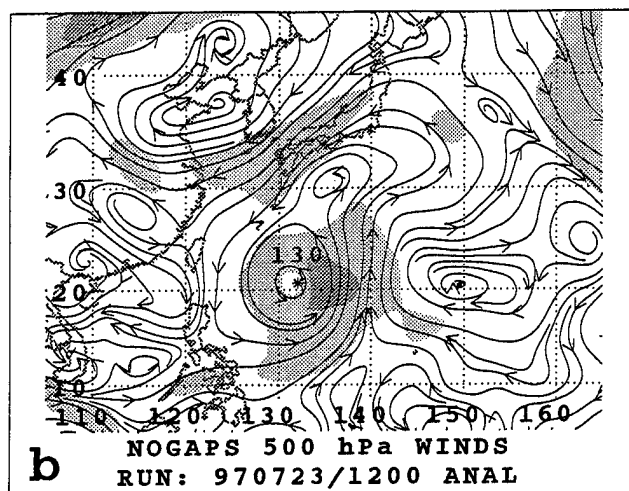
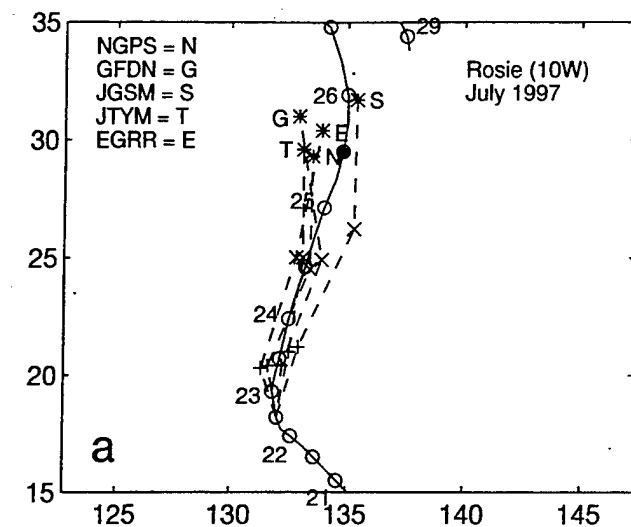


Fig. A.8. (a-l) As in Fig. A.1, except for 500-mb wind forecasts for Rosie initiated at 1200 and 1800 UTC 22 July 1997.

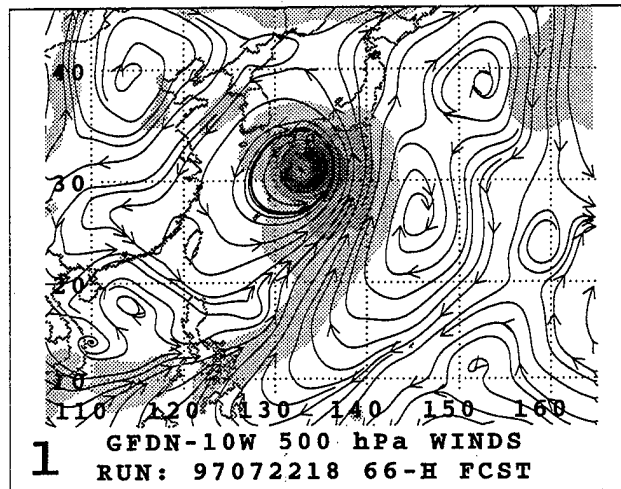
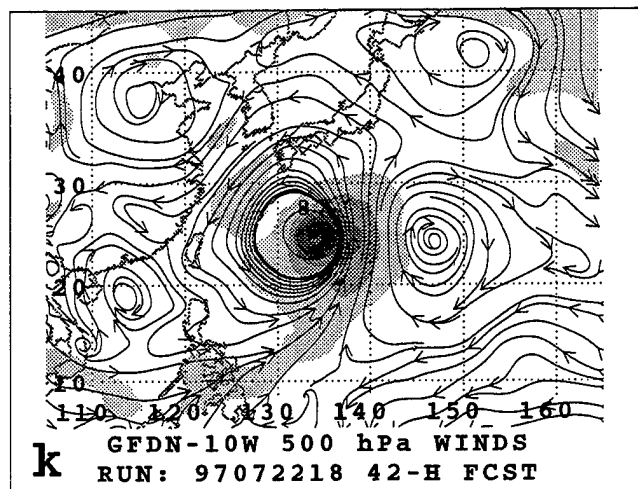
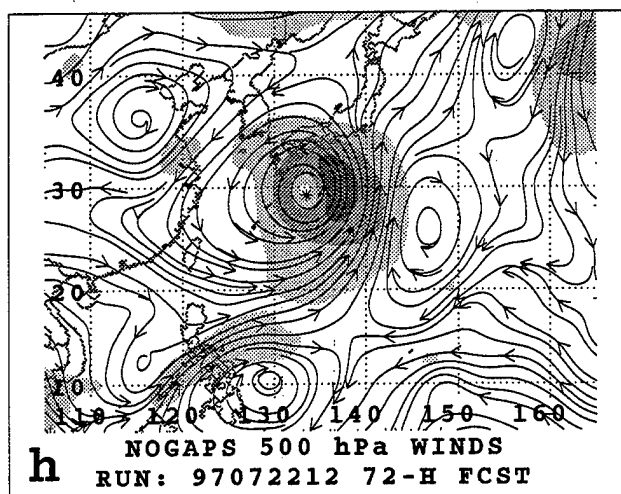
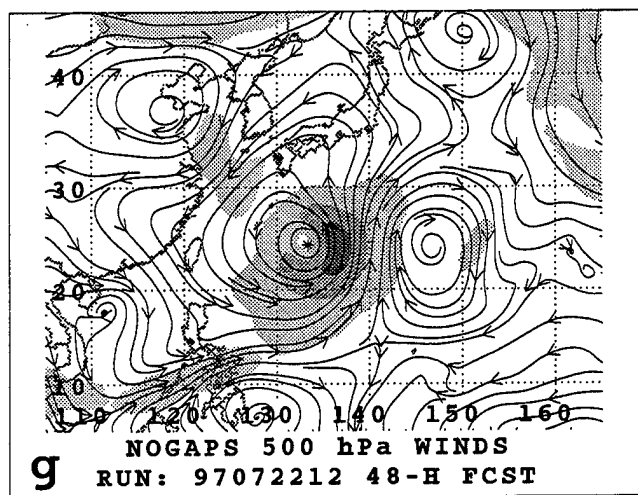
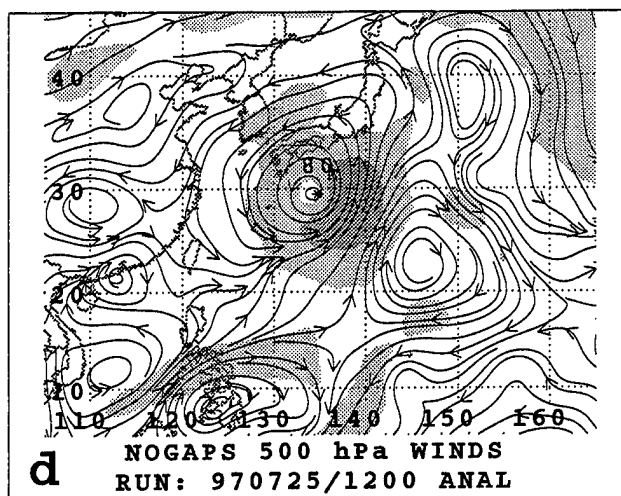
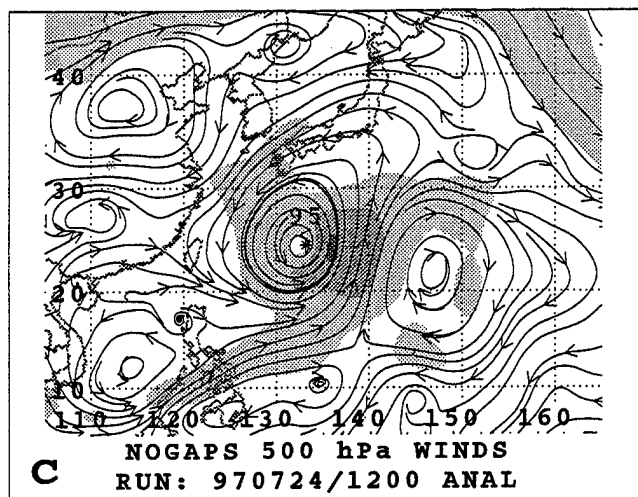


Fig. A.8. (continued)

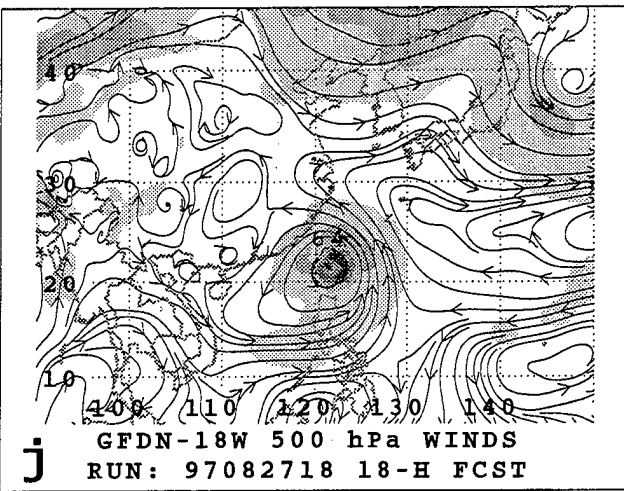
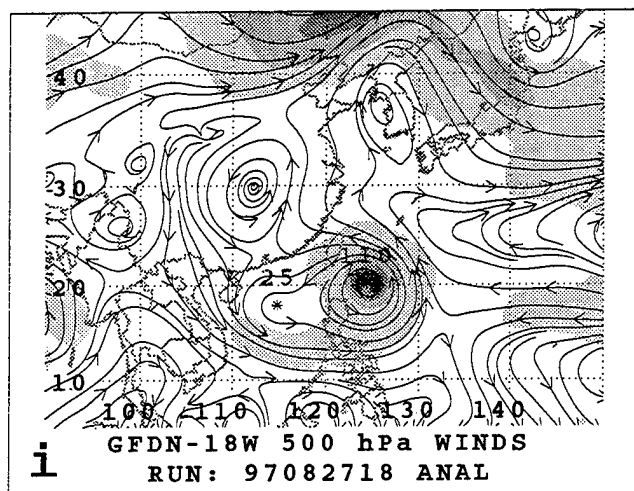
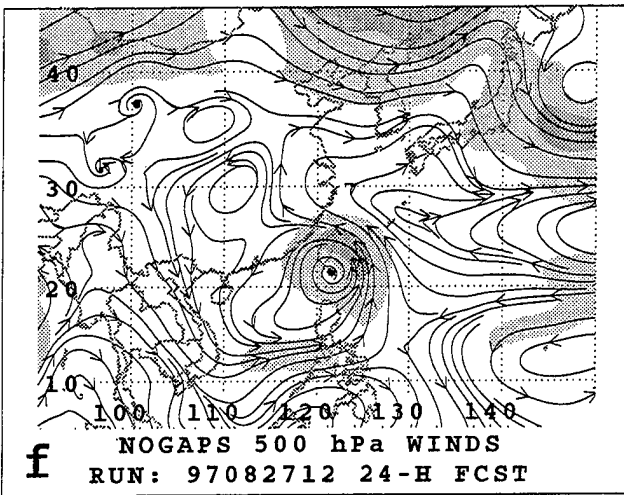
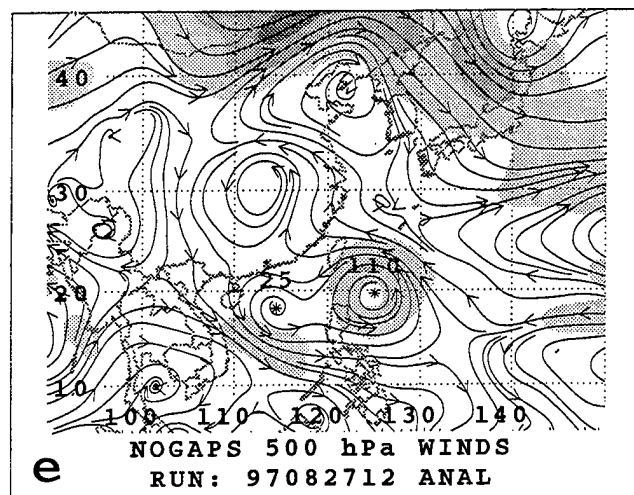
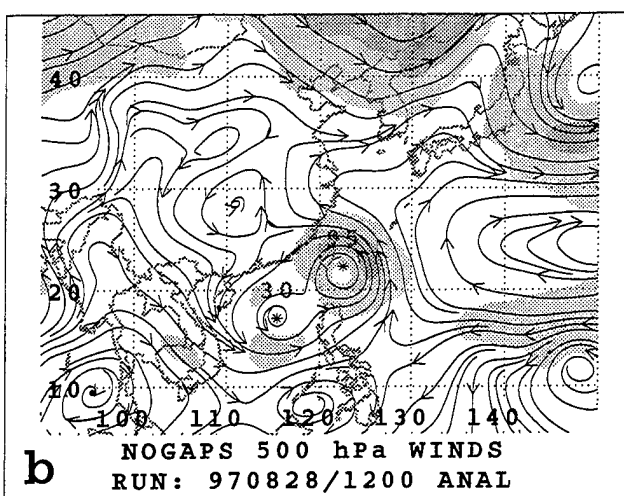
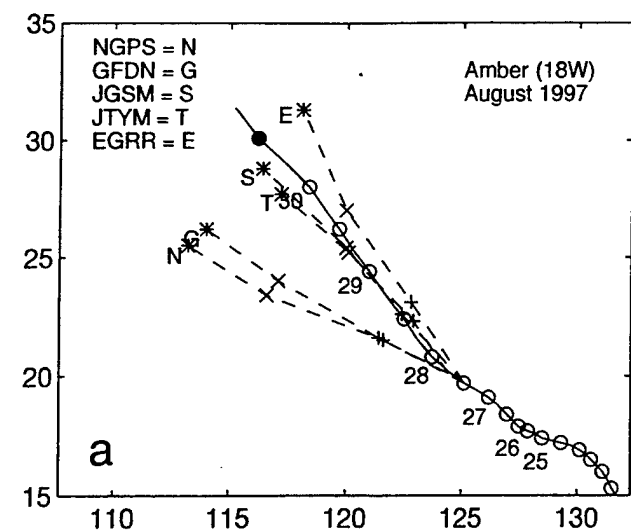


Fig. A.9. (a-l) As in Fig. A.1, except for 500-mb wind forecasts for Amber initiated at 1200 and 1800 UTC 27 August 1997.

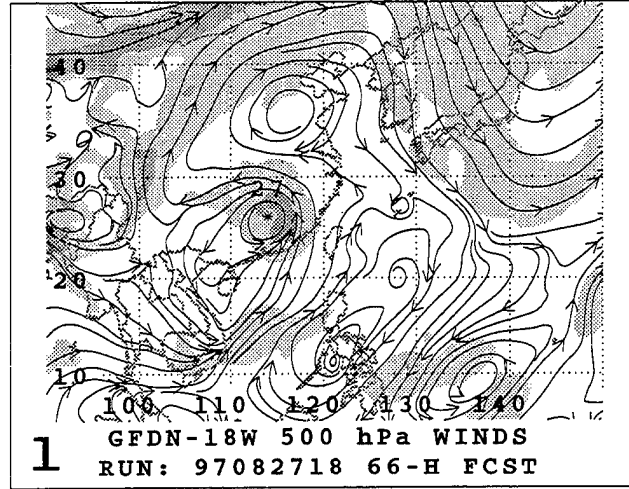
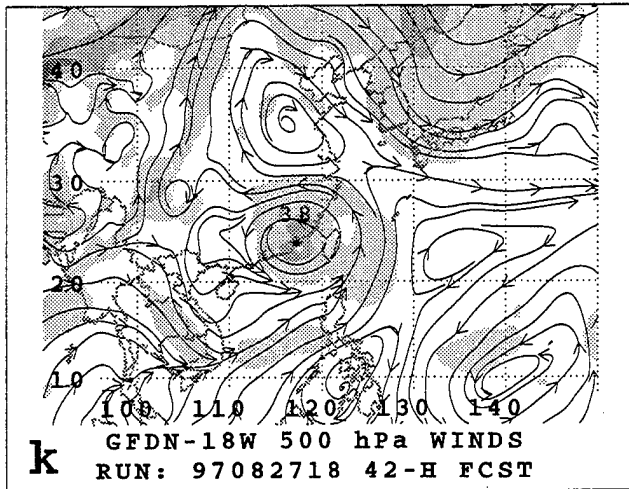
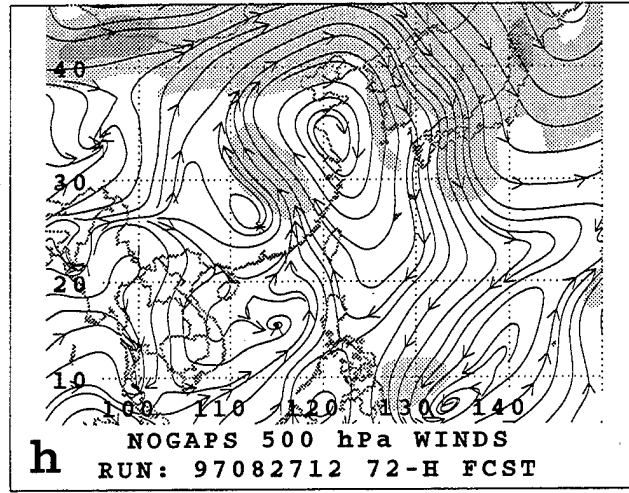
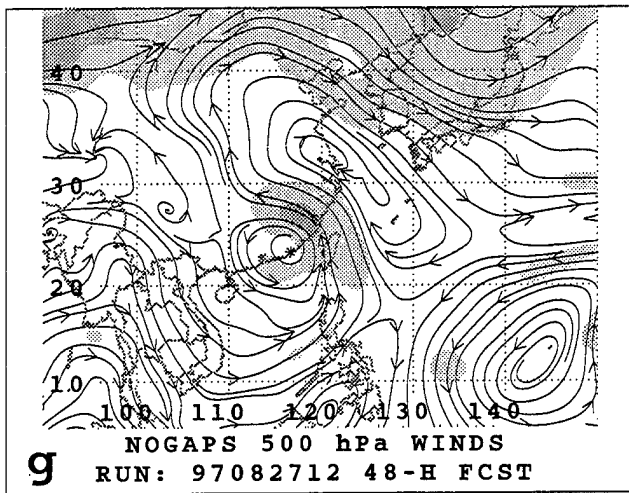
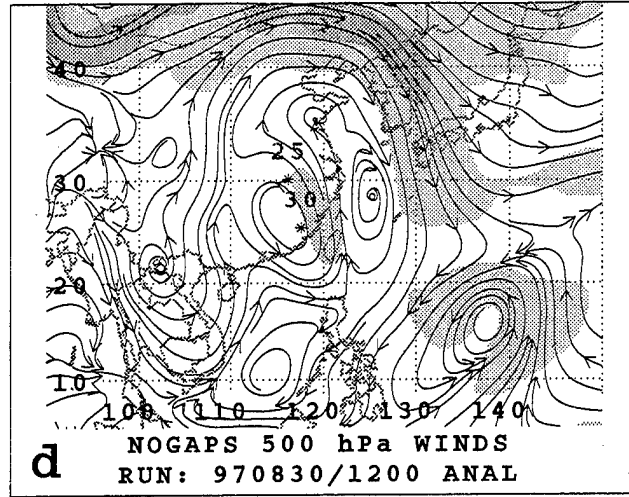
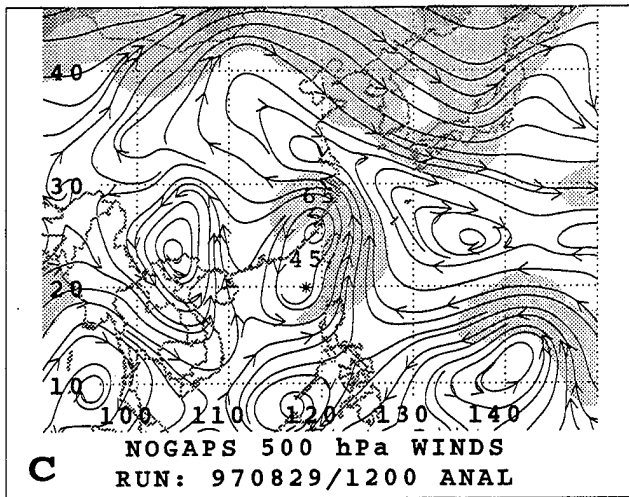


Fig. A.9. (continued)

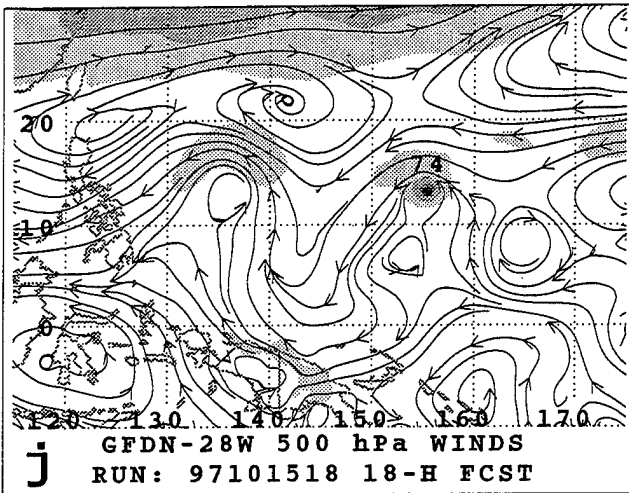
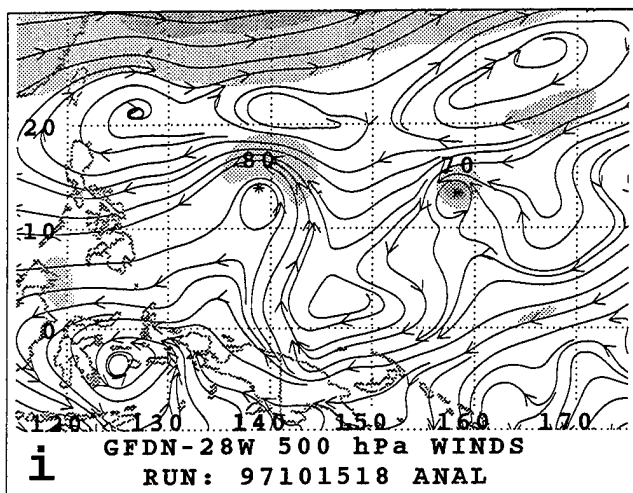
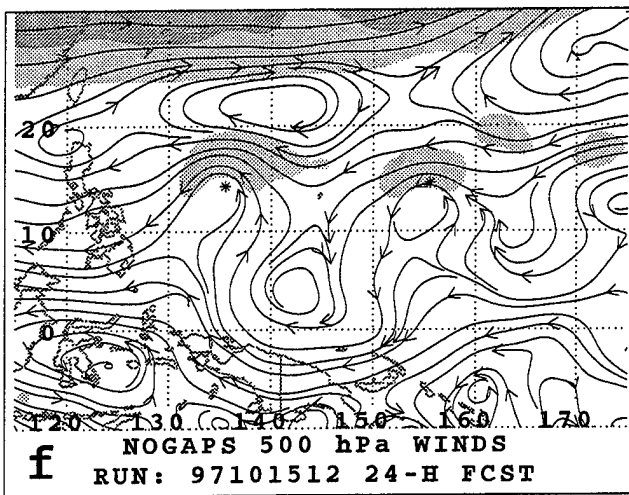
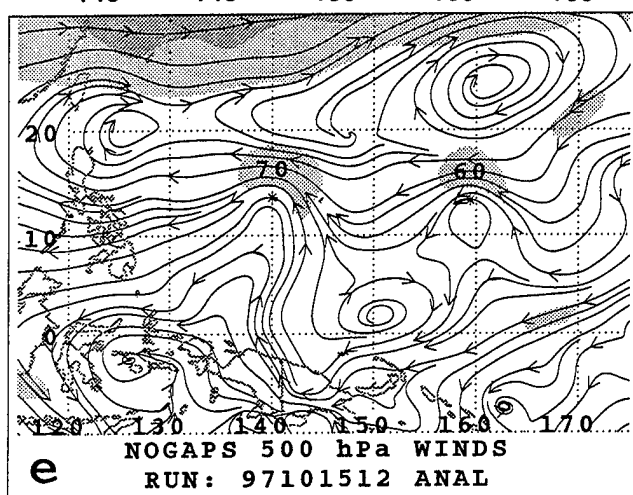
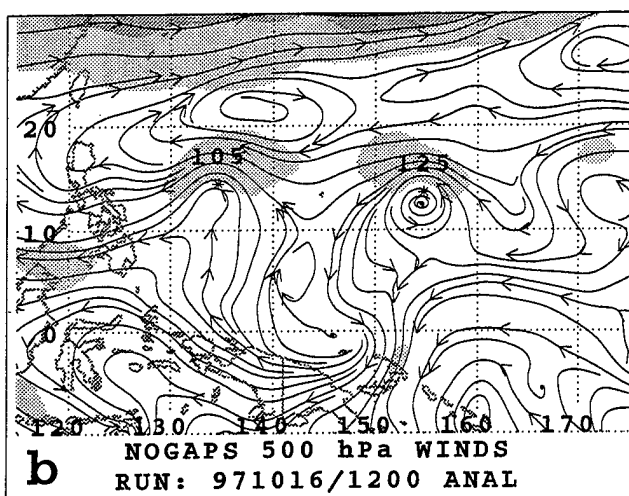
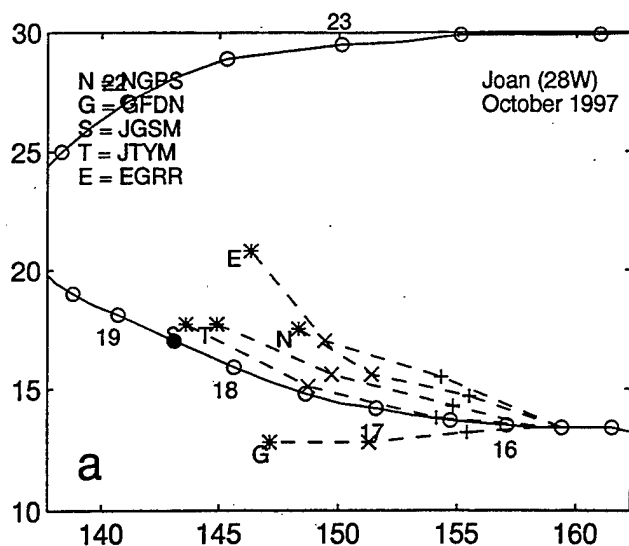


Fig. A.10. (a-l) As in Fig. A.1, except for 500-mb wind forecasts for Joan initiated at 1200 and 1800 UTC 15 October 1997.

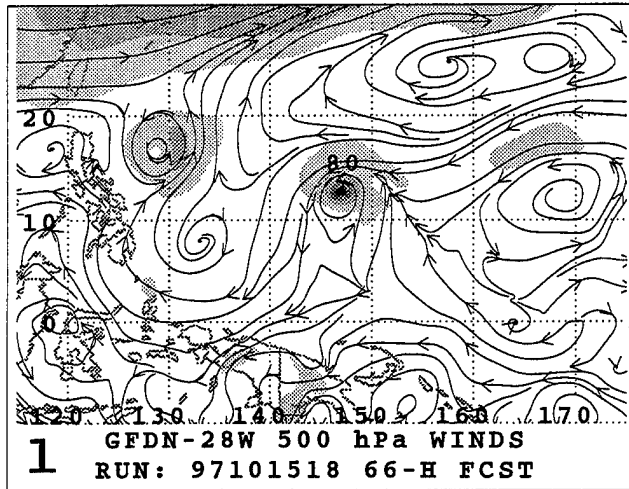
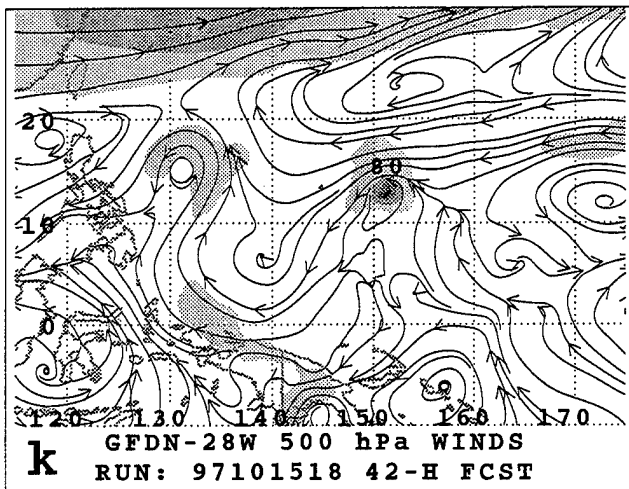
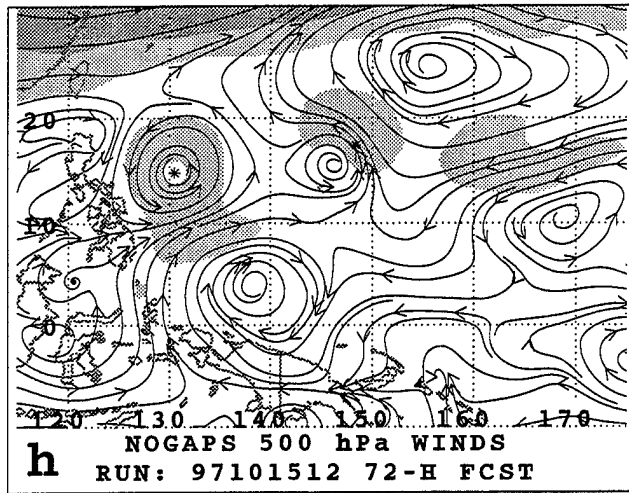
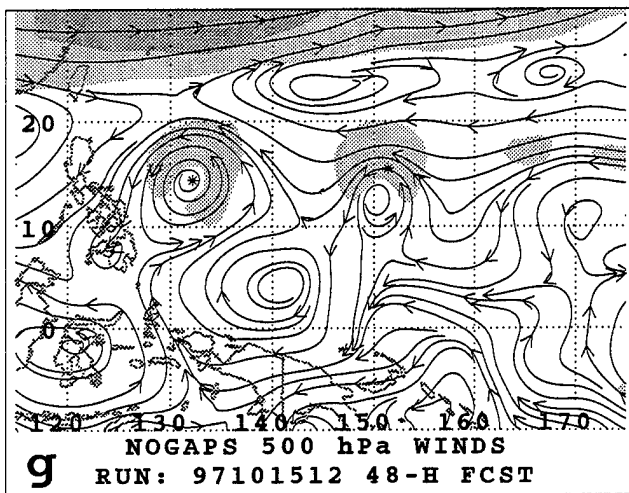
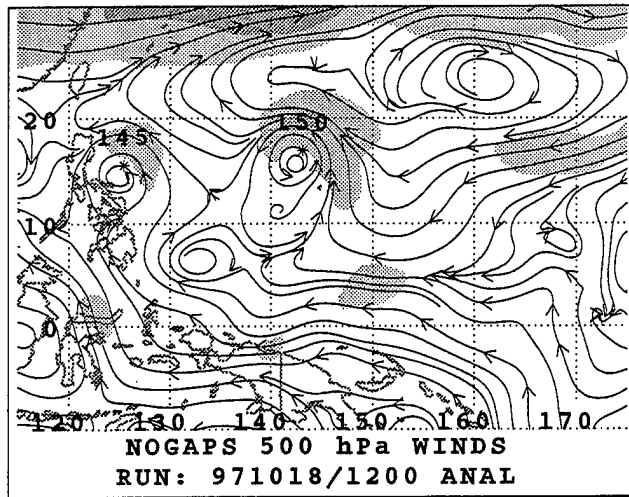
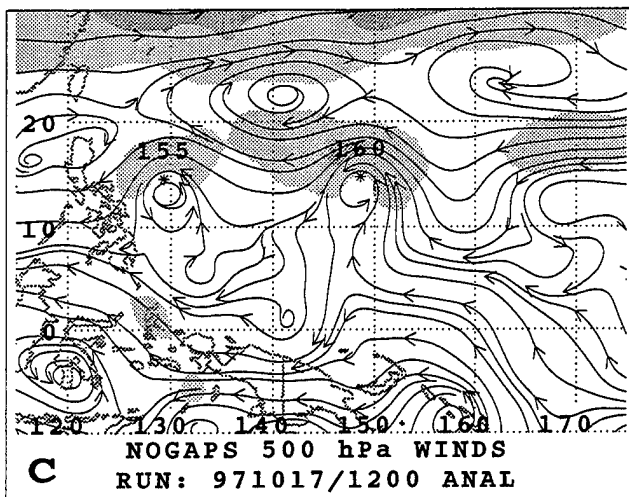


Fig. A.10. (continued)

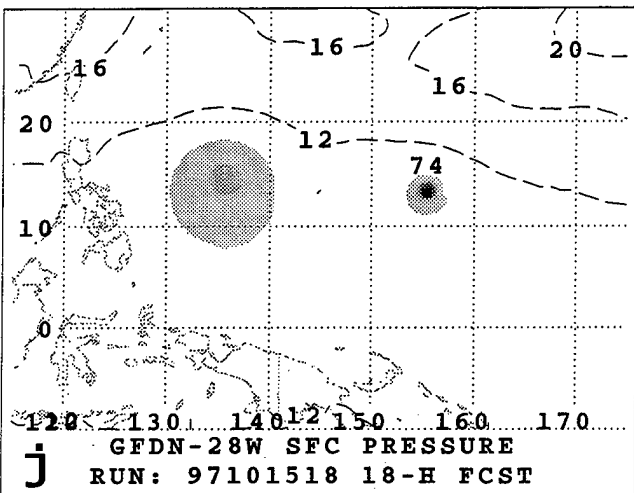
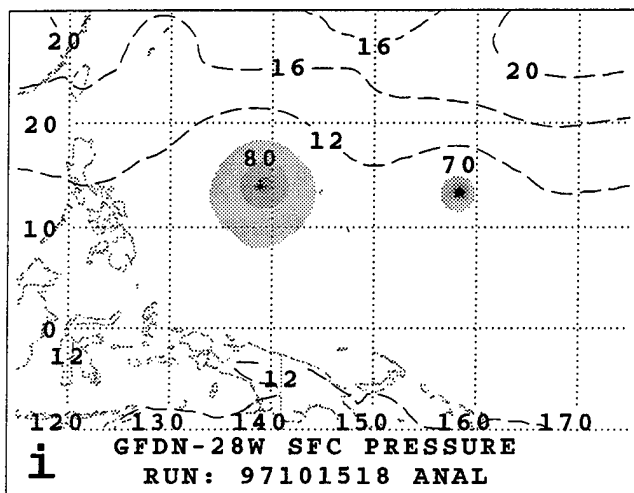
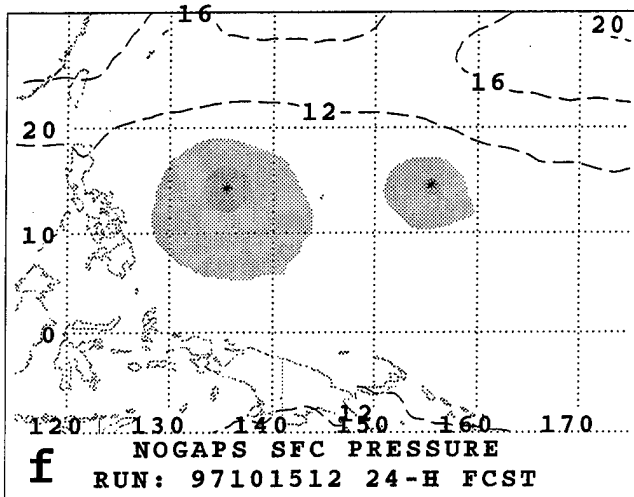
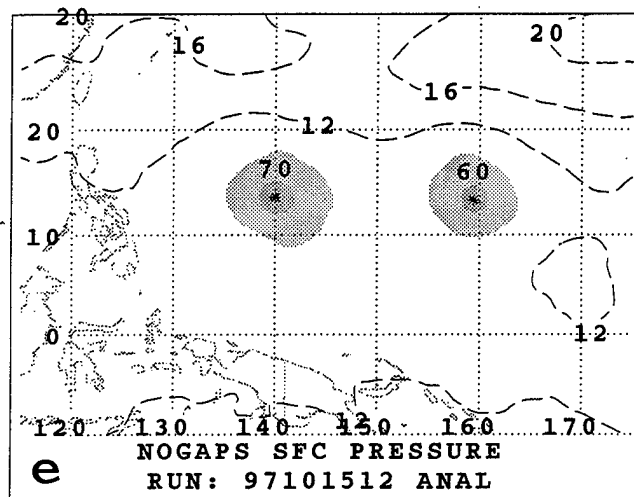
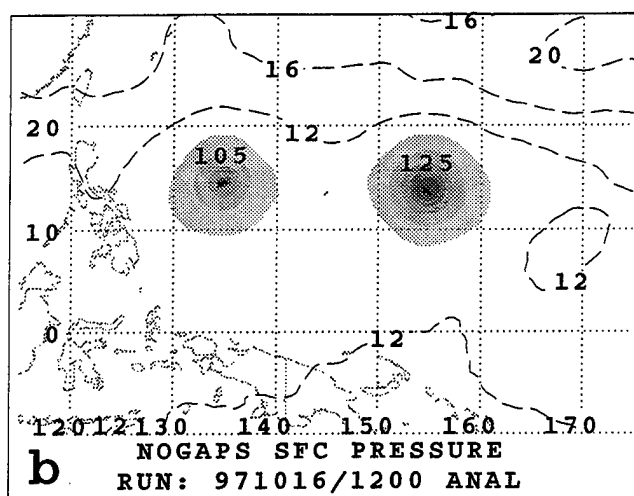
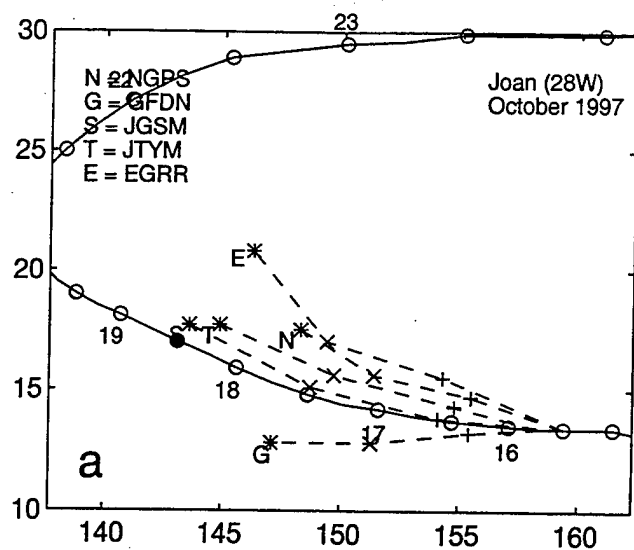


Fig. A.11. (a-l) As in Fig. A.1, except for sea-level pressure forecasts for Joan initiated at 1200 and 1800 UTC 15 October 1997.

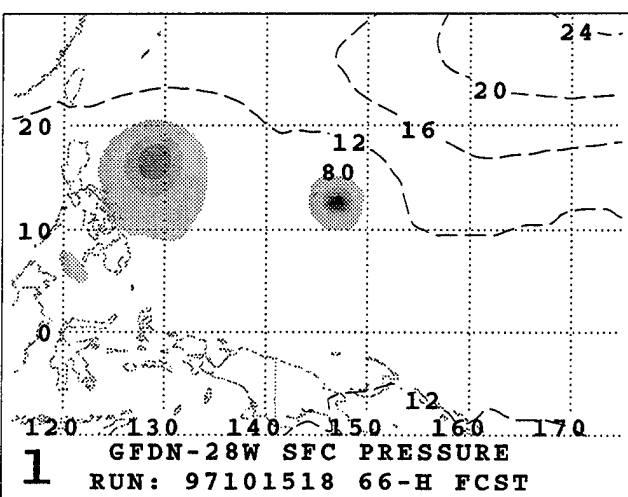
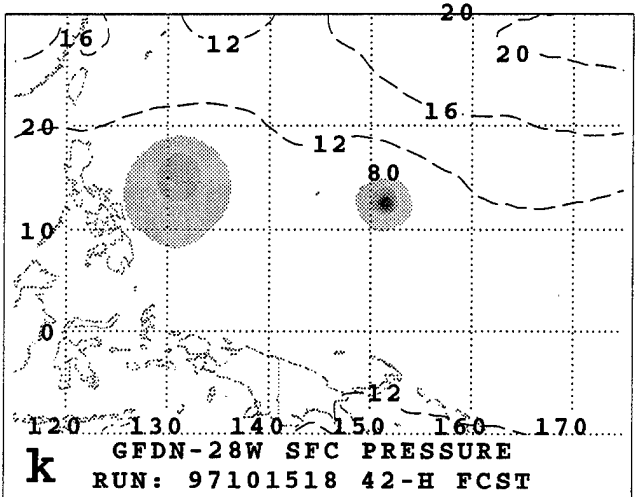
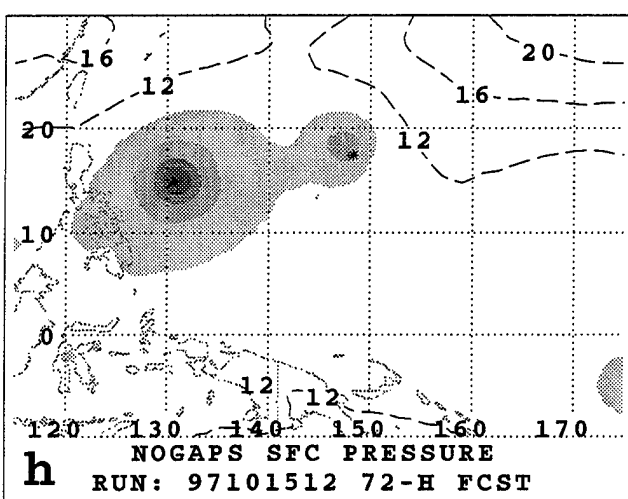
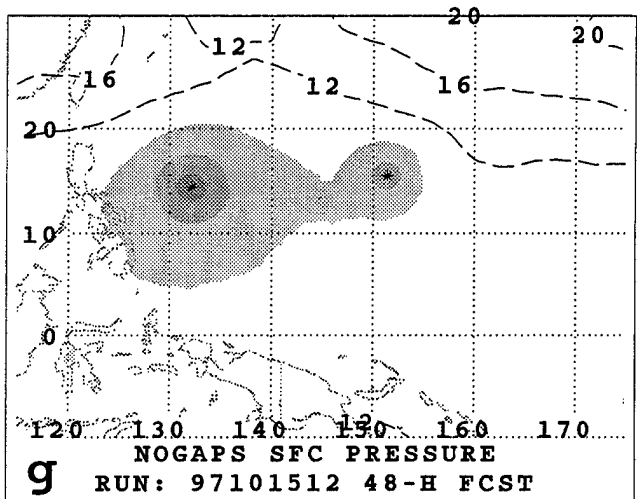
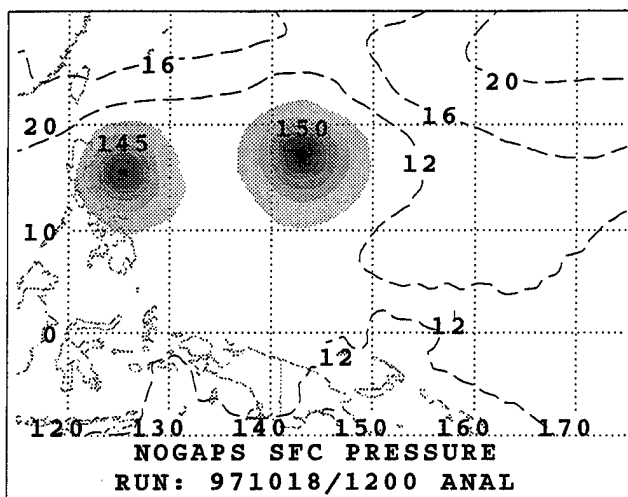
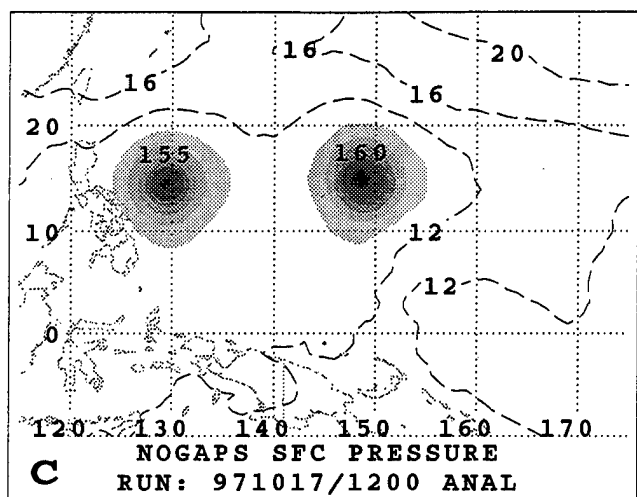


Fig. A.11. (continued)

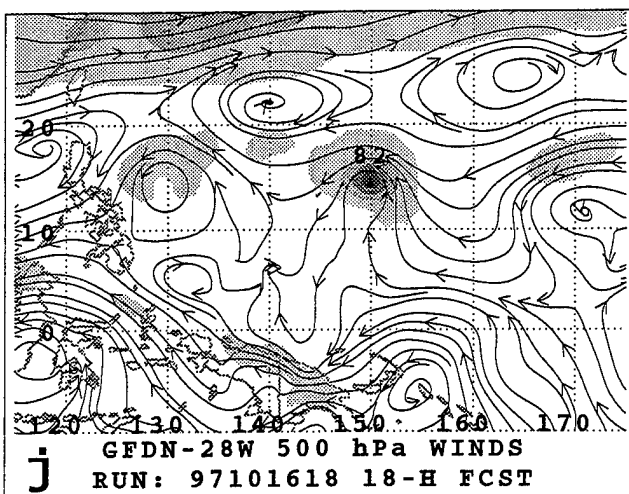
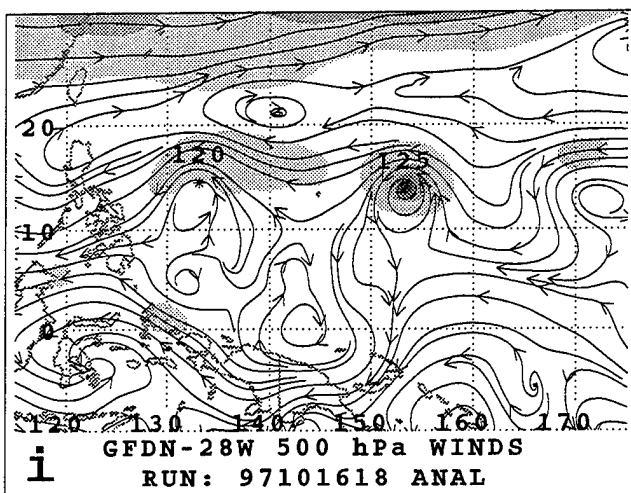
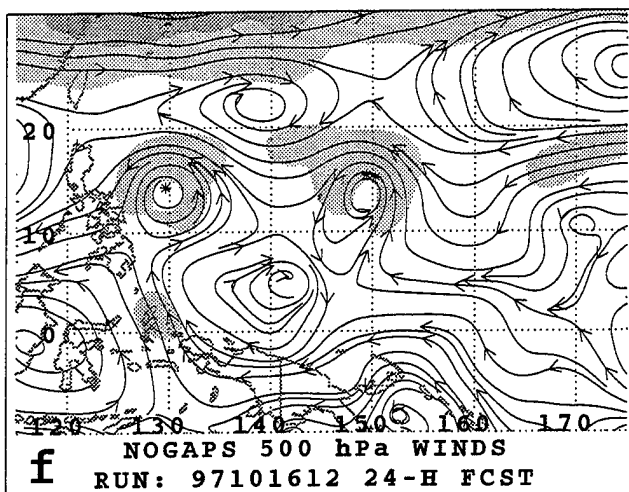
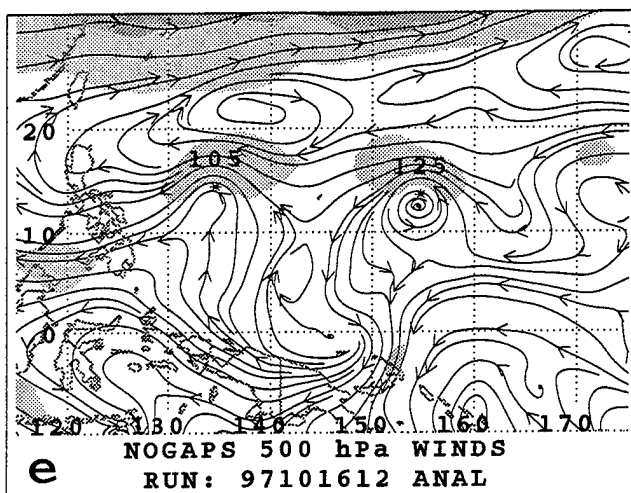
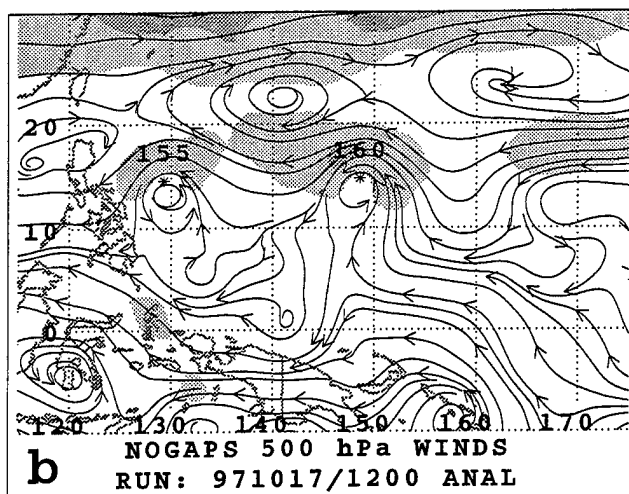
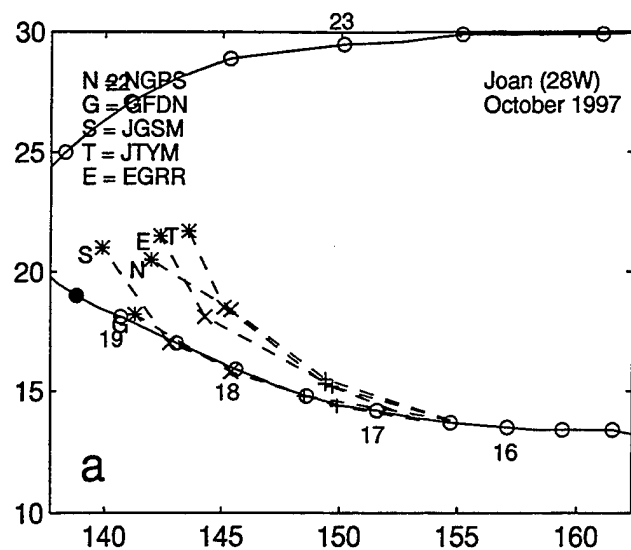


Fig. A.12. (a-l) As in Fig. A.1, except for 500-mb wind forecasts for Joan initiated at 1200 and 1800 UTC 16 October 1997.

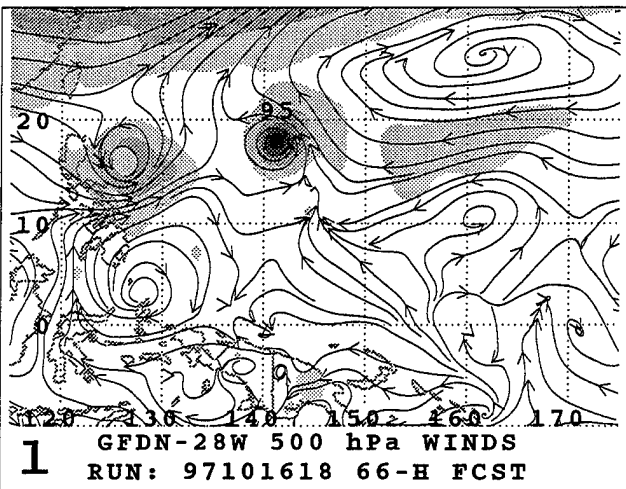
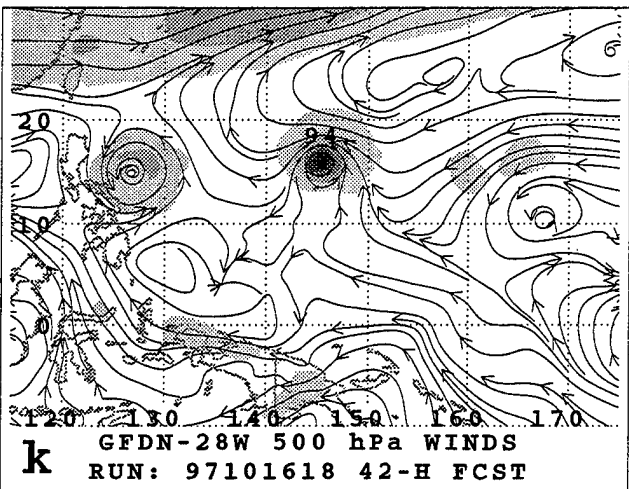
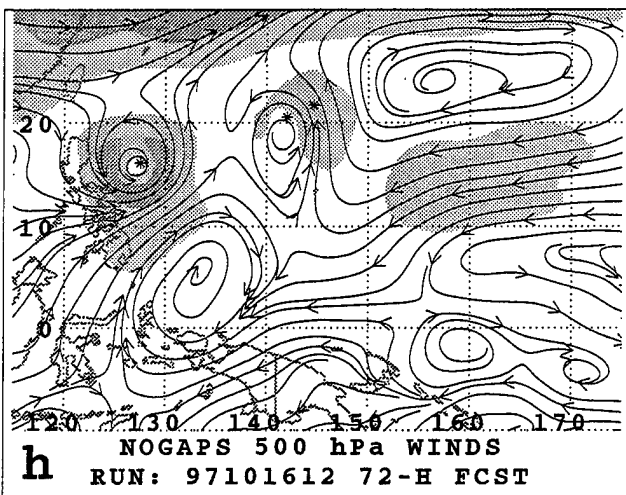
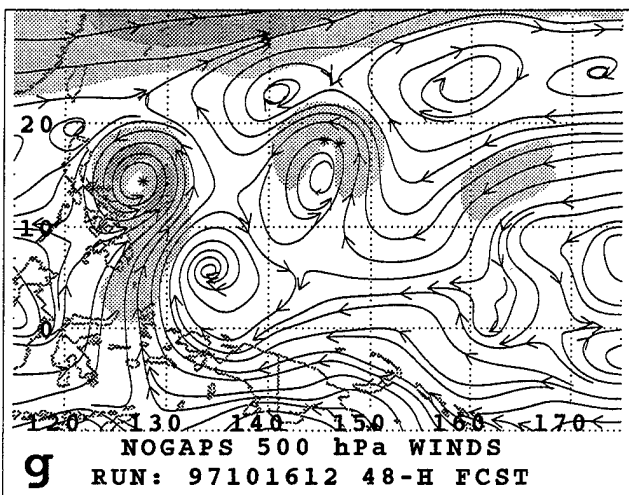
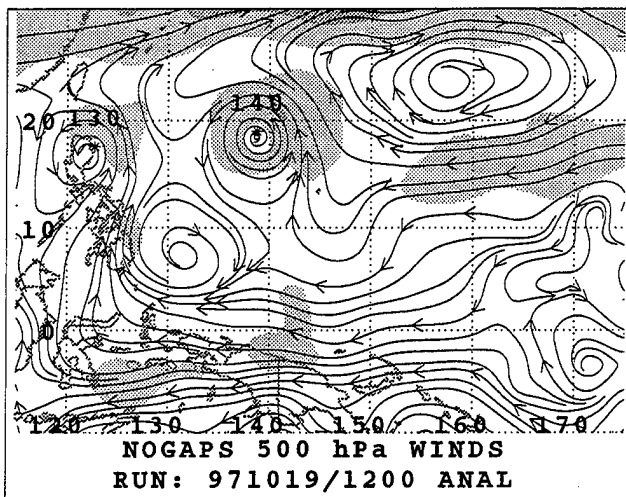
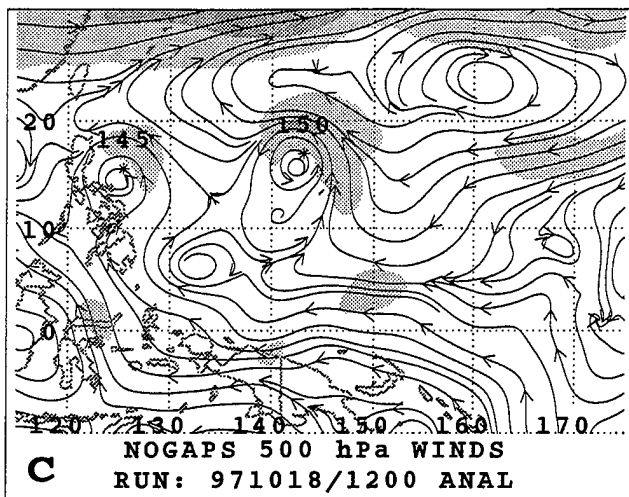


Fig. A.12. (continued)

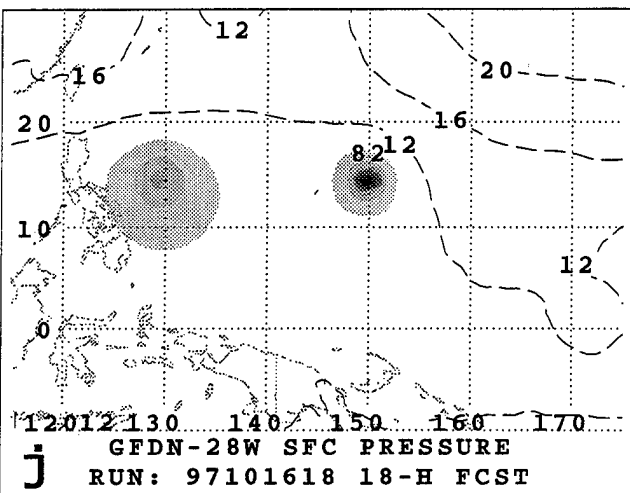
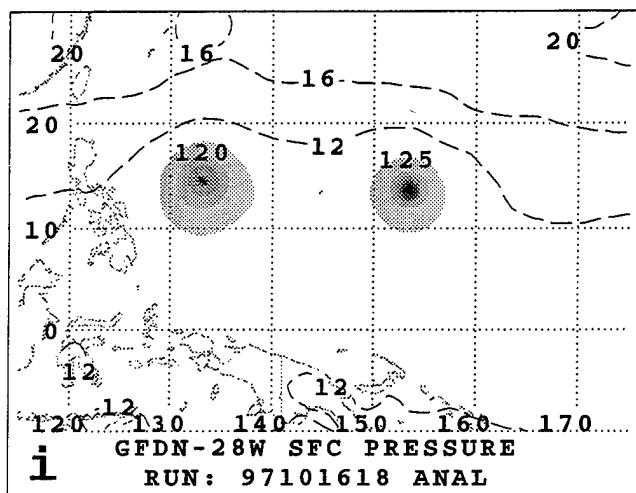
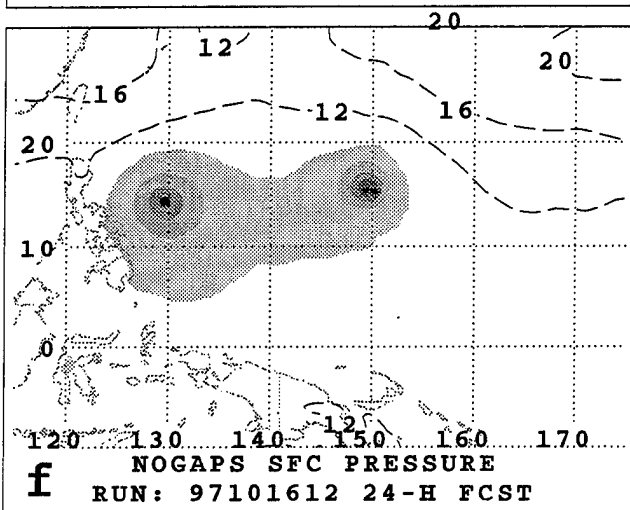
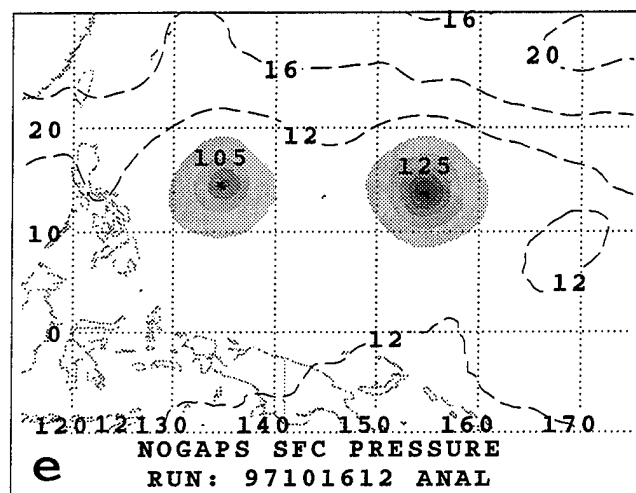
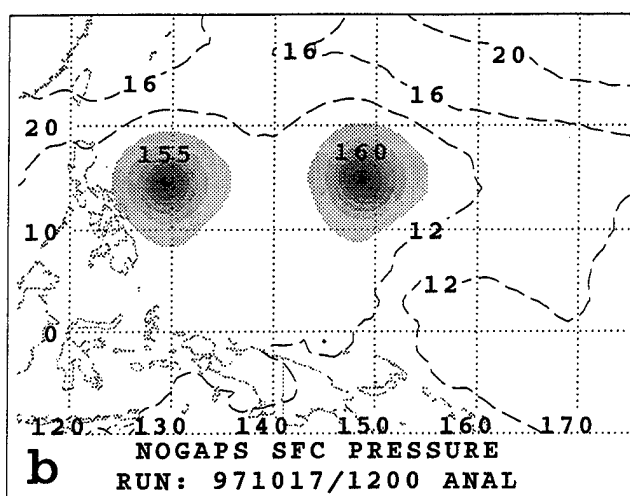
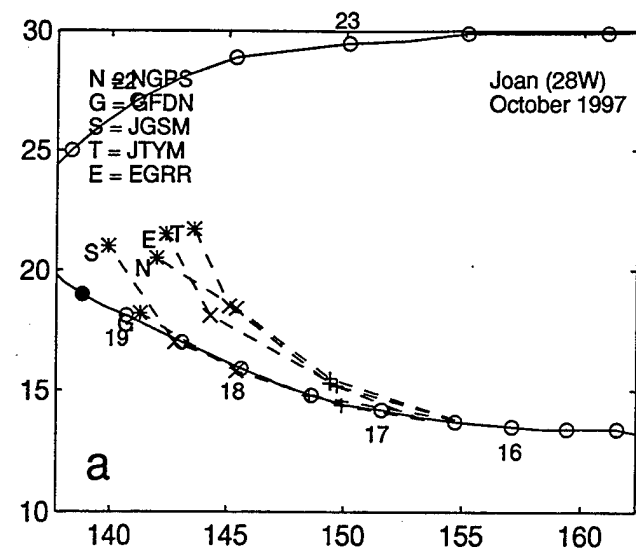


Fig. A.13. (a-l) As in Fig. A.1, except for sea-level pressure forecasts for Joan initiated at 1200 and 1800 UTC 16 October 1997.

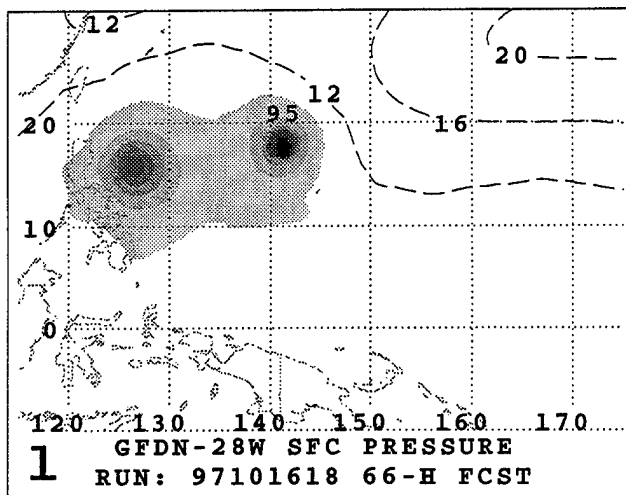
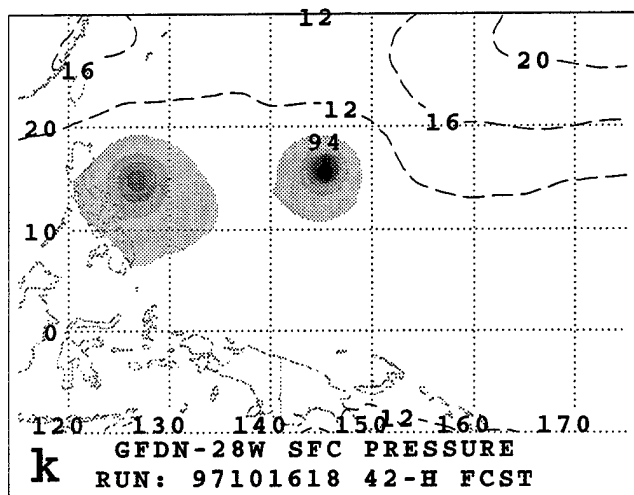
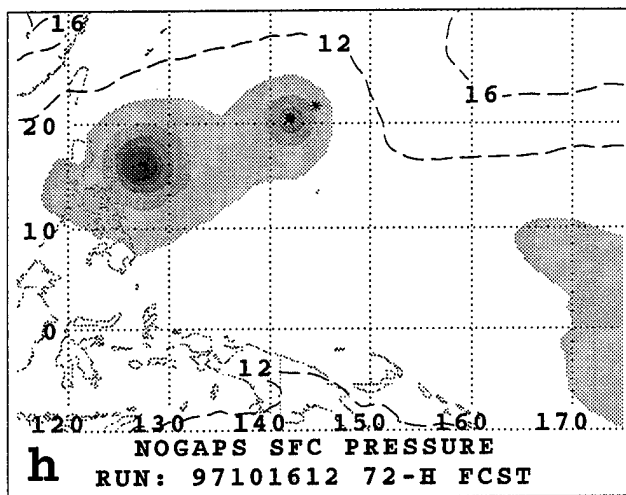
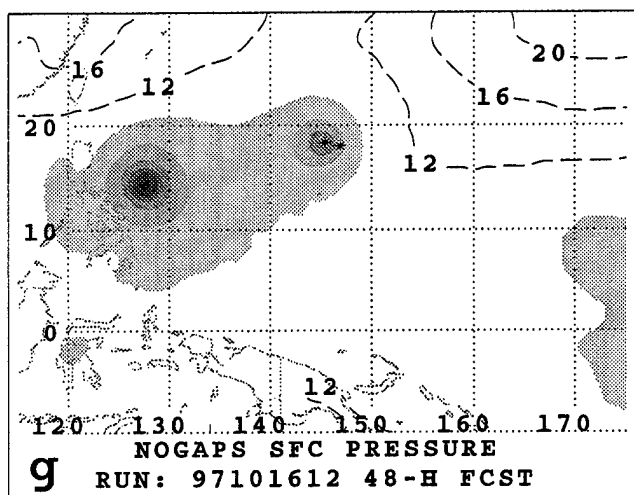
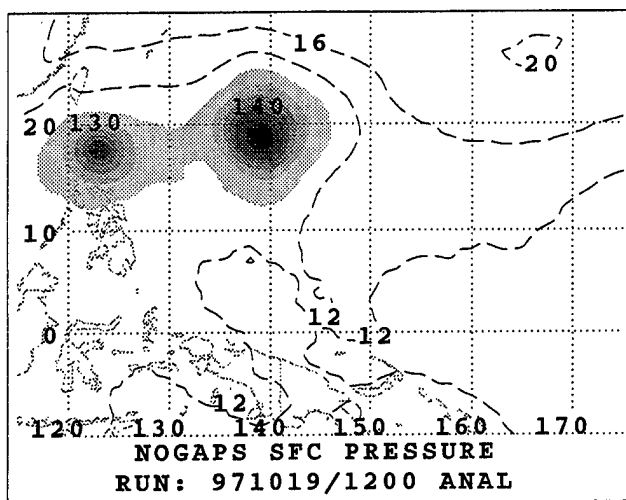
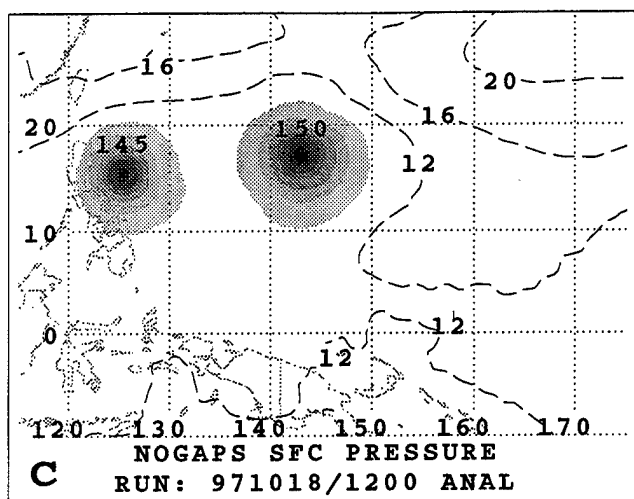


Fig. A.13. (continued)

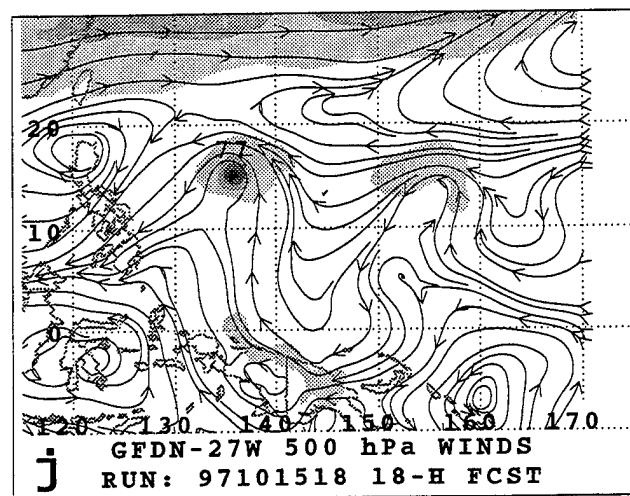
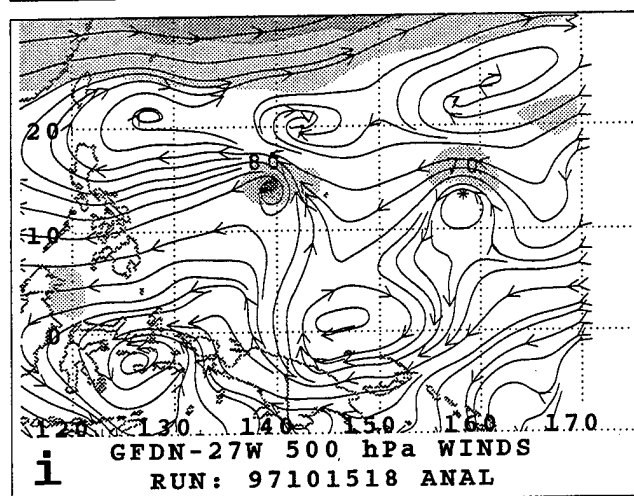
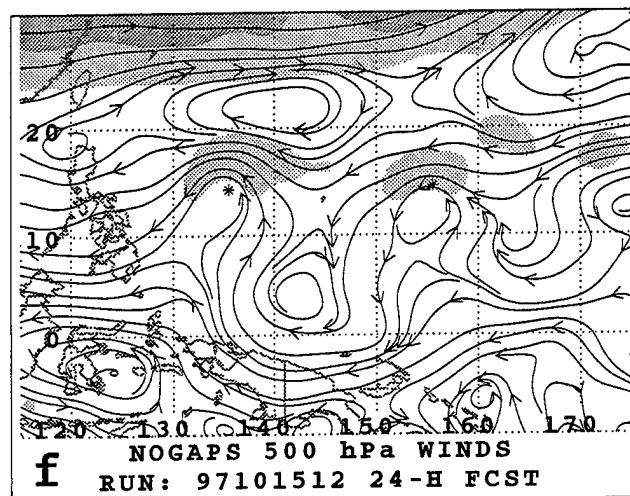
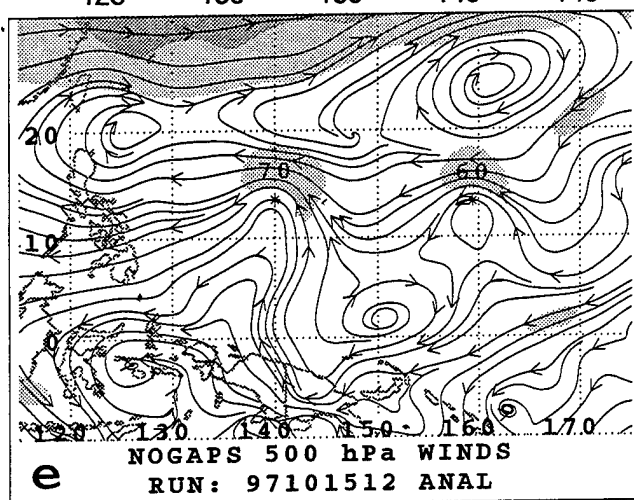
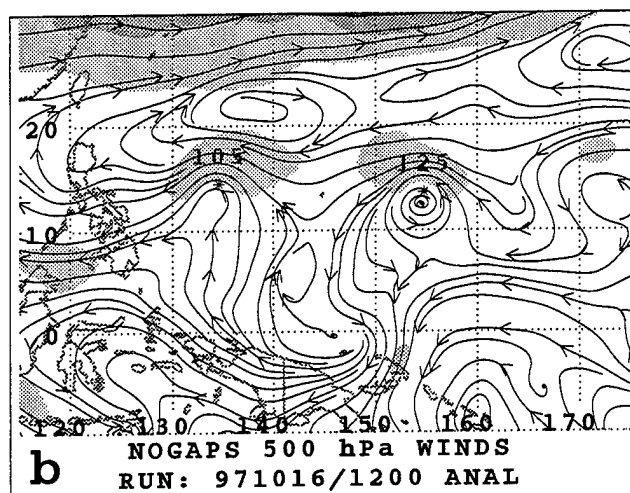
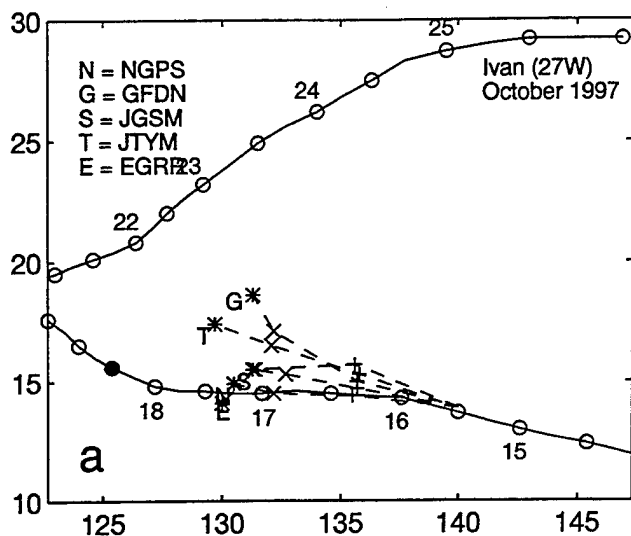


Fig. A.14. (a-l) As in Fig. A.1, except for 500-mb wind forecasts for Ivan initiated at 1200 and 1800 UTC 15 October 1997.

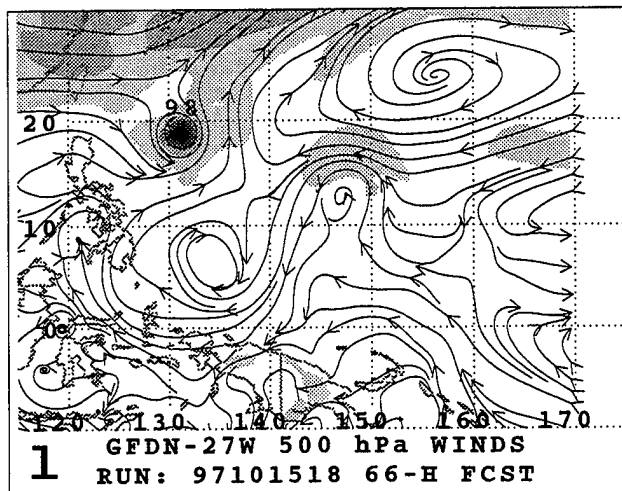
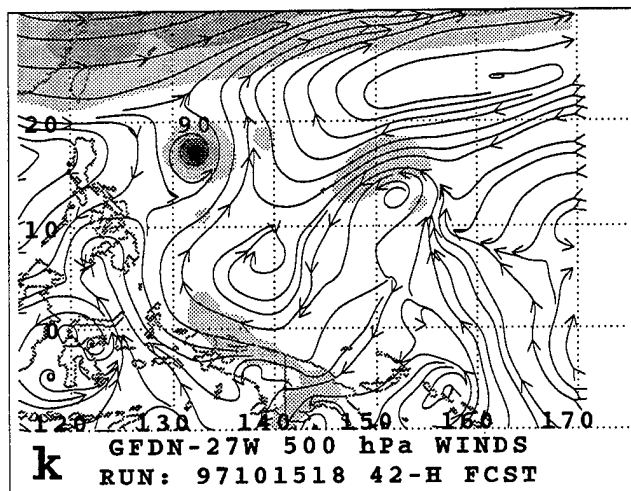
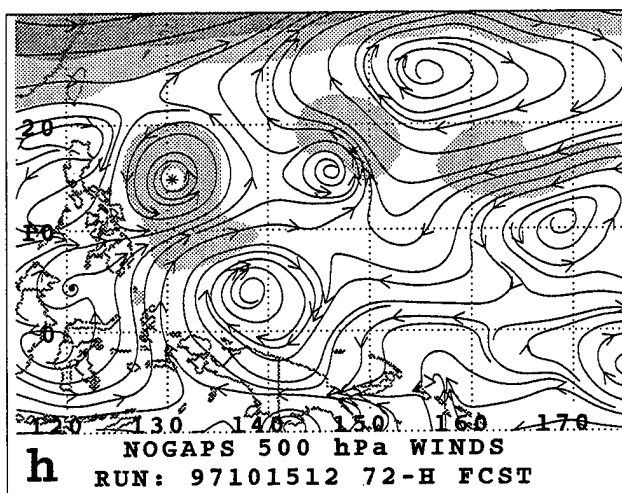
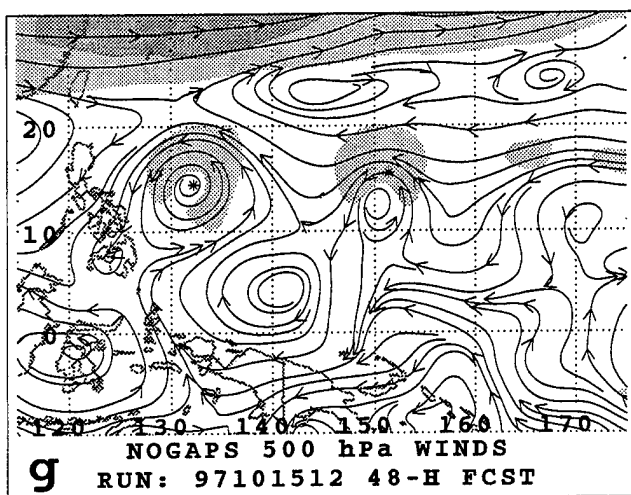
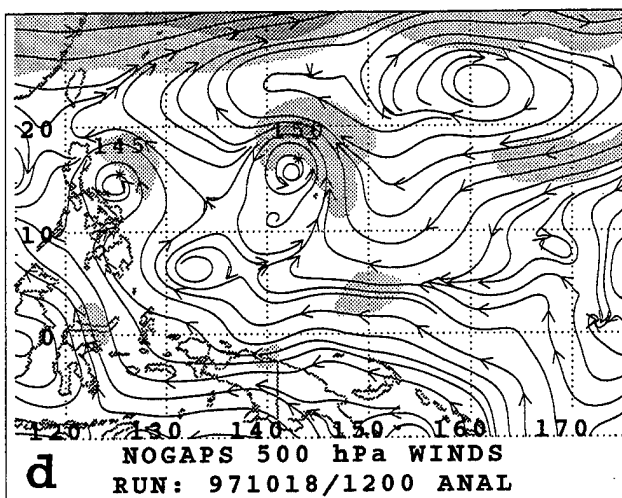
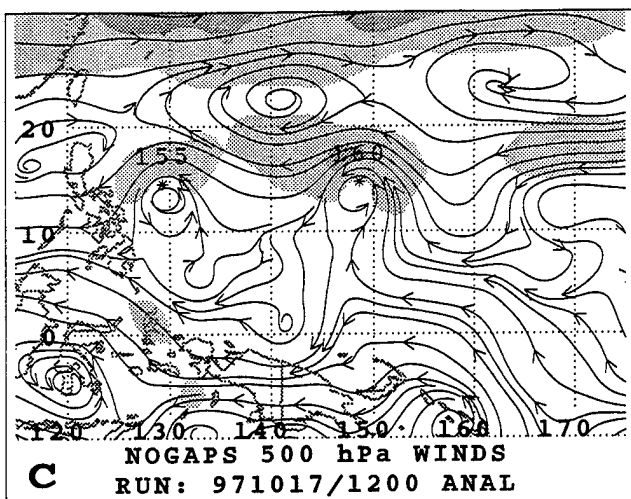


Fig. A.14. (continued)

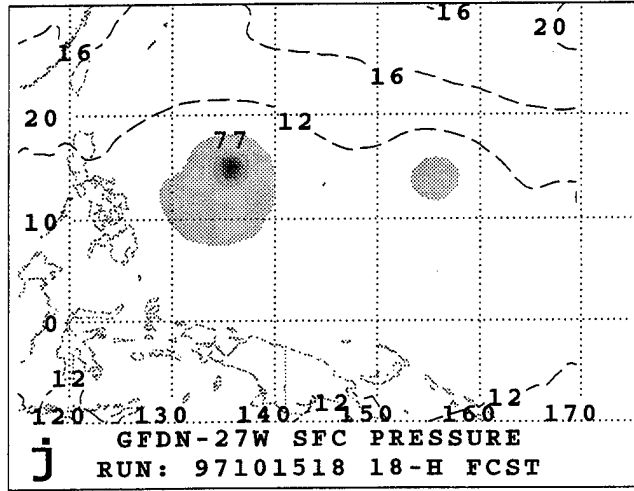
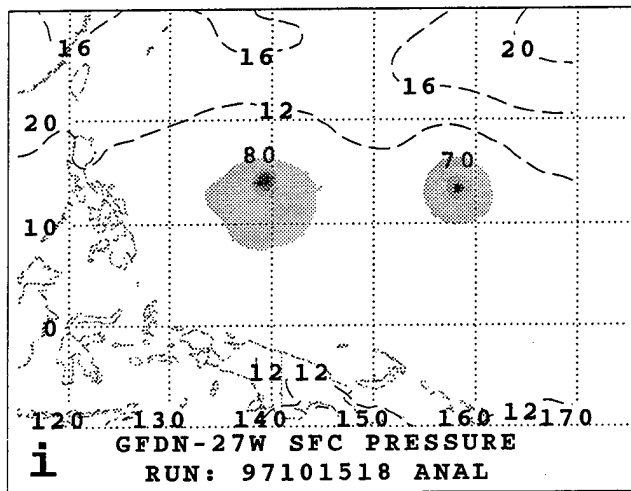
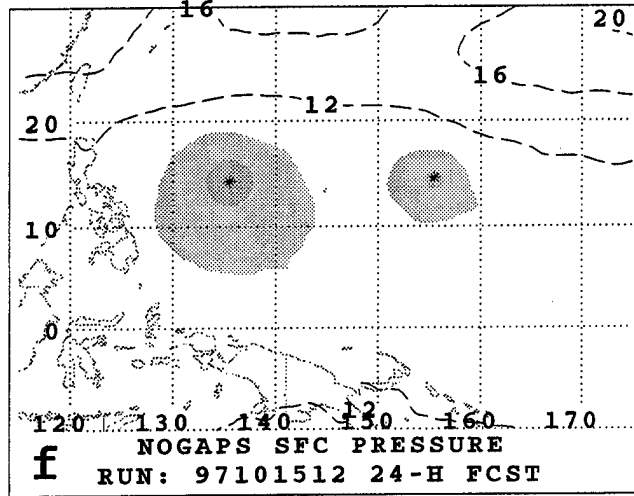
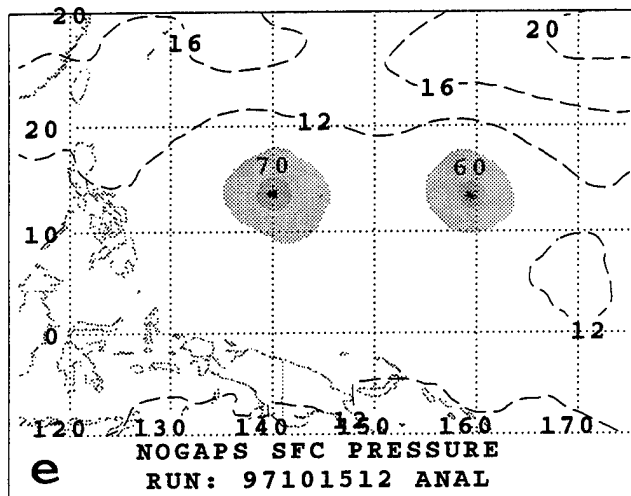
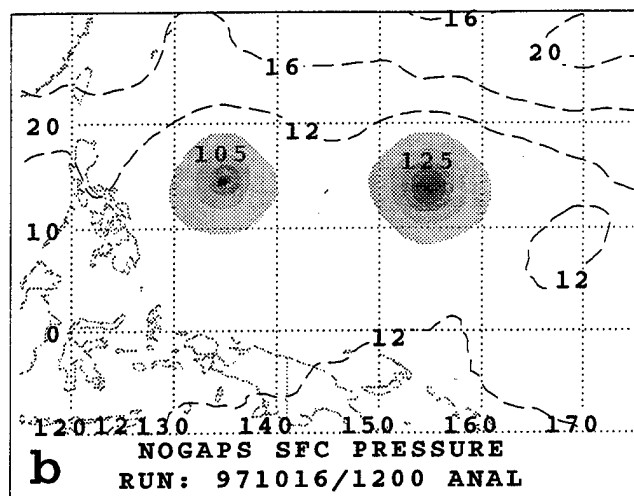
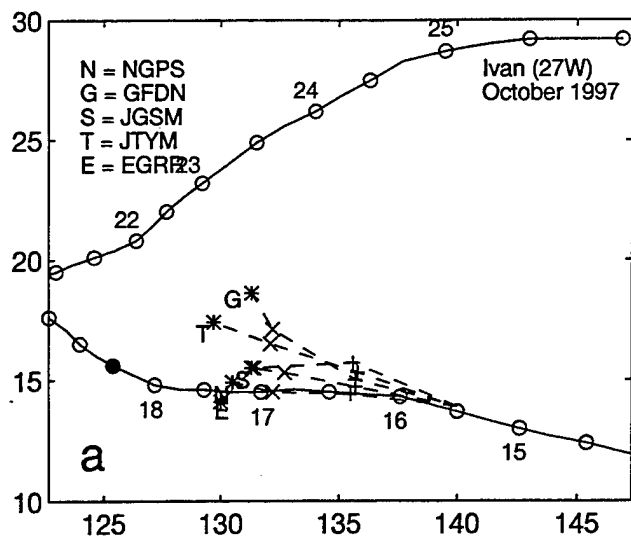


Fig. A.15. (a-l) As in Fig. A.1, except for sea-level pressure forecasts for Ivan initiated at 1200 and 1800 UTC 15 October 1997.

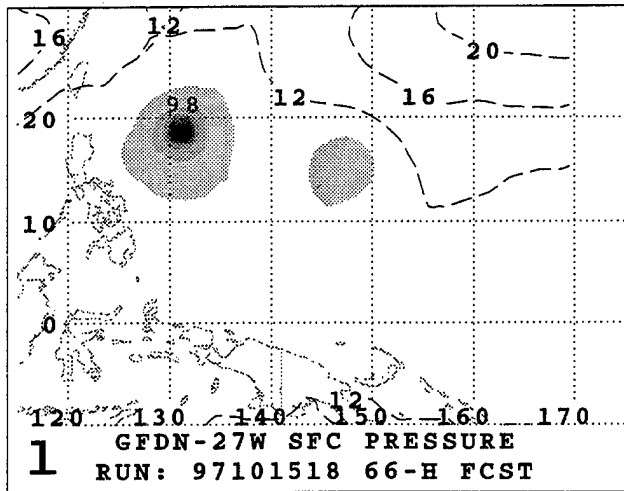
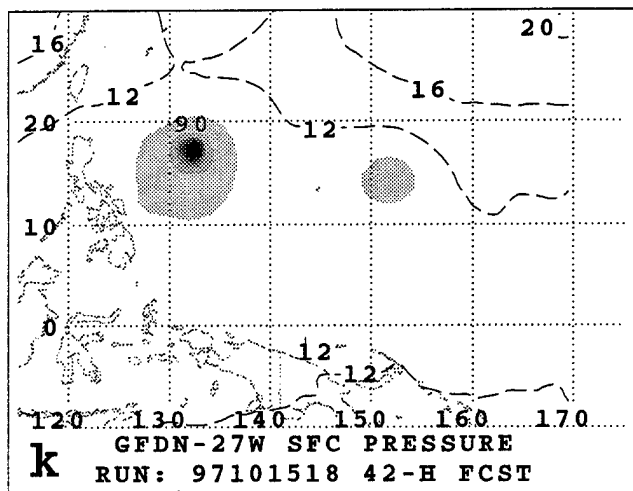
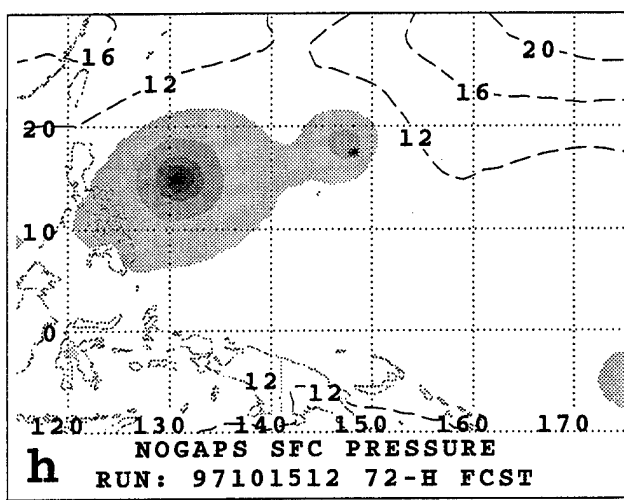
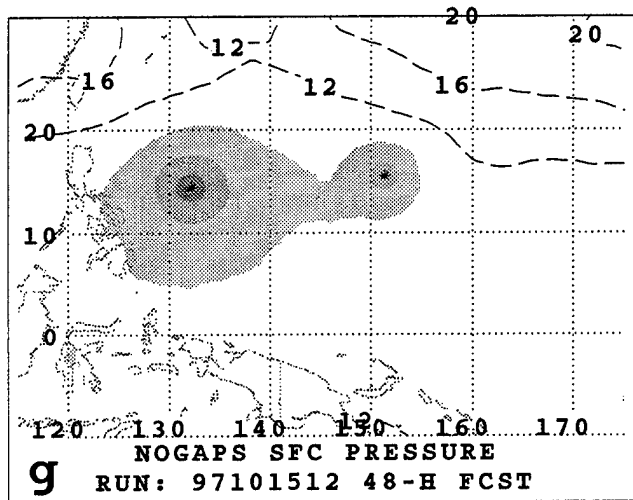
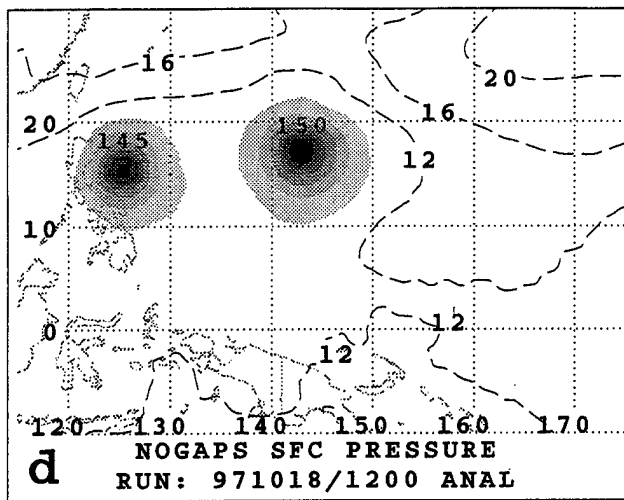
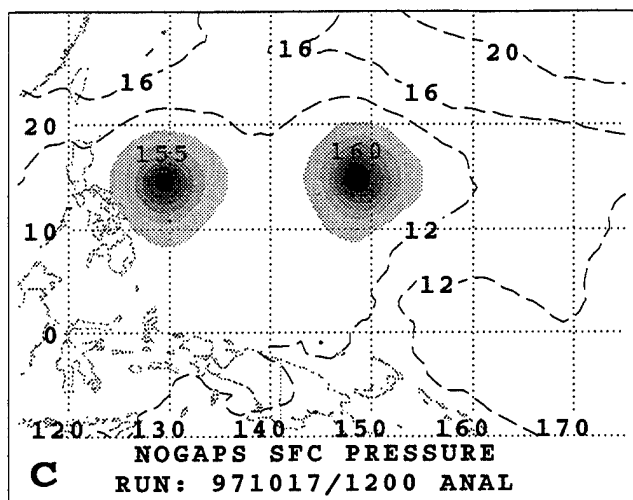


Fig. A.15. (continued)

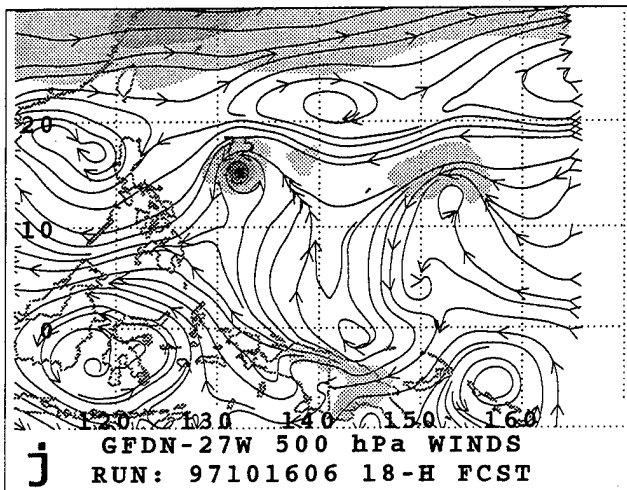
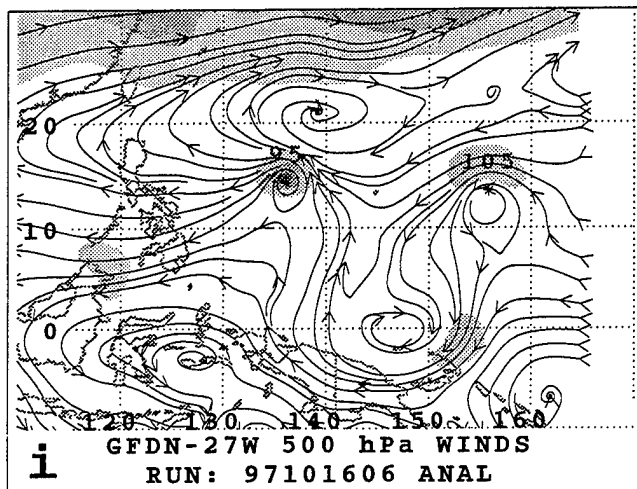
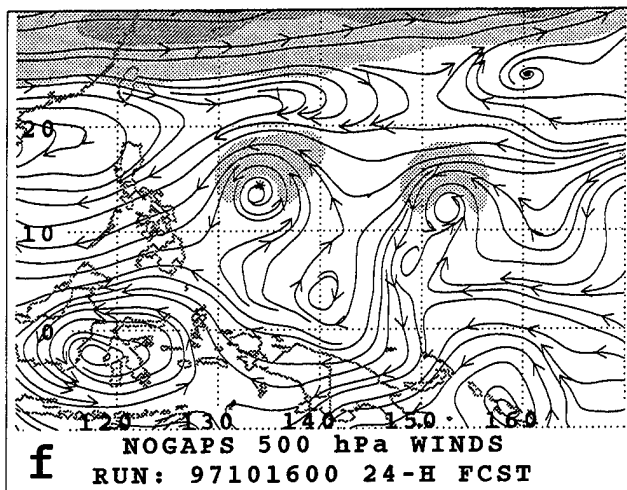
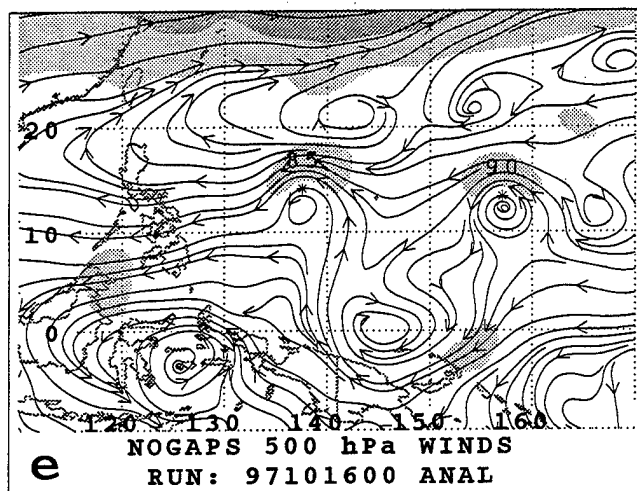
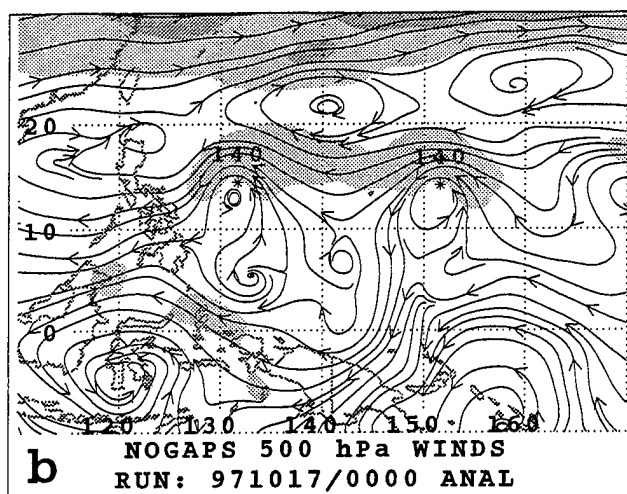
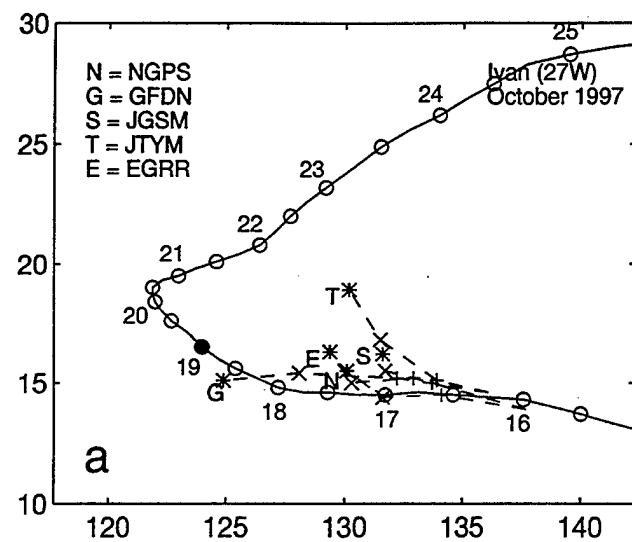


Fig. A.16. (a-l) As in Fig. A.1, except for 500-mb wind forecasts for Ivan initiated at 0000 and 0600 UTC 16 October 1997.

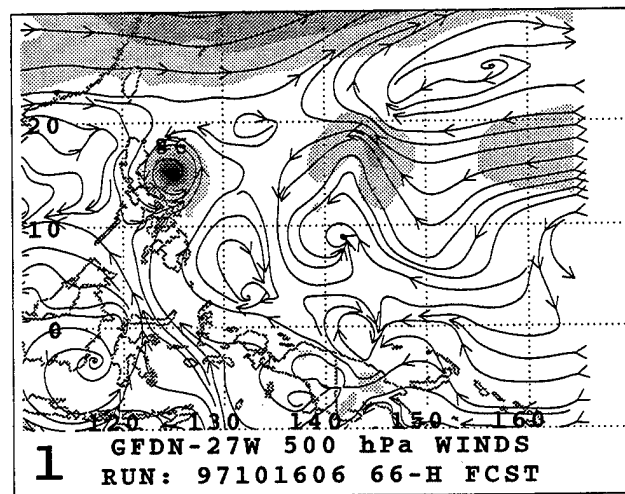
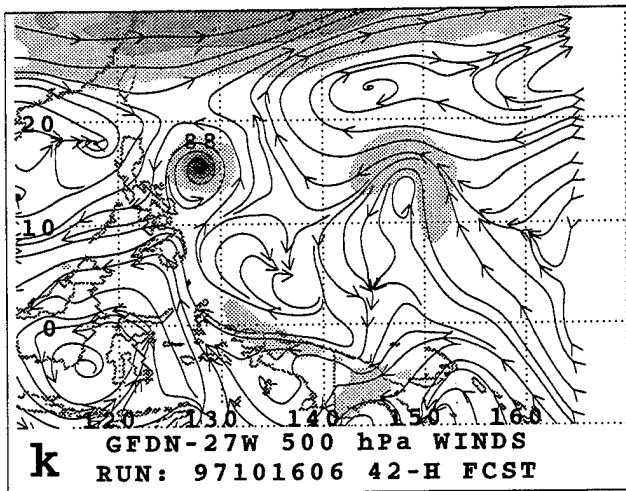
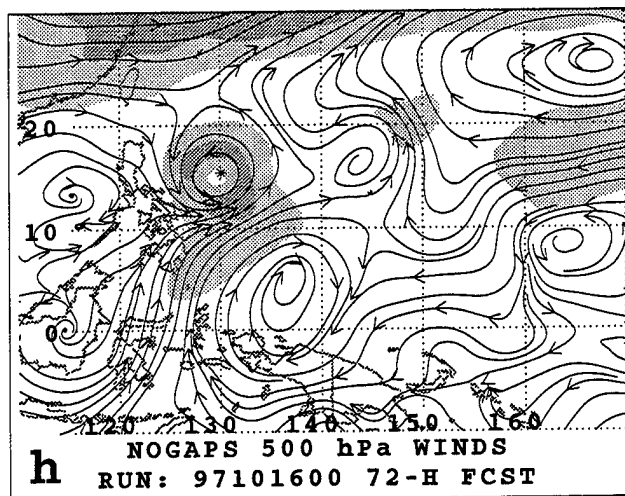
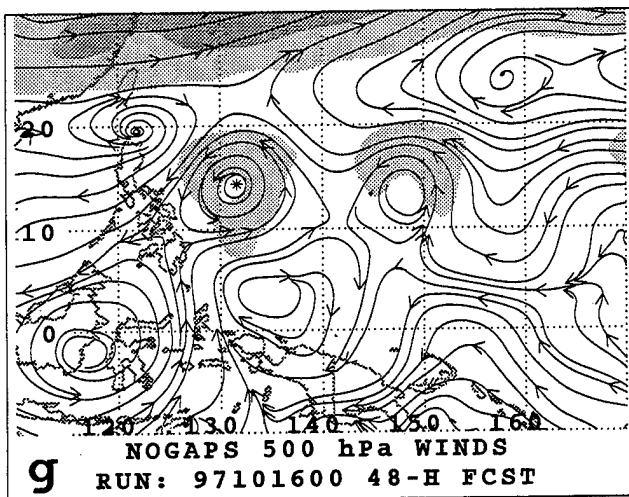
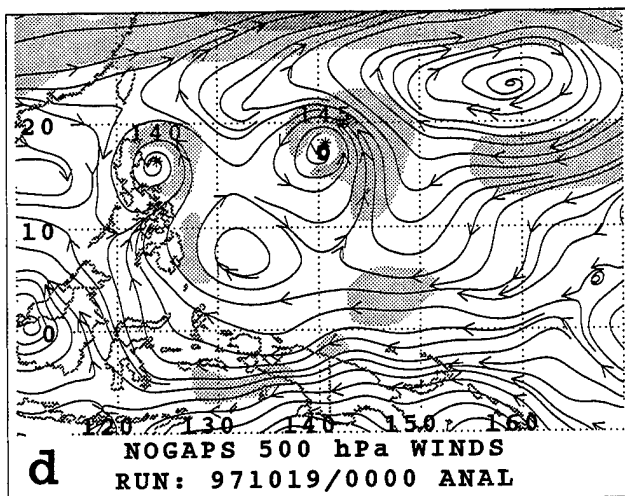
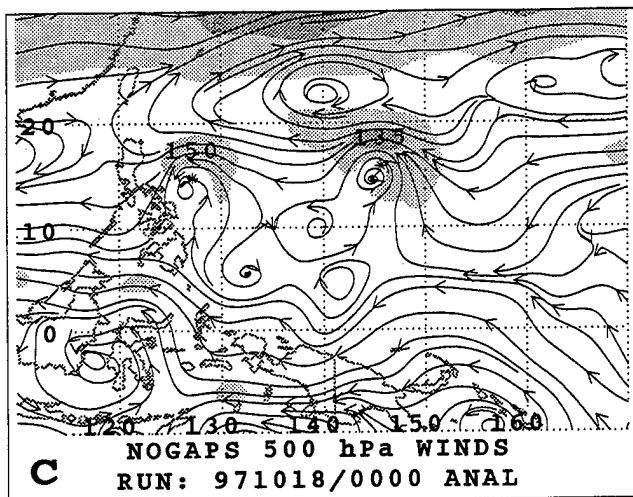


Fig. A.16. (continued)

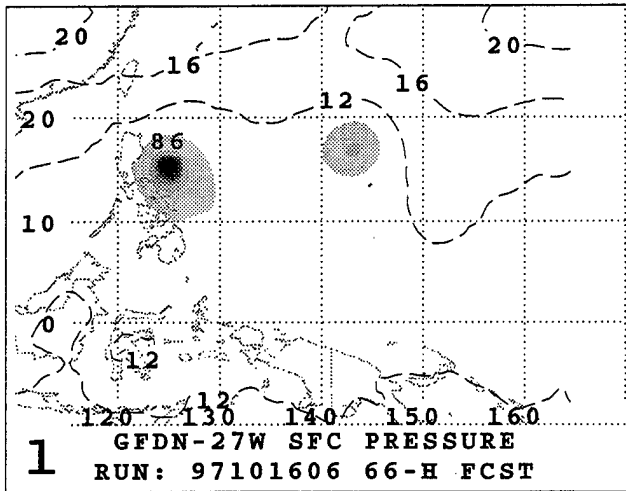
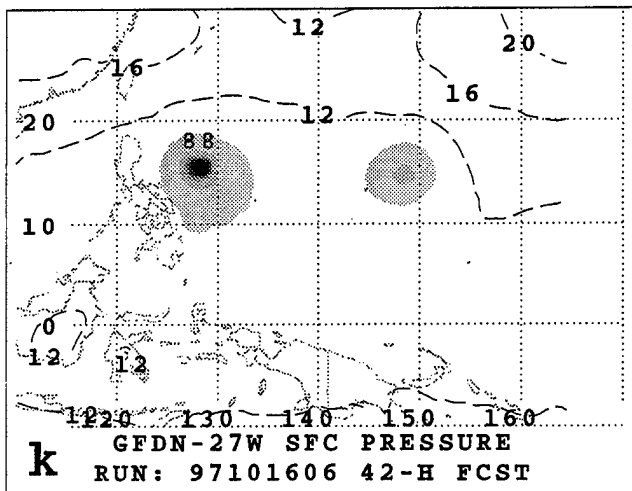
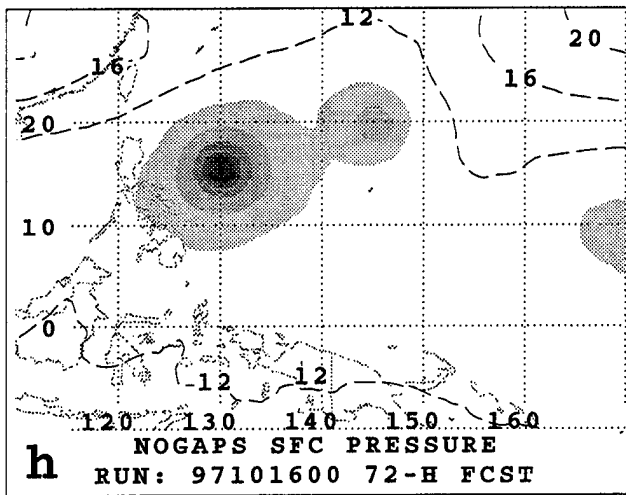
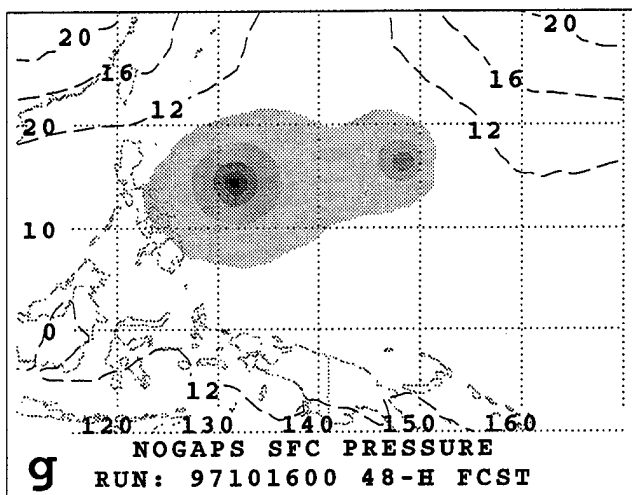
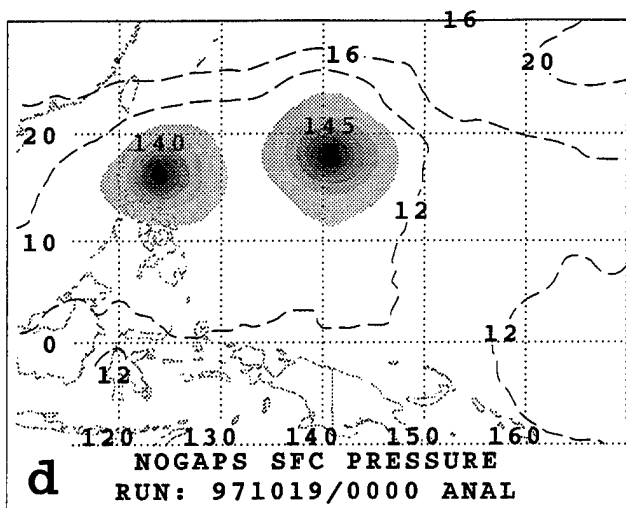
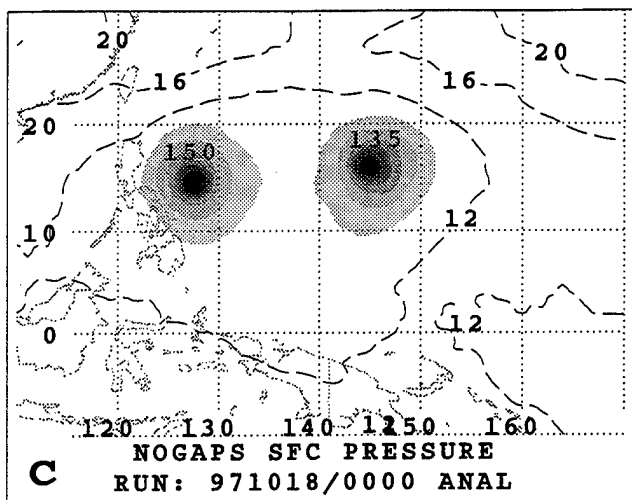


Fig. A.17. (continued)

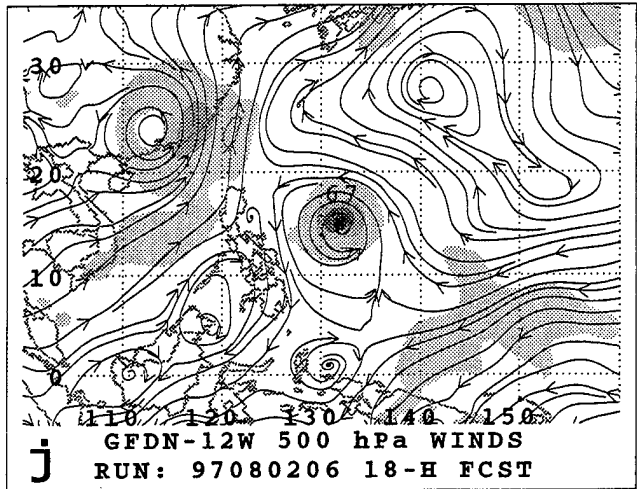
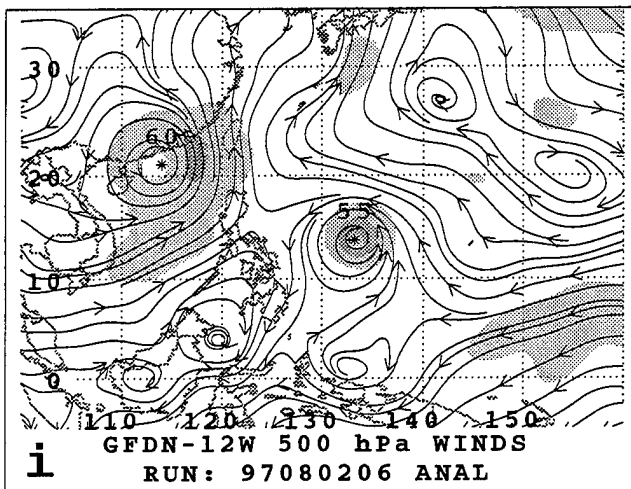
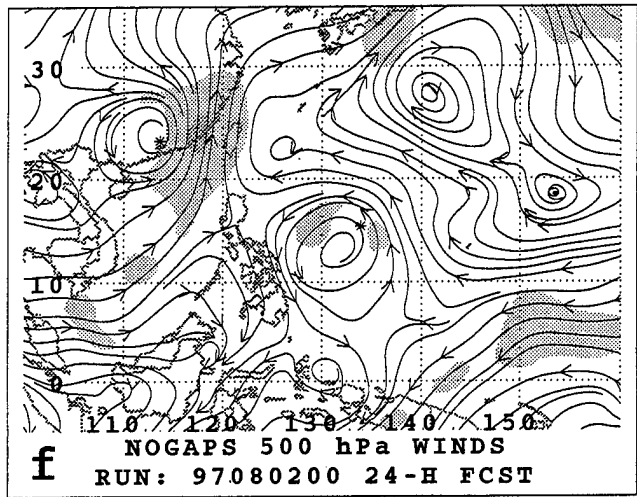
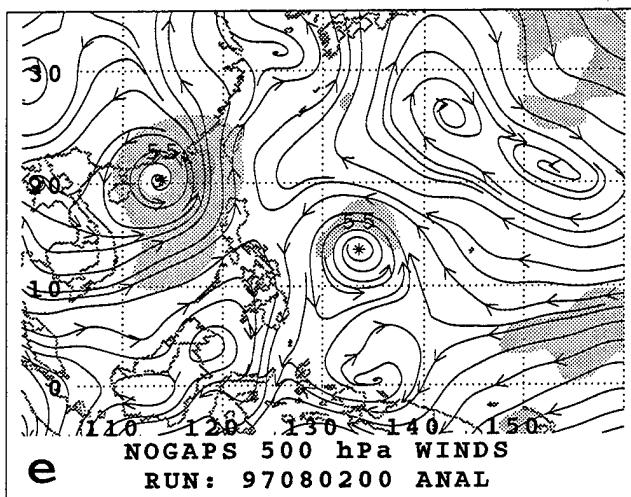
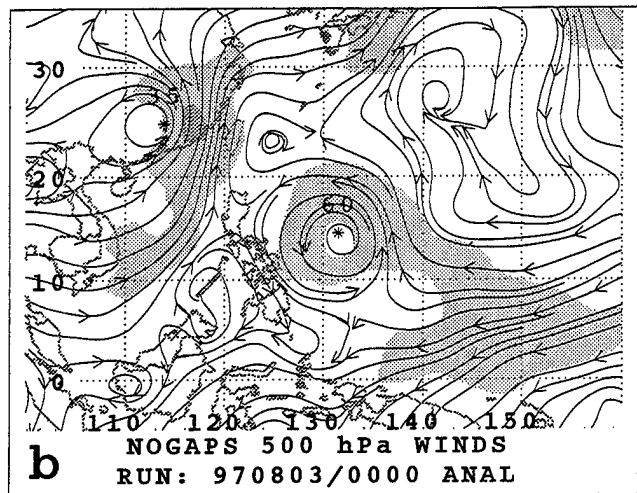
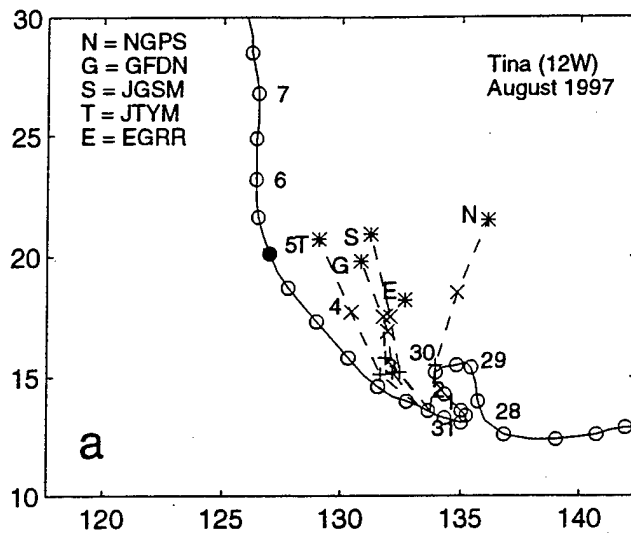


Fig. A.18. (a-l) As in Fig. A.1, except for 500-mb wind forecasts for Tina initiated at 0000 and 0600 UTC 2 August 1997.

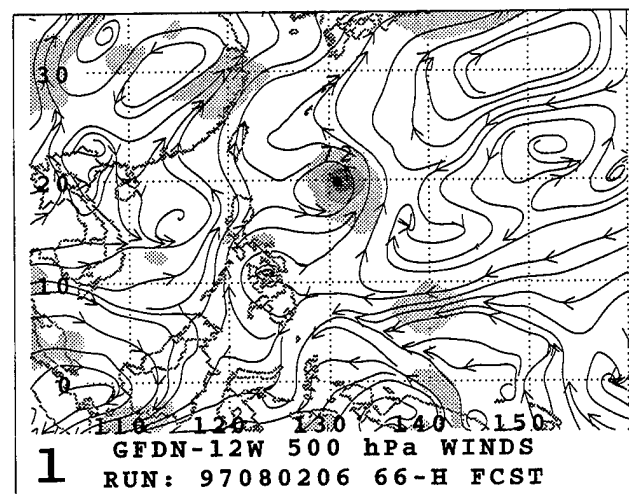
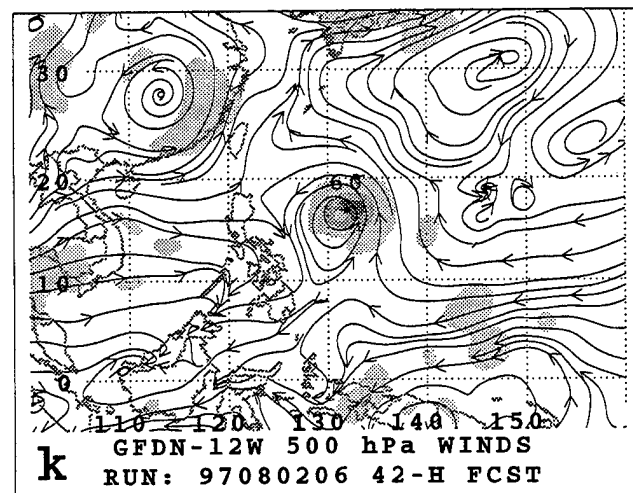
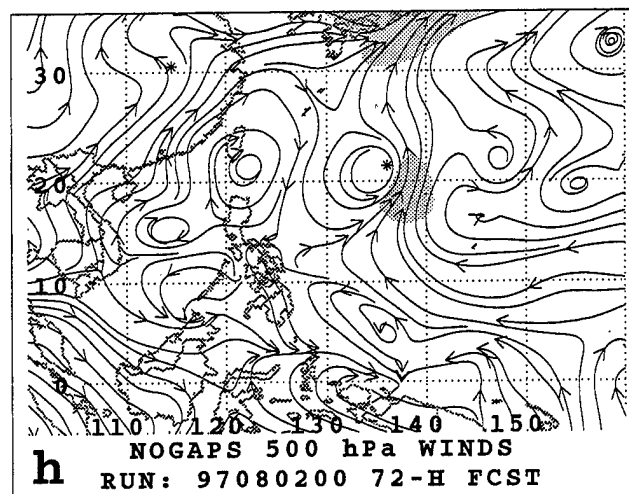
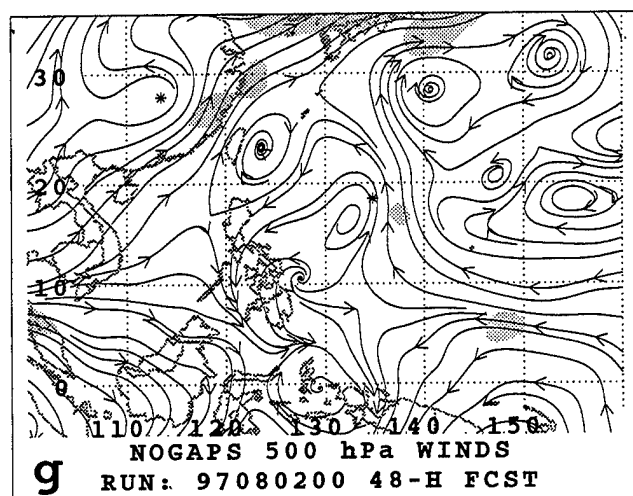
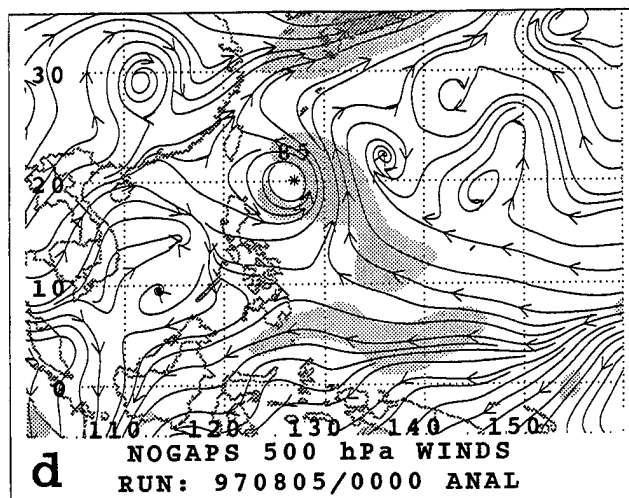
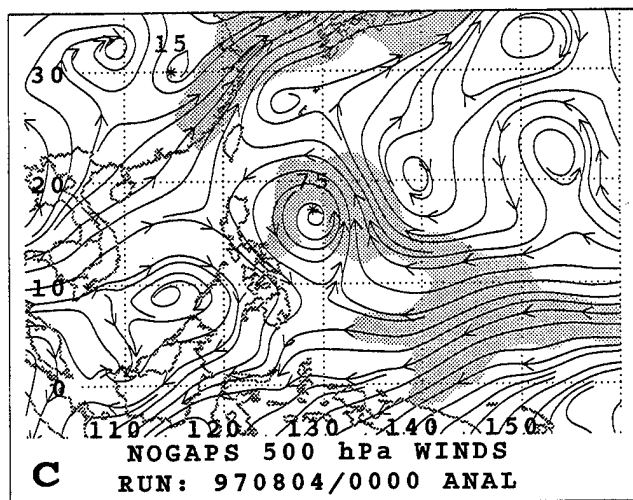


Fig. A.18. (continued)

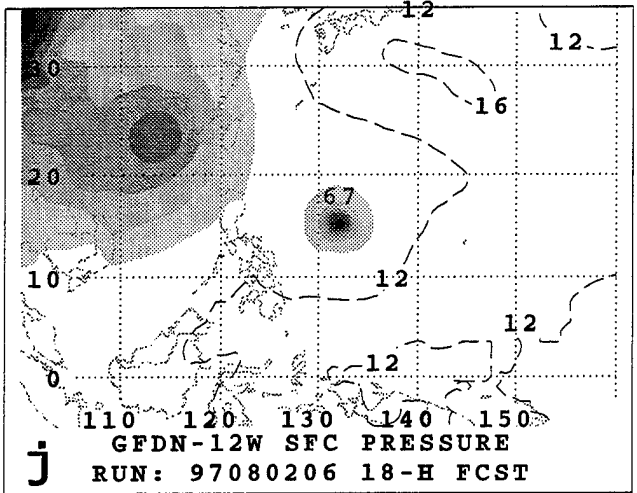
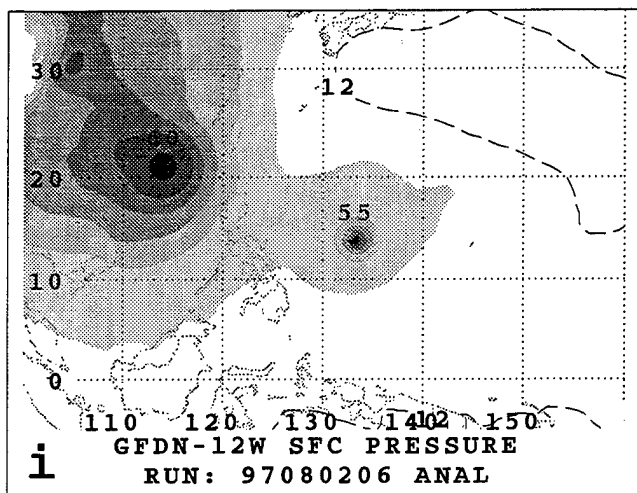
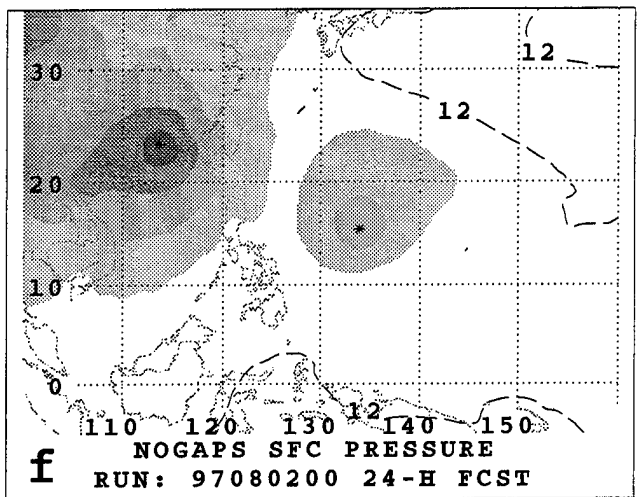
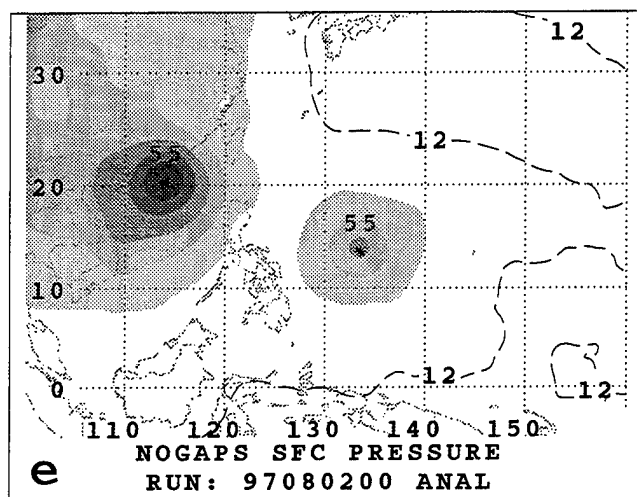
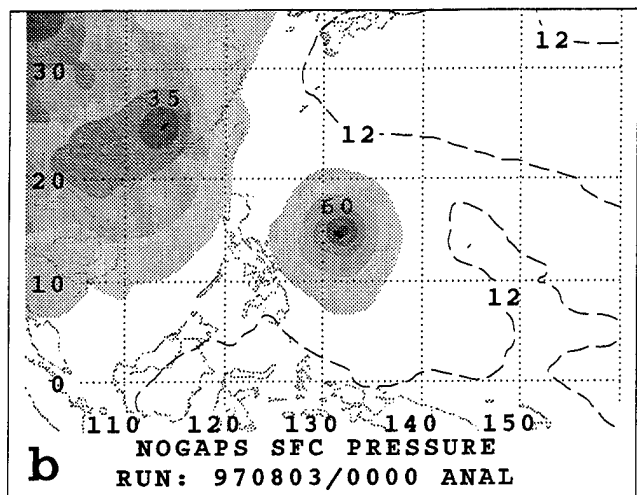
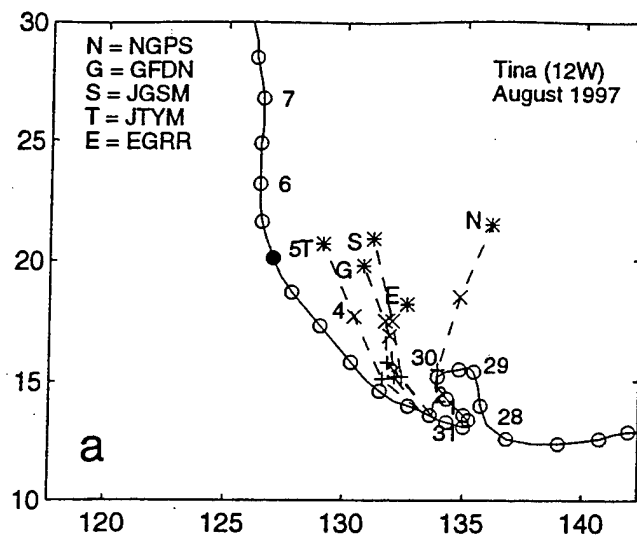


Fig. A.19. (a-l) As in Fig. A.1, except for sea-level pressure forecasts for Tina initiated at 0000 and 0600 UTC 2 August 1997.

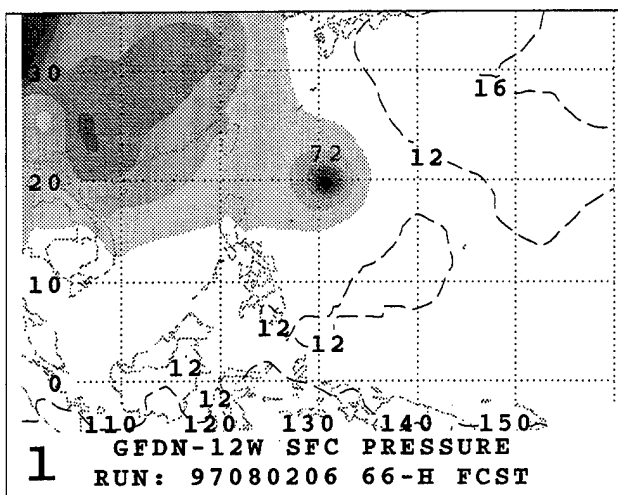
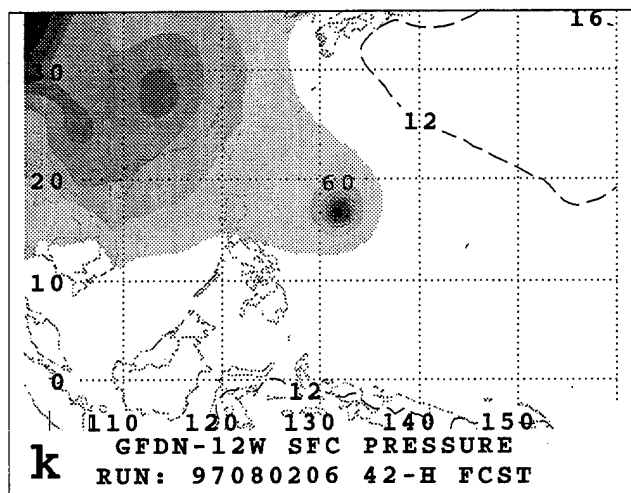
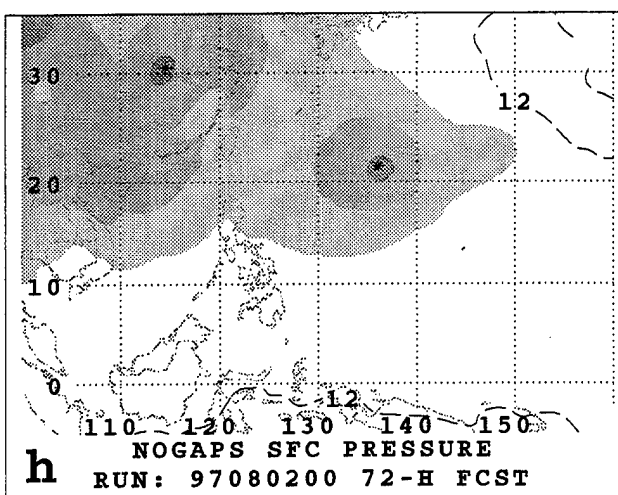
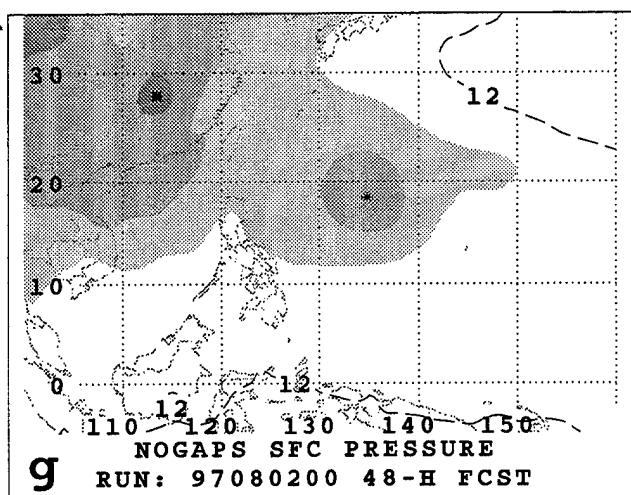
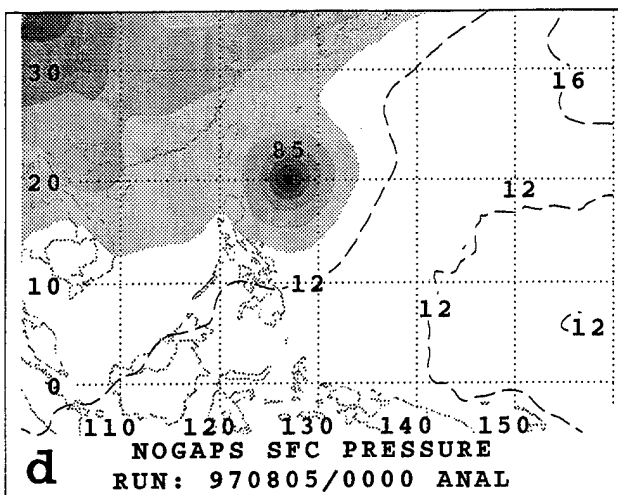
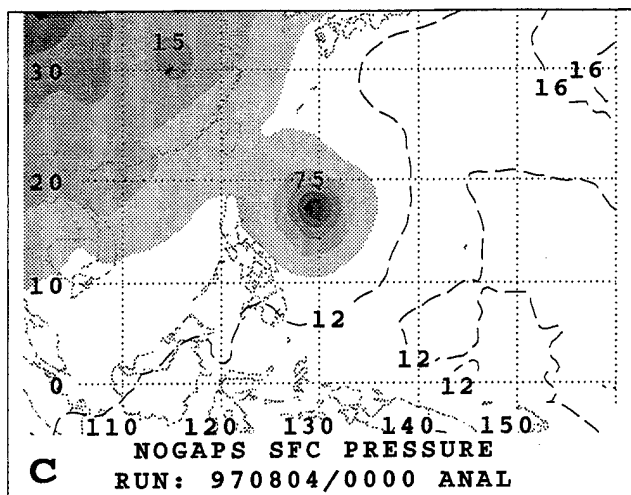


Fig. A.19. (continued)

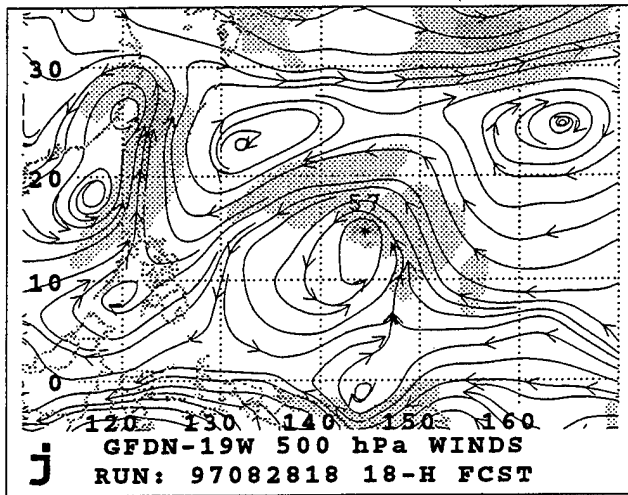
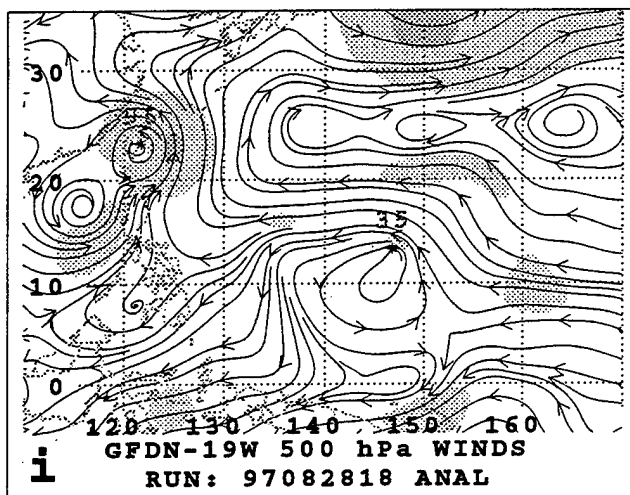
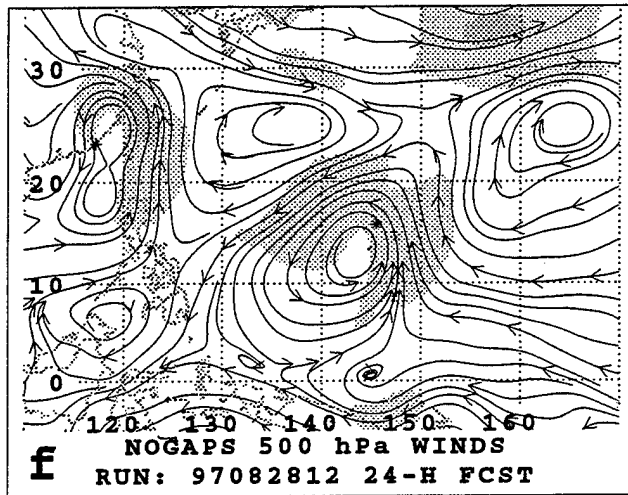
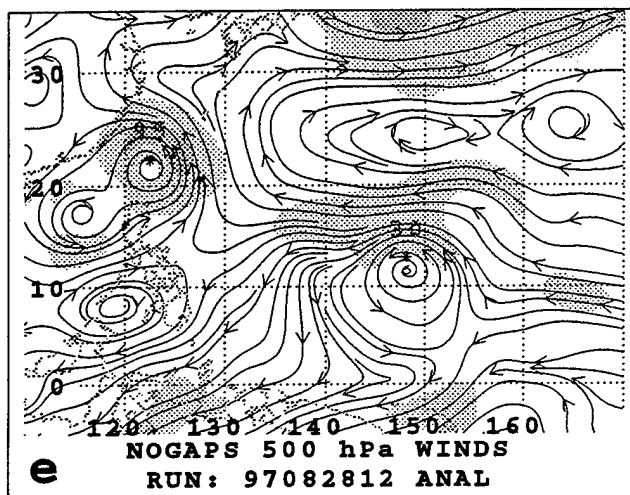
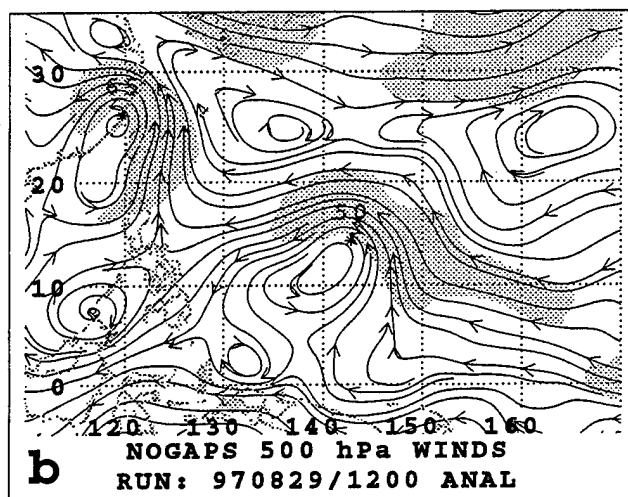
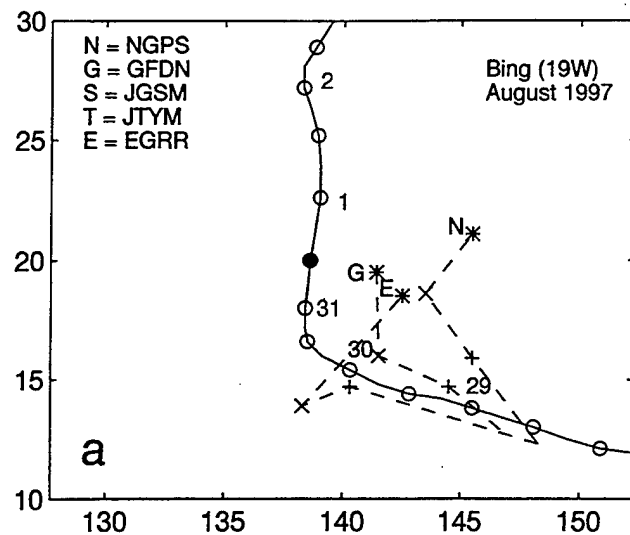


Fig. A.20. (a-l) As in Fig. A.1, except for 500-mb wind forecasts for Bing initiated at 1200 and 1800 UTC 28 August 1997.

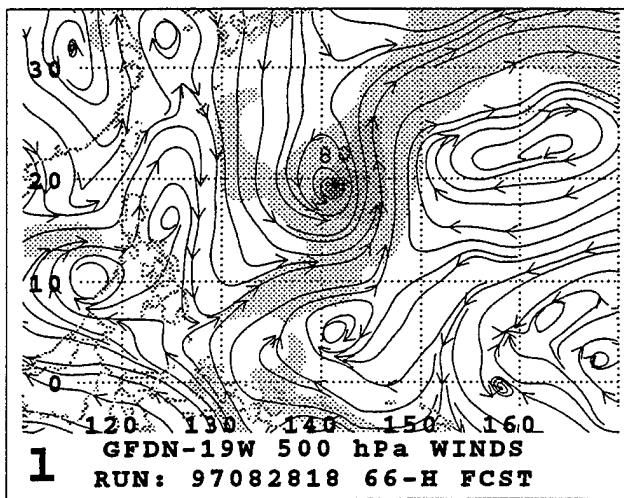
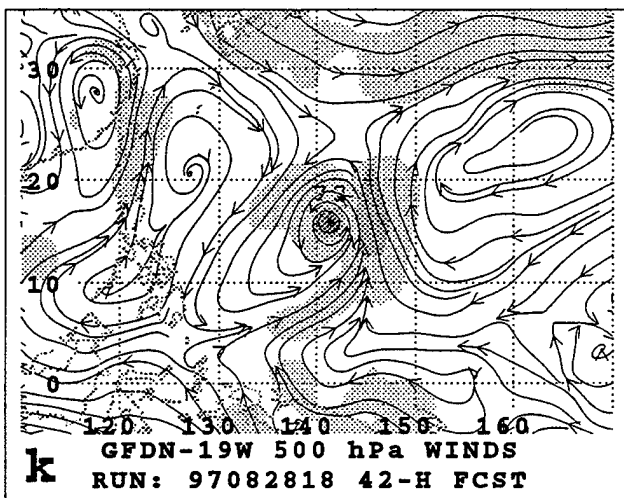
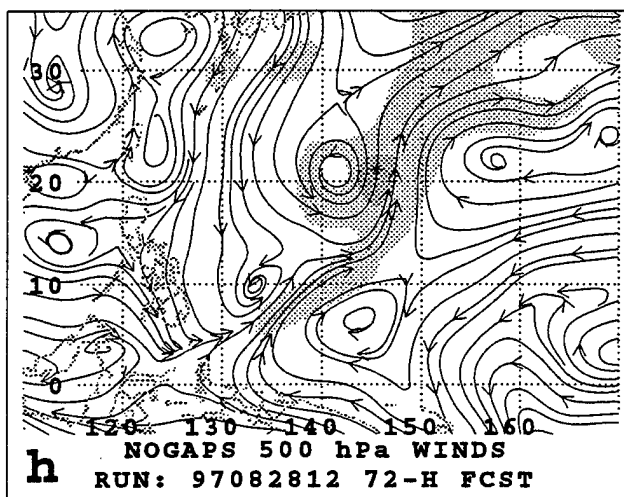
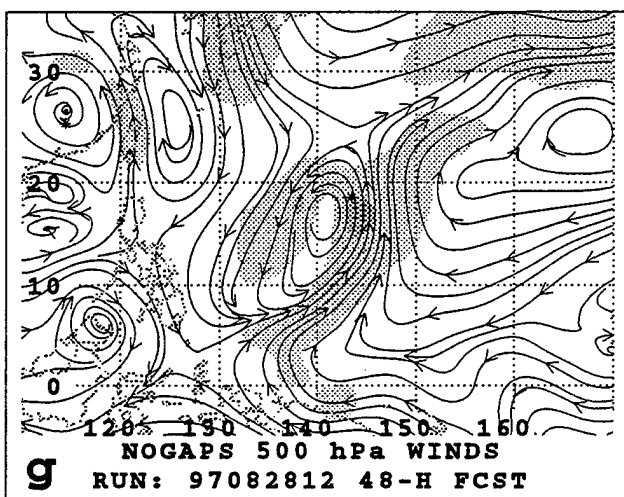
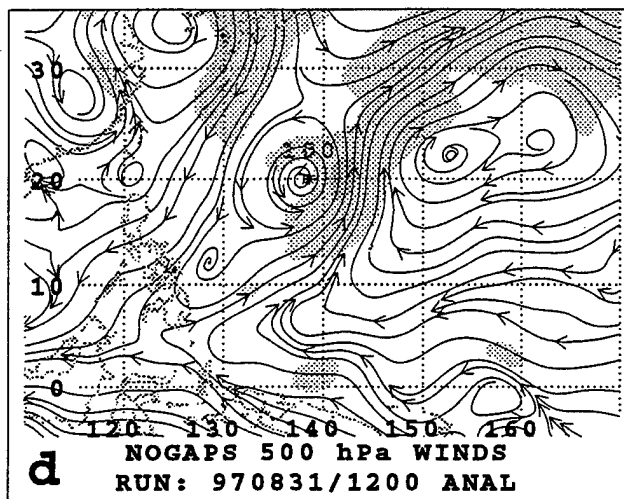
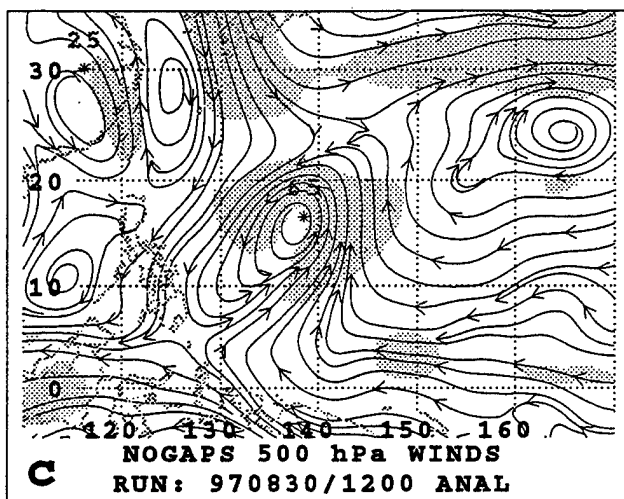


Fig. A.20. (continued)

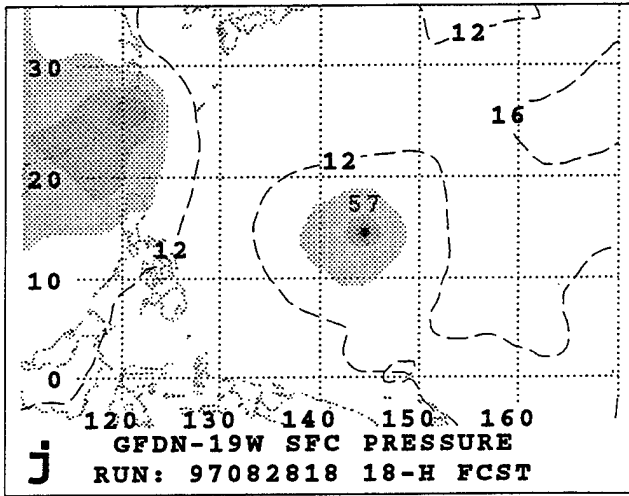
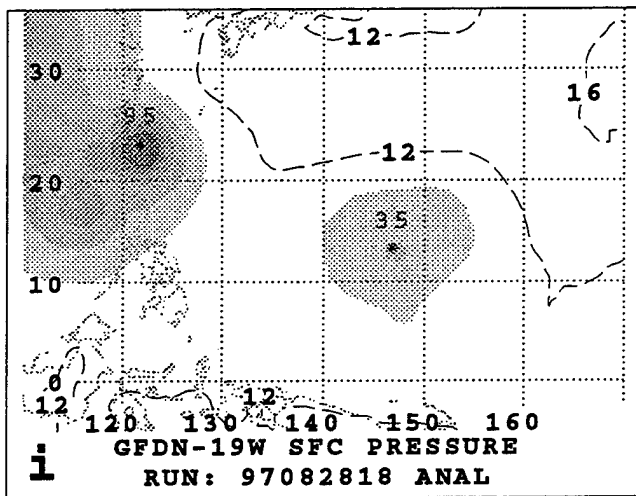
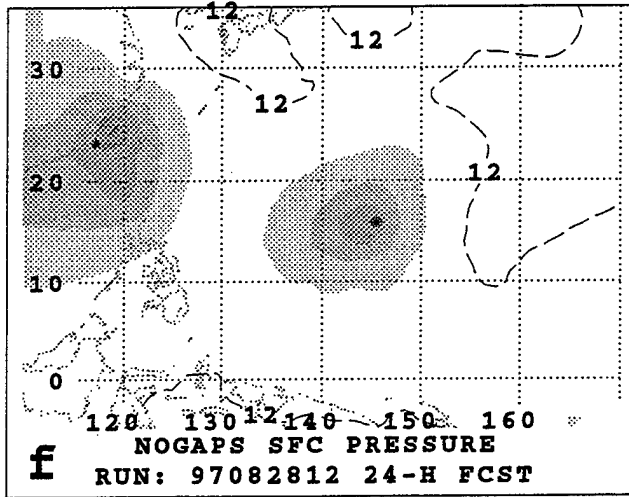
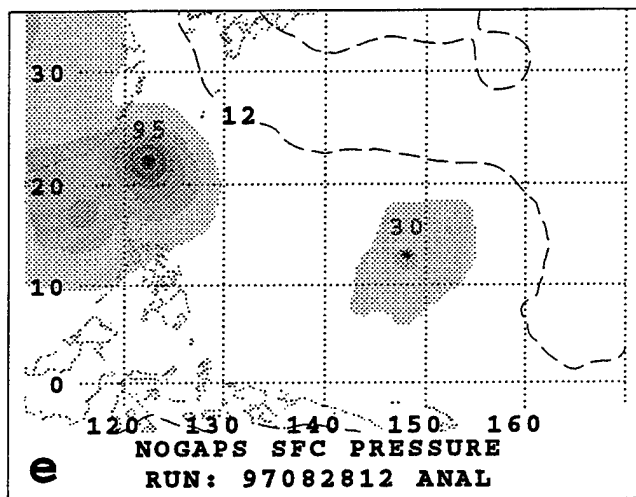
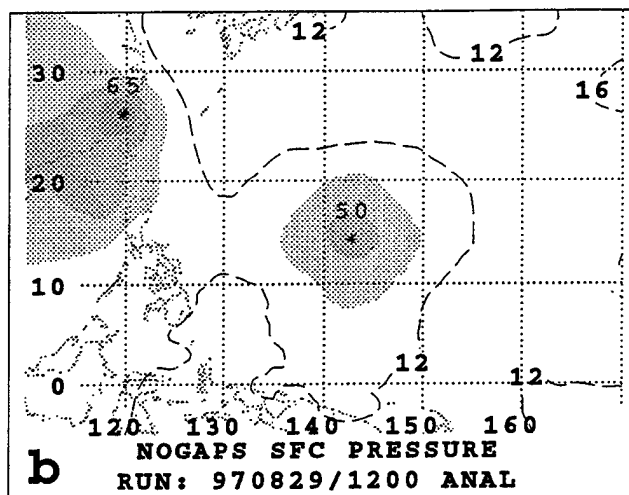
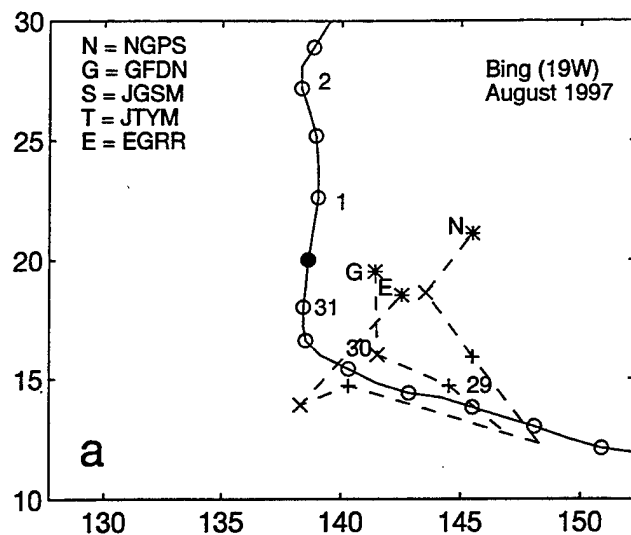


Fig. A.21. (a-l) As in Fig. A.1, except for sea-level pressure forecasts for Bing initiated at 1200 and 1800 UTC 28 August 1997.

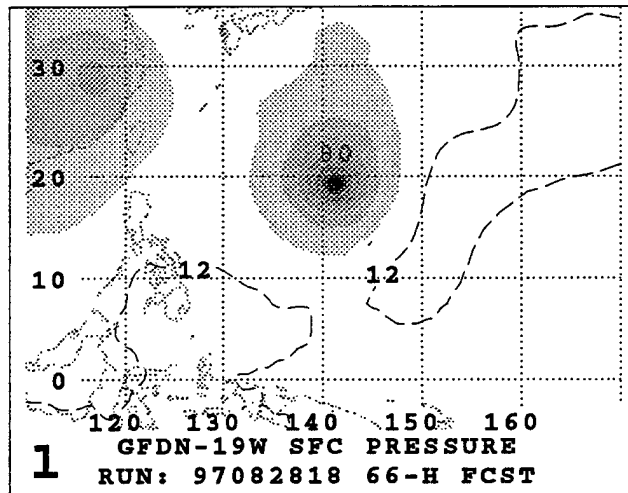
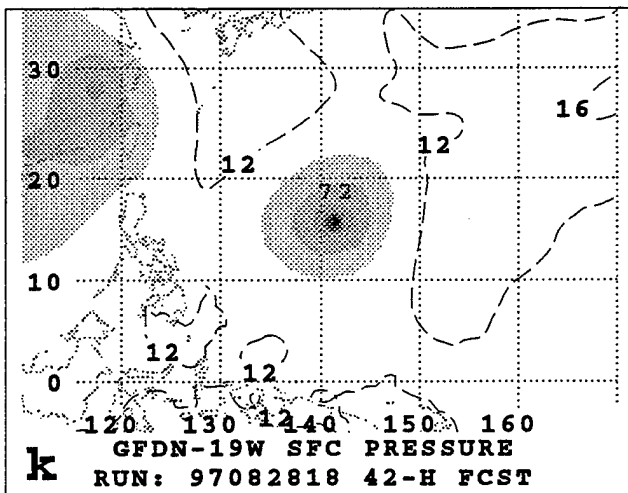
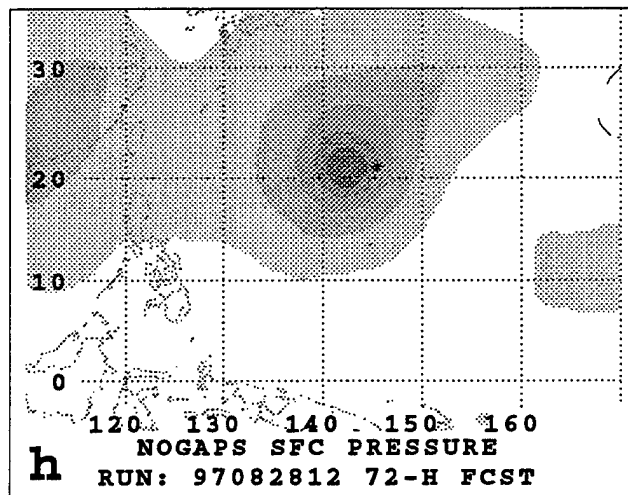
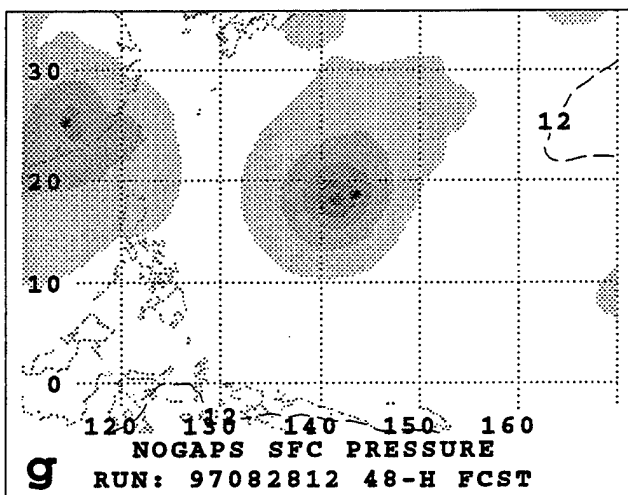
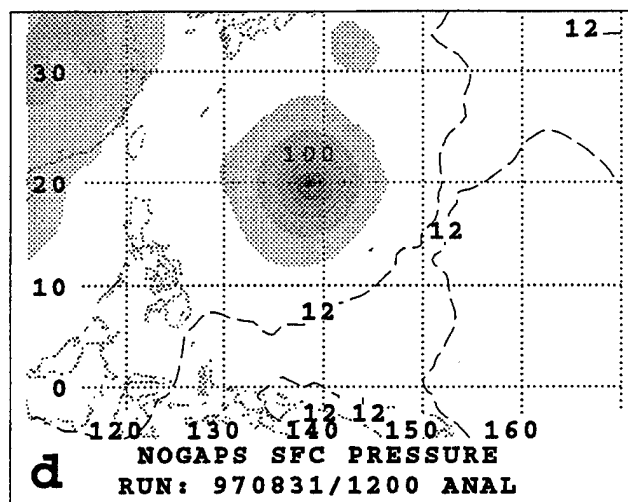
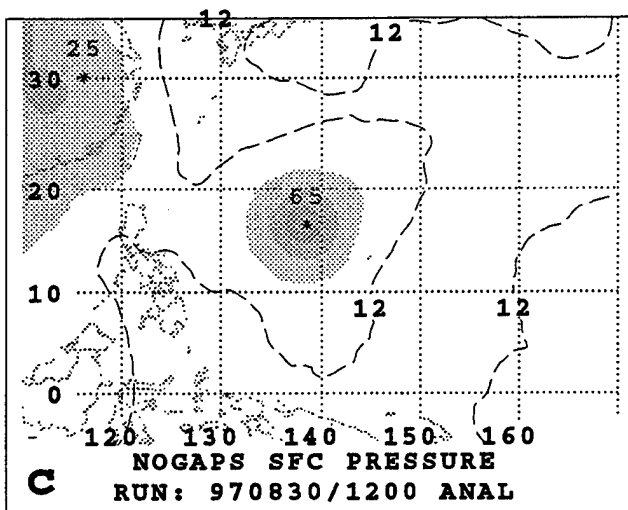


Fig. A.21. (continued)

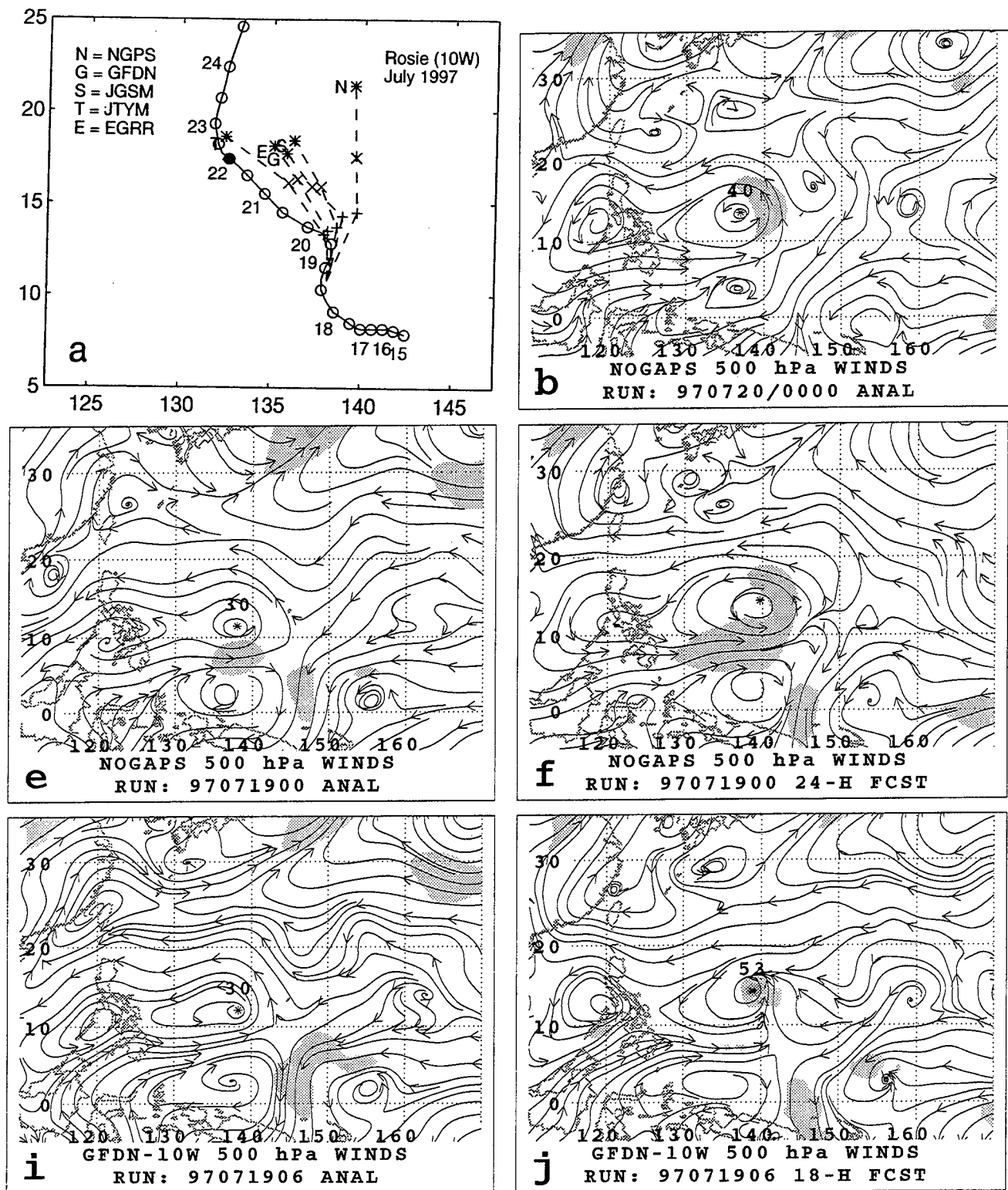


Fig. A.22. (a-l) As in Fig. A.1, except for 500-mb wind forecasts for Rosie initiated at 0000 and 0600 UTC 19 July 1997.

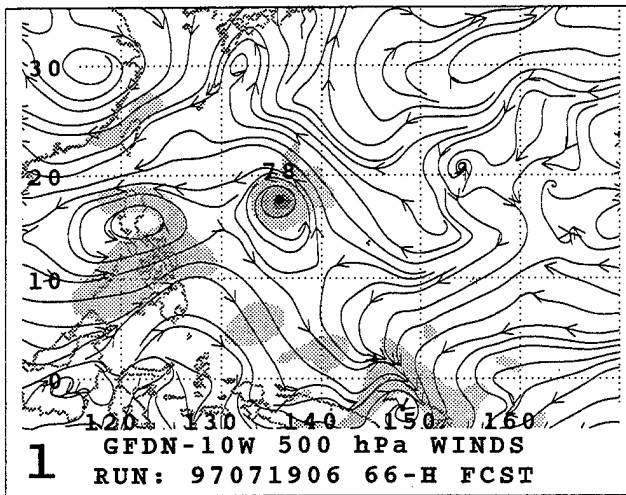
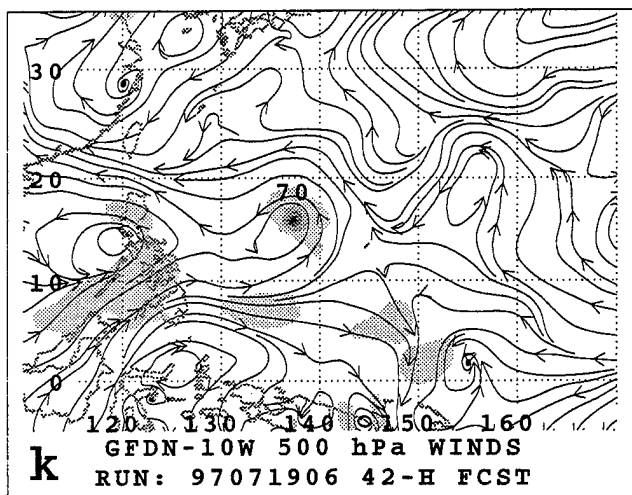
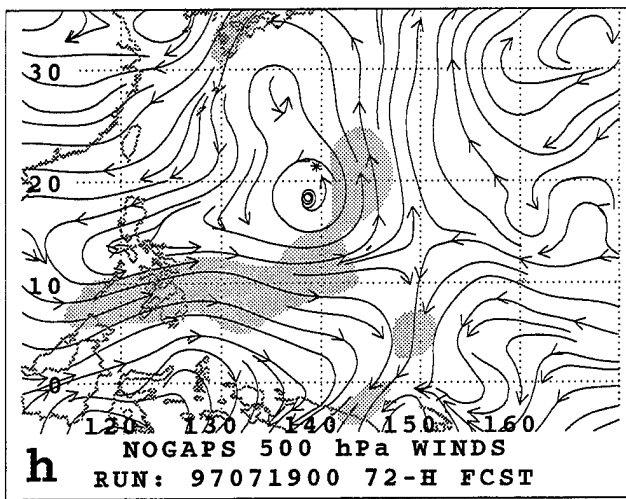
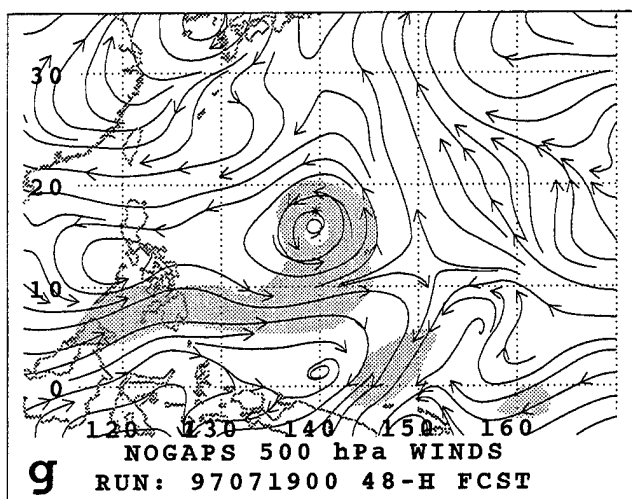
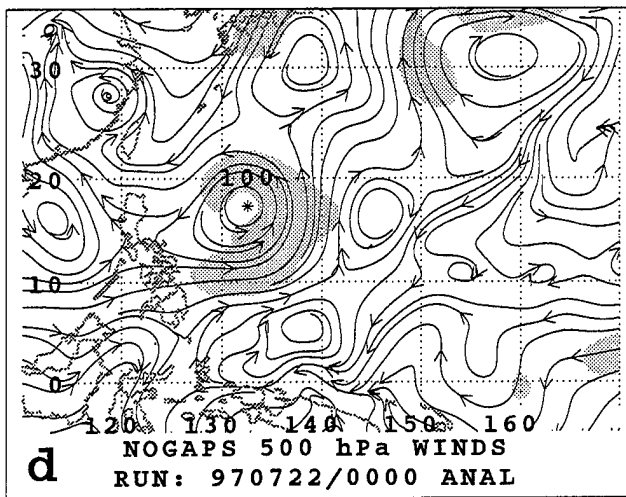
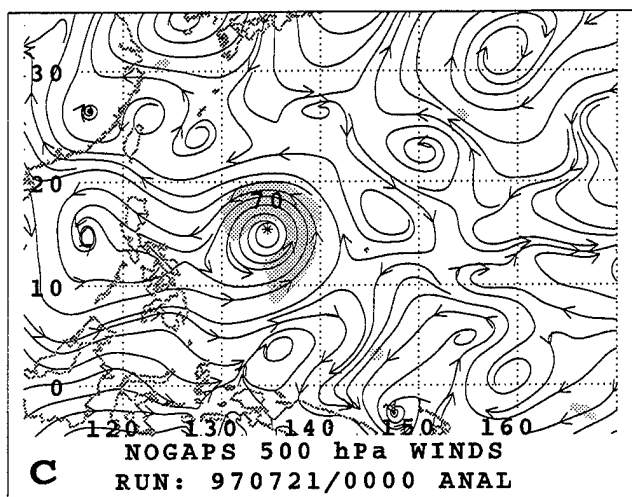


Fig. A.22. (continued)

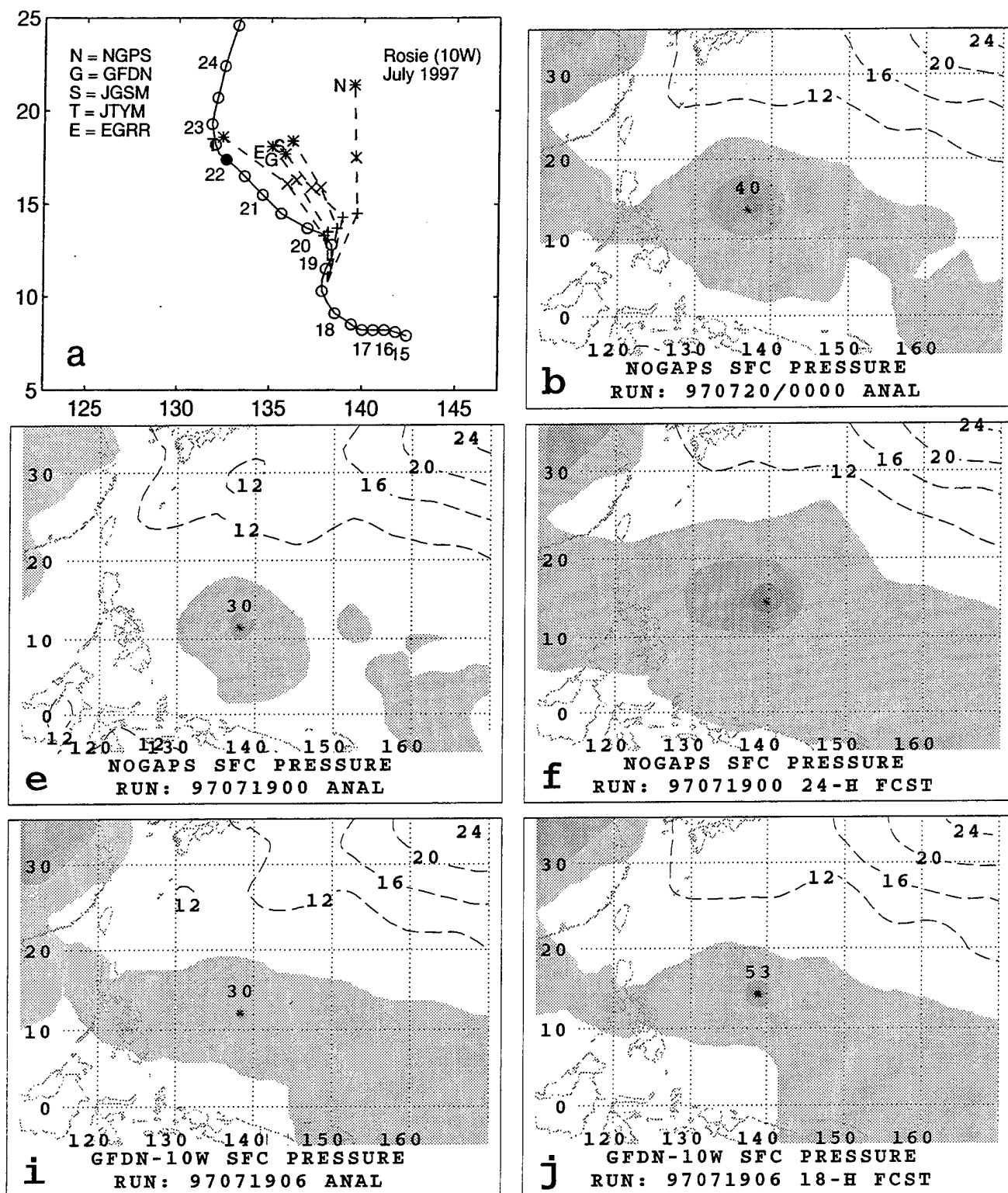


Fig. A.23. (a-l) As in Fig. A.1, except for sea-level pressure forecasts for Rosie initiated at 0000 and 0600 UTC 19 July 1997.

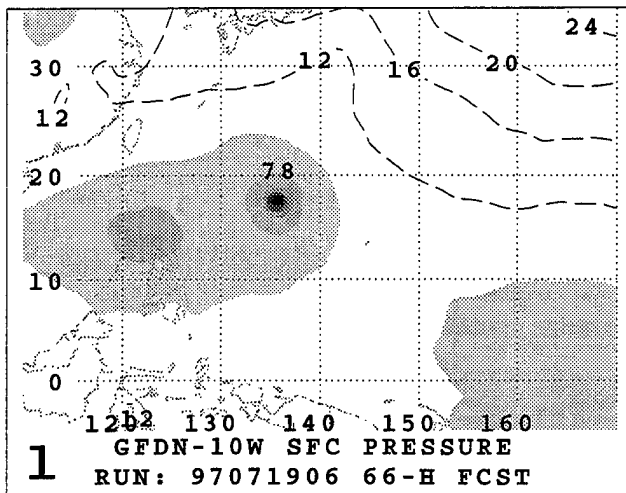
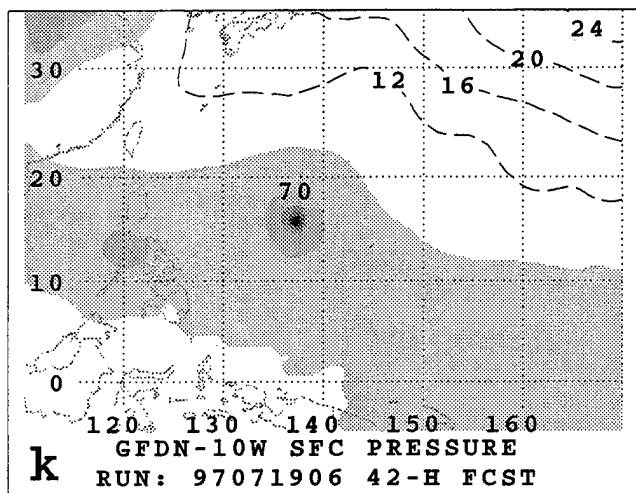
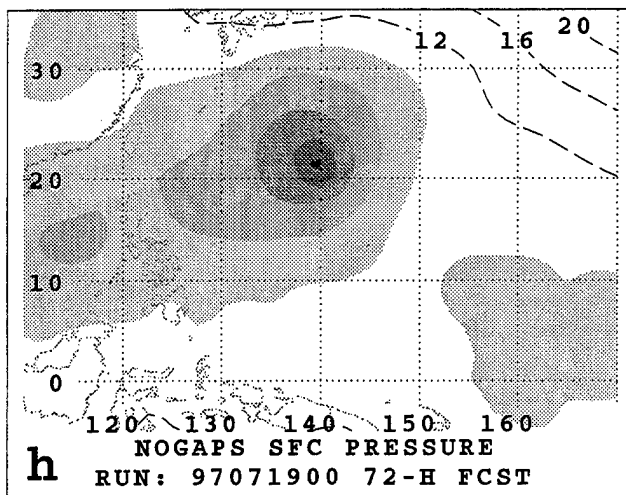
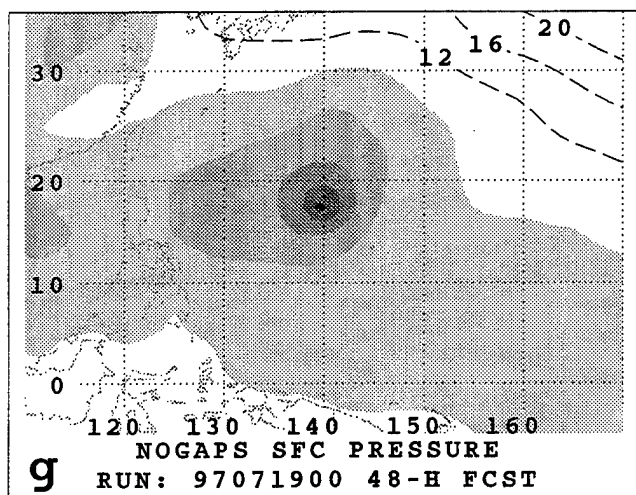
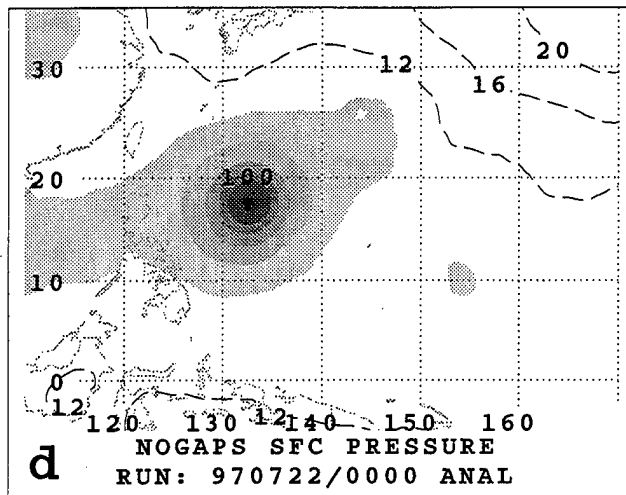
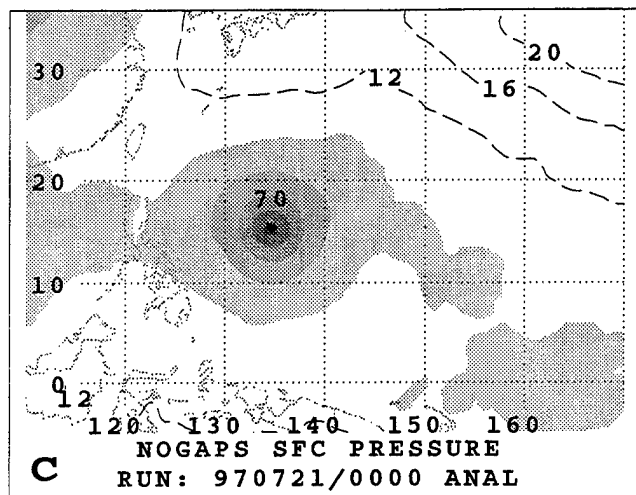


Fig. A.23. (continued)

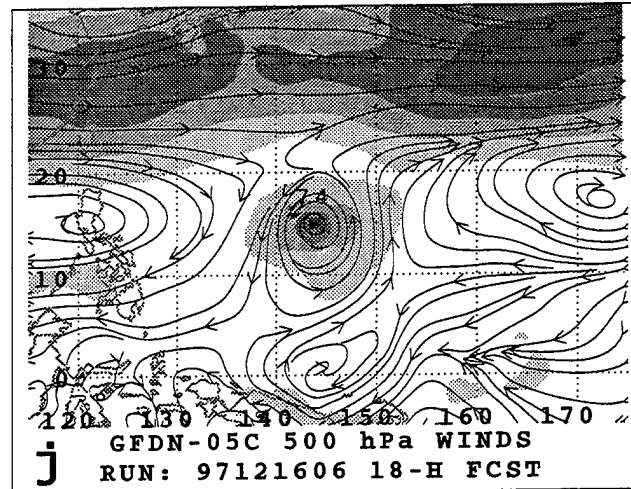
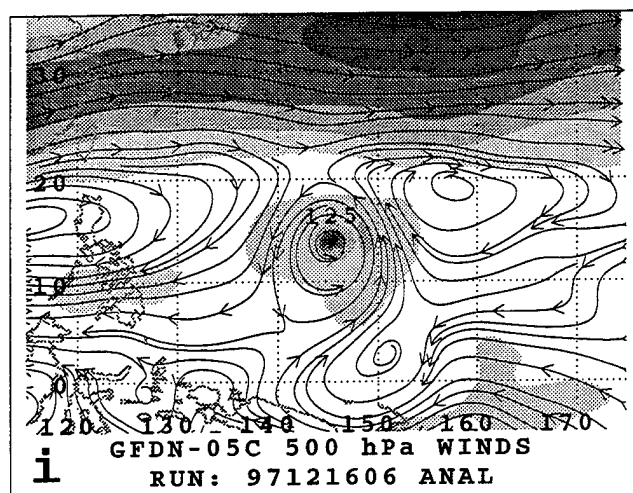
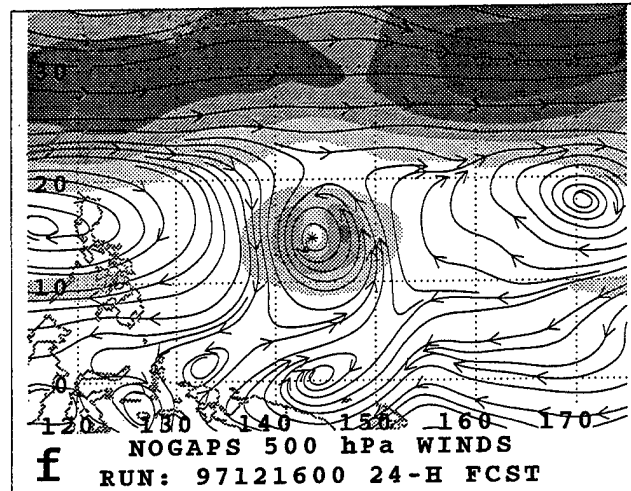
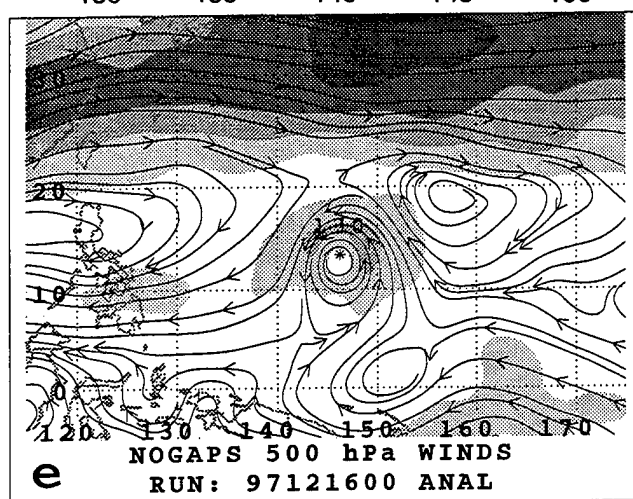
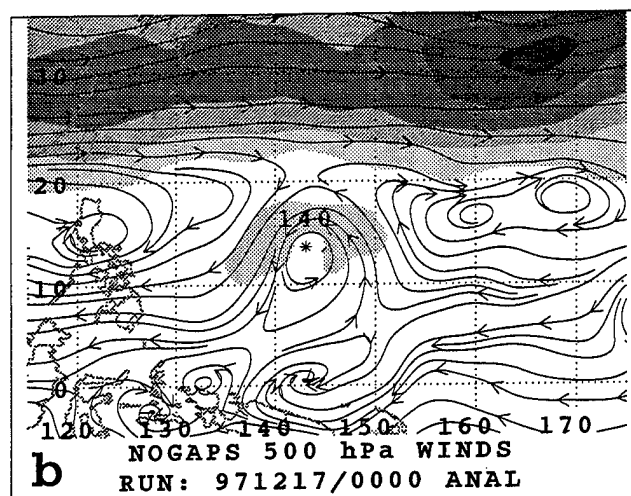
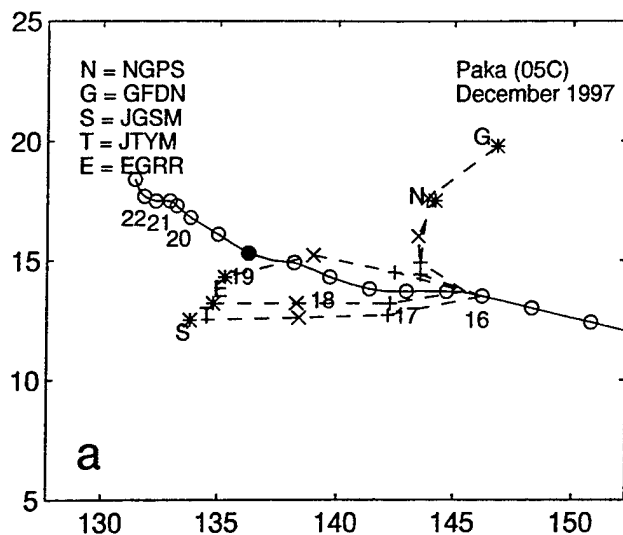


Fig. A.24. (a-l) As in Fig. A.1, except for 500-mb wind forecasts for Paka initiated at 0000 and 0600 UTC 16 December 1997.

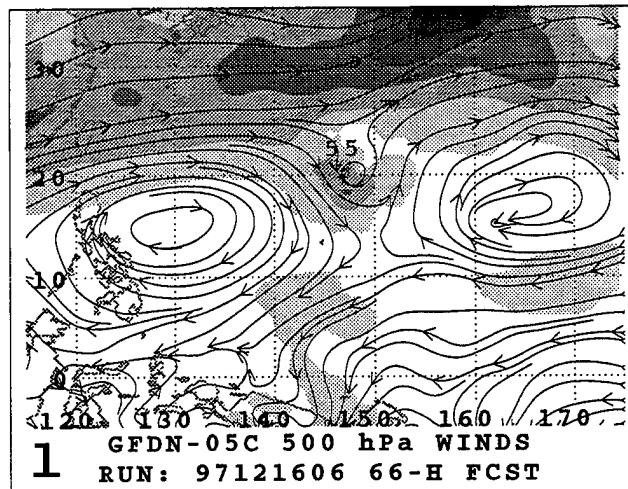
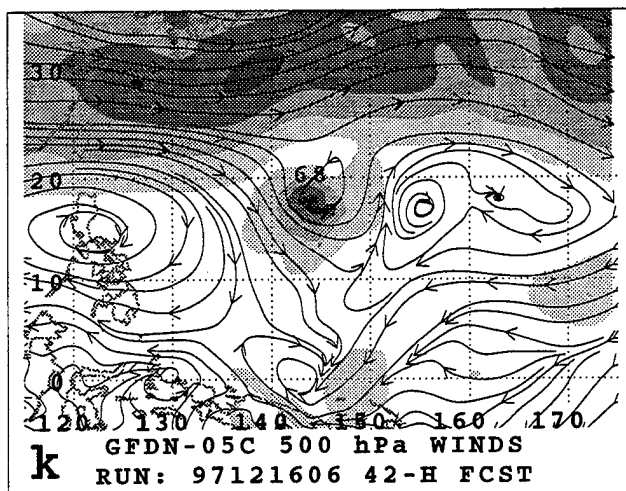
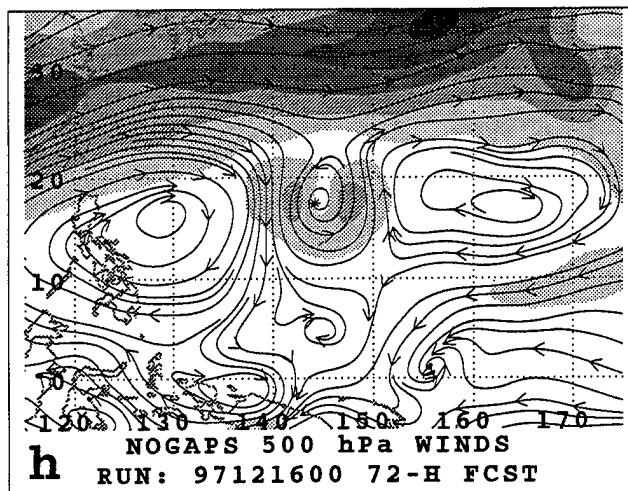
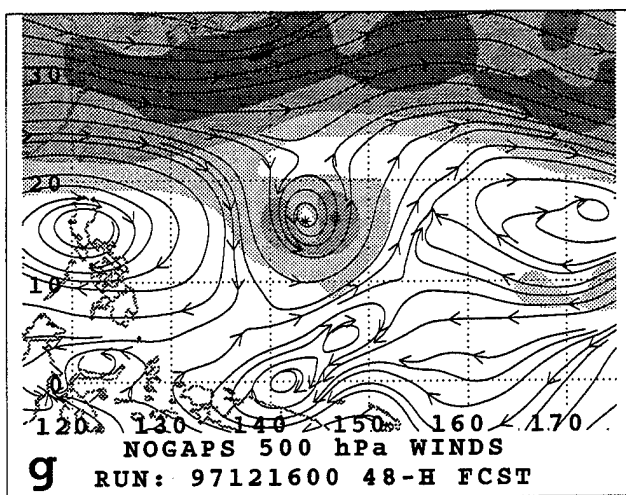
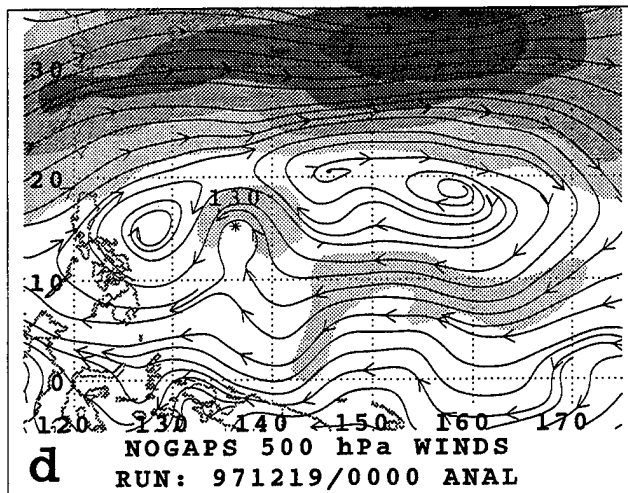
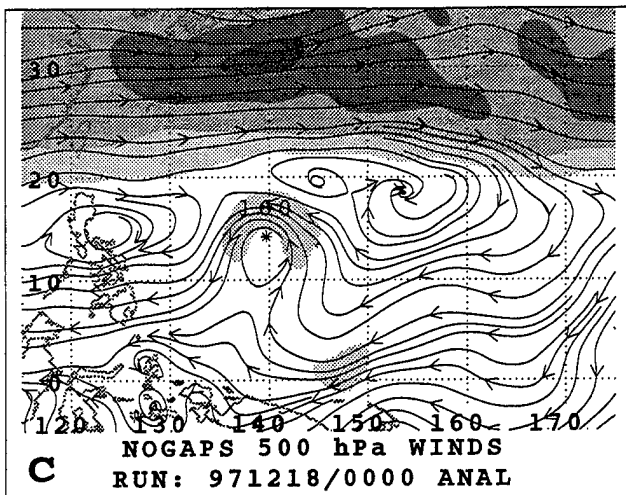


Fig. A.24. (continued)

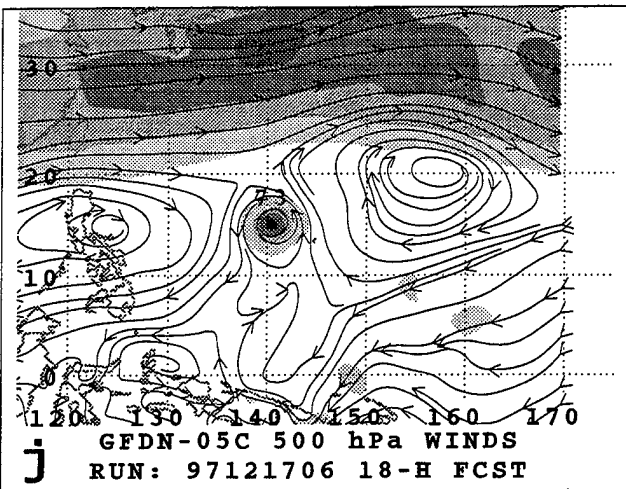
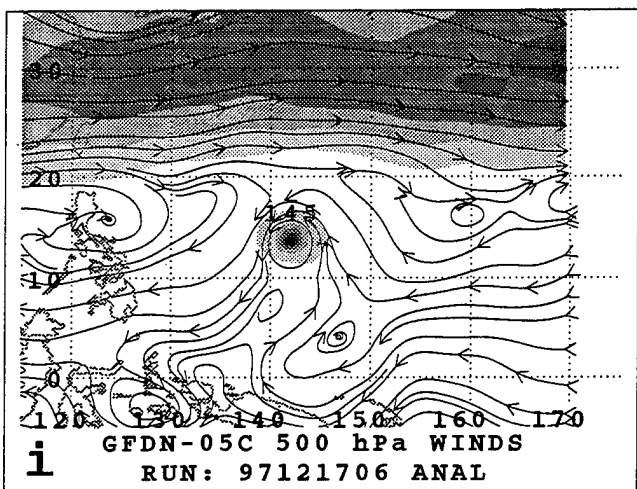
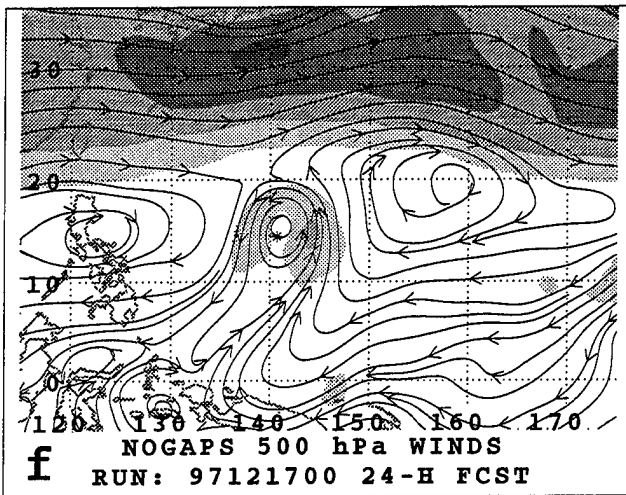
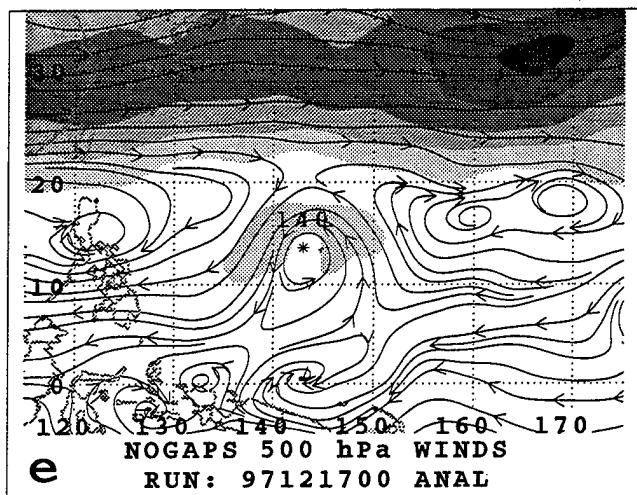
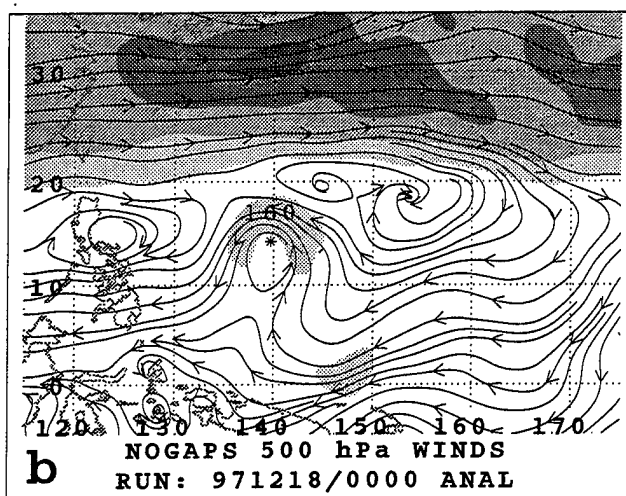
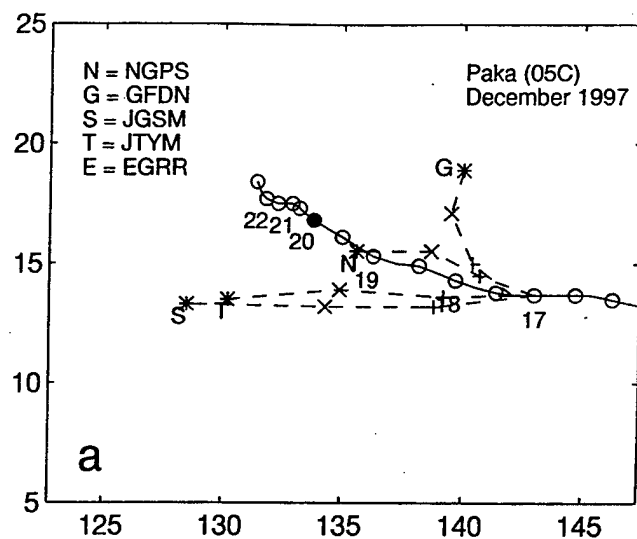


Fig. A.25. (a-l) As in Fig. A.1, except for 500-mb wind forecasts for Paka initiated at 0000 and 0600 UTC 17 December 1997.

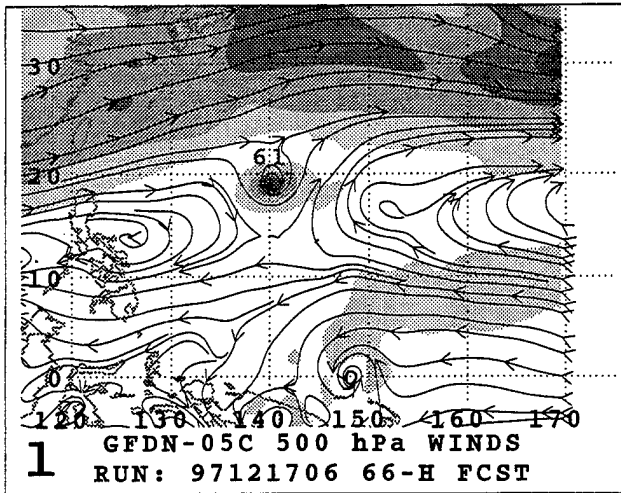
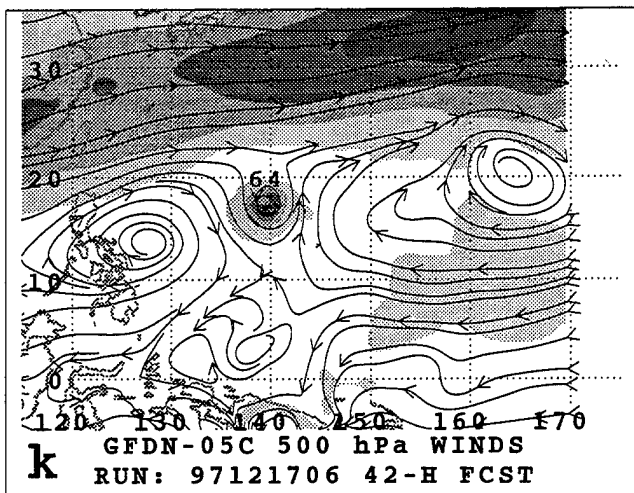
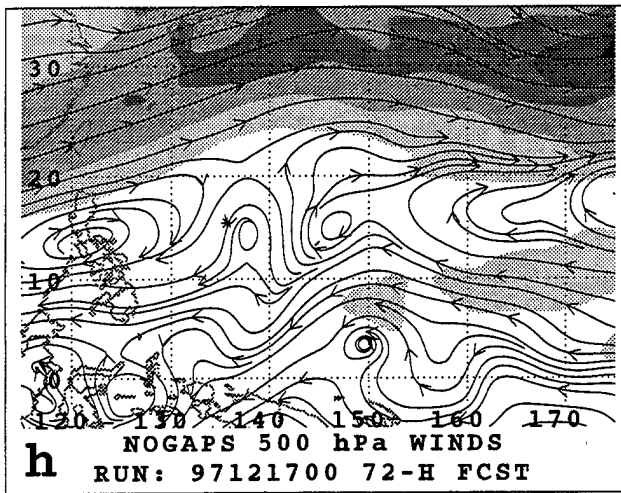
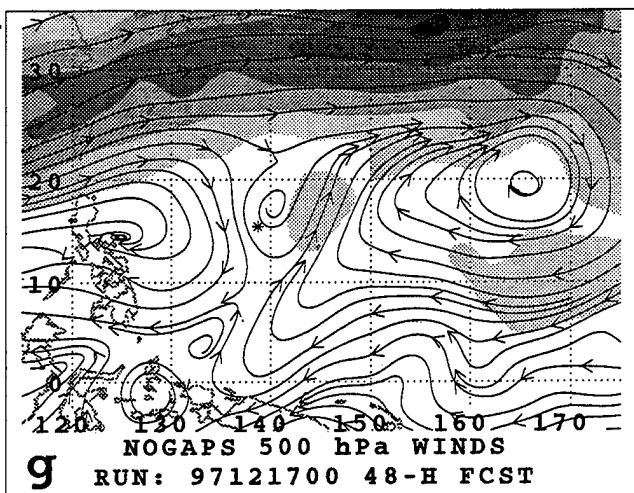
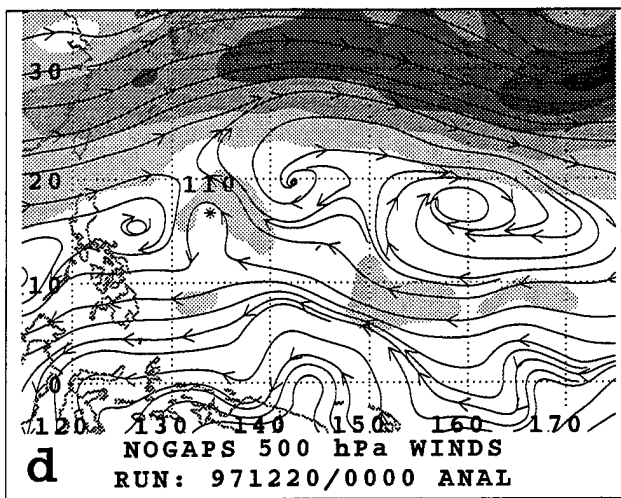
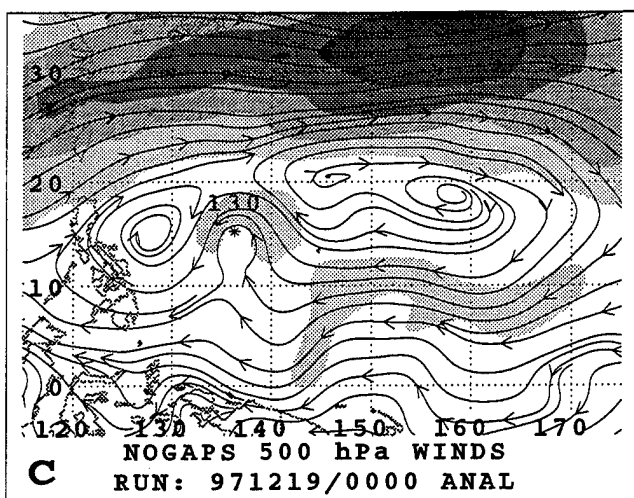


Fig. A.25. (continued)

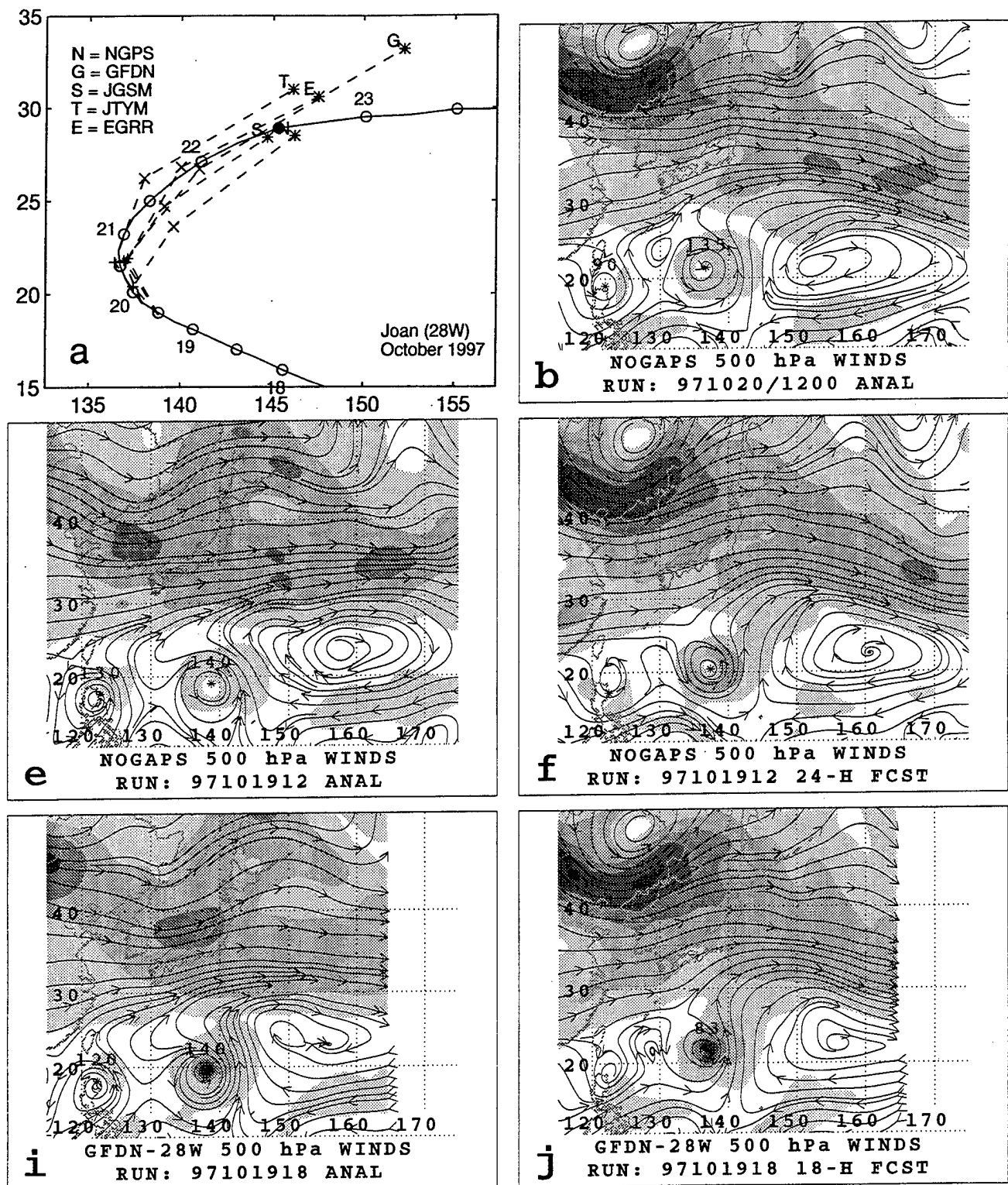


Fig. A.26. (a-l) As in Fig. A.1, except for 500-mb wind forecasts for Joan initiated at 1200 and 1800 UTC 19 October 1997.

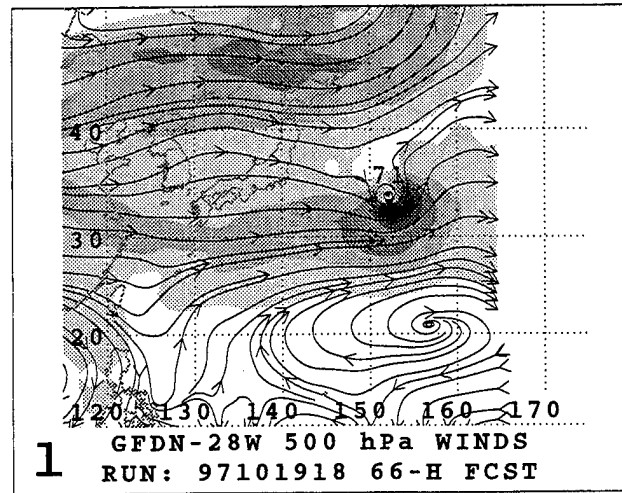
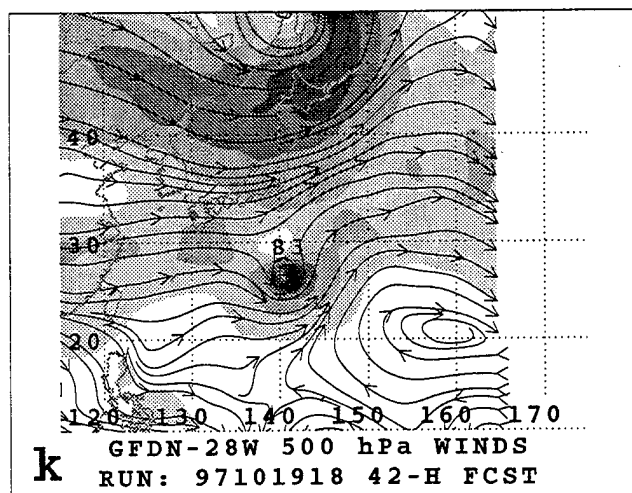
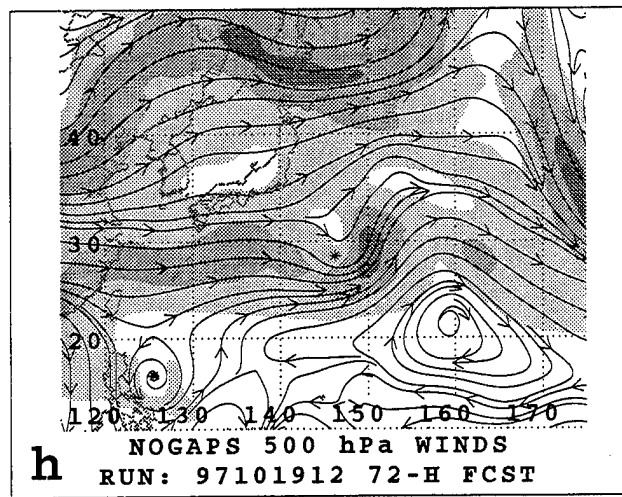
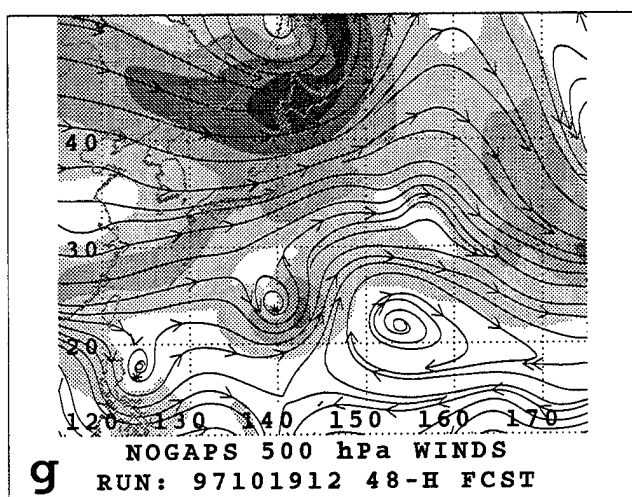
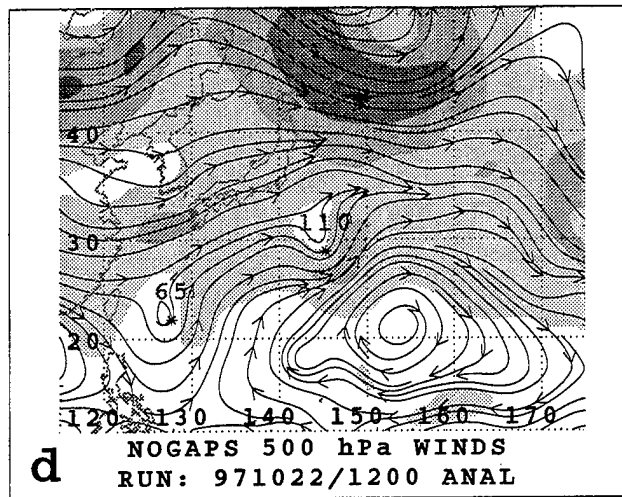
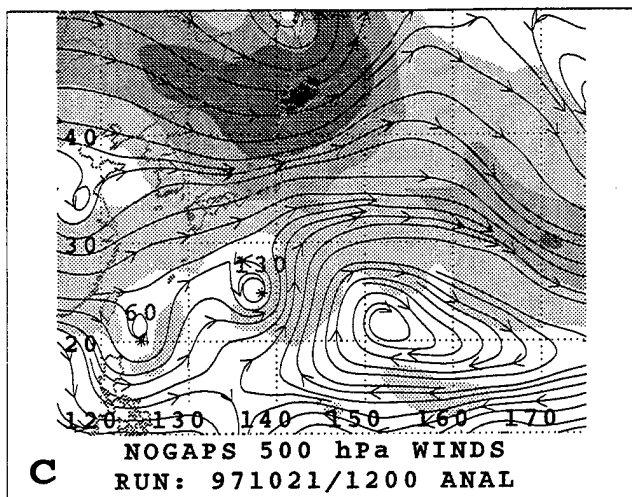


Fig. A.26. (continued)

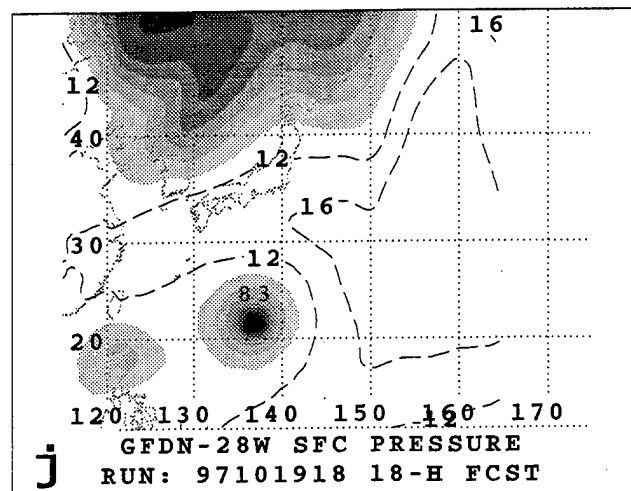
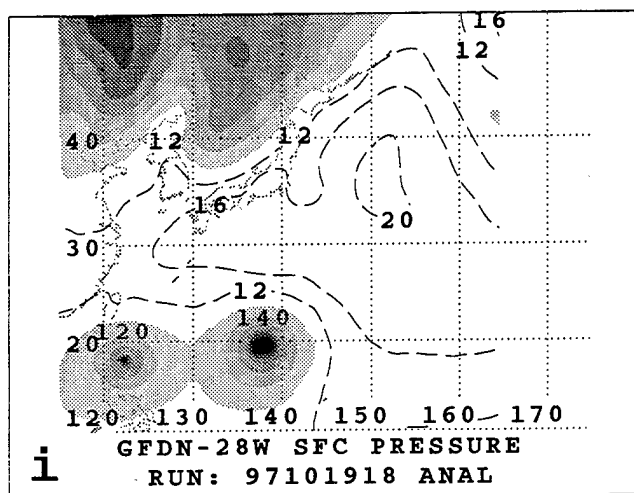
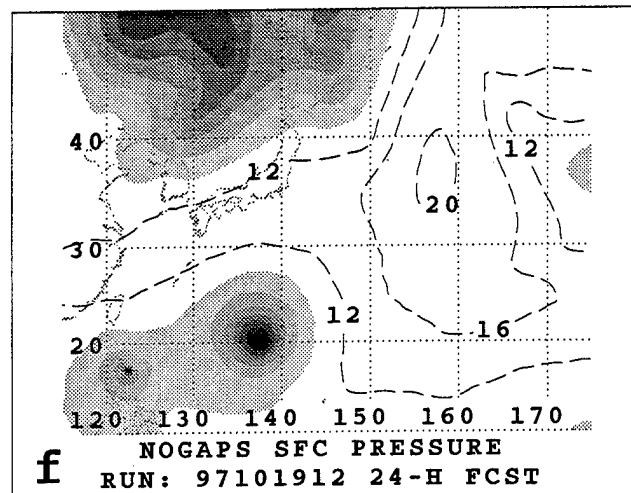
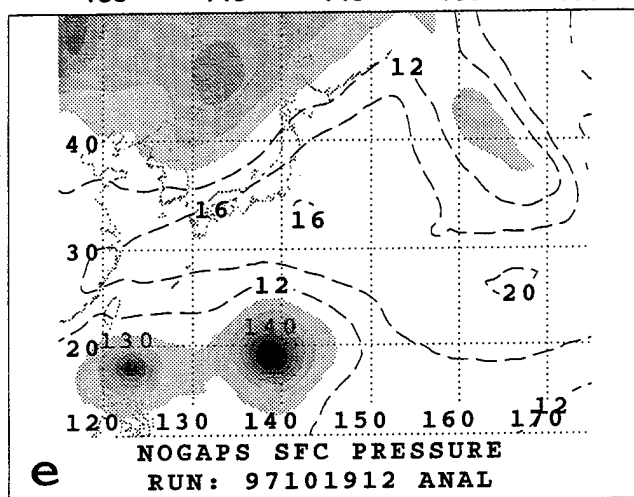
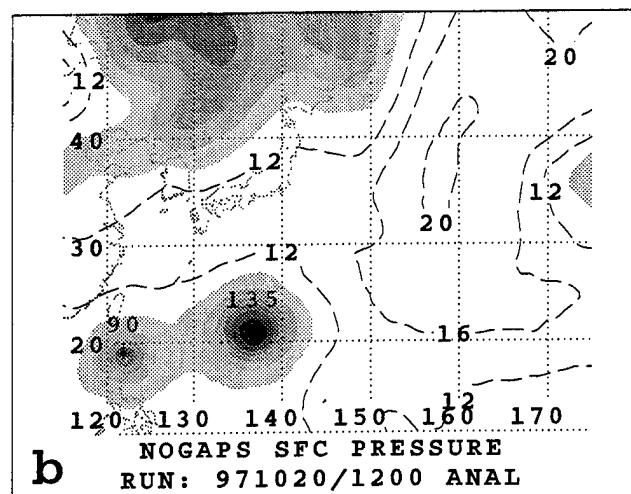
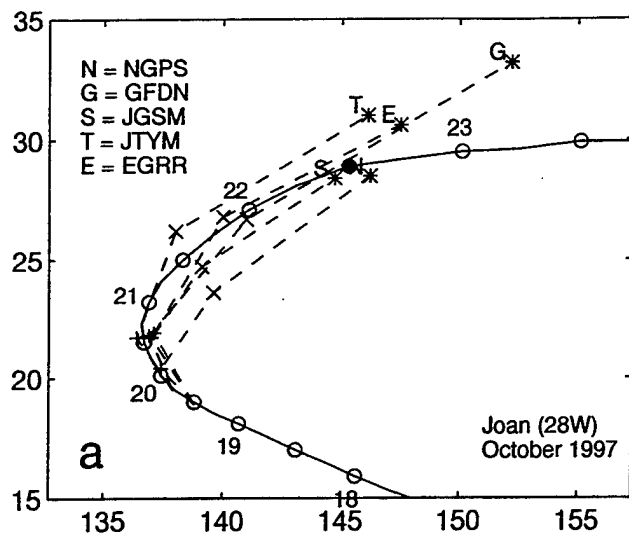


Fig. A.27. (a-l) As in Fig. A.1, except for sea-level pressure forecasts for Joan initiated at 1200 and 1800 UTC 19 October 1997.

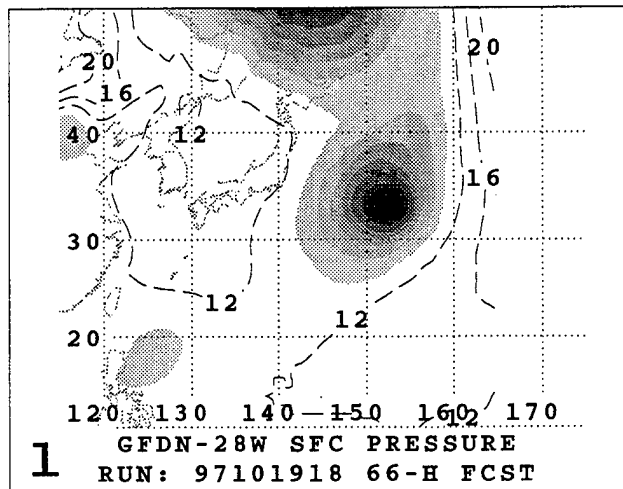
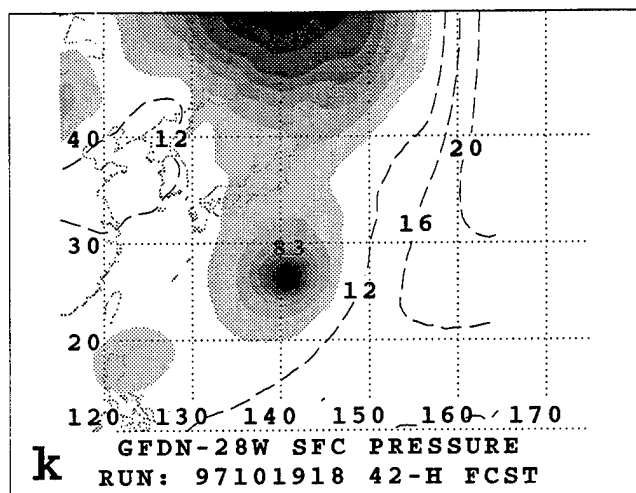
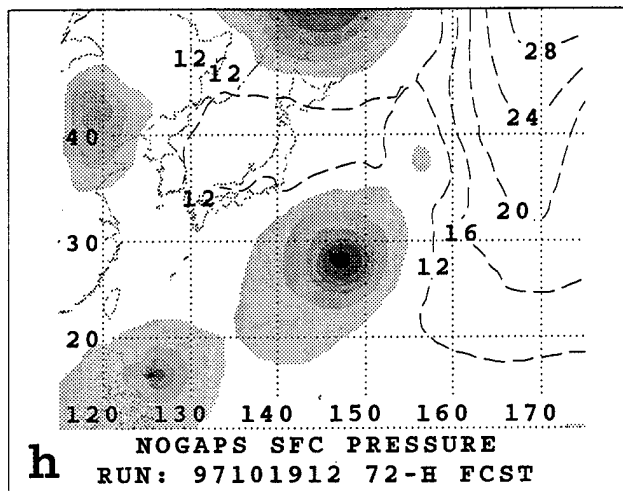
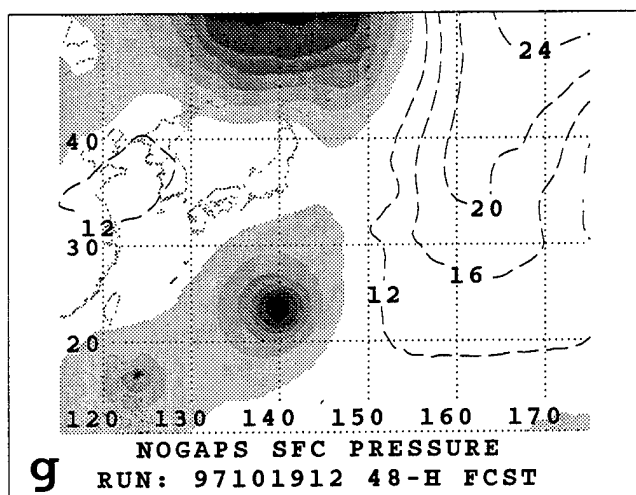
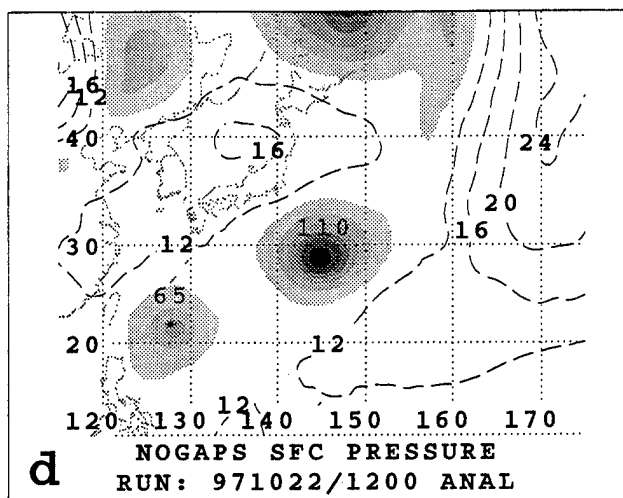
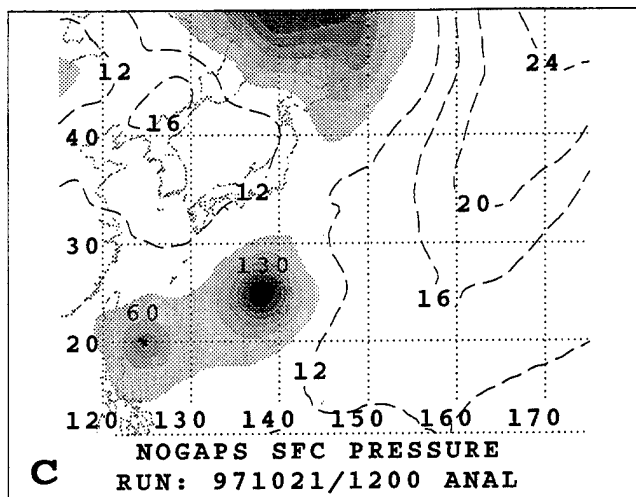


Fig. A.27. (continued)

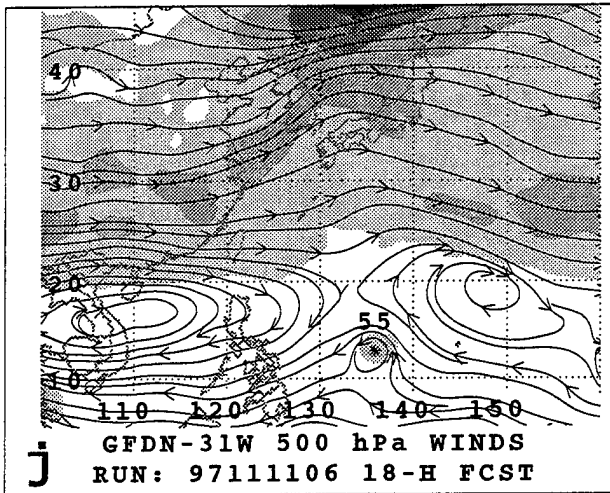
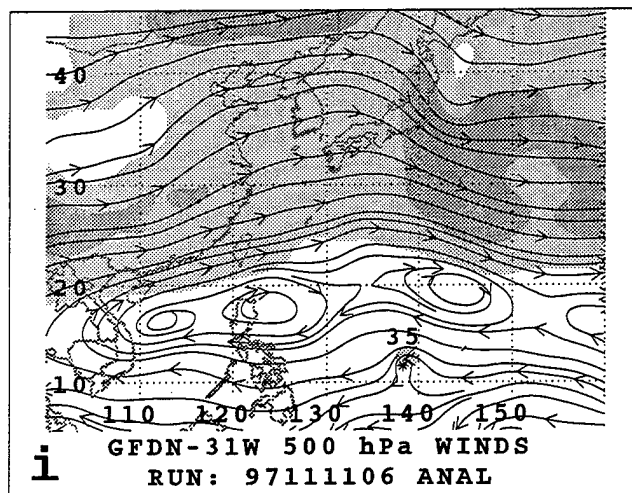
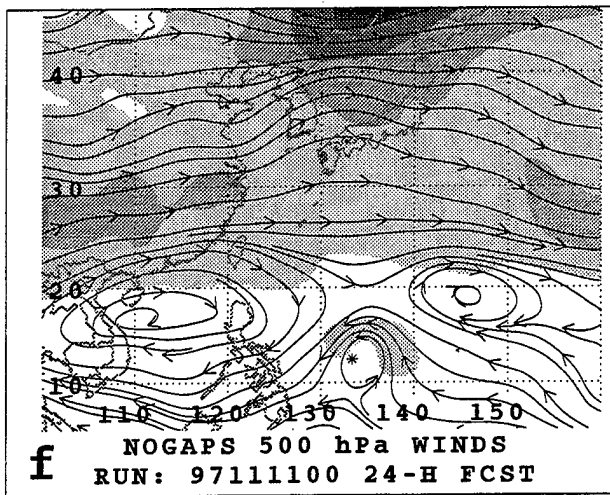
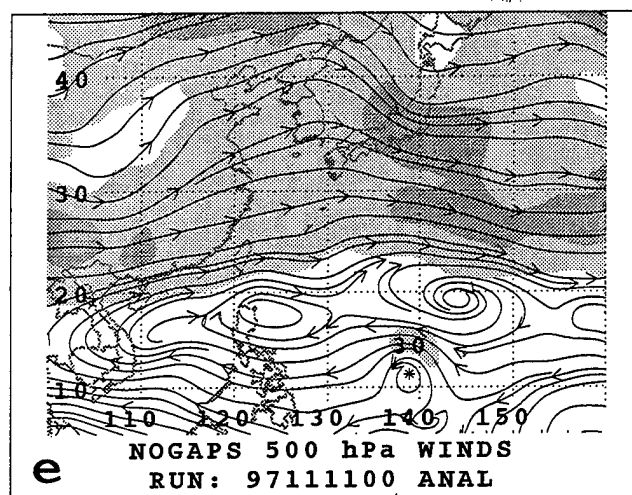
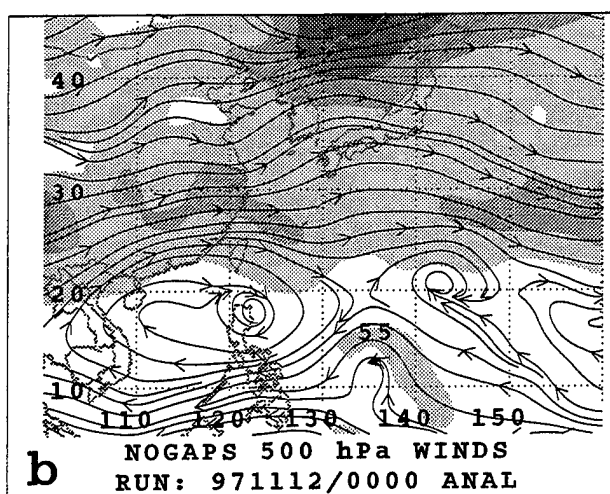
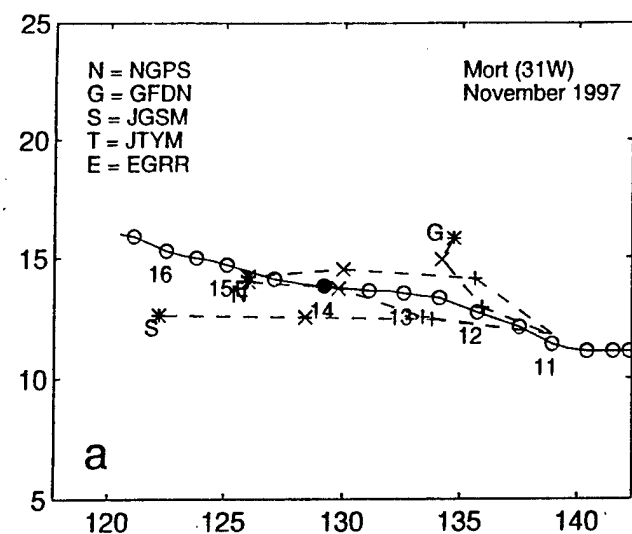


Fig. A.28. (a-l) As in Fig. A.1, except for 500-mb wind forecasts for Mort initiated at 0000 and 0600 UTC 11 November 1997.

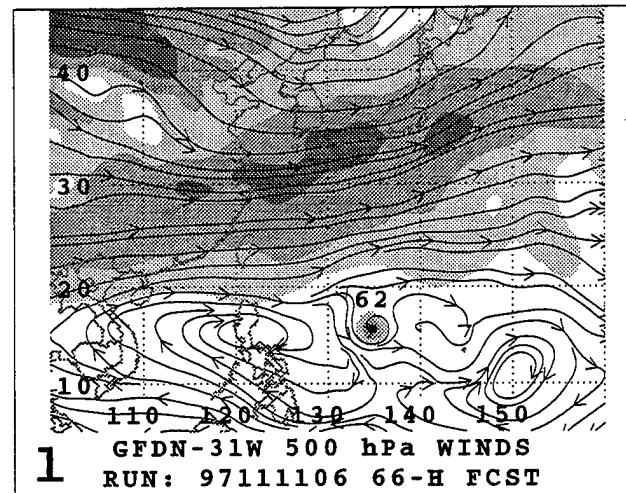
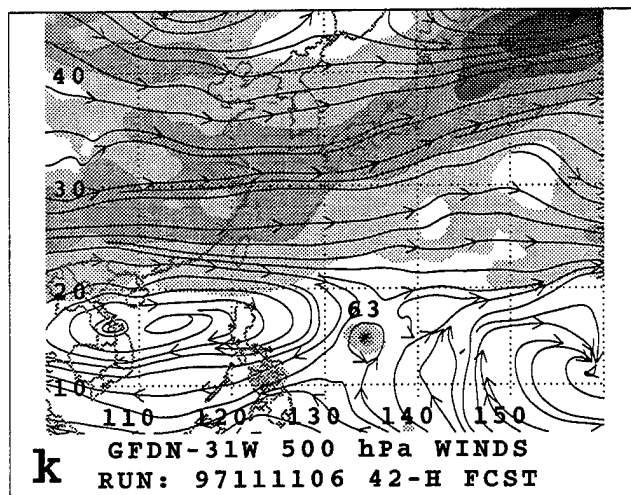
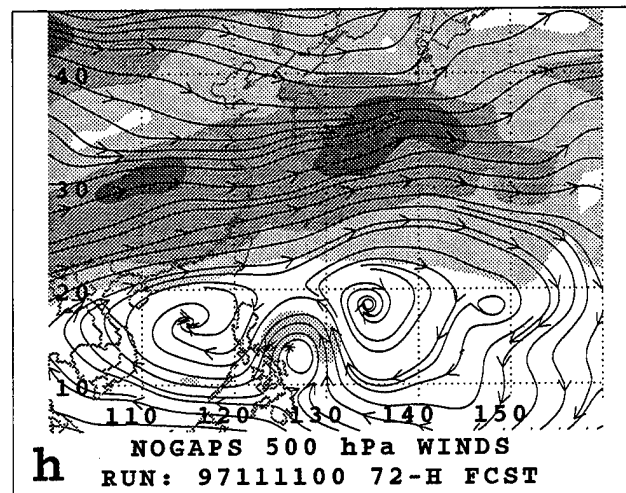
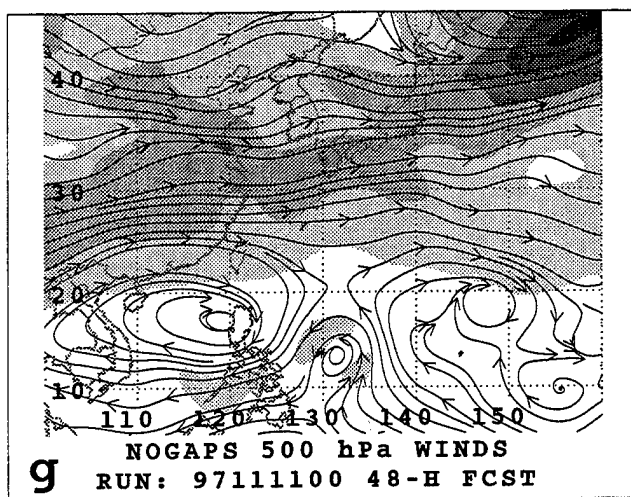
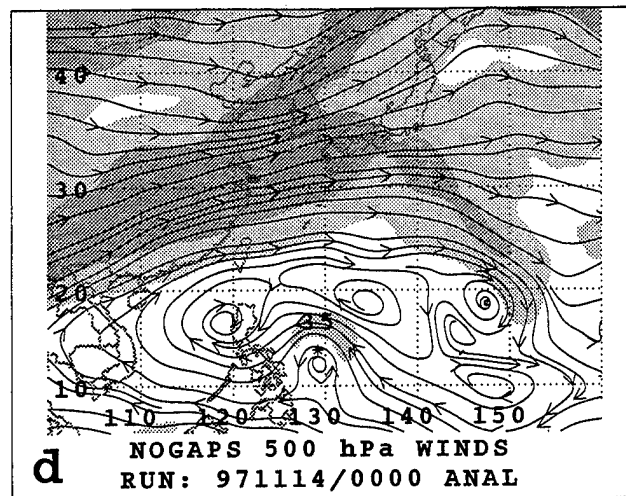
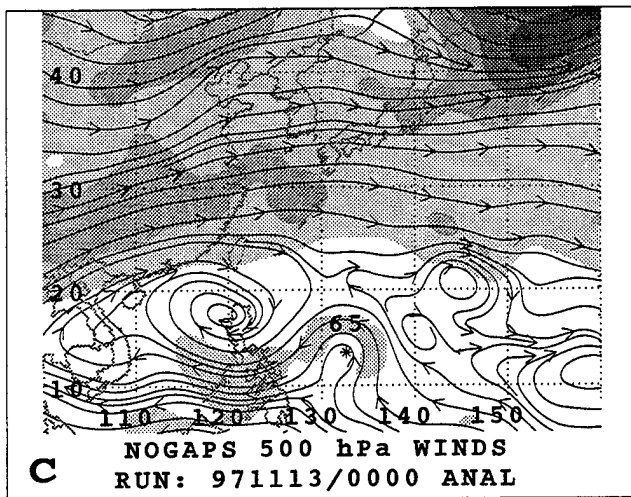


Fig. A.28. (continued)

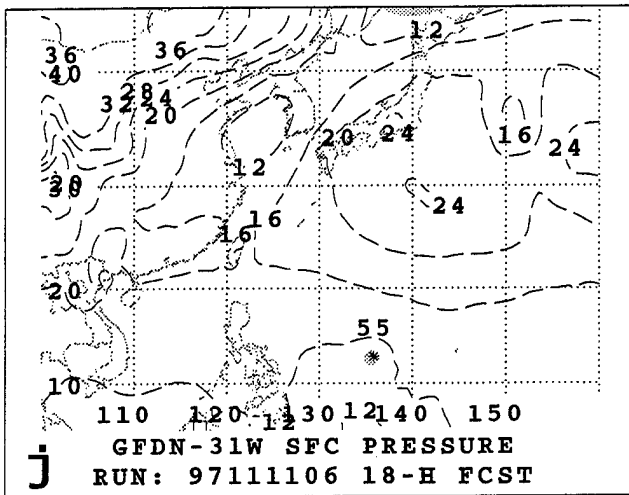
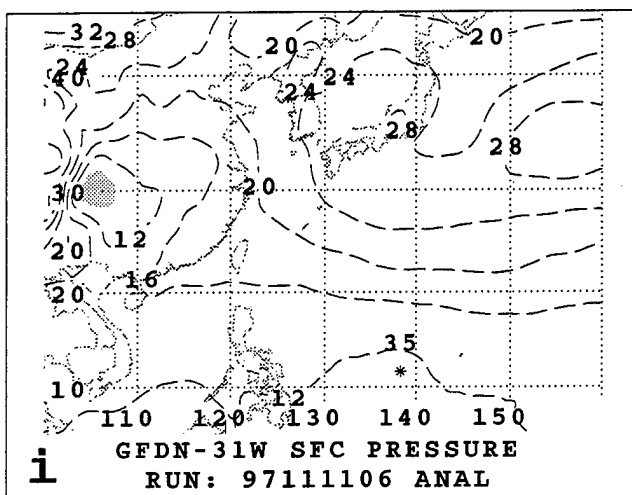
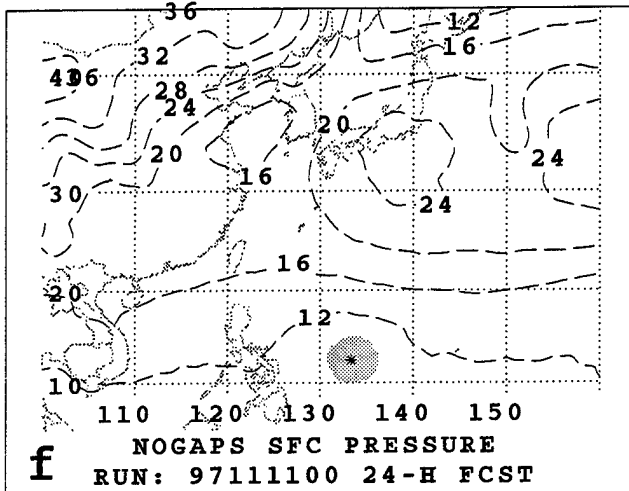
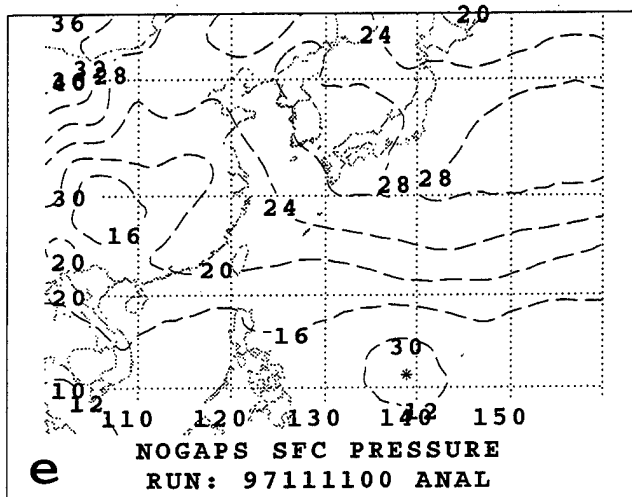
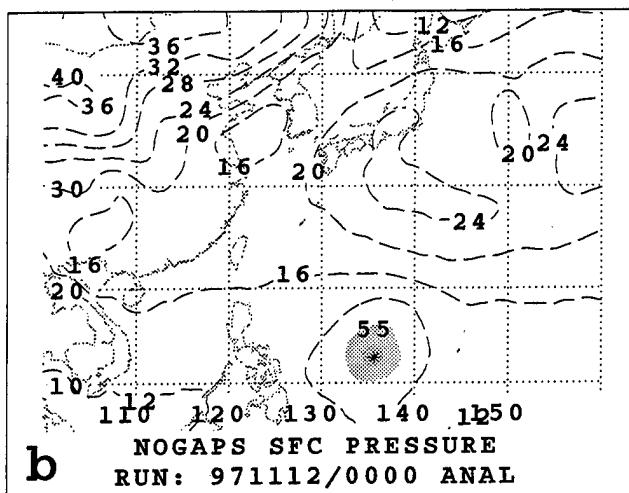
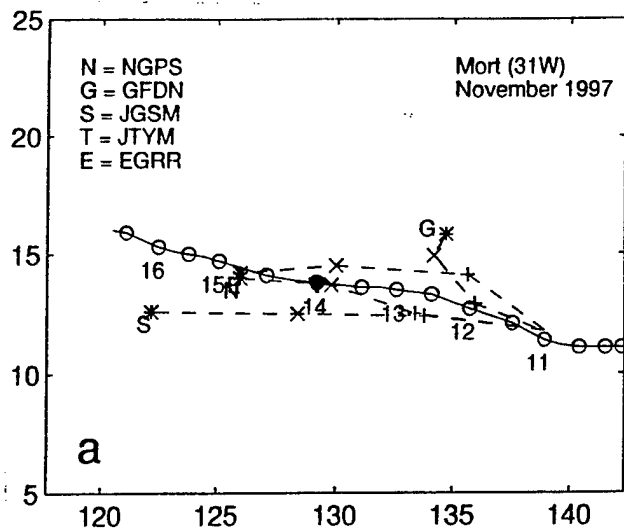


Fig. A.29. (a-l) As in Fig. A.1, except for sea-level pressure forecasts for Mort initiated at 0000 and 0600 UTC 11 December 1997.

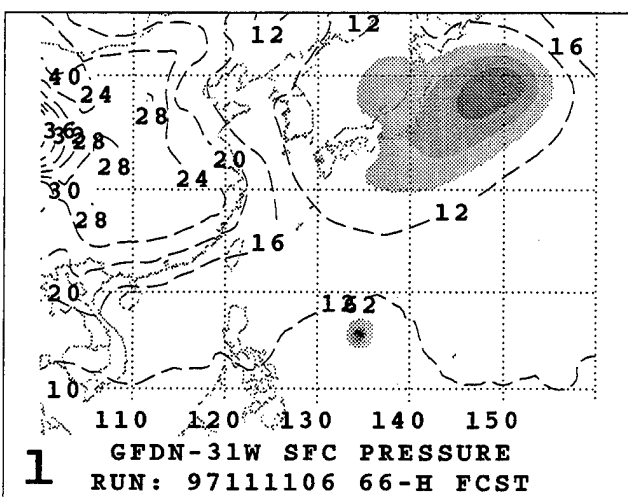
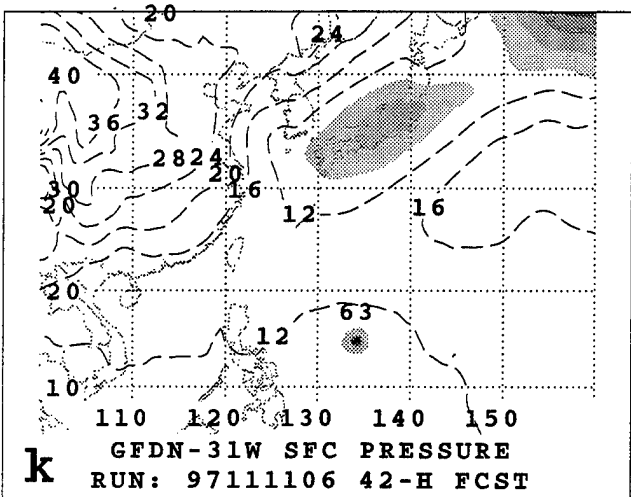
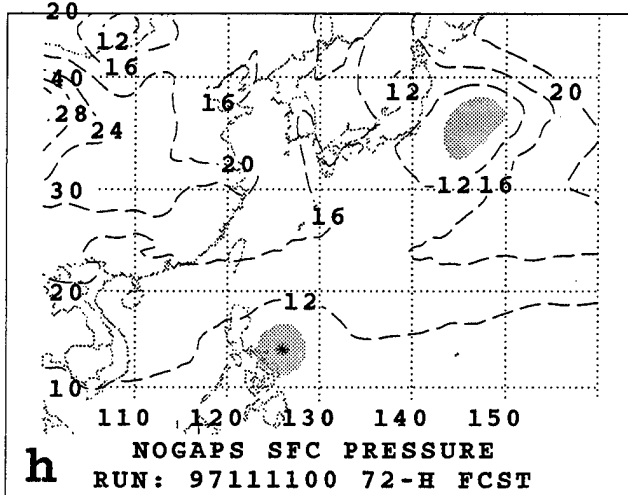
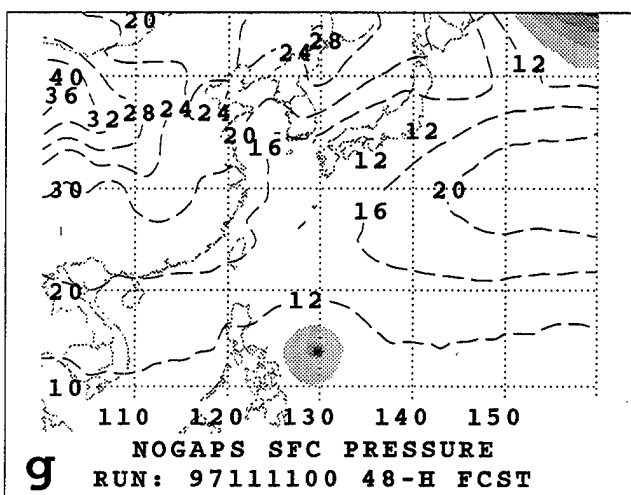
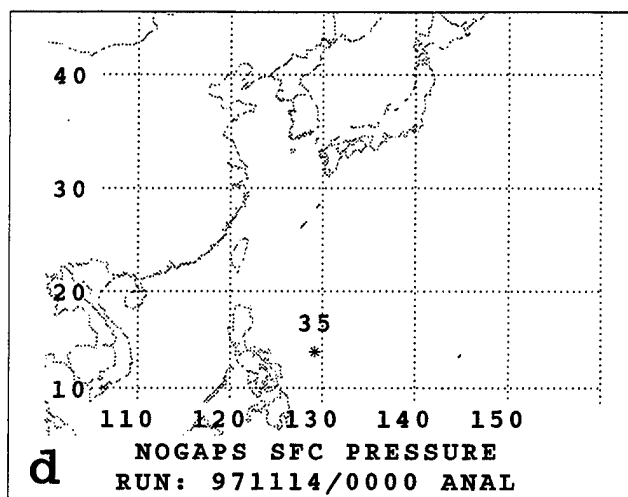
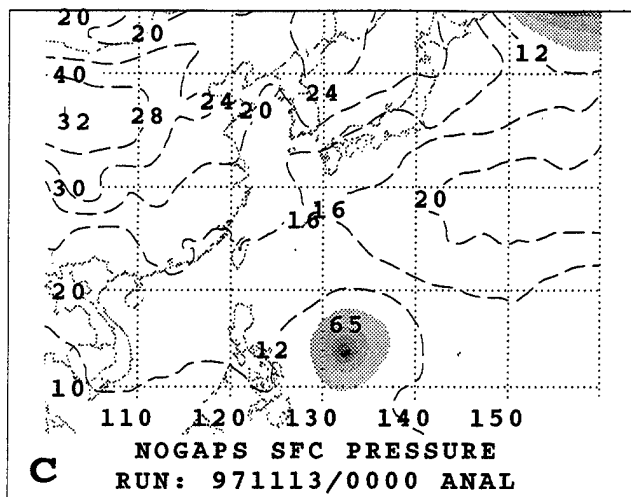


Fig. A.29. (continued)

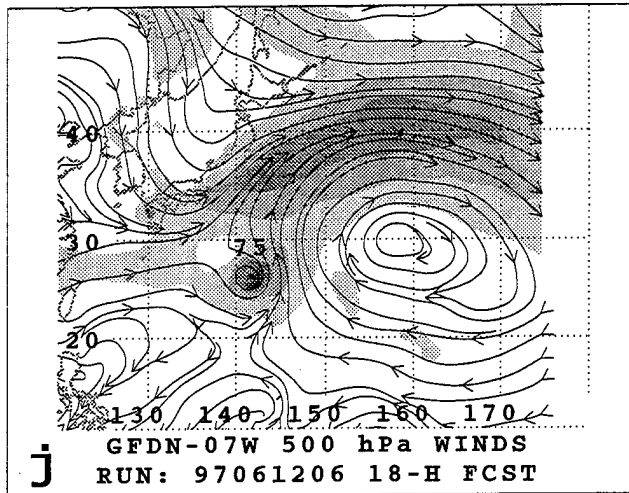
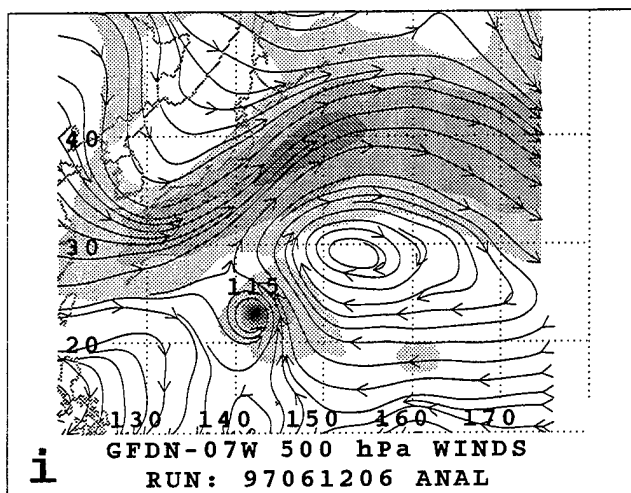
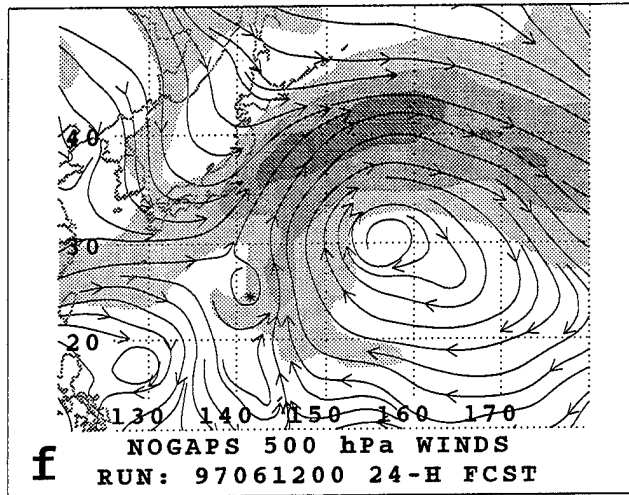
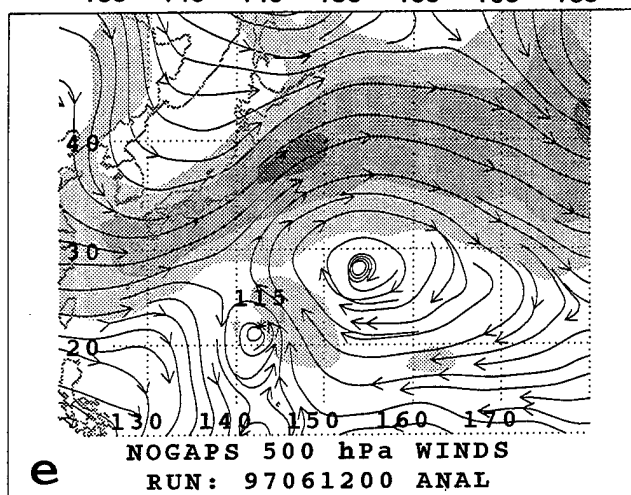
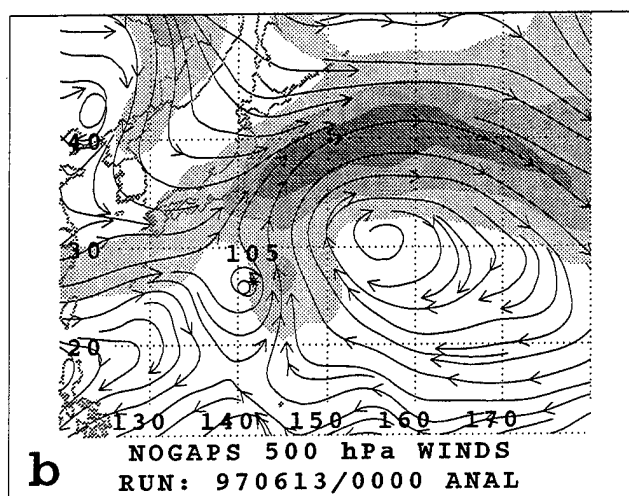
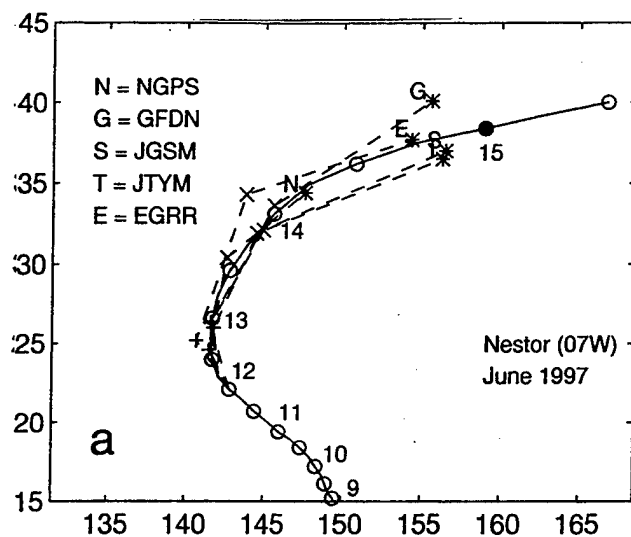


Fig. A.30. (a-l) As in Fig. A.1, except for 500-mb wind forecasts for Nestor initiated at 0000 and 0600 UTC 12 June 1997.

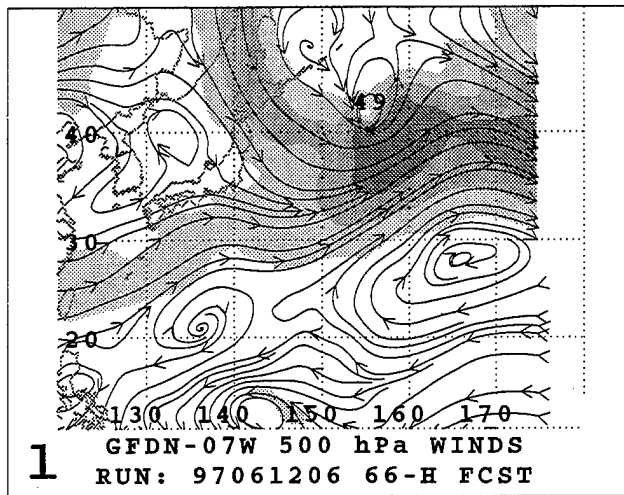
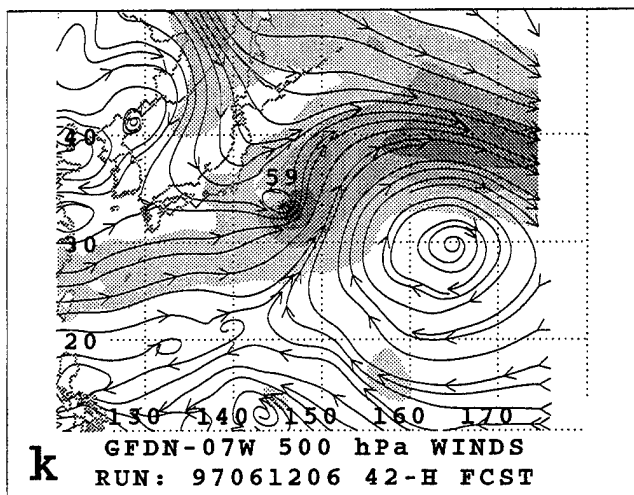
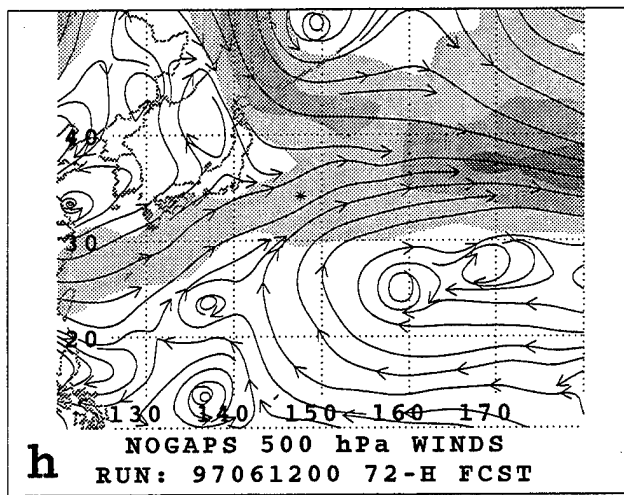
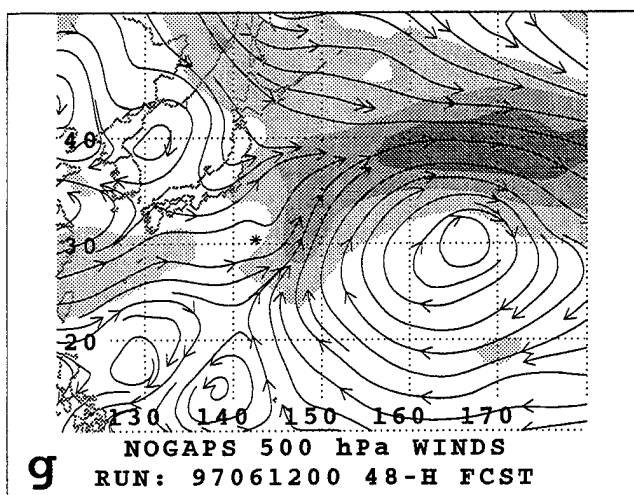
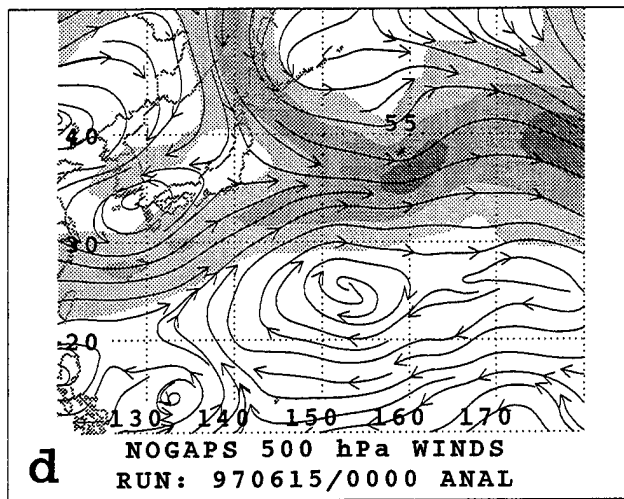
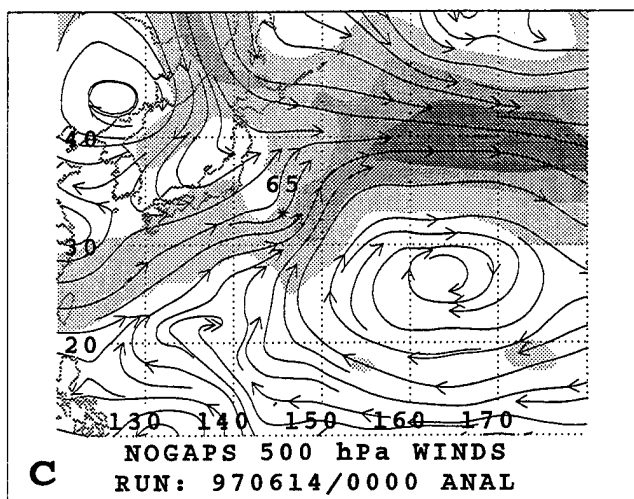


Fig. A.30. (continued)

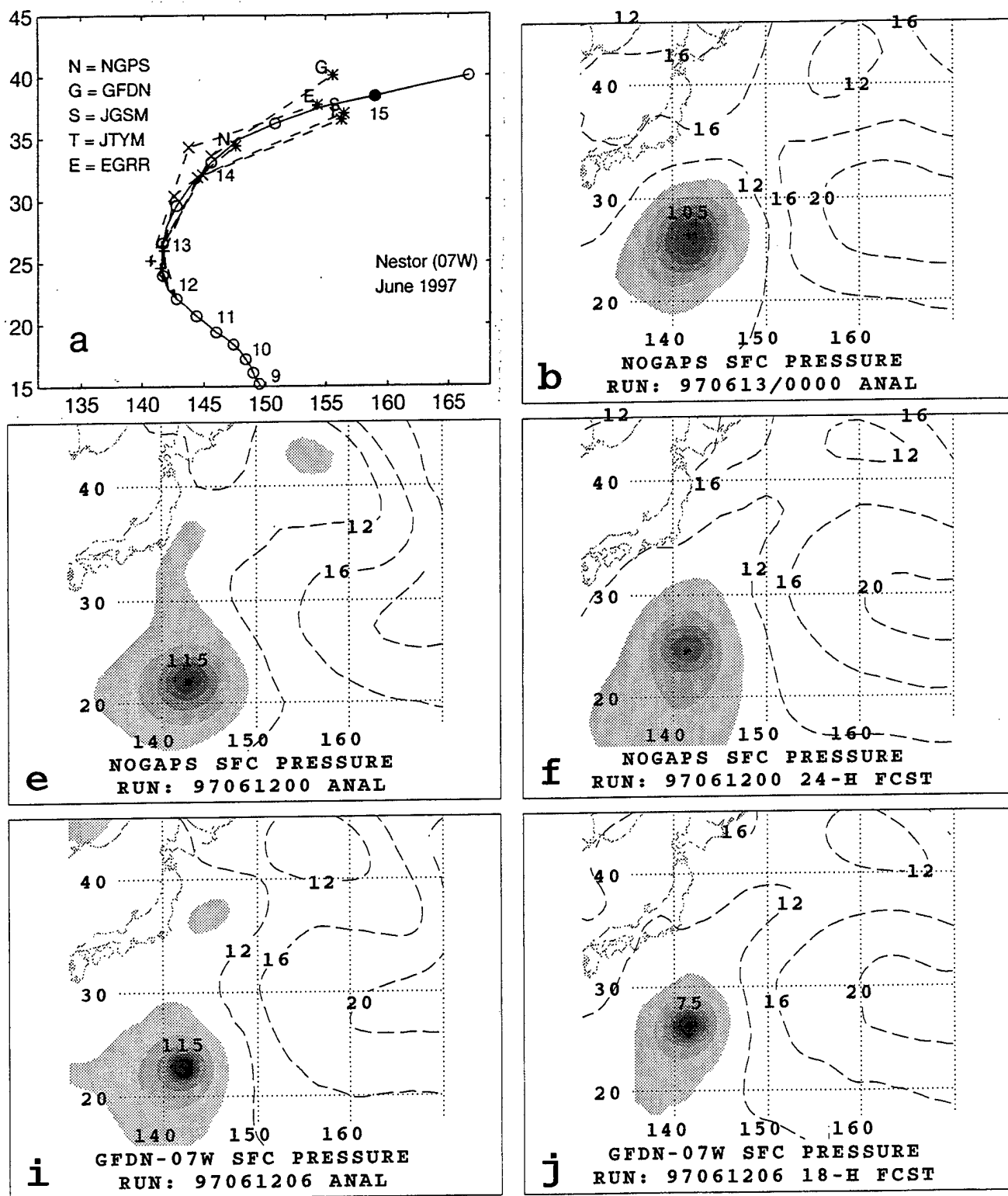


Fig. A.31. (a-l) As in Fig. A.1, except for sea-level pressure forecasts for Nestor initiated at 0000 and 0600 UTC 12 June 1997.

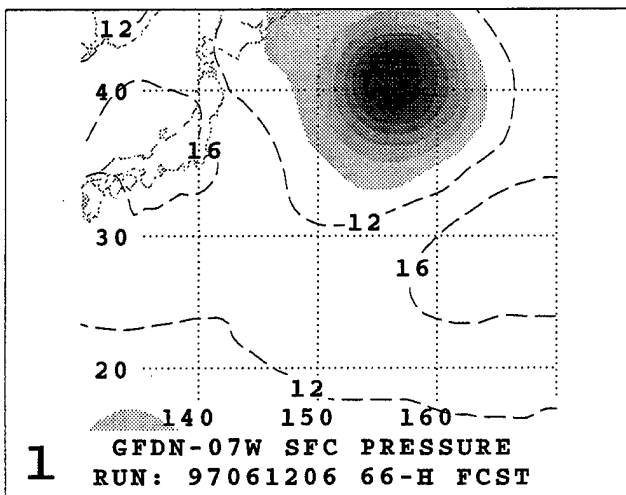
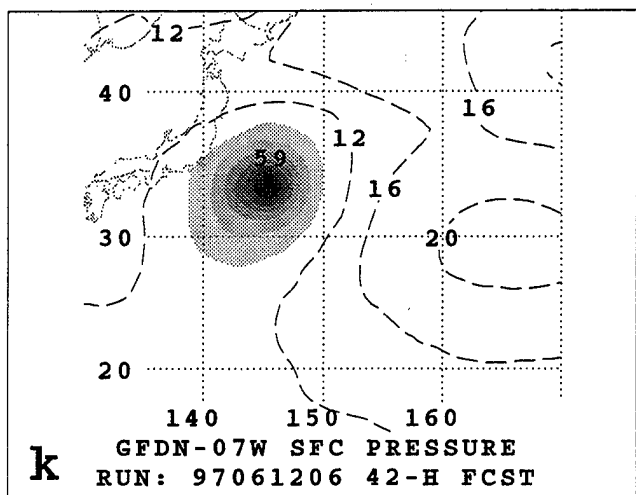
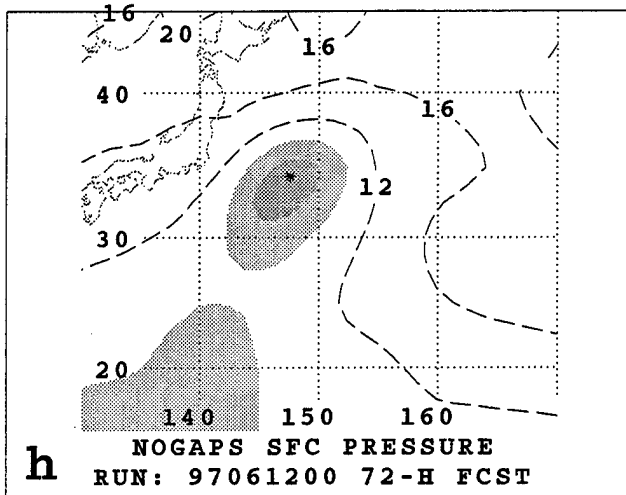
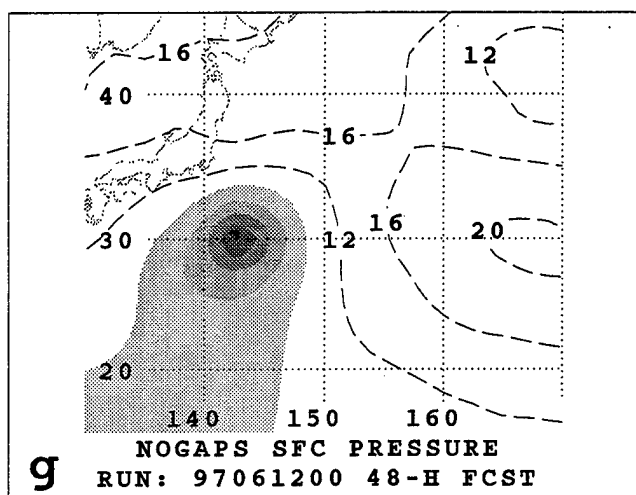
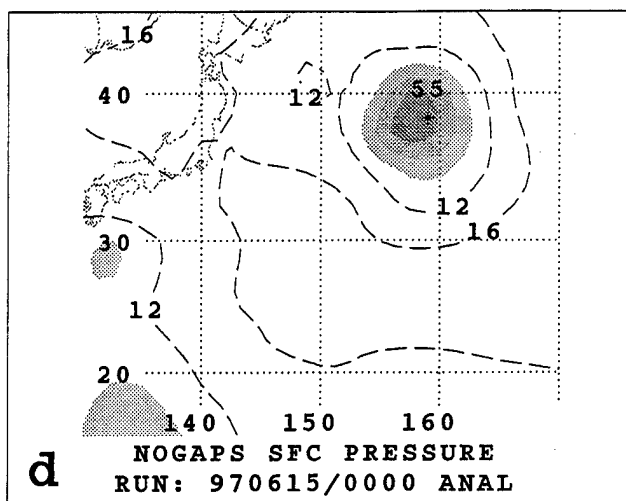
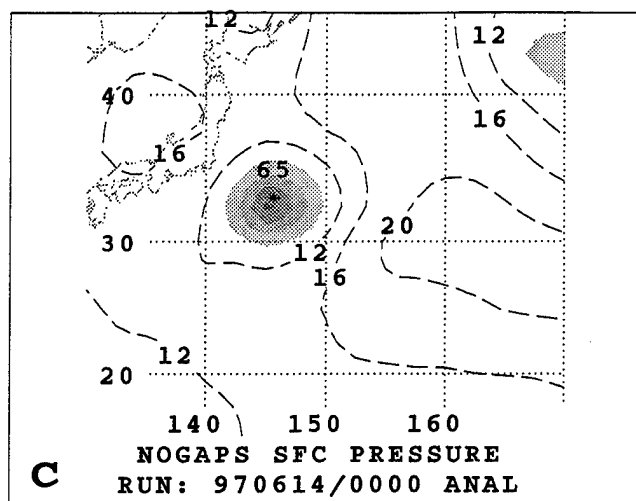


Fig. A.31. (continued)

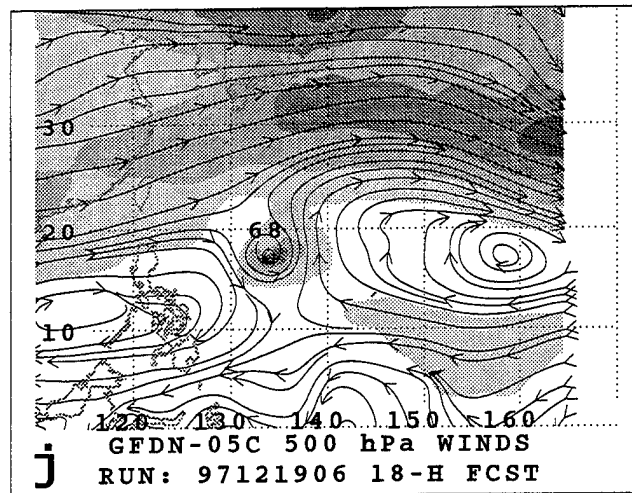
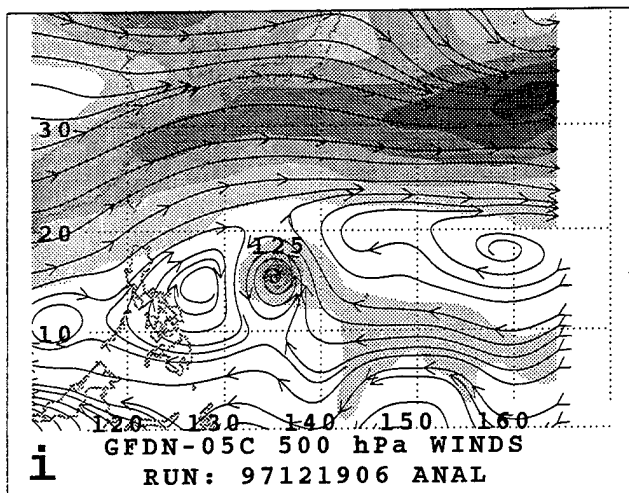
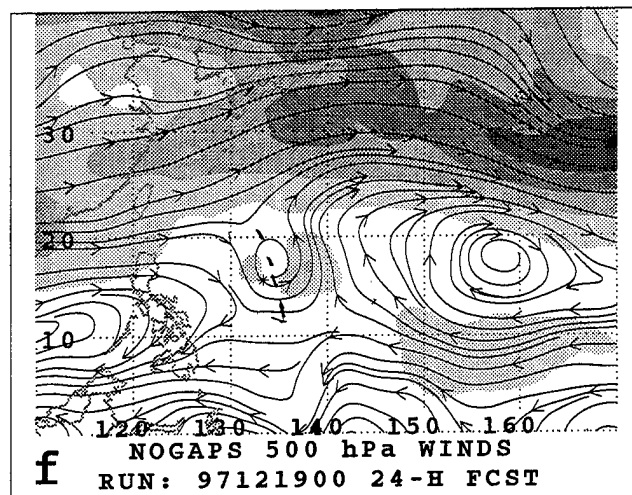
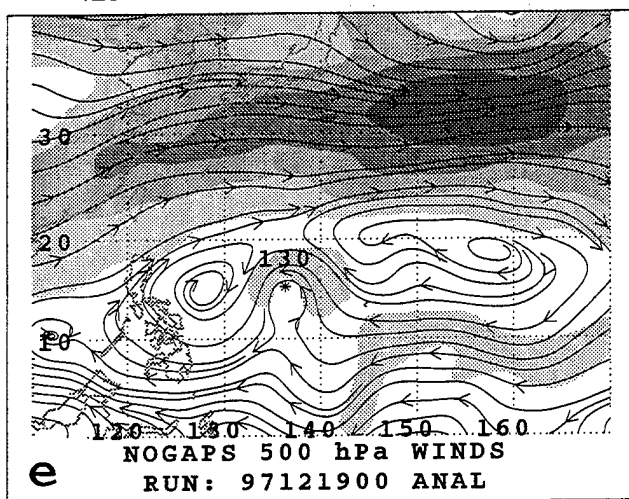
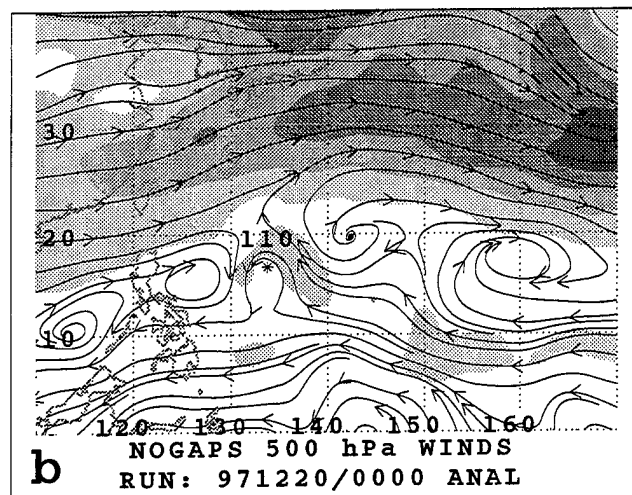
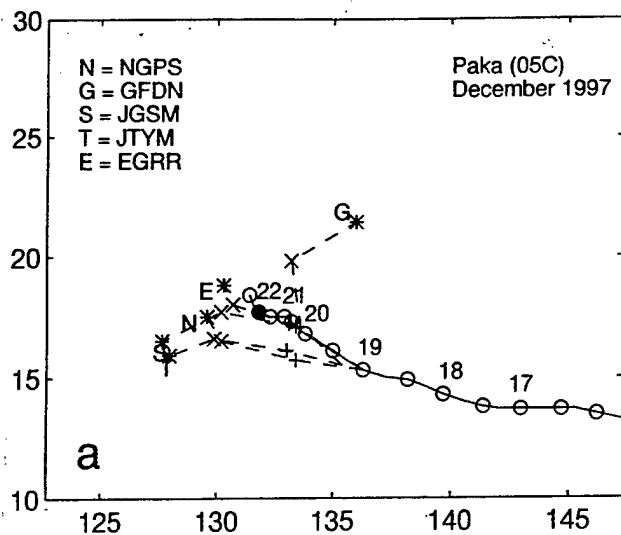


Fig. A.32. (a-l) As in Fig. A.1, except for 500-mb wind forecasts for Paka initiated at 0000 and 0600 UTC 19 December 1997.

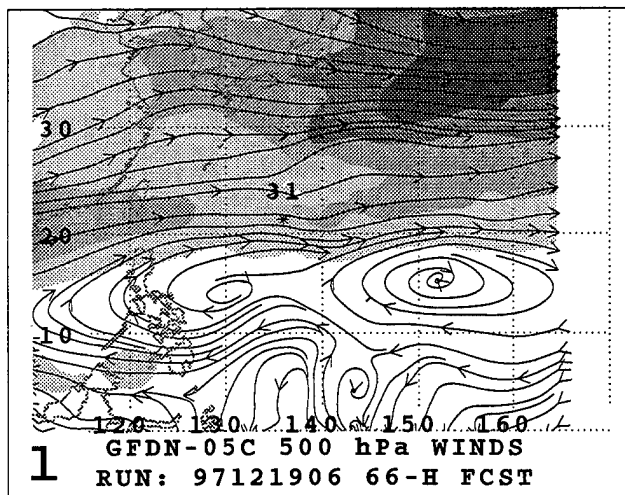
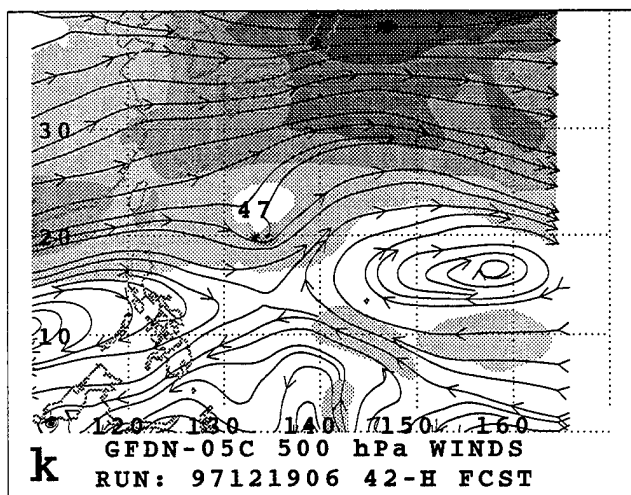
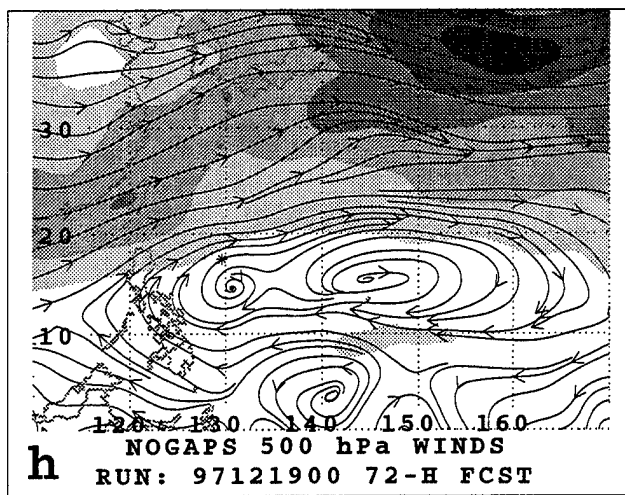
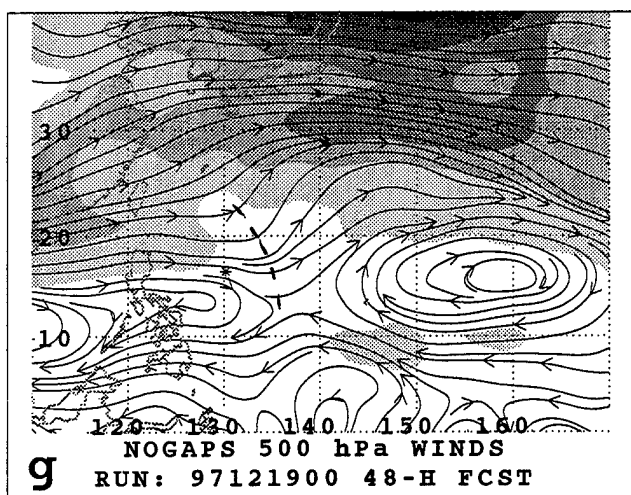
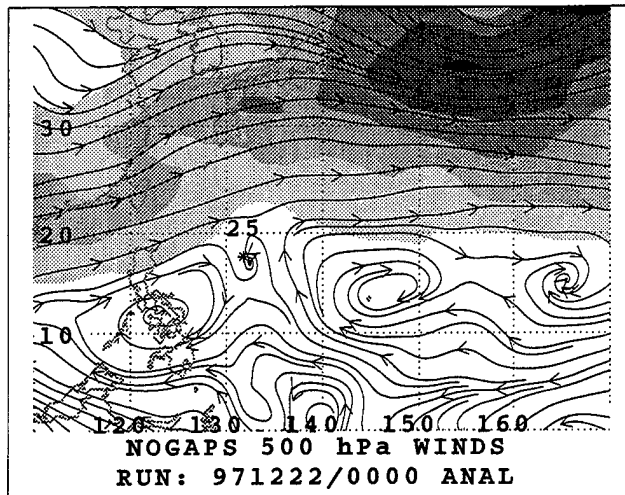
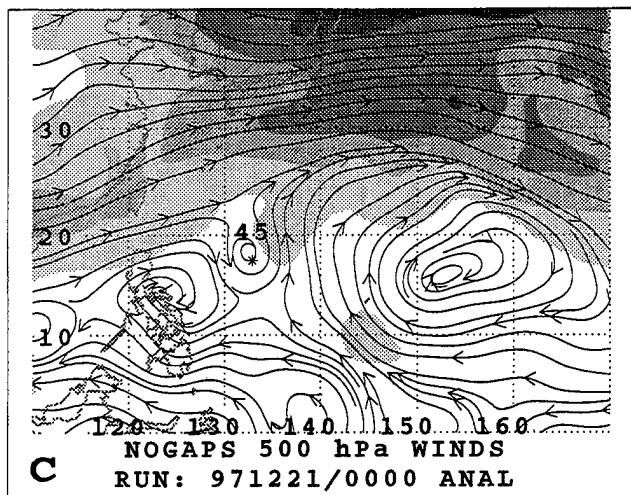


Fig. A.32. (continued)

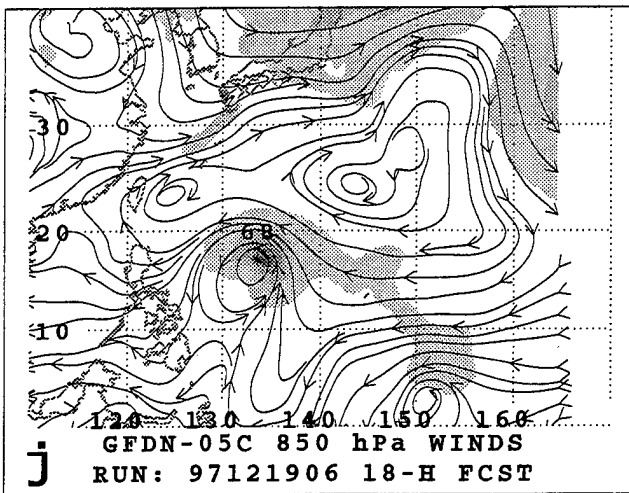
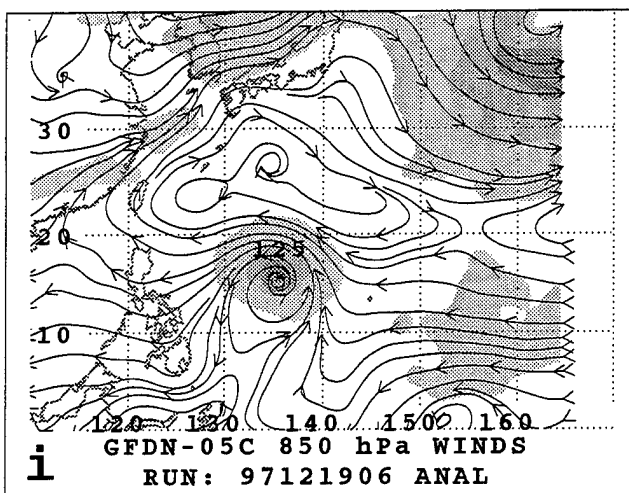
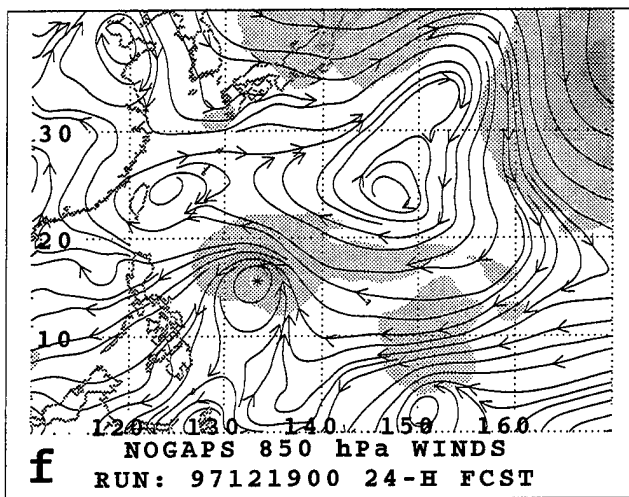
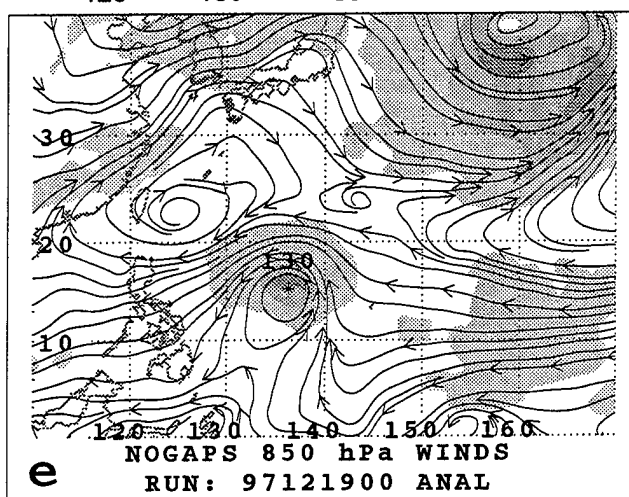
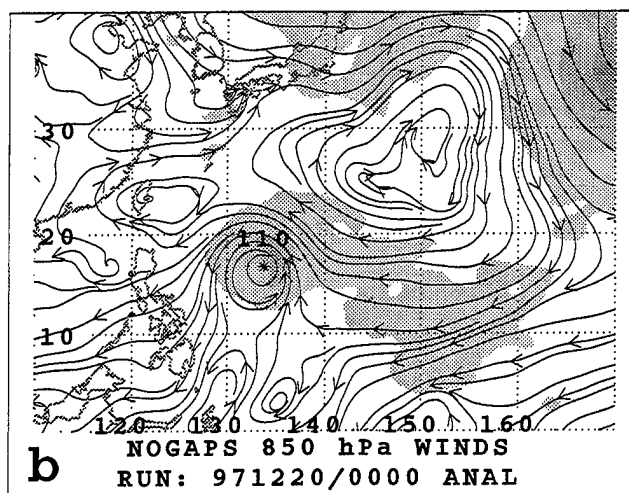
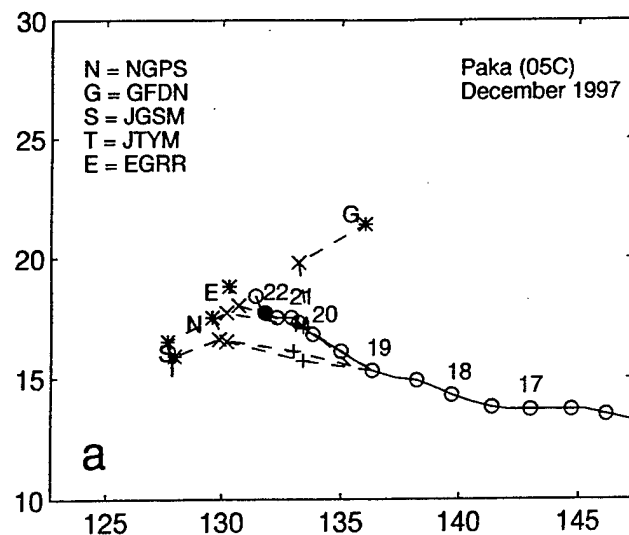


Fig. A.33. (a-l) As in Fig. A.1, except for 850-mb wind forecasts for Paka initiated at 0000 and 0600 UTC 19 December 1997.

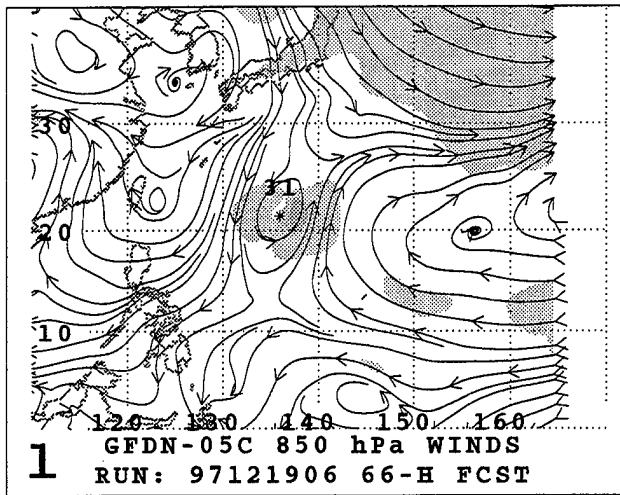
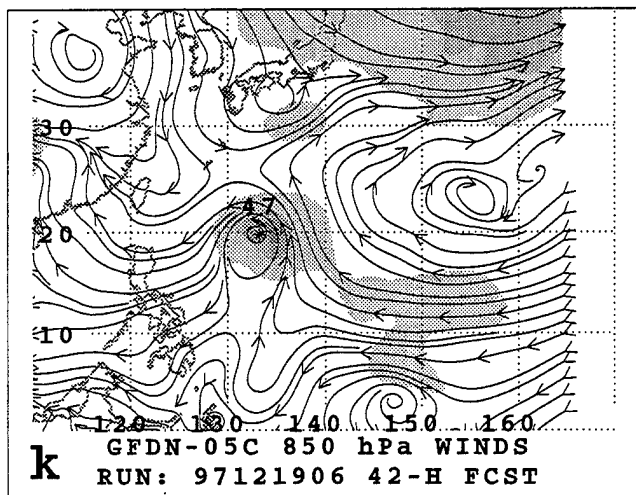
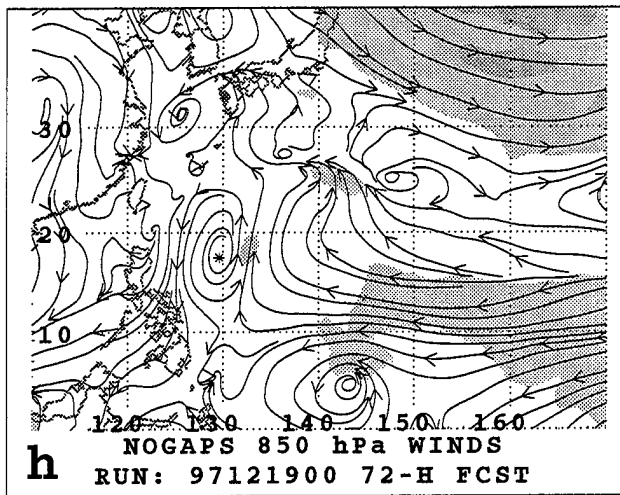
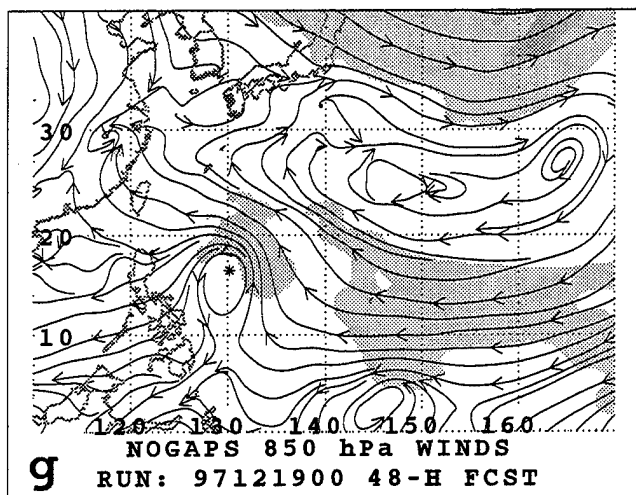
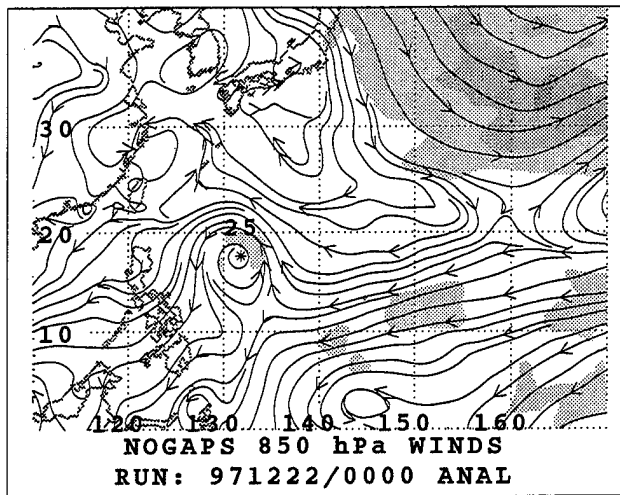
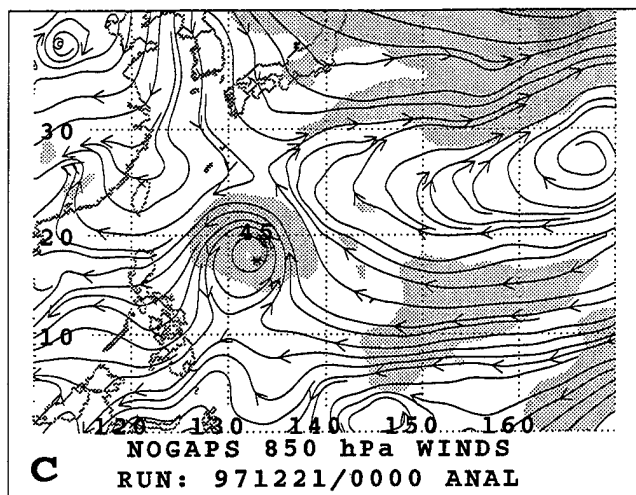


Fig. A.33. (continued)

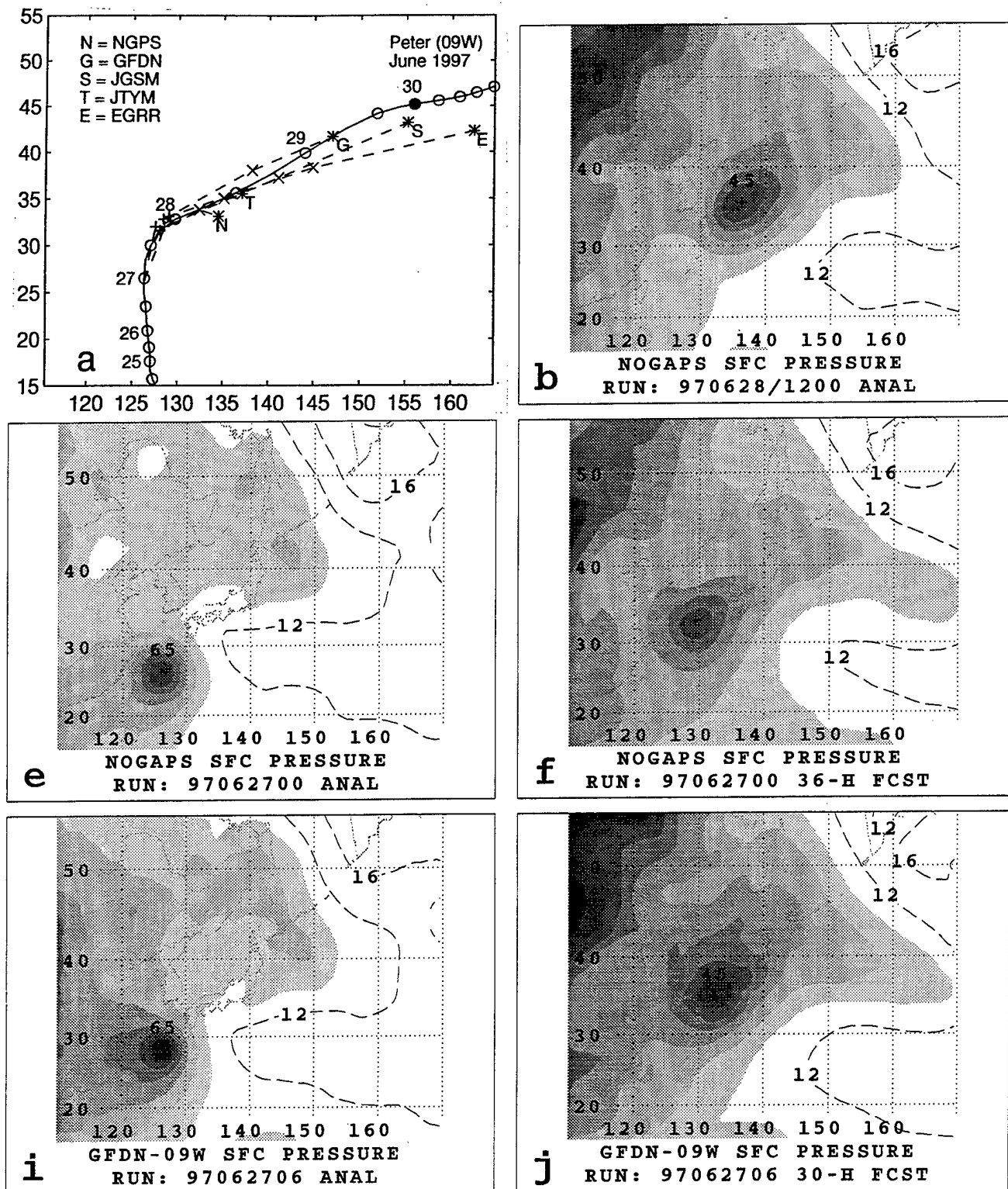


Fig. A.34. (a-l) As in Fig. A.1, except for sea-level pressure forecasts for Peter initiated at 0000 and 0600 UTC 27 June 1997.

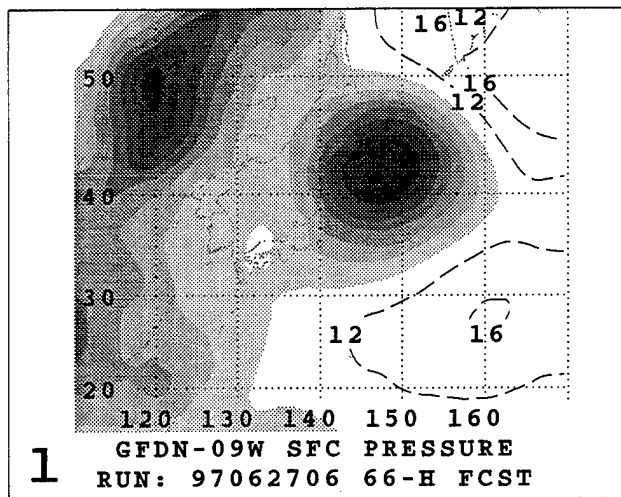
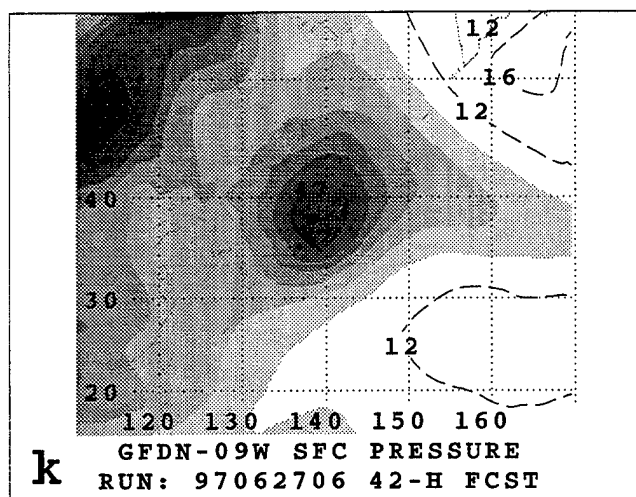
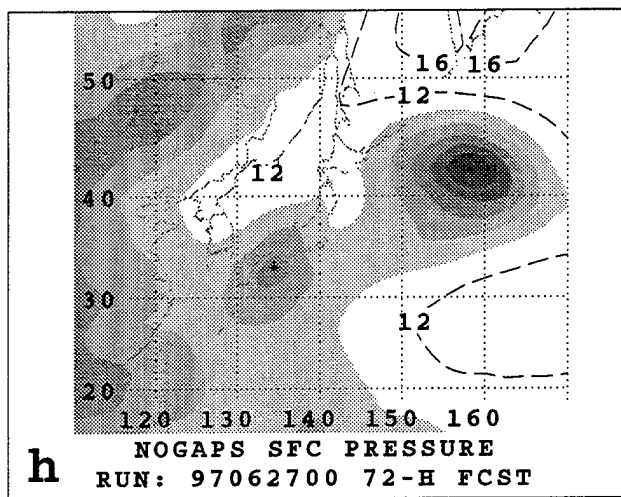
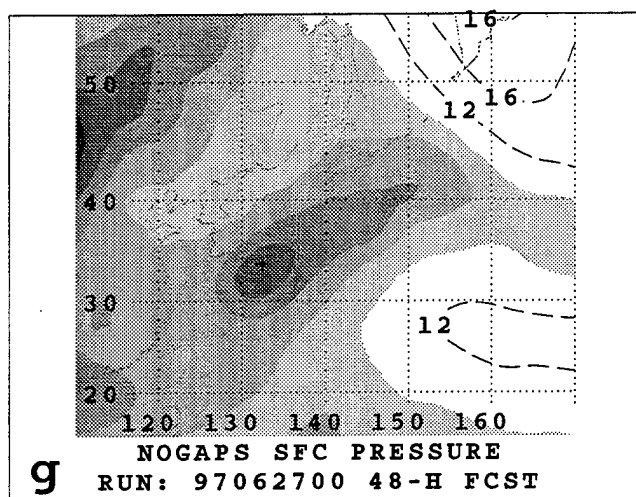
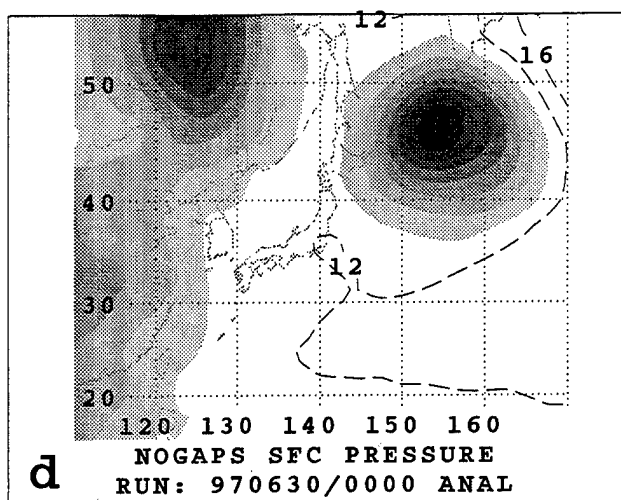
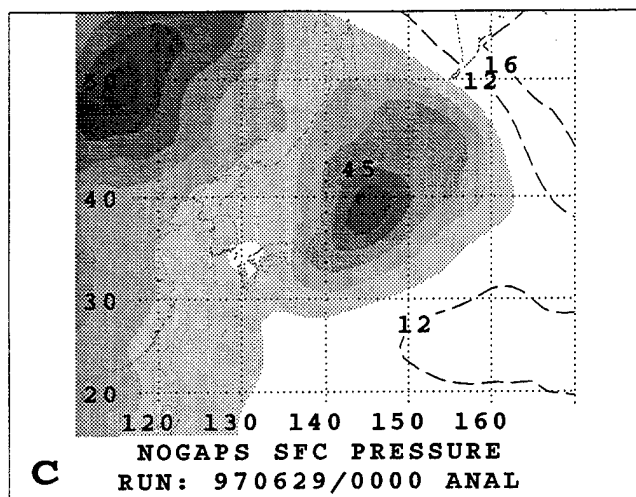


Fig. A.34. (continued)

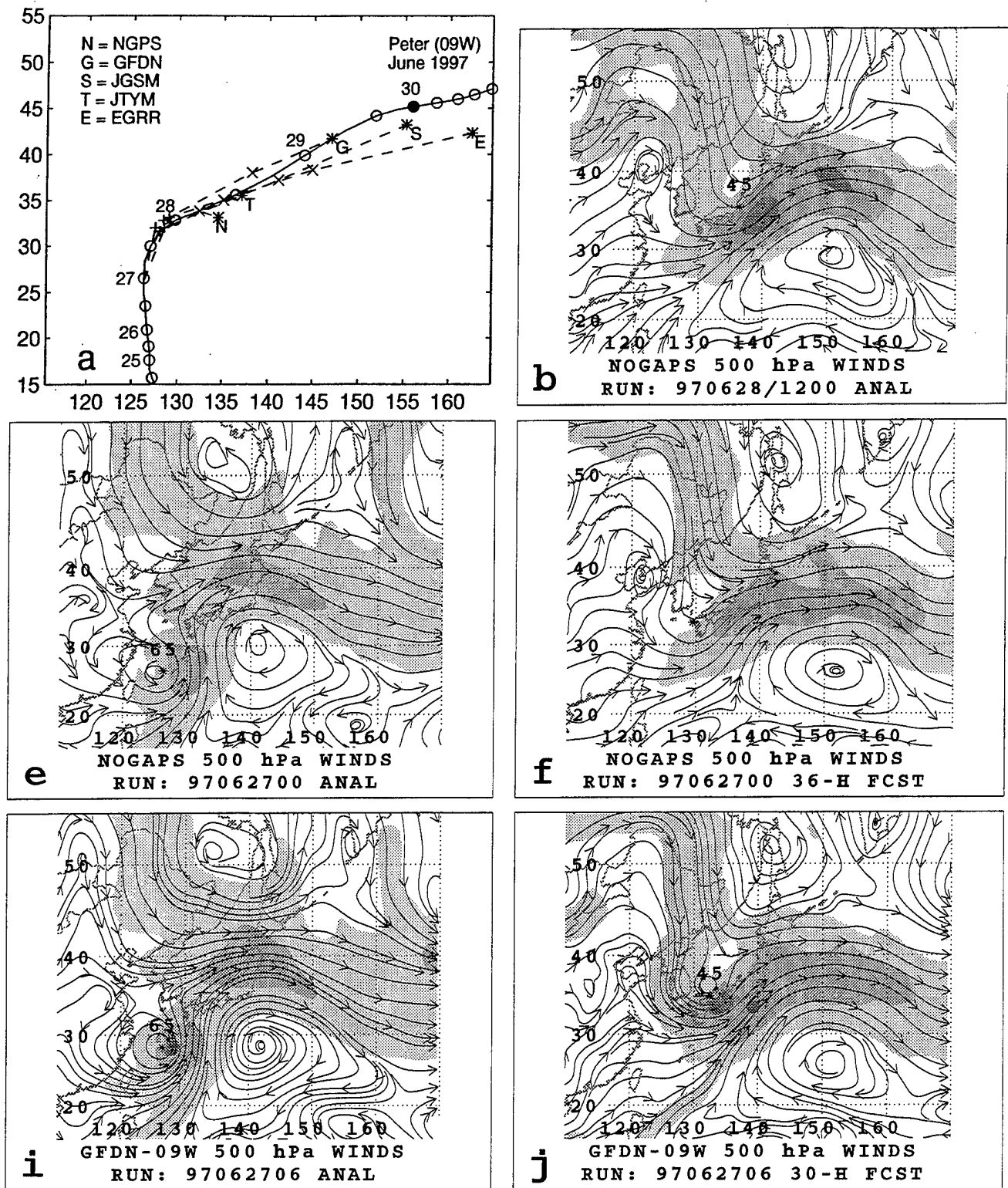


Fig. A.35. (a-l) As in Fig. A.1, except for 500-mb wind forecasts for Peter initiated at 0000 and 0600 UTC 27 June 1997.

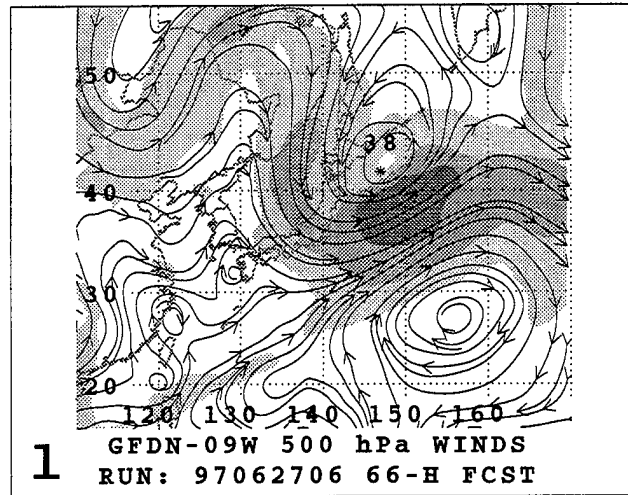
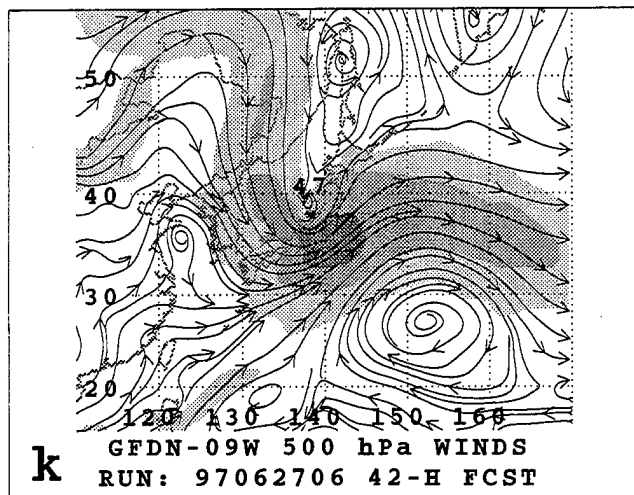
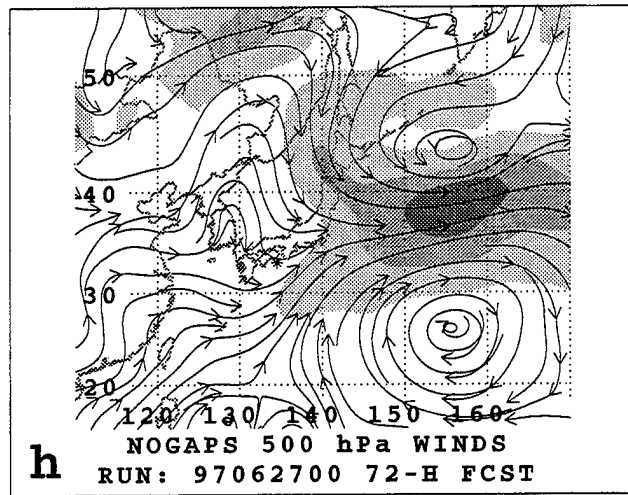
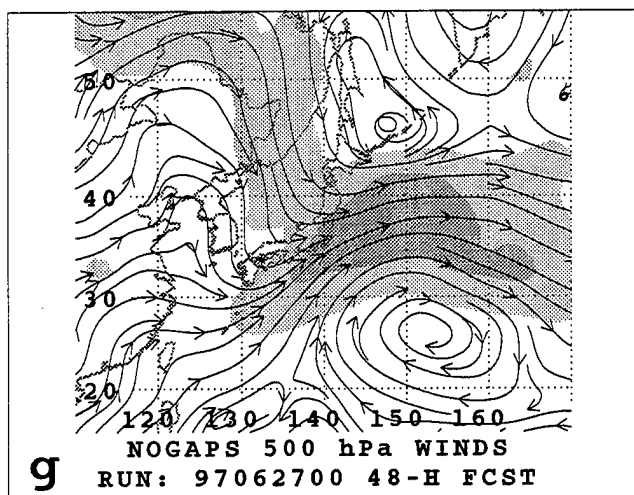
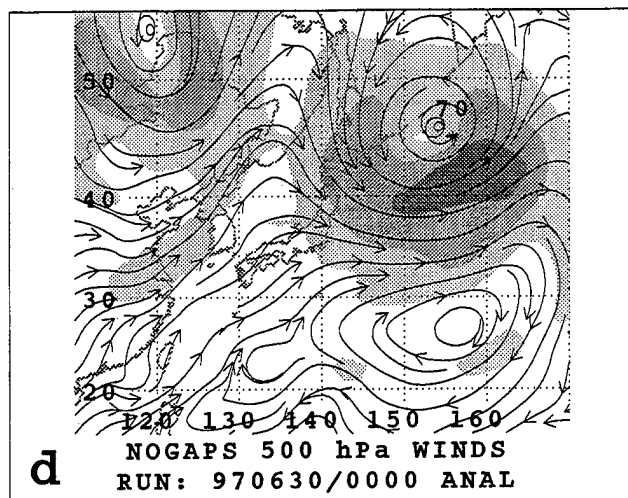
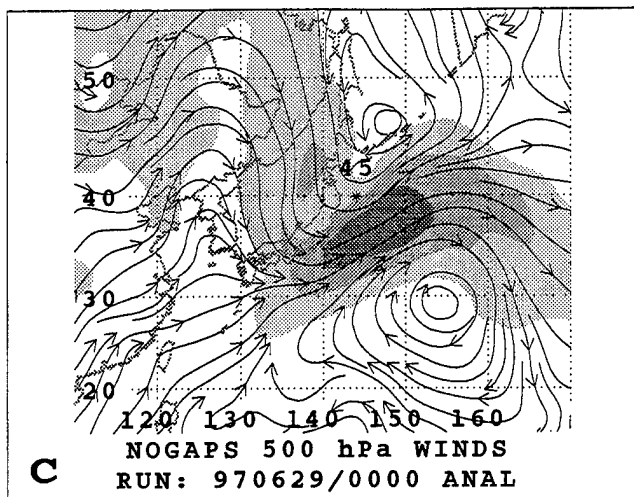


Fig. A.35. (continued)

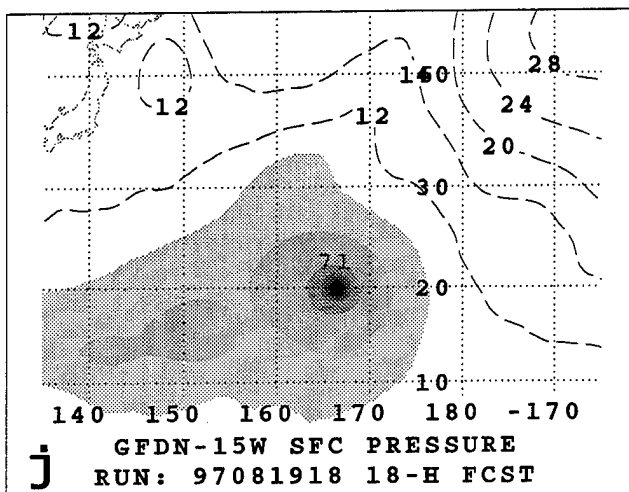
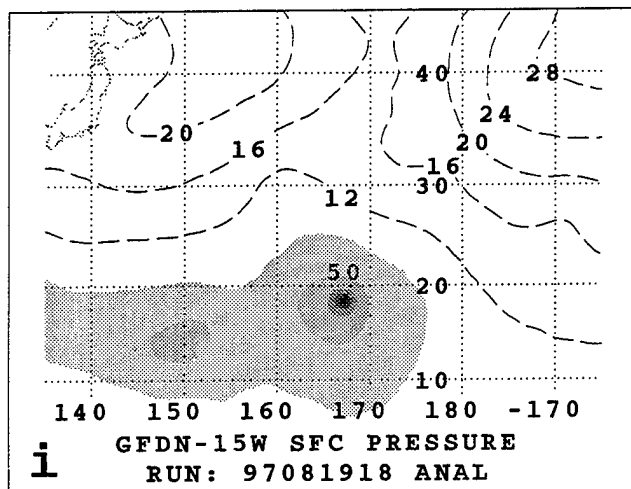
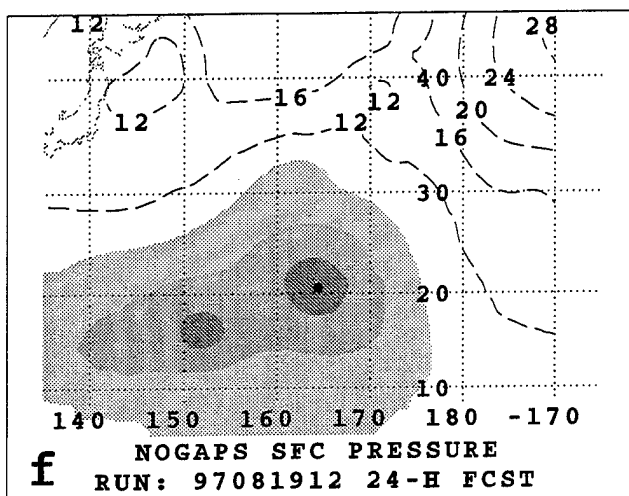
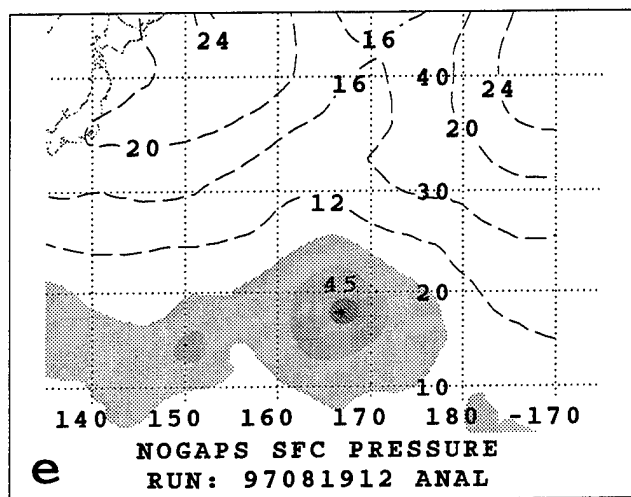
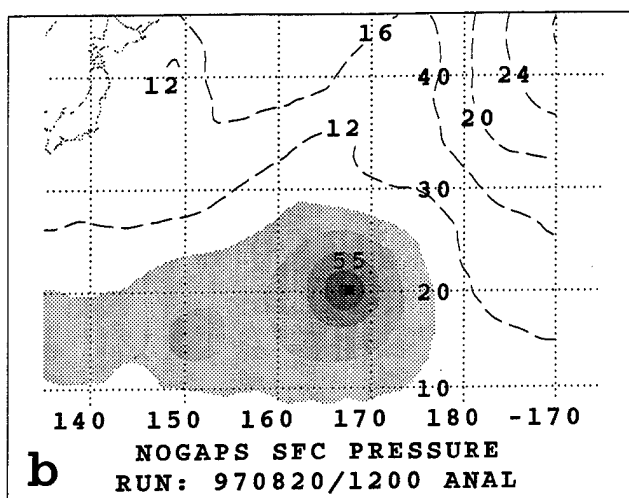
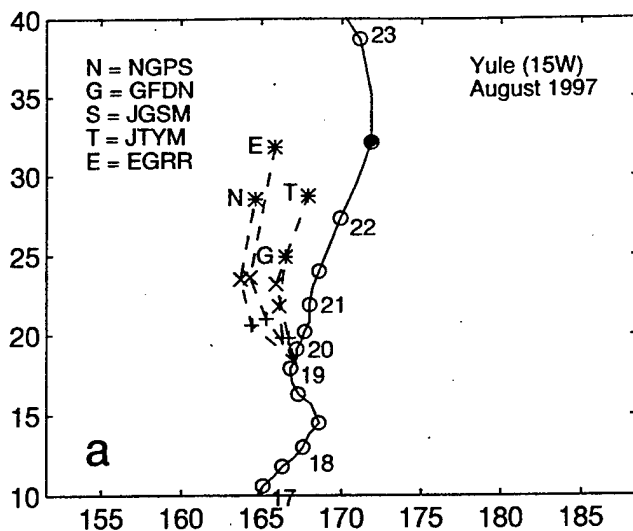


Fig. A.36. (a-l) As in Fig. A.1, except for sea-level pressure forecasts for Yule initiated at 1200 and 1800 UTC 19 August 1997.

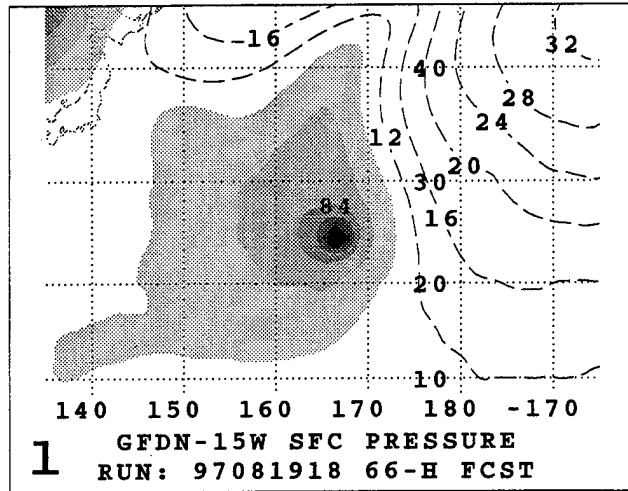
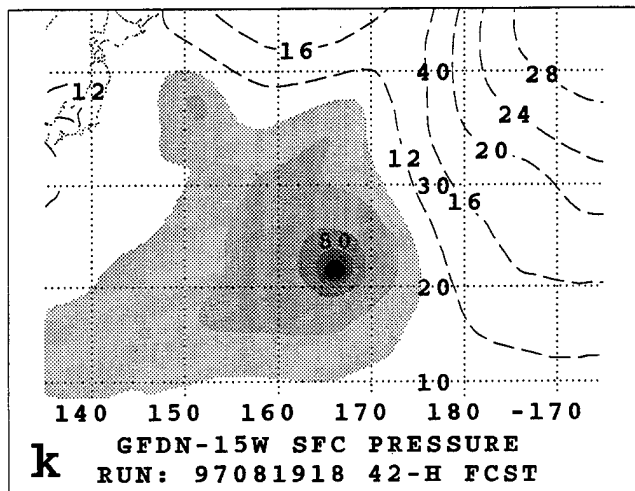
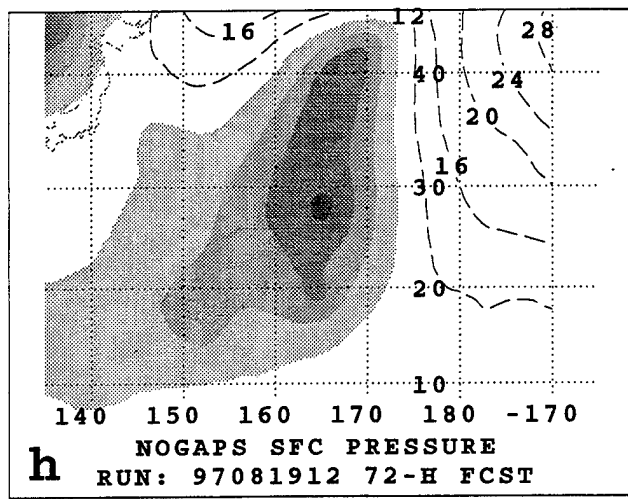
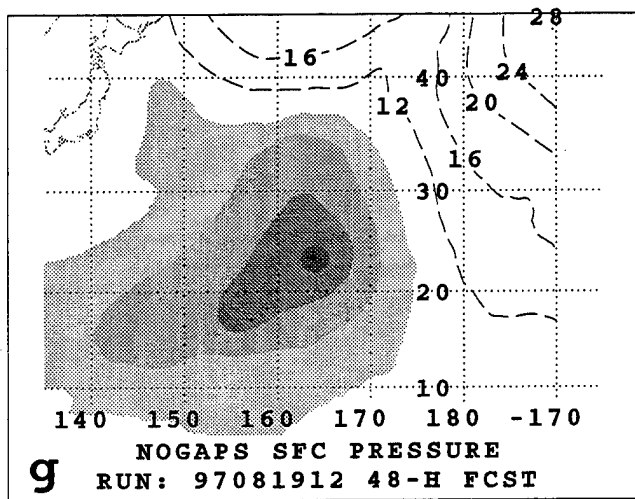
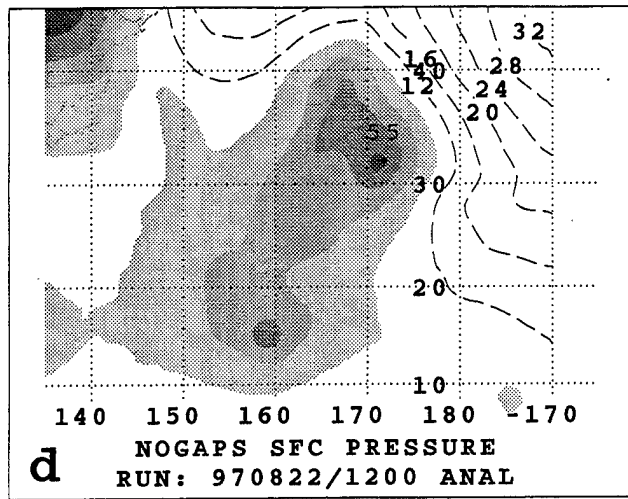
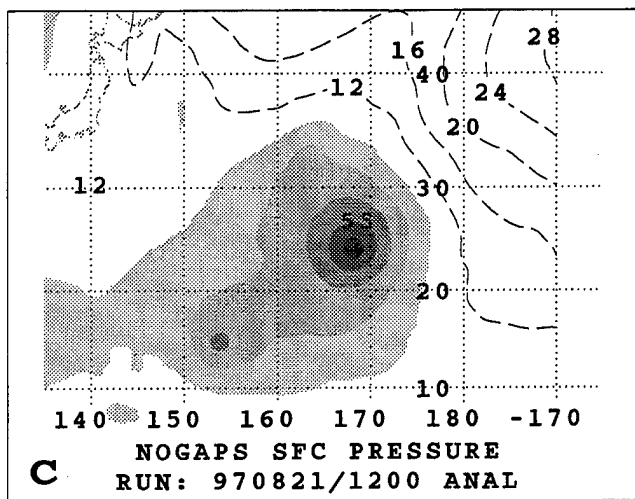


Fig. A.36. (continued)

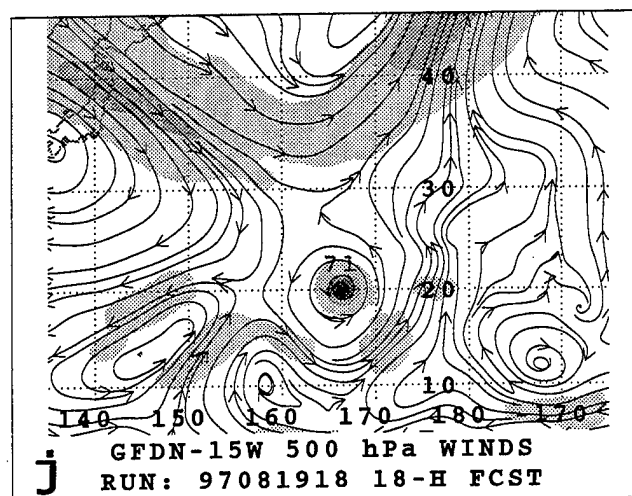
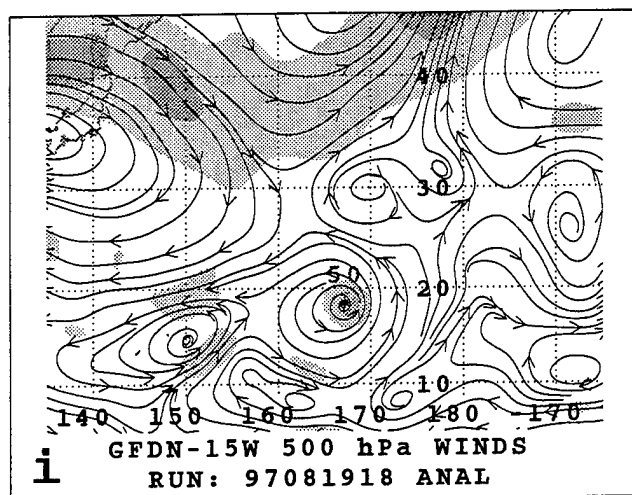
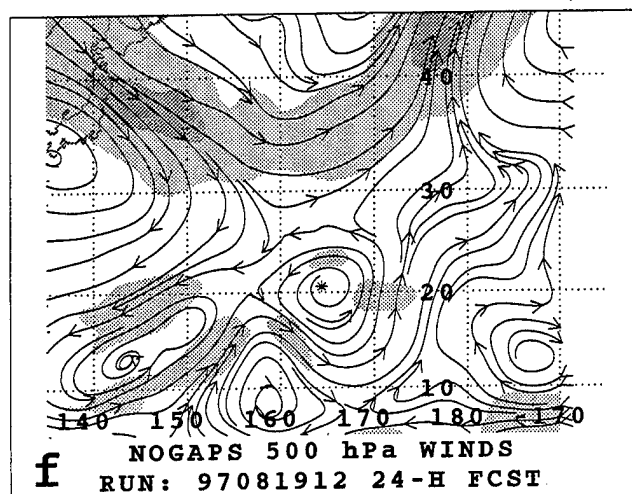
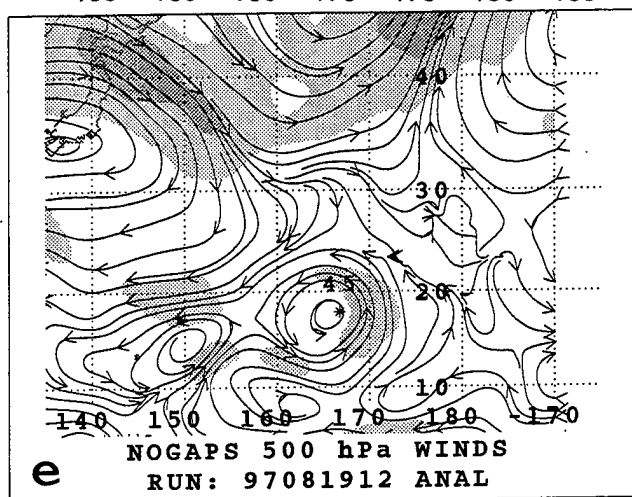
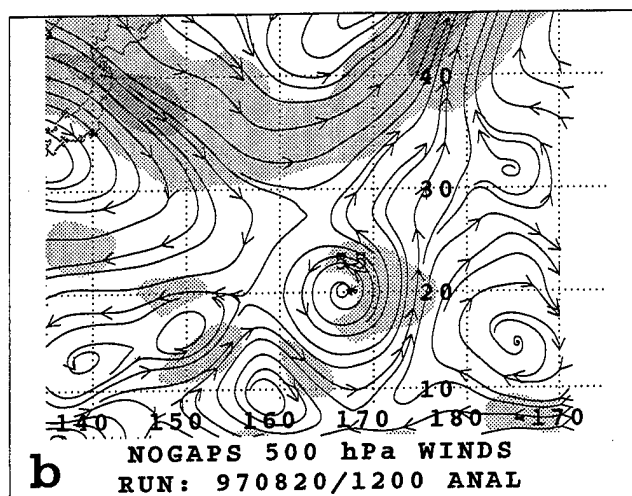
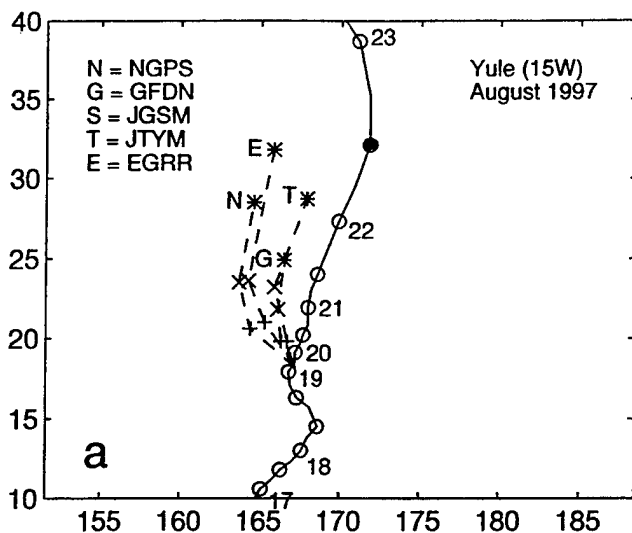


Fig. A.37. (a-l) As in Fig. A.1, except for 500-mb wind forecasts for Yule initiated at 1200 and 1800 UTC 19 August 1997.

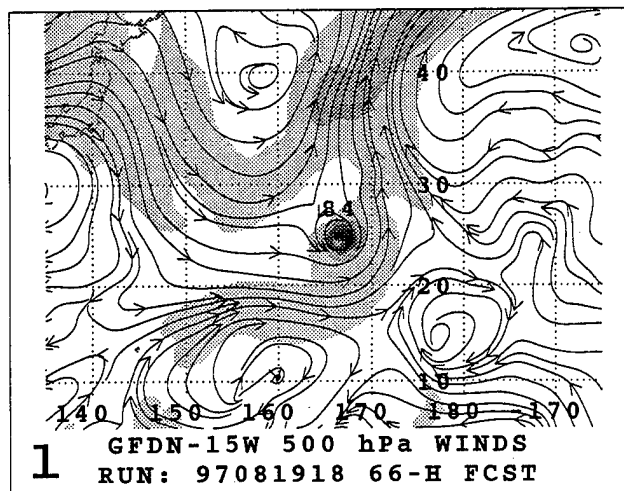
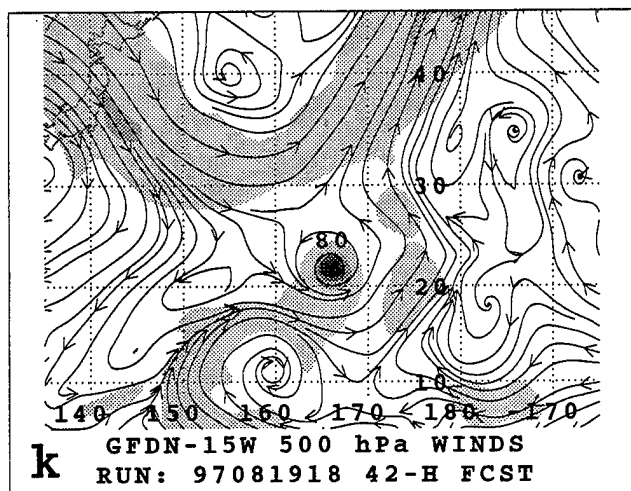
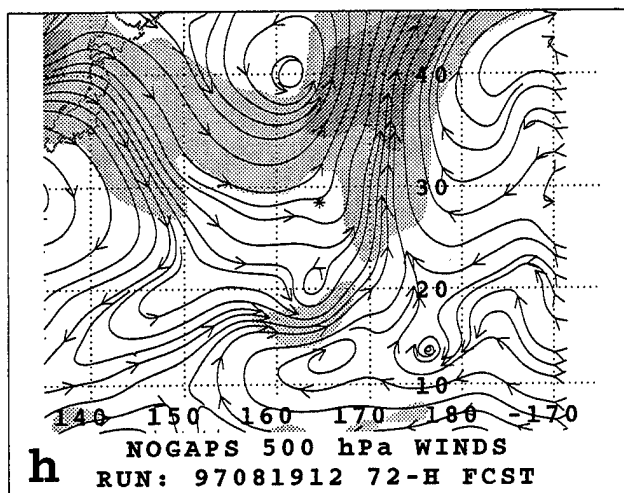
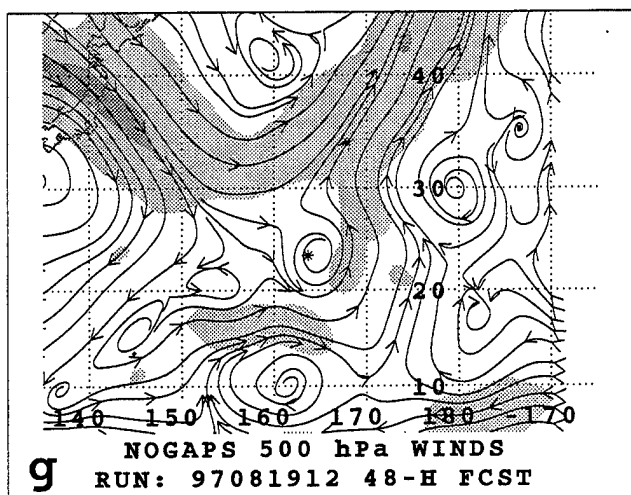
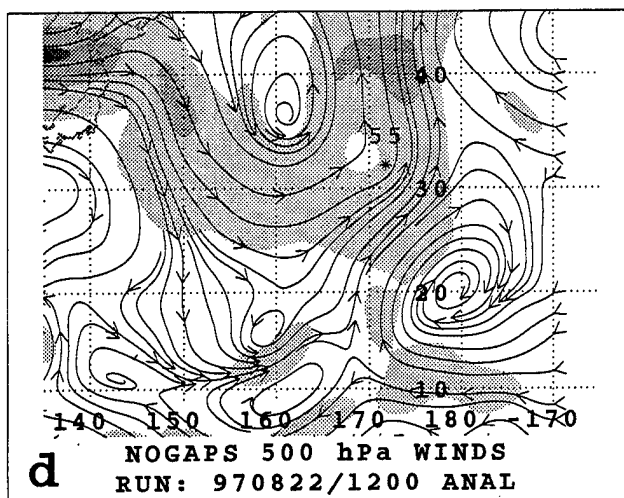
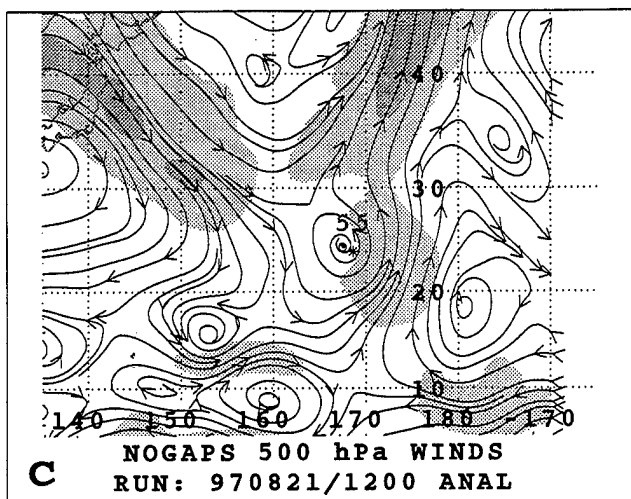


Fig. A.37. (continued)

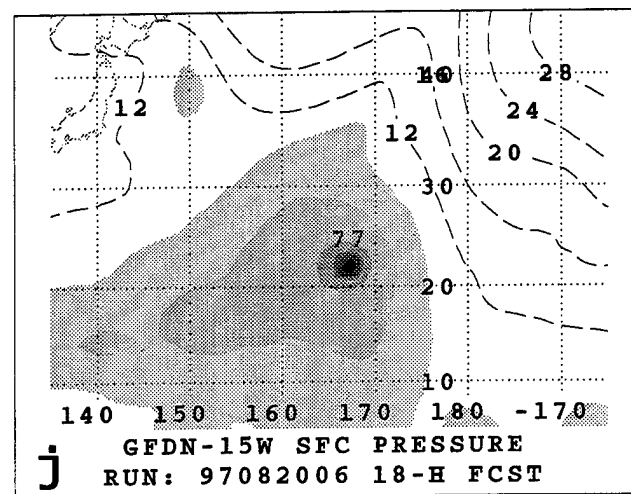
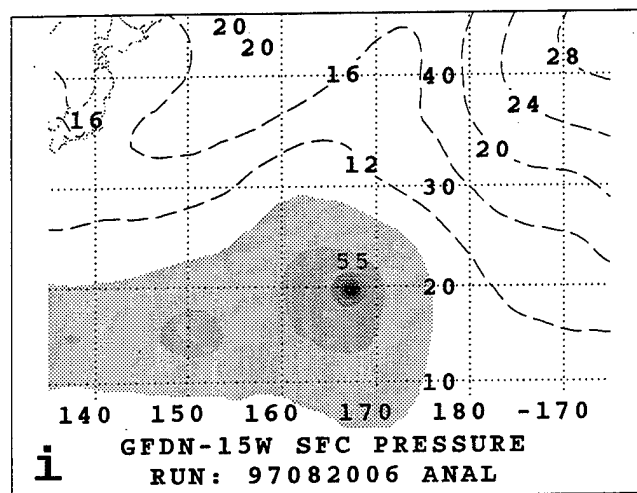
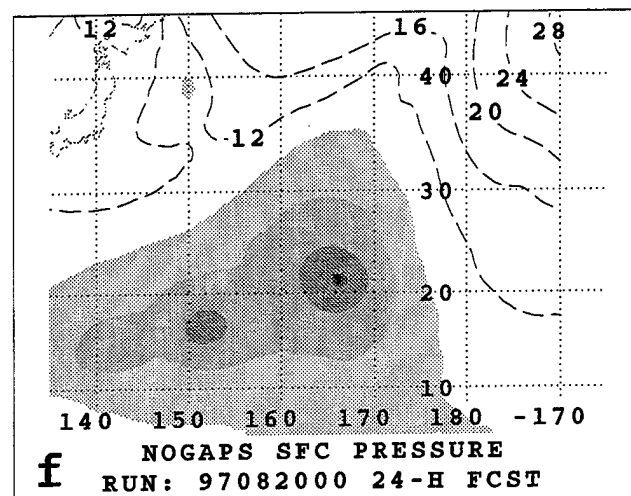
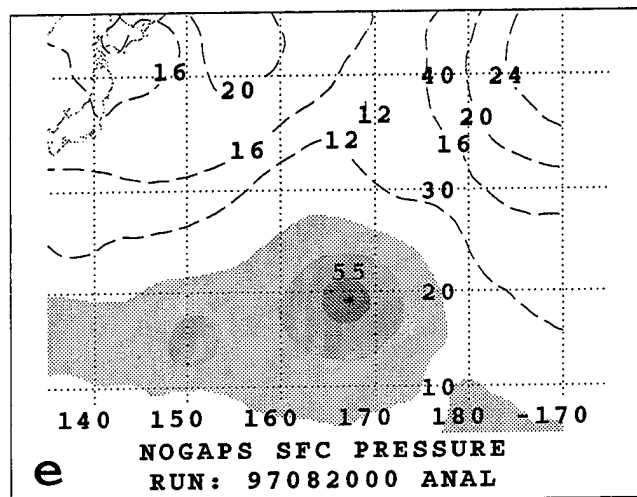
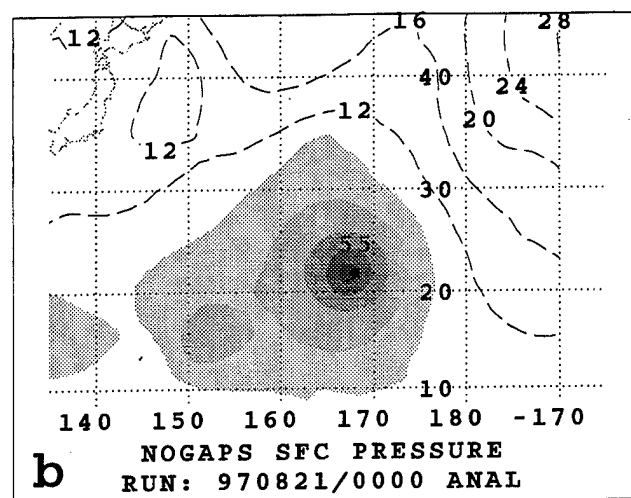
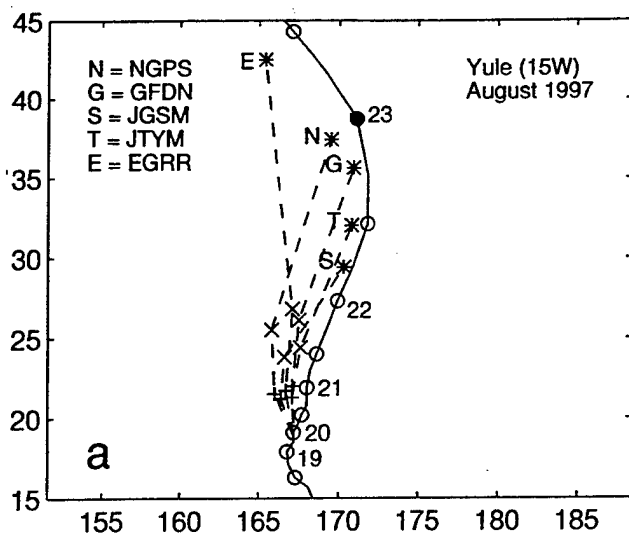


Fig. A.38. (a-l) As in Fig. A.1, except for sea-level pressure forecasts for Yule initiated at 0000 and 1200 UTC 20 August 1997.

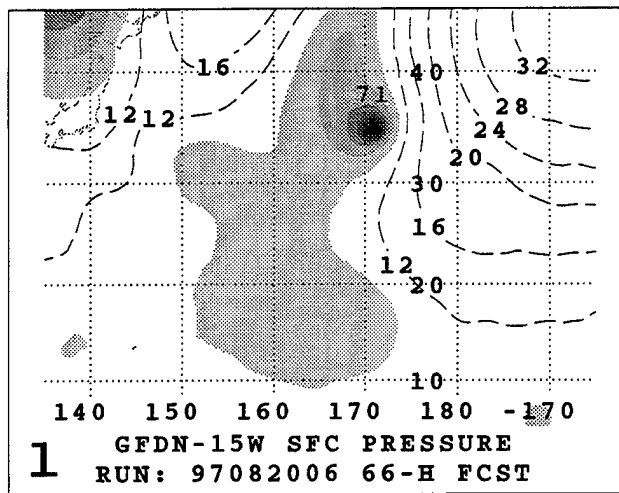
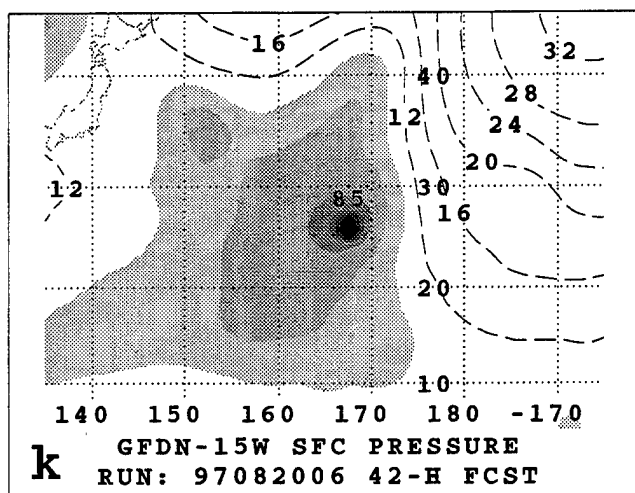
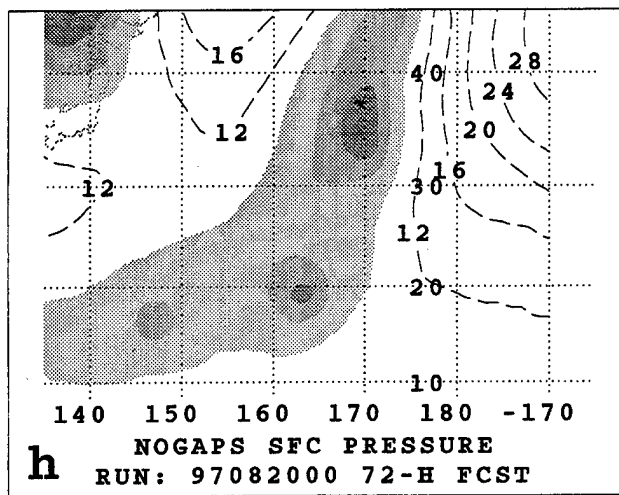
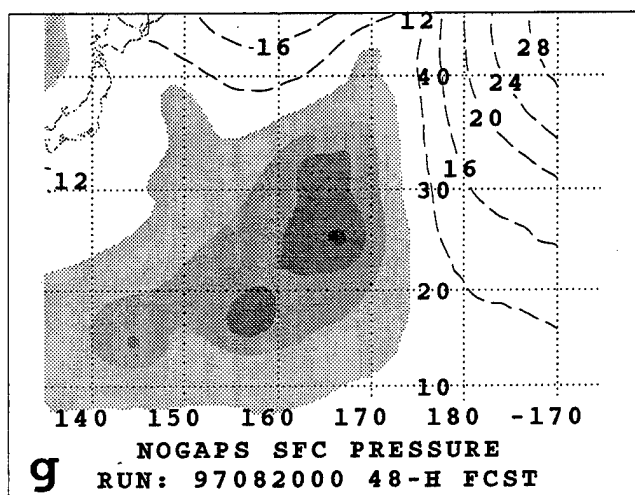
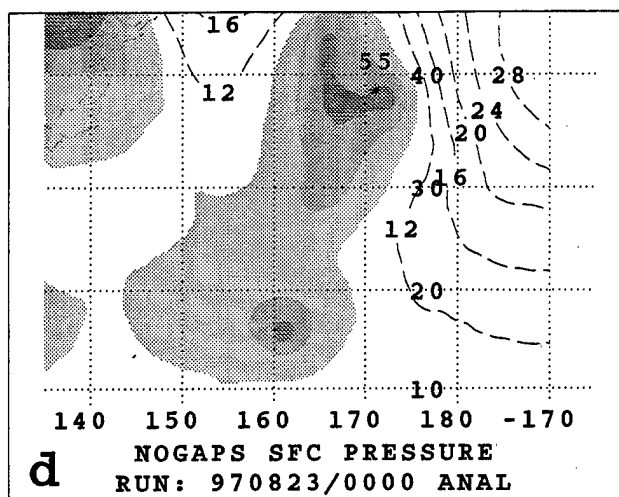
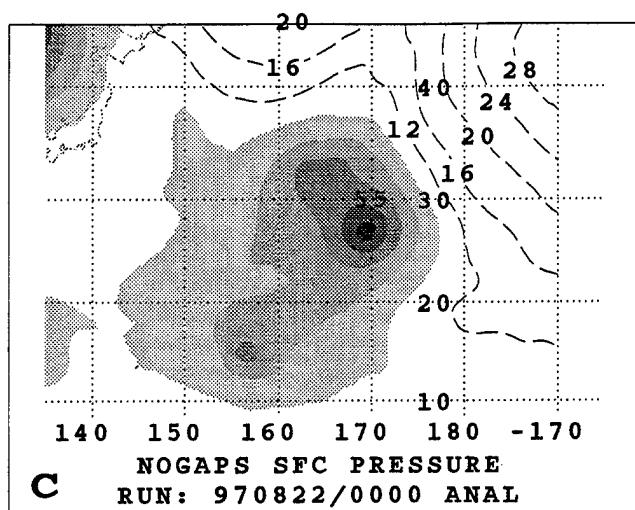


Fig. A.38. (continued)

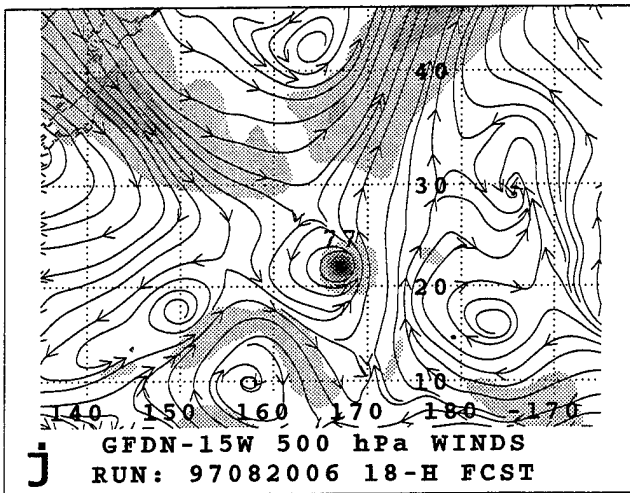
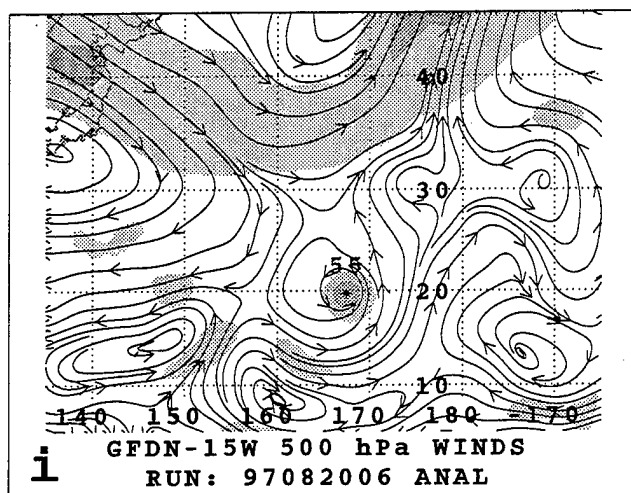
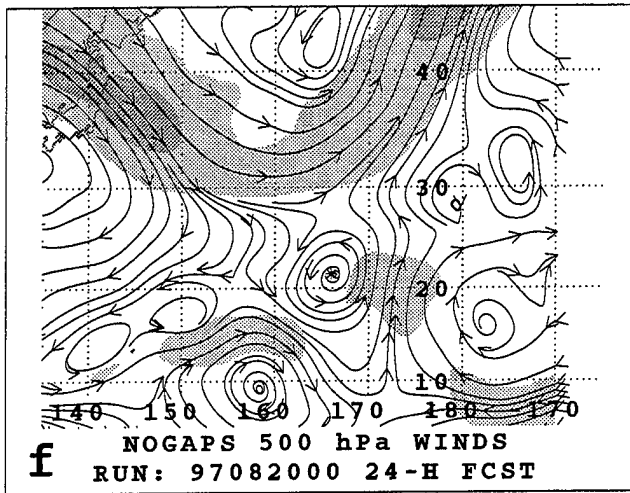
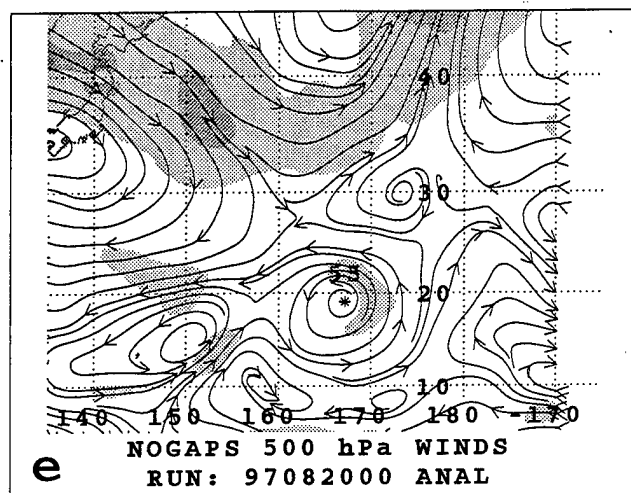
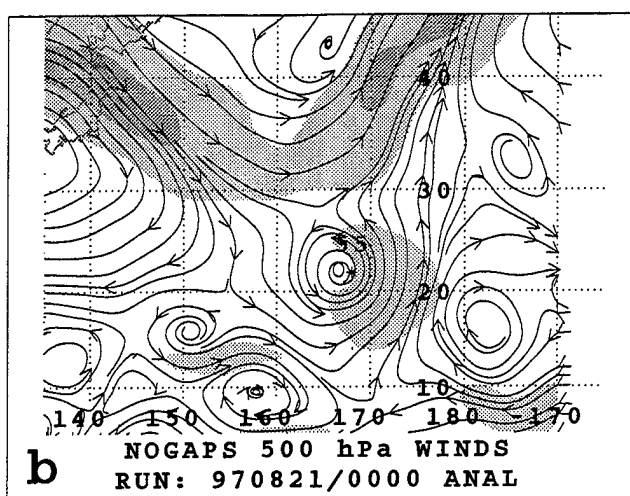
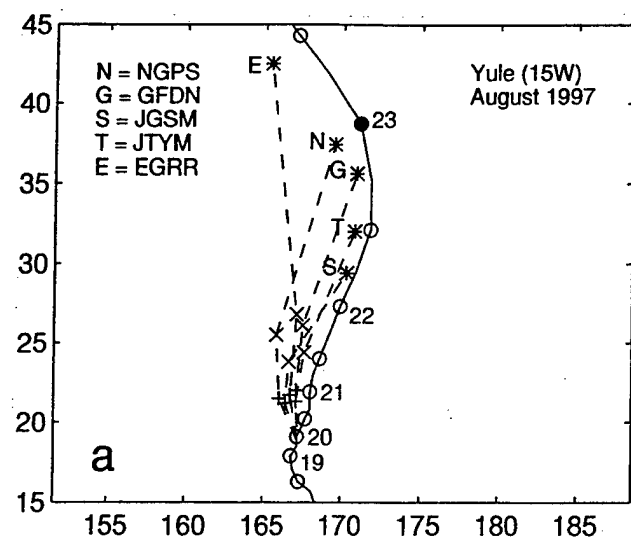


Fig. A.39. (a-l) As in Fig. A.1, except for 500-mb wind forecasts for Yule initiated at 1200 and 1800 UTC 19 August 1997.

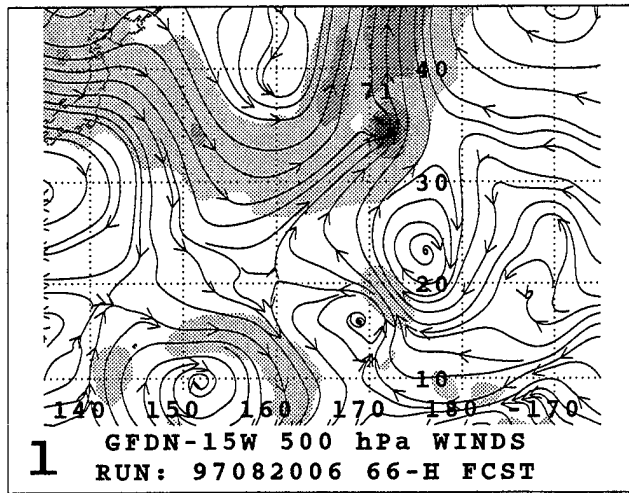
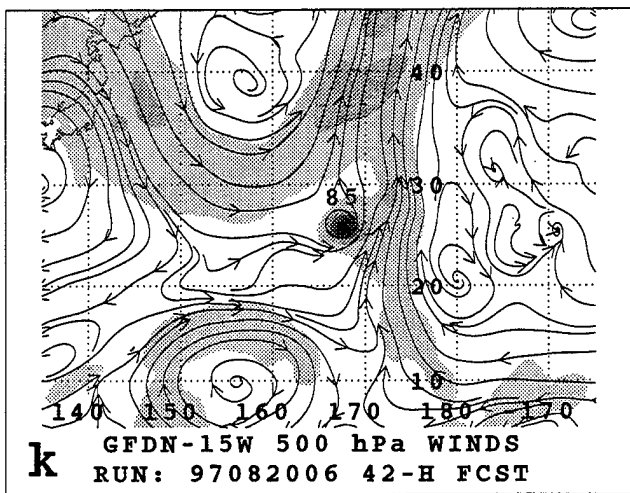
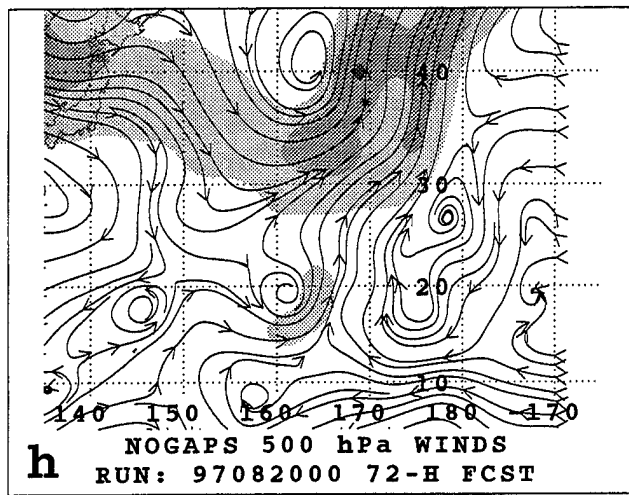
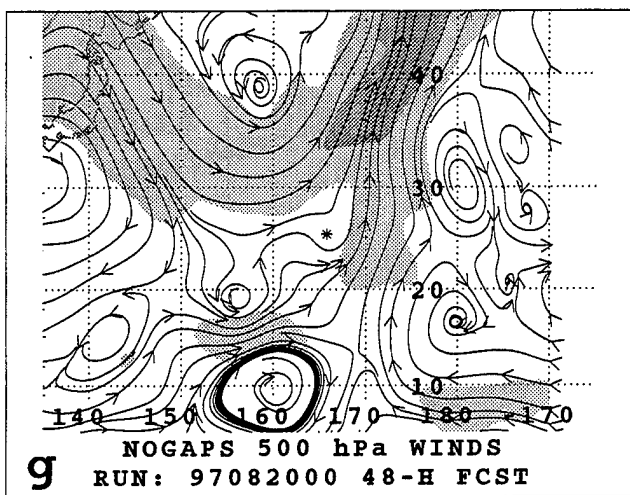
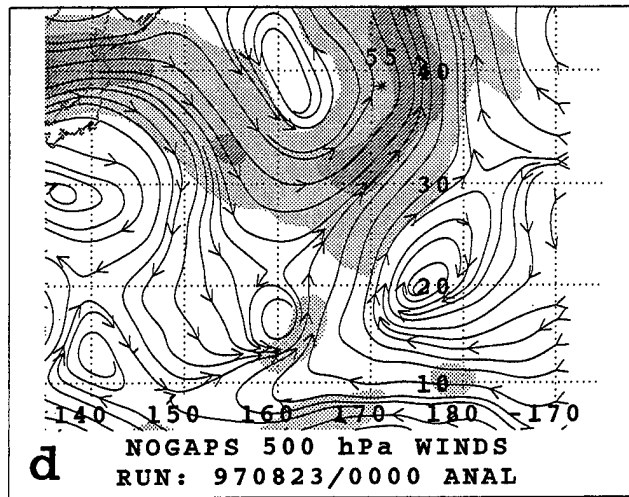
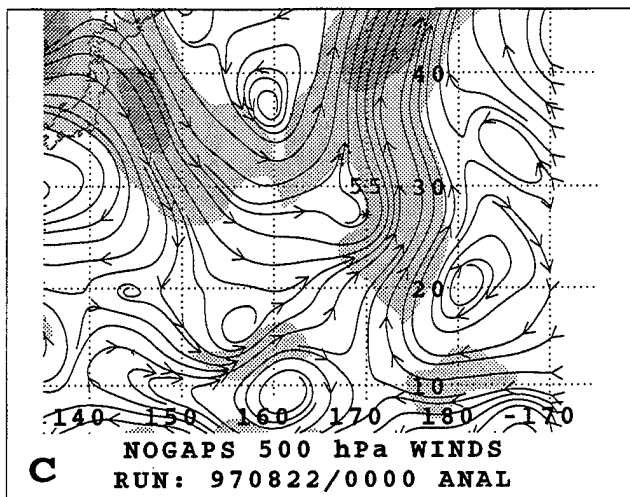


Fig. A.39. (continued)

THIS PAGE INTENTIONALLY LEFT BLANK

Appendix B

Case Study of Typhoon Rex (06W) in 1998

a. TC motion synopsis

Typhoon Rex existed from 23 August to 9 September 1998, and throughout that period followed a sinuous track to the northeast (Fig. B.1). Aspects of the track that complicated the track forecasting problem include: (i) the turn onto an eastward heading during 25-27 August; (ii) the turn onto an unusual east-southeastward heading during 30 August to 2 September; and (iii) a period of slowing during 3-5 September that was followed by a rapid acceleration during 6 September. Satellite infrared imagery during 24-29 August (Fig. B.2a-f) reveals that the first turn to the east occurred as a Tropical Upper Tropospheric Trough (TUTT) cell developed to the east-northeast of the TC (Fig. B.2a-c), and that the resumption of more poleward motion during 27-29 August (Fig. B.1) occurred as the TUTT cyclone weakened (Fig. B.2d-f).

Satellite imagery during 30 August - 2 September (Fig. B.3a-d) reveals that the second, larger turn during 30-31 August (Fig. B.1) also occurred as a second TUTT cell approached from the east. Notice that the convection under the diffluent region between the TUTT and the TC on 31 August (Fig. B.3b) undergoes a distinct shift to the northeast of the TC during 1-2 September (Fig. B.3c-d) and wraps around the TUTT cell, which reveals that the TUTT cell is quite close to the TC by 2 September (Fig. B.3d). Because this approach of the second TUTT cell from the east and the coincident equatorward turn of Rex has the appearance of a mutual cyclonic rotation, it has been suggested that direct TC interaction between the TC and the TUTT cell was responsible for the east-southeastward motion of Rex. Whereas the east-southeastward turn of Rex may have occurred in association with the approaching TUTT cell, it also may have been influenced by a mid-latitude trough and associated baroclinic zone just to the northwest of the TC on 30 August (Fig. B.3a). This midlatitude trough will be of critical importance in explaining some of the highly erroneous NOGAPS and GFDN forecasts for Rex.

Satellite imagery from 3-8 September reveals the development of another TUTT cell to the east of the TC (Fig. B.4a-c) that is coincident with the translational deceleration of the TC during 3-5 September (Fig. B.1). Finally, the rapid translational acceleration during 6 September and then a deceleration during 7-8 September occurred during the extratropical transition of Rex (Fig. B.4d-e) and the subsequent development of an occlusion (Fig. B.4e-f), respectively.

b. Error mechanism synopsis

A summary of the 72-h forecast track errors (FTEs) for the NOGAPS and GFDN models and the assigned error mechanisms is provided in Table B.1. Although the poor performance of both models during 28-30 August is of particular concern to the JTWC, it is important to recognize that poor performance by both models occurred throughout the existence of Rex and resulted in an unusually high percentage of large FTEs: 20 of 27 NOGAPS forecasts and 10 of 16 GFDN forecasts.

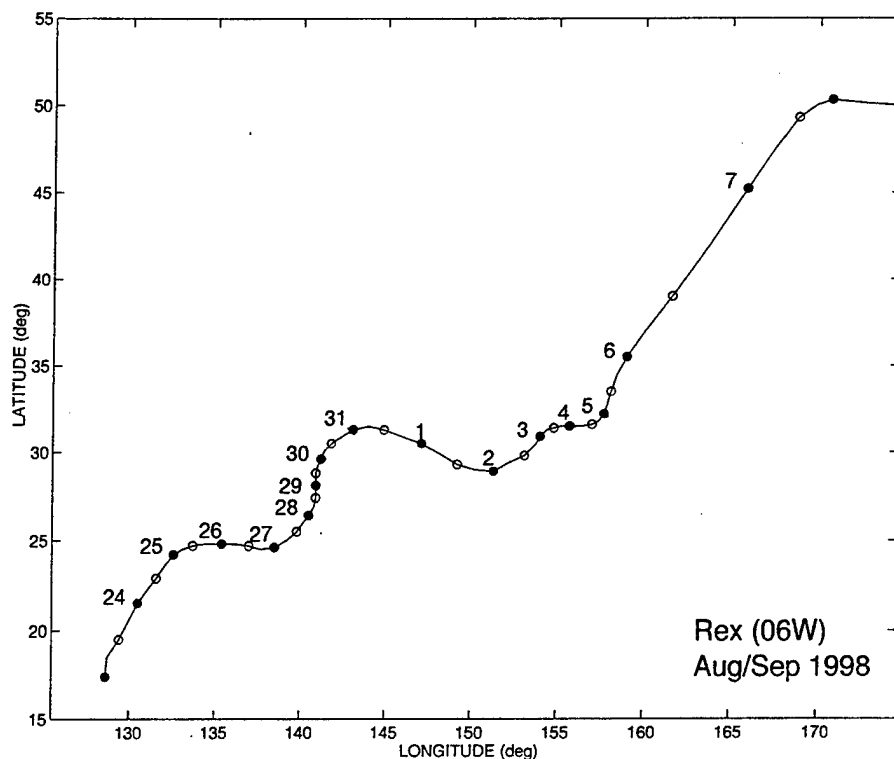


Fig. B.1. Best-track of TC Rex from 0000 UTC 23 August to 0000 UTC 8 September 1998.

The first period of degraded NOGAPS forecasts from 0000 UTC 24 to 1200 UTC 25 August is attributed to Excessive Ridge Modification by the TC (E-RMT). Whereas this E-RMT caused the NOGAPS (and presumably the EGRR) track to continue poleward (Fig. B.5a), Rex actually turned eastward. Although the GFDN track forecasts are not available for most of this period, the 1800 UTC 25 August GFDN forecast was considerably more accurate than the 1200 UTC 25 August NOGAPS forecast, and thus was not assigned an error mechanism in Table B.1. The presence of E-RMT in the NOGAPS forecasts, but not in the GFDN forecast for this one comparison, is consistent with the analysis of the model errors during 1997 (e.g., Table 1.3, row 6 and Table 5.1, column 2). This difference in sensitivity to the E-RMT error mechanism is presumably related to the significant differences in the horizontal resolution of the two models, and specifically the tendency for overly large TCs in the NOGAPS forecasts.

Excessive Baroclinic Cyclone Interaction (E-BCI) is assigned in Table B.1 as the error mechanism responsible for highly erroneous NOGAPS (GFDN) forecasts from 0000 UTC 26 (0600 UTC 27) August to 1200 UTC 31 August (0600 UTC 30 August). Representative NOGAPS and GFDN (and EGRR) forecast tracks during this period were for a rapid acceleration poleward (Fig. B.5b-d), whereas Rex moves slowly poleward and then turns east-southeast. The earlier onset of E-BCI in the NOGAPS forecast is consistent with the prior existence of E-RMT, which was associated with an excessive growth of the TC that then contributed to an early interaction of the

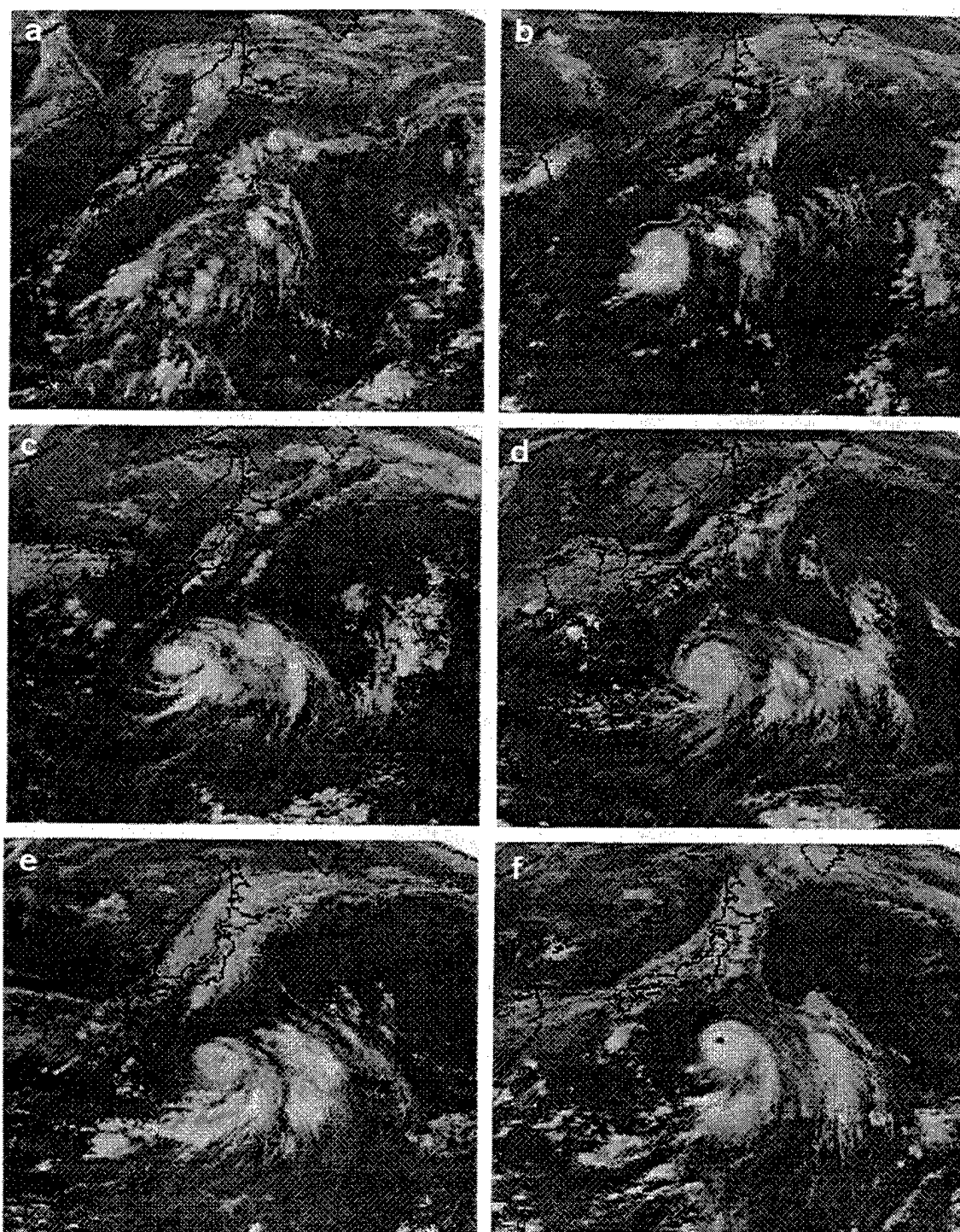


Fig. B.2. Satellite IR imagery as in Fig. 2.5, except for TC Rex at 0000 UTC on (a) 24, (b) 25, (c) 26, (d) 27, (e) 28, and (f) 29 August 1998.

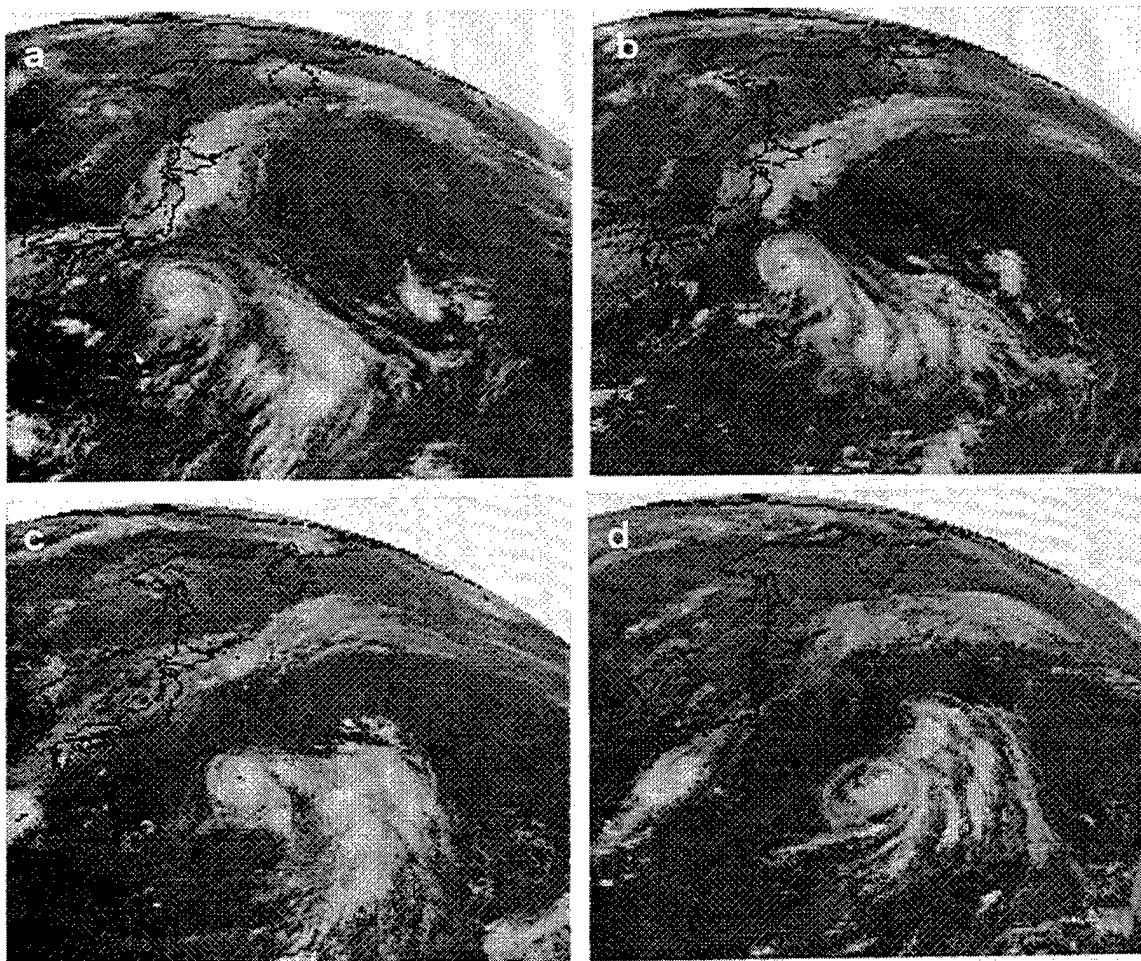


Fig. B.3. Continuation of the satellite IR imagery sequence in Fig. B.2 for (a) 30 and (b) 31 August, and (c) 1 and (d) 2 September 1998.

TC with a midlatitude system. During the period when E-BCI was occurring concomitantly in the NOGAPS and GFDN forecasts, Excessive Midlatitude CycloGenesis (E-MCG) was also a contributing factor (see columns 4 and 8 in Table B.1). Notice that the GFDN FTEs in Table B.1 are consistently larger than the NOGAPS FTEs at times when E-MCG is also identified as a contributing factor, which is consistent with the finding in section 4.a above that the GFDN forecast is much more likely to be significantly degraded by E-MCG (as the primary error mechanism) than the NOGAPS forecast.

Beginning with the 0600 UTC 1 September forecast, degradation of the GFDN track forecast is again attributed to E-BCI (Table B.1). Then after making at least five highly erroneous track forecasts, the GFDN forecast of the extratropical transition of Rex is remarkably accurate. After making three comparatively accurate track forecasts during 1-2 September, the NOGAPS model has two forecasts that are degraded by E-BCI, followed by two forecasts that are degraded by Insufficient BCI (BCI), and then four forecasts that are comparatively accurate (Table B.1). Recall that similar sporadic forecast-to-forecast fluctuations in the fidelity with which a numerical model represents

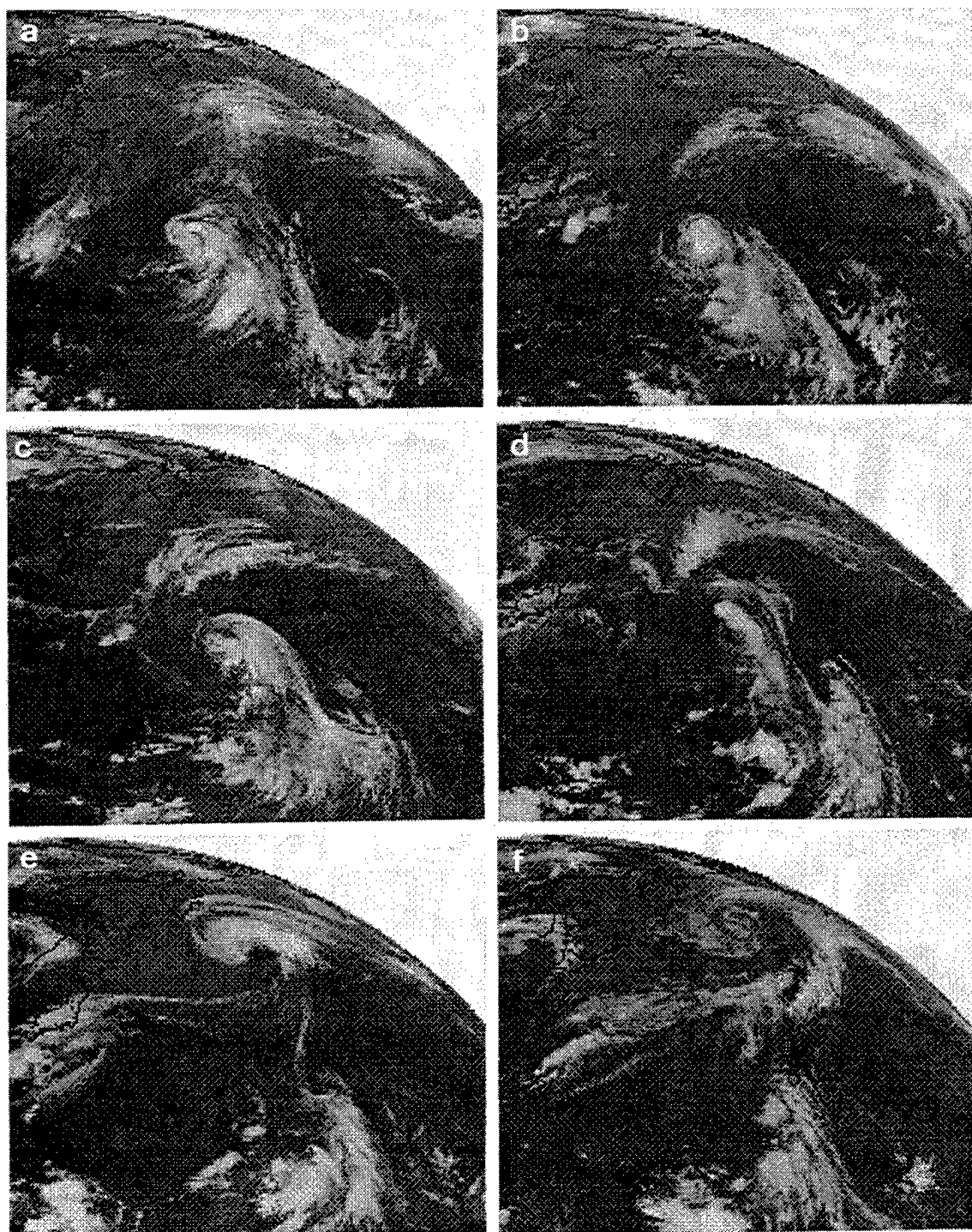


Fig. B.4. Continuation of satellite IR imagery sequence as in Fig. B.3 for (a) 3, (b) 4, (c) 5, (d) 6, (e) 7, and (f) 8 September 1998.

Table B.1 Summary of NOGAPS (left side) and GFDN (right side) 72-h FTEs and the responsible error mechanisms for 72-h FTEs > 300 n mi, and contributing factors to the degraded forecasts. In the NOGAPS FTE column: (i) asterisks denote approximate 72-h FTEs from manually determined 72-h positions when the vortex tracker lost the TC, although a closed low was evident in the 72-h sea-level pressure forecast; and (ii) numbers in parentheses indicate 48-h FTEs because the TC became too weak by 72 h to be tracked either objectively or manually. A notation of n/a means the GFDN forecast was either not made or failed to get into the JTWC data base.

DTG (UTC)	72-h FTE	Error Mech	Contributing factors	DTG (UTC)	72-h FTE	Error Mech	Contributing factors
24/00	515	E-RMT	TC growth forecast	24/06	N/a		
24/12	483		"	24/18	n/a		
25/00	472		"	25/06	n/a		
25/12	481		"	25/18	271		E-MCG evident
26/00	825	E-BCI	"	26/06	240		"
26/12	394		E-MCG contributing	26/18	n/a		"
27/00	(320)		"	27/06	505	E-BCI	E-MCG contributing
27/12	781*		"	27/18	852		"
28/00	375		"	28/06	909		"
28/12	553		"	28/18	722		"
29/00	742		"	29/06	1230		"
29/12	793		"	29/18	n/a		
30/00	856		"	30/06	1273		E-MCG contributing
30/12	(444)		"	30/18	n/a	?	
31/00	(493)		"	31/06	n/a	?	
31/12	371		"	31/18	n/a	?	
01/00	285			01/06	337	E-BCI	E-MCG contributing
01/12	215			01/18	437		"
02/00	175			02/06	649		"
02/12	587	E-BCI	E-MCG not evident	02/18	906		E-MCG not evident
03/00	592		"	03/06	789		"
03/12	380*	I-BCI		03/18	n/a	?	
04/00	743			04/06	65		
04/12	271			04/18	n/a		
05/00	14*			05/06	35		
05/12	67			05/18	94		
06/00	273			06/06	n/a		

the extratropical transition process occurred in the case of Yule in 1997 (see section 4.c.3.b). In the Yule case, it was the GFDN model that behaved sporadically. Representative NOGAPS and GFDN tracks (Fig. B.5e-f) show that the magnitude of the tracks errors depended critically on an accurate forecast of the timing of the TC acceleration to the northeast, and that the UKMO model and the JTVM also had difficulty in forecasting the extratropical transition of Rex.

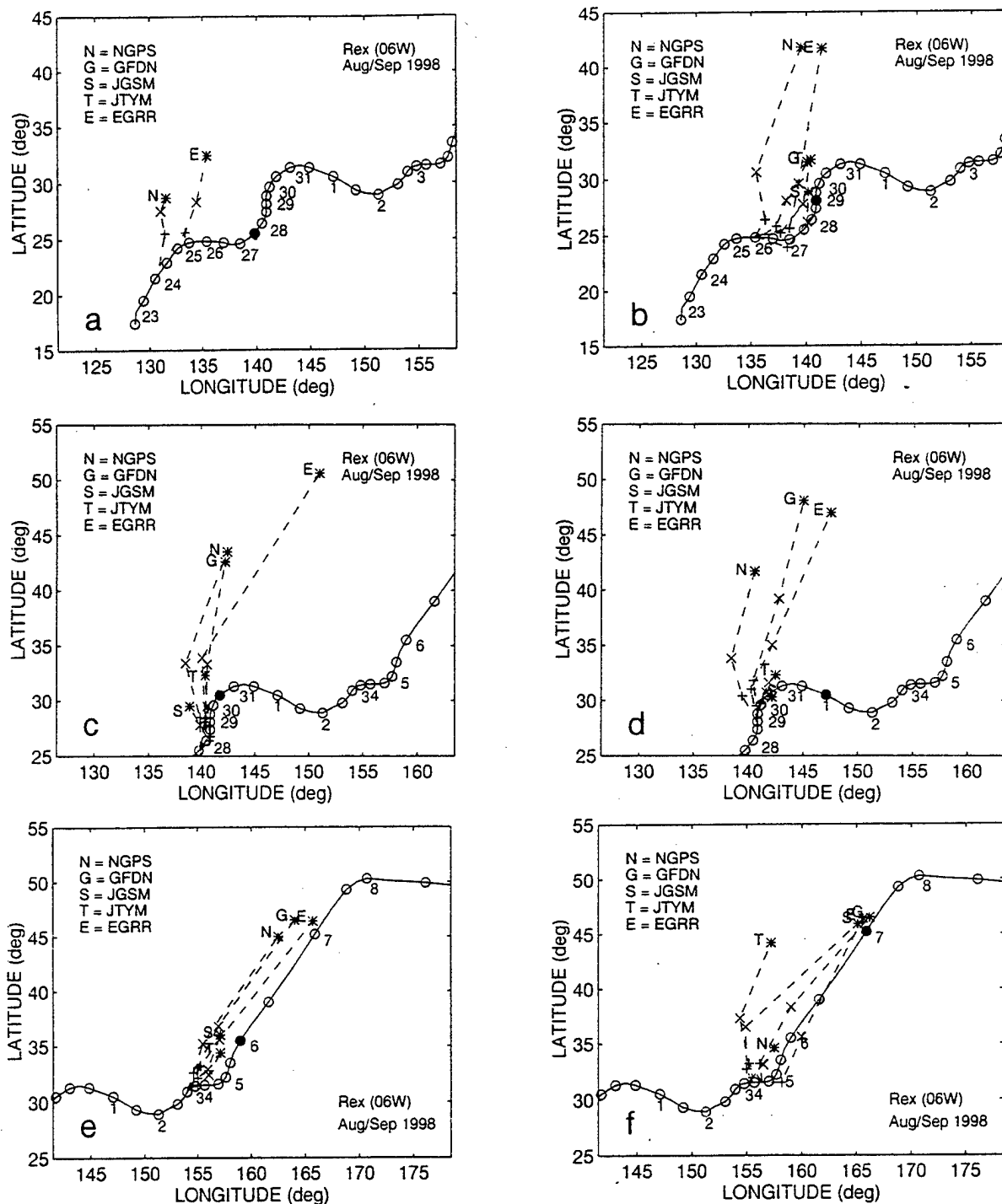


Fig. B.5. Best-track and selected model track forecasts (see inset) as in Fig. 2.7b, except for TC Rex at (a) 1200 UTC 24 August, (b) 0000 UTC 26 August, (c) 1200 UTC 27 August, (d) 0000 UTC 29 August, (e) 0000 UTC 3 September, and (f) 0000 UTC 4 September 1998.

Since the extratropical transition of Rex actually occurred on 7 September (Fig. B.4e), the first period of E-BCI in the NOGAPS forecast (and presumably GFDN¹) involved a truly false (vice premature) interaction of the TC with a midlatitude cyclone (see Fig. B.3). By contrast, the second period of E-BCI in both models represents a premature interaction of the TC with a different midlatitude short-wave trough, with which Rex did interact. All of the cases of E-BCI during 1997 conformed to the latter scenario. Because the false forecasts of extratropical transition situation was not encountered during the study of large NOGAPS and GFDN FTEs for the 1997 TCs, it is unknown how commonly this situation occurs.

Forecast tracks of the steering models and the CSUM are given in Fig. B.6a-f for the same times as in Fig. B.5a-f. As expected from the analysis of model errors during 1997, the character of the erroneous BAMS forecast tracks is qualitatively similar to that of the corresponding NOGAPS forecast tracks (recall Table 5.1). That is, whenever the NOGAPS track has a poleward and fast bias, the BAM tracks also have such a bias. For the one time when the NOGAPS track forecast has a slow bias owing to I-BCI (Fig. B.5f), the corresponding BAMs tracks are also slow. Although the MBAM track is not highly degraded, the fact that the FBAM track (which responds to more to the jet-level winds) is slower than the MBAM track should be a warning to the forecaster that the accuracy of the BAM tracks is suspect.

Although the 1200 UTC 24 August CSUM forecast (Fig. B.6a) fails to predict the eastward turn of Rex, that failure is most likely because such a non-climatological turn would be an extreme outlier in the CSUM developmental database. On the other hand, the consistent qualitative similarity of the CSUM and NOGAPS tracks when E-BCI was occurring in the NOGAPS forecast (compare Fig. B.5b-e and B.6b-e) is considered to be compelling evidence that errors in how the NOGAPS model forecasts the development of the midlatitude cyclones (E-MCG), which contributed to E-BCI in NOGAPS, also significantly degrades the CSUM forecast. This result is not consistent with the analysis for the 1997 TCs, which suggested that CSUM may not be frequently degraded by E-BCI in NOGAPS (Table 5.1). However, all of the cases of E-BCI in 1997 resulted in NOGAPS 72-h FTEs in the 300-500 n mi range, which is suggestive of rather moderate E-BCI. In the Rex case, repeated NOGAPS 72-h FTEs in the 700-900 n mi range were observed. Thus, the Rex case is clearly an outlier relative to the 1997 sample of E-BCI cases. A determination of whether the Rex case is an outlier in the absolute sense with regard to severity of E-BCI in the NOGAPS forecast, or whether the 1997 sample is unrepresentatively biased toward weaker incidents of E-BCI in the NOGAPS forecast, will require a larger database. For the present, the forecasters must simply be aware of the potential that the CSUM forecast may also be degraded when the possibility exists of an extreme E-BCI in the NOGAPS forecast.

c. Selected illustrations of error mechanisms

1) E-RMT in NOGAPS, but not in GFDN. The comparison/verification of the NOGAPS 500-mb wind and sea-level pressure fields (Fig. B.7a-l and B.8a-l, respectively) and TC track forecast initiated at 1200 UTC 24 August 1998, illustrates the impact of E-RMT. At 1200 UTC 24 August (Fig. B.7e), Rex is moving poleward (Fig. B.7a) in response to a poleward steering flow associated

¹ The absence of three GFDN forecasts from 1800 UTC 30 to 1800 31 August in Table B.1 creates some uncertainty as to whether there was one or two periods of E-BCI in the GFDN forecasts.

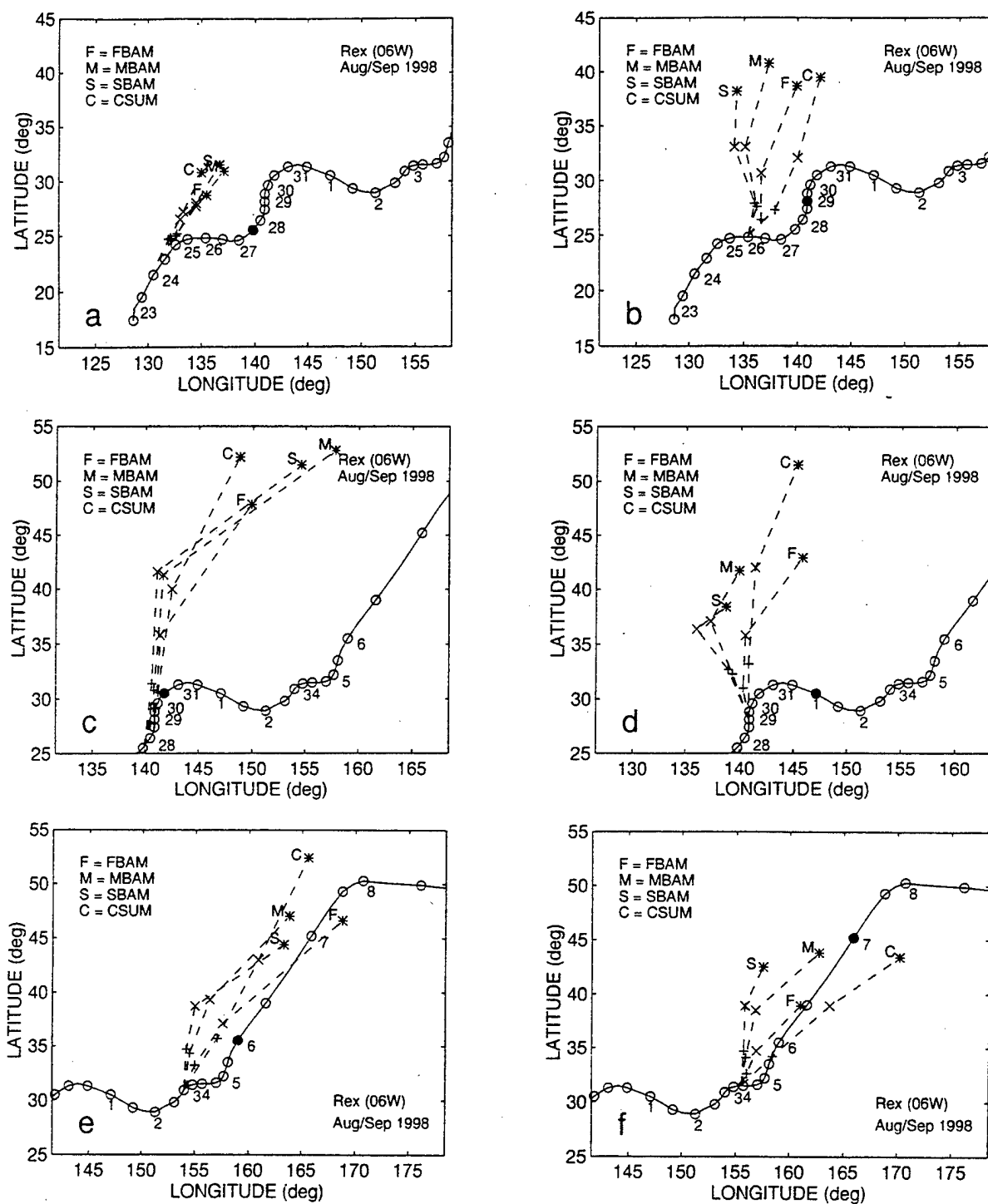


Fig. B.6. Best-track of TC Rex and selected objective technique track forecasts (see inset) for the same times as in Fig. B.5.

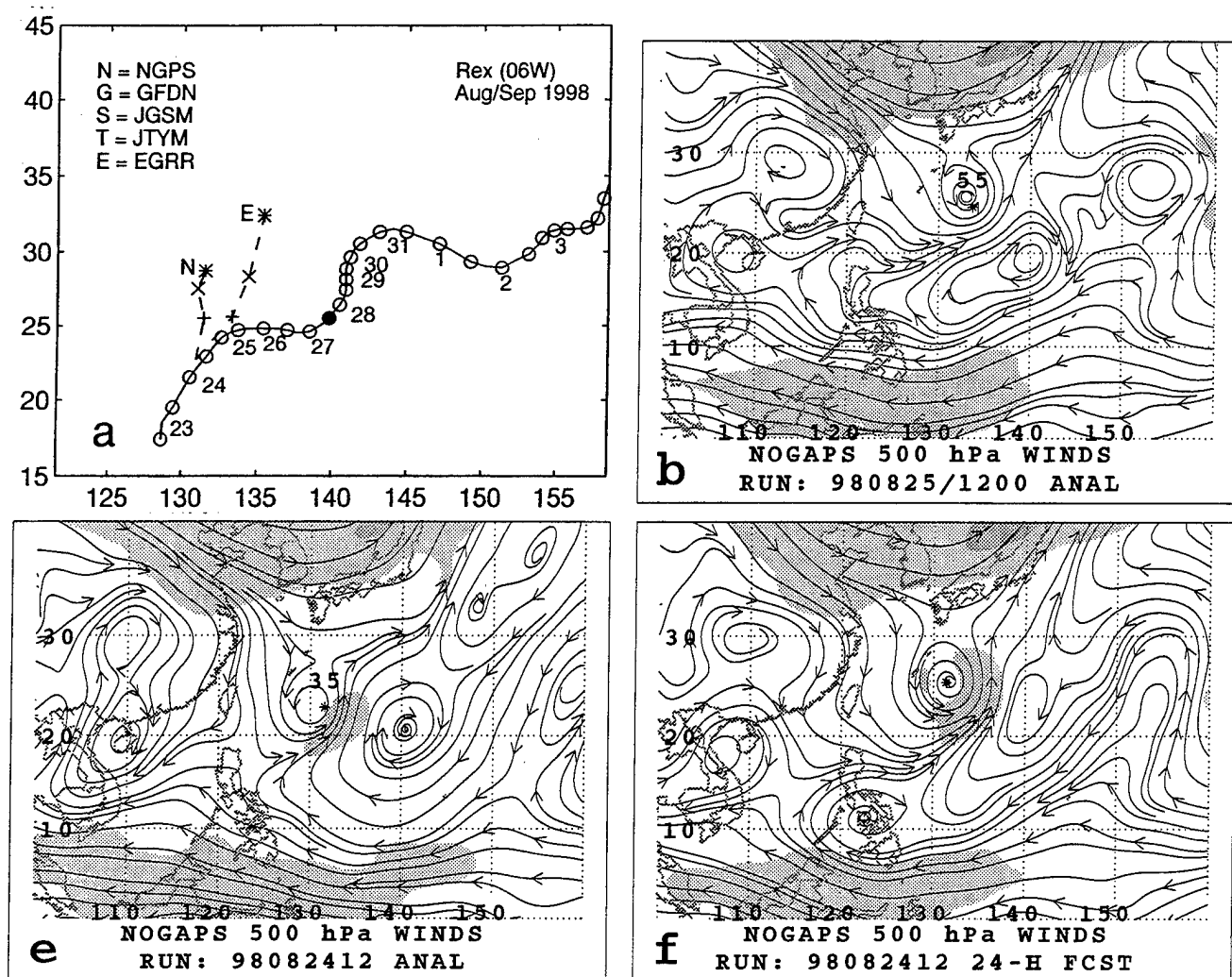


Fig. B.7. Dual page display of (a) best-track of Rex and selected numerical model forecasts (see inset) as in Appendix A, except only NOGAPS forecast initiated at 1200 UTC 24 August 1998.

with a peripheral anticyclone to the southeast that is part of an unbroken ridge extending to the northeast (Fig. B.7e). That is, Rex is in the PF region of a P pattern. Notice that the subtropical anticyclone to the west-northwest of Rex has an unusual meridional orientation, and that this anticyclone together with the Rex cyclonic circulation and the anticyclone southeast of Rex have the appearance of a Rossby wave train as in Fig. 3.2. The 500-mb reflection of the first TUTT cell (see Fig. B.2a and discussion) is to the east of Rex near 25°N, 158°E. In the 1200 UTC 25 August analysis (Fig. B.7b), the TUTT cell has moved westward to 28°N, 152°E and has deepened, which weakens the anticyclonic circulation to the east of Rex by separating the peripheral anticyclone to the southeast of Rex from the subtropical anticyclone. As a result, the steering flow over Rex becomes more westerly, as indicated by the shift of the isotach maximum from southeast (as in Fig. B.7e) to

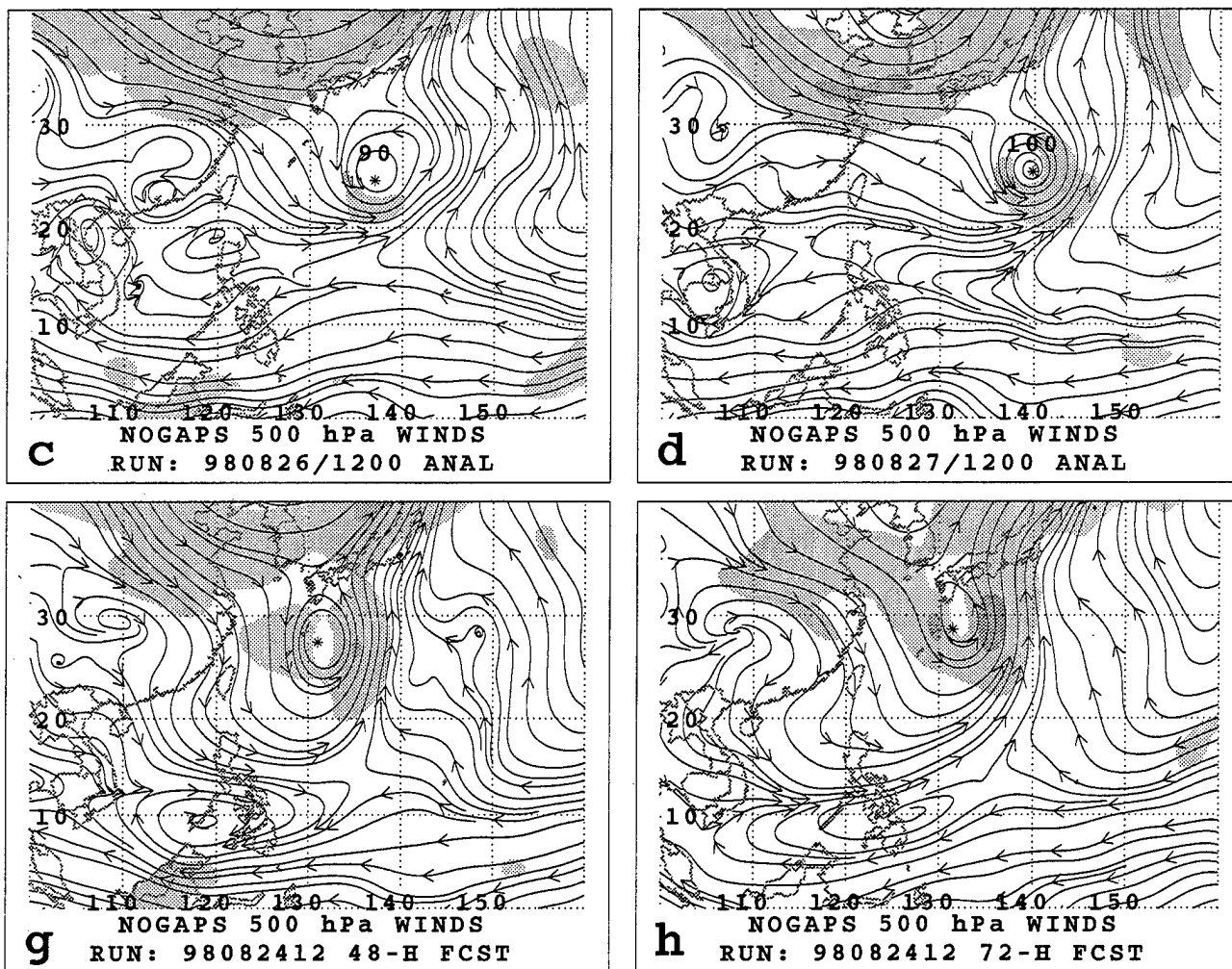


Fig. B.7. (continued).

south of Rex in the 1200 UTC 26 August analysis (Fig. B.7c). The indirect effect of the TUTT cell on the motion of Rex is an example of Indirect Cyclone Interaction on a western TC (ICIW) in the Meteorological Knowledge base (Fig. 1.3). This case is a somewhat atypical example of ICIW, since the eastern cyclone is not another TC, and the ICIW results in an eastward turn due to a midlatitude trough to the north, instead of a westward turn when a subtropical anticyclone is to the north. In the 1200 UTC 27 August NOGAPS analysis (Fig. B.7d), the TUTT cell weakens and is replaced by a ridge so that Rex is again subjected to a more poleward steering flow, as is manifest by a shift of the isotach maximum back to southeast of Rex.

In the NOGAPS 500-mb wind forecast fields (Fig. B.7f-h), the TC is subjected to increasingly poleward flow (as is manifest by the isotach maximum shifting from the southeast to the east of the TC). Thus, the NOGAPS forecast has the TC remaining in a P/PF pattern/region combination. Since the TUTT cell location and amplitude in the NOGAPS 500-mb forecast fields differs from the verifying analyses, the TUTT cell evidently had insufficient indirect effect on the TC motion to the west, which is then the I-ICIW error mechanism. In contrast to the more subtle differences between the forecast and analyzed structure of the TUTT cell, the NOGAPS sea-level pressure forecasts

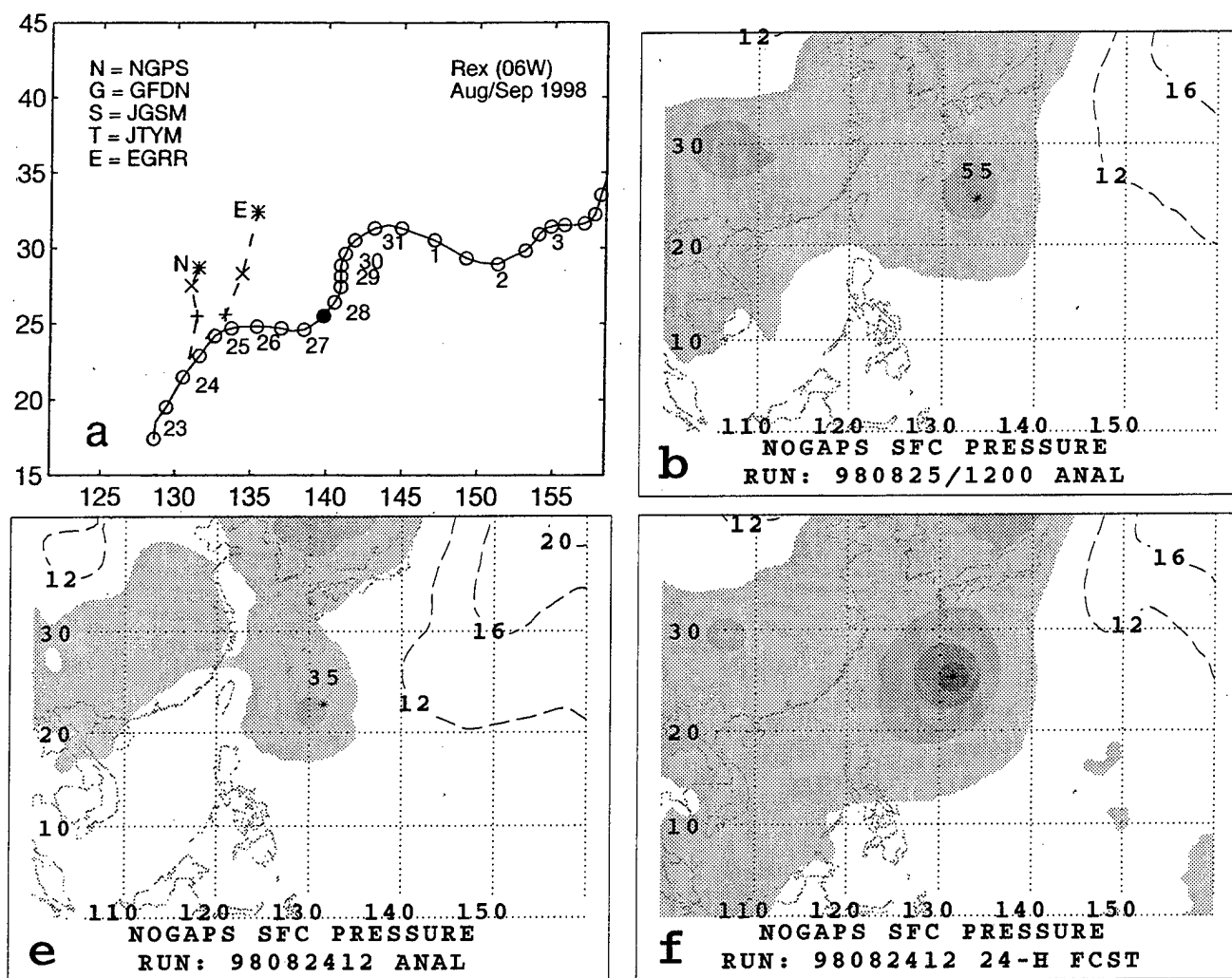


Fig. B.8. As in Fig. B.7, except for sea-level pressure analyses.

(Fig. B.8f-h) have a considerable increase in TC size compared to the verifying analyses (Fig. B.8b-d). In accordance with the RMT conceptual model (Fig. 3.1) and the supporting barotropic theory, the degree of ridge modification depends directly on the size of the TC. Thus, the overly large size of Rex in the NOGAPS forecasts would be expected to generate an overly strong peripheral anticyclone to the southeast of Rex, so that this anticyclone would tend to be resistant to the dissipative effect of the TUTT cell encroaching from the east. In short, the larger size of Rex in the NOGAPS forecast would render the TC more resistant to the ICIW from the encroaching TUTT cell, which in reality had contributed to Rex's turn onto an eastward track.

2) E-BCI in NOGAPS, but not in GFDN. The comparison/verification of the NOGAPS and GFDN sea-level pressure fields and TC track forecasts initiated at 0000 and 0600 UTC 26 August 1998 (Fig. B.9a-l, respectively) is illustrative of the period when forecast track degradation due to

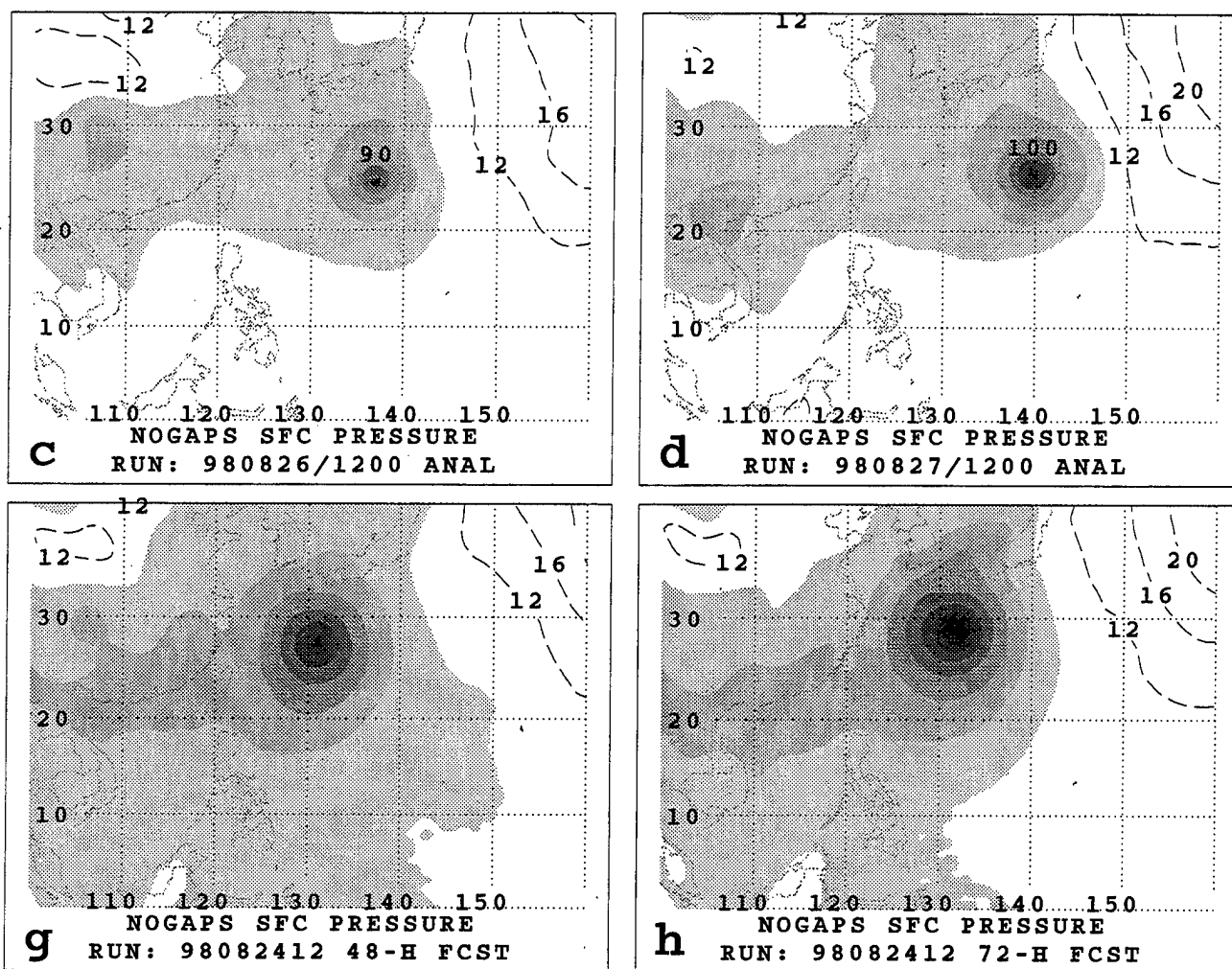


Fig. B.8. (continued) As in Fig. B.7 e-f, except for sea-level pressure forecasts.

E-BCI was occurring in the NOGAPS forecast, but not in the GFDN forecast (Fig. B.9a). Notice that the size of Rex is considerably larger in the NOGAPS 24-h forecast field (Fig. B.9f) than in the verifying analysis (Fig. B.9b). This erroneous growth of the TC is probably a continuation of the E-RMT process illustrated in subsection 1) above. In the NOGAPS 48-h and 72-h forecast fields (Fig. B.9g-h), the TC clearly undergoes a BCI with a midlatitude cyclogenesis to the north that is associated with a strong midlatitude cyclone at 500 mb (not shown). However, there is little indication of BCI in the verifying NOGAPS analyses (Fig. B.9c-d), even though some indication of midlatitude cyclogenesis is present to the north of the TC in the 0000 UTC 28 August analysis (Fig. B.9c). Support for the conclusion that the E-BCI in the NOGAPS forecast is at least partially due to a result of the overly large size of the model TC is that a compact TC structure is maintained throughout the GFDN forecast (Fig. B.9j-l) and no E-BCI occurs, even though Excessive Midlatitude CycloGenesis (E-MCG) is occurring to the north of the TC at 42 h (Fig. B.9k) compared to the verifying analysis (Fig. B.9c). As annotated in Table B.1, the presence of E-MCG in the GFDN forecast eventually contributed to extreme E-BCI and highly erroneous GFDN track forecasts.

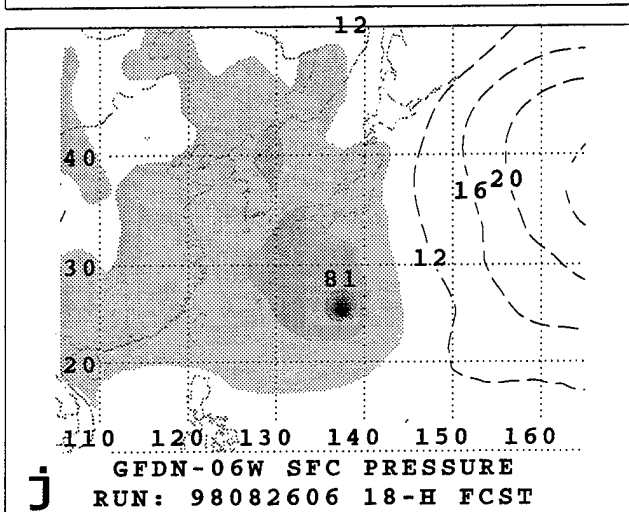
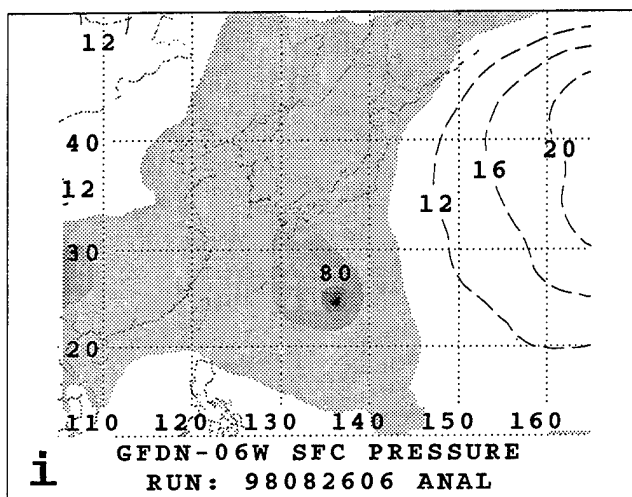
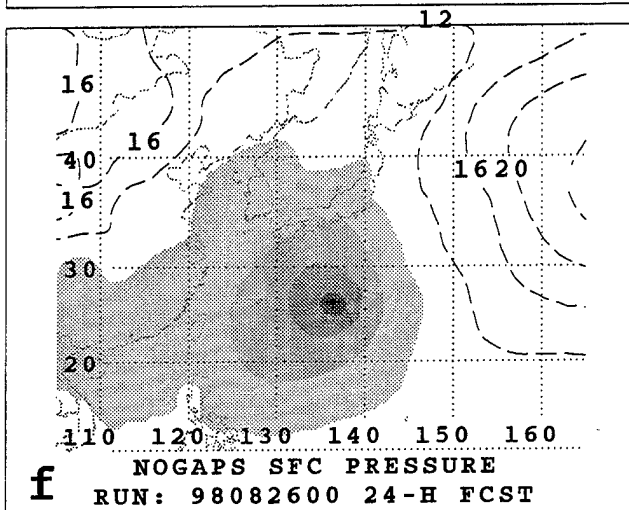
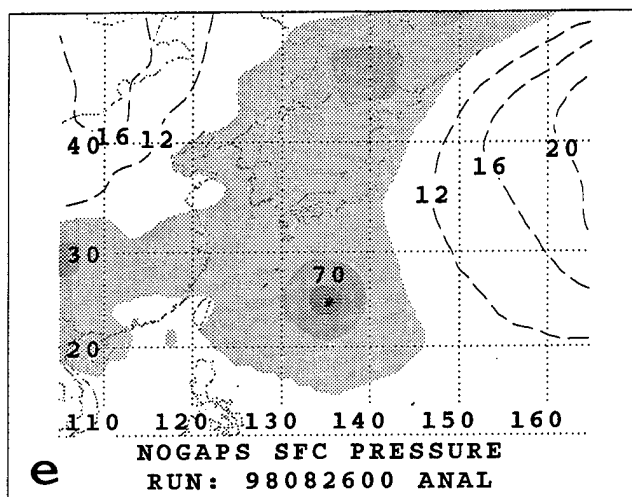
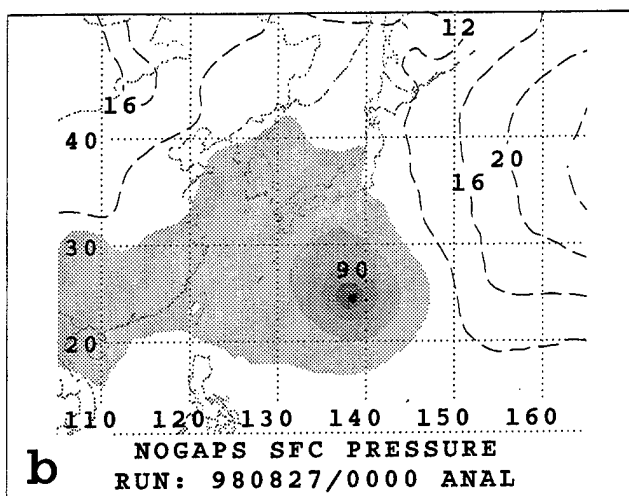
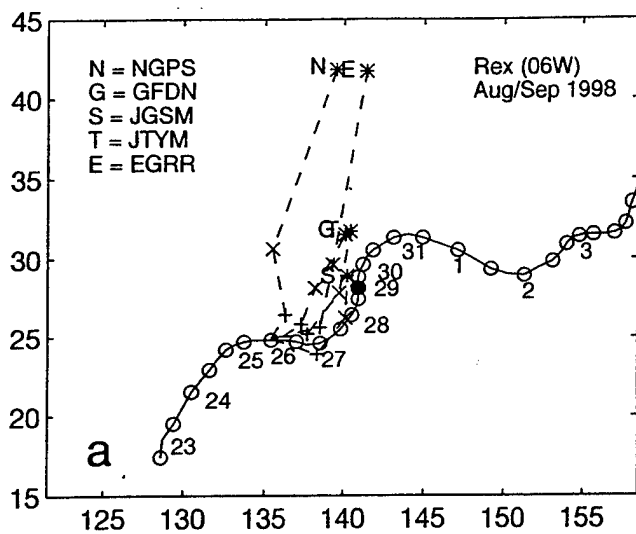


Fig. B.9. Dual page display of sea-level pressures and tracks as in Appendix A for TC Rex at initial time of 0000 UTC 26 August 1998 for NOGAPS and 0600 UTC 26 August for GFDN.

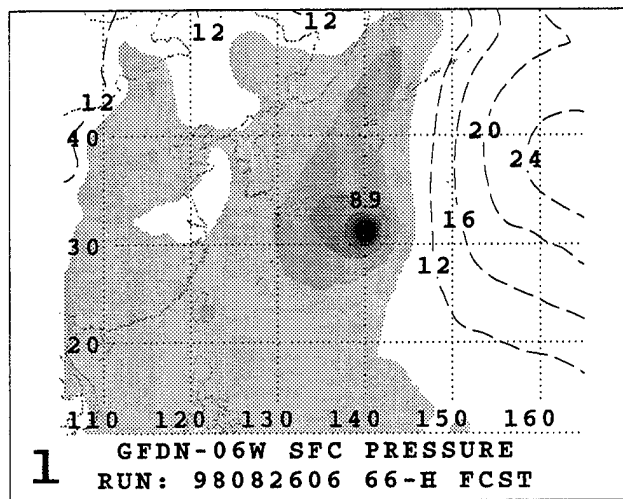
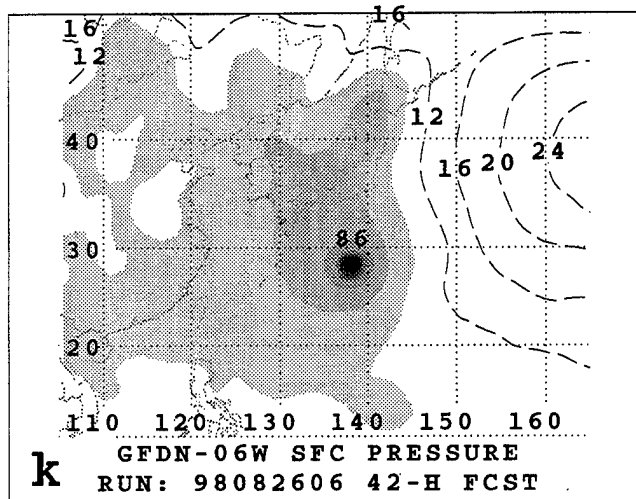
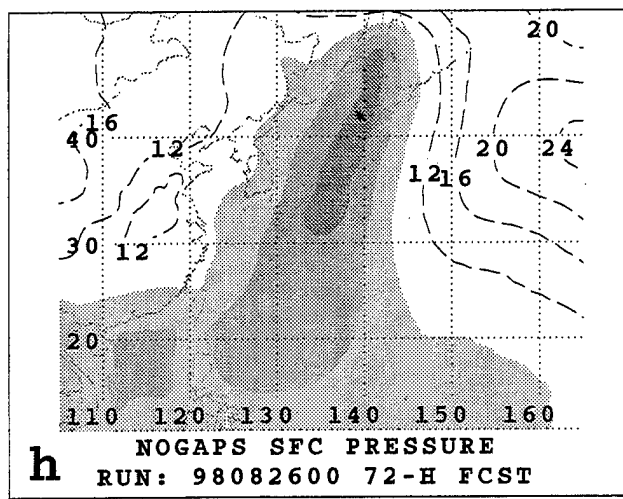
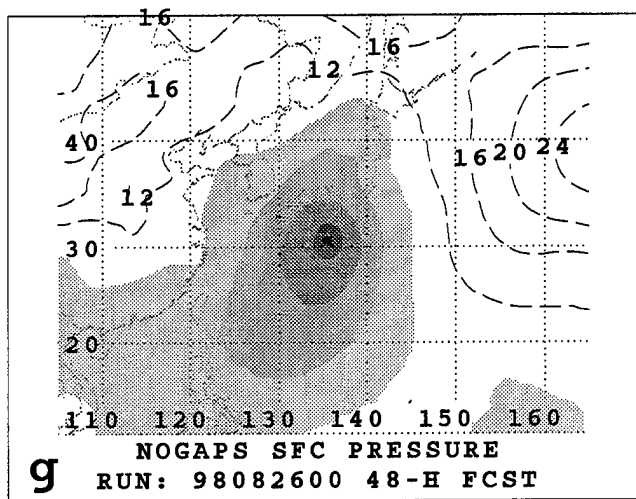
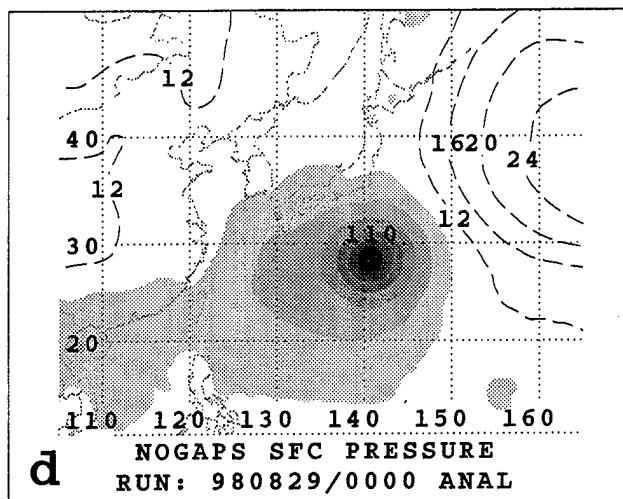
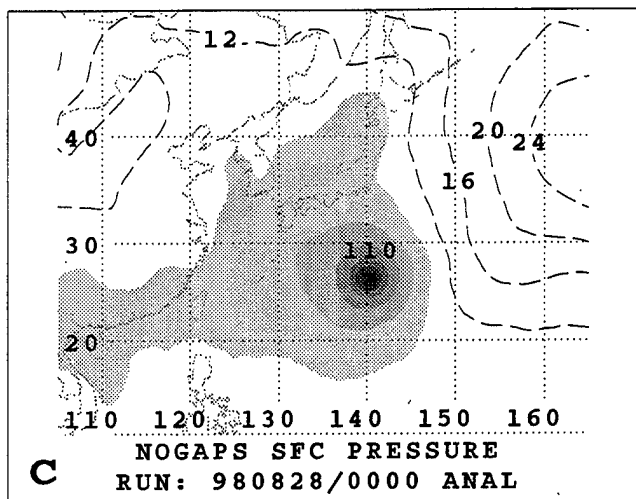


Fig. B.9 (continued).

3) E-BCI in both NOGAPS and GFDN. The comparison/verification of the NOGAPS and GFDN sea-level pressure and 500-mb wind fields and TC track forecasts initiated at 0000 and 0600 UTC 29 August 1998, respectively, is provided in Fig. B.10a-l and Fig. B.11a-l, respectively. This is a critical period during Rex when severe forecast track degradation due to E-BCI was occurring in the NOGAPS and GFDN (and presumably EGRR) forecasts, but Rex was actually turning onto a east-southeastward heading (Fig. B.10a). In both the NOGAPS and GFDN sea-level pressure forecasts (Fig. B.10f-k and j-l, respectively), the TC interacts with an area of excessive midlatitude cyclogenesis to the northeast, which is particularly evident in the NOGAPS 48-h forecast as a low pressure trough (Fig. B.10g) that is deeper than in the verifying analysis (Fig. B.10c). As a result of the E-BCI in the NOGAPS forecast, the TC is predicted to have a distinctively baroclinic structure by 72 h (Fig. B.10h) -- note the cold frontal trough extending south-southwest of TC. Whereas extreme deepening occurs by 66 h in the GFDN forecast (Fig. B.10l), the structure of Rex changes little in the verifying analyses (Fig. B.10b-d).

In the NOGAPS and GFDN 500-mb wind forecasts (Fig. B.11f-h and j-l, respectively), the TC interacts with, and becomes embedded in, a deep 500-mb midlatitude cyclone and associated jet maximum that is associated with the midlatitude cyclogenesis to the north of the TC in the sea-level forecasts of both models (e.g., Fig. B.10f and g). In the verifying NOGAPS 500-mb wind analyses (Fig. B.11b-d), the TC turns to the southeast and does not interact with the midlatitude cyclone to the northwest, which was fairly well forecast to 48 h (42 h) by the NOGAPS (GFDN) model.

Forecasters at JTWC have suggested:

(i) that the unusual turn to the east-southeast by Rex was primarily a result of a Direct Cyclone Interaction (DCI) between the TC and the approaching second TUTT cell (recall Fig. B.3), which is only a steadily weakening trough to the east of the TC in the verifying analyses (Fig. B.11b-d); and

(ii) that the failure of the NOGAPS and GFDN models to forecast this interaction was due to an under-representation of the TUTT cell amplitude and vertical extent in the both the initial analyses and forecast fields (Figs. B.11e-h and i-l).

However, the differences in the TUTT cell between the forecast fields and verifying analyses seem to be rather subtle. By contrast, a striking difference is found in the strength of a subtropical ridge (STR) circulation to the southwest of Rex in the 0000 UTC 1 September analysis (Fig. B.11d) compared to the NOGAPS 72-h and GFDN 66-h forecasts (Fig. B.11h and l, respectively). In the sequence of verifying analyses (Fig. B.11b-d), the steady amplification of this anticyclonic circulation would subject the TC to an increasingly strong northwesterly steering flow that accounts for the east-southeastward turn of Rex during this period. By contrast, this anticyclone does not develop in the corresponding NOGAPS and GFDN forecasts (Fig. B.10f-h and j-l, respectively). The combination of this anticyclone and the approaching TUTT cell may have contributed to an increasingly strong southeastward steering over Rex as the pressure gradient tightens between the low (TUTT) and the high (STR circulation). In the Systematic Approach Meteorological knowledge base, this effect is termed Semi-direct Cyclone Interaction of a Western TC (SCIW), which is analogous to the binary TC interaction effect called STIW in Carr *et al.* (1997) and CMKB (p. 97-101).

4) Alternating E-BCI and I-BCI in NOGAPS. The comparison/verification of the NOGAPS and GFDN sea-level pressure fields and TC track forecasts initiated at 0000 UTC and 0600 UTC, respectively, on 3 September and 4 September 1998 (Fig. B.12a-l and Fig. B.13a-l, respectively) illustrate a rapid change from E-BCI to I-BCI in the NOGAPS forecast. This variation occurred during a period of vigorous extratropical transition by Rex that was accompanied by a translational acceleration to the northeast (Fig. B.12a). In both of the 3 September NOGAPS and GFDN forecasts (Fig. B.12f-h and j-k, respectively), rapid northeastward movement of the TC is predicted in response to interaction between the TC and an area of midlatitude cyclogenesis that is manifest as a lobe of low pressure extending to the north-northeast of the TC in the NOGAPS 48-h and GFDN 42-h forecasts (Fig. B.12g and k, respectively). By contrast, significant interaction of the TC and the area of cyclogenesis does not occur in the verifying analyses (Fig. B.12b-d). That an E-BCI occurs in both the NOGAPS and GFDN forecasts by 72 h and 66 h, respectively, is remarkable considering that:

- (i) the size of the TC in the earlier NOGAPS and GFDN forecasts (Fig. B.12f-g and j-k, respectively) is smaller than in the verifying NOGAPS analyses (Fig. B.12b-c);
- (ii) it is difficult to see any definitive difference in the degree of midlatitude cyclogenesis to the northeast of the TC in the earlier NOGAPS and GFDN forecasts compared to the verifying analyses; and
- (iii) no differences are readily discerned between the development of the 500-mb midlatitude cyclone (not shown) in either of the model forecasts and verifying NOGAPS analyses.

Whereas extratropical transition again occurs in the 4 September GFDN sea-level pressure forecasts (Fig. B.13j-l), extratropical transition does not occur in the corresponding NOGAPS sea-level pressure forecasts (Fig. B.13f-h), despite more midlatitude cyclogenesis having occurred to the northeast of the TC in the 48-h forecast (Fig. B.13g) than in the verifying analysis (Fig. B.13c). Since extratropical transition and associated rapid translational acceleration does occur on 7 September (Fig. B.4e and Fig. B.13a, respectively), the degraded 4 September NOGAPS forecast is attributed to I-BCI, whereas just 24 h earlier the degradation was due to E-BCI.

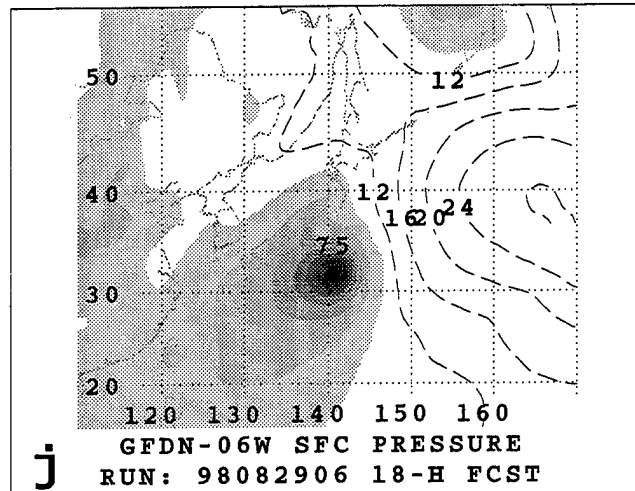
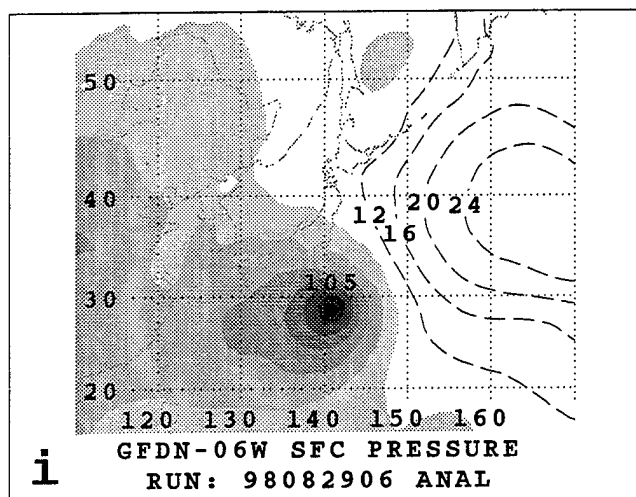
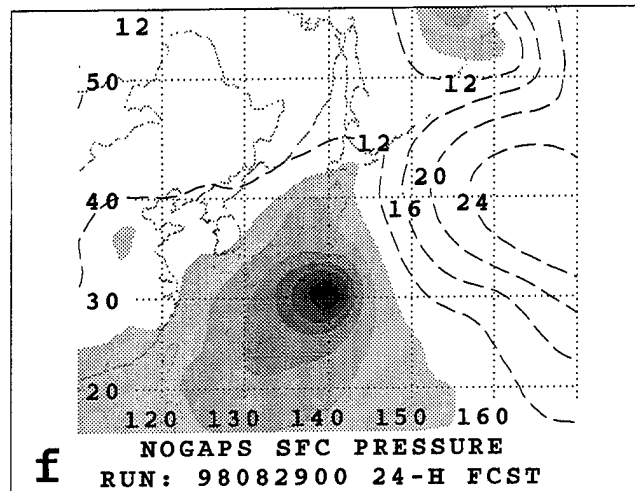
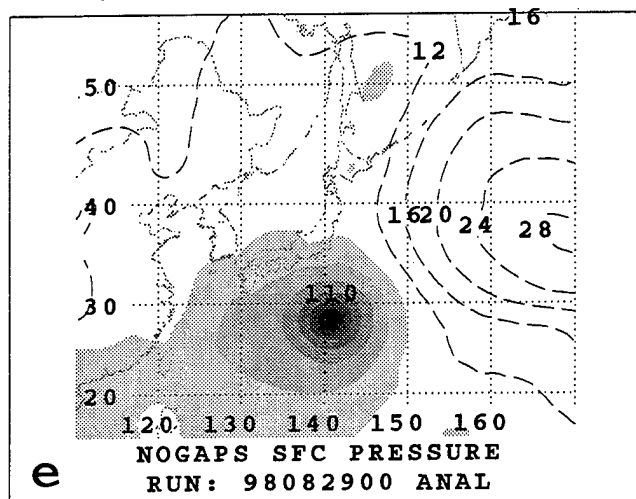
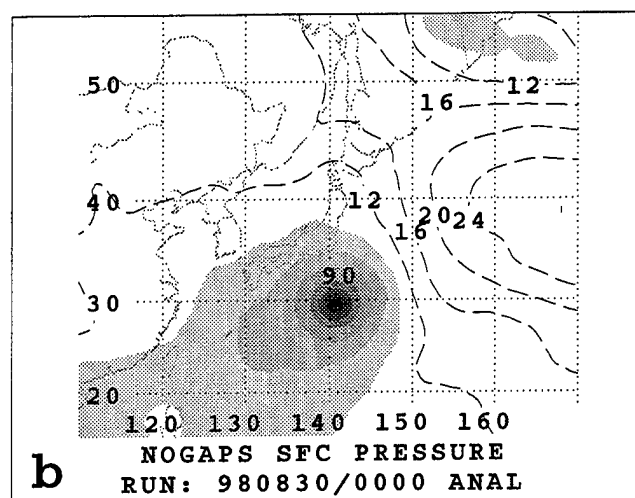
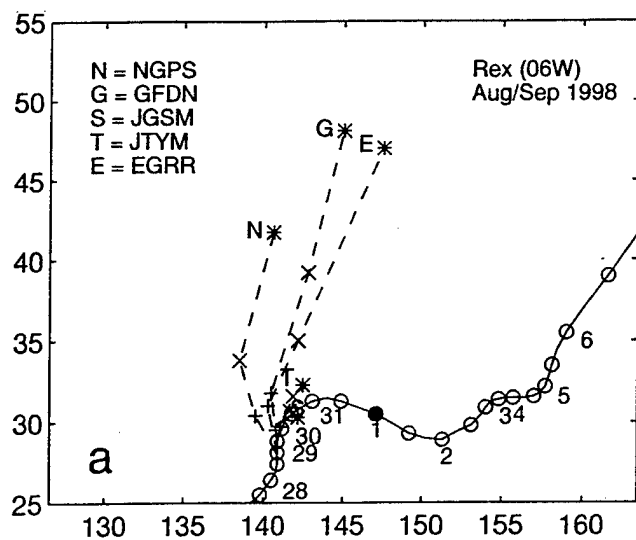


Fig. B.10. Dual page display of sea-level pressure analyses and forecasts and tracks as in Fig. B.9, except at initial time of 0000 UTC 29 August 1998 for NOGAPS and 0600 UTC 29 August for GFDN.

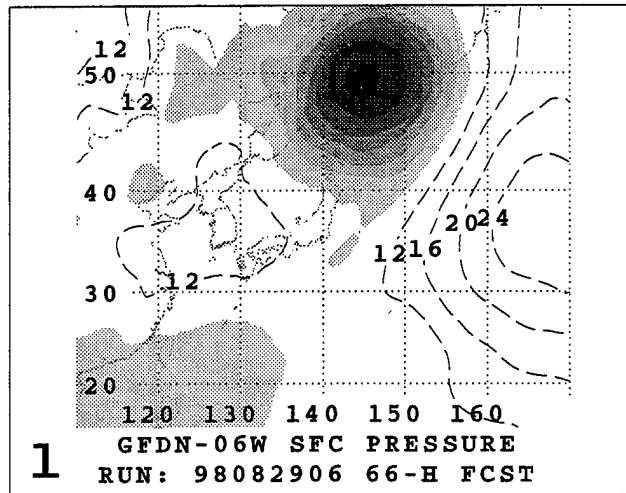
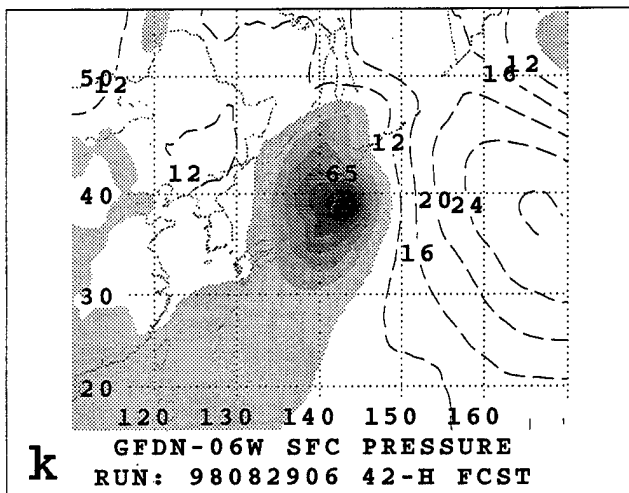
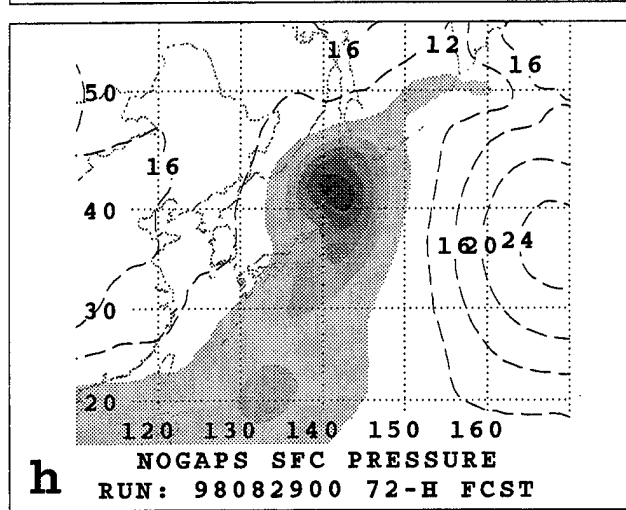
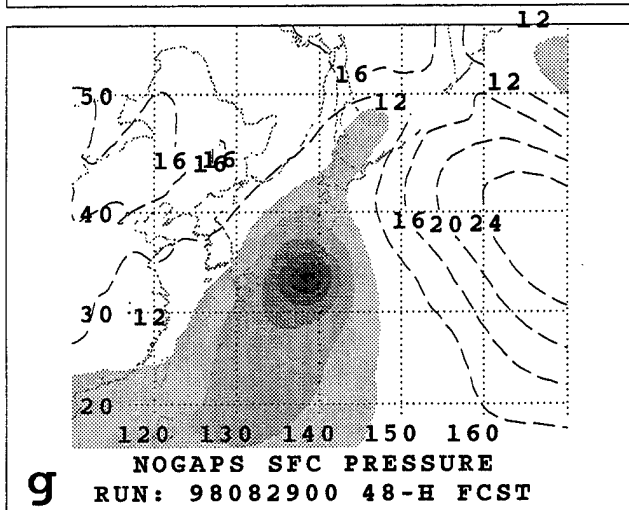
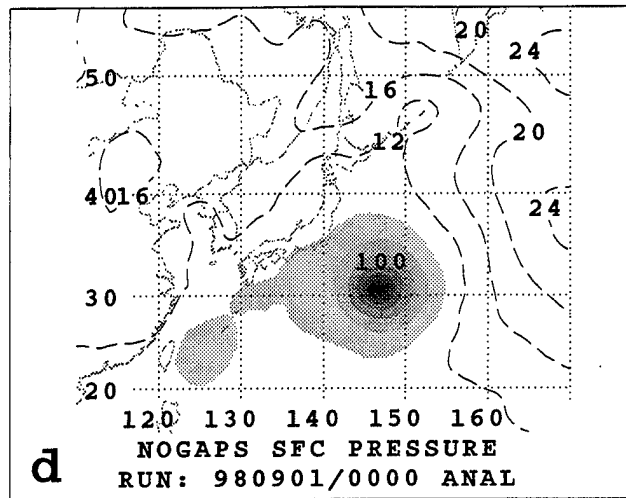
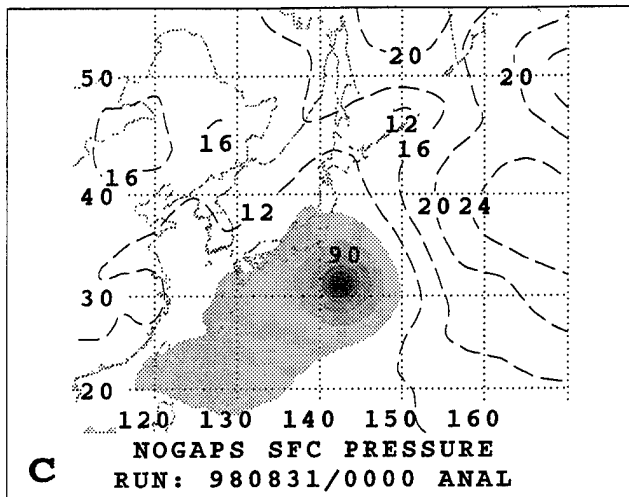


Fig. B.10. (continued).

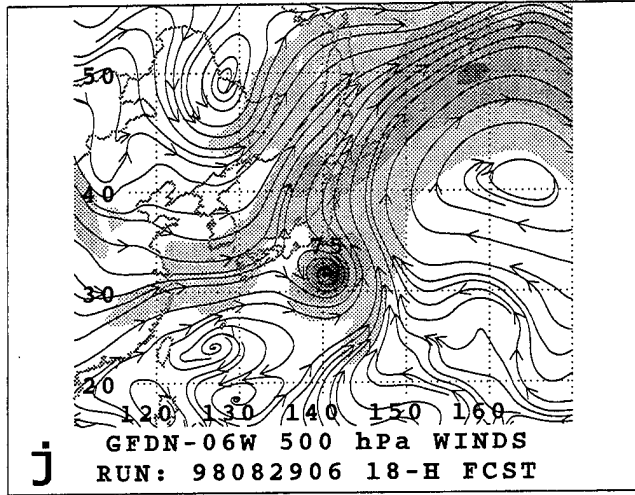
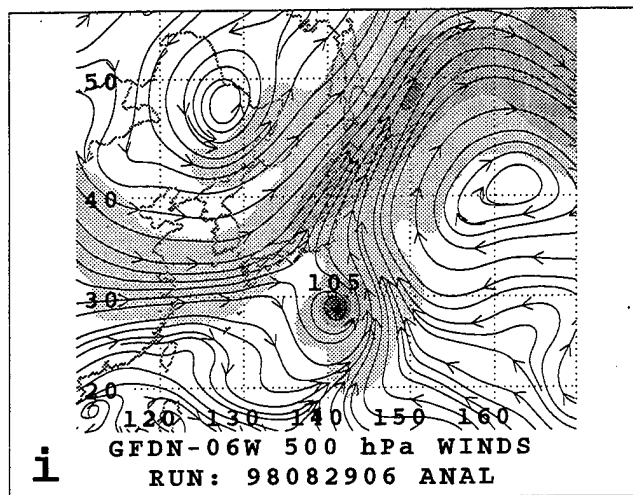
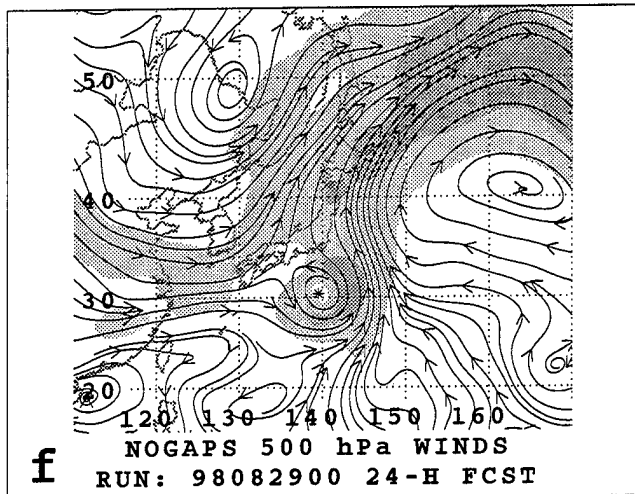
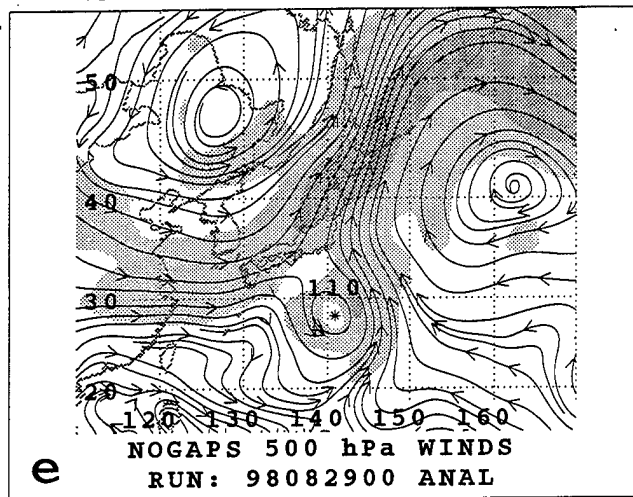
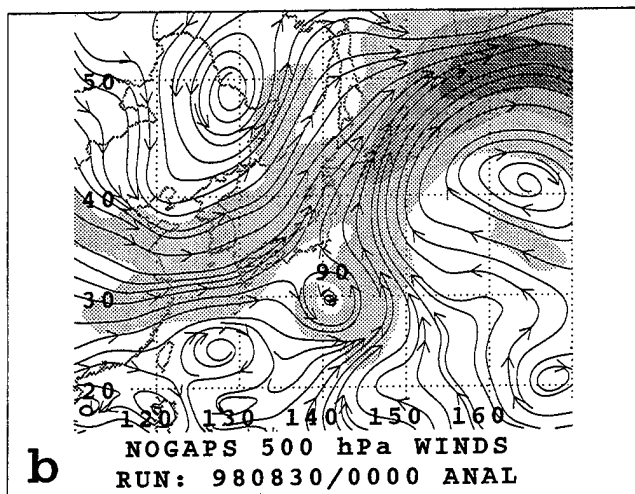
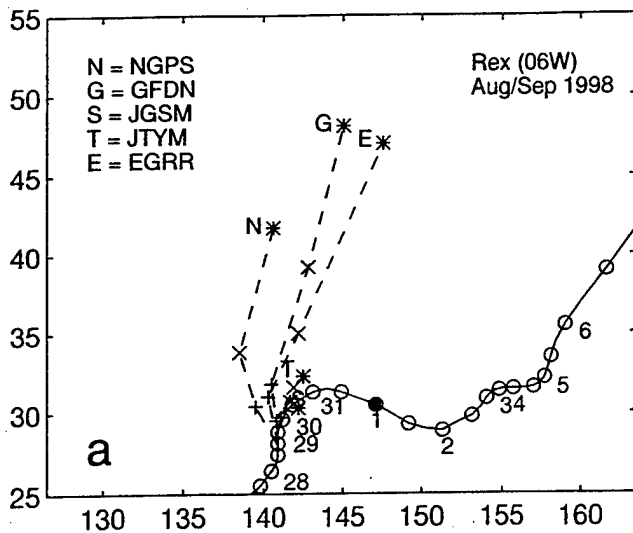


Fig. B.11. Dual page display of 500-mb wind analyses and forecasts and tracks as in Appendix A for TC Rex at initial time of 0000 UTC 29 August 1998 for NOGAPS and 0600 UTC 29 August for GFDN.

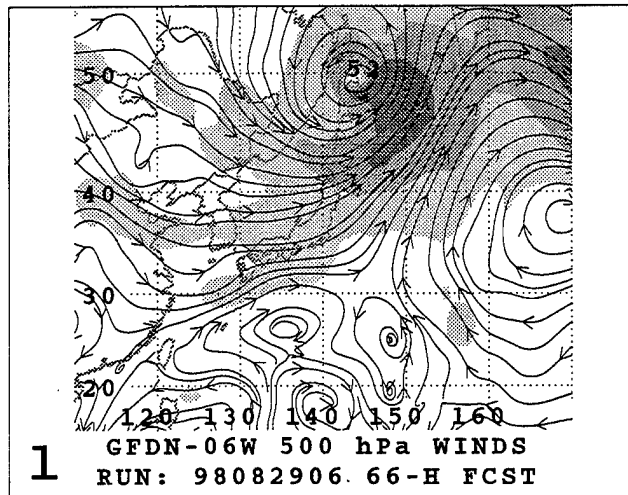
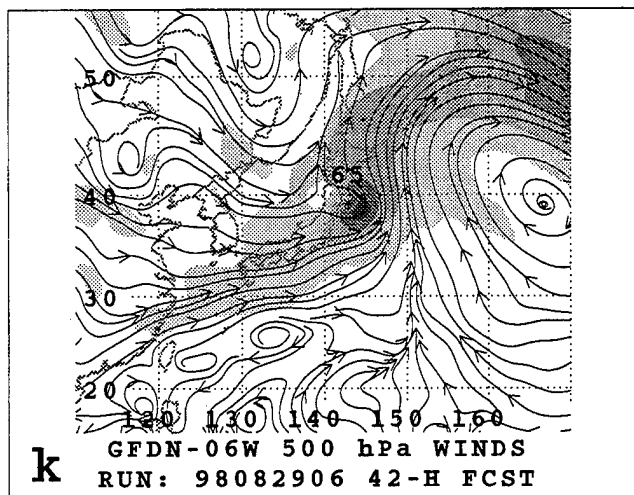
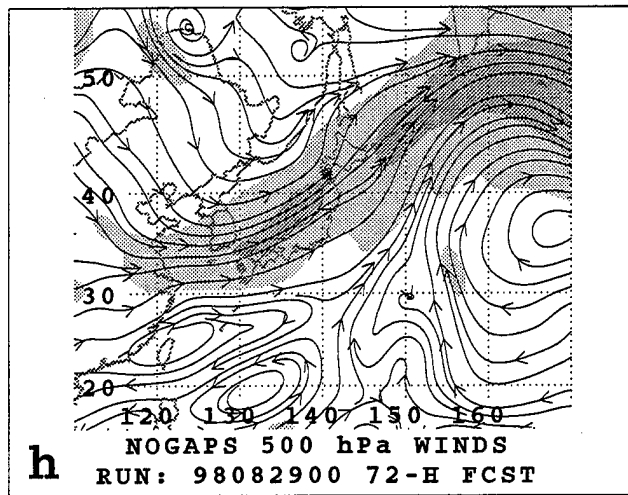
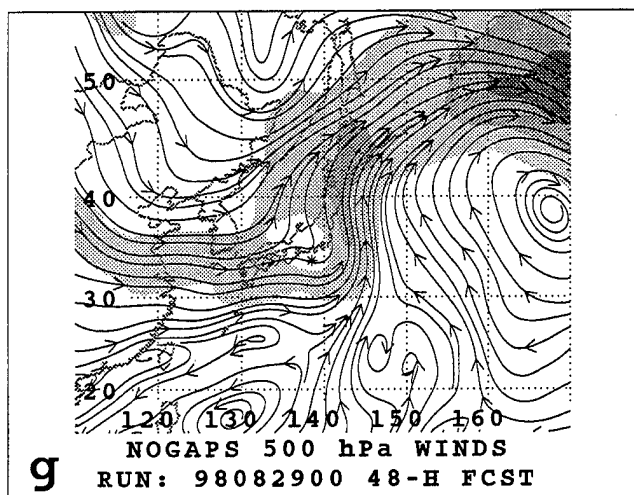
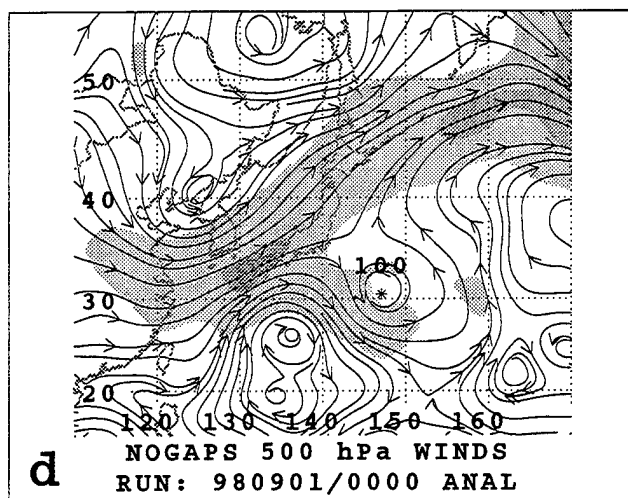
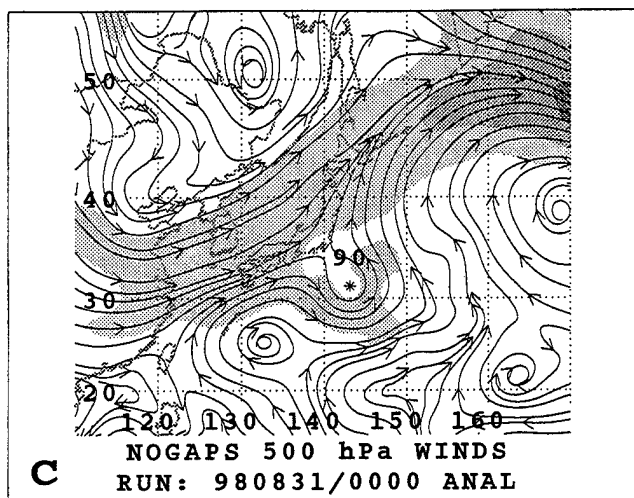


Fig. B.11. (continued).

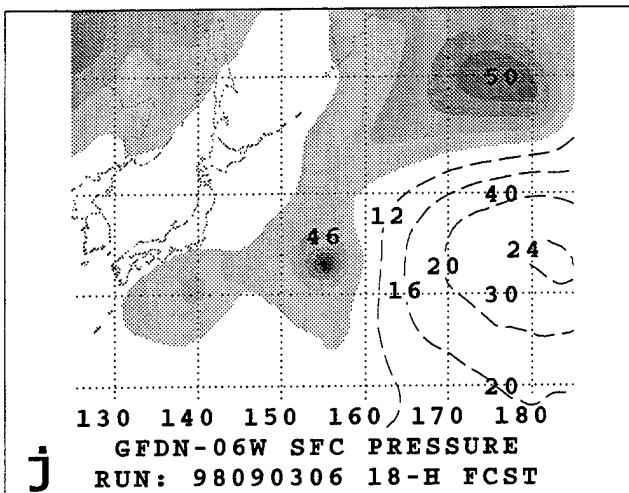
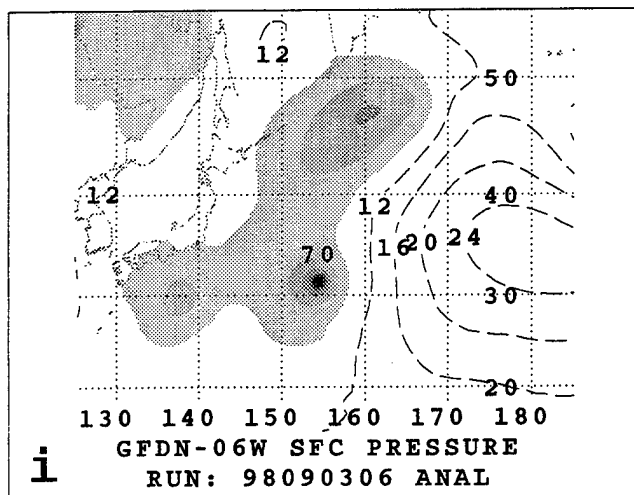
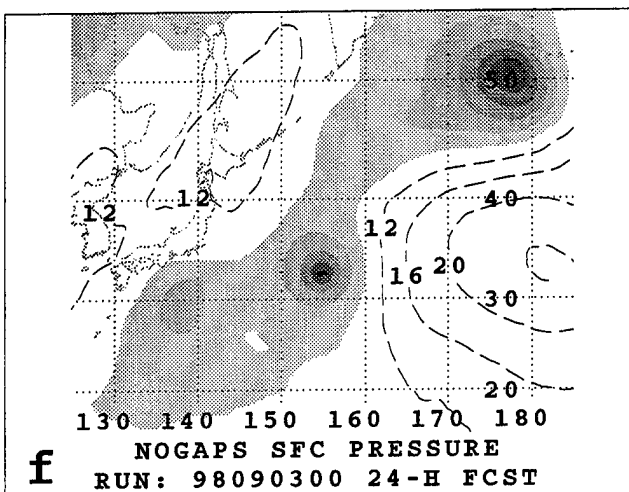
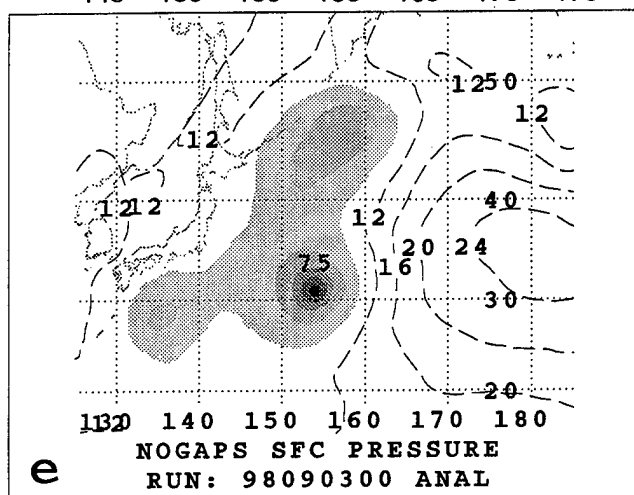
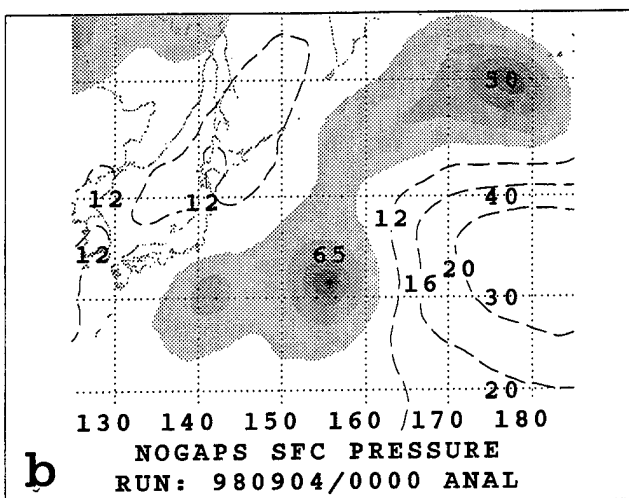
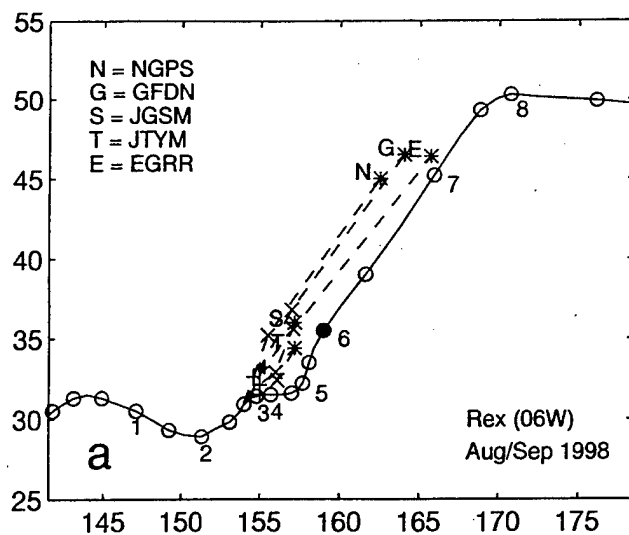


Fig. B.12. Dual page display of sea-level pressure analyses and forecasts and tracks as in Fig. 8.B, except at initial time of 0000 UTC 3 September 1998 for NOGAPS and 0600 UTC 3 September for GFDN.

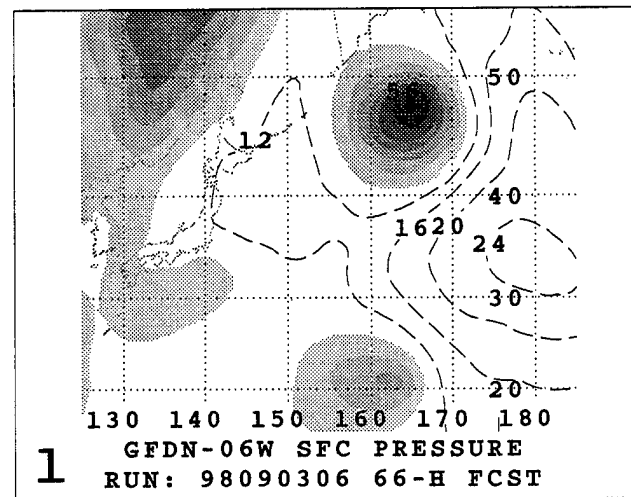
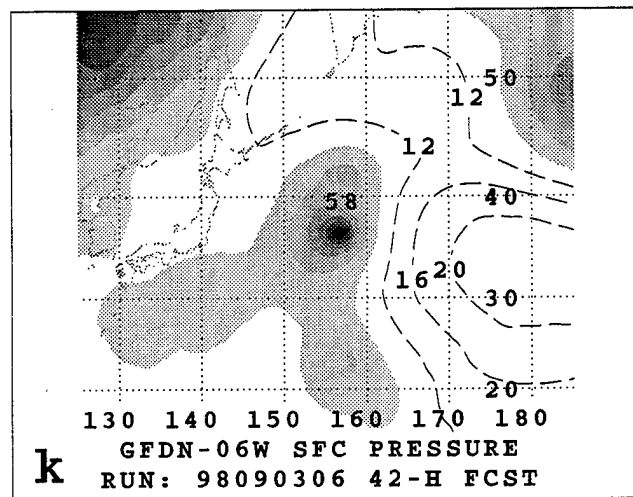
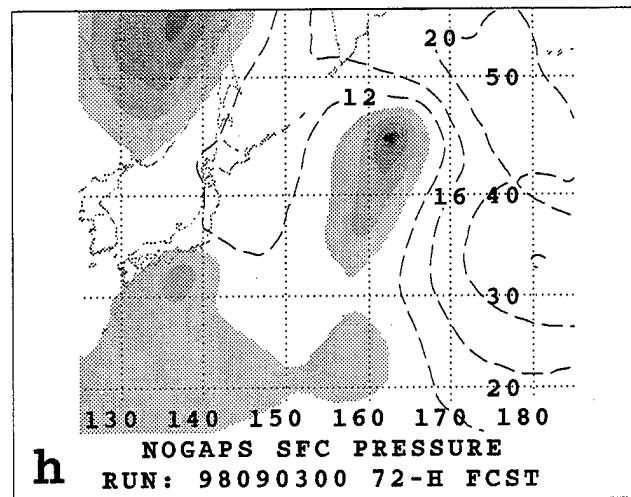
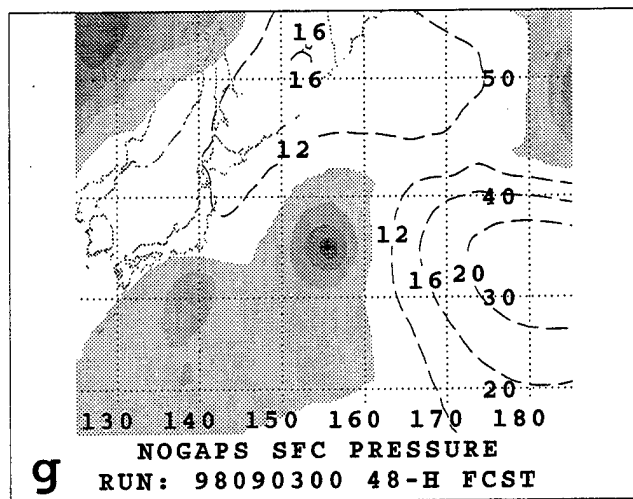
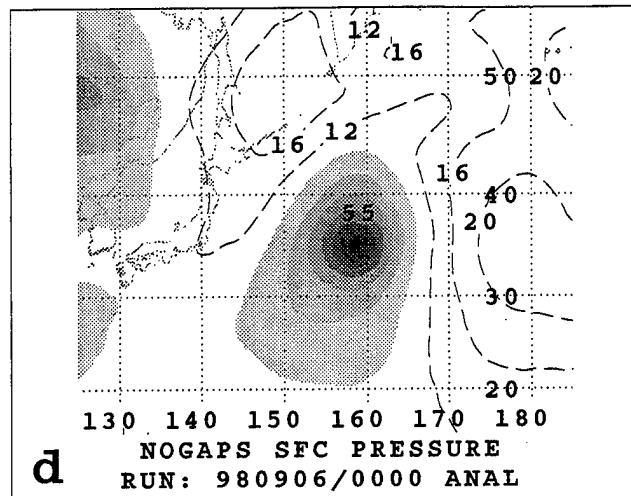
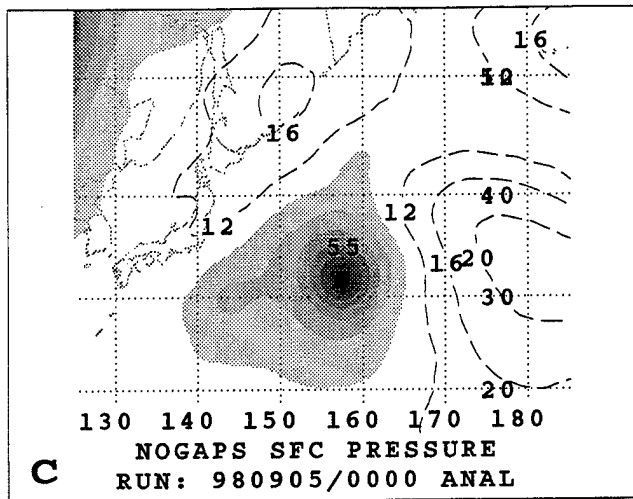


Fig. B.12. (continued).

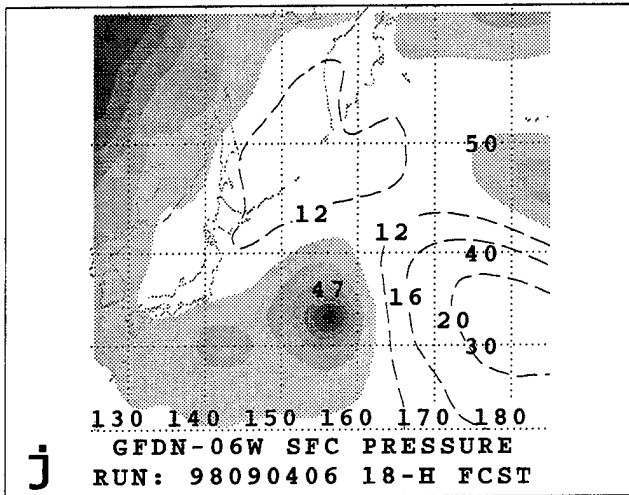
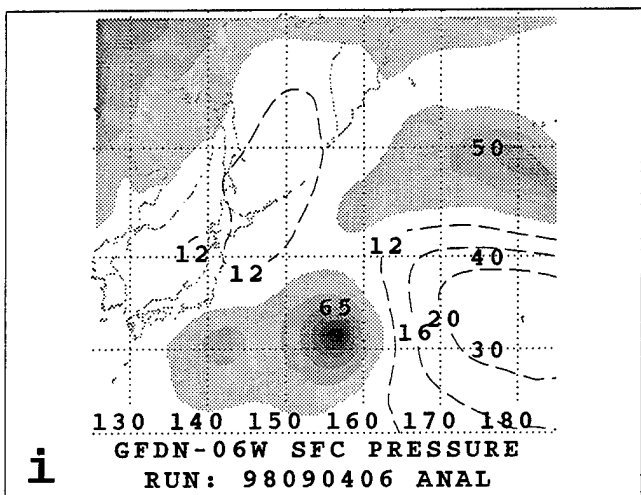
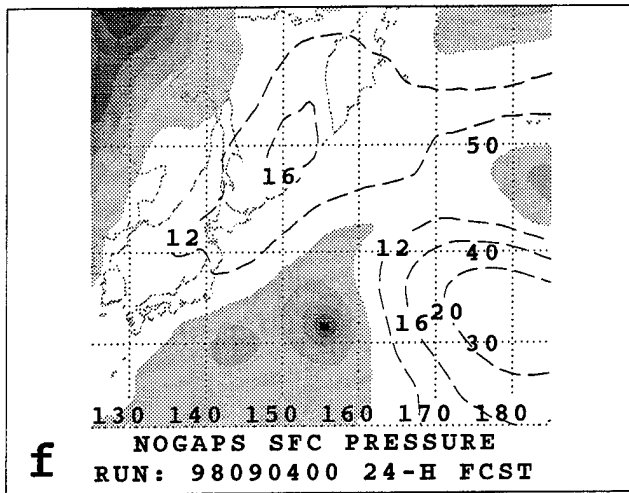
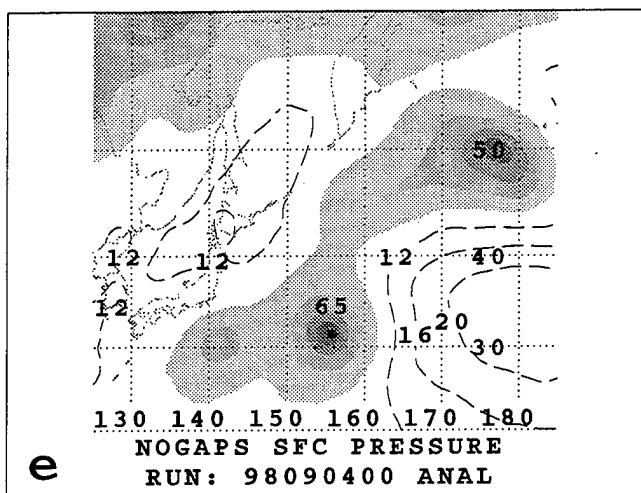
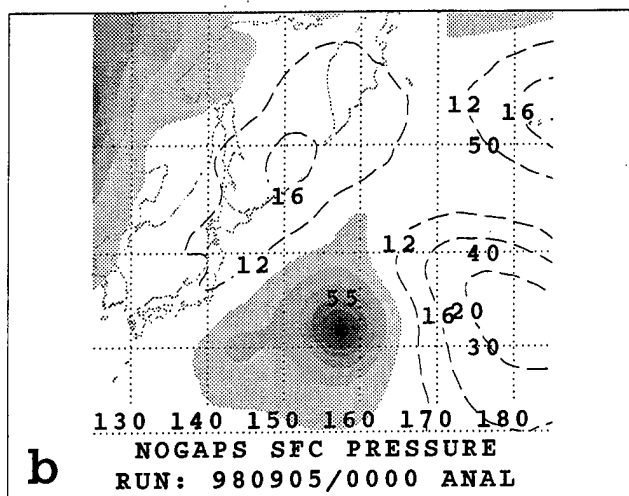
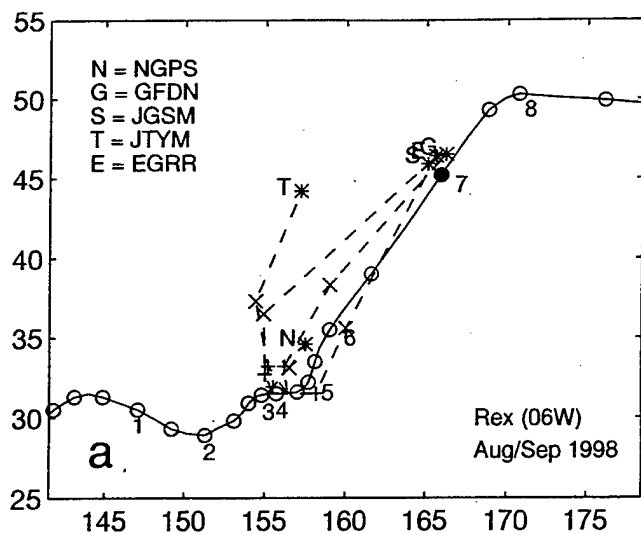


Fig. B.13. Dual page display of sea-level pressure analyses and forecasts and tracks as in Fig. B.9, except at initial time of 0000 UTC 4 September 1998 for NOGAPS and 0600 UTC 4 September for GFDN.

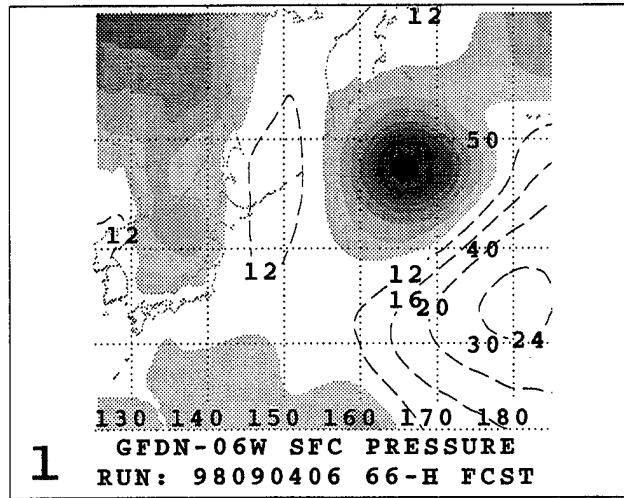
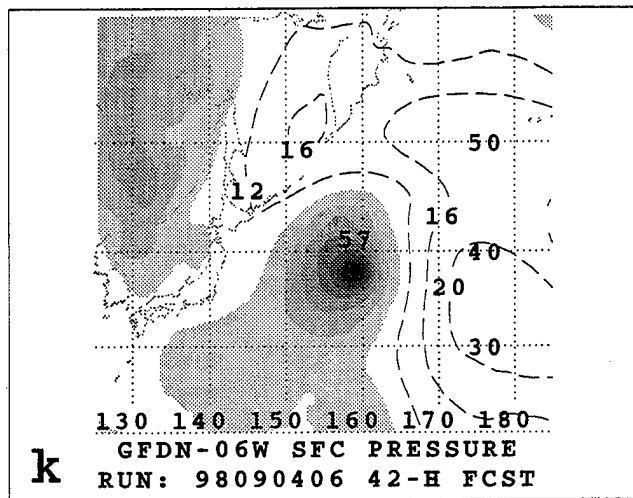
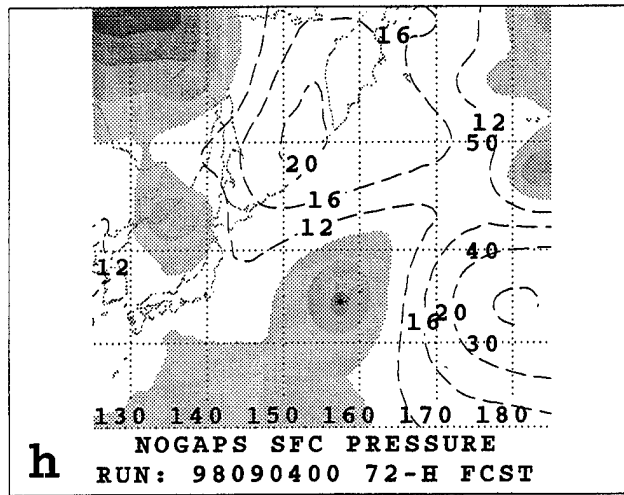
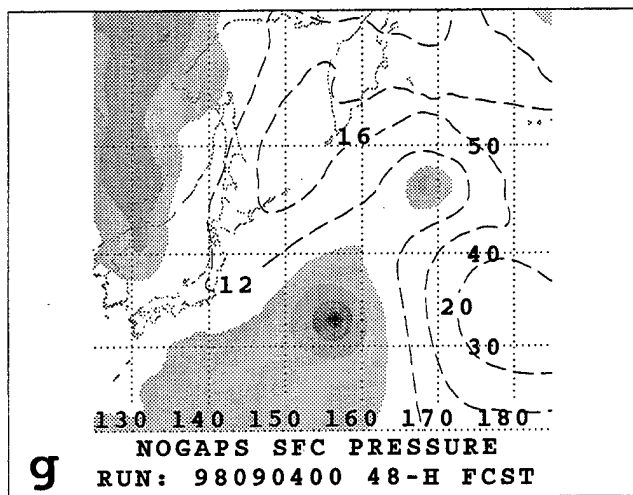
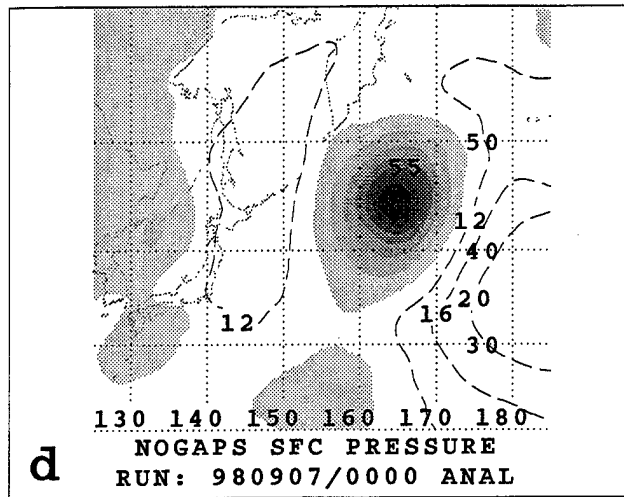
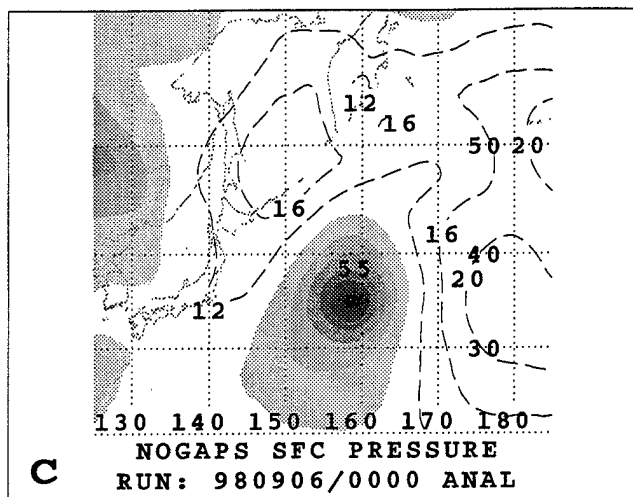


Fig. B.13. (continued).

d. Conclusion

Both the anomalous track of Rex and the highly erroneous NOGAPS and GFDN track forecasts have been evaluated and explained using the conceptual models from the Meteorological Knowledge base, and especially from the Model Traits Knowledge base of the Systematic Approach. Whereas the motion of Rex may have been influenced by encounters with several TUTT cells, the principal reason for all of the poor NOGAPS track forecasts except three E-RMT-related cases, and all of the poor GFDN track forecasts, was recurring erroneous Baroclinic Cyclone Interaction (BCI). Whereas two NOGAPS forecasts were degraded by I-BCI, the remainder of the degraded NOGAPS and all of the degraded GFDN forecasts were due to E-BCI (Table B.1). As with the case studies of Peter and Yule in section 4, the problem of E-BCI seems to depend sensitively of the positioning and structure of both the TC and midlatitude cyclone in the models versus in reality. As these are difficult forecast scenarios to explain retrospectively, it is expected that they will be even more difficult to diagnose in real-time. The complex interactions of Rex with the midlatitude circulation, the TUTT cell, and the subtropical anticyclone are unusual--general conclusions about dynamical model performance should not be made based on such unusual cases.

REFERENCES

- Bannister, A. J., M. A. Boothe, L. E. Carr, III, and R. L. Elsberry, 1997: Southern Hemisphere application of the systematic approach to tropical cyclone track forecasting. Part I. Environment structure characteristics. Tech. Rep. NPS-MR-98-001, Naval Postgraduate School, Monterey, CA 93943-5114, 96 pp.
- Bannister, A. J., M. A. Boothe, L. E. Carr, III, and R. L. Elsberry, 1998: Southern Hemisphere application of the systematic approach to tropical cyclone track forecasting. Part II. Climatology and refinement of meteorological knowledge base. Tech. Rep. NPS-MR-98-004, Naval Postgraduate School, Monterey, CA 93943-5114, 69 pp.
- Boothe, M. A., 1997: Extension of the systematic approach to tropical cyclone track forecasting in the eastern and central Pacific. Master's Thesis, Naval Postgraduate School, Monterey, CA 93943-5114, 133 pp.
- Carr, L. E., III, and R. L. Elsberry, 1994: Systematic and integrated approach to tropical cyclone track forecasting. Part I. Approach overview and description of meteorological basis. Tech. Rep. NPS-MR-94-002, Naval Postgraduate School, Monterey, CA 93943-5114, 273 pp.
- Carr, L. E., III, and R. L. Elsberry, 1995: Monsoonal interactions leading to sudden tropical cyclone track changes. *Mon. Wea. Rev.*, **123**, 265-289.
- Carr, L. E., III, and R. L. Elsberry, 1997: Models of tropical cyclone wind distribution and beta-effect propagation for application to tropical cyclone track forecasting. *Mon. Wea. Rev.*, **125**, 3190-3209.
- Carr, L. E., III, and R. L. Elsberry, 1998: Objective diagnosis of binary tropical cyclone interactions for the western North Pacific basin. *Mon. Wea. Rev.*, **126**, 1734-1740.
- Carr, L. E., III, M. A. Boothe, S. R. White, C. S. Kent, and R. L. Elsberry, 1995: Systematic and integrated approach to tropical cyclone track forecasting. Part II. Climatology, reproducibility, and refinement of meteorological data base. Tech. Rep. NPS-MR-95-001, Naval Postgraduate School, Monterey, CA 93943-5114, 96 pp.
- Carr, L. E., III, M. A. Boothe, and R. L. Elsberry, 1997a: Observational evidence for alternate modes of track-altering binary tropical cyclone scenarios. *Mon. Wea. Rev.*, **125**, 2094-2111.
- Carr, L. E., III, R. L. Elsberry, and M. A. Boothe, 1997b: Condensed and updated version of the systematic approach meteorological knowledge base western North Pacific. Tech. Rep. NPS-MR-98-002, Naval Postgraduate School, Monterey, CA 93943-5114, 167 pp.
- Kent, C. S. T., 1995: Systematic and integrated approach to tropical cyclone track forecasting in the North Atlantic. M. S. Thesis, Naval Postgraduate School, Monterey, CA 93943, 76 pp.

- Schnabel, R. G., 1998: A comparison of the NOGAPS and GFDN dynamical track prediction models during the 1997 western North Pacific typhoon season. M. S. Thesis, Naval Postgraduate School, Monterey, CA 93943, 137 pp.
- White, S. R., 1995: Systematic and integrated approach to tropical cyclone track forecasting in the eastern and central North Pacific. M. S. Thesis, Naval Postgraduate School, Monterey, CA 93943, 79 pp.

INITIAL DISTRIBUTION LIST

- | | | |
|----|---|----|
| 1. | Defense Technical Information Center
8725 John J. Kingman Rd., STE 0944
Ft. Belvoir, VA 22060-6218 | 2 |
| 2. | Dudley Knox Library, Code 013
Naval Postgraduate School
Monterey, CA 93943-5100 | 2 |
| 3. | Research Office, Code 09
Naval Postgraduate School
Monterey, CA 93943-5138 | 1 |
| 4. | Office of Naval Research
Marine Meteorology Division
800 N. Quincy St.
Arlington, VA 22217 | 2 |
| 5. | Space and Naval Warfare Systems Command
PMW 185
4301 Pacific Highway
San Diego, CA 92110-3127 | 5 |
| 6. | Dr. Carlyle H. Wash, Chairman
Department of Meteorology, MR/Wx
Naval Postgraduate School
589 Dyer Rd., Room 254
Monterey, CA 93943-5114 | 1 |
| 7. | Naval Pacific Meteorology and Oceanography Center/
Joint Typhoon Warning Center
Box 113
Pearl Harbor, HI 96860-5050 | 25 |
| 8. | Dr. Russell L. Elsberry
Department of Meteorology, MR/Es
Naval Postgraduate School
589 Dyer Rd., Room 254
Monterey, CA 93943-5114 | 85 |